

PDF hosted at the Radboud Repository of the Radboud University Nijmegen

The following full text is a publisher's version.

For additional information about this publication click this link.

<http://hdl.handle.net/2066/199057>

Please be advised that this information was generated on 2019-12-04 and may be subject to change.



Splice modulation as potential therapy for Usher syndrome IIa

RALPH W.N. SLIJKERMAN

Splice modulation as potential therapy for Usher syndrome IIa

Radulfus Willem Nicolaas Slijkerman

Ph.D.-thesis

January, 2019 – Nijmegen

Colophon

The work presented in this thesis was carried out within the Radboud Institute for Molecular Life Sciences. The research in this thesis was financially supported by the Netherlands Organisation for Health Research and Development (ZonMW E-rare grant 40-42900-98-1006 (EUR-USH)), the Netherlands Organisation for Scientific Research (grant Veni-016.136.091 to Erwin van Wyk), Stichting Ushersyndroom, Stichting Wetenschappelijk Onderzoek DoofBlindheid (SWODB), Gelderse Blindenstichting, Stichting Nederlands Oogheekundig Onderzoek, Stichting Blindenhulp, Stichting Researchfonds Nijmegen, Landelijke Stichting voor Blinden en Slechtzienden, the Foundation Fighting Blindness USA (grant number PPA-0517-0717-RAD) and Stichting AF Deutman Oogheekunde Researchfonds (SAFDOR). For publication of this thesis, a financial support by the Department of Otorhinolaryngology at the Radboudumc, Nijmegen – the Netherlands, was received.

Cover and lay-out design, and printing of this thesis was performed by Optima Grafische Communicatie, Rotterdam, the Netherlands.

© Ralph W.N. Slijkerman, 2019

ISBN: 978-94-92896-89-6

Splice modulation as potential therapy for Usher syndrome IIa

Proefschrift

ter verkrijging van de graad van doctor
aan de Radboud Universiteit Nijmegen
op gezag van de rector magnificus prof. dr. J.H.J.M. van Krieken,
volgens besluit van het college van decanen
in het openbaar te verdedigen op donderdag 17 januari 2019
om 12.30 uur precies

door

Radulfus Willem Nicolaas Slijkerman

geboren op 26 februari 1990

te Terneuzen

Promotor

Prof. dr. J.M.J. (Hannie) Kremer

Copromotoren

Dr. H.A.R. (Erwin) van Wijk

Dr. R.J.E. (Ronald) Pennings

Manuscriptcommissie

Prof. dr. R.E. (Roland) Brock (voorzitter)

Prof. dr. A.M. (Annemieke) Aartsma-Rus, Universiteit Leiden

Prof. dr. ir. J.P.W.M. (Jeroen) Bakkers, Universiteit Utrecht

Paranimfen

Muriël Messchaert

Tjeerd van Dijk

Splice modulation as potential therapy for Usher syndrome IIa

Doctoral Thesis

to obtain the degree of doctor
from Radboud University Nijmegen
on the authority of the Rector Magnificus prof. dr. J.H.J.M. van Krieken,
according to the decision of the Council of Deans
to be defended in public on Thursday, January 17, 2019
at 12.30 hours

by

Radulfus Willem Nicolaas Slijkerman

Born in Terneuzen, the Netherlands
on Februari, 26, 1990

Supervisor

Prof. dr. J.M.J. (Hannie) Kremer

Co-supervisors

Dr. H.A.R. (Erwin) van Wijk

Dr. R.J.E. (Ronald) Pennings

Doctoral Thesis Committee

Prof. dr. R.E. (Roland) Brock (chair)

Prof. dr. A.M. (Annemieke) Aartsma-Rus, Leiden University

Prof. dr. ir. J.P.W.M. (Jeroen) Bakkers, Utrecht University

Paranimphs

Muriël Messchaert

Tjeerd van Dijk

TABLE OF CONTENTS

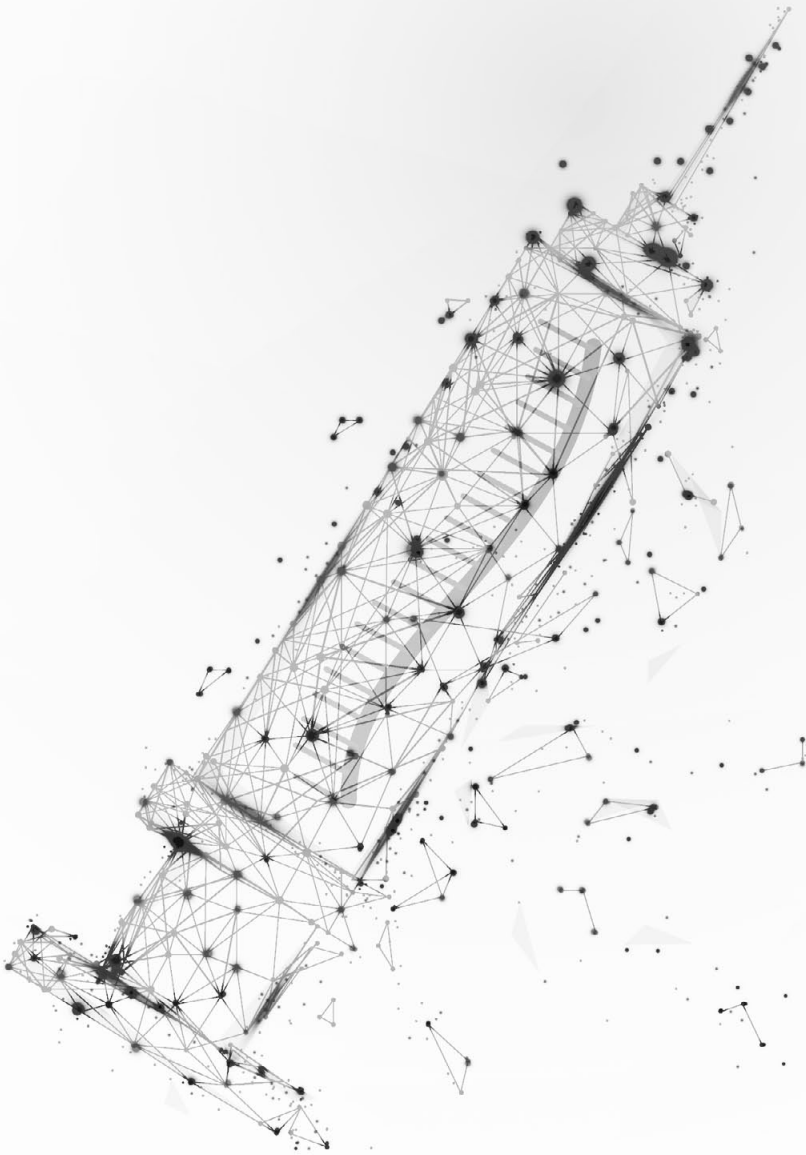
Chapter 1: General Introduction And Outline Of This Thesis	8
Chapter 1a: Molecular genetics of Usher syndrome: current state of understanding	10
Chapter 1b: Aim and outline of this thesis	30
Chapter 2: Zebrafish As Animal Model To Study Retinal Degeneration	40
Chapter 2a: The pros and cons of vertebrate animal models for functional and therapeutic research on inherited retinal dystrophies	42
Chapter 2b: Usherin defects lead to early-onset retinal dysfunction in zebrafish	104
Chapter 2c: Affinity purification of <i>in vivo</i> -assembled whirlin-associated protein complexes from the zebrafish retina	138
Chapter 3: A Splice-Based Therapy For <i>USH2A</i>-Associated Retinal Degeneration Due To The Deep Intronic c.7595-2144A>G Mutation That Activates PE40	166
Chapter 3a: Antisense oligonucleotide design and evaluation of splice-modulating properties using cell-based assays	168
Chapter 3b: Antisense oligonucleotide-based splice correction for <i>USH2A</i> -associated retinal degeneration caused by a frequent deep-intronic mutation.	182
Chapter 3c: Poor splice site recognition in a humanized zebrafish knock-in model for the recurrent deep-intronic c.7595-2144A>G mutation in <i>USH2A</i>	208
Chapter 4: Skipping Of <i>ush2a</i> Exon 13 Prevents Retinal Dysfunction In A Mutant Zebrafish Model	236
Chapter 5: General Discussion And Future Perspectives	260
Chapter 6: In Brief	288
Chapter 6a: Summary And Conclusions	290
Chapter 6b: Samenvatting En Conclusies	296
Chapter 7: About The Author	304
Chapter 7A: List Of Publications	306
Chapter 7B: Curriculum Vitae	312
Chapter 7C: Acknowledgements	316
Chapter 7D: RIMLS Portfolio	322

Chapter **1**

General Introduction And Outline Of This Thesis



Chapter **1** a



Molecular genetics of Usher syndrome: current state of understanding

Ralph W.N. Slijkerman^{a, b}, Hannie Kremer^{a, c} and Erwin van Wijk^a

^a Department of Otorhinolaryngology, Radboud University Medical Center, Geert Grooteplein 10, 6525 GA, Nijmegen, The Netherlands

^b Radboud Institute for Molecular Life Sciences, Radboud University Medical Center, Geert Grooteplein 10, 6525 GA, Nijmegen, The Netherlands

^c Department of Human Genetics, Radboud University Medical Center, Geert Grooteplein 10, 6525 GA, Nijmegen, The Netherlands

The majority of this chapter is published in eLS (*encyclopedia of Life Sciences*), 2017

doi: 10.1002/9780470015902.a0021456.pub2

Usher syndrome is an autosomal recessively inherited disorder that is characterized by (congenital) moderate-to-profound hearing loss combined with a progressive loss of vision. Also vestibular impairment can be associated with the syndrome. Usher syndrome is the most common cause of hereditary deaf-blindness in man, representing approximately 50% of cases, with a prevalence of about 1 in 20,000 individuals. Although the syndrome and its heredity were already described by Von Graefe in 1858 (Graefe 1858), shortly before Mendel proposed the principles of heredity and introduced the concepts of dominantly and recessively inherited traits, it was finally named after the Scottish ophthalmologist Charles Howard Usher in 1935.

THE EAR: ANATOMY AND SOUND PERCEPTION

With our ears we can perceive sounds in order to create awareness of our surroundings. Sound waves are captured by the outer ear (containing the external ear, also named the auricle, and the external auditory canal) and transported to the tympanic membrane (ear drum), which separates the outer ear from the middle ear. The middle ear contains the ossicles, the malleus (hammer), incus (anvil), and stapes (stirrup), the three smallest bones in the human body. The ossicles connect the tympanic membrane and the oval window of the inner ear. The inner ear is buried in the hardest bone of the human body, the temporal bone, and consists of a labyrinth of ducts that contain ion-rich fluids that move in response to sound waves and movements of the head. The inner ear can be divided into the balance organ (the vestibulum) and the hearing organ (the cochlea) (**Fig. 1**). The cochlea is spiraling around a cartilage structure, the modiolus, and is divided into three parallel ducts: the scala vestibule, the scala tympani and the scala media. Within the scala media the actual sensory epithelium is located within the Organ of Corti. This epithelium consists of three rows of outer hair cells, one row of inner hair cells and supporting cells. On top of the hair cells, actin-based protrusions are present, the stereocilia. Stereocilia are typically organized in a V-shaped staircase-like pattern. Upon deflection of the hair bundles, the hair cells convert mechanical signals (sound waves) into electrical signals (action potential) by the physical opening of mechano-transduction channels. In patients with Usher syndrome, however, the organization of hair bundles is affected and therefore lead to a reduced ability of sound perception. These patients are therefore often provided with hearing aids or cochlear implants. Patients with cochlear implants have shown to improve their speech intelligibility and report an improved quality of life (Hartel et al. 2017). The molecular composition of the hair bundles and the role of Usher-associated proteins in the process of hair bundle formation is explained later on in more detail.

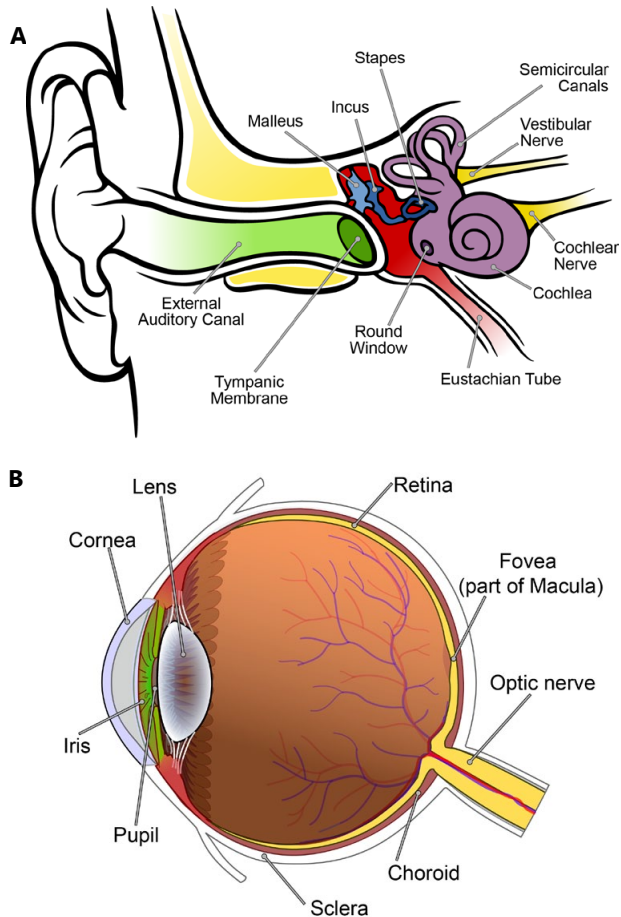


Figure 1. Anatomical overview of the ear (A) and eye (B). The ear overview is taken from (Chittka and Brockmann 2005) and the eye overview is adapted from Wikipedia (https://commons.wikimedia.org/wiki/File:Schematic_diagram_of_the_human_eye_en.svg).

THE EYE: ANATOMY AND LIGHT PERCEPTION

The eye is the sensory organ that is able to receive and convert light into an electrical signal that is processed by the brain. The anterior region of the eye, consisting of the cornea, the sclera, the iris and the pupil, is visible from outside the body. The lens, which is located behind the pupil, can accommodate to adjust the focal point of entering light beams. The retina, which decorates the back of the eye, will capture the light and has an organized layered structure that contains highly specialized cells. The actual light-sensitive cell is the photoreceptor. Two types of photoreceptor cells can be distinguished: cones and rods. The human retina contains three types of cones: blue (S-

cone), green (M-cone) and red (L-cone). Some vertebrates - such as the zebrafish - have an additional UV-light sensitive cone. Rods cannot distinguish between colors, but are responsible for dim-light (scotopic) vision. In rod photoreceptors, rhodopsin acts as the photopigment that initiates the phototransduction cascade. In cones, different types of photopsin molecules are present, depending on the cone subtype, which all have a different spectral sensitivity. In the human retina, cone photoreceptors are mostly clustered in the central region of the retina, called the fovea, whereas rod photoreceptors are more abundantly present in the peripheral retina. For a more detailed description of the retinal architecture and molecular processes that play a role in light perception, the reader is referred to **chapter 2a**. The role of Usher syndrome-associated proteins in the retina will be discussed in more detail below.

CLINICAL CHARACTERISTICS OF USHER SYNDROME

Clinical heterogeneity of Usher syndrome was recognized by Julia Bell. She reported differences in the severity of hearing loss among patients and these differences formed the basis for the present distinction of three clinical types: type I (USH1), type II (USH2) and type III (USH3). USH1 is characterized by congenital severe-to-profound hearing loss combined with the absence of vestibular function. RP is the type of retinal degeneration seen in Usher syndrome, most often starting with night blindness as the first clinical symptom. In patients with USH1, RP is generally diagnosed before puberty.

Typical for USH2 is congenital moderate-to-severe bilateral hearing loss, with high frequencies being most severely affected. For USH2a it has been shown that hearing impairment is more progressive in patients with two protein-truncating mutations as compared to patients with one or two missense mutations (Hartel et al. 2016). Vestibular function is within the normal range, as are motor milestones of the patients. However, also mildly abnormal vestibular function has been reported. The first clinical symptoms of RP in USH2a patients become apparent at an age of approximately 15 years, which is 10 years earlier than in nsRP cases with mutations in *USH2A* (Pierrache et al. 2016).

USH3 is more variable than USH1 and USH2. In USH3 the hearing loss is progressive with a variable age of onset. Also, the age at which RP is diagnosed is variable and can precede that of the hearing loss. Vestibular function can be normal, absent or partially impaired.

The majority of patients with Usher syndrome can be classified as USH1, USH2 or USH3. However, there are also patients with an atypical form of Usher syndrome with, for example, congenital severe-to-profound hearing loss and late onset or subclinical RP.

Besides hearing, balance and vision problems, also additional phenotypic traits have been reported in patients with Usher syndrome, including anosmia, ataxia, sperm abnormalities and osteopenia (Reiners et al. 2006, Ribeiro et al. 2016, Urano et al. 2012). Several of the Usher genes have been shown to be expressed in the mouse olfactory epithelium and the encoded proteins interact with olfactory signaling proteins (Jansen et al. 2016). Functional evaluation of mouse models showed that there was olfactory impairment in *SANS*- and *harmonin*-deficient mice (Jansen et al. 2016). In patients with Usher syndrome, only a reduced ciliary beat frequency of the nasal epithelia has been observed (Aparisi et al. 2013) without appearance of any functional impairment in a sniffing test (Dad et al. 2016). Although ataxia was mentioned as a feature in a patient clinically diagnosed with Usher syndrome, subsequent genetic screening led to a different - non-Usher syndrome - diagnosis. Since Usher genes are also expressed in the central nervous system and Usher patients with psychiatric symptoms have been reported, it has been proposed that Usher proteins fulfill a distinct role in the brain as well (reviewed by Domanico et al. 2015). However, underlying mechanisms are not known and psychiatric symptoms might be of secondary nature as a consequence of the (partial) loss of the two major sensory systems.

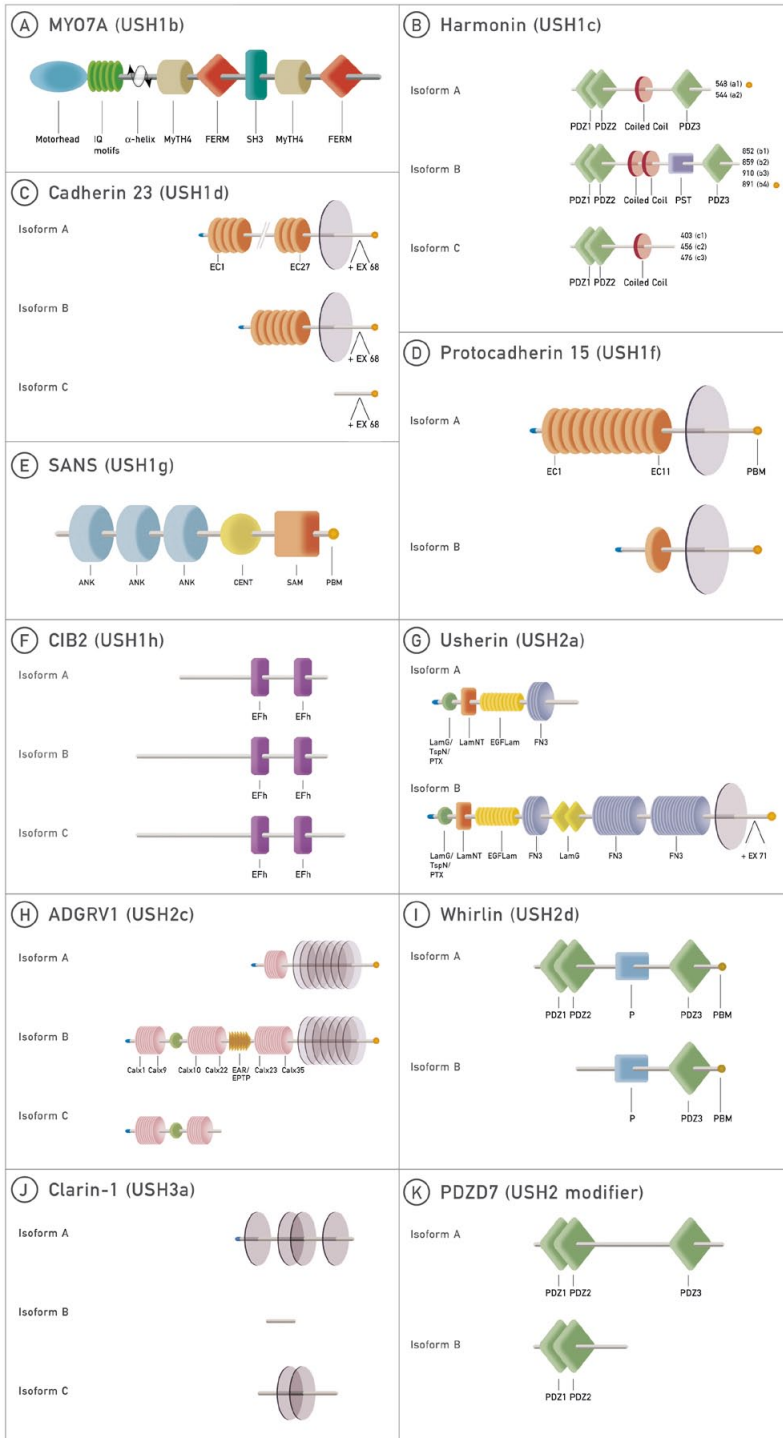
USHER SYNDROME IS GENETICALLY HETEROGENEOUS

Besides being clinically heterogeneous, Usher syndrome also exhibits genetic heterogeneity (**Table 1**). For *USH1*, nine genetic loci have been described so far, *USH1b*–*USH1h*, *USH1j* and *USH1k*. For *USH2*, three loci are known, *USH2a*, *USH2c* and *USH2d*. So far, two loci have been described for *USH3*: *USH3a* and *USH3b*. In addition, defects of other genes than those listed here might contribute to an Usher-like phenotype. Mutations in *PDZD7* have been shown to modify the retinal phenotype in *USH2A* patients. Furthermore, *PDZD7* has been proposed as a contributor to digenic Usher syndrome in combination with *ADGRV1* or *USH2A* mutations (Ebermann et al. 2010). Mutations in *HARS*, associated with *USH3b*, and a combination of mutations in *CEP250* and *C2ORF71* are also associated with (atypical) Usher syndrome (Aparisi et al. 2014).

USH1b, caused by mutations in *MYO7A*, is the most common type of *USH1* accounting for 30–50% of *USH1* cases. Mutations in the *USH2A* gene, encoding usherin, are the most common cause of Usher syndrome, explaining ~50% of all *USH* cases and up to 85% of *USH2* patients. Apart from deaf-blindness, mutations in the *USH1* genes *MYO7A*, *USH1C*, *CDH23*, *PCDH15*, *USH1G*, *CIB2* and *USH* modifier *PDZD7* can also result in non-syndromic hearing loss (Ebermann et al. 2010, Cosgrove and Zallocchi 2014). Defects in *USH2A* are associated with nsRP when at least one ‘retinal disease-specific’ *USH2A* allele is present, resulting in the preservation of normal hearing (Lenassi, Vincent, et al.

Table 1. Types of Usher syndrome and associated genes and proteins, with their corresponding animal models and therapeutical progress.

USH type	Locus	Location	Gene	Protein	Animal model		Therapeutic progress	
					Mouse	Fruit fly	Zebrafish	Fruit fly
USH 1	USH1b	11q13.5	MYO7A	MYO7A	Shaker-1 (sh1)	<i>crinkled</i>	<i>mariner</i>	<ul style="list-style-type: none"> • Transplicing therapy in mice • Gene augmentation in mice and humans (UshStat®)
	USH1c	11p15.1	USH1C	harmonin	Deaf circler (dfcr); deaf circler 2 Jackson (dfcr-2J)	<i>ush1c^{h293}</i>	<i>CG5921</i>	<ul style="list-style-type: none"> • Gene augmentation in mice • Splice correction in mice • Translational read-through inducing drugs (TRIDs) <i>in vivo</i> • Gene correction <i>in vitro</i>
	USH1d	10q22.1	CDH23	cadherin-23	Waltzer (v)		<i>sputnik</i>	
	USH1e	21q21	unknown	unknown				
	USH1f	10q21.1	PCDH15	protocadherin-15	Ames waltzer (av)		<i>orbiter</i>	<i>Cad99C</i>
	USH1g	17q25.1	USH1G	SANS	Jackson shaker (js)			<i>Sans</i>
	USH1h	15q22-q23	unknown	unknown				• TRIDs <i>in vitro</i>
	USH1j	15q25.1	CIB2	CIB2				
	USH1k	10p11.21-q21.1	unknown	unknown				
	USH2	USH2a	1q41	USH2A	usherin	<i>ush2a^{-/-}</i>	<i>ush2a^{p1245}</i> , <i>ush2a^{mc1}</i>	
USH2c	5q14.3	ADGRV1	ADGRV1		<i>gpr98^{-/-}</i> ;			
					<i>vlg1/del7TM</i> ; <i>Frings/Mass1^{4B/8V}</i>			
USH2d	9q32	WHRN	whirlin	Whirlter (wt); whirlin long isoform ^{-/-}				<ul style="list-style-type: none"> • Gene augmentation in mice
USH3	USH3a	3q25.1	CLRN1	clarin-1	<i>Clrn1^{-/-}</i> ;	<i>hCLRN1^{N48K}</i>		
					<i>Clrn1^{N48K/N48K}</i>			<ul style="list-style-type: none"> • Small molecules
USH modifier	-	10q24.31	PDZD7	PDZD7				



2015). However, there is one report of a patient having compound heterozygous mutations in *USH2A* leading to isolated hearing impairment, whereas her brother with the same mutations developed Usher syndrome (Lenassi, Robson, et al. 2015). However, the distinct phenotypic differences between brother and sister question the pathogenicity of either one of the reported variants.

Usher syndrome is nowadays often genetically diagnosed after failure of the Newborn Hearing Screening Test. Standard DNA diagnostic efforts include the analysis of exonic sequences, splice sites and chromosomal aberrations. In a research setting, whole genome sequencing could be used to reveal not only known genetic defects, but also previously unknown mutations in both exonic and (deep-)intronic regions. For instance,

Figure 2 (previous page). Schematic representation of the architecture of Usher proteins and their different isoforms.

(A) The *USH1b* protein, *MYO7A*, is composed of a motor head domain, five calmodulin-binding IQ motifs, two FERM domains, two MyTH4 domains and a Src homology 3 (SH3) domain. **(B)** Three different classes of isoforms of the *USH1c* protein, harmonin, are identified. All three isoforms consist of two PDZ (PSD95, discs large, ZO-1) domains (PDZ1 and 2) and one coiled-coil domain. Class A isoforms contain an additional PDZ domain (PDZ3). The class B isoforms contain also this third PDZ domain, a second coiled-coil domain and a proline, serine, threonine-rich region (PST). Isoform A1 and B4 contain a C-terminal class I PDZ binding motif (PBM). **(C)** Representation of the three different isoforms of cadherin 23 (*USH1d*). Isoform A is composed of 27 Ca²⁺-binding extracellular cadherin domains (EC1-27), a transmembrane domain (TM) and a short intracellular region with a C-terminal class I PBM. Isoform B is similar to isoform A, but lacks the first 21 EC domains. Isoform C only consists of the intracellular region and C-terminal PBM. **(D)** Like cadherin 23, the nonclassical cadherin protocadherin 15 (*USH1f*) consists of either 11 (isoform A) or 1 (isoform B) EC domains, a transmembrane domain and a C-terminal class I PBM. **(E)** The scaffold protein SANS (*USH1G*) consists of three ankyrin domains (ANK), a central region (CENT), a sterile alpha motif (SAM) and a C-terminal class I PBM. **(F)** Three isoforms are known for *CIB2*, the *USH1j* protein. All three isoforms contain two EF-hand domains (EFh). Variation in protein length is determined by alternative splicing in the 5' and 3' end of *CIB2* transcripts, resulting in isoform A, B and C. **(G)** Isoform A of the *USH2a* protein contains an N-terminal thrombospondin/pentaxin/laminin G-like domain, a laminin N-terminal (LamNT) domain, ten laminin-type EGF-like (EGF Lam) and four fibronectin type III (FN3) domains. In addition to the domain structure of isoform A, isoform B contains two laminin G (LamG), 28 FN3, a transmembrane domain and an intracellular region with a C-terminal class I PBM. **(H)** Three isoforms of the adhesion G protein-coupled receptor V1 (*ADGRV1*, *USH2c*), are identified. The longest isoform, isoform B, consists of a thrombospondin/pentaxin/laminin G-like domain (depicted in green), 35 Ca²⁺-binding calcium exchanger b (Calx) domains, seven EAR/EPTP repeats, a seven transmembrane region and an intracellular region containing a C-terminal class I PBM. Isoform A is composed of the last six C-terminal Calx domains, the seven transmembrane region and the intracellular region with the C-terminal class I PBM. The predicted extracellular isoform C only contains the first 16 N-terminal Calx domains and the thrombospondin/pentaxin/laminin G-like domain. **(I)** Isoform A of whirlin, the *USH2d* protein, contains three PDZ domains and a proline-rich region (indicated by 'P'). Isoform B lacks the two N-terminal PDZ domains. Both isoforms contain a C-terminal class II PBM. **(J)** The protein product of *USH3a*, *Clarin-1*, is present in three isoforms. Isoform A is the longest and consists of four transmembrane domains. Isoform C consists of two of these transmembrane domains, whereas isoform B consists of none of the transmembrane domains. **(K)** The *USH2* modifier PDZD7 is structurally related to harmonin and whirlin and consists of three PDZ domains (isoform A). The smaller isoform B lacks the third PDZ domain. This figure was adapted from (Kremer et al. 2006).

four deep-intronic mutations have been identified in *USH2A*, all leading to pseudoexon inclusion into the mature mRNA transcript and a subsequent disruption of the reading frame (Vache et al. 2012, Liquori et al. 2016).

USH PROTEIN STRUCTURE AND ISOFORMS

USH proteins (**Fig. 2**) are members of protein families with very diverse functions (for review see Cosgrove and Zallocchi 2014). *MYO7A* is an actin-based motor protein, whereas cadherin-23 and protocadherin-15 are members of the cadherin protein superfamily that consists of cell adhesion molecules (Geng et al. 2013). *ADGRV1* and usherin are both transmembrane proteins with large extracellular regions consisting of domains that suggest a role in outside-in signaling. The extracellular region of *ADGRV1* is mainly built up by CalX- β domains, whereas usherin contains stretches of EGF-Lam and fibronectin type3 (FN3) motifs in its extracellular region. Whirlin, harmonin, *PDZD7* and *SANS* function as scaffold proteins, of which the first three are structurally related. *Clarin-1* is predicted to be a four-transmembrane protein and part of the vertebrate-specific clarin protein family. The most recently identified Usher protein *CIB2* is named after its calcium- and integrin-binding capacity (Giese et al. 2017). Except for *USH1G*, alternative transcripts are known for all USH genes that (are predicted to) encode several protein isoforms.

USH PROTEINS ARE PART OF USH PROTEIN NETWORKS

At first sight, the diverse nature of the USH proteins seems surprising in view of the limited phenotypic differences that are observed between the genetic subtypes of Usher syndrome. These clinical similarities suggest that all associated genes encode proteins that function in a common process or pathway.

Indeed, USH proteins have been found to interact with each other in highly dynamic protein networks (Pan and Zhang 2012, Maerker et al. 2008, Sorusch et al. 2017). USH-associated proteins have PDZ (PSD95, Discs large, ZO-1) domains, that are able to form protein-protein interactions with a PDZ-binding motif (PBM). Indeed, a complex consisting of the USH1 proteins cadherin-23, harmonin and *MYO7A* for instance, is mediated by PDZ-PBM interactions and is pre-assembled in the ER. Misfolding or lack of one of the three proteins leads to disruption of the protein complex and consequently to ER-stress and photoreceptor degeneration (Blanco-Sanchez et al. 2014). Like cadherin-23, also protocadherin-15 uses its intracellular C-terminal PDZ-binding motif to interact with harmonin (Reiners, Marker, et al. 2005). In 2004, we identified the transmembrane

isoform of usherin with a PBM at the C-terminus suggesting a link with the USH1 protein network. We confirmed this link for both usherin and ADGRV1 (Reiners, van Wijk, et al. 2005). The similarity between harmonin and whirlin then directed us to test whirlin as a candidate interaction partner of these USH2 proteins, with positive results (van Wijk et al. 2006). Also harmonin and SANS are connected by a PDZ-PBM interaction, synergistically strengthened by interactions of the PDZ domains of harmonin with SANS' SAM domain (Zou et al. 2017). Also a PDZ domain-mediated interaction is present between the USH2 scaffold protein whirlin and SANS (Maerker et al. 2008). The USH protein network, as it has been unraveled so far, is schematically depicted in **Fig. 3**. Interactions between multiple Usher and non-Usher proteins depend on the same protein domains, for instance whirlin's PDZ1 and 2 domains associate with usherin, ADGRV1 and SANS (Maerker et al. 2008, van Wijk et al. 2006), suggesting that the USH protein network is highly dynamic. Spatiotemporal differences in network composition have

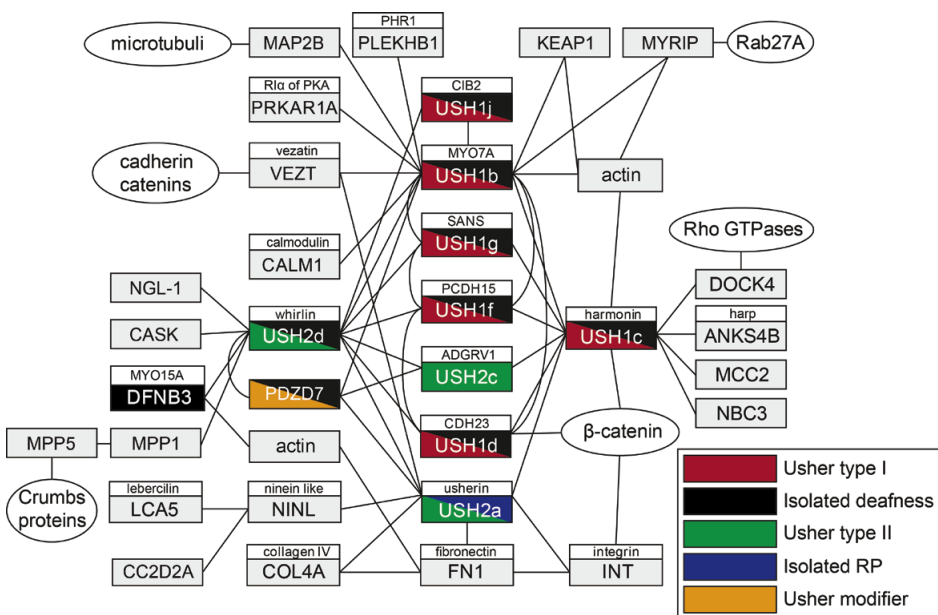


Figure 3. Schematic representation of the Usher protein network. All identified protein–protein interactions are indicated (references: see text). Boxes in red indicate an association with Usher syndrome type I (USH1), green indicates association with Usher syndrome type II (USH2), blue indicates association with isolated retinitis pigmentosa (RP), black indicates association with isolated deafness and orange indicates association as an Usher syndrome modifier. This figure was adapted from (Kremer et al. 2006).

been observed, possibly needed to fulfill distinct roles at separate subcellular locations and during different stages of retinal and inner ear development.

THE USH PROTEIN NETWORK IN THE INNER EAR: LOCALIZATION AND FUNCTION

In the inner ear, the main localization of USH proteins is in the neurosensory hair cells, that mediate mechanotransduction (**Fig. 4**) (for review see Cosgrove and Zallochi 2014). Hair cells, present in both the cochlea and the vestibular system are named after the 'hair bundles' that are located at the apical surface of these cells. Bending of the hair bundle as the result of sound waves in the cochlea or displacement of fluid in the vestibulum, leads to the opening of mechano-electrical transducer (MET)-channels. A

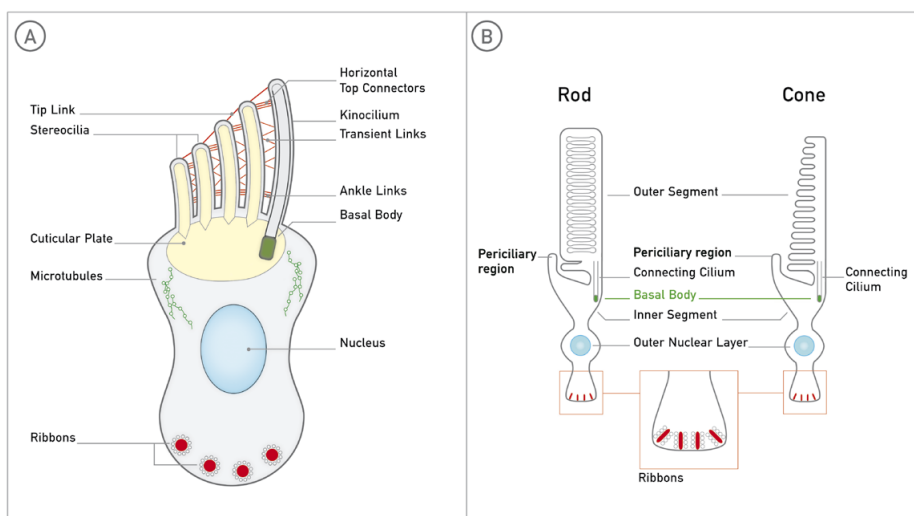


Figure 4. Schematic representation of the sensory cells in the inner ear and retina. (A) The apical side of the inner ear hair cell carries the highly organized, actin filled stereocilia, in which the mechanotransduction takes place. The stereocilia are connected by the tip links, horizontal links, transient links and ankle links. The stereocilia are anchored in the actin-rich cuticular plate. The only true cilium, the kinocilium, is located lateral to the largest stereocilium and extends from the basal body. The synaptic junctions between hair cells (mainly in inner hair cells) and afferent neurons at the basal side of the hair cell, contain the synaptic ribbons. **(B)** The rod and cone photoreceptors, which are the main morphological subtypes of photoreceptors, are highly polarized. The photoreceptor outer segment, a highly modified cilium containing the phototransduction proteins, is separated from the inner segment by the connecting cilium. The periciliary region is situated next to the connecting cilium and the proximal outer segment. The nuclei of the photoreceptors are situated in the outer nuclear layer. The synaptic terminals, containing the ribbons, connect the photoreceptors with horizontal cells, bipolar cells and ganglion cells. This figure was adapted from (Kremer et al. 2006).

signaling cascade is initiated culminating in the release of neurotransmitter at the base of the hair cell. The hair bundle consists of actin-based microvilli, the stereocilia. Every bundle contains one true, microtubule-based, cilium that is known as the kinocilium. The kinocilium in mammals is required for proper hair bundle formation and orientation and disappears at the end of hair cell development in the cochlea. Hair bundles maintain their cohesion by fibrous interstereociliar links and by links between the tallest stereocilia and the kinocilium. The pattern of these fibrous links in cochlear hair cells changes during development in a species- and hair cell type-specific manner.

Cochlear development and formation of stereocilia bundles has been extensively studied in mice. Mice with mutations in orthologous USH genes exhibit abnormally developed hair bundles in which the stereocilia are splayed (e.g. Waltzer and Ames Waltzer) or shorter (e.g. Deaf circler and Whirler) (El-Amraoui and Petit 2005). This points towards a function of the USH proteins in hair bundle development and cohesion. The picture that emerged from extensive immunohistochemistry and immunoelectronmicroscopy in normal mice and mice with mutations in USH genes, is that the fibrous links are (partially) composed of transmembranous USH proteins that are anchored via scaffold proteins and MYO7A to the actin core of the stereocilia. During cochlear hair cell differentiation, before the hair bundle has developed, the kinocilium repositions to the periphery of the cell. This is essential for correct positioning and orientation of the hair bundle. The studies of Lefevre and coworkers (Lefevre et al. 2008) suggest a link between hair bundle orientation and the formation of the links between stereocilia and kinocilium as well as the interstereociliar links. The first steps of polarization of the hair bundle does not seem to be affected in mice deficient for USH1 proteins, as is the case for the localization of proteins involved in planar cell polarity. It has been hypothesized that the disturbance of differential elongation of different rows of stereocilia (staircase pattern) in mice deficient for USH1 genes is caused by a lack of tension forces from the tip link of the tallest stereocilia on the tips of the rows of smaller stereocilia (Lefevre et al. 2008). These tip links between stereocilia are formed by heteromeric interactions of the extracellular fragments of cadherin-23 and protocadherin-15, the former at the upper part and the latter at the lower part of the link (Geng et al. 2013). At the upper tip link density (UTLD) cadherin-23 is linked to the actin skeleton by an interaction with MYO7A, aided by harmonin and SANS (Bahloul et al. 2010). In mice deficient for either MYO7A, harmonin or SANS, tip links were present but sparser (Lefevre et al. 2008). At the lower tip link density (LTLD), protocadherin-15 is connected to the MET-channel (Fettiplace and Kim 2014). Probably also SANS is present in this complex, since SANS interacts with protocadherin-15 *in vitro* and SANS is missing from stereocilia in either protocadherin-15 or cadherin-23 knock-out mice (Caberlotto et al. 2011). In order to function properly, the interaction between MET-channels and CIB2 is essential (Giese et al. 2017).

Ankle links are temporal and disappear after hair bundle development is completed. The spatio-temporal expression pattern of usherin, ADGRV1, whirlin and also vezatin, a MYO7A- and usherin-interacting protein, suggests that these molecules are associated with the ankle links (Toms et al. 2015). This is supported by the absence of ankle links in *Adgrv1* knock-out (*gpr98^{-/-}*) mice and the lack of usherin, whirlin and vezatin at the base of stereocilia in developing cochlear hair cells of these mice (Mathur and Yang 2015). However, the localization of whirlin at the tip of the stereocilia is unaltered in *gpr98^{-/-}* mice. In addition, with the exception of mice lacking MYO7A, all mice that are deficient for USH1 proteins still have the ability to form ankle links (Lefevre et al. 2008, Zou et al. 2017).

Besides at the UTLD, SANS is also localized beneath the cuticular plate, especially below the basal body of the kinocilium where the cuticular plate is thinner (El-Amraoui and Petit 2005). Because of the enrichment of vesicles and microtubules in the apical peri- and subcuticular regions including the subkinociliar region, SANS has been suggested to be involved in the trafficking of USH proteins along microtubules and actin filaments towards the stereocilia (El-Amraoui and Petit 2005). Supporting evidence comes from experiments that reveal an association between SANS and the microtubules in photoreceptors (Maerker et al. 2008). Furthermore, harmonin accumulates in the apical region of the hair cell and is no longer detected in the stereocilia of mice lacking SANS (El-Amraoui and Petit 2005).

USH proteins have also been suggested to play an important role in hair bundle formation and stereocilia elongation. Harmonin, for example, has actin-bundling activity that is needed for hair bundle and hair cell morphogenesis (Phillips et al. 2011). Both SANS and whirlin, present at the tip of stereocilia during hair bundle development, are essential for stereocilia elongation (Caberlotto et al. 2011). ADGRV1 has been detected in the peripheral microvilli at the apical surface of hair cells. These microvilli do not develop into stereocilia and degenerate in normal hair cells. In *gpr98^{-/-}* mice, these microvilli undergo stereocilia-like maturation and therefore ADGRV1 is suggested to be required for the regression of peripheral microvilli during hair cell development (Michalski et al., 2007).

Several of the USH proteins have also been identified in the synaptic region of hair cells (reviewed by Cosgrove and Zallochi 2014). Mouse hair cell synaptogenesis was shown to be (partially) orchestrated by a complex comprising of clarin-1 and specific isoforms of the Usher proteins cadherin-23, protocadherin-15 and ADGRV1 (Zallochi et al. 2012). Usherin, ADGRV1, harmonin and SANS were found to be present in the pre- and postsynaptic region of both inner and outer hair cells and whirlin in the synaptic region of outer hair cells only (van Wijk et al. 2006, Zallochi et al. 2012). It has been postulated that the large extracellular fragments of usherin and ADGRV1 are involved in maintaining a proper spacing between pre- and postsynaptic membranes, similar to

their role in the ankle link complex at the base of stereocilia and as one of their proposed roles at the periciliary membrane of photoreceptors (Maerker et al. 2008, Yang et al. 2010). In inner hair cells, harmonin was shown to have a multifaceted presynaptic role in regulating cell surface $\text{Ca}_v1.3 \text{ Ca}^{2+}$ -channel levels and exocytosis (Gregory et al. 2013).

THE USH PROTEIN NETWORK IN RETINAL PHOTORECEPTORS

In photoreceptors, light is captured in the outer segment (OS) by disc-shaped membranes that contain the components of the phototransduction cascade. The OS is connected to the inner segment (IS) via the connecting cilium. The OS and connecting cilium together are regarded as a highly specialized non-motile cilium that develops from a basal body during photoreceptor differentiation. The photoreceptor IS contains the organelles necessary for eukaryotic cell metabolism, including the machinery for protein synthesis. Consequently, all OS proteins are synthesized in the IS and have to be transported through the connecting cilium.

The USH proteins most prominently localize at the photoreceptor connecting cilium region, more specifically in the basal body, the accessory centriole, the calyceal processes and at the periciliary membrane (**Fig. 4**; reviewed by Mathur and Yang 2015, Kremer et al. 2006). The b isoforms of harmonin are specifically found in rod OS, potentially anchored by protocadherin-15, and act as a scaffold (Reiners et al. 2006). Protocadherin-15 is indeed present in the membranes of OS and calyceal processes, where it has been recently hypothesized to connect the calyceal processes with each other and to the OS by heteromeric interactions with cadherin-23 similar as in stereociliary tip-links (Schietroma et al. 2017). Knockdown of *Pcdh15* in *Xenopus* leads to disorganization of calyceal processes and uncontrolled outgrowth of parts of the photoreceptor OS, indicating a role in photoreceptor development and/or maintenance (Schietroma et al. 2017). Additionally, like in hair cells, Usher proteins are found in the ribbon synapses of photoreceptors.

The apical part of the inner segment is shaped as a periciliary collar that surrounds the connecting cilium in mammalian photoreceptors. It has been suggested that this collar corresponds to the amphibian periciliary ridge complex, consisting of ridges and grooves (Maerker et al. 2008). Usherin, ADGRV1, SANS and whirlin are detected in the periciliary collar in mouse photoreceptors and in the ridges of the periciliary ridge complex in *Xenopus* (Maerker et al. 2008, Yang et al. 2010, Kremer et al. 2006). Also in macaque and human photoreceptors, the USH2 proteins are found at the periciliary collar that is wrapped around the connecting cilium (Sahly et al. 2012, Sorusch et al. 2017). Fibrous links connect the membranes of the connecting cilium and the periciliary collar in mammals. The fibrous links that connect these membranes are absent from

homozygous *vlgr1/del7TM* mice lacking ADGRV1 (Maerker et al. 2008). Therefore, the links in the periciliary region of photoreceptor cells are probably homologous to the ankle links in hair cells, composed of the extracellular regions of ADGRV1 and usherin. The scaffold proteins whirlin and SANS are thought to anchor these links in the opposed cytoplasmic compartments of the connecting cilium and the periciliary region.

The USH protein networks in the periciliary region and at the basal body and the accessory centriole have not only a function in providing structural support. Evidence is also pointing towards a concept in which Usher and Bardet-Biedl syndrome (BBS) proteins co-function in the organization of planar cell polarity (Giese, Riazuddin, and Ahmed 2013). Furthermore, Usher proteins have been implicated in intracellular transport mechanisms. MYO7A, for instance, was found to function in the transport of (rhod)opsin and RPE65 in photoreceptors and in the migration of melanosomes and phagosomes in the RPE (Mathur and Yang 2015). SANS can bind to the microtubule cytoskeleton and is proposed to be involved - together with myomegalin - in transport of cargo vesicles from the trans-Golgi network towards the outer segment, either via direct entering into the connecting cilium or after docking and fusion of transport vesicles to the periciliary membrane (Overlack et al. 2011, Maerker et al. 2008, Yang et al. 2010, Mathur and Yang 2015). Whirlin interacts with RPGR, a protein known to be involved in protein trafficking through the connecting cilium (Cosgrove and Zallocchi 2014). Usherin is transported by the NINL-associated vesicle transport complex. This transport complex also involves proteins associated with Leber congenital amaurosis (lebercilin) and Joubert/Meckel syndrome (CC2D2A) (van Wijk et al. 2009, Bachmann-Gagescu et al. 2015). Although Usher proteins have been implicated to aid in targeting and/or docking of vesicular transport mechanisms through the connecting cilium, photoreceptors can develop normally when one of the USH proteins is defective. This makes the role of Usher proteins difficult to interpret, since their contribution to transport mechanisms during development seems compensatory.

The protein domain architecture of several Usher molecules, such as usherin and ADGRV1, also suggests a role in outside-in-signaling. Besides harmonin, whirlin was also shown to directly interact with the calcium channel $Ca_v1.3$ and both proteins colocalize in the synapse and the connecting cilium region of mouse photoreceptors (reviewed by Cosgrove and Zallocchi 2014). This suggests that Usher proteins are involved in Ca^{2+} -signaling and signal transduction at both the synapse and connecting cilium region of photoreceptors (Sorusch et al. 2017). In addition, ADGRV1, regulated by PDZD7 and Ca^{2+} , has been shown to be involved in G-protein signaling via coupling to G_i , G_q and G_s proteins as has been observed after overexpression in HEK293 cells (Hu et al. 2014). However, an *in vivo* role for Usher proteins in inner ear or retinal signaling cascades has so far not been confirmed (Mathur and Yang 2015).

CELLULAR AND ANIMAL MODELS FOR USHER SYNDROME

In order to study the function of Usher proteins or to evaluate therapeutic strategies, suitable models are needed. Usher proteins have a distinct expression pattern in mostly difficult to obtain tissues such as retina, brain and inner ear. Nevertheless, alternative cell types and tissues that express Usher genes and can be collected semi-invasively, such as human nasal epithelium or hair roots, have been identified and used for limited applications (Vache et al. 2010, Nakanishi et al. 2010). Also, patient-derived fibroblasts with compound heterozygous *USH2A* mutations have been dedifferentiated into induced pluripotent stem cells and subsequently differentiated into photoreceptor-like cells to examine the mechanism of disease (Tucker et al. 2013). However, these cultured photoreceptors are not completely functional and lack retinal architecture and surrounding cells. Therefore, to understand the role of Usher proteins at the functional level and to evaluate therapeutic strategies it will be essential to study animal models. Nowadays, for almost all known Usher genes a corresponding mouse knock-out model has been generated and characterized (**Table 1**) (summarized by Toms et al. 2015). Although showing hearing impairment to various degrees, these knock-out mice sporadically recapitulate the retinal phenotype as observed in Usher syndrome patients, probably as a consequence of absent calyceal processes and an underdeveloped periciliary membrane in mouse photoreceptors (**Chapter 2a**). An alternative model organism used in Usher syndrome research is zebrafish (*Danio rerio*). Several zebrafish Usher knock-down and knock-out models have been generated and characterized. All of them show early-onset retinal dysfunction resulting in reduced electroretinogram (ERG) traces in *ush2a*, *Pcdh15b*, *Myo7a* (*mariner*) and *ush1c* (*ush1c^{fh293}*) models (Blanco-Sanchez et al. 2017, **Chapter 2b**). Due to an ancient genome duplication in teleost fish, orthologs of approximately 30% of mammalian genes are now present in two copies in the zebrafish genome. The expressed proteins from both gene copies often have obtained a split function. In zebrafish, *PCDH15* for instance has two paralogs: *Pcdh15a* and *Pcdh15b*. *Pcdh15a* knock-out zebrafish (*Ush1f*, *orbiter*) display hearing impairment and vestibular dysfunction without visual defects, while knock-down of *Pcdh15b* only results in impaired visual function (Seiler et al. 2005). Next to mice and zebrafish, also fruit fly (*Drosophila melanogaster*) knock-out models for the orthologous Usher genes *MYO7A* (*crinkled*; showing dentritic cap morphology defects in the Johnston's organ), *PCDH15* (*Cad99C*; having shorter and disorganized microvilli in the fly), *USH1G* (*Sans*; having no obvious phenotype), *CDH23* (*Cad88C*; uncharacterized) and *USH1C* (*CG5921*; uncharacterized) have been used to study the function of Usher proteins (Demontis and Dahmann 2009). With animal models that recapitulate visual defects as seen in Usher syndrome patients becoming available, it can be expected that the role of Usher proteins in the photoreceptor will be better understood.

THERAPEUTIC DEVELOPMENTS FOR USHER SYNDROME

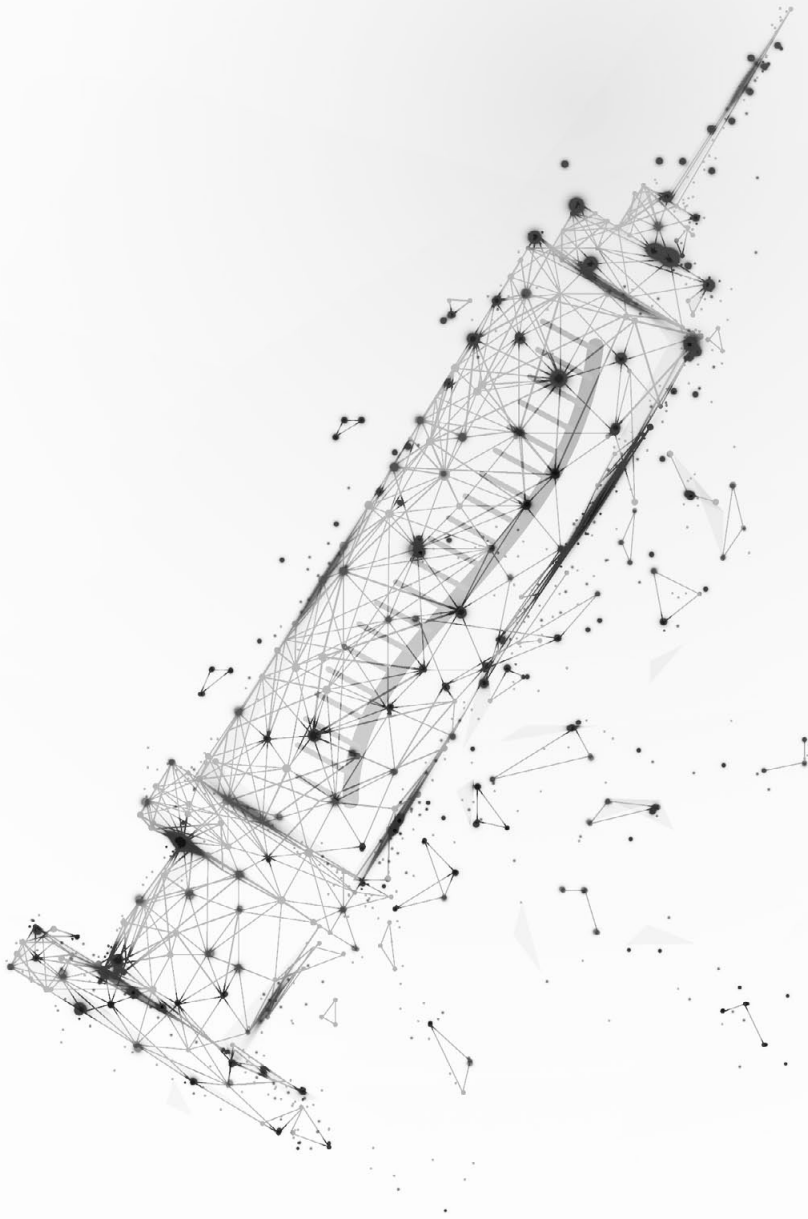
During the past five years, a range of preclinical therapeutic strategies has been developed for the different types of Usher syndrome. Recently, gene augmentation in an *Ush1c* knock-out mouse model shortly after birth was shown to restore sensory and vestibular hair cell function (Pan et al. 2017). Likewise, supplementing a healthy *Whrn* cDNA copy prevented auditory and vestibular problems in the Whirler mouse (Isgrig et al. 2017). Prior to this study, augmentation of *Whrn* in the retina of a *Whrn* knock-out mouse rescued the disrupted USH2 protein complex (whirlin, usherin and ADGRV1) in photoreceptors (Zou et al. 2011). In these three studies, researchers employed adeno-associated virus (AAV)-derived particles as a vehicle for delivery. Although these AAV vectors have been optimized to transduce specific target cells, their cargo capacity of 4.7 kb make them only potentially suitable for a subset of Usher genes. The limited cargo capacity led to the development of a dual or triple AAV vector approach. Different vectors each contain parts of a large transgene expression cassette which can recombine in target cells and thereby double or triple the total cargo capacity. This approach has been exemplified for *MYO7A* (Dyka et al. 2014). Alternatively, it is possible to use different viral gene delivery vehicles with larger cargo capacities, such as lentiviruses. *MYO7A* for instance, is packaged into a lentivirus (known as UshStat®) and effectively expressed in the retina of the *shaker1* mouse model for USH1b (Zalocchi et al. 2014). Currently, UshStat® is being evaluated in a phase I/II clinical trial (ClinicalTrials.gov Identifier: NCT01505062).

Although gene augmentation has been shown to hold promising therapeutic potential, there are drawbacks that limit clinical application. The large coding sequence of several Usher genes, the difficulty to control correct temporal and spatial gene expression and the presence of alternatively spliced transcripts with unknown significance obstruct a gene augmentation approach for several Usher genes. Consequently, other therapeutic strategies for the future treatment of Usher syndrome, such as splice correction using antisense oligonucleotides (AONs), translational read-through inducing drugs (TRIDs) or gene editing, are under development. AONs are small, RNA-like oligomers that are complementary to their target sequence. Upon binding their target pre-mRNA, it depends on the AON chemistry whether they initiate RNase H-mediated degradation of their target or interfere with splicing. For Usher syndrome, AONs have shown to hold great promise as splice correcting molecules in fibroblasts of patients with the frequent deep-intronic c.7595-2144A>G mutation in *USH2A* (**Chapter 3b**). Also, morpholino-induced skipping of the mutated *ush2a* exon13 in zebrafish larvae restored visual function (**Chapter 4**). In addition, treatment of neonatal mice with a single systemic dose of splice modulating AONs partially corrected aberrant *Ush1c* pre-mRNA splicing caused by the c.216G>A mutation, thereby rescuing vestibular function

and low-frequency hearing in mice (Vijayakumar et al. 2017). For nonsense mutations resulting in pre-mature termination of translation, the applicability of TRIDs is being explored. TRIDs are effective in reading through nonsense mutations in *USH1G* *in vitro* (Sorusch et al. 2017) and *USH1C* both *in vitro* and *in vivo* (reviewed by Nagel-Wolfrum et al. 2014). Gene repair would be the most elegant way to treat a genetic disorder, since it solves the primary problem. The CRISPR/Cas9 system is a widely used gene editing method that could be tailored for different target sequences relatively easy (overview in **Chapter 2a**). However, observed off-target effects and low on-target efficiencies so far hamper clinical application of gene editing approaches. Nevertheless, Overlack and colleagues have initiated an *in vitro Ush1c* gene correction strategy using zinc finger nucleases (Overlack et al. 2012). Besides that, targeted animal knock-out (performed in **chapter 2b**) as well as targeted knock-in (performed in **chapter 3c**) (animal) models can be generated when using CRISPR/Cas9.

All therapeutic approaches discussed so far, depend on the presence of sensory cells. The early genetic diagnosis of Usher syndrome prior to the manifestation of retinal dysfunction, provides a window of opportunity in which treatment can be initiated. In contrast to the retina, Usher proteins are essential for inner ear hair bundle development. Therefore, it is expected that effective genetic therapies for the inner ear defects will need to be applied prior to or during cochlear development, which occurs *in utero*. A more feasible option is the postnatal stabilization of mutant Usher proteins using small molecules, potentially resulting in the presence of protein with enough residual function to alleviate the hearing phenotype. This strategy was proven to be protective against rapid deterioration of hearing as a result of the clarin-1 p.N48K mutation in a mouse model for USH3a (Alagramam et al. 2016). Similarly, the retina of an USH2 patient was supplemented with ciliary neurotrophic factor (CNTF) which is known to promote neuronal survival and to protect against retinal degeneration. Although a reduction of cone photoreceptor loss was observed after CNTF treatment, deterioration of visual function was not significantly prohibited in this clinical study (Talcott et al. 2011). In contrast, injection of neuronal progenitor cells into the subretinal space appeared to be protective against the decline of visual acuity in the *Ush2a*-mouse model for Usher syndrome (Lu et al. 2010). However, when RP has progressed into a more advanced state, treatment options are limited to retinal implants or cell replacement therapies. *In vitro* differentiated and grown retinal cells can be transplanted into the defective retina. Although some early studies show the promise of cell replacement therapies, challenges such as the robust *in vitro* generation of donor cells, the survival of donor cells in a degenerated retina and the ability of donor cells to properly connect with the existing circuitry, need to be addressed before patients can benefit from this therapeutic option (reviewed by Jayakody et al. 2015).

Chapter **1** b



Aim and outline of this thesis

Usher syndrome is a devastating disease affecting both visual and auditory function. In this thesis, I describe the research that I have performed with the ultimate goal to better understand the underlying molecular pathogenesis and to preclinically develop a potential splice modulating therapy to halt or delay the progression of retinal degeneration in (a subset of) patients with Usher syndrome.

In order to learn more about the function of Usher syndrome proteins and to elucidate the pathogenic mechanism underlying the disease, as well as the evaluation of novel therapeutic strategies, a suitable animal model is needed. In **chapter 2a**, an overview of pros and cons of different vertebrate animal models that are being used in functional and therapeutic research on inherited retinal dystrophies is presented. **Chapter 2b** shows the characterization of two targeted usherin knock-out zebrafish models (*ush2a^{mc1}* and *ush2a^{b1245}*), both showing an early-onset retinal dysfunction. **Chapter 2c** describes the isolation and characterization of USH2d-associated proteins and protein complexes from the adult zebrafish retina.

Chapter 3 describes the pre-clinical development of an AON-based splice correction strategy to prevent aberrant splicing of *USH2A* pre-mRNA as a consequence of the c.7595-2144A>G mutation. First, a protocol for an optimal design and *in vitro* validation of the exon-skipping or retention potential of AONs is presented (**Chapter 3a**). **Chapter 3b** shows the design of AONs targeting *USH2A* pseudoexon 40 that effectively correct aberrant *USH2A* splicing in fibroblasts of patients having the c.7595-2144A>G mutation. Splice correction is expected to result in the restoration of wild-type usherin protein translation. **Chapter 3c** describes the generation and characterization of a humanized *USH2A* pseudoexon 40 knock-in zebrafish model using CRISPR/Cas9 technology in order to validate this hypothesis. As clear differences in the recognition of human *USH2A* pseudoexon 40 splice sites between human and zebrafish are observed, a novel pipeline for the generation of future knock-in zebrafish models to study human splice defects is proposed.

Chapter 4 shows that skipping of mutated *ush2a* exon13 in zebrafish larvae restores ERG-traces in our previously generated and characterized *ush2a^{mc1}* knock-out model. In patients with retinitis pigmentosa, *USH2A* exon13 is the most frequently mutated exon in which two founder mutations (c.2299delG; p.Glu767SerfsTer21 and c.2276G>T; p.Cys759Phe) have been identified.

Finally, **chapter 5** provides a general discussion and future directions for follow-up research.

REFERENCES

- Alagramam, K. N., S. R. Gopal, R. Geng, D. H. Chen, I. Nemet, R. Lee, G. Tian, M. Miyagi, K. F. Malagu, C. J. Lock, W. R. Esmieu, A. P. Owens, N. A. Lindsay, K. Ouwehand, F. Albertus, D. F. Fischer, R. W. Burli, A. M. MacLeod, W. E. Harte, K. Palczewski, and Y. Imanishi. 2016. "A small molecule mitigates hearing loss in a mouse model of Usher syndrome III." *Nat Chem Biol* 12 (6):444-51. doi: 10.1038/nchembio.2069.
- Aparisi, M. J., E. Aller, C. Fuster-García, G. García-García, R. Rodrigo, R. P. Vazquez-Manrique, F. Blanco-Kelly, C. Ayuso, A. F. Roux, T. Jaijo, and J. M. Millan. 2014. "Targeted next generation sequencing for molecular diagnosis of Usher syndrome." *Orphanet J Rare Dis* 9:168. doi: 10.1186/s13023-014-0168-7.
- Aparisi, M. J., G. García-García, E. Aller, M. D. Sequedo, C. Martínez-Fernández de la Cámara, R. Rodrigo, M. Armengot, J. Cortijo, J. Milara, L. Llopis, M. Diaz, T. Jaijo, and J. M. Millan. 2013. "Study of USH1 splicing variants through minigenes and transcript analysis from nasal epithelial cells." *PLoS One* 8 (2):e57506. doi: 10.1371/journal.pone.0057506.
- Bachmann-Gagescu, R., M. Dona, L. Hetterschijt, E. Tonnaer, T. Peters, E. de Vrieze, D. A. Mans, S. E. van Beersum, I. G. Phelps, H. H. Arts, J. E. Keunen, M. Ueffing, R. Roepman, K. Boldt, D. Doherty, C. B. Moens, S. C. Neuhauss, H. Kremer, and E. van Wijk. 2015. "The Ciliopathy Protein CC2D2A Associates with NINL and Functions in RAB8-MICAL3-Regulated Vesicle Trafficking." *PLoS Genet* 11 (10):e1005575. doi: 10.1371/journal.pgen.1005575.
- Bahloul, A., V. Michel, J. P. Hardelin, S. Nouaille, S. Hoos, A. Houdusse, P. England, and C. Petit. 2010. "Cadherin-23, myosin VIIa and harmonin, encoded by Usher syndrome type I genes, form a ternary complex and interact with membrane phospholipids." *Hum Mol Genet* 19 (18):3557-65. doi: 10.1093/hmg/ddq271.
- Blanco-Sanchez, B., A. Clement, J. Fierro, Jr., P. Washbourne, and M. Westerfield. 2014. "Complexes of Usher proteins preassemble at the endoplasmic reticulum and are required for trafficking and ER homeostasis." *Dis Model Mech* 7 (5):547-59. doi: 10.1242/dmm.014068.
- Blanco-Sanchez, B., A. Clement, J. B. Phillips, and M. Westerfield. 2017. "Zebrafish models of human eye and inner ear diseases." *Methods Cell Biol* 138:415-467. doi: 10.1016/bs.mcb.2016.10.006.
- Caberlotto, E., V. Michel, I. Foucher, A. Bahloul, R. J. Goodyear, E. Pepermans, N. Michalski, I. Perfettini, O. Alegria-Prevot, S. Chardenoux, M. Do Cruzeiro, J. P. Hardelin, G. P. Richardson, P. Avan, D. Weil, and C. Petit. 2011. "Usher type 1G protein sans is a critical component of the tip-link complex, a structure controlling actin polymerization in stereocilia." *Proc Natl Acad Sci U S A* 108 (14):5825-30. doi: 10.1073/pnas.1017114108.
- Chittka, L., and A. Brockmann. 2005. "Perception space--the final frontier." *PLoS Biol* 3 (4):e137. doi: 10.1371/journal.pbio.0030137.
- Cosgrove, D., and M. Zallocchi. 2014. "Usher protein functions in hair cells and photoreceptors." *Int J Biochem Cell Biol* 46:80-9. doi: 10.1016/j.biocel.2013.11.001.
- Dad, S., N. D. Rendtorff, L. Tranenjaerg, K. Gronskov, H. G. Karstensen, V. Brox, O. Nilssen, A. F. Roux, T. Rosenberg, H. Jensen, and L. B. Moller. 2016. "Usher syndrome in Denmark: mutation spectrum and some clinical observations." *Mol Genet Genomic Med* 4 (5):527-539. doi: 10.1002/mgg3.228.
- Demontis, F., and C. Dahmann. 2009. "Characterization of the Drosophila ortholog of the human Usher Syndrome type 1G protein sans." *PLoS One* 4 (3):e4753. doi: 10.1371/journal.pone.0004753.

- Domanico, D., S. Fragiotta, A. Cutini, P. L. Grenga, and E. M. Vingolo. 2015. "Psychosis, Mood and Behavioral Disorders in Usher Syndrome: Review of the Literature." *Med Hypothesis Discov Innov Ophthalmol* 4 (2):50-5.
- Dyka, F. M., S. L. Boye, V. A. Chiodo, W. W. Hauswirth, and S. E. Boye. 2014. "Dual adeno-associated virus vectors result in efficient in vitro and in vivo expression of an oversized gene, MYO7A." *Hum Gene Ther Methods* 25 (2):166-77. doi: 10.1089/hgtb.2013.212.
- Ebermann, I., J. B. Phillips, M. C. Liebau, R. K. Koenekoop, B. Schermer, I. Lopez, E. Schafer, A. F. Roux, C. Dafinger, A. Bernd, E. Zrenner, M. Claustres, B. Blanco, G. Nurnberg, P. Nurnberg, R. Ruland, M. Westerfield, T. Benzing, and H. J. Bolz. 2010. "PDZD7 is a modifier of retinal disease and a contributor to digenic Usher syndrome." *J Clin Invest* 120 (6):1812-23. doi: 10.1172/JCI39715.
- El-Amraoui, A., and C. Petit. 2005. "Usher I syndrome: unravelling the mechanisms that underlie the cohesion of the growing hair bundle in inner ear sensory cells." *J Cell Sci* 118 (Pt 20):4593-603. doi: 10.1242/jcs.02636.
- Fettiplace, R., and K. X. Kim. 2014. "The physiology of mechano-electrical transduction channels in hearing." *Physiol Rev* 94 (3):951-86. doi: 10.1152/physrev.00038.2013.
- Geng, R., M. Sotomayor, K. J. Kinder, S. R. Gopal, J. Gerka-Stuyt, D. H. Chen, R. E. Hardisty-Hughes, G. Ball, A. Parker, R. Gaudet, D. Furness, S. D. Brown, D. P. Corey, and K. N. Alagramam. 2013. "Noddy, a mouse harboring a missense mutation in protocadherin-15, reveals the impact of disrupting a critical interaction site between tip-link cadherins in inner ear hair cells." *J Neurosci* 33 (10):4395-404. doi: 10.1523/JNEUROSCI.4514-12.2013.
- Giese, A. P. J., Y. Q. Tang, G. P. Sinha, M. R. Bowl, A. C. Goldring, A. Parker, M. J. Freeman, S. D. M. Brown, S. Riazuddin, R. Fettiplace, W. R. Schafer, G. I. Frolenkov, and Z. M. Ahmed. 2017. "CIB2 interacts with TMC1 and TMC2 and is essential for mechanotransduction in auditory hair cells." *Nat Commun* 8 (1):43. doi: 10.1038/s41467-017-00061-1.
- Giese, A., S. Riazuddin, and Z.M. Ahmed. 2013. "Usher and bardet biedl syndrome proteins: new pieces in the planar cell polarity puzzle."
- Graefe, A von. 1858. "Exceptionelles Verhalten des Gesichtsfeldes bei Pigmententartung der Netzhaut." *Archiv für Ophthalmologie* 1858 (250).
- Gregory, F. D., T. Pangrsic, I. E. Calin-Jageman, T. Moser, and A. Lee. 2013. "Harmonin enhances voltage-dependent facilitation of Cav1.3 channels and synchronous exocytosis in mouse inner hair cells." *J Physiol* 591 (13):3253-69. doi: 10.1113/jphysiol.2013.254367.
- Hartel, B. P., M. Lofgren, P. L. M. Huygen, I. Guchelaar, N. L. A. N. Kort, A. M. Sadeghi, E. van Wijki, L. Tranebjaerg, H. Kremer, W. J. Kimberling, C. W. R. J. Cremers, C. Moller, and R. J. E. Penning. 2016. "A combination of two truncating mutations in *USH2A* causes more severe and progressive hearing impairment in Usher syndrome type IIa." *Hearing Research* 339:60-68. doi: 10.1016/j.heares.2016.06.008.
- Hartel, B. P., J. W. I. van Nierop, W. J. Huinck, L. J. C. Rotteveel, E. A. M. Mylanus, A. F. Snik, H. P. M. Kunst, and R. J. E. Penning. 2017. "Cochlear Implantation in Patients With Usher Syndrome Type IIa Increases Performance and Quality of Life." *Otol Neurotol* 38 (6):e120-e127. doi: 10.1097/MAO.0000000000001441.
- Hu, Q. X., J. H. Dong, H. B. Du, D. L. Zhang, H. Z. Ren, M. L. Ma, Y. Cai, T. C. Zhao, X. L. Yin, X. Yu, T. Xue, Z. G. Xu, and J. P. Sun. 2014. "Constitutive Galphai coupling activity of very large G protein-coupled receptor 1 (VLGR1) and its regulation by PDZD7 protein." *J Biol Chem* 289 (35):24215-25. doi: 10.1074/jbc.M114.549816.

- Isgrig, K., J. W. Shteamer, I. A. Belyantseva, M. C. Drummond, T. S. Fitzgerald, S. Vijayakumar, S. M. Jones, A. J. Griffith, T. B. Friedman, L. L. Cunningham, and W. W. Chien. 2017. "Gene Therapy Restores Balance and Auditory Functions in a Mouse Model of Usher Syndrome." *Mol Ther* 25 (3):780-791. doi: 10.1016/j.ymthe.2017.01.007.
- Jansen, F., B. Kalbe, P. Scholz, M. Mikosz, K. A. Wunderlich, S. Kurtenbach, K. Nagel-Wolfrum, U. Wolfrum, H. Hatt, and S. Osterloh. 2016. "Impact of the Usher syndrome on olfaction." *Hum Mol Genet* 25 (3):524-33. doi: 10.1093/hmg/ddv490.
- Jayakody, S. A., A. Gonzalez-Cordero, R. R. Ali, and R. A. Pearson. 2015. "Cellular strategies for retinal repair by photoreceptor replacement." *Prog Retin Eye Res* 46:31-66. doi: 10.1016/j.preteyeres.2015.01.003.
- Kremer, H., E. van Wijk, T. Marker, U. Wolfrum, and R. Roepman. 2006. "Usher syndrome: molecular links of pathogenesis, proteins and pathways." *Hum Mol Genet* 15 Spec No 2:R262-70. doi: 10.1093/hmg/ddl205.
- Lefevre, G., V. Michel, D. Weil, L. Lepelletier, E. Bizard, U. Wolfrum, J. P. Hardelin, and C. Petit. 2008. "A core cochlear phenotype in USH1 mouse mutants implicates fibrous links of the hair bundle in its cohesion, orientation and differential growth." *Development* 135 (8):1427-37. doi: 10.1242/dev.012922.
- Lenassi, E., A. G. Robson, L. M. Luxon, M. Bitner-Glindzicz, and A. R. Webster. 2015. "Clinical Heterogeneity in a Family With Mutations in USH2A." *Jama Ophthalmology* 133 (3):352-355. doi: 10.1001/jamaophthalmol.2014.5163.
- Lenassi, E., A. Vincent, Z. Li, Z. Saihan, A. J. Coffey, H. B. Steele-Stallard, A. T. Moore, K. P. Steel, L. M. Luxon, E. Heon, M. Bitner-Glindzicz, and A. R. Webster. 2015. "A detailed clinical and molecular survey of subjects with nonsyndromic USH2A retinopathy reveals an allelic hierarchy of disease-causing variants." *European Journal of Human Genetics* 23 (10):1318-1327. doi: 10.1038/ejhg.2014.283.
- Liquori, A., C. Vache, D. Baux, C. Blanchet, C. Hamel, S. Malcolm, M. Koenig, M. Claustres, and A. F. Roux. 2016. "Whole USH2A Gene Sequencing Identifies Several New Deep Intronic Mutations." *Hum Mutat* 37 (2):184-93. doi: 10.1002/humu.22926.
- Lu, B., S. Wang, P. J. Francis, T. Li, D. M. Gamm, E. E. Capowski, and R. D. Lund. 2010. "Cell transplantation to arrest early changes in an *ush2a* animal model." *Invest Ophthalmol Vis Sci* 51 (4):2269-76. doi: 10.1167/iovs.09-4526.
- Maerker, T., E. van Wijk, N. Overlack, F. F. Kersten, J. McGee, T. Goldmann, E. Sehn, R. Roepman, E. J. Walsh, H. Kremer, and U. Wolfrum. 2008. "A novel Usher protein network at the periciliary reloading point between molecular transport machineries in vertebrate photoreceptor cells." *Hum Mol Genet* 17 (1):71-86. doi: 10.1093/hmg/ddm285.
- Mathur, P., and J. Yang. 2015. "Usher syndrome: Hearing loss, retinal degeneration and associated abnormalities." *Biochim Biophys Acta* 1852 (3):406-20. doi: 10.1016/j.bbadis.2014.11.020.
- Nagel-Wolfrum, K., F. Moller, I. Penner, and U. Wolfrum. 2014. "Translational read-through as an alternative approach for ocular gene therapy of retinal dystrophies caused by in-frame nonsense mutations." *Vis Neurosci* 31 (4-5):309-16. doi: 10.1017/S0952523814000194.
- Nakanishi, H., M. Ohtsubo, S. Iwasaki, Y. Hotta, K. Mizuta, H. Mineta, and S. Minoshima. 2010. "Hair roots as an mRNA source for mutation analysis of Usher syndrome-causing genes." *J Hum Genet* 55 (10):701-3. doi: 10.1038/jhg.2010.83.
- Overlack, N., T. Goldmann, U. Wolfrum, and K. Nagel-Wolfrum. 2012. "Gene repair of an Usher syndrome causing mutation by zinc-finger nuclease mediated homologous recombination." *Invest Ophthalmol Vis Sci* 53 (7):4140-6. doi: 10.1167/iovs.12-9812.

- Overlack, N., D. Kilić, K. Bauss, T. Marker, H. Kremer, E. van Wijk, and U. Wolfrum. 2011. "Direct interaction of the Usher syndrome 1G protein SANS and myomegalin in the retina." *Biochim Biophys Acta* 1813 (10):1883-92. doi: 10.1016/j.bbamcr.2011.05.015.
- Pan, B., C. Askew, A. Galvin, S. Heman-Ackah, Y. Asai, A. A. Indzhykulia, F. M. Jodelka, M. L. Hastings, J. J. Lentz, L. H. Vandenberghe, J. R. Holt, and G. S. Geleoc. 2017. "Gene therapy restores auditory and vestibular function in a mouse model of Usher syndrome type 1c." *Nat Biotechnol* 35 (3):264-272. doi: 10.1038/nbt.3801.
- Pan, L., and M. Zhang. 2012. "Structures of usher syndrome 1 proteins and their complexes." *Physiology (Bethesda)* 27 (1):25-42. doi: 10.1152/physiol.00037.2011.
- Phillips, J. B., B. Blanco-Sanchez, J. J. Lentz, A. Tallafuss, K. Khanobdee, S. Sampath, Z. G. Jacobs, P. F. Han, M. Mishra, T. A. Titus, D. S. Williams, B. J. Keats, P. Washbourne, and M. Westerfield. 2011. "Harmonin (Ush1c) is required in zebrafish Muller glial cells for photoreceptor synaptic development and function." *Dis Model Mech* 4 (6):786-800. doi: 10.1242/dmm.006429.
- Pierrache, L. H. M., B. P. Hartel, E. van Wijk, M. A. Meester-Smoor, F. P. M. Cremers, E. de Baere, J. de Zaeytijd, M. J. van Schooneveld, C. W. R. J. Cremers, G. Dagnelie, C. B. Hoyng, A. A. Bergen, B. P. Leroy, R. J. E. Pennings, L. I. van den Born, and C. C. W. Klaver. 2016. "Visual Prognosis in USH2A-Associated Retinitis Pigmentosa Is Worse for Patients with Usher Syndrome Type IIa Than for Those with Nonsyndromic Retinitis Pigmentosa." *Ophthalmology* 123 (5):1151-1160. doi: 10.1016/j.ophtha.2016.01.021.
- Reiners, J., T. Marker, K. Jurgens, B. Reidel, and U. Wolfrum. 2005. "Photoreceptor expression of the Usher syndrome type 1 protein protocadherin 15 (USH1F) and its interaction with the scaffold protein harmonin (USH1C)." *Mol Vis* 11:347-55.
- Reiners, J., K. Nagel-Wolfrum, K. Jurgens, T. Marker, and U. Wolfrum. 2006. "Molecular basis of human Usher syndrome: deciphering the meshes of the Usher protein network provides insights into the pathomechanisms of the Usher disease." *Exp Eye Res* 83 (1):97-119. doi: 10.1016/j.exer.2005.11.010.
- Reiners, J., E. van Wijk, T. Marker, U. Zimmermann, K. Jurgens, H. te Brinke, N. Overlack, R. Roepman, M. Knipper, H. Kremer, and U. Wolfrum. 2005. "Scaffold protein harmonin (USH1C) provides molecular links between Usher syndrome type 1 and type 2." *Hum Mol Genet* 14 (24):3933-43. doi: 10.1093/hmg/ddi417.
- Ribeiro, J. C., B. Oliveiros, P. Pereira, N. Antonio, T. Hummel, A. Paiva, and E. D. Silva. 2016. "Accelerated age-related olfactory decline among type 1 Usher patients." *Sci Rep* 6:28309. doi: 10.1038/srep28309.
- Sahly, I., E. Dufour, C. Schietroma, V. Michel, A. Bahloul, I. Perfettini, E. Pepermans, A. Estivalet, D. Carette, A. Aghaie, I. Ebermann, A. Lelli, M. Iribarne, J. P. Hardelin, D. Weil, J. A. Sahel, A. El-Amraoui, and C. Petit. 2012. "Localization of Usher 1 proteins to the photoreceptor calyceal processes, which are absent from mice." *J Cell Biol* 199 (2):381-99. doi: 10.1083/jcb.201202012.
- Schietroma, C., K. Parain, A. Estivalet, A. Aghaie, J. Boutet de Monvel, S. Picaud, J. A. Sahel, M. Perron, A. El-Amraoui, and C. Petit. 2017. "Usher syndrome type 1-associated cadherins shape the photoreceptor outer segment." *J Cell Biol* 216 (6):1849-1864. doi: 10.1083/jcb.201612030.
- Seiler, C., K. C. Finger-Baier, O. Rinner, Y. V. Makhankov, H. Schwarz, S. C. Neuhaus, and T. Nicolson. 2005. "Duplicated genes with split functions: independent roles of protocadherin15 orthologues in zebrafish hearing and vision." *Development* 132 (3):615-23. doi: 10.1242/dev.01591.

- Sorusch, N., K. Bauss, J. Plutniok, A. Samanta, B. Knapp, K. Nagel-Wolfrum, and U. Wolfrum. 2017. "Characterization of the ternary Usher syndrome SANS/ush2a/whirlin protein complex." *Hum Mol Genet* 26 (6):1157-1172. doi: 10.1093/hmg/ddx027.
- Talcott, K. E., K. Ratnam, S. M. Sundquist, A. S. Lucero, B. J. Lujan, W. Tao, T. C. Porco, A. Roorda, and J. L. Duncan. 2011. "Longitudinal study of cone photoreceptors during retinal degeneration and in response to ciliary neurotrophic factor treatment." *Invest Ophthalmol Vis Sci* 52 (5):2219-26. doi: 10.1167/iovs.10-6479.
- Toms, Maria, Maria Bitner-Glindzicz, Andrew Webster, and Mariya Moosajee. 2015. "Usher syndrome: a review of the clinical phenotype, genes and therapeutic strategies." *Expert Review of Ophthalmology* 10 (3):241-256. doi: 10.1586/17469899.2015.1033403.
- Tucker, B. A., R. F. Mullins, L. M. Streb, K. Anfinson, M. E. Eyestone, E. Kaalberg, M. J. Riker, A. V. Drack, T. A. Braun, and E. M. Stone. 2013. "Patient-specific iPSC-derived photoreceptor precursor cells as a means to investigate retinitis pigmentosa." *Elife* 2:e00824. doi: 10.7554/eLife.00824.
- Urano, T., M. Shiraki, H. Yagi, M. Ito, N. Sasaki, M. Sato, Y. Ouchi, and S. Inoue. 2012. "GPR98/Gpr98 gene is involved in the regulation of human and mouse bone mineral density." *J Clin Endocrinol Metab* 97 (4):E565-74. doi: 10.1210/jc.2011-2393.
- Vache, C., T. Besnard, C. Blanchet, D. Baux, L. Larrieu, V. Faugere, M. Mondain, C. Hamel, S. Malcolm, M. Claustres, and A. F. Roux. 2010. "Nasal epithelial cells are a reliable source to study splicing variants in Usher syndrome." *Hum Mutat* 31 (6):734-41. doi: 10.1002/humu.21255.
- Vache, C., T. Besnard, P. le Berre, G. Garcia-Garcia, D. Baux, L. Larrieu, C. Abadie, C. Blanchet, H. J. Bolz, J. Millan, C. Hamel, S. Malcolm, M. Claustres, and A. F. Roux. 2012. "Usher syndrome type 2 caused by activation of an *USH2A* pseudoexon: implications for diagnosis and therapy." *Hum Mutat* 33 (1):104-8. doi: 10.1002/humu.21634.
- van Wijk, E., F. F. Kersten, A. Kartono, D. A. Mans, K. Brandwijk, S. J. Letteboer, T. A. Peters, T. Marker, X. Yan, C. W. Cremers, F. P. Cremers, U. Wolfrum, R. Roepman, and H. Kremer. 2009. "Usher syndrome and Leber congenital amaurosis are molecularly linked via a novel isoform of the centrosomal ninein-like protein." *Hum Mol Genet* 18 (1):51-64. doi: 10.1093/hmg/ddn312.
- van Wijk, E., B. van der Zwaag, T. Peters, U. Zimmermann, H. Te Brinke, F. F. Kersten, T. Marker, E. Aller, L. H. Hoefsloot, C. W. Cremers, F. P. Cremers, U. Wolfrum, M. Knipper, R. Roepman, and H. Kremer. 2006. "The DFNB31 gene product whirlin connects to the Usher protein network in the cochlea and retina by direct association with *USH2A* and *VLGR1*." *Hum Mol Genet* 15 (5):751-65. doi: 10.1093/hmg/ddi490.
- Vijayakumar, S., F. F. Depreux, F. M. Jodelka, J. J. Lentz, F. Rigo, T. A. Jones, and M. L. Hastings. 2017. "Rescue of peripheral vestibular function in Usher syndrome mice using a splice-switching antisense oligonucleotide." *Hum Mol Genet*. doi: 10.1093/hmg/ddx234.
- Yang, J., X. Liu, Y. Zhao, M. Adamian, B. Pawlyk, X. Sun, D. R. McMillan, M. C. Liberman, and T. Li. 2010. "Ablation of whirlin long isoform disrupts the *USH2* protein complex and causes vision and hearing loss." *PLoS Genet* 6 (5):e1000955. doi: 10.1371/journal.pgen.1000955.
- Zallocchi, M., K. Binley, Y. Lad, S. Ellis, P. Widdowson, S. Iqbal, V. Scripps, M. Kelleher, J. Loader, J. Miskin, Y. W. Peng, W. M. Wang, L. Cheung, D. Delimont, K. A. Mitrophanous, and D. Cosgrove. 2014. "EIAV-based retinal gene therapy in the shaker1 mouse model for usher syndrome type 1B: development of UshStat." *PLoS One* 9 (4):e94272. doi: 10.1371/journal.pone.0094272.
- Zallocchi, M., D. T. Meehan, D. Delimont, J. Rutledge, M. A. Gratton, J. Flannery, and D. Cosgrove. 2012. "Role for a novel Usher protein complex in hair cell synaptic maturation." *PLoS One* 7 (2):e30573. doi: 10.1371/journal.pone.0030573.

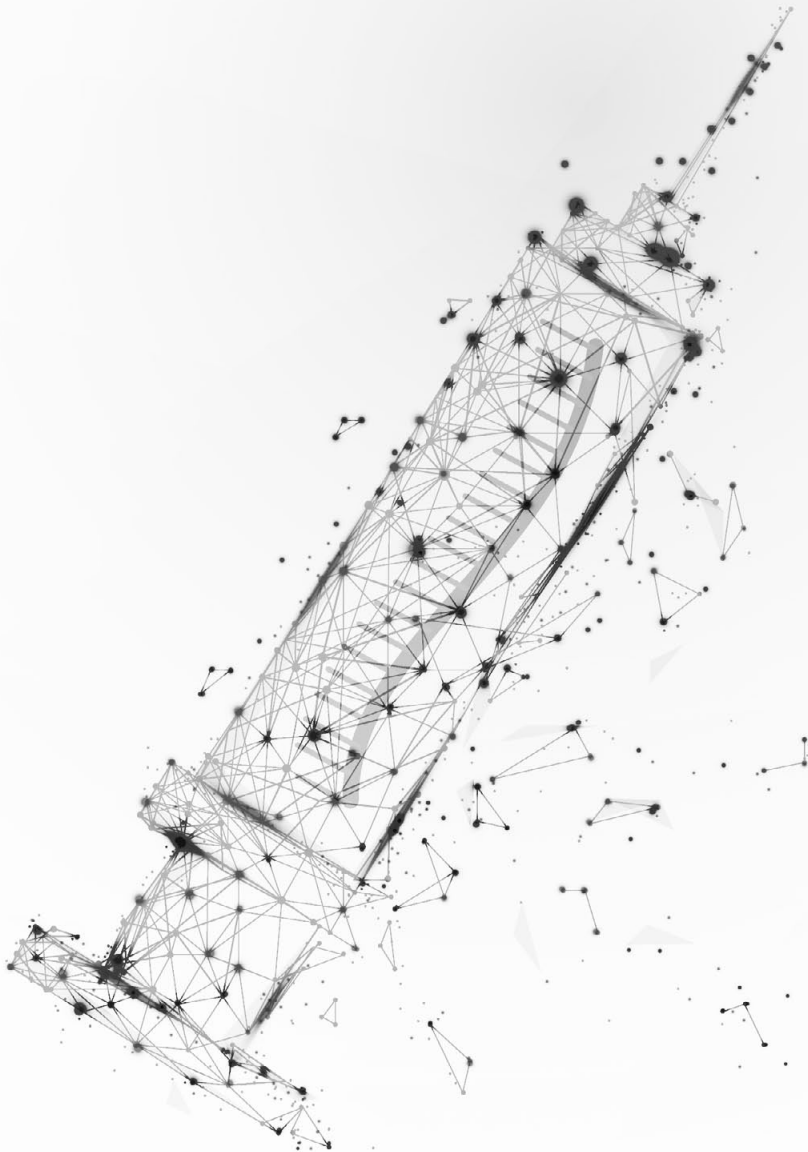
- Zou, J., Q. Chen, A. Almishaal, P. D. Mathur, T. Zheng, C. Tian, Q. Y. Zheng, and J. Yang. 2017. "The roles of USH1 proteins and PDZ domain-containing USH proteins in USH2 complex integrity in cochlear hair cells." *Hum Mol Genet* 26 (3):624-636. doi: 10.1093/hmg/ddw421.
- Zou, J., L. Luo, Z. Shen, V. A. Chiodo, B. K. Ambati, W. W. Hauswirth, and J. Yang. 2011. "Whirlin replacement restores the formation of the USH2 protein complex in whirlin knockout photoreceptors." *Invest Ophthalmol Vis Sci* 52 (5):2343-51. doi: 10.1167/iovs.10-6141.

Chapter 2

Zebrafish As Animal Model To Study Retinal Degeneration



Chapter **2**^a



The pros and cons of vertebrate animal models for functional and therapeutic research on inherited retinal dystrophies

Ralph W.N. Slijkerman^{a,d,1}, **Fei Song**^{e,1}, **Galuh D.N. Astuti**^{b,d,f,1}, **Martijn A. Huynen**^{c,d},
Erwin van Wijk^{a,d,2}, **Knut Stieger**^{e,2} and **Rob W.J. Collin**^{b,d,2}

¹ Three first authors have contributed equally.

² Three last authors have contributed equally.

^a Department of Otorhinolaryngology, Radboud University Medical Center, Geert Grooteplein 10, 6525 GA, Nijmegen, The Netherlands

^b Department of Human Genetics, Radboud University Medical Center, Geert Grooteplein 10, 6525 GA, Nijmegen, The Netherlands

^c Center for Molecular and Biomolecular Informatics, Radboud University Medical Center, Geert Grooteplein 10, 6525 GA, Nijmegen, The Netherlands

^d Radboud Institute for Molecular Life Sciences, Radboud University Medical Center, Geert Grooteplein 10, 6525 GA, Nijmegen, The Netherlands

^e Department of Ophthalmology, Justus-Liebig-University, Friedrichstrabe 18, 35392, Gießen, Germany

^f Center for Biomedical Research, Diponegoro University, dr. Soetomo 18, 50321, Semarang, Indonesia

Published in *Progress in Retinal Eye Research*, 2015

doi: 10.1016/j.preteyeres.2015.04.004

PMID: 25936606

ABSTRACT

Over the last decade, huge progress has been made in the understanding of the molecular mechanisms underlying inherited retinal dystrophy (IRD), as well as in the development and implementation of novel therapies, especially in the field of gene therapy. The use of mutant animal models, either naturally occurring or generated by genetic modification, have contributed greatly to our knowledge on IRD. Yet, these mutant animal models do not always mimic the retinal phenotype that is observed in humans with mutations in the orthologous gene, often due to species-specific characteristics of the retina, and/or diverse functions of the gene products in different species. In this manuscript, we compare general and ocular characteristics of a series of widely used vertebrate animal models, i.e. zebrafish, chicken, rodents, cats, dogs, sheep, pigs and monkeys, in terms of genetic architecture and sequence homology, methods to modify genomes, anatomy of the eye, and structural details of the retina. Furthermore, we present an overview of mutant vertebrate animal models that have been used to study or develop treatments for the various genetic subtypes of IRD, and correlate the suitability of these models to the specific characteristics of each animal. Herewith, we provide tools that will help to select the most suitable animal model for specific research questions on IRDs in the future, and thereby assist in an optimal use of animals and resources to further increase our understanding of inherited retinal dystrophies, and develop novel treatments for these disorders.

1. INTRODUCTION

Inherited retinal dystrophies (IRDs) are a group of heterogeneous disorders characterized by a progressive loss of visual function due to degeneration of the light-sensing photoreceptor cells in the retina, often resulting in complete blindness. Over the past two decades, the molecular and phenotypic characterization of mutant animal models resembling IRD has contributed greatly to our understanding of the physiological processes that regulate vision and of the pathophysiological mechanisms that underlie IRD. In addition, several of these models have shown to be instrumental for the development of novel treatments, such as gene augmentation therapies that are now in clinical trials (Bainbridge et al., 2008; Hauswirth et al., 2008; MacLaren et al., 2014; Maguire et al., 2008). On many occasions however, animal models that carry mutations in genes underlying IRD in humans do not, or only partially, mimic the human phenotype. Why is that? Do the gene products have diverse functions in different species? Is this due to structural differences in the retinal cells of the various animals? In this manuscript, we will describe the general and ocular characteristics of a series of vertebrate species commonly used in functional and/or therapeutic research on IRDs. In addition, we provide a comprehensive overview of currently existing IRD models, and assess whether they resemble the human phenotype. With this, we aim to provide insight in the utility of the various different animal models for IRD, and why some species may be particularly suited for certain types of functional or therapeutic research in the future.

1.1. *The retina*

Vision is a complex and highly regulated biological process. When light enters the eye through the cornea and the pupil, it is refracted by the lens and focused onto the retina that lines the inner surface of the eye. In the retina, light is converted into an electrical signal that is transmitted via the optic nerve to the visual cortex in the brain where the actual images are formed. The retina is a thin, multilayered and highly structured tissue composed of several different cell types that each play a crucial role in the conversion and amplification of light to electrical signals (Marc, 2008). The light-sensing photoreceptor cells are arranged in a defined layer, that at one end contacts the retinal pigment epithelium (RPE) and at the other end feeds into the outer plexiform layer (OPL). Here, the photoreceptor terminals form synapses with the second order neurons (bipolar cells, horizontal cells and amacrine cells), the nuclei of which together with the nuclei of the Müller cells define the inner nuclear layer (INL). These neurons again form synapses in the inner plexiform layer (IPL) with the ganglion cells, whose nuclei are situated within the ganglion cell layer (GCL). The axons of the ganglion cells define the retinal nerve fiber layer (RNFL) and exit the retina through the optic nerve head (ONH) or papilla. The borders of the Müller cells delineate the internal (ILM) and

external limiting membrane (ELM). A cartoon describing the layered structure of the human retina is provided in **Fig. 1A**.

When light reaches the retina, it first passes through the ganglion and inner nuclear cell layer to reach the photoreceptor cells. In the photoreceptor cells, photons are captured by the photopigment molecules after which the phototransduction cascade is initiated, a complex chain of events that results in the closing of voltage-gated ion channels producing a change in membrane potential. Subsequently, this electrical signal is structured and specifically amplified by the different cell types in the inner retina to be ultimately transported to the brain via the retinal ganglion cells for the generation of images. Oxygen and nutrients for the outer retina (i.e. the photoreceptors) are provided through diffusion from the choroidal vessels via the RPE. The inner retina is supplied by the retinal vasculature consisting of a superficial (within the RNFL) and a deep (within the INL, IPL) plexus. Therefore, the human retina is classified as holangiotic (different forms of vascularised retinae exist in certain animals, see section 2). The most important features of the human retina are the macular zone and the foveal pit in the centre of the macula, both being specific for the primate retina, containing an avascular zone around the most sensitive cones and considered to be necessary for high-contrast vision. The avascularity of the fovea is possible because the inner retinal layers have moved aside, thus forming the macular wall with a high density of ganglion cells.

1.1.1. Photoreceptor cells

Morphologically, photoreceptor cells can be segmented into different parts, i.e. a synaptic end that faces the bipolar cells, the cell body that contains the nucleus, an inner segment where protein synthesis occurs and a large outer segment where the actual phototransduction takes place (**Fig. 1B**). The inner and outer segments are linked by the connecting cilium (CC), a microtubule-based structure that is crucial for the transport of proteins into the outer segments (Satir and Christensen, 2008). Near the connecting cilium, cellular extensions are formed, the calyceal processes, which can be found at other ciliated cells as well (e.g. hair cells in the inner ear).

All the proteins needed to initiate phototransduction are present in the outer segments of the photoreceptor cells. When light reaches the photoreceptors, photons are captured by the opsin molecules, initiating a complex chain of events that includes conformational changes in the chromophores, activation of G-proteins and the closing of voltage-gated ion channels causing a hyperpolarisation of the membrane potential that ultimately results in a decreased neurotransmitter secretion at the synaptic terminal of the photoreceptor cells (Cruce et al., 1996; Dell'Orco and Koch, 2011). A similarly complex chain of molecular events is needed to re-open the cation channels and prepare the photoreceptor cell for another round of phototransduction. Every night, the upper 10% of all outer segment discs are phagocytised by the RPE cells (see section

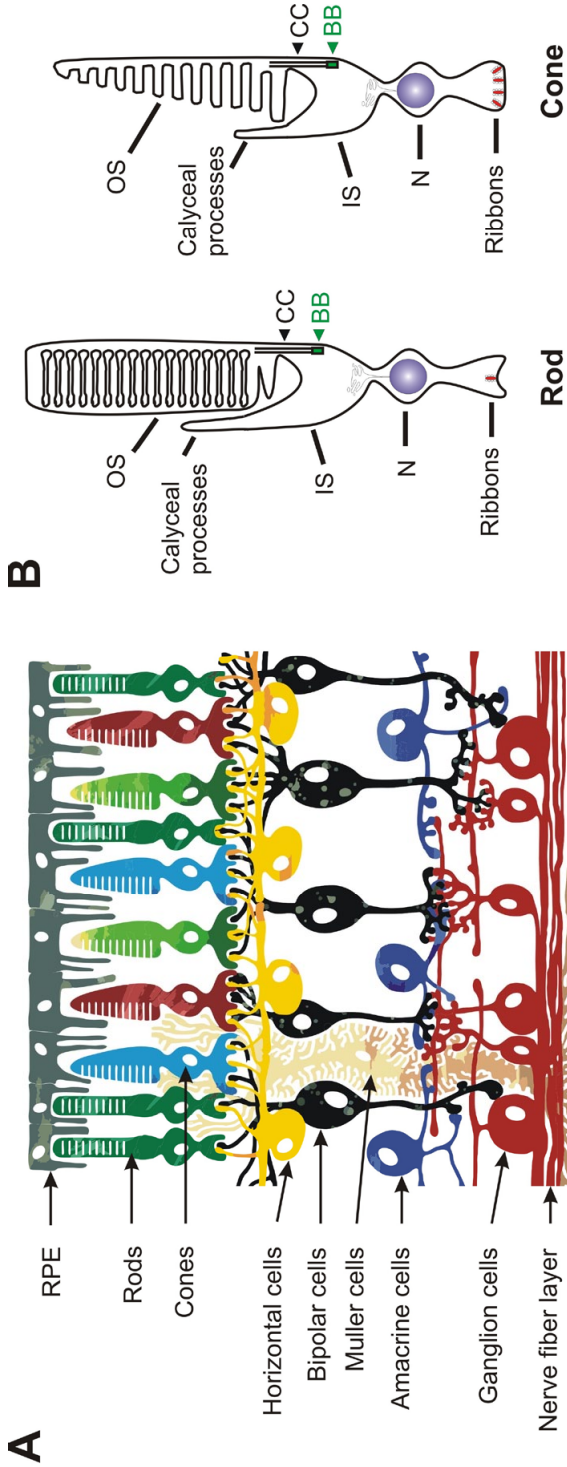


Figure 1. Schematic representation of the retina and light-sensitive photoreceptor cells. (A) The retina consists of different cell types. The retinal pigment epithelium is involved in the phagocytosis of shed photoreceptor outer segment discs. The photoreceptor cells (rods and cones) convert light into an electrical signal. The interneuronal cells (bipolar, amacrine and horizontal cells) combine and subsequently transmit these signals to the ganglion cells. The Müller cells are radial cells that are present throughout the entire retina, thereby connecting all retinal cell types at adherence junctions. They function in photopigment recycling, maintaining retinal extracellular environment homeostasis, providing neurons with nutrients and removal of their waste products. (B) The rod and cone photoreceptor cells consist of an outer segment (OS), where the primary signal transduction takes place, and a separated inner segment (IS) connected via the connecting cilium (CC). The calyceal processes are situated next to the proximal outer segment. The nuclei (N) of the photoreceptor cells are situated in the outer nuclear layer. The synaptic terminals, containing the ribbons, connect the photoreceptor cells with horizontal cells, bipolar cells and neurons. BB: basal body of the connecting cilium.

1.1.2), and new discs are evaginated from the connecting cilium region at the base of the outer segment.

In the human eye, two types of photoreceptor cells can be distinguished, i.e. rods and cones, named such based on the shape of their outer segments (**Fig. 1B**). Rods are very sensitive to low levels of light, and are most abundant in the peripheral retina, whereas cone photoreceptor cells function well under bright light conditions, and are mostly present in the central part of the retina, i.e. the macula. Hence, cones mainly mediate our central vision, including color vision, and allow high visual acuity, whereas rods are responsible for peripheral vision and vision under dim light conditions, i.e. night vision, in addition to sensing contrast and motion. Besides a difference in spatial distribution, rods and cones also differ to some extent in their molecular content, for instance with regard to their photopigment molecules. In rod photoreceptor cells, rhodopsin acts as the key molecule initiating the phototransduction cascade, whereas in cone cells different types of photopsin molecules are present, depending on the cone subtype. In the human eye, three different types of cones can be distinguished, each sensitive to light of a different wavelength, i.e. the S-cones (short wavelength), M-cones (medium wavelength) and L-cones (long wavelength) (Roorda and Williams, 1999; Solomon and Lennie, 2007). Even within the macula, there are local differences in the distribution of each of the different cone photoreceptor subtypes (Curcio et al., 1990), illustrating the complexity of the human retina. The synapses formed between photoreceptors and the bipolar and amacrine cells within the OPL are either invaginating or non-invaginating, depending on the impact they play in the forwarding of the light-triggered signal. Invaginating synapses form specialized ribbon synapse structures, one per rod spherule and several per cone pedicule (**Fig. 1B**). A fully developed retina contains approximately 92 million rods and 4.6 million cones (Curcio et al., 1990), that are post-mitotic and therefore do not divide or regenerate following injury.

1.1.2. RPE cells

The retinal pigment epithelium (RPE) consists of a monolayer of hexagonally shaped cells that are in direct contact with the photoreceptor outer segments (**Fig. 1A**), and has several distinct and important functions in the retina. As mentioned above, the RPE cells are responsible for the phagocytosis of the most upper part of outer segment discs that contain the highest concentration of toxic by-products resulting from many cycles of phototransduction (Anderson et al., 1978; Steinberg et al., 1980). In addition, the RPE plays an important role in the visual cycle, a molecular cascade that allows to replenish the photoreceptor cells with chromophore molecules following a series of enzymatic reactions that also partially takes place in the photoreceptor cells (Kiser et al., 2012). Other functions of the RPE include the maintenance of the outer blood-retina barrier by the formation of tight junctions between adjacent RPE cells, and the active transport of

metabolites, nutrients and waste products between the choriocapillaris and the photoreceptor cells and vice versa (Hughes et al., 1998). The pigmented nature of the RPE is caused by melanosomes, melanin-containing organelles that have the ability to absorb light. As such, the RPE can absorb scattered light and thereby minimize phototoxic damage to the retina (Sarna, 1992), revealing yet another important function of the RPE.

1.2. Inherited retinal dystrophies

As indicated in section 1.1, the molecular processes in the retina that initiate vision, including the phototransduction cascade and the visual cycle, involve hundreds of different proteins in any of the different retinal cells. Because many of these proteins are retina specific mutations in the encoding genes often result in dysfunction of retinal cells and concomitantly cause a retinal phenotype. Depending on the severity of the mutations, the cell type that is primarily affected by the mutation (RPE, cone and/or rod photoreceptors, or one of the other cells in the retina) and the function of the protein that is encoded by the corresponding gene, IRDs can be divided into different clinical subtypes with a varying age of onset, rate of progression and clinical hallmarks. The most severe subtype of IRD is Leber congenital amaurosis (LCA), with an onset of symptoms in the first year of life and resulting in complete blindness in childhood. Other subtypes of IRD include retinitis pigmentosa (RP, also known as rod-cone dystrophy), cone-rod dystrophy (CRD), cone dystrophy (CD), achromatopsia (ACHM) or congenital stationary night blindness (CSNB) that all display a large degree of clinical and genetic heterogeneity. In addition, there are some other subtypes of IRD that are caused by mutations in only a single gene, e.g. Stargardt disease (caused by mutations in *ABCA4*), choroideremia (caused by mutations in *CHM*) or Best disease (caused by mutations in *BEST1*). IRDs can be inherited in an autosomal recessive, autosomal dominant, or X-linked fashion, whereas mitochondrial or digenic inheritance also have been reported occasionally. To date, more than 200 genes are collectively known to be mutated in one or more of these IRD subtypes (<https://sph.uth.edu/retnet/>). Retinal dystrophies can manifest either as the sole clinical symptom (non-syndromic IRD) or in conjunction with other abnormalities elsewhere in the human body (syndromic IRD). Examples of syndromic types of IRD include Bardet-Biedl syndrome (BBS), Joubert syndrome (JBTS), Usher syndrome (USH) or Senior-Løken syndrome (SLS). Often, the genes mutated in these syndromes can also underlie non-syndromic IRD. Although the more severe (i.e. protein-truncating) mutations might be more often causative for syndromic forms, establishing a clear genotype-phenotype correlation is not trivial. Given this extreme genetic (and clinical) heterogeneity, establishing the correct molecular or clinical diagnosis can be complicated. Yet, finding the genetic cause underlying IRD has become increasingly important, due to several new treatment options that have reached the clinical trial phase over the last few years, or are currently emerging.

1.3. Therapeutic interventions in IRD

For many years, IRDs have been considered incurable diseases. Yet, from a therapeutic perspective, the eye has several key advantages including its accessibility and its immune-privileged nature that is ensured by the blood-retina barrier, which would allow a robust delivery of therapeutic molecules that remain within the eye and thereby reducing the probability of unwanted side effects. In general, IRDs are progressive disorders that, following the onset of visual complaints in individuals with IRD, become more severe with age. In the early phases of the disease, the cells in the retina are not functioning well but are still structurally intact, while as the disease progresses, cells start to degenerate. Most of the genes in which mutations have been found to underlie IRD are expressed in the RPE or photoreceptor cells, inducing cell death in these cell types as the primary cause of the IRD-associated vision loss. Other neuronal cell types such as the bipolar, amacrine, horizontal and retinal ganglion cells remain intact for a longer period of time, or are even spared. The stage of the disease therefore has repercussions for selecting the most promising therapeutic approach. When the photoreceptor or RPE cells (mostly the primarily affected cell type in IRD) are still structurally intact, gene therapy appears to be the most promising therapeutic strategy, often involving a (virus-based) delivery of the wild-type cDNA of the gene that is mutated to the right retinal cell type via subretinal injections. This strategy has already revealed its promise in IRD patients with mutations in *RPE65* (Bainbridge et al., 2008; Bennett et al., 2012; Hauswirth et al., 2008; Maguire et al., 2009; Maguire et al., 2008), and more recently, in patients with choroideremia and mutations in *CHM* (MacLaren et al., 2014). However, if the RPE or photoreceptor cells are fully degenerated, gene therapy can no longer be considered an option, and alternative strategies need to be employed such as cell replacement therapy (Tucker et al., 2014; Wiley et al., 2015), optogenetic therapy (Roska et al., 2013), or, at a very advanced stage of the disease, retinal implants (Zrenner et al., 2011). Ideally however, one would like to treat IRDs as early as possible when the majority of RPE and photoreceptor cells are still intact, i.e. with gene therapeutic approaches. As this requires the development of independent tailor-made therapies for each gene, suitable cellular and animal models that mimic the molecular and clinical defects observed in patients are needed to assess therapeutic efficacy and safety. In this review, we aim to provide a comprehensive overview of the currently existing vertebrate animal models, their characteristics, and their suitability for functional and therapeutic research on IRDs. We will focus our attention on animal models carrying mutations in genes that have been associated with non-syndromic IRD in humans.

2. VERTEBRATE ANIMALS FOR IRD RESEARCH

2.1. General characteristics

A wide variety of animal models have so far played an important role in the field of IRD, either for increasing our understanding of the molecular mechanisms underlying these disorders, or for the pre-clinical development of novel therapies. Vertebrate animals that will be subject to investigation are macaque, mouse, rat, dog, cat, pig, sheep, chicken and zebrafish, as these are the most commonly used models to study retinal function, the mechanisms underlying IRD and/or in the development of novel treatments. Besides detailed genetic, ocular and retinal characteristics, a range of general aspects need to be considered when selecting the ideal animal model, including breeding time and techniques, the time needed to complete embryonic development and to reach fertility, and housing costs and requirements. As shown in **Table 1**, these general characteristics differ heavily between species, with the general observation that smaller animals are easier to maintain, have a shorter life cycle and generally produce a larger number of offspring. One other advantage of for instance zebrafish over avian and mammalian species is that offspring develops *ex utero* and therefore the development of the eye can be monitored more easily. On the other hand, (larger) mammalian species more closely resemble humans in terms of genetic architecture and sequence, or gross retinal anatomy. In the paragraphs below, we will discuss the ocular (section 2.2) and genomic features (section 2.3) of each of the selected animals compared to the human eye and genome, respectively.

2.2. Ocular and retinal characteristics

As discussed in section 1.1, humans possess a retina that consists of several layers of neurons and interneuronal connections closely connected to the RPE. Three highly specific mechanisms are unique or almost unique to the photoreceptor/RPE complex: the visual cycle, the phototransduction cascade, and the ciliary transport through the connecting cilium. As described in section 1.2, the majority of genes mutated in IRD encode proteins participating in one of these pathways. To be used in preclinical research on IRD, animal models should ideally display similar anatomic features and mechanisms of light transduction as humans. Such anatomic features include specificities at the cellular level (i.e. photoreceptor inner segments, outer segments, synaptic terminals and connecting cilium) as well as at the tissue organisation level (i.e. presence of a macula, fovea). Most currently used animal models for therapeutic research on IRDs lack one or more of these specific features of the human retina and/or have other specific features instead. These are important to consider when deciding on which animal model to use in future IRD research, and to include in the analysis of unexpected but nonetheless frequently occurring results, such as a lack of phenotype or difficulties in therapeutic applications.

Below, an overview is provided of the specific ocular features of the selected animal models starting with the evolutionary most distantly related species (zebrafish and chicken), and moving along the mammalian evolutionary tree to the most closely related animal model, the nonhuman primate. All these animals fulfil the most important request of a suitable model: they possess a morphologically very similar retinal structure with all discernible retinal layers and neuronal cell types. Yet, specific and important differences exist that in some cases determine their suitability to be used in IRD research. A graphical overview of the retinal structure and species-specific features of each animal is provided in **Fig. 2** and ocular characteristics together with general reproductive peculiarities of each species are summarized in **Table 1**, based on our own investigations and data published by others (Bailey et al., 2012; Bawa et al., 2013; Chopovska et al., 2011; Collery et al., 2014; Ferguson et al., 2013; Gekeler et al., 2007; Gelatt, 2007; Hernandez-Merino et al., 2011; Howland et al., 2004; Iribarren et al., 2014; Lozano and Twa, 2012; McKibbin et al., 2014; Montiani-Ferreira et al., 2003; Puk et al., 2006; Williams, 2004).

2.2.1. Zebrafish

Morphologically, the zebrafish retina is composed of all major cell and tissue layers that can be found in humans. The retina lacks a cone-rich structure and is considered holangiotoxic since one plexus of retinal vessels is present at the ILM (Alvarez et al., 2007). The zebrafish is diurnal and contains four diverse cone subtypes which by far outnumber the rod population. In addition to cones receptive to the three color wavelengths perceived by humans, a fourth UV-sensitive cone is present (Fadool and Dowling, 2008). The M- and L-cones form double cones which consist of a principle (L-cone) and an accessory segment (M-cone), and the nuclei of the accessory cones form a morphologically distinguishable cell layer. Rods, cones and double cones possess calyceal processes surrounding the OS and an accessory outer segment (Hodel et al., 2014; Tarboush et al., 2012). Photoreceptor terminals form ribbon synaptic connections with bipolar and horizontal cells (Tarboush et al., 2012). In contrast to mammals, the IS contain megamitochondria, the function of which is currently unknown (Tarboush et al., 2012).

Unlike any of the mammalian species mentioned below, zebrafish are well known to have a remarkable capability to regenerate their retina after damage (Goldman, 2014). Damaged retinal cells will be replaced by newly differentiated cells originating from de-differentiated Müller glia cells (Goldman, 2014). As described in section 1.1 and **Fig. 1A**, Müller glia cells physically span all three different retinal cell layers (ONL, INL until GCL) with their nuclei residing in the INL, making them suitable for sensing and responding to retinal damage from any retinal cell (Fausett and Goldman, 2006; Goldman, 2014). The molecular mechanism underlying the activation of the regeneration process is still largely unknown (Nelson et al., 2013).

2.2.2. Chicken

The avian retina is highly specialized and varies among birds. Raptors, such as the common buzzard, possess one or several foveal structures, while other birds like chicken, do not. Because chicken are diurnal birds, their retina contains a relatively high number of cones (considered cone-dominated). The chicken retina is avascular (anangiomatic) but contains a specific structure called *pecten oculi* (Wolburg et al., 1999). This structure is highly vascularised and responsible for oxygen and nutrient supply to the retina. Concerning the overall morphological structure of the retina, a wide IPL layer is observed together with a prominent INL layer, both being generally thicker compared to the human or mammalian retina (Rauscher et al., 2013). In contrast, the ONL is rather thin and contains, similar to the zebrafish retina, double cones (Kram et al., 2010). These double cones are considered to be responsible for motion detection in birds. A specific feature of the avian photoreceptor is the oil droplet within the single and most double cones, right at the border between the IS and OS and spanning the entire width of the photoreceptor. These droplets consist of lipids in which carotenoid pigments are dissolved (Goldsmith et al., 1984). The precise function of the droplets, which are coloured according to the opsin expressed within the cell, is still unknown, but they may serve as cut-off filters in order to optimize light input to the OS. The RPE possesses long, slender cytoplasmic processes filled with melanosomes that surround the OS (Gelatt, 2007).

The chick retina is believed not to have any retinal regeneration capacities. However, postnatal chicks can regenerate damaged neuronal cells via differentiation of their Müller glia cells (Fischer and Reh, 2001; Luz-Madriral et al., 2014). This capacity is lost in adulthood, although retinal progenitor cells have been found in the retinal peripheral edge (Fischer and Reh, 2000, 2002).

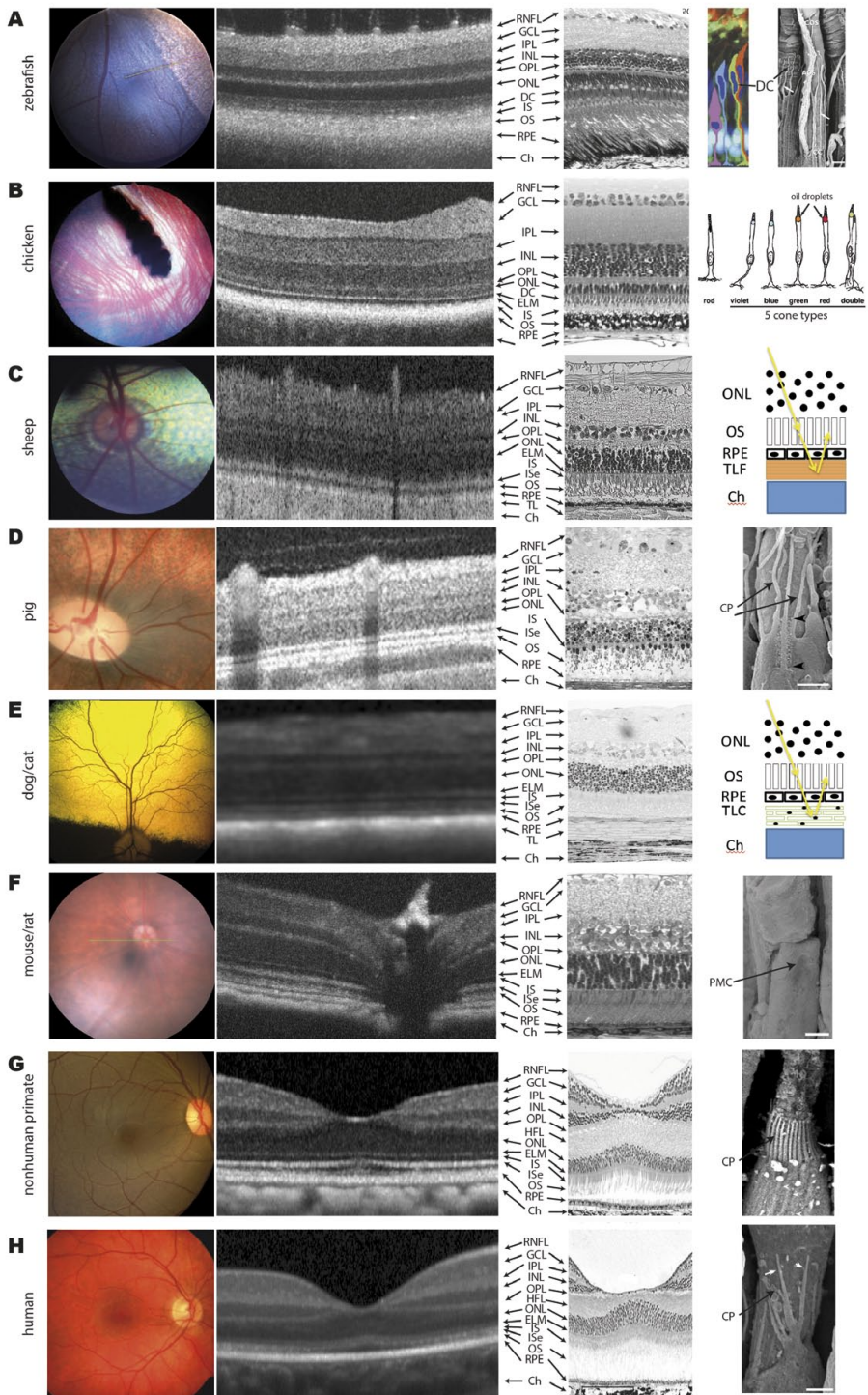
2.2.3. Sheep

Sheep belong to the order ungulata and possess a tapetum lucidum between the RPE and the choroid, that is composed of collagenous fibers, in contrast to carnivores (Ollivier et al., 2004). This special layer between the RPE and choroid reflects the light in order to increase photon capture of the photoreceptors. The retina is holangiomatic. Sheep are diurnal animals and their retina contains rods and two different types of cones (S and M/L cones) (Jacobs et al., 1998). The cones are found in higher numbers in the visual streak and area centralis in the dorsotemporal retina, which is also the region of highest ganglion cell density (Shinozaki et al., 2010).

Table 1. Summary of ocular and reproductive characteristics of the vertebrate animal models used in IRD research

Characteristic	Zebrafish	Chicken	Sheep	Pig	Cat	Dog	Mouse	Rat	NHP	Human
Eye size (visual axis, mm)	~1.2 ¹	~12.5 ⁴	26 ⁵	24.8 ⁵	21.9 ⁵	16-22 ⁵	3.5 ⁶	5.6 ⁵	17.6 ⁵	24.5 ⁵
Lens Thickness (mm)	~0.75 ¹	3.5	10 ¹⁰	8 ⁹	7.8 ⁹	6.7 ⁸	2.1 ⁶	3.8 ⁷	3	4
VA/Lens ratio	1.6	3.5	2.6	3.1	2.8	2.4-3.3	1.67	1.5	5.8	6.125
Retinal thickness on OCT (µm)	191±9 ²	280±10.8 ³	261±2.5 ^{**}	239±0.005 [^]	1:245±21 ^{§13} 2:204±11 ^{§13} 3:182±11 ^{§13}	1:198±9.6 ^{§14} 2:164.4±6 ^{§14}	204±5 ¹¹	192±7 ¹²	1:270±6 [°] 2:348±5.5 [°] 3:310±4.5 [°]	1:226.9±14.3 ^{°15} 2:348.6±14.9 ^{°15} 3:311.5±16.5 ^{°15}
Activity profile	diurnal	diurnal	diurnal	diurnal	both (n/d)	both (n/d)	nocturnal	nocturnal	diurnal	diurnal
Dominant PR	rods	cones	rods	rods	rods	rods	rods	rods	rods	rods
Cone dominant structure	no	no	area centralis	area centralis	area centralis	area centralis	no	no	fovea	fovea
Presence of macular pigment	no	no	no	no	no	no	no	no	yes	yes
# of diff. opsins	four	five	two	two	two	two	two	two	three	three
Special cones [*]	yes	yes	no	no	no	no	yes	yes	no	no
PR structure ^{&}	yes, (CP, DB)	yes (DB, OD)	not known	yes (CP)	not known	not known	no	no	yes (CP)	yes (CP)
Pigmented RPE	no	no	inferior part	yes	inferior part	inferior part	depends [†]	depends [†]	yes	yes
Tapetum lucidum	no	no	yes	no	yes	yes	no	no	no	no
Body weight	0.5-0.7g	1-1.5kg	30-90kg	65-150kg	2-8kg	~5-50kg	20-50g	200-400g	2-8kg	~50-120kg
Reprod. cycle	12-14 weeks	21-25 weeks	6-12 months	6 months	6 months	6 months	9-12 weeks	9-12 weeks	12 months	12-15 months
Females fecund	10-14 weeks	18-22 weeks	5-12 months	4-8 months	4-12 months	7-14 months	6-8 weeks	4-6 weeks	3-4 years	12-14 years

NHP: non human primate; VA: visual axis; (n/d): nocturnal/diurnal
‡: 1: peripapillary; 2: periphery; 3: area centralis
§: 1: superior retina; 2: inferior retina
¶: UV cones or mixed cones
‡: CP: calyceal processes; DB: double cones; OD: oil droplets
‡: depends on pigmentation of strain
∞: 1: foveal minimum; 2: superior inner macula; 3: superior outer macula
** : data kindly provided by Dr. M.H. Greenlee, Iowa State University, US
^ : data kindly provided by Dr. C. Kostic, University of Lausanne, Suisse.
References used in the table: ¹ Collerey et al., 2014, ² Bailey et al., 2012, ³ McKibbin et al., 2014, ⁴ Montiani-Ferreira et al., 2003, ⁵ Howard et al., 2004, ⁶ Puk et al., 2006, ⁷ Bawa et al., 2013, ⁸ Williams et al., 2004, ⁹ Gellat, 2007, ¹⁰ Iribarren et al., 2014, ¹¹ Ferguson et al., 2013, ¹² Lozano and Twa, 2012, ¹³ Gekeler et al., 2007, ¹⁴ Hernandez-Merino et al., 2011, ¹⁵ Chopovska et al., 2010.



2.2.4. Pigs

Since the pig is a diurnal mammal, the porcine retina is optimized for day vision, consisting of a large population of cones with highest density within the *area centralis* dorsal to the optic nerve head (Chandler et al., 1999). The retina is holangiotic and pigs do not possess a tapetal structure (Ollivier et al., 2004). The cones comprise calyceal processes around the CC and OS similar to the human retina (Sahly et al., 2012). The cone IS are usually large and can be easily identified on histological sections. Overall, due to the cone-rich nature of the retina, the presence of an *area centralis* and the lack of a tapetal zone, the porcine retina is considered to be a ideal model for studying IRDs, especially cone-dominated disorders.

Figure 2. Comparative description of ocular features in vertebrate animal models. (A) Fundus image, OCT scan, histological section and special features of the zebrafish retina. Special features include the presence of double cones (DC), calyceal processes (CP), and accessory outer segments (AOS). CP and AOS start at the level of the connecting cilium (CC) (TEM image adapted from Hodel et al., 2014). Retinal vessels located at the border of the RNFL within the OCT scan. Fundus image and OCT scan courtesy of Phoenix Research Labs, La Jolla, US. Histological section shows the long and pigmented RPE microvilli extending into the OS layer (adapted from Schonthaler et al., 2010). **(B)** Fundus image, OCT scan, histological section and special features of the chicken (bird) retina. Special features include the presence of five different cone subtypes, double cones (DC) and oil droplets (adapted from Kram et al., 2010). Note the presence of the pecten oculi within the fundus image (<http://people.eku.edu>). OCT scan adapted from Moyaed et al., 2011. Histological section reveals the wide IPL and INL layer and the comparatively thin ONL layer (adapted from Bueno et al., 2011). **(C)** Fundus image, OCT scan, histological section and special features of the sheep retina. Special features include the presence of a tapetum lucidum fibrosum (cartoon modified after Ollivier et al., 2004). Fundus image adapted from (Galan et al., 2006). OCT scan and histological section kindly provided by Dr. M.H. Greenlee (Iowa State University, US). The retinal vessels are very prominent at the border of the RNFL within the OCT scan. **(D)** Fundus image, OCT scan, histological section and special features of the porcine retina. Special features include the presence of calyceal processes (TEM image adapted from Sahly et al., 2012) and large cone inner segments (histological section from Ross et al., 2012). Fundus image adapted from (<http://www.ocularservices.com>). OCT scan adapted from (McLellan and Rassmussen, 2012). The retinal vessels are very prominent at the border of the RNFL within the OCT scan. **(E)** Fundus image, OCT scan, histological section and special features of the dog retina. Special features include the presence of a tapetum lucidum celluloseum (TLC) (Cartoon modified after Ollivier et al., 2004). **(F)** Fundus image, OCT scan, histologic section and special features of the rodent (mouse) retina. Special features include large outer segments and the absence of calyceal processes. Instead, a periciliary membrane complex (PMC) is present at the CC (TEM image adapted from Sahly et al., 2012). **(G)** Fundus image, OCT scan, histological section and special features of the macaque retina. Special features include the presence the foveal pit, Henle fiber layer and calyceal processes (CP) (TEM image from Sahly et al., 2012). OCT scan kindly provided by Dr. F. Rolling (University of Nantes, Fr). **(H)** Fundus image, OCT scan, histological section and special features of the human retina. Special features include the presence the foveal pit, Henle fiber layer and calyceal processes (CP) (TEM image from Sahly et al., 2012). Histologic section adapted from (<http://webvision.med.utah.edu>). RNFL: retinal nerve fibre layer; GCL: ganglion cell layer; IPL: inner plexiform layer; INL: inner nuclear layer; OPL: outer plexiform layer; ONL: outer nuclear layer; HFL: Henle fiber layer; ELM: external limiting membrane; IS: inner segments; ISe: inner segment ellipsoids; OS: outer segments; RPE: retinal pigment epithelium; Ch: choroid.

2.2.5 Cats & dogs

Cats and dogs are originally nocturnal carnivores. Their retinas are holangiomatic. Both species possess in the superior part of the retina a tapetal zone that contains cells, the iridocytes, that harbor crystals rich in zinc cysteins in dogs and riboflavin in cats (Ollivier et al., 2004). The tapetal zone is almost triangular in form and the RPE adjacent to it is unpigmented. The remaining part of the retina is attached to a pigmented RPE and therefore, the retina can be divided into two areas, depending on the pigmentation of the fundus. The presence of the tapetal zone renders examination methods that depend on light reflectivity such as OCT more challenging.

Most parts of the dog retina are dominated by rods. Cones are not evenly distributed, but their retinas have a central area with a high density of cones (Mowat et al., 2008). This area centralis can be found in the superior temporal retina and is defined by an increased number of ganglion cells (Peichl, 1992). A recent study even described a fovea-like structure composed exclusively of cones within the *area centralis*, albeit without a foveal pit (Beltran et al., 2014). Overall, the cat retina has similar characteristics.

2.2.6. Rodents (mouse & rat)

The rodent retina is optimized for activity at night (nocturnal). Like most mammals, the retinal vasculature is holangiomatic. The retina contains highly sensitive rods with long outer segments loaded with many discs and cones that are not evenly dispersed throughout the retina but do not form a defined cone-rich region such as the human macula. This characteristic has largely challenged the generation of animal models for cone disorders, as the phenotype may not reflect the human situation. However, in the *Nrl^{-/-}* mouse, the lack of transcription factor neural retina leucine zipper drives the cell fate of rod photoreceptors to become cone-like photoreceptors (Oh et al., 2007). Moreover, rodents are dichromats, since the cones are either UV-sensitive or sensitive to long-wavelength light (Gouras and Ekesten, 2004). L/M cones are distributed mostly in the superior hemisphere of the retina, while the UV cones are found mostly in the inferior hemisphere (Szel et al., 1992). Some cones may express both types of opsins. The CC of cones is surrounded by a periciliary membrane complex (PMC) instead of calyceal processes, which may hamper studies on IRDs related to ciliary transport (Sahly et al., 2012).

2.2.7. Nonhuman primates (macaque)

Nonhuman primates that are used in research on the treatment of IRDs belong most often to the species macaque and are classified, like humans, to the suborder haplorhini. Members of this group have evolved vision as one of their main senses and have among other specifications forward facing eyes positioned on the front of the skull, thus enabling optimized binocular (i.e. three-dimensional) vision. Like humans, macaques see

with three different cone subtypes (trichromatic) and have a cone-only foveal pit in the centre of the macula. While there are no IRDs so far described in nonhuman primates, the presence of the specific macular structures makes this model crucial for developing treatment strategies.

2.3 Genomic architecture and evolution of IRD genes

In addition to anatomic and morphological features of the eye and the retina, one very important aspect in determining the suitability of an animal model is the genomic architecture and gene content of each species. As illustrated in **Fig. 3**, between 20 and 100 million years of evolution separate humans from most vertebrate species. The evolutionary distance to chicken is more than 300 million years whereas the human and zebrafish lineages have separated 450 million years ago (Hedges, 2002). Hence, in terms of genetic architecture and sequence identity, mammalian models resemble human more closely than chicken and fish. The complexity of genomic evolution is further illustrated by several events that result in copy number differences, i.e. deletions or duplications of certain genes in the genome of particular species (Katju and Bergthorsson, 2013). One vision-related example of this is the primate-specific copy number polymorphism of the *OPN1LW* and *OPN1MW* gene cluster on the X-chromosome. This variation in copy number, combined with specific amino acid sequence changes in some of these copies contributes to the trichromatic nature of primate vision, and is thought to be the result of convergent evolution as a consequence of visual adaptation to the environment (Hunt et al., 1998).

In order to assess the degree of evolutionary conservation and copy number of genes associated with IRD amongst the selected species, we studied the amino acid sequence and orthology relationships for all genes currently listed in the RetNet database that are associated with any form of monogenic IRD (<https://sph.uth.edu/retnet/>). The percentages of identity at the amino acid or nucleotide level were based on those levels as recorded in Ensembl (Cunningham et al., 2015). To obtain an average across the various proteins, their levels of identity were weighted by their sequence length. In case multiple orthologous proteins were present in one species (i.e. deriving from duplicated genes), the one with the highest level of identity to the human protein was used to calculate the average. The orthology relationships are based on the annotation in the ENSEMBL database (Vilella et al., 2009). For all genes that were absent or predicted to be duplicated in any given species, we manually checked whether this was indeed consistent with other datasources of orthology. Specifically, for genes predicted to be duplicated, we examined Treefam (Ruan et al., 2008) for orthology relationships, including examining the existence of RNA transcripts for inferred species-specific duplications. For species not present in Treefam, Blast analysis was performed to find homologues that were used to create Neighbor Joining phylogenies after which we

inferred orthology relationships from those. For genes that appeared to be missing in the genomes from certain species, we examined the nucleotide collection for those species at the NCBI database fusing tBlastn (Altschul et al., 1990), i.e. to detect genes that may have gone unnoticed in the DNA or that have only been sequenced as cDNAs.

When comparing the sequence identity of the selected 215 genes at the amino acid level, zebrafish proteins show an overall identity of 54% to their human counterparts, a number that increases up to 92% for the macaque (**Fig. 3**). In terms of absent and duplicated genes, it immediately becomes apparent that zebrafish shows a high number of duplicated genes (**Fig. 3** and **Supplemental Table 1**). This is due to the ancient genome

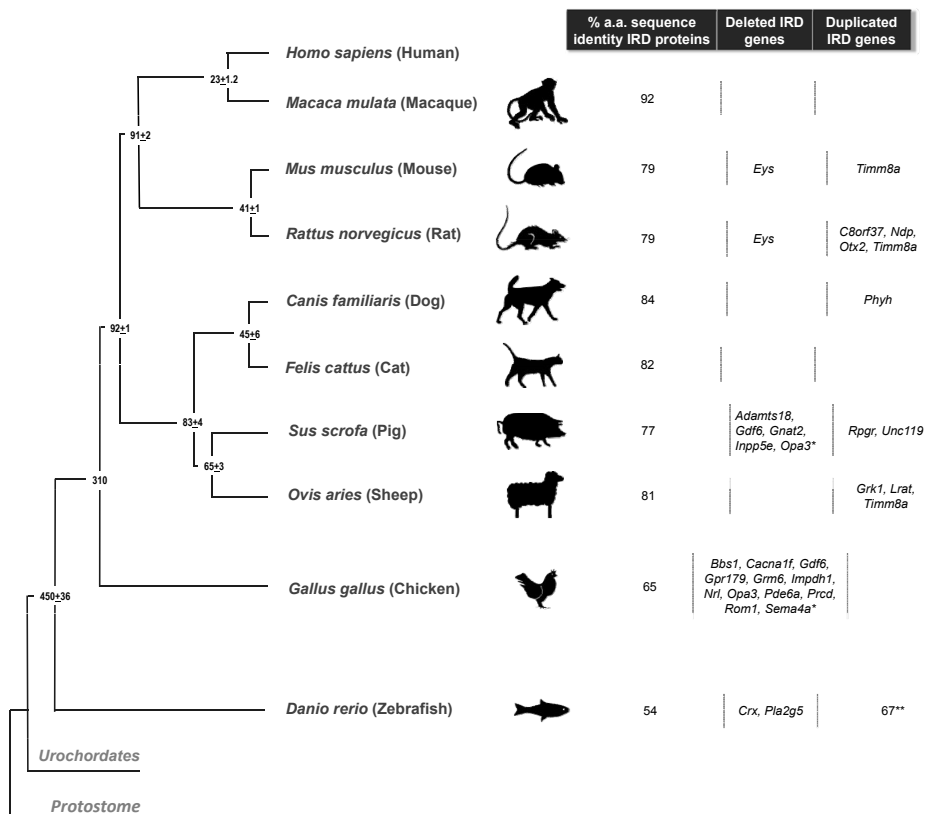


Figure 3. Comparative genomics and evolutionary distance genes involved in IRD. Phylogeny and divergence time of the selected animals. The numbers on branches indicate the evolutionary divergence time in million years. The average percentage of amino acid (a.a.) sequence identity of proteins encoded by IRD genes was calculated, and ranges from 92% in macaque to 54% in zebrafish. Genes that are predicted to be deleted or duplicated in the genome of certain species are indicated. *Due to the poor quality annotation of the chicken and porcine genome, some genes that are predicted to be deleted may in fact be missed in our analysis. **Given the high number of duplicated genes in the zebrafish genome ($n = 67$), these genes are listed separately in **Supplementary table 1**.

duplication event in the teleost fish that gave rise to many genes with two copies in the present day zebrafish genome (Meyer and Schartl, 1999). In contrast, only two genes appear to be deleted in zebrafish, among which the transcription factor *Crx* that plays a crucial role in photoreceptor development in mammals. A relatively large number of genes appear absent in the genomes of chicken and pig (**Fig. 3**), although we cannot rule out that these are not actually lost but rather the result of the incompleteness of the genomes. Intriguingly, *EYS*, one of the most frequently mutated arRP genes in humans (Abd El-Aziz et al., 2008; Collin et al., 2008) has no orthologues in the rodent genomes, i.e. in mouse and rats. Interesting duplications are those of *TIMM8A* in three species (sheep, mouse and rats) and *RPGR*, in which mutations are a recurrent cause of X-linked RP, in pig. Whether these deletions and duplications have any functional relevance or selective advantage in the corresponding species needs to be established, but most certainly they are important when one considers generating a mutant animal model for a particular gene or genetic defect.

3. GENETIC MODIFICATION AND NATURALLY OCCURRING MUTANT ANIMAL MODELS

In order to study IRD, many different animal models have been used. Some animals have developed IRD as the result of a naturally occurring mutation, whereas in others, specific mutations have been introduced in their genomes, via different ways, i.e. either non-targeted or targeted. Attempts have been undertaken to systematically create mutant animals independent of the genomic sequence by using mutagenic chemicals such as N-Ethyl-N-nitrosourea (ENU) or by disruption of genes with a viral DNA insertion or transposons. Employing such forward genetic screens can be advantageous for mutating lots of different loci at the same time, in order to obtain as many different mutant animals as possible. Because of the high number of animals to be screened, such screens are only cost- and labor-effective for small animals with a large offspring and short regeneration times. In contrast, reverse genetic screens can be used to specifically modify a genomic region of interest in a cost-effective way for nearly all animals, because of its targeted approach. The characteristics of the different approaches to modify a genome (non-targeted vs. targeted) that are described in this chapter are listed in **Table 2**. A summary of the use of these methods per species is provided in **Table 3**.

3.1. Naturally occurring models

Like in humans, naturally occurring mutations can result in the disruption of gene function and a concomitant phenotype. Especially in mice, many naturally occurring models have been identified and used for research over the last three decades (Veleri et

Table 2. Characteristics of different genome modifying methods. Characteristics of different genome modifying methods. Each method has been described in the text and is classified into non-targeted, used in forward genetic screens, or targeted, used in reverse genetic studies. Practical characteristics mentioned which are used to choose a method of choice are compared by giving them an artificial score from ++ to --. ++ very well applicable; + well applicable; ± moderately applicable; - less applicable; -- hardly/not applicable.

	Non-targeted (forward genetics)			Targeted (reverse genetics)			
	ENU mutagenesis	Viral inserted mutagenesis	Transposon mediated mutagenesis	Homologous recombination	ZFNs	TALENs	Crispr/Cas9
High throughput / large scale	+	+	+	-	-	-	-
Efficiency in genome modification	++	++	+	±	+	+	+
Specificity in genome modification	--	--	--	+	+	+	++
Cost/labour intensity	-- [#]	-	-- [#]	+	±	±	++
Sequence specificity	-	-	-	+	+	+	+
Identification specific mutational events	--	++	++	++	++	++	++
Genotoxicity	+	+	+	-	±	±	±
Off-target effects	+	+	+	-	±	±	± [§]

[§] Large linkage studies and sequence efforts are needed to identify causative mutations.

[#] Improvements have been made, resulting in minimal off-target effects (Fu et al., 2014).

al., 2015). A prerequisite for employing these animals however is the identification of the causative genetic defect, which in the past was often done by linkage analysis combined with Sanger sequencing of candidate genes. In some species, this has been very challenging, due to the relative lack of knowledge on polymorphic regions (e.g. SNPs and CA-repeats) within their genome, and/or little knowledge on the exact genomic sequence. Nowadays, the method of exome sequencing, when possible in combination with linkage analysis, is generally applied to identify naturally occurring variants, also in pigs and dogs (Ahonen et al., 2013; Robert et al., 2014). The poor annotation of the genome of some species however still complicates matters, as for instance exome sequencing data cannot be robustly analyzed. Once the causative mutation has been identified, these animals are ideal for experimental research since no genetic modification and, as a result of that, potential off-target effects are involved. Exome sequencing data derived from blind pet canines are nowadays employed in order to find suitable large animal models for gene characterization and gene therapy trials (Ahonen et al., 2013). Visually impaired chickens suffering from naturally occurring founder mutations have been identified and are nowadays used for research purposes (Hocking and Guggenheim, 2013). Furthermore, retinal degenerative disorders have been observed occasionally in cats and sheep.

Table 3. Genome modifying methods used in different species. Each genome modifying method has been described in the text and is classified into non-targeted, used in forward genetic screens, or targeted, used in reverse genetic studies. The species mentioned in the text are summed and examples that are applied marked with "X". Information in this table is derived from literature and is not restricted to IRD genes.

	Non-targeted (forward genetics)				Targeted (reverse genetics)		
	ENU mutagenesis	Viral inserted mutagenesis	Transposon mediated mutagenesis	Homologous recombination	ZFNs	TALENs	Crispr/Cas9
Zebrafish	X	X	X	X	X	X	X
Chick	X		X		X	X	
Sheep					X	X	X
Pig			X	X	X	X	X
Cat							
Dog			X				
Rat	X	X	X	X	X	X	X
Mouse	X	X	X	X	X	X	X
Macaque	X					X	X

3.2. Forward genetic approaches / phenotype-based screens

3.2.1. ENU mutagenesis

ENU is an efficient mutagenic agent used in the premeiotic male germ line, where it is estimated to induce one sequence change per 100 kb on average (Beier, 2000). However, only ten percent of these mutations are thought to have functional consequences, i.e. the induced point mutations lead to a nonsense, missense or splice site mutation resulting in a phenotype (Beier, 2000; Kettleborough et al., 2013; Zan et al., 2003). A subsequent assessment of visual function in these mutant animals can reveal many new suitable model systems for retinal degeneration, e.g. in zebrafish and mice (Li, 2001; Maaswinkel et al., 2005; Won et al., 2011). An unavoidable coincidence of using such mutagenic agents however, is the chance of having multiple induced mutations per genome, potentially leading to a combined phenotype or the involvement of different genes contributing to one phenotype in some cases. A large ENU-screen on the zebrafish genome covered over 38% of the protein-coding genes and revealed 10,043 genes to be mutated (Kettleborough et al., 2013). The identification of affected genes and corresponding mutations as such remains challenging in using ENU-treated mutant animals.

3.2.2. *Viral and transposon-based insertions*

Insertional mutagenesis is another approach for large mutagenic screens. By using viral DNA, capable of randomly integrating into a host genome, some genes will be targeted by chance and thereby deregulated. Nowadays the mostly used viral vectors are pseudotyped retroviruses, which are able to introduce their cDNA into a host genome. For example, zebrafish embryos infected with a pseudotyped murine leukemia (MLV)-based virus at the 1,000 to 2,000 cell stage, gave rise to an average of 63 integrations per cell (Wang et al., 2007). The mosaic male parent animals are then outcrossed with wildtype females to generate heterozygote F1 fish with on average 10.4 ± 5.0 proviral insertions per genome (Wang et al., 2007). In this zebrafish study, approximately twenty percent of the viral integrations led to more than 70% reduction in mRNA levels, originating from viral integrations into exons, introns or sites close to annotated genes (Wang et al., 2007). Intriguingly, from all insertions into introns, by far (59%) the most hits were in the first intron of the corresponding gene (Wang et al., 2007). Offspring animals are phenotyped to identify specific functional and/or morphogenetic defects, such as defects in optokinetic responses (Gross et al., 2005). For mutants with the desired phenotype, the identification of disrupted genes can be easily done using the inserted DNA sequence as a molecular tag, which is a huge advantage over other mutagenic screening methods. Such forward genetic-driven research has yielded animal models for studying several retinal defects (Gross et al., 2005). In a similar way, also transposon elements can be used to integrate foreign DNA in a genome for genome-modifying purposes (Izsvak et al., 2010). However, the reason why transposon-based methods are not often used is the lack of active transposon elements for the vertebrate genome. One exception is the *tol2* element derived from the medaka fish, which is found to be naturally and autonomously active in all tested vertebrate genomes (Kawakami, 2007). The Tol2 system can be modified to incorporate a sequence of interest very efficiently into the genome of at least zebrafish, frog or mouse (Hamlet et al., 2006; Keng et al., 2009; Kotani et al., 2006). In addition, researchers have activated another transposon element from teleost fish, named Sleeping Beauty (SB), to randomly integrate into the human genome, which therefore can be used for insertional mutagenesis as well as for gene delivery by pronuclear injections in at least zebrafish, mouse and rats (Ivics et al., 2004; Kitada et al., 2007; Lu et al., 2007). Transposon elements, such as the Tol2 system, SB and also the PiggyBac system, are now used in preclinical studies as an alternative for viral gene therapy delivery (Chénais, 2013).

3.3. Reverse genetic approaches

3.3.1. Homologous recombination

Homologous recombination is naturally used by cells to repair DNA double-stranded breaks and interstrand crosslinks, but can also be used to introduce foreign DNA into the genome of a host cell, e.g. embryonic stem cells, by using two flanking homologous arms allowing a targeted way of integration. Once the DNA sequence of the gene of interest is known, homologous recombination can exchange or introduce DNA up to several kilobases of DNA. With the same mechanism, also knock-out or knock-in animals can be generated. For screening purposes of the growing stem cell colonies, mostly a selection gene (e.g. neomycin resistance) is co-incorporated within the homologous flanking arms. The surviving cells can be injected into a fertilized blastocyst and implanted in a pseudo-pregnant female animal to generate chimeric offspring (Tong et al., 2011). Because the homology arms are sequence-specific, the major limitation of homologous recombination is the low ability (<1%) of targeting some loci (Osterwalder et al., 2010). Nevertheless, the European Conditional Mouse Mutagenesis (EUCOMM) and the National Institutes of Health Knockout Mouse (KOMP) consortia are using homologous recombination in a high throughput and systematic manner to generate knock-out mice (Skarnes et al., 2011). Additionally, gene trap methods have been using homologous recombination to insert DNA cassettes into genes of interest (Osterwalder et al., 2010).

3.3.2. Sequence-specific endonucleases: zinc-finger nucleases and TALENs

Large mutagenesis screens are all based on the introduction of random mutations and are phenotype-driven. Since more detailed genetic information becomes apparent from patients, also the need for generating models with specific mutations arose with it. One of the first approaches of targeted gene modification made use of one class of specific DNA binding proteins, zinc fingers, that are peptides that can recognize and bind 3-bp DNA motifs. These peptides are usually clustered into three to six DNA binding domains capable of recognizing around 9 to 18 bps. The fusion of zinc-fingers with the endonuclease enzyme *FokI* into a zinc finger nuclease (ZFN) complex led to the possibility of targeted DNA cleavage. Cellular non-homologous end-joining (NHEJ) repair processes will join the DNA ends, sometimes introducing mutations such as insertions and/or deletions at this position (Sander et al., 2011). The nucleotide specificity remains critical, since off-target effects can result in false phenotypes. The targeting options using *FokI*, however, were limited to its DNA restriction motifs. In order to increase DNA restriction possibilities, a more flexible form of DNA cleavage was used. By fusing a transcription activator-like (TAL) effector DNA-binding domain to a general DNA cleavage domain, a wide range of possible restriction motifs is estimated to be present

once in every 35 bp of DNA (Sander et al., 2011). The encoded amino acids of the DNA binding domain of these artificial endonucleases are easier to design than previously used ZFNs and are, together with an endonuclease domain, referred to as transcription activator-like effector nucleases (TALENs). TALENs have been shown to be suitable for gene-specific mutagenesis in zebrafish (Huang et al., 2011), rat (Ponce de Leon et al., 2014; Tesson et al., 2011), mouse (Davies et al., 2013) or human derived embryonic stem cells and induced pluripotent cells (Hockemeyer et al., 2011). Attempts to make a less genotoxic TALEN-mediated endonuclease system recently yielded a re-engineered very specific endonuclease (I-SceI) without efficiency loss compared to traditional TALENs (Lin et al., 2014). Following induction of DSBs by either ZFNs or TALENs, repair can also be directed towards homologous recombination by the addition of donor template DNAs (section 3.3.1.).

3.3.3. *Crispr/Cas9*

Over the last two years, a new tool has become available to efficiently modify a genome. Although the principle has not changed, clustered regulatory interspaced short palindromic repeat (CRISPR)/Cas9-based RNA-guided DNA endonucleases are very easy in both design and use, and have increased efficiencies compared to previously used methods like ZFNs or TALENs (Smith et al., 2014). CRISPR arrays were first discovered in the *Escherichia coli* genome (Ishino et al., 1987) and were found to play a role in the adaptive immune system by protecting bacteria from invading viruses when combined with Cas9 genes (Barrangou et al., 2007). The transition of this system from a biological phenomenon to a genome engineering tool was the result of combining targeted specificity (crRNA) with the structural Cas9-binding properties of the tracrRNA in a chimeric single guide RNA (gRNA) (Jinek et al., 2012). The Crispr/Cas9 system has been adapted for efficient use in a wide variety of organisms, including zebrafish, mouse, rat, human, pig and sheep (Han et al., 2014; Sander and Joung, 2014; Whitworth et al., 2014; Wu et al., 2013). Two recent studies however, show major off-target binding of catalytically active Cas9 endonuclease, leading to possible genotoxicity (Fu et al., 2013; Wu et al., 2014). Although only a few off-target mutations were found in one of these two studies, the other shows higher off-target mutagenesis efficiency in some cases, even when Cas9 was targeted to positions with up to five nucleotide mismatches compared to the ~20-nucleotide guide RNA sequence (Fu et al., 2013). A method which can improve the target specificity of active endonucleases to the genome is needed for future use. Shortening guide RNAs to less than twenty nucleotides can reduce off-target binding up to 5,000 fold or more, without reducing any on-target functionality (Fu et al., 2014). Another improvement, which can be combined with truncated guide RNAs, was made when researchers introduced the use of a Cas9 endonuclease mutant able to induce only a single strand break called nickase (Ran et al., 2013). Targeting two nickases to

the same genomic position is thus required for a double strand break, via which the specificity can be increased by 50- to 1,500-fold, as two different guide RNAs can be used (Ran et al., 2013). Since the genome-directed Cas9 nickases are catalytically active, they will still induce single-strand breaks, contributing to genotoxicity and potential mutations. To circumvent these limitations, a *FokI* endonuclease can be fused to a catalytically dead Cas9 protein used by guide RNAs to target the desired genomic location (Tsai et al., 2014). The advantage of using *FokI* over previous versions of the Crispr/cas9 system is that *FokI* endonucleases are only catalytically active after dimerization, overcoming therefore all earlier mentioned genotoxicity. Following the induction of the double strand break by the cas9 endonuclease activity, the break can be repaired by either nonhomologous endjoining (NHEJ) or homology-directed repair. NHEJ will induce insertions and/or deletions since no template is present, while homology directed repair can use any template to repair the breaks (see section 3.3.1.). Thus, by providing Crispr/cas9 treated genomes with an organism-foreign DNA donor fragment containing DNA of interest, the possibilities for genome editing are enormous. Indeed, this is an established technique and larger DNA templates have been successfully incorporated in genomes of zebrafish (Auer et al., 2014) or mouse (Yang et al., 2013). With higher specificities, it now becomes possible to not only mutate a gene, but also to repair a mutated allele back to the wild-type sequence. First tests in a mouse model for cataracts showed successful repair of the mutated *Crygc* gene by using its healthy counterpart as a template, which led to fertile wildtype mice (Wu et al., 2013). Along the same line, researchers have been able to repair mutations in human derived induced pluripotent stem cells (Smith et al., 2014).

4. MUTANT VERTEBRATE ANIMAL MODELS USED IN IRD RESEARCH

4.1 Historical overview on the use of mutant IRD animal models

For centuries, scientists have attempted to better understand human physiology and pathology by employing animals in research. Already in the first half of the 20th century, the first studies on retinal degeneration in animals were published (Bourne et al., 1938; Chatzinoff et al., 1958), and soon after that, the first animal models displaying retinal degeneration segregating in a Mendelian fashion were identified, i.e. the *rd* (retinal degeneration) mice, and the *rds* (retinal degeneration slow) mice (Sanyal et al., 1980; Sidman and Green, 1965). Although the genomic regions harbouring the causative genetic defects were mapped, it took until the late eighties before the actual genes carrying these mutations were identified, i.e. *Prph2* in the *rds* mice (Travis et al., 1989; Travis et al., 1991) and *Pde6b* in the *rd* mice (Bowes et al., 1990). From that point on, the genetic defect underlying retinal degeneration in many mouse models was

elucidated, and mutations in the human orthologous genes were identified at a very rapid pace. At the same time, positional cloning combined with sequencing analysis in humans revealed other genes to be mutated in IRDs (Cremers et al., 1990; Dryja et al., 1990), genes that automatically served as good candidates to be mutated in animal models with naturally occurring types of IRD, not only in mice but for instance also in dogs (Clements et al., 1993) and, somewhat later, in rats (D’Cruz et al., 2000). Ever since, many different animal models carrying spontaneous mutations in genes associated with IRD have been identified, and studied in great detail to increase our understanding on retinal function and dysfunction. The discovery of homologous recombination in mouse embryonic stem cells upon transfection of exogenous DNA (Thomas and Capecchi, 1987) and possibilities to use this technology for the generation of genetically modified mice (Koller and Smithies, 1989) led to novel opportunities to study the function of proteins encoded by the various genes that are mutated in IRDs. Targeted disruption (knock-out) or targeted insertion of specific pieces of endogenous or exogenous DNA (knock-in) via homologous recombination in mouse ES cells, has resulted in the generation of many animal models with genetic defects in genes underlying IRD in humans. The development of other novel technologies to modify genomes (see **Chapter 3**) has even further expanded the number of animal models for IRD, and to date, more than 250 different animal models have been described (**Supplemental Table 2**). Yet, in several animal models, the phenotype does not (exactly) resemble the phenotype that one would expect based on the clinical characteristics of human IRD patients with mutations in the corresponding gene. Below, we discuss these discrepancies, and aim to find correlations between the disparity of the phenotype and the molecular, anatomical or retinal characteristics of the particular animals.

4.2 Mutant IRD models that do not mimic the human phenotype

Comparing the clinical characteristics of a mutant animal model with those of IRD patients with mutations in the orthologous gene is complicated due to intrinsic differences in retinal development and structure, as well as by the different procedures that are applied to describe this phenotype. Hence, establishing whether a mutant animal model exactly mimics the human phenotype is not always straightforward. In several cases however, a detailed molecular or phenotypical analysis of the mutant animal models clearly shows the absence of any, or presence of unexpectedly mild, retinal abnormalities (**Supplemental Table 2**). In the following paragraphs, we cluster these discrepancies into groups, describe several examples, and hypothesize on the molecular, or retinal structure-related reasons for the differences in phenotypic outcome.

4.2.1. Gene- or mutation-related discrepancies

As described in section 2.3, the genomic architecture of the selected species can differ significantly, resulting in the absence of certain genes in some species, or the presence of multiple copies of one gene in a given genome (**Fig. 3** and **Supplemental Table 1**). In addition, supported by alternative splicing, the same or slightly different protein products derived from the same gene can have diverse functions, in different organisms, within the same organism, and even within the same cell. It is therefore not surprising that different mutations can result in various molecular defects, either because the mutation affects only a single isoform of the gene, or because the type of mutation results in complete loss-of-function, partial loss-of-function, a gain-of-function, or has a dominant-negative effect on the wild-type allele in case of heterozygous mutations. In several cases, a discordance between a mutant animal model and the clinical phenotype in humans can be explained by such gene- or mutation specific reasons, as illustrated below.

4.2.1.1. Embryonic lethality

In case a particular mutation, or compound heterozygous mutations, in humans result in only a partial loss-of-function, this may affect the function of only one or a few specific organs or tissues, resulting in for instance IRD. If the corresponding genes are ubiquitously or broadly expressed in the human body, a complete loss-of-function of these genes could result in a much more severe phenotype, or even be incompatible with life. Similarly, a targeted disruption of the orthologous mouse genes can result in embryonic lethality, as has been shown for *Chm*, *Elovl4*, *Prpf3* and *Prpf8* (**Supplemental Table 2**). In some cases, this embryonic lethality is unexpected, for instance in *Chm*, since the mutations that cause choroideremia in humans are also true loss-of-function mutations. Further studies revealed that this observation is most likely explained by preferential inactivation of the paternal X-chromosome in murine extraembryonic membranes, together with a crucial function for the Rep-1 protein (encoded by *Chm*) during early embryonic development (van den Hurk et al., 1997).

4.2.1.2. Differences in mutational mechanisms

One other explanation for discrepancies in the phenotypic outcome between humans and animals are differences in the mutational mechanisms, which is particularly true for disorders that are inherited in an autosomal dominant manner. When causative heterozygous missense mutations are identified, the pathophysiological mechanisms underlying IRD in those cases could be haploinsufficiency in case of loss-of-function mutations, the mutation could act in a dominant-negative way, or the mutation can cause a gain-of-function. Without a clear understanding on these exact mechanisms,

correlating the phenotype observed in mutant animal models with different mutations in the same gene to the human situation is challenging.

Mutations in the *cone-rod homeobox-containing (CRX)* gene, encoding a transcription factor essential for the development of photoreceptor cells, in humans are associated with different subtypes of IRD, depending on the type and zygosity of the mutations, i.e. Leber congenital amaurosis, cone-rod dystrophy or RP (Freund et al., 1997; Freund et al., 1998; Sohocki et al., 1998; Swain et al., 1997; Swaroop et al., 1999). The majority of these mutations are thought to act in a dominant-negative manner, i.e. the mutant CRX protein impairs the transcriptional activity of the wild-type copy.

Homozygous $Crx^{-/-}$ mice clearly demonstrate a functional impairment of photoreceptor cells, resulting in a progressive photoreceptor degeneration (Furukawa et al., 1999). This knock-out mouse however fails to model the dominant inheritance of CRX-associated IRD in humans, as heterozygous mice display only a mild phenotype and normal retinal morphology (Furukawa et al., 1999). Thereafter, the generation of mouse models carrying mechanistically distinct mutations has further revealed the complexity of studying CRX-associated phenotypes. Crx^{R90W} knock-in mice, carrying the exact missense mutation associated with autosomal recessive LCA in humans (Swaroop et al., 1999), appear healthy in heterozygous state, whereas the phenotype in homozygous mutant mice closely resembles that of the $Crx^{-/-}$ mice (Tran et al., 2014). In contrast, studies in Crx^{E168d2} mice carrying a frame-shift mutation, have revealed that a truncation in the CRX trans-activation domain will preserve DNA-binding activity and disrupts the trans-activation activity of the wild type protein (Tran et al., 2014). As a result, both $Crx^{E168d2/+}$ and $Crx^{E168d2/E168d2}$ mice show clear signs of retinal degeneration, although more severe in the homozygous mutant mice. The characterization of a spontaneous heterozygous frameshift mutation in the Crx^{Rip} mice with congenital blindness (Roger et al., 2014), and a naturally occurring cat model Crx^{Rdy} with a frameshift mutation more closely resembling the human CRX-associated phenotype (Menotti-Raymond et al., 2010) has further revealed the complexity of modeling phenotypes caused by mutations in the same gene that display different mutational mechanisms.

Another example is the diversity of mutations in *RHO* that encodes rhodopsin. IRD-associated mutations in *RHO* can be subdivided into two classes. Some mutations, clustering in the first transmembrane domain or near the carboxy-terminal end of the protein, like the Q334* mutation tend to aggregate at the plasmamembrane of the photoreceptor cell body, as was shown in a mutant mouse model with this mutation (Sung et al., 1994), as well as in transgenic zebrafish carrying the exact same mutation (Raghupathy et al., 2013). Likewise, knock-in mice expressing rhodopsin with a *349Q mutation demonstrate a severe and early-onset retinal degeneration with mislocalization and improper disc formation (Hollingsworth and Gross, 2013).

The majority of *RHO* mutations however, including the most recurrent mutation P23H, are predicted to undergo protein misfolding, thereby accumulating in the endoplasmic reticulum and inducing apoptotic cell death. Studies in transgenic mice, rats, dogs and, more recently, pigs with this mutation indeed supported this pathophysiological mechanism (Kijas et al., 2002; Olsson et al., 1992; Roof et al., 1994; Ross et al., 2012), again illustrating that different mutations in the same gene can exert different pathophysiological mechanisms, in humans as well as in different animal models.

4.2.1.3. Isoform-specific expression and differential pre-mRNA splicing

As described in section 4.2.1, the majority of protein-coding genes encode several protein isoforms that are the result of alternative splicing, a process that determines the inclusion or exclusion of specific exons in the mature transcript. For several genes that are associated with IRD, retina-specific isoforms have been described that often contain exons exclusively present in these isoforms, e.g. *CERKL*, *RPGR*, and *BBS3* (Garanto et al., 2011; Kirschner et al., 1999; Pretorius et al., 2010). The use of alternative promoters driving the expression of one or more of these isoforms complicates matters even further. For genes with such a complex transcriptional profile, generating a mutant animal model that mimics the human phenotype can be a challenging task. For instance, attempts to knock-out *Cerkl* in mice revealed only very mild phenotypic abnormalities, and further studies revealed the use of several promoters driving the expression of a multitude of *Cerkl* transcripts, in mice as well as in humans (Garanto et al., 2011; Garanto et al., 2012).

Besides naturally occurring alternative splicing, many mutations have been described that somehow affect the recognition of splice sites by the spliceosome, and thereby alter the composition of the transcript and final protein product. One example of such a mutation is a recurrent change in *CEP290*, a deep-intronic mutation c.2991+1655A>G that activates a cryptic splice donor site in intron 26, and results in the inclusion of a pseudo-exon to ~50% of all *CEP290* transcripts these LCA patients (den Hollander et al., 2006). Attempts to mimic this recurrent mutation and the associated phenotype in a humanized knock-in mouse model failed, apparently because the mouse splicing machinery did not effectively recognize the pseudo-exon present in LCA patients with this mutation (Garanto et al., 2013). Further studies recently showed that the recognition of such cryptic splice sites can vary heavily in different species (Garanto et al., 2015).

Another intriguing relationship between splicing and IRD exists through the *PRPF*-associated retinal dystrophies. Proteins encoded by *PRPF* genes are an essential component of the spliceosome in all cells of the human body, yet mutations in several of these genes cause a phenotype that appears to be restricted to the retina (Chakarova et al., 2002; Chen et al., 2014; McKie et al., 2001; Tanackovic et al., 2011; Vithana et al., 2001). Hypotheses to explain this phenomenon include dual, retina-specific functions for these proteins, a higher demand of splicing in retinal cells, or specific mis-splicing

of some key components within the retina. Many studies involving animal models have attempted to uncover the molecular mechanisms involved in the retinal-restricted phenotype caused by mutations in these *PRPF* genes (Bujakowska et al., 2009; Chakarova et al., 2002; Graziotto et al., 2011; Graziotto et al., 2008; McKie et al., 2001; Vithana et al., 2001), yet these studies were severely hampered by either early lethality or severe phenotypes not restricted to the eye. A more recent study demonstrated the RPE to be the primary retinal cell type affected by these mutations, thereby revealing new insights into the pathophysiology of splice factor-associated IRD (Farkas et al., 2014).

4.2.1.4. Genetic redundancy

Genetic redundancy is occurring when the protein products of two different genes have an identical or at least overlapping function in the same biological process. In such cases, defects in one of the two genes could have a less detrimental effect on the phenotypic outcome of the organism than what could be expected based on the physiological function of the encoded proteins. Redundant genes are found in almost all signaling, developmental, or metabolic contexts (Kafri et al., 2009). The fact that these genes are believed to originate from a single ancestral gene, explains why there might be overlapping functions remaining (Kafri et al., 2009).

Due to an ancient genome duplication event, the zebrafish genome is largely duplicated, giving rise to many genes with two copies (Meyer and Schartl, 1999). Some of these duplicated genes have acquired split functions. One example is *protocadherin-15* (*PCDH15*), a gene that in zebrafish has two orthologues (*pcdh15a* and *pcdh15b*). Zebrafish lacking *Pcdh15a* (*orbiter*) reveal no defects in optokinetic responses, whereas the absence of *Pcdh15b* results in reduced optokinetic and ERG responses (Seiler et al., 2005). It might therefore be expected that genes for which one of the copies has been lost following the genome duplication, or duplicated genes with a clear split function, are less tolerant to mutations and would therefore be overrepresented in the non-targeted screens that most of the mutant zebrafish models originate from (**Supplemental Table 2**). Yet, only four out of the seven zebrafish IRD models carry mutations in genes that are not duplicated when compared to the human genome. However, as exemplified above, some of the genes that are assigned as being duplicated indeed might actually have acquired a split function or are at least not fully redundant in the zebrafish retina anymore, such as *gc1/gc3* or *Cacna1fa/b*, as described below.

One example of two functionally redundant genes in humans that have arisen after a gene duplication event in humans are *GUCA1A* (expression in cones and only weakly in rods) and *GUCA1B* (expression in both rods and cones) (Imanishi et al., 2002; Kachi et al., 1999; Surguchov et al., 1997). These two genes, that share more than 90% sequence similarity, are sequentially located tail-to-tail at human chromosome 6 and encode the calcium-sensing part of guanylate cyclase enzyme (GC) that is involved in the recovery

phase of the phototransduction cascade (Subbaraya et al., 1994; Surguchov et al., 1997). Mouse models with a disruption in only one of the two *Guca* genes do not show any abnormal histological retinas (**Supplemental Table 2: *Guca1a*^{tm1Itl} and *Guca1b*^{tm1Amd}**), although single *Guca* knock-out rods became more sensitive to flashes and to steps of illumination as a result of reduced calcium sensitivity (Makino et al., 2008; Mendez et al., 2001). However, the combined loss of both genes does result in a clear and severe photoreceptor degeneration (Mendez et al., 2001) which is indicative for Gcap1 and Gcap2 (encoded by *Guca1a* and *-1b*, respectively) being functionally redundant. This was further strengthened by the complete rescue of the *Guca1a/Guca1b* double knockout phenotype with a healthy copy of only the *Guca1a* gene (Howes et al., 2002; Pennesi et al., 2003). Intriguingly however, expression of only *Guca1b* was not enough to completely restore the phenotype (Mendez et al., 2001). In humans, *GUCA1A* mutations result in cone-dystrophy, with *GUCA1B* apparently not being fully redundant in these cones (Payne et al., 1998). Mutations in *GUCA1B* in contrast have been reported to lead to autosomal dominant retinitis pigmentosa (Sato et al., 2005), although the exact involvement of these mutations in retinal disease remains controversial (Kitiratschky et al., 2011). One other difference between mice and human cone photoreceptor cells that could influence the phenotypic outcome, is the presence of a third calcium sensing domain (GCAP3) in human, but not in mouse, cone photoreceptors (Imanishi et al., 2002). A similar mechanism for reduced guanylate cyclase activity is also seen in the rd chickens that carry a spontaneous mutation in the *GC1* gene (Semple-Rowland et al., 1998). Mechanistically, this phenotype can be explained by the same mechanism as seen with mutations in *GUCA1A*. Already before any pathological disruption can be observed, the retinal cGMP levels are below normal (Semple-Rowland et al., 1998). Altogether, these data suggest that there is some redundancy between GCAP1 and GCAP2 (and perhaps also GCAP3 in humans), but GCAP1 seems to be the main actor which cannot be fully replaced by GCAP2 (or GCAP3).

Following rhodopsin activation and the conformational change of 11-cis-retinal to all-trans-retinal, this all-trans-retinal can be re-converted into 11-cis-retinol via the visual cycle. The rate-limiting step in this cycle is the enzymatic conversion of all-trans-retinal into all-trans-retinol. This process is performed by retinal dehydrogenases: RDH8, RDH12 and retSDR1 (retinal short-chain dehydrogenase reductase 1) in photoreceptor outer segments, and RDH10 in the RPE (Maeda et al., 2007). Oxidation of 11-cis-retinol in the RPE is catalyzed by 11-cis-RDHs (RDH5 and RDH11) to yield 11-cis-retinal. Since the two enzymes RDH8 + RDH12 and RDH5 + RDH11 in fact catalyze the same reaction, one might expect that a functional loss in one of these enzymes due to mutations can be compensated for by the other unaffected gene. Indeed, knocking out either *Rdh5* (Driessen et al., 2000; Shang et al., 2002) or *Rdh11* (Kim et al., 2005), and *Rdh8* or *Rdh12* (Maeda et al., 2007) in mice for example only results in a delayed dark adaptation

after high bleaching levels. In contrast, the double (Rdh5&Rdh11 or Rdh8&Rdh12) or triple (Rdh5, Rdh8 & Rdh12) knock-out mice do indeed suffer from rod-cone dystrophy, indicating that the different RDHs are functionally redundant in the mouse retina (Kim et al., 2005; Maeda et al., 2007). In humans however, mutations in either *RDH5* (fundus albipunctatus) Yamamoto et al., 1999), *RDH11* (Retinal Dystrophy, Juvenile Cataracts and Short Stature Syndrome (RDJCSS), or *RDH12* (LCA) do already result in apparent phenotypes (Janecke et al., 2004; Perrault et al., 2004; Xie et al., 2014; Yamamoto et al., 1999).

4.2.2. Retinal function- & structure-related discrepancies

As described in 2.2, differences in retinal architecture and the presence or absence of anatomical structures in retinal cells are apparent in the selected species. It is therefore not surprising that animal models with a differential distribution of rod vs. cone cells, mainly due to a difference in nocturnal versus diurnal activity, as well as models for IRDs in which the human pathology resides in anatomical structures that are underdeveloped or even absent, will not entirely mimic the human clinical phenotype. In the next paragraphs, some examples will be outlined in which a different clinical outcome in mutant animal models as compared to the human situation can be explained by retinal structure-related differences.

4.2.2.1. Calyceal processes in rodent Usher models

Calyceal processes are axially oriented microvillus-like structures that emerge from the inner segment and form a collar around the base of both rod and cone outer segments. Scanning electron-microscopy analyses revealed that these F-actin-rich structures are conserved in at least NHP, pigs and zebrafish, (Allwardt and Dowling, 2001; Cohen, 1963), but absent in mice and rats. Recently all five known proteins involved in Usher syndrome type 1 (myosin7a, harmonin (=Ush1c), cadherin-23 (=Cdh23), protocadherin-15 (=Pcdh15) and Sans (=Ush1g) were shown to co-localize to the junction between the inner and outer segment of retinal photoreceptors in human and macaque but not in mouse. Closer examination by electron microscopy revealed that these proteins localize to the photoreceptor calyceal processes (Sahly et al., 2012). The differential distribution in photoreceptors of humans and rodents strongly supports evidence that the difference in phenotypic outcome of mutations in these genes are explained by the presence/absence of these calyceal processes. Although their exact function remains elusive, they have been proposed to serve a structural role by providing the outer segment strength and rigidity (Sahly et al., 2012). Another attractive hypothesis, that was raised based on the presence of the fastest known neuronal Ca^{2+} pump (PMCA2), is that the calyceal processes might be mechanosensitive, similar to the inner ear hair cells and therefore fulfill a role in signaling (Caride et al., 2001).

The membrane of the periciliary region, a collar-like extension of the apical inner segment that surrounds the connecting cilium, is also thought to function in the organization of the transport of post-Golgi-derived vesicles which are indicated to dock at the membrane of the periciliary membrane (Maerker et al., 2008). All known Usher syndrome type 1 and type 2 proteins are located in this (peri)ciliary region (Goodyear and Richardson, 1999; Maerker et al., 2008; McGee et al., 2006; Sahly et al., 2012), which is also underdeveloped in rodents as compared to humans (Petit, 2001). Fibrous links connect the membrane of the periciliary region to the membrane of the connecting cilium. Gpr98 (Ush2c) was found to be essential for the formation of these links because they were absent in *Gpr98*-deficient (*Vlgr1/del7TM*) mice (Maerker et al., 2008). Since also usherin (*Ush2a*) and whirlin (*Ush2d*) are present in this periciliary region the fibrous links are thought to be the analogs of the ankle links in the hair bundle of cochlear hair cells. The fibrous links may be formed by homo- and/or heteromeric binding of the extracellular domains of *Ush2a* and *Gpr98* which are intracellularly tethered by whirlin. SANS and whirlin directly interact and SANS thereby may provide the molecular link to the microtubule transport machinery (Maerker et al., 2008; van Wijk et al., 2006). The fibrous links may function as structural support of the periciliary region and the connecting cilium (Maerker et al., 2008) and analogous to the function of the links in the hair bundle, they could play a role in development of this region of the photoreceptor. However there are no, or in case of *Ush2a*^{-/-} and *whirlin*^{-/-} mouse mutants only with very mild (Liu et al., 2007; Yang et al., 2010), retinal aberrations due to ablation of the Usher genes. In addition to their structural role, it was postulated that these proteins play a role in defining the membranous regions and thereby contribute to the control of vesicle docking and cargo transfer from the inner segment transport system to that of the cilium (Maerker et al., 2008) or play a role in outer segment disk formation and renewal (Sahly et al., 2012). Since whirlin associates with the calcium channel subunit Cav1.3 it is likely to have a role either in the transport to or the organization of the voltage-gated calcium channels at the plasma membrane and thus contributes to the control of vesicle docking and/or fusion via regulation of local Ca²⁺ concentrations (Kersten et al., 2010).

4.2.2.2. Differential distribution of cone and rod photoreceptor cells

Cones and rods serve different functions in the retina and are differentially distributed amongst species. As described in this review, the human retina contains a cone-rich area (fovea centralis) whereas in zebrafish the retina is built up almost exclusively by cones that are distributed throughout their entire retina. Moreover, rod development is not matured until 20 days post fertilization (dpf) which therefore gives rise to a retina overrepresented by cones at 5 dpf when functional measurements in forward genetic screens are often conducted (Branchek and Bremiller, 1984). However, the overall anat-

omy of the retina is similar in both species. This would make rod-specific degeneration less pronounced in the zebrafish retina as compared to other species such as humans. A cone and rod difference is for example seen in the zebrafish *cacna1fa* mutant. In both humans and mice, the *CACNA1F* gene is expressed in both rods and cones, whereas zebrafish contains two *cacna1f* orthologues that are differentially expressed: *cacna1fa* (cone-specific) and *cacna1fb* (rod-specific). This is most probably also the reason that, in contrast to the *cacna1fa* zebrafish mutant, *Cacna1f* knock-out mice mimic the human ERG measurements and congenital stationary night blindness (Chang et al., 2006; Jia et al., 2014). On the other hand, when comparing animal models for genes specifically expressed in cones (*PDE6C* or *GNAT2*), a similar phenotype is observed in case of any mutation. Humans, dogs, mouse and zebrafish all show cone-specific degeneration and therefore suffer from achromatopsia (**Supplemental Table 2**).

A more subtle difference between cone and rod photoreceptor cells amongst species is observed with mutations in the PDE6 complex. In the rod photoreceptor cells, PDE6 forms a heterotetrameric complex of PDE6 α , PDE6 β and two PDE6 γ subunits to make an active cGMP phosphodiesterase capable of cGMP hydrolysis.

Both mice and dogs have a relatively rod dominated retina, which is the result of their high nocturnal activity as compared to the more cone-rich human retina. As a result, one could expect that rod-specific null alleles have a great impact on vision in mice and dogs as compared to humans. Indeed, it can be observed that mutations in the mouse and dog *Pde6b* gene lead to rapid rod photoreceptor degeneration and eventually to complete retinal degeneration and loss of visual function (Hart et al., 2005; Suber et al., 1993). Also, in humans with *PDE6B* mutations, the initial symptoms include night blindness as a result of rod-specific dysfunction and eventually show a more advanced retinal degradation probably induced by the proposed bystander effect (Ripps, 2002), but with a progression rate that is significantly slower than in mice and dogs (Hart et al., 2005). However, phenotypic variability in terms of disease progression often occurs even within the same species. For instance, the rd1 mouse carrying nonsense mutation displays a rapid photoreceptor degeneration at postnatal day 8, and absence of nearly all rods by week 3 (Pittler and Baehr, 1991). In comparison, rd10 mice with a *Pde6b* missense mutation (p.R560C) show a relatively slower disease progression, starting at postnatal day 16 and complete absence of photoreceptor cells within 2 months (Chang et al., 2007). A *PDE6B* nonsense mutation in *rcd1* Irish setter dogs leads to a rapid disease progression, which starts one month after birth and continues until 3 months (Suber et al., 1993). In contrast, *crd1* American Staffordshire terrier dogs carrying an *in-frame* deletion have a milder phenotype and later onset compare to *rcd1* dogs. Histological examination of the retina at 11 weeks shows that photoreceptors and the ONL in homzygous *crd1* dogs are more preserved compared to those in *crd1/rcd1* or *rcd1/rcd1* dogs (Goldstein et al., 2013). Similar results were seen in *Pde6a* mutant mouse

and dog models, encoding the other PDE6 rod-specific subunit (Petersen-Jones et al., 1999; Sakamoto et al., 2009). These studies highlight the importance of considering genetic background, and the type of mutation when selecting suitable animal models that mimic the human phenotype.

5. MUTANT ANIMAL MODELS FOR THERAPEUTIC STUDIES ON IRD

As outlined above and shown in **Supplemental Table 2**, the vast majority of vertebrate animal models for IRD research at least to a significant part mimics the phenotype present in humans. Most models can be found in the mouse, since this species has several practical advances in terms of generating, maintaining and analysing the underlying pathologic mechanisms. Consequently, over the last years a growing number of pharmacologic and gene therapeutic studies have been performed in these mouse models, demonstrating the conceptual possibility to treat the mimicked human retinal disorders (Boye et al., 2013; Stieger et al., 2010). Most often, viral vectors were employed as vehicles for the transfer of genes, with AAV- and lentivirus-based vectors being the most regularly used ones (Trapani et al., 2014). Zebrafish models have also been used to study pharmacological interventions, such as translational read-through approaches, but have so far not been used for gene therapeutic applications (Moosajee et al., 2008). Gene therapeutic approaches were described in one chicken model carrying mutations in *GUCY2D* (Williams et al., 2006).

However, when translating these results to humans, several key features cannot be sufficiently modelled in small animal models and, therefore, large animal models become more and more important (Komaromy, 2010; Kostic et al., 2013; Petersen-Jones, 2013). Successful proof-of-principle therapeutic studies have been published in several canine models of IRD (Acland et al., 2001; Beltran et al., 2012; Komaromy, 2010; Le Meur et al., 2007; Lheriteau et al., 2014; Narfstrom et al., 2003; Petit et al., 2012). But even in large animal models, certain features cannot be comprehensively analysed due to interspecies-related differences. These features include the limited similarity of the retinal anatomy among the different species and humans (primates), as well as major differences concerning efficacy and cellular tropism of viral vectors between species. The published use of animal models for different types of experimental therapeutic approaches is summarized in **Table 4**. In the following paragraphs, the different vertebrate animal models will be discussed with regard to the current hot topics in retinal gene therapy research, i.e. viral vector tropism and gene transfer approaches with regard to the varying retinal anatomy.

Table 4. Overview on therapeutic and vector-related studies on IRD in the various animals

Model	Treatment approach / Vectorology				
	Pharmacologic [§]	Optokinetics	Cell therapy	Gene therapy [§]	Vectorology*
Zebrafish	X				
Chicken				X	
Sheep					
Pig					X
Cat					X
Dog	X			X	X
Rat			X	X	X
Mouse	X	X	X	X	X
NHP					X

[§]: includes translational read through drugs, retinoids, neuroprotection.

[§]: includes gene addition, gene silencing, gene editing.

*: includes studies on cellular tropism, vector distribution, and host immune responses to AAV-, lentivirus-, adenovirus- and nanoparticle-mediated gene transfer.

5.1 Vector tropism in different species

For specific as well as non-specific gene therapeutic approaches, subretinal viral vector-mediated gene transfer is still considered to be the most efficient way to enable transgene expression in retinal cells. While AAV-based vectors are considered the gold standard due to their varying cellular tropism depending on the serotype, its limited packaging capacity represents a major roadblock for the development of therapeutic strategies for IRDs in which the disease-causing mutations are often located in genes that have open reading frames larger than 4kb. For those genes, lentivirus-based vectors have been generated and successfully tested in mouse models for several IRDs, such as Usher syndrome type 1B or Stargardt disease (Binley et al., 2012; Zallocchi et al., 2014). In order to evaluate safety aspects, the authors also included data on non-human primates (NHP) in these papers. Since an efficient uptake of most vectors is dependent on receptor-mediated endocytosis, the tropism of a vector is usually defined by the presence or absence of cell surface receptors. For AAV, a large number of different receptors have been defined that interact with the different serotypes (Akache et al., 2006; Di Pasquale et al., 2003; Kaludov et al., 2001; Summerford and Samulski, 1998; Walters et al., 2001). Knowledge about these capsid-surface interactions led to the development of tyrosine-mutated capsid variants with better transduction efficiencies (Petr-Silva et al., 2009). Nonetheless, the efficacy of serotypes to transduce a given cell type varies among species, which makes it crucial to test all serotypes in the species in which a treatment strategy is to be explored. For example, the expression profiles of the serotypes currently considered to be most efficient for photoreceptors in mice, AAV2/5,

2/8, and 2/9 (either tyrosine-mutated or not), differ among several large animal model species such as cat, dog and pig (Manfredi et al., 2013; Minella et al., 2014; Mowat et al., 2014; Stieger et al., 2008).

Thanks to the experiences gained with different viral vectors in the aforementioned species, a set of AAV vector tools is now present for targeting photoreceptor cells and RPE, and researchers are able to choose among more than a dozen different serotypes and isolates. With the increasing focus of translating preclinical proof-of-concept studies to the clinic, it becomes more and more an issue to identify the most optimal AAV serotype for expression of transgenes in primate photoreceptors. Following several studies with sometimes contradictory results, it seems that AAV serotype 9 may be the most efficient vector to target photoreceptors (both rods and cones) and RPE cells following subretinal injection (Vandenberghe et al., 2013). Targeting exclusively RPE cells was shown to be possible using AAV serotype 4 in all species tested so far (Weber, 2003). There is at present no vector known to exclusively target photoreceptor cells following subretinal injection.

Lentivirus-based vectors are usually pseudotyped with the vesicular stomatitis virus glycoprotein (VSVG), which has been shown to target predominantly RPE cells, but also allows photoreceptor transduction in mice and rats (Calame et al., 2011; Duisit et al., 2002). Other pseudotyping approaches, such as hemagglutinin (HA) or venezuelean equine encephalitis virus (VEEG), did so far not show an advantage, regardless of the species tested (Duisit et al., 2002; Lipinski et al., 2014).

Since subretinal injections only allow to target a locally defined area of the retinal surface, the treatment of the entire retina by this transfer approach is not possible. A second way of introducing vectors to the retina represents the intravitreal approach, through which at least theoretically the entire retina can be brought into contact with the vector. Unfortunately, none of the standard AAV serotypes or lentivirus-based vectors is capable of transducing a significant number of photoreceptor or RPE cells via this approach. The AAV serotype 2 showed significant transduction of retinal ganglion cells, which does not help for specific gene therapy of photoreceptor or RPE cells (Dudus et al., 1999). The reason is seen in the ILM barrier, which hampers an efficient invasion of the retina by most AAV serotypes (Dalkara et al., 2009). Recently however, *in vivo* directed evolution of AAV capsids allowed the generation of AAV vectors with the capacity to target most retinal cell types panretinally in mice and at certain spots in NHP following intravitreal injection (Dalkara et al., 2013). At least in mice, transgene expression in photoreceptor cells was sufficiently high to change the phenotype of several IRD models (*rs1h*^{-/-} and *rd12*). However, since there is no IRD model in NHP, it is unknown how the efficacy of intravitreal injection concerning photoreceptor transduction would be in degenerative retinæ of humans. A different approach, using again capsid-modified variants where tyrosine or phenylalanine residues were mutated, likewise yielded AAV

capsid mutants able to transduce photoreceptors following intravitreal injection in mice (Kay et al., 2013).

Although a panretinal transduction of retinal cells is likely only possible following intravitreal injection, this transfer approach may be blocked by the immune system, which is more effective in responding to foreign proteins in the vitreous compared to the subretinal space. Especially in NHPs, where the immune system is similar to the human one, immune reactions against capsid proteins following intravitreal injection were recently observed (Kotterman et al., 2014).

5.2 The impact of anatomical differences on gene transfer

As discussed in sections 1 and 2, primates possess a foveal depression that exclusively contains cones with long dendrites (Henle fibers) and the inner retinal layers, and have a comparably large eye and a small lens, which results in a high axial length ratio between eye globe and lens (**Table 1**). These anatomical differences hinder the advancement of preclinical studies and are currently at the height of translational research.

Since there is no foveal depression in any of the animal models for IRD, the subretinal injection cannot be studied preclinically in diseased retinæ and therefore always poses an unknown risk factor. While foveal subretinal injections in healthy primates do not result in significant destruction, the data from clinical trials on *RPE65* gene augmentation therapy indicate that a foveal treatment may not be beneficial (Jacobson et al., 2012). In contrast, another study related to treatment of patients with choroideremia observed no unwanted side effects in treated patients (MacLaren et al., 2014).

While a panretinal transduction is possible in mice following intravitreal injection of AAV serotype 2 or the newly generated capsids, the situation in NHP is more complex. Here, a relatively strong transduction of the macular ring of ganglion cells surrounding the fovea can be observed, which may be due to a different molecular composition of the ILM in this zone compared to more peripheral parts of the retina (Yin et al., 2011). Alternatively, the tyrosine-mutated AAV serotype 9 vector was shown to transduce the central nervous system following systemic administration in mice, and combined with a rhodopsin promoter, transgene expression was limited to retinal photoreceptor cells (Dalkara et al., 2012). It remains to be seen, whether this observation is similar in large animal models.

6. CONCLUDING REMARKS

In this review, we have attempted to provide a comprehensive overview on the use of animal models in functional and therapeutic research on IRD, and discuss the lessons learned so far by comparing the genetic architecture, and the gross and fine

structural and functional characteristics of the retina in different species. Obviously, the human retina has clear anatomical differences with most animal models considered so far. However, the anatomy is not the only major feature important for deciding which model species would be the ideal one for a given question. The possibilities to generate transgenic or genetically modified animals may sometimes outweigh the differences in ocular and retinal anatomy. Or, the absence of a phenotype in a certain species may prevent this model from being used for therapeutic research. While the pros and cons of each animal model are summarized in **Fig. 4**, the following section attempts to address a number of questions that need to be answered when deciding for the optimal model species for a given research question.









Pros							
<ul style="list-style-type: none"> - Genetic modification - Housing - Lots of offspring - Generation time - Animal laws (55 dpi) - Ex utero development 	<ul style="list-style-type: none"> - Generation time - Lots of offspring - Egg incubation into any desired stage - Ex utero development 	<ul style="list-style-type: none"> - Human eye size - Area centralis - Genetic modification 	<ul style="list-style-type: none"> - Human eye size - Cone-dominant retina - Genetic modification 	<ul style="list-style-type: none"> - Human eye size - Area centralis 	<ul style="list-style-type: none"> - Many naturally occurring models - Human eye size - Area centralis - Mutations similar to humans 	<ul style="list-style-type: none"> - Many naturally occurring models - Genetic modification - Lots of offspring - Generation time 	<ul style="list-style-type: none"> - Human eye size - Anatomically similar to humans
							
Zebrafish	Chick	Sheep	Pig	Cat	Dog	Rat/Mouse	Macaque
<ul style="list-style-type: none"> - Evolutionary distinct from human - Largely duplicated genome - Retinal regeneration capacity - Ectothermic 	<ul style="list-style-type: none"> - Evolutionary distinct from human - Photoreceptor anatomy (oil droplets) - Poorly annotated genome 	<ul style="list-style-type: none"> - Housing - Regeneration time - Tapetal structure complicates imaging - Moderately annotated genome 	<ul style="list-style-type: none"> - Housing - Regeneration time - Poorly annotated genome 	<ul style="list-style-type: none"> - Housing - Regeneration time - Tapetal structure complicates imaging - Moderately annotated genome 	<ul style="list-style-type: none"> - Housing - Regeneration time - Tapetal structure complicates imaging - Moderately annotated genome 	<ul style="list-style-type: none"> - Nocturnal - Photoreceptor anatomy (calyceal processes) 	<ul style="list-style-type: none"> - No IRD model existing - Moderately annotated genome - Ethical restrictions
Cons							

Figure 4. Summary of pros and cons of nine species for research on IRD. Per species, the most prominent pros and cons are listed. These include general characteristics, as well as retina- or IRD-specific features.

When studying the phenotype of IRDs, the eye size or the ratio between lens and visual axis may not impact the outcome as much as it would be the case when studying therapeutic approaches. However, since most animal models for IRDs will be used at some point for therapeutic applications, this question needs to be answered in the beginning. Generally, from the mouse onwards, techniques have been developed to reliably perform gene transfer to retinal cells. This may not be the case for the zebrafish, and was only once performed in chicken.

Apart from their different gross anatomy of the eye, zebrafish and chicken possess a higher number of cone photoreceptors, have double cones and oil droplets (chicken) which may interfere with the interpretation of data in cone-related disorders. On the other hand, all mammalian models except NHP only have two cone types and thus less than humans, which again may complicate analysis of cone-related disorders. In

addition, only the large animal models cat, dog, sheep, and pig possess an area centralis corresponding at least in part to the cone-only foveal region in humans. Studying cone-rod or pure cone dystrophies will always be biased in the remaining model species, since a cone-enriched region does not exist and the interaction between rods and cones may complicate analysis of data.

Several animal models possess a tapetal structure behind the retina that increases photon capture by the photoreceptors through the reflection of light. This may increase photopic stress to the diseased retina and results in localized differences of neuronal cell death among the different photoreceptor cell types, which was at least suggested by a recent study in a dog model of *RPE65* insufficiency (Klein et al., 2014). In addition, the presence of this reflecting structure renders OCT imaging, which is more and more accepted as a tool for *in vivo* thickness measurements, problematic (McLellan and Rasmussen, 2012).

A major drawback for IRD research in large animal models is the slow reproduction rate and the high costs of housing of these animals. While it takes only few weeks to generate hundreds of zebrafish or chicken, and few months to have double-digit numbers of mice and rats, it takes between 6 months and a year to generate a small number of offspring in cats, dogs, sheep or pigs. Hence, research on the phenotype of IRDs, let alone therapeutic research in these large animal species is cost-intensive and requires a significant time investment. However, the human size of their eye, the similarity of their immune system to the human one, and the possibility to work with vector titers close to what will be injected in human patients warrants the use of large animals for therapeutic research.

Special features related to the photoreceptor structure such as calyceal processes can be found in species that are considered to be closely related to humans (pig) but also in evolutionary distant species like zebrafish. Since this structure has recently gained attention in the scientific community due to the localization of certain Usher syndrome proteins, it became clear that when working on these disorders, choosing the right models species is crucial. Mice do not possess such calyceal processes and a lack of phenotype development in mouse models of the disease became understandable.

As discussed in section 2.3, and shown in **Fig. 3**, certain genes are either duplicated or not present at all in the genome of some species, and therefore cannot be studied in these species. For instance, *EYS*, one of the most frequently mutated genes in patients with autosomal recessive RP (Abd El-Aziz et al., 2008; Collin et al., 2008) is not present in the rodent genome, and has prevented a better understanding on the mechanisms underlying *EYS*-associated IRD. A detailed knowledge on the absent and duplicated genes in the selected vertebrate species as provided here (**Fig. 3** and **Supplemental Table 1**) may potentially avoid the generation of animal models without a phenotype, and instead guide scientists to using alternative model species.

Because vertebrate animal models all have limitations in their use to study IRDs, the search for alternatives to model ocular disorders is a very active one. With the development of a technique to induce pluripotency in somatic cells (i.e. to generate induced pluripotent stem cell (ipSC) out of adult somatic cells) and differentiate these into any given cell type, and thus to have the principal capacity to generate photoreceptor or RPE cells from patients suffering from IRDs has gained much attention in recent years (Wiley et al., 2015). These cells contain the exact same mutation present in the human patients and therefore, the specific consequences can be studied in the affected cell type. Furthermore, gene editing technology allows to correct the mutation and to observe the consequences this treatment has on the intracellular pathways. Over all, the use of ipSCs to study pathomechanisms of IRD represents an important alternative to *in vivo* animal studies, but limitations are also eminent. While the advantage of this technique is obvious, the organ-specific influences and the interaction with other cells, the consequences of altered cell function on the surrounding cells and the immune system cannot be extensively studied using this approach, and it will therefore not be able to fully replace animal experimentation.

With the increasing knowledge about the genetic causes of retinal blinding disorders in men, the use of vertebrate animal models becomes more and more important, not only for studying the pathophysiological mechanisms but also to develop therapeutic strategies. While a number of different species have been used for modeling IRDs, it became clear that not every species can be used for a given genetic defect. The present review aimed at generating a comprehensive overview on the currently used animal models and to identify pros and cons for each species. Only when the ideal animal model system for a given question is chosen, optimal output can be generated from *in vivo* experiments, which will serve both human health and will prevent unnecessary research on animals, an ethically important goal to achieve.

ACKNOWLEDGMENTS

We gratefully acknowledge Pavel Cizek, Armen Karapeteyan and Rozan Vrooman for their contributions to this manuscript, and drs. Frans Cremers and Birgit Lorenz for critical reading of the manuscript. This work was supported by the Directorate General for Higher Education in Indonesia (DIKTI) of the Ministry for National Education of Indonesia (to G.D.N.A), by the Foundation Fighting Blindness USA (grants C-CMM-0811-0547-RAD03 to E.v.W., and TAGT-0912-0582-RAD to R.W.J.C), by The Netherlands Organisation for Scientific Research (grant Veni-016.136.091 to E.v.W.), and by the Netherlands Organisation for Health Research and Development (ZonMW E-rare grant 40-42900-98-1006 (EUR-USH) to E.v.W.).

REFERENCES

- Abd El-Aziz, M.M., Barragan, I., O'Driscoll, C.A., Goodstadt, L., Prigmore, E., Borrego, S., Mena, M., Pieras, J.I., El-Ashry, M.F., Safieh, L.A., Shah, A., Cheetham, M.E., Carter, N.P., Chakarova, C., Ponting, C.P., Bhattacharya, S.S., Antinolo, G., 2008. EYS, encoding an ortholog of *Drosophila* spacemaker, is mutated in autosomal recessive retinitis pigmentosa. *Nat Genet* 40, 1285-1287.
- Acland, G.M., Aguirre, G.D., Ray, J., Zhang, Q., Aleman, T.S., Cideciyan, A.V., Pearce-Kelling, S.E., Anand, V., Zeng, Y., Maguire, A.M., Jacobson, S.G., Hauswirth, W.W., Bennett, J., 2001. Gene therapy restores vision in a canine model of childhood blindness. *Nat Genet* 28, 92-95.
- Ahonen, S.J., Arumilli, M., Lohi, H., 2013. A CNGB1 frameshift mutation in Papillon and Phalene dogs with progressive retinal atrophy. *PLoS one* 8, e72122.
- Akache, B., Grimm, D., Pandey, K., Yant, S.R., Xu, H., Kay, M.A., 2006. The 37/67-kilodalton laminin receptor is a receptor for adeno-associated virus serotypes 8, 2, 3, and 9. *Journal of virology* 80, 9831-9836.
- Allwardt, B.A., Dowling, J.E., 2001. The pineal gland in wild-type and two zebrafish mutants with retinal defects. *Journal of neurocytology* 30, 493-501.
- Altschul, S.F., Gish, W., Miller, W., Myers, E.W., Lipman, D.J., 1990. Basic local alignment search tool. *Journal of molecular biology* 215, 403-410.
- Alvarez, Y., Cederlund, M.L., Cottell, D.C., Bill, B.R., Ekker, S.C., Torres-Vazquez, J., Weinstein, B.M., Hyde, D.R., Vihtelic, T.S., Kennedy, B.N., 2007. Genetic determinants of hyaloid and retinal vasculature in zebrafish. *BMC developmental biology* 7, 114.
- Anderson, D.H., Fisher, S.K., Steinberg, R.H., 1978. Mammalian cones: disc shedding, phagocytosis, and renewal. *Invest Ophthalmol Vis Sci* 17, 117-133.
- Auer, T.O., Duroure, K., De Cian, A., Concordet, J.P., Del Bene, F., 2014. Highly efficient CRISPR/Cas9-mediated knock-in in zebrafish by homology-independent DNA repair. *Genome research* 24, 142-153.
- Bailey, T.J., Davis, D.H., Vance, J.E., Hyde, D.R., 2012. Spectral-domain optical coherence tomography as a noninvasive method to assess damaged and regenerating adult zebrafish retinas. *Invest Ophthalmol Vis Sci* 53, 3126-3138.
- Bainbridge, J.W., Smith, A.J., Barker, S.S., Robbie, S., Henderson, R., Balaggan, K., Viswanathan, A., Holder, G.E., Stockman, A., Tyler, N., Petersen-Jones, S., Bhattacharya, S.S., Thrasher, A.J., Fitzke, F.W., Carter, B.J., Rubin, G.S., Moore, A.T., Ali, R.R., 2008. Effect of gene therapy on visual function in Leber's congenital amaurosis. *N Engl J Med* 358, 2231-2239.
- Barrangou, R., Fremaux, C., Deveau, H., Richards, M., Boyaval, P., Moineau, S., Romero, D.A., Horvath, P., 2007. CRISPR provides acquired resistance against viruses in prokaryotes. *Science* 315, 1709-1712.
- Bawa, G., Tkatchenko, T.V., Avrutsky, I., Tkatchenko, A.V., 2013. Variational analysis of the mouse and rat eye optical parameters. *Biomedical optics express* 4, 2585-2595.
- Beier, D.R., 2000. Sequence-based analysis of mutagenized mice. *Mammalian genome : official journal of the International Mammalian Genome Society* 11, 594-597.
- Beltran, W.A., Cideciyan, A.V., Guziewicz, K.E., Iwabe, S., Swider, M., Scott, E.M., Savina, S.V., Ruthel, G., Stefano, F., Zhang, L., Zorger, R., Sumaroka, A., Jacobson, S.G., Aguirre, G.D., 2014. Canine retina has a primate fovea-like bouquet of cone photoreceptors which is affected by inherited macular degenerations. *PLoS one* 9, e90390.

- Beltran, W.A., Cideciyan, A.V., Lewin, A.S., Iwabe, S., Khanna, H., Sumaroka, A., Chiodo, V.A., Fajardo, D.S., Roman, A.J., Deng, W.T., Swider, M., Aleman, T.S., Boye, S.L., Genini, S., Swaroop, A., Hauswirth, W.W., Jacobson, S.G., Aguirre, G.D., 2012. Gene therapy rescues photoreceptor blindness in dogs and paves the way for treating human X-linked retinitis pigmentosa. *Proceedings of the National Academy of Sciences of the United States of America* 109, 2132-2137.
- Bennett, J., Ashtari, M., Wellman, J., Marshall, K.A., Cyckowski, L.L., Chung, D.C., McCague, S., Pierce, E.A., Chen, Y., Bennicelli, J.L., Zhu, X., Ying, G.S., Sun, J., Wright, J.F., Auricchio, A., Simonelli, F., Shindler, K.S., Mingozzi, F., High, K.A., Maguire, A.M., 2012. AAV2 gene therapy readministration in three adults with congenital blindness. *Science translational medicine* 4, 120ra115.
- Binley, K., Widdowson, P.S., Kelleher, M., de Belin, J., Loader, J., Ferrige, G., Carlucci, M., Esapa, M., Chipchase, D., Angell-Manning, D., Ellis, S., Mitrophanous, K., Miskin, J., Bantseev, V., Nork, T.M., Miller, P., Naylor, S., 2012. Safety and biodistribution of an equine infectious anemia virus-based gene therapy, RetinoStat((R)), for age-related macular degeneration. *Hum Gene Ther* 23, 980-991.
- Bourne, M.C., Campbell, D.A., Tansley, K., 1938. Hereditary Degeneration of the Rat Retina. *The British journal of ophthalmology* 22, 613-623.
- Bowes, C., Li, T., Danciger, M., Baxter, L.C., Applebury, M.L., Farber, D.B., 1990. Retinal degeneration in the rd mouse is caused by a defect in the beta subunit of rod cGMP-phosphodiesterase. *Nature* 347, 677-680.
- Boye, S.E., Alexander, J.J., Boye, S.L., Witherspoon, C.D., Sandefer, K.J., Conlon, T.J., Erger, K., Sun, J., Ryals, R., Chiodo, V.A., Clark, M.E., Girkin, C.A., Hauswirth, W.W., Gamlin, P.D., 2012. The human rhodopsin kinase promoter in an AAV5 vector confers rod- and cone-specific expression in the primate retina. *Hum Gene Ther* 23, 1101-1115.
- Boye, S.E., Boye, S.L., Lewin, A.S., Hauswirth, W.W., 2013. A comprehensive review of retinal gene therapy. *Molecular therapy : the journal of the American Society of Gene Therapy* 21, 509-519.
- Branchek, T., Bremiller, R., 1984. The development of photoreceptors in the zebrafish, *Brachydanio rerio*. I. Structure. *The Journal of comparative neurology* 224, 107-115.
- Bueno, J.M., Giakoumaki, A., Gualda, E.J., Schaeffel, F., Artal, P., 2011. Analysis of the chicken retina with an adaptive optics multiphoton microscope. *Biomedical optics express* 2, 1637-1648.
- Bujakowska, K., Maubaret, C., Chakarova, C.F., Tanimoto, N., Beck, S.C., Fahl, E., Humphries, M.M., Kenna, P.F., Makarov, E., Makarova, O., Paquet-Durand, F., Ekstrom, P.A., van Veen, T., Leveillard, T., Humphries, P., Seeliger, M.W., Bhattacharya, S.S., 2009. Study of Gene-Targeted Mouse Models of Splicing Factor Gene Prpf31 Implicated in Human Autosomal Dominant Retinitis Pigmentosa (RP). *Invest Ophth Vis Sci* 50, 5927-5933.
- Calame, M., Cachafeiro, M., Philippe, S., Schouwey, K., Tekaya, M., Wanner, D., Sarkis, C., Kostic, C., Arsenijevic, Y., 2011. Retinal degeneration progression changes lentiviral vector cell targeting in the retina. *PLoS one* 6, e23782.
- Caride, A.J., Penheiter, A.R., Filoteo, A.G., Bajzer, Z., Enyedi, A., Penniston, J.T., 2001. The plasma membrane calcium pump displays memory of past calcium spikes. Differences between isoforms 2b and 4b. *The Journal of biological chemistry* 276, 39797-39804.

- Chakarova, C.F., Hims, M.M., Bolz, H., Abu-Safieh, L., Patel, R.J., Papaioannou, M.G., Inglehearn, C.F., Keen, T.J., Willis, C., Moore, A.T., Rosenberg, T., Webster, A.R., Bird, A.C., Gal, A., Hunt, D., Vithana, E.N., Bhattacharya, S.S., 2002. Mutations in HPRP3, a third member of pre-mRNA splicing factor genes, implicated in autosomal dominant retinitis pigmentosa. *Human molecular genetics* 11, 87-92.
- Chandler, M.J., Smith, P.J., Samuelson, D.A., MacKay, E.O., 1999. Photoreceptor density of the domestic pig retina. *Veterinary ophthalmology* 2, 179-184.
- Chang, B., Hawes, N.L., Pardue, M.T., German, A.M., Hurd, R.E., Davisson, M.T., Nusinowitz, S., Rengarajan, K., Boyd, A.P., Sidney, S.S., Phillips, M.J., Stewart, R.E., Chaudhury, R., Nickerson, J.M., Heckenlively, J.R., Boatright, J.H., 2007. Two mouse retinal degenerations caused by missense mutations in the beta-subunit of rod cGMP phosphodiesterase gene. *Vision research* 47, 624-633.
- Chang, B., Heckenlively, J.R., Bayley, P.R., Brecha, N.C., Davisson, M.T., Hawes, N.L., Hirano, A.A., Hurd, R.E., Ikeda, A., Johnson, B.A., McCall, M.A., Morgans, C.W., Nusinowitz, S., Peachey, N.S., Rice, D.S., Vessey, K.A., Gregg, R.G., 2006. The nob2 mouse, a null mutation in *Cacna1f*: anatomical and functional abnormalities in the outer retina and their consequences on ganglion cell visual responses. *Visual neuroscience* 23, 11-24.
- Chatzinoff, A., Millman, N., Oroshnik, W., Rosen, F., 1958. 11-Cis vitamin A in the prevention of retinal rod degeneration; an animal study. *American journal of ophthalmology* 46, 205-209; discussion 209-210.
- Chen, X., Liu, Y., Sheng, X., Tam, P.O., Zhao, K., Chen, X., Rong, W., Liu, Y., Liu, X., Pan, X., Chen, L.J., Zhao, Q., Vollrath, D., Pang, C.P., Zhao, C., 2014. PRPF4 mutations cause autosomal dominant retinitis pigmentosa. *Human molecular genetics* 23, 2926-2939.
- Chénais, B., 2013. Vectors for gene therapy: A place for DNA transposon. *Open Journal of Genetics* 3, 1-11.
- Chopovska, Y., Jaeger, M., Rambow, R., Lorenz, B., 2011. Comparison of central retinal thickness in healthy children and adults measured with the Heidelberg Spectralis OCT and the zeiss Stratus OCT 3. *Ophthalmologica. Journal international d'ophtalmologie. International journal of ophthalmology. Zeitschrift fur Augenheilkunde* 225, 27-36.
- Clements, P.J., Gregory, C.Y., Peterson-Jones, S.M., Sargan, D.R., Bhattacharya, S.S., 1993. Confirmation of the rod cGMP phosphodiesterase beta subunit (PDE beta) nonsense mutation in affected *rcd-1* Irish setters in the UK and development of a diagnostic test. *Current eye research* 12, 861-866.
- Cohen, A.I., 1963. Vertebrate retinal cell and their organisation. *Biological Reviews* 38, 427-459.
- Collery, R.F., Veth, K.N., Dubis, A.M., Carroll, J., Link, B.A., 2014. Rapid, accurate, and non-invasive measurement of zebrafish axial length and other eye dimensions using SD-OCT allows longitudinal analysis of myopia and emmetropization. *PloS one* 9, e110699.
- Collin, R.W.J., Littink, K.W., Klevering, B.J., van den Born, L.I., Koenekoop, R.K., Zonneveld, M.N., Blokland, E.A., Strom, T.M., Hoyng, C.B., den Hollander, A.I., Cremers, F.P.M., 2008. Identification of a 2 Mb human ortholog of *Drosophila* eyes shut/spacemaker that is mutated in patients with retinitis pigmentosa. *American journal of human genetics* 83, 594-603.
- Cremers, F.P., van de Pol, D.J., van Kerkhoff, L.P., Wieringa, B., Ropers, H.H., 1990. Cloning of a gene that is rearranged in patients with choroideraemia. *Nature* 347, 674-677.
- Cruce, M., Cruce, R., Tanasescu, D., 1996. The molecular mechanism of visual transduction. *Oftalmologia* 40, 201-209.

- Cunningham, F., Amode, M.R., Barrell, D., Beal, K., Billis, K., Brent, S., Carvalho-Silva, D., Clapham, P., Coates, G., Fitzgerald, S., Gil, L., Giron, C.G., Gordon, L., Hourlier, T., Hunt, S.E., Janacek, S.H., Johnson, N., Juettemann, T., Kahari, A.K., Keenan, S., Martin, F.J., Maurel, T., McLaren, W., Murphy, D.N., Nag, R., Overduin, B., Parker, A., Patricio, M., Perry, E., Pignatelli, M., Riat, H.S., Sheppard, D., Taylor, K., Thormann, A., Vullo, A., Wilder, S.P., Zadissa, A., Aken, B.L., Birney, E., Harrow, J., Kinsella, R., Muffato, M., Ruffier, M., Searle, S.M., Spudich, G., Trevanion, S.J., Yates, A., Zerbino, D.R., Flicek, P., 2015. Ensembl 2015. *Nucleic acids research* 43, D662-669.
- Curcio, C.A., Sloan, K.R., Kalina, R.E., Hendrickson, A.E., 1990. Human photoreceptor topography. *J Comp Neurol* 292, 497-523.
- D’Cruz, P.M., Yasumura, D., Weir, J., Matthes, M.T., Abderrahim, H., LaVail, M.M., Vollrath, D., 2000. Mutation of the receptor tyrosine kinase gene *Mertk* in the retinal dystrophic RCS rat. *Human molecular genetics* 9, 645-651.
- Dalkara, D., Byrne, L.C., Klimczak, R.R., Visel, M., Yin, L., Merigan, W.H., Flannery, J.G., Schaffer, D.V., 2013. In vivo-directed evolution of a new adeno-associated virus for therapeutic outer retinal gene delivery from the vitreous. *Science translational medicine* 5, 189ra176.
- Dalkara, D., Byrne, L.C., Lee, T., Hoffmann, N.V., Schaffer, D.V., Flannery, J.G., 2012. Enhanced gene delivery to the neonatal retina through systemic administration of tyrosine-mutated AAV9. *Gene therapy* 19, 176-181.
- Dalkara, D., Kolstad, K.D., Caporale, N., Visel, M., Klimczak, R.R., Schaffer, D.V., Flannery, J.G., 2009. Inner limiting membrane barriers to AAV-mediated retinal transduction from the vitreous. *Molecular therapy: the journal of the American Society of Gene Therapy* 17, 2096-2102.
- Davies, B., Davies, G., Preece, C., Puliyadi, R., Szumska, D., Bhattacharya, S., 2013. Site specific mutation of the *Zic2* locus by microinjection of TALEN mRNA in mouse CD1, C3H and C57BL/6J oocytes. *PloS one* 8, e60216.
- Dell’Orco, D., Koch, K.W., 2011. A dynamic scaffolding mechanism for rhodopsin and transducin interaction in vertebrate vision. *The Biochemical journal* 440, 263-271.
- den Hollander, A.I., Koenekoop, R.K., Yzer, S., Lopez, I., Arends, M.L., Voeseenek, K.E., Zonneveld, M.N., Strom, T.M., Meitinger, T., Brunner, H.G., Hoyng, C.B., van den Born, L.I., Rohrschneider, K., Cremers, F.P., 2006. Mutations in the CEP290 (NPHP6) gene are a frequent cause of Leber congenital amaurosis. *American journal of human genetics* 79, 556-561.
- Di Pasquale, G., Davidson, B.L., Stein, C.S., Martins, I., Scudiero, D., Monks, A., Chiorini, J.A., 2003. Identification of PDGFR as a receptor for AAV-5 transduction. *Nature medicine* 9, 1306-1312.
- Driessen, C.A., Winkens, H.J., Hoffmann, K., Kuhlmann, L.D., Janssen, B.P., Van Vugt, A.H., Van Hooser, J.P., Wieringa, B.E., Deutman, A.F., Palczewski, K., Ruether, K., Janssen, J.J., 2000. Disruption of the 11-cis-retinol dehydrogenase gene leads to accumulation of cis-retinols and cis-retinyl esters. *Molecular and cellular biology* 20, 4275-4287.
- Dryja, T.P., McGee, T.L., Hahn, L.B., Cowley, G.S., Olsson, J.E., Reichel, E., Sandberg, M.A., Berson, E.L., 1990. Mutations within the rhodopsin gene in patients with autosomal dominant retinitis pigmentosa. *N Engl J Med* 323, 1302-1307.
- Dudus, L., Anand, V., Acland, G.M., Chen, S.J., Wilson, J.M., Fisher, K.J., Maguire, A.M., Bennett, J., 1999. Persistent transgene product in retina, optic nerve and brain after intraocular injection of rAAV. *Vision research* 39, 2545-2553.

- Duisit, G., Conrath, H., Saleun, S., Folliot, S., Provost, N., Cosset, F.L., Sandrin, V., Moullier, P., Rolling, F., 2002. Five recombinant simian immunodeficiency virus pseudotypes lead to exclusive transduction of retinal pigmented epithelium in rat. *Molecular therapy : the journal of the American Society of Gene Therapy* 6, 446-454.
- Fadool, J.M., Dowling, J.E., 2008. Zebrafish: a model system for the study of eye genetics. *Progress in retinal and eye research* 27, 89-110.
- Farkas, M.H., Lew, D.S., Sousa, M.E., Bujakowska, K., Chatagnon, J., Bhattacharya, S.S., Pierce, E.A., Nandrot, E.F., 2014. Mutations in Pre-mRNA Processing Factors 3, 8, and 31 Cause Dysfunction of the Retinal Pigment Epithelium. *Am J Pathol* 184, 2641-2652.
- Fausett, B.V., Goldman, D., 2006. A role for alpha1 tubulin-expressing Muller glia in regeneration of the injured zebrafish retina. *The Journal of neuroscience : the official journal of the Society for Neuroscience* 26, 6303-6313.
- Ferguson, L.R., Dominguez li, J.M., Balaiya, S., Grover, S., Chalam, K.V., 2013. Retinal Thickness Normative Data in Wild-Type Mice Using Customized Miniature SD-OCT. *PloS one* 8, e67265.
- Fischer, A.J., Reh, T.A., 2000. Identification of a proliferating marginal zone of retinal progenitors in postnatal chickens. *Developmental biology* 220, 197-210.
- Fischer, A.J., Reh, T.A., 2001. Muller glia are a potential source of neural regeneration in the postnatal chicken retina. *Nature neuroscience* 4, 247-252.
- Fischer, A.J., Reh, T.A., 2002. Exogenous growth factors stimulate the regeneration of ganglion cells in the chicken retina. *Developmental biology* 251, 367-379.
- Freund, C.L., Gregory-Evans, C.Y., Furukawa, T., Papaioannou, M., Looser, J., Ploder, L., Bellingham, J., Ng, D., Herbrick, J.A., Duncan, A., Scherer, S.W., Tsui, L.C., Loutradis-Anagnostou, A., Jacobson, S.G., Cepko, C.L., Bhattacharya, S.S., McInnes, R.R., 1997. Cone-rod dystrophy due to mutations in a novel photoreceptor-specific homeobox gene (CRX) essential for maintenance of the photoreceptor. *Cell* 91, 543-553.
- Freund, C.L., Wang, Q.L., Chen, S., Muskat, B.L., Wiles, C.D., Sheffield, V.C., Jacobson, S.G., McInnes, R.R., Zack, D.J., Stone, E.M., 1998. De novo mutations in the CRX homeobox gene associated with Leber congenital amaurosis. *Nature genetics* 18, 311-312.
- Fu, Y., Foden, J.A., Khayter, C., Maeder, M.L., Reyon, D., Joung, J.K., Sander, J.D., 2013. High-frequency off-target mutagenesis induced by CRISPR-Cas nucleases in human cells. *Nature biotechnology* 31, 822-826.
- Fu, Y., Sander, J.D., Reyon, D., Cascio, V.M., Joung, J.K., 2014. Improving CRISPR-Cas nuclease specificity using truncated guide RNAs. *Nat Biotech* 32, 279-284.
- Furukawa, T., Morrow, E.M., Li, T., Davis, F.C., Cepko, C.L., 1999. Retinopathy and attenuated circadian entrainment in Crx-deficient mice. *Nature genetics* 23, 466-470.
- Galan, A., Martin-Suarez, E.M., Granados, M.M., Gallardo, J.M., Molleda, J.M., 2006. Comparative fluorescein angiography of the normal sheep and goat ocular fundi. *Veterinary ophthalmology* 9, 7-15.
- Garanto, A., Duijkers, L., Collin, R.W.J., 2015. Species-dependent splice recognition of a cryptic exon resulting from a recurrent deep-intronic mutation in CEP290 that causes congenital blindness. *Int J Mol Sci* 16, 5285-5298.
- Garanto, A., Riera, M., Pomares, E., Permanyer, J., de Castro-Miro, M., Sava, F., Abril, J.F., Marfany, G., Gonzalez-Duarte, R., 2011. High transcriptional complexity of the retinitis pigmentosa CERKL gene in human and mouse. *Invest Ophth Vis Sci* 52, 5202-5214.

- Garanto, A., van Beersum, S.E.C., Peters, T.A., Roepman, R., Cremers, F.P.M., Collin, R.W.J., 2013. Unexpected CEP290 mRNA Splicing in a Humanized Knock-In Mouse Model for Leber Congenital Amaurosis. *Plos One* 8.
- Garanto, A., Vicente-Tejedor, J., Riera, M., de la Villa, P., Gonzalez-Duarte, R., Blanco, R., Marfany, G., 2012. Targeted knockdown of Cerkl, a retinal dystrophy gene, causes mild affectation of the retinal ganglion cell layer. *Biochimica et biophysica acta* 1822, 1258-1269.
- Gekeler, F., Gmeiner, H., Volker, M., Sachs, H., Messias, A., Eule, C., Bartz-Schmidt, K.U., Zrenner, E., Shinoda, K., 2007. Assessment of the posterior segment of the cat eye by optical coherence tomography (OCT). *Veterinary ophthalmology* 10, 173-178.
- Gelatt, K.N., 2007. *Veterinary Ophthalmology*, 4th ed. Blackwell, Ames, Iowa.
- Goldman, D., 2014. Muller glial cell reprogramming and retina regeneration. *Nature reviews. Neuroscience* 15, 431-442.
- Goldsmith, T.H., Collins, J.S., Licht, S., 1984. The cone oil droplets of avian retinas. *Vision research* 24, 1661-1671.
- Goldstein, O., Mezey, J.G., Schweitzer, P.A., Boyko, A.R., Gao, C., Bustamante, C.D., Jordan, J.A., Aguirre, G.D., Acland, G.M., 2013. IQCB1 and PDE6B mutations cause similar early onset retinal degenerations in two closely related terrier dog breeds. *Invest Ophth Vis Sci* 54, 7005-7019.
- Goodyear, R., Richardson, G., 1999. The ankle-link antigen: an epitope sensitive to calcium chelation associated with the hair-cell surface and the calycal processes of photoreceptors. *The Journal of neuroscience: the official journal of the Society for Neuroscience* 19, 3761-3772.
- Gouras, P., Ekesten, B., 2004. Why do mice have ultra-violet vision? *Experimental eye research* 79, 887-892.
- Graziotto, J.J., Farkas, M.H., Bujakowska, K., Deramautd, B.M., Zhang, Q., Nandrot, E.F., Inglehearn, C.F., Bhattacharya, S.S., Pierce, E.A., 2011. Three Gene-Targeted Mouse Models of RNA Splicing Factor RP Show Late-Onset RPE and Retinal Degeneration. *Invest Ophth Vis Sci* 52, 190-198.
- Graziotto, J.J., Inglehearn, C.F., Pack, M.A., Pierce, E.A., 2008. Decreased levels of the RNA splicing factor Prpf3 in mice and zebrafish do not cause photoreceptor degeneration. *Invest Ophth Vis Sci* 49, 3830-3838.
- Gross, J.M., Perkins, B.D., Amsterdam, A., Egana, A., Darland, T., Matsui, J.I., Sciascia, S., Hopkins, N., Dowling, J.E., 2005. Identification of zebrafish insertional mutants with defects in visual system development and function. *Genetics* 170, 245-261.
- Hamlet, M.R., Yergeau, D.A., Kulyev, E., Takeda, M., Taira, M., Kawakami, K., Mead, P.E., 2006. Tol2 transposon-mediated transgenesis in *Xenopus tropicalis*. *Genesis* 44, 438-445.
- Han, H., Ma, Y., Wang, T., Lian, L., Tian, X., Hu, R., Deng, S., Li, K., Wang, F., Li, N., Liu, G., Zhao, Y., Lian, Z., 2014. One-step generation of myostatin gene knockout sheep via the CRISPR/Cas9 system. *Frontiers of Agricultural Science and Engineering* 1, 2-5.
- Hart, A.W., McKie, L., Morgan, J.E., Gautier, P., West, K., Jackson, I.J., Cross, S.H., 2005. Genotype-phenotype correlation of mouse *pde6b* mutations. *Invest Ophth Vis Sci* 46, 3443-3450.
- Hauswirth, W.W., Aleman, T.S., Kaushal, S., Cideciyan, A.V., Schwartz, S.B., Wang, L., Conlon, T.J., Boye, S.L., Flotte, T.R., Byrne, B.J., Jacobson, S.G., 2008. Treatment of leber congenital amaurosis due to RPE65 mutations by ocular subretinal injection of adeno-associated virus gene vector: short-term results of a phase I trial. *Hum Gene Ther* 19, 979-990.
- Hedges, S.B., 2002. The origin and evolution of model organisms. *Nature reviews. Genetics* 3, 838-849.

- Hernandez-Merino, E., Kecova, H., Jacobson, S.J., Hamouche, K.N., Nzokwe, R.N., Grozdanic, S.D., 2011. Spectral domain optical coherence tomography (SD-OCT) assessment of the healthy female canine retina and optic nerve. *Veterinary ophthalmology* 14, 400-405.
- Hockemeyer, D., Wang, H., Kiani, S., Lai, C.S., Gao, Q., Cassady, J.P., Cost, G.J., Zhang, L., Santiago, Y., Miller, J.C., Zeitler, B., Cherone, J.M., Meng, X., Hinkley, S.J., Rebar, E.J., Gregory, P.D., Urnov, F.D., Jaenisch, R., 2011. Genetic engineering of human pluripotent cells using TALE nucleases. *Nature biotechnology* 29, 731-734.
- Hocking, P.M., Guggenheim, J.A., 2013. The chick as an animal model of eye disease. *Drug Discovery Today: Disease Models* 10, e225-e230.
- Hodel, C., Niklaus, S., Heidemann, M., Klooster, J., Kamermans, M., Biehlmaier, O., Gesemann, M., Neuhaus, S.C., 2014. Myosin VIIA is a marker for the cone accessory outer segment in zebrafish. *Anatomical record* 297, 1777-1784.
- Hollingsworth, T.J., Gross, A.K., 2013. The severe autosomal dominant retinitis pigmentosa rhodopsin mutant Ter349Glu mislocalizes and induces rapid rod cell death. *The Journal of biological chemistry* 288, 29047-29055.
- Howes, K.A., Pennesi, M.E., Sokal, I., Church-Kopish, J., Schmidt, B., Margolis, D., Frederick, J.M., Rieke, F., Palczewski, K., Wu, S.M., Detwiler, P.B., Baehr, W., 2002. GCAP1 rescues rod photoreceptor response in GCAP1/GCAP2 knockout mice. *The EMBO journal* 21, 1545-1554.
- Howland, H.C., Merola, S., Basarab, J.R., 2004. The allometry and scaling of the size of vertebrate eyes. *Vision research* 44, 2043-2065.
- Huang, P., Xiao, A., Zhou, M., Zhu, Z., Lin, S., Zhang, B., 2011. Heritable gene targeting in zebrafish using customized TALENs. *Nature biotechnology* 29, 699-700.
- Hughes, B.A., Gallemore, R.P., Miller, S.S., 1998. *Transport mechanisms in the retinal pigment epithelium*, 1st ed. Oxford University Press, New York.
- Hunt, D.M., Dulai, K.S., Cowing, J.A., Julliot, C., Mollon, J.D., Bowmaker, J.K., Li, W.H., Hewett-Emmett, D., 1998. Molecular evolution of trichromacy in primates. *Vision research* 38, 3299-3306.
- Imanishi, Y., Li, N., Sokal, I., Sowa, M.E., Lichtarge, O., Wensel, T.G., Saperstein, D.A., Baehr, W., Palczewski, K., 2002. Characterization of retinal guanylate cyclase-activating protein 3 (GCAP3) from zebrafish to man. *The European journal of neuroscience* 15, 63-78.
- Iribarren, R., Rozema, J.J., Schaeffel, F., Morgan, I.G., 2014. Calculation of crystalline lens power in chickens with a customized version of Bennett's equation. *Vision research* 96, 33-38.
- Ishino, Y., Shinagawa, H., Makino, K., Amemura, M., Nakata, A., 1987. Nucleotide sequence of the *iap* gene, responsible for alkaline phosphatase isozyme conversion in *Escherichia coli*, and identification of the gene product. *Journal of bacteriology* 169, 5429-5433.
- Ivics, Z., Kaufman, C.D., Zayed, H., Miskey, C., Walisko, O., Izsvak, Z., 2004. The Sleeping Beauty transposable element: evolution, regulation and genetic applications. *Current issues in molecular biology* 6, 43-55.
- Izsvak, Z., Frohlich, J., Grabundzija, I., Shirley, J.R., Powell, H.M., Chapman, K.M., Ivics, Z., Hamra, F.K., 2010. Generating knockout rats by transposon mutagenesis in spermatogonial stem cells. *Nature methods* 7, 443-445.
- Jacobs, G.H., Deegan, J.F., 2nd, Neitz, J., 1998. Photopigment basis for dichromatic color vision in cows, goats, and sheep. *Vis Neurosci* 15, 581-584.

- Jacobson, S.G., Cideciyan, A.V., Ratnakaram, R., Heon, E., Schwartz, S.B., Roman, A.J., Peden, M.C., Aleman, T.S., Boye, S.L., Sumaroka, A., Conlon, T.J., Calcedo, R., Pang, J.J., Erger, K.E., Olivares, M.B., Mullins, C.L., Swider, M., Kaushal, S., Feuer, W.J., Iannaccone, A., Fishman, G.A., Stone, E.M., Byrne, B.J., Hauswirth, W.W., 2012. Gene therapy for leber congenital amaurosis caused by RPE65 mutations: safety and efficacy in 15 children and adults followed up to 3 years. *Archives of ophthalmology* 130, 9-24.
- Janecke, A.R., Thompson, D.A., Utermann, G., Becker, C., Hubner, C.A., Schmid, E., McHenry, C.L., Nair, A.R., Ruschendorf, F., Heckenlively, J., Wissinger, B., Nurnberg, P., Gal, A., 2004. Mutations in RDH12 encoding a photoreceptor cell retinol dehydrogenase cause childhood-onset severe retinal dystrophy. *Nat Genet* 36, 850-854.
- Jia, S., Muto, A., Orisme, W., Henson, H.E., Parupalli, C., Ju, B., Baier, H., Taylor, M.R., 2014. Zebrafish *Cacna1fa* is required for cone photoreceptor function and synaptic ribbon formation. *Human molecular genetics* 23, 2981-2994.
- Jinek, M., Chylinski, K., Fonfara, I., Hauer, M., Doudna, J.A., Charpentier, E., 2012. A programmable dual-RNA-guided DNA endonuclease in adaptive bacterial immunity. *Science* 337, 816-821.
- Kachi, S., Nishizawa, Y., Olshevskaya, E., Yamazaki, A., Miyake, Y., Wakabayashi, T., Dizhoor, A., Usukura, J., 1999. Detailed localization of photoreceptor guanylate cyclase activating protein-1 and -2 in mammalian retinas using light and electron microscopy. *Experimental eye research* 68, 465-473.
- Kafri, R., Springer, M., Pilpel, Y., 2009. Genetic redundancy: new tricks for old genes. *Cell* 136, 389-392.
- Kaludov, N., Brown, K.E., Walters, R.W., Zabner, J., Chiorini, J.A., 2001. Adeno-associated virus serotype 4 (AAV4) and AAV5 both require sialic acid binding for hemagglutination and efficient transduction but differ in sialic acid linkage specificity. *Journal of virology* 75, 6884-6893.
- Katju, V., Bergthorsson, U., 2013. Copy-number changes in evolution: rates, fitness effects and adaptive significance. *Frontiers in genetics* 4, 273.
- Kawakami, K., 2007. Tol2: a versatile gene transfer vector in vertebrates. *Genome biology* 8 Suppl 1, S7.
- Kay, C.N., Ryals, R.C., Aslanidi, G.V., Min, S.H., Ruan, Q., Sun, J., Dyka, F.M., Kasuga, D., Ayala, A.E., Van Vliet, K., Agbandje-McKenna, M., Hauswirth, W.W., Boye, S.L., Boye, S.E., 2013. Targeting photoreceptors via intravitreal delivery using novel, capsid-mutated AAV vectors. *PLoS one* 8, e62097.
- Keng, V.W., Ryan, B.J., Wangensteen, K.J., Balciunas, D., Schmedt, C., Ekker, S.C., Largaespada, D.A., 2009. Efficient transposition of Tol2 in the mouse germline. *Genetics* 183, 1565-1573.
- Kersten, F.F., van Wijk, E., van Reeuwijk, J., van der Zwaag, B., Marker, T., Peters, T.A., Katsanis, N., Wolftrum, U., Keunen, J.E., Roepman, R., Kremer, H., 2010. Association of whirlin with Cav1.3 (alpha1D) channels in photoreceptors, defining a novel member of the usher protein network. *Invest Ophthalmol Vis Sci* 51, 2338-2346.
- Kettleborough, R.N., Busch-Nentwich, E.M., Harvey, S.A., Dooley, C.M., de Bruijn, E., van Eeden, F., Sealy, I., White, R.J., Herd, C., Nijman, I.J., Fenyes, F., Mehroke, S., Scahill, C., Gibbons, R., Wali, N., Carruthers, S., Hall, A., Yen, J., Cuppen, E., Stemple, D.L., 2013. A systematic genome-wide analysis of zebrafish protein-coding gene function. *Nature* 496, 494-497.

- Kijas, J.W., Cideciyan, A.V., Aleman, T.S., Pianta, M.J., Pearce-Kelling, S.E., Miller, B.J., Jacobson, S.G., Aguirre, G.D., Acland, G.M., 2002. Naturally occurring rhodopsin mutation in the dog causes retinal dysfunction and degeneration mimicking human dominant retinitis pigmentosa. *Proceedings of the National Academy of Sciences of the United States of America* 99, 6328-6333.
- Kim, T.S., Maeda, A., Maeda, T., Heinlein, C., Kedishvili, N., Palczewski, K., Nelson, P.S., 2005. Delayed dark adaptation in 11-cis-retinol dehydrogenase-deficient mice: a role of RDH11 in visual processes in vivo. *The Journal of biological chemistry* 280, 8694-8704.
- Kirschner, R., Rosenberg, T., Schultz-Heienbrok, R., Lenzner, S., Feil, S., Roepman, R., Cremers, F.P., Ropers, H.H., Berger, W., 1999. RPGR transcription studies in mouse and human tissues reveal a retina-specific isoform that is disrupted in a patient with X-linked retinitis pigmentosa. *Human molecular genetics* 8, 1571-1578.
- Kiser, P.D., Golczak, M., Maeda, A., Palczewski, K., 2012. Key enzymes of the retinoid (visual) cycle in vertebrate retina. *Biochimica et biophysica acta* 1821, 137-151.
- Kitada, K., Ishishita, S., Tosaka, K., Takahashi, R., Ueda, M., Keng, V.W., Horie, K., Takeda, J., 2007. Transposon-tagged mutagenesis in the rat. *Nature methods* 4, 131-133.
- Kitiratschky, V.B., Glockner, C.J., Kohl, S., 2011. Mutation screening of the GUCA1B gene in patients with autosomal dominant cone and cone rod dystrophy. *Ophthalmic genetics* 32, 151-155.
- Klein, D., Mendes-Madeira, A., Schlegel, P., Rolling, F., Lorenz, B., Haverkamp, S., Stieger, K., 2014. Immunohistochemical analysis of rod and cone reaction to RPE65 deficiency in the inferior and superior canine retina. *PloS one* 9, e86304.
- Koller, B.H., Smithies, O., 1989. Inactivating the beta 2-microglobulin locus in mouse embryonic stem cells by homologous recombination. *Proceedings of the National Academy of Sciences of the United States of America* 86, 8932-8935.
- Komaromy, A.M., 2010. Day blind sheep and the importance of large animal disease models. *Veterinary journal* 185, 241-242.
- Kostic, C., Lillico, S.G., Crippa, S.V., Grandchamp, N., Pilet, H., Philippe, S., Lu, Z., King, T.J., Mallet, J., Sarkis, C., Arsenijevic, Y., Whitelaw, C.B., 2013. Rapid cohort generation and analysis of disease spectrum of large animal model of cone dystrophy. *PloS one* 8, e71363.
- Kotani, T., Nagayoshi, S., Urasaki, A., Kawakami, K., 2006. Transposon-mediated gene trapping in zebrafish. *Methods* 39, 199-206.
- Kotterman, M.A., Yin, L., Strazzeri, J.M., Flannery, J.G., Merigan, W.H., Schaffer, D.V., 2014. Antibody neutralization poses a barrier to intravitreal adeno-associated viral vector gene delivery to non-human primates. *Gene therapy*.
- Kram, Y.A., Mantey, S., Corbo, J.C., 2010. Avian cone photoreceptors tile the retina as five independent, self-organizing mosaics. *PloS one* 5, e8992.
- Le Meur, G., Stieger, K., Smith, A.J., Weber, M., Deschamps, J.Y., Nivard, D., Mendes-Madeira, A., Provost, N., Pereon, Y., Cherel, Y., Ali, R.R., Hamel, C., Moullier, P., Rolling, F., 2007. Restoration of vision in RPE65-deficient Briard dogs using an AAV serotype 4 vector that specifically targets the retinal pigmented epithelium. *Gene therapy* 14, 292-303.
- Lheriteau, E., Petit, L., Weber, M., Le Meur, G., Deschamps, J.Y., Libeau, L., Mendes-Madeira, A., Guihal, C., Francois, A., Guyon, R., Provost, N., Lemoine, F., Papal, S., El-Amraoui, A., Colle, M.A., Moullier, P., Rolling, F., 2014. Successful gene therapy in the RPGRIP1-deficient dog: a large model of cone-rod dystrophy. *Molecular therapy : the journal of the American Society of Gene Therapy* 22, 265-277.

- Li, L., 2001. Zebrafish mutants: behavioral genetic studies of visual system defects. *Developmental dynamics: an official publication of the American Association of Anatomists* 221, 365-372.
- Lin, J., Chen, H., Luo, L., Lai, Y., Xie, W., Kee, K., 2014. Creating a monomeric endonuclease TALE-1-Scel with high specificity and low genotoxicity in human cells. *Nucleic acids research*.
- Lipinski, D.M., Barnard, A.R., Charbel Issa, P., Singh, M.S., De Silva, S.R., Trabalza, A., Eleftheriadou, I., Ellison, S.M., Mazarakis, N.D., MacLaren, R.E., 2014. Vesicular stomatitis virus glycoprotein- and Venezuelan equine encephalitis virus-derived glycoprotein-pseudotyped lentivirus vectors differentially transduce corneal endothelium, trabecular meshwork, and human photoreceptors. *Hum Gene Ther* 25, 50-62.
- Liu, X., Bulgakov, O.V., Darrow, K.N., Pawlyk, B., Adamian, M., Liberman, M.C., Li, T., 2007. Usherin is required for maintenance of retinal photoreceptors and normal development of cochlear hair cells. *Proceedings of the National Academy of Sciences of the United States of America* 104, 4413-4418.
- Lozano, D.C., Twa, M.D., 2012. Quantitative evaluation of factors influencing the repeatability of SD-OCT thickness measurements in the rat. *Invest Ophth Vis Sci* 53, 8378-8385.
- Lu, B., Geurts, A.M., Poirier, C., Petit, D.C., Harrison, W., Overbeek, P.A., Bishop, C.E., 2007. Generation of rat mutants using a coat color-tagged Sleeping Beauty transposon system. *Mammalian genome: official journal of the International Mammalian Genome Society* 18, 338-346.
- Luz-Madrigal, A., Grajales-Esquivel, E., McCorkle, A., DiLorenzo, A.M., Barbosa-Sabanero, K., Tsonis, P.A., Del Rio-Tsonis, K., 2014. Reprogramming of the chick retinal pigmented epithelium after retinal injury. *BMC biology* 12, 28.
- Maaswinkel, H., Riesbeck, L.E., Riley, M.E., Carr, A.L., Mullin, J.P., Nakamoto, A.T., Li, L., 2005. Behavioral screening for nightblindness mutants in zebrafish reveals three new loci that cause dominant photoreceptor cell degeneration. *Mechanisms of ageing and development* 126, 1079-1089.
- MacLaren, R.E., Groppe, M., Barnard, A.R., Cottrill, C.L., Tolmachova, T., Seymour, L., Clark, K.R., Durning, M.J., Cremers, F.P., Black, G.C., Lotery, A.J., Downes, S.M., Webster, A.R., Seabra, M.C., 2014. Retinal gene therapy in patients with choroideremia: initial findings from a phase 1/2 clinical trial. *Lancet* 383, 1129-1137.
- Maeda, A., Maeda, T., Sun, W., Zhang, H., Baehr, W., Palczewski, K., 2007. Redundant and unique roles of retinol dehydrogenases in the mouse retina. *Proceedings of the National Academy of Sciences of the United States of America* 104, 19565-19570.
- Maerker, T., van Wijk, E., Overlack, N., Kersten, F.F., McGee, J., Goldmann, T., Sehn, E., Roepman, R., Walsh, E.J., Kremer, H., Wolfrum, U., 2008. A novel Usher protein network at the periciliary reloading point between molecular transport machineries in vertebrate photoreceptor cells. *Human molecular genetics* 17, 71-86.
- Maguire, A.M., High, K.A., Auricchio, A., Wright, J.F., Pierce, E.A., Testa, F., Mingozzi, F., Bencicelli, J.L., Ying, G.S., Rossi, S., Fulton, A., Marshall, K.A., Banfi, S., Chung, D.C., Morgan, J.I., Hauck, B., Zelenia, O., Zhu, X., Raffini, L., Coppieters, F., De Baere, E., Shindler, K.S., Volpe, N.J., Surace, E.M., Acerra, C., Lyubarsky, A., Redmond, T.M., Stone, E.M., Sun, J., McDonnell, J.W., Leroy, B.P., Simonelli, F., Bennett, J., 2009. Age-dependent effects of RPE65 gene therapy for Leber's congenital amaurosis: a phase 1 dose-escalation trial. *Lancet* 374, 1597-1605.

- Maguire, A.M., Simonelli, F., Pierce, E.A., Pugh, E.N., Jr., Mingozzi, F., Bennicelli, J., Banfi, S., Marshall, K.A., Testa, F., Surace, E.M., Rossi, S., Lyubarsky, A., Arruda, V.R., Konkle, B., Stone, E., Sun, J., Jacobs, J., Dell'Osso, L., Hertle, R., Ma, J.X., Redmond, T.M., Zhu, X., Hauck, B., Zelenia, O., Shindler, K.S., Maguire, M.G., Wright, J.F., Volpe, N.J., McDonnell, J.W., Auricchio, A., High, K.A., Bennett, J., 2008. Safety and efficacy of gene transfer for Leber's congenital amaurosis. *N Engl J Med* 358, 2240-2248.
- Makino, C.L., Peshenko, I.V., Wen, X.H., Olshevskaya, E.V., Barrett, R., Dizhoor, A.M., 2008. A role for GCAP2 in regulating the photoresponse. Guanylyl cyclase activation and rod electrophysiology in GUC1A1B knock-out mice. *The Journal of biological chemistry* 283, 29135-29143.
- Manfredi, A., Marrocco, E., Puppo, A., Cesi, G., Sommella, A., Della Corte, M., Rossi, S., Giunti, M., Craft, C.M., Bacci, M.L., Simonelli, F., Surace, E.M., Auricchio, A., 2013. Combined rod and cone transduction by adeno-associated virus 2/8. *Hum Gene Ther* 24, 982-992.
- Marc, R.E., 2008. *Functional neuroanatomy of the retina*, 3rd ed. Elsevier, New York.
- McGee, J., Goodyear, R.J., McMillan, D.R., Stauffer, E.A., Holt, J.R., Locke, K.G., Birch, D.G., Legan, P.K., White, P.C., Walsh, E.J., Richardson, G.P., 2006. The very large G-protein-coupled receptor VLGR1: a component of the ankle link complex required for the normal development of auditory hair bundles. *The Journal of neuroscience : the official journal of the Society for Neuroscience* 26, 6543-6553.
- McKibbin, M., Ali, M., Inglehearn, C., Shires, M., Boyle, K., Hocking, P.M., 2014. Spectral domain optical coherence tomography imaging of the posterior segment of the eye in the retinal dysplasia and degeneration chicken, an animal model of inherited retinal degeneration. *Veterinary ophthalmology* 17, 113-119.
- McKie, A.B., McHale, J.C., Keen, T.J., Tartelin, E.E., Goliath, R., van Lith-Verhoeven, J.J., Greenberg, J., Ramesar, R.S., Hoyng, C.B., Cremers, F.P., Mackey, D.A., Bhattacharya, S.S., Bird, A.C., Markham, A.F., Inglehearn, C.F., 2001. Mutations in the pre-mRNA splicing factor gene PRPC8 in autosomal dominant retinitis pigmentosa (RP13). *Human molecular genetics* 10, 1555-1562.
- McLellan, G.J., Rasmussen, C.A., 2012. Optical coherence tomography for the evaluation of retinal and optic nerve morphology in animal subjects: practical considerations. *Veterinary ophthalmology* 15 Suppl 2, 13-28.
- Mendez, A., Burns, M.E., Sokal, I., Dizhoor, A.M., Baehr, W., Palczewski, K., Baylor, D.A., Chen, J., 2001. Role of guanylate cyclase-activating proteins (GCAPs) in setting the flash sensitivity of rod photoreceptors. *Proceedings of the National Academy of Sciences of the United States of America* 98, 9948-9953.
- Menotti-Raymond, M., Deckman, K.H., David, V., Myrkalov, J., O'Brien, S.J., Narfstrom, K., 2010. Mutation discovered in a feline model of human congenital retinal blinding disease. *Invest Ophthalmol Vis Sci* 51, 2852-2859.
- Meyer, A., Schartl, M., 1999. Gene and genome duplications in vertebrates: the one-to-four (-to-eight in fish) rule and the evolution of novel gene functions. *Current opinion in cell biology* 11, 699-704.
- Minella, A.L., Mowat, F.M., Willett, K.L., Sledge, D., Bartoe, J.T., Bennett, J., Petersen-Jones, S.M., 2014. Differential targeting of feline photoreceptors by recombinant adeno-associated viral vectors: implications for preclinical gene therapy trials. *Gene therapy* 21, 913-920.
- Moayed, A.A., Hariri, S., Song, E.S., Choh, V., Bizheva, K., 2011. In vivo volumetric imaging of chicken retina with ultrahigh-resolution spectral domain optical coherence tomography. *Biomedical optics express* 2, 1268-1274.

- Montiani-Ferreira, F., Li, T., Kiupel, M., Howland, H., Hocking, P., Curtis, R., Petersen-Jones, S., 2003. Clinical features of the retinopathy, globe enlarged (rge) chick phenotype. *Vision research* 43, 2009-2018.
- Moosajee, M., Gregory-Evans, K., Ellis, C.D., Seabra, M.C., Gregory-Evans, C.Y., 2008. Translational bypass of nonsense mutations in zebrafish *rep1*, *pax2.1* and *lamb1* highlights a viable therapeutic option for untreatable genetic eye disease. *Human molecular genetics* 17, 3987-4000.
- Mowat, F.M., Gornik, K.R., Dinculescu, A., Boye, S.L., Hauswirth, W.W., Petersen-Jones, S.M., Bartoe, J.T., 2014. Tyrosine capsid-mutant AAV vectors for gene delivery to the canine retina from a subretinal or intravitreal approach. *Gene therapy* 21, 96-105.
- Mowat, F.M., Petersen-Jones, S.M., Williamson, H., Williams, D.L., Luthert, P.J., Ali, R.R., Bainbridge, J.W., 2008. Topographical characterization of cone photoreceptors and the area centralis of the canine retina. *Molecular vision* 14, 2518-2527.
- Narfstrom, K., Katz, M.L., Bragadottir, R., Seeliger, M., Boulanger, A., Redmond, T.M., Caro, L., Lai, C.M., Rakoczy, P.E., 2003. Functional and structural recovery of the retina after gene therapy in the RPE65 null mutation dog. *Invest Ophthalmol Vis Sci* 44, 1663-1672.
- Nelson, C.M., Ackerman, K.M., O'Hayer, P., Bailey, T.J., Gorsuch, R.A., Hyde, D.R., 2013. Tumor necrosis factor-alpha is produced by dying retinal neurons and is required for Muller glia proliferation during zebrafish retinal regeneration. *The Journal of neuroscience : the official journal of the Society for Neuroscience* 33, 6524-6539.
- Oh, E.C., Khan, N., Novelli, E., Khanna, H., Strettoi, E., Swaroop, A., 2007. Transformation of cone precursors to functional rod photoreceptors by bZIP transcription factor NRL. *Proceedings of the National Academy of Sciences of the United States of America* 104, 1679-1684.
- Ollivier, F.J., Samuelson, D.A., Brooks, D.E., Lewis, P.A., Kallberg, M.E., Komaromy, A.M., 2004. Comparative morphology of the tapetum lucidum (among selected species). *Veterinary ophthalmology* 7, 11-22.
- Olsson, J.E., Gordon, J.W., Pawlyk, B.S., Roof, D., Hayes, A., Molday, R.S., Mukai, S., Cowley, G.S., Berson, E.L., Dryja, T.P., 1992. Transgenic mice with a rhodopsin mutation (Pro23His): a mouse model of autosomal dominant retinitis pigmentosa. *Neuron* 9, 815-830.
- Osterwalder, M., Galli, A., Rosen, B., Skarnes, W.C., Zeller, R., Lopez-Rios, J., 2010. Dual RMCE for efficient re-engineering of mouse mutant alleles. *Nature methods* 7, 893-895.
- Payne, A.M., Downes, S.M., Bessant, D.A., Taylor, R., Holder, G.E., Warren, M.J., Bird, A.C., Bhattacharya, S.S., 1998. A mutation in guanylate cyclase activator 1A (GUCA1A) in an autosomal dominant cone dystrophy pedigree mapping to a new locus on chromosome 6p21.1. *Human molecular genetics* 7, 273-277.
- Peichl, L., 1992. Morphological types of ganglion cells in the dog and wolf retina. *The Journal of comparative neurology* 324, 590-602.
- Pennesi, M.E., Howes, K.A., Baehr, W., Wu, S.M., 2003. Guanylate cyclase-activating protein (GCAP) 1 rescues cone recovery kinetics in GCAP1/GCAP2 knockout mice. *Proceedings of the National Academy of Sciences of the United States of America* 100, 6783-6788.
- Perrault, I., Hanein, S., Gerber, S., Barbet, F., Ducroq, D., Dollfus, H., Hamel, C., Dufier, J.L., Munnich, A., Kaplan, J., Rozet, J.M., 2004. Retinal dehydrogenase 12 (RDH12) mutations in leber congenital amaurosis. *American journal of human genetics* 75, 639-646.
- Petersen-Jones, S.M., 2013. Drug and gene therapy of hereditary retinal disease in dog and cat models. *Drug Discovery Today: Disease Models* 10, e215-e223.

- Petersen-Jones, S.M., Entz, D.D., Sargan, D.R., 1999. cGMP phosphodiesterase-alpha mutation causes progressive retinal atrophy in the Cardigan Welsh corgi dog. *Invest Ophth Vis Sci* 40, 1637-1644.
- Petit, C., 2001. Usher syndrome: from genetics to pathogenesis. *Annual review of genomics and human genetics* 2, 271-297.
- Petit, L., Lheriteau, E., Weber, M., Le Meur, G., Deschamps, J.Y., Provost, N., Mendes-Madeira, A., Libeau, L., Guihal, C., Colle, M.A., Moullier, P., Rolling, F., 2012. Restoration of vision in the pde6beta-deficient dog, a large animal model of rod-cone dystrophy. *Molecular therapy : the journal of the American Society of Gene Therapy* 20, 2019-2030.
- Peters-Silva, H., Dinculescu, A., Li, Q., Min, S.H., Chiodo, V., Pang, J.J., Zhong, L., Zolotukhin, S., Srivastava, A., Lewin, A.S., Hauswirth, W.W., 2009. High-efficiency transduction of the mouse retina by tyrosine-mutant AAV serotype vectors. *Molecular therapy : the journal of the American Society of Gene Therapy* 17, 463-471.
- Pittler, S.J., Baehr, W., 1991. Identification of a nonsense mutation in the rod photoreceptor cGMP phosphodiesterase beta-subunit gene of the rd mouse. *Proceedings of the National Academy of Sciences of the United States of America* 88, 8322-8326.
- Ponce de Leon, V., Merillat, A.M., Tesson, L., Anegon, I., Hummler, E., 2014. Generation of TALEN-mediated GRdim knock-in rats by homologous recombination. *PLoS one* 9, e88146.
- Pretorius, P.R., Baye, L.M., Nishimura, D.Y., Searby, C.C., Bugge, K., Yang, B., Mullins, R.F., Stone, E.M., Sheffield, V.C., Slusarski, D.C., 2010. Identification and functional analysis of the vision-specific BBS3 (ARL6) long isoform. *PLoS genetics* 6, e1000884.
- Puk, O., Dalke, C., Favor, J., de Angelis, M.H., Graw, J., 2006. Variations of eye size parameters among different strains of mice. *Mammalian genome: official journal of the International Mammalian Genome Society* 17, 851-857.
- Raghupathy, R.K., McCulloch, D.L., Akhtar, S., Al-mubrad, T.M., Shu, X., 2013. Zebrafish model for the genetic basis of X-linked retinitis pigmentosa. *Zebrafish* 10, 62-69.
- Ran, F.A., Hsu, P.D., Lin, C.Y., Gootenberg, J.S., Konermann, S., Trevino, A.E., Scott, D.A., Inoue, A., Matoba, S., Zhang, Y., Zhang, F., 2013. Double nicking by RNA-guided CRISPR Cas9 for enhanced genome editing specificity. *Cell* 154, 1380-1389.
- Rauscher, F.G., Azmanis, P., Korber, N., Koch, C., Hubel, J., Vetterlein, W., Werner, B., Thielebein, J., Dawczynski, J., Wiedemann, P., Reichenbach, A., Francke, M., Krautwald-Junghanns, M.E., 2013. Optical coherence tomography as a diagnostic tool for retinal pathologies in avian ophthalmology. *Invest Ophth Vis Sci* 54, 8259-8269.
- Ripps, H., 2002. Cell death in retinitis pigmentosa: gap junctions and the 'bystander' effect. *Experimental eye research* 74, 327-336.
- Robert, C., Fuentes-Utrilla, P., Troup, K., Loecherbach, J., Turner, F., Talbot, R., Archibald, A.L., Mileham, A., Deeb, N., Hume, D.A., Watson, M., 2014. Design and development of exome capture sequencing for the domestic pig (*Sus scrofa*). *BMC genomics* 15, 550.
- Roger, J.E., Hiriyan, A., Gotoh, N., Hao, H., Cheng, D.F., Ratnapriya, R., Kautzmann, M.A., Chang, B., Swaroop, A., 2014. OTX2 loss causes rod differentiation defect in CRX-associated congenital blindness. *The Journal of clinical investigation* 124, 631-643.
- Roof, D.J., Adamian, M., Hayes, A., 1994. Rhodopsin accumulation at abnormal sites in retinas of mice with a human P23H rhodopsin transgene. *Invest Ophth Vis Sci* 35, 4049-4062.
- Roorda, A., Williams, D.R., 1999. The arrangement of the three cone classes in the living human eye. *Nat New Biol* 397, 520-522.

- Roska, B., Busskamp, V., Sahel, J.A., Picaud, S., 2013. Retinitis pigmentosa: eye sight restoration by optogenetic therapy. *Biologie aujourd'hui* 207, 109-121.
- Ross, J.W., Fernandez de Castro, J.P., Zhao, J., Samuel, M., Walters, E., Rios, C., Bray-Ward, P., Jones, B.W., Marc, R.E., Wang, W., Zhou, L., Noel, J.M., McCall, M.A., DeMarco, P.J., Prather, R.S., Kaplan, H.J., 2012. Generation of an inbred miniature pig model of retinitis pigmentosa. *Invest Ophthalmol Vis Sci* 53, 501-507.
- Ruan, J., Li, H., Chen, Z., Coghlan, A., Coin, L.J., Guo, Y., Heriche, J.K., Hu, Y., Kristiansen, K., Li, R., Liu, T., Moses, A., Qin, J., Vang, S., Vilella, A.J., Ureta-Vidal, A., Bolund, L., Wang, J., Durbin, R., 2008. TreeFam: 2008 Update. *Nucleic acids research* 36, D735-740.
- Sahly, I., Dufour, E., Schietroma, C., Michel, V., Bahloul, A., Perfettini, I., Pepermans, E., Estivalet, A., Carette, D., Aghaie, A., Ebermann, I., Lelli, A., Iribarne, M., Hardelin, J.P., Weil, D., Sahel, J.A., El-Amraoui, A., Petit, C., 2012. Localization of Usher 1 proteins to the photoreceptor calyceal processes, which are absent from mice. *The Journal of cell biology* 199, 381-399.
- Sakamoto, K., McCluskey, M., Wensel, T.G., Naggert, J.K., Nishina, P.M., 2009. New mouse models for recessive retinitis pigmentosa caused by mutations in the *Pde6a* gene. *Human molecular genetics* 18, 178-192.
- Sander, J.D., Cade, L., Khayter, C., Reyon, D., Peterson, R.T., Joung, J.K., Yeh, J.R., 2011. Targeted gene disruption in somatic zebrafish cells using engineered TALENs. *Nature biotechnology* 29, 697-698.
- Sander, J.D., Joung, J.K., 2014. CRISPR-Cas systems for editing, regulating and targeting genomes. *Nature biotechnology* 32, 347-355.
- Sanyal, S., De Ruiter, A., Hawkins, R.K., 1980. Development and degeneration of retina in *rds* mutant mice: light microscopy. *The Journal of comparative neurology* 194, 193-207.
- Sarna, T., 1992. Properties and function of the ocular melanin—a photobiophysical view. *J Photochem Photobiol B* 12, 215-258.
- Satir, P., Christensen, S.T., 2008. Structure and function of mammalian cilia. *Histochemistry and cell biology* 129, 687-693.
- Sato, M., Nakazawa, M., Usui, T., Tanimoto, N., Abe, H., Ohguro, H., 2005. Mutations in the gene coding for guanylate cyclase-activating protein 2 (*GUCA1B* gene) in patients with autosomal dominant retinal dystrophies. *Graefes' archive for clinical and experimental ophthalmology = Albrecht von Graefes Archiv fur klinische und experimentelle Ophthalmologie* 243, 235-242.
- Schonthaler, H.B., Franz-Odenaal, T.A., Hodel, C., Gehring, I., Geisler, R., Schwarz, H., Neuhaus, S.C., Dahm, R., 2010. The zebrafish mutant bumper shows a hyperproliferation of lens epithelial cells and fibre cell degeneration leading to functional blindness. *Mechanisms of development* 127, 203-219.
- Seiler, C., Finger-Baier, K.C., Rinner, O., Makhankov, Y.V., Schwarz, H., Neuhaus, S.C., Nicolson, T., 2005. Duplicated genes with split functions: independent roles of protocadherin15 orthologues in zebrafish hearing and vision. *Development* 132, 615-623.
- Semple-Rowland, S.L., Lee, N.R., Van Hooser, J.P., Palczewski, K., Baehr, W., 1998. A null mutation in the photoreceptor guanylate cyclase gene causes the retinal degeneration chicken phenotype. *Proceedings of the National Academy of Sciences of the United States of America* 95, 1271-1276.
- Shang, E., Lai, K., Packer, A.I., Paik, J., Blaner, W.S., de Moraes Vieira, M., Gouras, P., Wolgemuth, D.J., 2002. Targeted disruption of the mouse *cis*-retinol dehydrogenase gene: visual and nonvisual functions. *Journal of lipid research* 43, 590-597.

- Shinozaki, A., Hosaka, Y., Imagawa, T., Uehara, M., 2010. Topography of ganglion cells and photoreceptors in the sheep retina. *The Journal of comparative neurology* 518, 2305-2315.
- Sidman, R.L., Green, M.C., 1965. Retinal Degeneration in the Mouse: Location of the Rd Locus in Linkage Group Xvii. *The Journal of heredity* 56, 23-29.
- Skarnes, W.C., Rosen, B., West, A.P., Koutsourakis, M., Bushell, W., Iyer, V., Mujica, A.O., Thomas, M., Harrow, J., Cox, T., Jackson, D., Severin, J., Biggs, P., Fu, J., Nefedov, M., de Jong, P.J., Stewart, A.F., Bradley, A., 2011. A conditional knockout resource for the genome-wide study of mouse gene function. *Nature* 474, 337-342.
- Smith, C., Abalde-Atristain, L., He, C., Brodsky, B.R., Braunstein, E.M., Chaudhari, P., Jang, Y.Y., Cheng, L., Ye, Z., 2014. Efficient and Allele-Specific Genome Editing of Disease Loci in Human iPSCs. *Molecular therapy : the journal of the American Society of Gene Therapy*.
- Sohocki, M.M., Sullivan, L.S., Mintz-Hittner, H.A., Birch, D., Heckenlively, J.R., Freund, C.L., McInnes, R.R., Daiger, S.P., 1998. A range of clinical phenotypes associated with mutations in CRX, a photoreceptor transcription-factor gene. *American journal of human genetics* 63, 1307-1315.
- Solomon, S.G., Lennie, P., 2007. The machinery of colour vision. *Nat Rev Neurosci* 8, 276-286.
- Steinberg, R.H., Fisher, S.K., Anderson, D.H., 1980. Disc morphogenesis in vertebrate photoreceptors. *J Comp Neurol* 190, 501-508.
- Stieger, K., Chauveau, C., Rolling, F., 2010. Preclinical studies on specific gene therapy for recessive retinal degenerative diseases. *Current gene therapy* 10, 389-403.
- Stieger, K., Colle, M.A., Dubreil, L., Mendes-Madeira, A., Weber, M., Le Meur, G., Deschamps, J.Y., Provost, N., Nivard, D., Cherel, Y., Moullier, P., Rolling, F., 2008. Subretinal delivery of recombinant AAV serotype 8 vector in dogs results in gene transfer to neurons in the brain. *Molecular therapy: the journal of the American Society of Gene Therapy* 16, 916-923.
- Subbaraya, I., Ruiz, C.C., Helekar, B.S., Zhao, X., Gorczyca, W.A., Pettenati, M.J., Rao, P.N., Palczewski, K., Baehr, W., 1994. Molecular characterization of human and mouse photoreceptor guanylate cyclase-activating protein (GCAP) and chromosomal localization of the human gene. *The Journal of biological chemistry* 269, 31080-31089.
- Suber, M.L., Pittler, S.J., Qin, N., Wright, G.C., Holcombe, V., Lee, R.H., Craft, C.M., Lolley, R.N., Baehr, W., Hurwitz, R.L., 1993. Irish setter dogs affected with rod/cone dysplasia contain a nonsense mutation in the rod cGMP phosphodiesterase beta-subunit gene. *Proceedings of the National Academy of Sciences of the United States of America* 90, 3968-3972.
- Summerford, C., Samulski, R.J., 1998. Membrane-associated heparan sulfate proteoglycan is a receptor for adeno-associated virus type 2 virions. *Journal of virology* 72, 1438-1445.
- Sung, C.H., Makino, C., Baylor, D., Nathans, J., 1994. A rhodopsin gene mutation responsible for autosomal dominant retinitis pigmentosa results in a protein that is defective in localization to the photoreceptor outer segment. *The Journal of neuroscience : the official journal of the Society for Neuroscience* 14, 5818-5833.
- Surguchov, A., Bronson, J.D., Banerjee, P., Knowles, J.A., Ruiz, C., Subbaraya, I., Palczewski, K., Baehr, W., 1997. The human GCAP1 and GCAP2 genes are arranged in a tail-to-tail array on the short arm of chromosome 6 (p21.1). *Genomics* 39, 312-322.
- Swain, P.K., Chen, S., Wang, Q.L., Affatigato, L.M., Coats, C.L., Brady, K.D., Fishman, G.A., Jacobson, S.G., Swaroop, A., Stone, E., Sieving, P.A., Zack, D.J., 1997. Mutations in the cone-rod homeobox gene are associated with the cone-rod dystrophy photoreceptor degeneration. *Neuron* 19, 1329-1336.

- Swaroop, A., Wang, Q.L., Wu, W., Cook, J., Coats, C., Xu, S., Chen, S., Zack, D.J., Sieving, P.A., 1999. Leber congenital amaurosis caused by a homozygous mutation (R90W) in the homeodomain of the retinal transcription factor CRX: direct evidence for the involvement of CRX in the development of photoreceptor function. *Human molecular genetics* 8, 299-305.
- Szel, A., Rohlich, P., Caffè, A.R., Juliusson, B., Aguirre, G., Van Veen, T., 1992. Unique topographic separation of two spectral classes of cones in the mouse retina. *The Journal of comparative neurology* 325, 327-342.
- Tanackovic, G., Ransijn, A., Ayuso, C., Harper, S., Berson, E.L., Rivolta, C., 2011. A missense mutation in PRPF6 causes impairment of pre-mRNA splicing and autosomal-dominant retinitis pigmentosa. *American journal of human genetics* 88, 643-649.
- Tarboush, R., Chapman, G.B., Connaughton, V.P., 2012. Ultrastructure of the distal retina of the adult zebrafish, *Danio rerio*. *Tissue & cell* 44, 264-279.
- Tesson, L., Usal, C., Menoret, S., Leung, E., Niles, B.J., Remy, S., Santiago, Y., Vincent, A.I., Meng, X., Zhang, L., Gregory, P.D., Anegón, I., Cost, G.J., 2011. Knockout rats generated by embryo microinjection of TALENs. *Nature biotechnology* 29, 695-696.
- Thomas, K.R., Capecchi, M.R., 1987. Site-directed mutagenesis by gene targeting in mouse embryonic stem cells. *Cell* 51, 503-512.
- Tong, C., Huang, G., Ashton, C., Li, P., Ying, Q.L., 2011. Generating gene knockout rats by homologous recombination in embryonic stem cells. *Nature protocols* 6, 827-844.
- Tran, N.M., Zhang, A., Zhang, X., Huecker, J.B., Hennig, A.K., Chen, S., 2014. Mechanistically distinct mouse models for CRX-associated retinopathy. *PLoS genetics* 10, e1004111.
- Trapani, I., Puppo, A., Auricchio, A., 2014. Vector platforms for gene therapy of inherited retinopathies. *Progress in retinal and eye research* 43, 108-128.
- Travis, G.H., Brennan, M.B., Danielson, P.E., Kozak, C.A., Sutcliffe, J.G., 1989. Identification of a photoreceptor-specific mRNA encoded by the gene responsible for retinal degeneration slow (rds). *Nature* 338, 70-73.
- Travis, G.H., Sutcliffe, J.G., Bok, D., 1991. The retinal degeneration slow (rds) gene product is a photoreceptor disc membrane-associated glycoprotein. *Neuron* 6, 61-70.
- Tsai, S.Q., Wyvekens, N., Khayter, C., Foden, J.A., Thapar, V., Reyon, D., Goodwin, M.J., Aryee, M.J., Joung, J.K., 2014. Dimeric CRISPR RNA-guided FokI nucleases for highly specific genome editing. *Nature biotechnology* 32, 569-576.
- Tucker, B.A., Mullins, R.F., Stone, E.M., 2014. Stem cells for investigation and treatment of inherited retinal disease. *Human molecular genetics* 23, R9-R16.
- Van den Hurk, J.A., Hendriks, W., van de Pol, D.J., Oerlemans, F., Jaissle, G., Ruther, K., Kohler, K., Hartmann, J., Zrenner, E., van Bokhoven, H., Wieringa, B., Ropers, H.H., Cremers, F.P., 1997. Mouse choroideremia gene mutation causes photoreceptor cell degeneration and is not transmitted through the female germline. *Human molecular genetics* 6, 851-858.
- Van Wijk, E., van der Zwaag, B., Peters, T., Zimmermann, U., Te Brinke, H., Kersten, F.F., Marker, T., Aller, E., Hoefsloot, L.H., Cremers, C.W., Cremers, F.P., Wolfrum, U., Knipper, M., Roepman, R., Kremer, H., 2006. The DFNB31 gene product whirlin connects to the Usher protein network in the cochlea and retina by direct association with USH2A and VLGR1. *Human molecular genetics* 15, 751-765.
- Vandenbergh, L.H., Bell, P., Maguire, A.M., Xiao, R., Hopkins, T.B., Grant, R., Bennett, J., Wilson, J.M., 2013. AAV9 targets cone photoreceptors in the nonhuman primate retina. *PLoS one* 8, e53463.

- Veleri, S., Lazar, C.H., Chang, B., Sieving, P.A., Banin, E., Swaroop, A., 2015. Biology and therapy of inherited retinal degenerative disease: insights from mouse models. *Disease models & mechanisms* 8, 109-129.
- Vilella, A.J., Severin, J., Ureta-Vidal, A., Heng, L., Durbin, R., Birney, E., 2009. EnsemblCompara GeneTrees: Complete, duplication-aware phylogenetic trees in vertebrates. *Genome research* 19, 327-335.
- Vithana, E.N., Abu-Safieh, L., Allen, M.J., Carey, A., Papaioannou, M., Chakarova, C., Al-Maghteh, M., Ebenezer, N.D., Willis, C., Moore, A.T., Bird, A.C., Hunt, D.M., Bhattacharya, S.S., 2001. A human homolog of yeast pre-mRNA splicing gene, PRP31, underlies autosomal dominant retinitis pigmentosa on chromosome 19q13.4 (RP11). *Molecular cell* 8, 375-381.
- Walters, R.W., Yi, S.M., Keshavjee, S., Brown, K.E., Welsh, M.J., Chiorini, J.A., Zabner, J., 2001. Binding of adeno-associated virus type 5 to 2,3-linked sialic acid is required for gene transfer. *The Journal of biological chemistry* 276, 20610-20616.
- Wang, D., Jao, L.E., Zheng, N., Dolan, K., Ivey, J., Zonies, S., Wu, X., Wu, K., Yang, H., Meng, Q., Zhu, Z., Zhang, B., Lin, S., Burgess, S.M., 2007. Efficient genome-wide mutagenesis of zebrafish genes by retroviral insertions. *Proceedings of the National Academy of Sciences of the United States of America* 104, 12428-12433.
- Weber, M., 2003. Recombinant adeno-associated virus serotype 4 mediates unique and exclusive long-term transduction of retinal pigmented epithelium in rat, dog, and nonhuman primate after subretinal delivery. *Molecular Therapy* 7, 774-781.
- Whitworth, K.M., Lee, K., Benne, J.A., Beaton, B.P., Spate, L.D., Murphy, S.L., Samuel, M.S., Mao, J., O'Gorman, C., Walters, E.M., Murphy, C.N., Driver, J., Mileham, A., McLaren, D., Wells, K.D., Prather, R.S., 2014. Use of the CRISPR/Cas9 system to produce genetically engineered pigs from in vitro-derived oocytes and embryos. *Biology of reproduction* 91, 78.
- Wiley, L.A., Burnight, E.R., Songstad, A.E., Drack, A.V., Mullins, R.F., Stone, E.M., Tucker, B.A., 2015. Patient-specific induced pluripotent stem cells (iPSCs) for the study and treatment of retinal degenerative diseases. *Progress in retinal and eye research* 44, 15-35.
- Williams, D.L., 2004. Lens morphometry determined by B-mode ultrasonography of the normal and cataractous canine lens. *Veterinary ophthalmology* 7, 91-95.
- Williams, M.L., Coleman, J.E., Haire, S.E., Aleman, T.S., Cideciyan, A.V., Sokal, I., Palczewski, K., Jacobson, S.G., Semple-Rowland, S.L., 2006. Lentiviral expression of retinal guanylate cyclase-1 (RetGC1) restores vision in an avian model of childhood blindness. *PLoS medicine* 3, e201.
- Wolburg, H., Liebner, S., Reichenbach, A., Gerhardt, H., 1999. The pecten oculi of the chicken: a model system for vascular differentiation and barrier maturation. *International review of cytology* 187, 111-159.
- Won, J., Shi, L.Y., Hicks, W., Wang, J., Hurd, R., Naggert, J.K., Chang, B., Nishina, P.M., 2011. Mouse model resources for vision research. *Journal of ophthalmology* 2011, 391384.
- Wu, X., Scott, D.A., Kriz, A.J., Chiu, A.C., Hsu, P.D., Dadon, D.B., Cheng, A.W., Trevino, A.E., Konermann, S., Chen, S., Jaenisch, R., Zhang, F., Sharp, P.A., 2014. Genome-wide binding of the CRISPR endonuclease Cas9 in mammalian cells. *Nature biotechnology* 32, 670-676.
- Wu, Y., Liang, D., Wang, Y., Bai, M., Tang, W., Bao, S., Yan, Z., Li, D., Li, J., 2013. Correction of a genetic disease in mouse via use of CRISPR-Cas9. *Cell stem cell* 13, 659-662.
- Xie, Y.A., Lee, W., Cai, C., Gambin, T., Noupou, K., Sujirakul, T., Ayuso, C., Jhangiani, S., Muzny, D., Boerwinkle, E., Gibbs, R., Greenstein, V.C., Lupski, J.R., Tsang, S.H., Allikmets, R., 2014. New syndrome with retinitis pigmentosa is caused by nonsense mutations in retinol dehydrogenase RDH11. *Human molecular genetics* 23, 5774-5780.

- Yamamoto, H., Simon, A., Eriksson, U., Harris, E., Berson, E.L., Dryja, T.P., 1999. Mutations in the gene encoding 11-cis retinol dehydrogenase cause delayed dark adaptation and fundus albipunctatus. *Nat Genet* 22, 188-191.
- Yang, H., Wang, H., Shivalila, C.S., Cheng, A.W., Shi, L., Jaenisch, R., 2013. One-step generation of mice carrying reporter and conditional alleles by CRISPR/Cas-mediated genome engineering. *Cell* 154, 1370-1379.
- Yang, J., Liu, X., Zhao, Y., Adamian, M., Pawlyk, B., Sun, X., McMillan, D.R., Liberman, M.C., Li, T., 2010. Ablation of whirlin long isoform disrupts the USH2 protein complex and causes vision and hearing loss. *PLoS genetics* 6, e1000955.
- Yin, L., Greenberg, K., Hunter, J.J., Dalkara, D., Kolstad, K.D., Masella, B.D., Wolfe, R., Visel, M., Stone, D., Libby, R.T., Diloreto, D., Jr., Schaffer, D., Flannery, J., Williams, D.R., Merigan, W.H., 2011. Intravitreal injection of AAV2 transduces macaque inner retina. *Invest Ophth Vis Sci* 52, 2775-2783.
- Zalocchi, M., Binley, K., Lad, Y., Ellis, S., Widdowson, P., Iqbal, S., Scripps, V., Kelleher, M., Loader, J., Miskin, J., Peng, Y.W., Wang, W.M., Cheung, L., Delimont, D., Mitrophanous, K.A., Cosgrove, D., 2014. ElAV-based retinal gene therapy in the shaker1 mouse model for usher syndrome type 1B: development of UshStat. *PLoS one* 9, e94272.
- Zan, Y., Haag, J.D., Chen, K.S., Shepel, L.A., Wigington, D., Wang, Y.R., Hu, R., Lopez-Guajardo, C.C., Brose, H.L., Porter, K.I., Leonard, R.A., Hitt, A.A., Schommer, S.L., Elegbede, A.F., Gould, M.N., 2003. Production of knockout rats using ENU mutagenesis and a yeast-based screening assay. *Nature biotechnology* 21, 645-651.
- Zrenner, E., Bartz-Schmidt, K.U., Benav, H., Besch, D., Bruckmann, A., Gabel, V.P., Gekeler, F., Greppmaier, U., Harscher, A., Kibbel, S., Koch, J., Kusnyerik, A., Peters, T., Stingl, K., Sachs, H., Stett, A., Szurman, P., Wilhelm, B., Wilke, R., 2011. Subretinal electronic chips allow blind patients to read letters and combine them to words. *Proc Biol Sci* 278, 1489-1497.

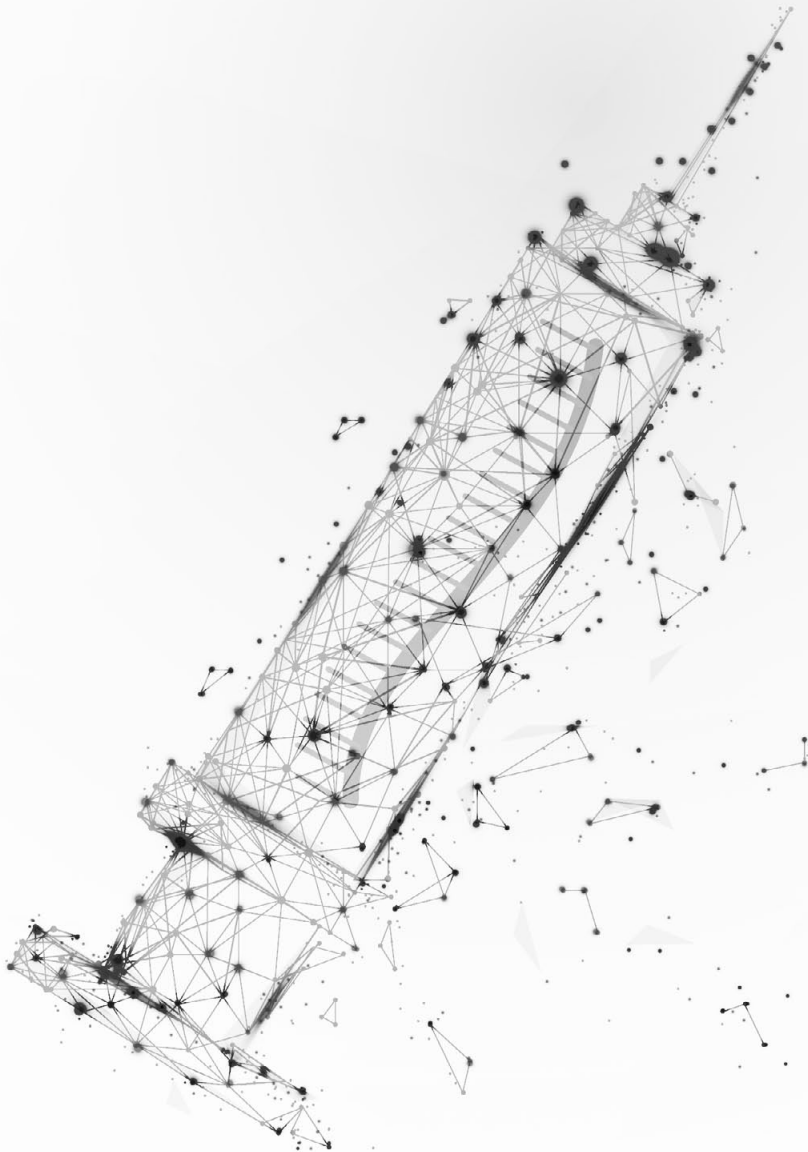
SUPPLEMENTAL TABLES

Supplemental Table 1. Duplicated IRD genes in the zebrafish genome.

<i>ABCA4</i>	<i>KIAA1549</i>
<i>ACBD5</i>	<i>LRIT3</i>
<i>C12orf65</i>	<i>MYO7A</i>
<i>CA4</i>	<i>NR2F1</i>
<i>CACNA1F</i>	<i>OPA1</i>
<i>CACNA2D4</i>	<i>OPN1LW</i>
<i>CAPN5</i>	<i>OPN1MW</i>
<i>CDHR1</i>	<i>PAX2</i>
<i>CNGA1</i>	<i>PCDH15</i>
<i>CNGA3</i>	<i>PCYT1A</i>
<i>CNGB1</i>	<i>PDZD7</i>
<i>CNGB3</i>	<i>PROM1</i>
<i>CNNM4</i>	<i>PRPH2</i>
<i>COL11A1</i>	<i>RGR</i>
<i>COL2A1</i>	<i>RGS9</i>
<i>COL9A1</i>	<i>RIMS1</i>
<i>CSPP1</i>	<i>RLBP1</i>
<i>CYP4V2</i>	<i>ROM1</i>
<i>DFNB31</i>	<i>RPE65</i>
<i>EFEMP1</i>	<i>RPGR</i>
<i>ELOVL4</i>	<i>RS1</i>
<i>FSCN2</i>	<i>SAG</i>
<i>GDF6</i>	<i>SEMA4A</i>
<i>GPR179</i>	<i>SLC7A14</i>
<i>GPR98</i>	<i>TEAD1</i>
<i>GRK1</i>	<i>TMEM237</i>
<i>GRM6</i>	<i>TOPORS</i>
<i>GUCA1A</i>	<i>TRPM1</i>
<i>GUCY2D</i>	<i>TULP1</i>
<i>IMPDH1</i>	<i>UNC119</i>
<i>IMPG1</i>	<i>USH1G</i>
<i>ITM2B</i>	<i>VCAN</i>
<i>JAG1</i>	<i>WFS1</i>
<i>KCNV2</i>	

Supplemental Table 2. Overview of vertebrate mutant animal models used in IRD research. This table can be found online using the following link: <https://doi.org/10.1016/j.preteyeres.2015.04.004>

Chapter 2^b



Usherin defects lead to early-onset retinal dysfunction in zebrafish

M. Dona^{1,2*}, R.W.N. Slijkerman^{1,2*}, K.M. Lerner³, S. Broekman^{4,5}, J. Wegner³, T.A. Howat³, T. Peters^{1,5}, L. Hetterschijt^{1,5}, N. Boon⁴, E. de Vrieze^{1,5}, N. Sorousch⁶, U. Wolfrum⁶, H. Kremer^{1,4,5}, S.C. Neuhaus⁷, J. Zang⁷, M. Kamermans⁸, M. Westerfield^{3,#}, J.B. Phillips^{3,#} and E. van Wijk^{1,5,#}

* The first two authors are co-first authors.

The last three authors are co-last authors.

¹ Department of Otorhinolaryngology, Radboud university medical centre, Nijmegen, the Netherlands.

² Radboud Institute for Molecular Life Sciences, Nijmegen, the Netherlands.

³ Institute of Neuroscience, University of Oregon, Eugene, Oregon, United States of America.

⁴ Department of Human Genetics, Radboudumc, Nijmegen, the Netherlands.

⁵ Donders Institute for Brain, Cognition, and Behaviour, Nijmegen, the Netherlands.

⁶ Institute of Molecular Physiology, Johannes Gutenberg University, Mainz, Germany.

⁷ University of Zurich, Institute of Molecular Life Sciences, Zurich, Switzerland.

⁸ Retinal Signal Processing Lab, Netherlands Institute for Neuroscience, Amsterdam, The Netherlands.

Published in *Experimental Eye Research*, 2018

doi: <https://doi.org/10.1016/j.exer.2018.05.015>

PMID: 29777677

ABSTRACT

Mutations in *USH2A* are the most frequent cause of Usher syndrome and autosomal recessive nonsyndromic retinitis pigmentosa. To unravel the pathogenic mechanisms underlying *USH2A*-associated retinal degeneration and to evaluate future therapeutic strategies that could potentially halt the progression of this devastating disorder, an animal model is needed. The available *Ush2a* knock-out mouse model does not mimic the human phenotype, because it presents with only a mild and late-onset retinal degeneration. Using CRISPR/Cas9-technology, we introduced protein-truncating germline lesions into the zebrafish *ush2a* gene (*ush2a^{mcc1}*: c.2337_2342delinsAC; p.Cys780GlnfsTer32 and *ush2a^{b1245}*: c.15520_15523delinsTG; p.Ala5174fsTer). Homozygous mutants were viable and displayed no obvious morphological or developmental defects. Immunohistochemical analyses with antibodies recognizing the N- or C-terminal region of the *ush2a*-encoded protein, usherin, demonstrated complete absence of usherin in photoreceptors of *ush2a^{mcc1}*, but presence of the ectodomain of usherin at the periciliary membrane of *ush2a^{b1245}*-derived photoreceptors. Furthermore, defects of usherin led to a reduction in localization of USH2 complex members, whirlin and *Adgrv1*, at the photoreceptor periciliary membrane of both mutants. Significantly elevated levels of apoptotic photoreceptors could be observed in both mutants when kept under constant bright illumination for three days. Electroretinogram (ERG) recordings revealed a significant and similar decrease in both a- and b-wave amplitudes in *ush2a^{mcc1}* as well as *ush2a^{b1245}* larvae as compared to strain- and age-matched wild-type larvae. In conclusion, this study shows that mutant *ush2a* zebrafish models present with early-onset retinal dysfunction that is exacerbated by light exposure. These models provide a better understanding of the pathophysiology underlying *USH2A*-associated RP and a unique opportunity to evaluate future therapeutic strategies.

INTRODUCTION

Usher syndrome is a rare genetic condition characterized by hearing impairment and a progressive loss of visual function as a consequence of Retinitis Pigmentosa (RP). The latter often results in legal blindness by the sixth decade of life (Sandberg et al., 2008). Currently there are no treatments for retinal degeneration in patients with Usher syndrome, although they benefit from hearing aids or cochlear implants. Usher syndrome is classified into three types (USH1, USH2 and USH3), varying in severity of hearing impairment, age at which RP is diagnosed, and presence or absence of vestibular dysfunction (Tazetdinov et al., 2008). Approximately two-thirds of USH patients present with USH2 (Millan et al., 2011), up to 85% of whom can be explained by mutations in *USH2A* (McGee et al., 2010; Yan and Liu, 2010). Mutations in *USH2A* are also the most frequent cause of autosomal recessive RP (arRP), accounting for 7-23% of arRP cases (McGee et al., 2010). Approximately 600 different, mostly private, mutations are evenly distributed over the gene and include point-nonsense, frame-shift, splice-modulating, and missense variants⁶. However, there are a number of mutations that originate from a common ancestor and are therefore observed more frequently (Aller et al., 2010; Baux et al., 2014; Pennings et al., 2004). The two most commonly found *USH2A* mutations are c.2299delG; p.Glu767fs and c.2276G>T; p.Cys759Phe, both residing in exon 13. Bi-allelic truncating defects of *USH2A* (nonsense mutations, frameshift mutations, or mutations that affect splicing), most often result in USH2, whereas the presence of at least one hypomorphic *USH2A* allele generally results in non-syndromic arRP (Lenassi et al., 2015). The distribution of known mutations and neutral variants from the LOVD database for *USH2A* does not reveal a particular mutation tolerant or intolerant region of the gene that could pinpoint particularly important functional domains (Baux et al., 2014). Despite ongoing efforts, little is known about either the physiological role(s) of the usherin protein in photoreceptors or the pathophysiological mechanism underlying *USH2A*-associated RP (Hartong et al., 2006; McGee et al., 2010).

The *USH2A* transcript in retina consists of 72 exons and encodes a protein of 5,202 amino acids (usherin) (Adato et al., 2005; van Wijk et al., 2004). Moreover, a cochlea-specific exon has been identified between exons 70 and 71 that encodes 24 additional amino acids (Adato et al., 2005). Usherin contains an N-terminal signal peptide, a Lam-G like domain, a LamNT domain, 10 EGF-lam domains, 4 FN3 domains, two laminin G (LamG) domains, 28 FN3 domains, a transmembrane domain, and a short intracellular region with a C-terminal class I PDZ-binding motif. It is generally thought that usherin has a structural role at the periciliary region of the photoreceptor, where it is held in place via its interactions with harmonin (*USH1C* encoded), SANS (*USH1G* encoded) and whirlin (*WHRN* encoded, USH2d) (Chen et al., 2014; Reiners et al., 2005; Sorusch et al., 2017; van Wijk et al., 2006; Yang et al., 2010; Zou et al., 2011). At the periciliary region,

usherin possibly stabilizes the photoreceptor connecting cilium by an extracellular interaction with Adhesion G protein-coupled receptor V1 (ADGRV1; previously known as GPR98 or VLGR1) (Adato et al., 2005; Liu et al., 2007; Maerker et al., 2008; Overlack et al., 2011).

Understanding the molecular mechanisms underlying photoreceptor dysfunction in *USH2A*-associated RP and the development of treatment strategies have been severely hampered by the absence of suitable cellular or animal models mimicking the human phenotype. Although mutant mouse models are commonly used to study RP and test therapeutic strategies, for USH and several other types of RP the retinal phenotypes in mouse models do not mimic that of patients with defects in the orthologous genes (Slijkerman et al., 2015). In contrast, retinal dysfunction from a very young age is observed in zebrafish *USH1* gene mutants (Blanco-Sanchez et al., 2017). Zebrafish larvae lacking *Myo7aa* (*USH1b*), harmonin (*USH1c*) or *Pcdh15b* (*USH1f*) function show reduced electroretinogram (ERG) traces by 5 to 7 days post fertilization (dpf) (Phillips et al., 2011; Seiler et al., 2005; Wasfy et al., 2014). Additionally, photoreceptor-specific degeneration has been shown to occur in *ush2a* depleted morphant larvae (Ebermann et al., 2010) as well as in *myo7aa* mutant larvae exposed to elevated light levels (Wasfy et al., 2014).

In this study, we generated and characterized two *ush2a* mutant zebrafish models (*ush2a^{rmc1}*: c.2337_2342delinsAC; p.Cys780GlnfsTer32 and *ush2a^{b1245}*: c.15520_15523delinsTG; p.Ala5174fsTer) to study usherin function in the retina. Subsequent functional analyses showed that usherin is absent from photoreceptors in *ush2a^{rmc1}*, but that the extracellular domain of usherin can still be detected at the periciliary membrane of *ush2a^{b1245}*-derived photoreceptors. The levels of usherin interaction partners *Whrna* and *Whrnb* (*whirlin*) are reduced at the photoreceptor periciliary membrane of homozygous *ush2a^{rmc1}* larvae, whereas in homozygous *ush2a^{b1245}* larvae only the level of *Whrna* is affected. Furthermore, mutant zebrafish display elevated levels of apoptotic cells in the outer retina as compared to strain and age-matched wild-type zebrafish upon constant light rearing. We further found that ERG traces are notably attenuated in both mutants, indicating impaired outer retinal function. These mutants are the first genetic animal models for *ush2a* that present with early-onset retinal dysfunction.

MATERIALS AND METHODS

Zebrafish maintenance and husbandry

Experimental procedures were conducted in accordance with international and institutional guidelines (Dutch guidelines, protocol #RU-DEC 2012-301; Swiss guidelines, Veterinäramt Zürich TV4206 and University of Oregon IACUC guidelines). Wild type adult Tupfel Long fin (TLF) or Oregon AB* zebrafish were used. The zebrafish eggs were

obtained from natural spawning of wild-type or mutant breeding fish. Larvae were maintained and raised by standard methods (Kimmel et al., 1995).

CRISPR/Cas9 design and microinjection

For the *ush2a^{rmc1}* allele, oligos for generating guide RNAs were designed using the ZiFiT targeter software (Sander et al., 2007). Oligos were subsequently ordered from Integrated DNA Technologies. Annealing of oligos was performed in a buffer (1 M NaCl, 10 mM EDTA and 100 mM Tris-HCl pH7.5) by incubation at 90°C for four minutes, followed by a ten minute-incubation step at 70°C and gradual cooling (5°C per two minutes) to 16°C. The annealed oligos were immediately ligated into the a BsaI (New England Biolabs, #R0535S) linearized pDR271 vector (Addgene plasmid #42250) using T4 ligase (New England Biolabs, #M0202). The oligo and surrounding sequences were excised from the pDR274 vector using DraI (New England Biolabs, #R0129S). The excised DNA band (284 basepairs) was subsequently used as a template for *in vitro* transcription using the MAXIscript® T7 Transcription Kit (Ambion life technologies, #AM1314) according to the manufacturer's protocol. Obtained transcripts were purified using the MEGAclean™ Transcription Clean-Up Kit (Ambion life technologies, #AM1908). For the *ush2a^{b1245}* allele, gene specific oligos were designed by flanking the 20 bp target sequence with T7 promoter and gRNA sequence: 5'-AATTAATACGACTCACTATA-[20 bp Target Sequence]-GTTT TAGAGCTAGAAATAGC-3'. The templates for gRNA syntheses were PCR amplified using the gene specific oligo with a gRNA scaffolding primer: 5'-GATCCGCACCGACTCGGTGCCACTTTTTCAAGTTGATAACGGACTAGCCTTATTTAACTTGCTATTTCTAGCTCTAAAC-3'. As input 13.4 µl water, 4ul 5x Phusion DNA polymerase buffer, 0.4 µl dNTPs (10 µM), 1 µl of gene specific oligo (10 µM), 1 µl of gRNA scaffold oligo (10 µM), 0.2 µl Phusion DNA polymerase. The cycling conditions were as follows: 98°C 30 seconds, 40 cycles of 98°C 10 seconds, 60°C 10 seconds, 72°C 15 seconds and 72°C 10 minutes. PCR products were column purified and used to prepare gRNA with the Ambion T7 megascript kit (AM1344) as per manufacturer's instructions. A zebrafish codon-optimized Cas9 containing vector (pT3TS-nCas9n; Addgene plasmid #46757) was used to generate Cas9 mRNA. The vector was linearized using XbaI (NEB, #R0145S) and used as a template for an *in vitro* transcription reaction using the mMESSAGING mMACHINE® T3 Transcription Kit (Ambion life technologies, #AM1348) according to manufacturer's instructions. Transcripts were purified using the MEGAclean™ Transcription Clean-Up Kit (#AM1908). Zebrafish embryos at a 1-cell stage were injected with 1 nl of a mixture containing gRNA (6 ng/µl), Cas9 mRNA (150 ng/µl), KCl (0.2 M) and phenol red (0.05%) using a Pneumatic PicoPump pv280 (World Precision Instruments) for the generation of the *ush2a^{rmc1}* allele. To generate the *ush2a^{b1245}* allele, one-cell stage zebrafish embryos were injected with 1 nl of a mixture containing gRNA (100 ng/µl), Cas9 mRNA (150 ng/µl), KCl (0.2 M) and phenol red (0.05%) using an MPPI-2 Pressure Injector with a BP-15

Back Pressure Unit (Applied Scientific Instrumentation, Oregon USA). After injection, embryos were raised at 28.5°C in E3 embryo medium (5 mM NaCl, 0.17 mM KCl, 0.33 mM CaCl₂, 0.33 mM MgSO₄), supplemented with 0.1% (v/v) methylene blue. At 2.5 days post fertilization, part of the injected embryos were analyzed for the presence of desired mutational events. When mutations could be detected, the remainder of injected embryos was raised.

Genotyping

Genomic DNA was isolated from pools of 15 larvae after incubation in 75 µl lysis buffer (10 mM Tris HCl pH=8.2, 10 mM EDTA, 100 mM NaCl and 0.5 % SDS) supplemented with freshly added proteinase K (final concentration of 0.20 mg/ml, Invitrogen #25530049) at 55°C for two hours. The isolated genomic DNA was subsequently used as a template in a PCR. Primers used for the amplification of *ush2a* exon13 are 5'-TC-CACCAACAGAATCTAAATCTTTC-3' and 5'-CTGATTTGTAAATGGTGTGGG-3' and primers used for the amplification of *ush2a* exon71 are 5'-CATGTTTTGGTTATCTGTTCTTCT-3' and 5'-GACAGCGGAATGGTGAGATAAAC-3'. The obtained amplicons were cloned into a pCR®4-TOPO® vector (Invitrogen, #450030) according to manufacturer's instructions. Individual clones were analyzed for the presence of mutational events using the ABI PRISM Big Dye Terminator Cycle Sequencing V2.0 Ready Reaction kit and the ABI PRISM 3730 DNA analyzer (Applied Biosystems).

Transcript analysis

Pools of 15 larvae were snap frozen in liquid nitrogen and subsequently homogenized in 500 µl QIAzol (Qiagen, #79306) using a 25 gauge 16 mm needle. Total RNA was isolated using phenol:chloroform extraction and precipitated using isopropanol. Extracted total RNA was further purified and DNase treated using a NucleoSpin® RNA II Isolation kit (Macherey-Nagel, #740955.50, Düren, Germany) according to manufacturer's protocol. Subsequently, 0.5-1.0 µg of total RNA was used as a template for cDNA synthesis using SuperScript III RT (Life Technologies, #11755050, Carlsbad (California) - United States). An *ush2a* amplicon (1096 bp) of homozygous *rmc1* larvae was amplified using with primers located in exon11 (5'-AGCGCTGTCGGAGTCTCTTC-3') and exon14 (5'-CCATCACTGACCGGTACAG-3'). An *ush2a* amplicon (710 bp) of homozygous *b1245* larvae was amplified using primers located in exon68 (5'-TGGACTGGAGTGGCTCTTTC-3') and exon73 (5'-GATGAGGACTTTGGAGAGACCA-3').

Antibodies and Immunohistochemistry

Dissected adult eyes (12-18 mpf) and larval zebrafish (4-6 dpf) from homozygous *ush2a^{rmc1}* and *ush2a^{b1245}* mutants and their age and strain-matched wild-type controls were cryoprotected with 10% sucrose in PBS for 30 minutes prior to embedding in

OCT compound (Tissue-Tek, 4583, Sakura). After embedding, samples were slowly frozen down using melting isopentane. To assess retinal morphology, cryosections (seven μm thickness along the lens/optic nerve axis) were fixed for 10 minutes with paraformaldehyde (PFA) 4%, stained with hematoxylin and eosin and analysed on a Zeiss Axioskop light microscope. For analysis by scanning confocal microscope, embryos were fixed in 4% PFA overnight at 4°C, washed 3x in PBS-T, dehydrated in 100% methanol, rehydrated in descending methanol series and washed several times in PBS-T before being cryoprotected in 30% sucrose for several hours at room temperature. Larvae were then embedded in molten agarose blocks, frozen, and sectioned on a cryomicrotome. For immunofluorescence on unfixed cryosections (seven μm thickness) were permeabilised for 20 minutes with 0.01% Tween20 in PBS. Sections were rinsed 3 times for 5 minutes with PBS and blocked for 1 hour with blocking buffer (10% normal goat serum and 2% bovine serum albumin in PBS). Antibodies diluted in blocking buffer were incubated overnight at 4 °C. Secondary antibodies were also diluted in blocking buffer and incubated together with DAPI (1:8000; D1306; Molecular Probes) for 1 hour. Sections were post fixed with PFA 4% for 10 minutes and mounted with Prolong Gold Anti-fade (P36930; Molecular Probes). For immunofluorescence on fixed cryosectioned tissue (16 μm thickness), slides were hydrated 10 minutes in PBS-T, then immersed in Sodium Citrate solution at pH 8.5 and heated in a pressure cooker for 10 minutes. After cooling to 37°C, slides were washed twice in PBS-T, blocked in 10% NFDm in PBS-T and incubated with primary antibodies. The following primary antibodies and dilutions were used: rabbit anti-active caspase 3 (1:500; #559565; BD Pharmingen), rabbit anti-Whrn (1:300; #42690002 Cip98a; Novus Biological), rabbit anti-Whrna (1:300; #42700002 Cip98b; Novus Biological), rabbit anti-usherin-C (1:500; #27640002; Novus Biological), rabbit anti-Adgrv1 (1:1000) (Ebermann et al., 2010) and as marker for connecting cilium region in photoreceptor cells we used mouse anti-centrin (1:500; # 04-1624; Millipore) or acetylated α -tubulin (Sigma T7451). Secondary antibodies (Alexa Fluor 568 goat anti-rabbit (A11011), Alexa Fluor 488 goat anti-guinea pig (A11073) and Alexa Fluor 488 goat anti-mouse (A11029)), derived from Molecular Probes, were used in a 1:800 dilution. Images were taken using a Zeiss Axio Imager fluorescence microscope equipped with an AxioCam MRC5 camera (Zeiss) or a Zeiss LSM5 Confocal. The intensity of Whrna and Whrn immunofluorescence was measured in FIJI version 1.47v⁵⁸. First, the outer segment layer was isolated based on the centrin immunostaining. Subsequently, a mask was made based on the centrin staining using the "Find Maxima" option (noise=50), and dilated five times. To find the exact location of Whrna or Whrn staining, the centrin mask and Whrn layer were combined. Find Maxima (noise=10) was used to identify the Whrn staining within the Centrin mask. The resulting mask was dilated three times and touching objects were separated using the watershed option. Subsequently, the maximum gray value of the identified regions was measured on the original image of Whrn

immunofluorescence (Analyze Particles option; size=0-50, pixel circularity=0.00-1.00). Active caspase-3 labeled cells were analyzed on a Zeiss fluorescence microscope by manually counting positively stained cells in the ONL.

Constant light rearing

For constant light treatment, embryos were raised in transparent 10-cm petri dishes under normal conditions and were placed under constant light from 5-8 dpf. From 5 dpf onwards, *ush2a^{rmc1}* larvae were either maintained in facility conditions of 300 lux white light in a 14/10h day/night rhythm or were exposed to continuous white light with an intensity of 3000 lux, using a 150 W LED light source (Zeiss). *ush2a^{b1245}* larvae were either maintained in facility conditions of 300 lux white light in a 14/10h day/night rhythm or were exposed to continuous white light with an intensity of 3000 lux using two LED strips (Westek) mounted in parallel. Light input: 12V DC, transformer input 120V ~60Hz, transformer output 12V DC, 6W max. Light intensities were measured at water level using a lumino meter (Testo 540, Lenzkirch, Germany or Advanced Light Meter 840022, Sper Scientific, Arizona, USA).

Fixation and pre-embedding labeling for immunoelectron microscopy

For immunoelectron microscopy of adult zebrafish retinas, we followed the previously published protocol for pre-embedding labeling (Maerker et al., 2008; Sedmak et al., 2009; Sedmak and Wolfrum, 2010). In brief, rabbit anti-usherin C (1:500; #27640002; Novus Biological) was applied on vibratome sections of pre-fixed (4% PFA) murine eye-cups, followed by incubation with biotinylated secondary antibodies. Antibody reactions were visualized by a Vectastain ABC-Kit (Vector Laboratories) and 0.01% hydrogen peroxide to 0.05 M diaminobenzidine (DAB) solution was added. Stained retinas were fixed in 2.5% glutaraldehyde in 0.1 M cacodylate buffer (pH 7.4), followed by silver enhancement of DAB precipitates and post-fixation in cacodylate buffered 0.5% OsO₄ on ice. Dehydrated specimens were flat-mounted between two sheaths of ACLAR-films (Ted Pella Inc., Redding, USA) in Araldite resin. Ultrathin sections were made using a Reichert Ultracut S ultramicrotome (Leica), collected on Formvar-coated copper or nickel grids and counterstained with 2% uranyl acetate in 50% ethanol and aq. 2% lead citrate. Ultrathin sections were analysed in a Tecnai 12 BioTwin transmission electron microscope (FEI, Eindhoven, The Netherlands). Images were obtained with a CCD camera (charge-coupled-device camera; SIS MegaView3; Surface Imaging Systems, Herzogenrath, Germany) and processed with Adobe Photoshop CS (Adobe Systems).

Electroretinogram (ERG) recordings

ERG recordings were performed on isolated larval eyes (5-7 dpf) as previously described (Sirisi et al., 2014). Larvae were dark-adapted for a minimum of 30 min prior to

the measurements and subsequently handled under dim red illumination. The isolated eye was positioned to face the light source. Under visual control via a standard microscope equipped with red illumination (Stemi 2000C, Zeiss, Oberkochen, Germany), the recording electrode with an opening of approximately 20 μm at the tip was positioned at the center of the cornea. This electrode was filled with E3 embryo medium (5 mM NaCl, 0.17 mM KCl, 0.33 mM CaCl₂, and 0.33 mM MgSO₄). The electrode was positioned using a micromanipulator (M330R, World Precision Instruments Inc., Sarasota, USA). A custom-made stimulator was invoked to provide light pulses of 100 ms duration, with a light intensity of 6000 lux. It uses a ZEISS XBO 75W light source and a fast shutter (Uni-Blitz Model D122, Vincent Associates, Rochester, NY, USA) driven by a delay unit interfaced to the main ERG recording setup. Electronic signals were amplified 1000 times by a pre-amplifier (P55 A.C. Preamplifier, Astro-Med. Inc, Grass Technology) with a band pass between 0.1 and 100 Hz, digitized by DAQ Board NI PCI-6035E (National Instruments) via NI BNC-2090 accessories and displayed via a self-developed NI Labview program (Rinner et al., 2005). Statistical analysis was performed using SPSS Statistics 22 (IBM) All the experiments were performed at room temperature ($\sim 22^\circ\text{C}$).

Statistical analyses

The Graphpad Prism software (version 5.03 for Windows, GraphPad Software, La Jolla California USA, www.graphpad.com) was used to generate scatter plots, calculate mean values, and perform statistical analysis using two-tailed unpaired Student's t-tests or two-tailed Mann-Whitney tests.

RESULTS

Zebrafish and human usherin are highly conserved

Bioinformatic analyses of the zebrafish and human usherin protein sequence revealed that the proteins have a high degree of sequence similarity (52% identity; 68% similarity) and share a similar protein domain architecture (**Fig. 1**). We characterized the subcellular localization of usherin in the zebrafish retina with an antibody directed against the intracellular C-terminal region of usherin (anti-usherin-C). In adult zebrafish retina, usherin is not only present at the periciliary membrane of both cones and rods, but also apical to the cone connecting cilium (**Fig. 2A, B, C** and **Supplemental Fig. 1**). Subsequent immunoelectron microscopy identified these structures as cone accessory outer segments (AOS) (**Fig. 2D, E**). AOS are structures that run along the photoreceptor outer segment and are predominantly found in cone photoreceptors of adult frogs and teleost fish (Januschka et al., 1987).

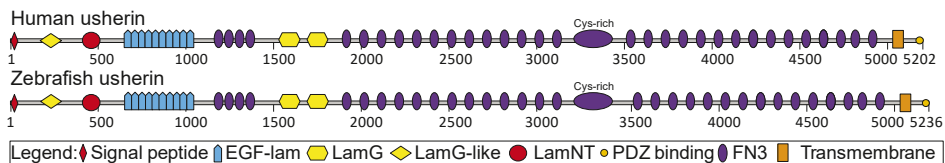


Figure 1. Schematic presentation of zebrafish usherin. Motif alignment of human and zebrafish usherin. Both proteins have an identical predicted domain architecture. EGF-lam, laminin-type epidermal growth factor-like domain; LamG, laminin G domain; LamG-like, LamG-like jellyroll fold domain; LamNT, laminin N-terminal domain; FN3, fibronectin type 3 domain.

Generation of zebrafish *ush2a^{rmc1}* and *ush2a^{b1245}* mutants

Using CRISPR/Cas9 technology, we generated two *ush2a* mutant alleles (sequences in **Supplemental Fig. 3**). *ush2a^{rmc1}* contains a frameshift mutation in *ush2a* exon13 (c.2337_2344delinsAC; p.Cys780GlnfsTer32), that is predicted to result in the premature termination of translation of usherin (**Fig. 3A**). *ush2a^{b1245}* harbors a frameshift mutation in *ush2a* exon71 (ENSDART00000086201.4; c.15520_15523delinsTG; p.Ala5174fsTer), predicted to encode an usherin protein that retains the transmembrane domain but lacks the C-terminal 62 amino acids of the intracellular region including the class I PDZ binding motif. This allele provides an opportunity to assess the functional importance of the intracellular region, including the PDZ-binding motif, relative to the ectodomain of usherin (**Fig. 3A**). Both homozygous mutants were viable and no abnormalities in morphology, development, or swimming behavior were observed.

ush2a^{rmc1} and *ush2a^{b1245}* do not affect *ush2a* pre-mRNA splicing

In patient-derived fibroblasts, the *USH2A* c.2299delG mutation results in skipping of *USH2A* exon12 and exon13 in some transcripts, or in skipping of exon13 only (Lenassi et al., 2014). Recent studies showed that CRISPR/Cas9-induced exonic lesions could also induce an (in-frame) skipping of the targeted exon thereby preventing generation of a functional knock-out model (Mou et al., 2017). If the lesion introduced in the *ush2a^{rmc1}* mutant causes an in-frame skipping of exon 13, this could potentially result in expression of a shortened usherin with residual function. Similarly, the c.15520_15523delinsTG (*ush2a^{b1245}*) mutation is predicted to disrupt an exonic splice enhancer site and potentially induce skipping of exon71, thereby also leaving the *ush2a* open reading frame intact. We, thus, analyzed *ush2a* transcripts in homozygous *ush2a^{rmc1}* and *ush2a^{b1245}* larvae to assess whether the introduced lesions would result in alternative *ush2a* pre-mRNA splicing events. Amplicons spanning exon13 or exon71 and their surrounding exons were amplified by RT-PCR. Because no alternatively spliced *ush2a* transcripts were amplified from cDNA derived from homozygous *ush2a^{rmc1}* or *ush2a^{b1245}* larvae (**Fig. 3B, C**), we expect that the introduced mutations in the *rmc1* and *b1245* alleles result in premature termination of usherin translation.

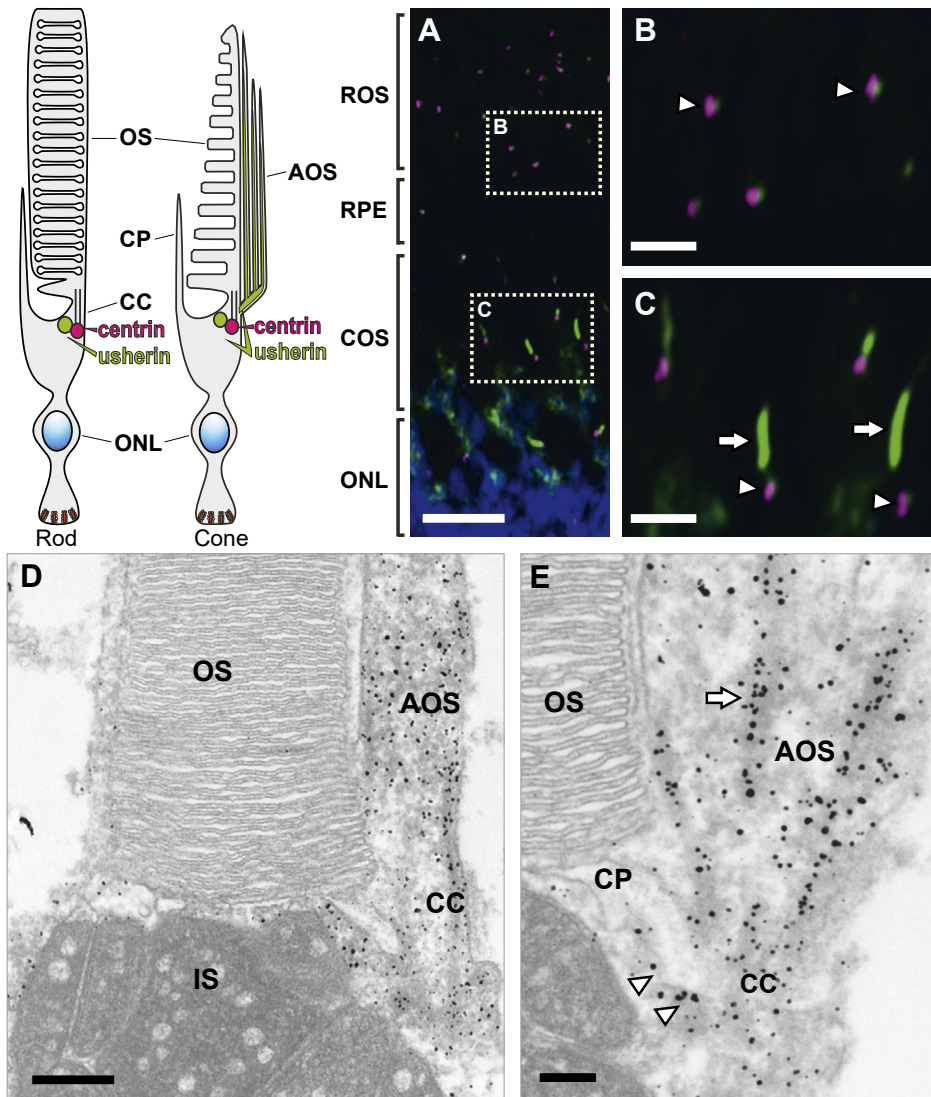


Figure 2. Usherin localizes at the periciliary membrane and accessory outer segments of adult zebrafish photoreceptor cells. (A) Retinal sections of wild-type adult zebrafish are labeled for usherin (green signal) and the connecting cilium marker centrin (magenta signal). (B) Usherin labeling at the periciliary region of rod photoreceptors is present adjacent to the connecting cilium marked by centrin (indicated by an arrow head). (C) In cones, usherin is also detected at the periciliary region (arrow heads) as well as apical to the connecting cilium marked by centrin labeling (arrows). Nuclei were stained with DAPI (blue signal). (D, E) Electron microscopy images of adult zebrafish retinas show that usherin localizes at the periciliary membrane (arrowheads) as well as in the accessory outer segments (AOS; arrow) of cone photoreceptors. Scale bars in A: 10 μm ; B: 3 μm ; C: 3 μm ; D: 1 μm ; E: 0.1 μm . CC: connecting cilium, COS: cone outer segment, CP: calyceal processes, ONL: outer nuclear layer, OS: outer segment, ROS: rod outer segment, RPE: retinal pigment epithelium.

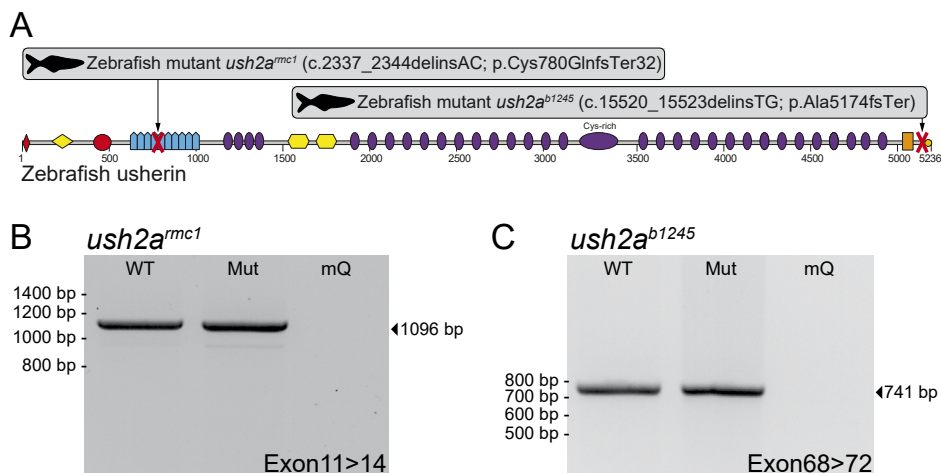


Figure 3. *ush2a* transcript analyses in homozygous *ush2a^{rmc1}* and *ush2a^{b1245}* mutant zebrafish. (A) The locations of the mutations in *ush2a^{rmc1}* and *ush2a^{b1245}* are schematically depicted. (B) RT-PCR analyses of *ush2a* transcripts derived from homozygous *ush2a^{rmc1}* or (C) homozygous *ush2a^{b1245}* larvae (5 dpf) provided no indications for an effect of the introduced lesions on pre-mRNA splicing. WT: wild-type, Mut: homozygous mutant, mQ: milliQ water.

Ush2a^{rmc1} leads to absence of usherin, whereas *ush2a^{b1245}* results in truncated usherin at the periciliary region

Using zebrafish-specific anti-usherin antibodies directed against the N- or C-terminus of the protein, we evaluated the presence of usherin in the retina of homozygous *ush2a^{rmc1}* and *ush2a^{b1245}* larvae and strain-matched (TLF or AB*, respectively) wild-type larvae at 5 dpf. Anti-usherin-N is directed against an amino acid sequence present at the N-terminus of usherin. In wild-type larvae, both antibodies detected usherin adjacent to the basal body and connecting cilium marker, centrin (**Fig. 4**). In contrast, no usherin signal was detected in the retina of *ush2a^{rmc1}* mutant larvae using either anti-usherin antibody. Also in the retina of *ush2a^{b1245}* larvae, no signal was detected when using anti-usherin-C antibodies (**Fig. 4A, B**). However, a signal at the photoreceptor periciliary region of homozygous *ush2a^{b1245}* larvae was obtained when using anti-usherin-N antibodies. These results suggest that the truncated usherin protein still localizes appropriately at the membrane even though it lacks the C-terminal intracellular region and the PDZ binding motif (**Fig. 4A, B**). We conclude that *ush2a^{rmc1}* mutants completely lack usherin at the photoreceptor periciliary region and the mutation should be considered a true null allele, whereas *ush2a^{b1245}* should be considered a hypomorphic allele with potential residual function.

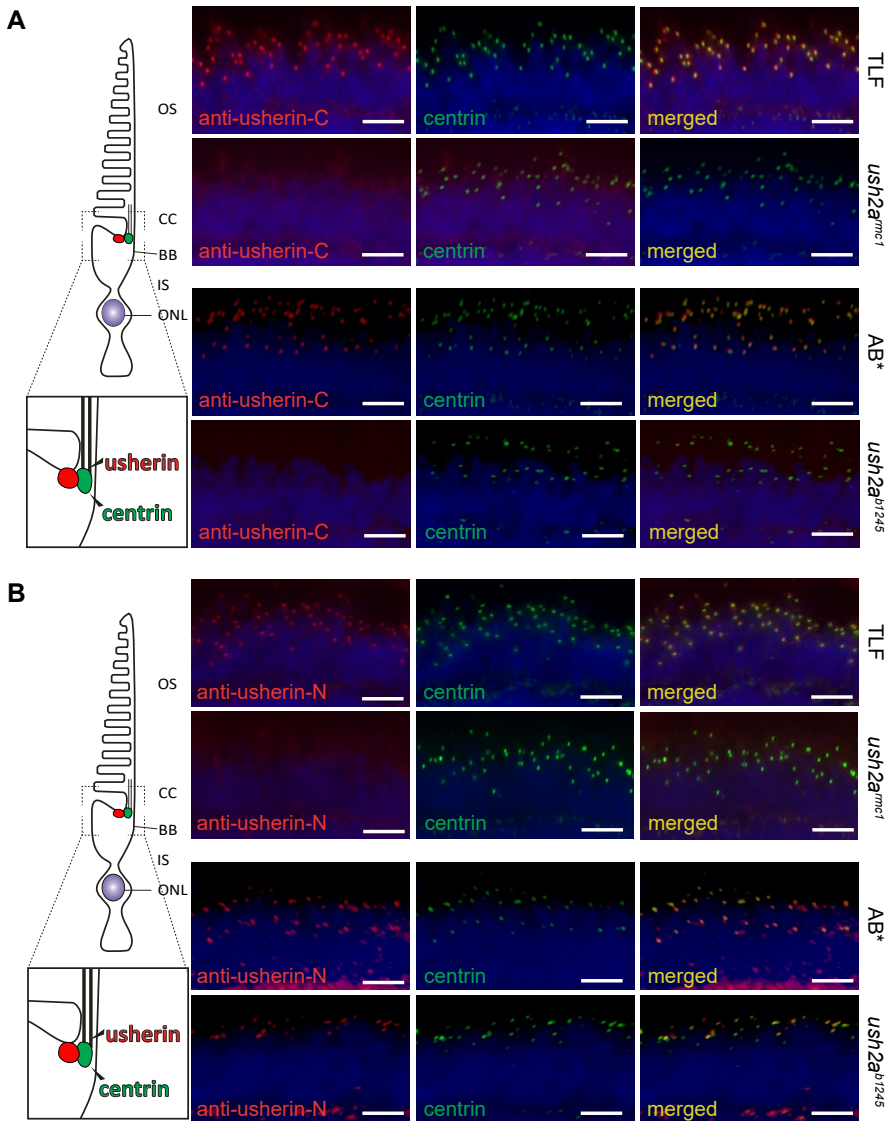


Figure 4. Localization of usherin in frontal cryosections of wild-type and mutant zebrafish retinas (5 dpf). Zebrafish-specific anti-usherin-C (**A**) or anti-usherin-N (**B**) antibodies are employed (red signal). (**A**) In *ush2a^{mc1}* as well as *ush2a^{b1245}* homozygous mutant larvae no signal was detected with the anti-usherin-C antibody, whereas in both TLF and AB* wild-type controls usherin was present adjacent to the connecting cilium marked by centrin (green signal). (**B**) No signal was detected in the retina of homozygous *ush2a^{mc1}* mutants using the anti-usherin-N antibody, however, a signal at the photoreceptor periciliary region was observed in the retina of homozygous *ush2a^{b1245}* larvae when this antibody was used. In wild-type controls, the anti-usherin-N antibody also detected usherin at the photoreceptor periciliary region. (n= 35 larvae, from 5 biological replicates with TLF and *ush2a^{mc1}* larvae, n= 64, from 8 biological replicates with AB* and *ush2a^{b1245}* larvae). Nuclei are stained with DAPI (blue signal). Scale bars: 10 μ m.

Ablation of usherin affects the localization of Whrna and Whrnb in the retina

Human usherin was previously shown to interact directly with whirlin *in vitro* (van Wijk et al., 2006). The biological relevance of this interaction was confirmed by the absence of whirlin at the photoreceptor periciliary membrane of *Ush2a* knock-out mice (Yang et al., 2010). Here, we determined whether or not whirlin localization was also affected in the retina of homozygous *ush2a^{rmc1}* and *ush2a^{b1245}* zebrafish larvae (5 dpf). The zebrafish genome harbors two whirlin-encoding orthologs. *whrna* (previously known as *dfnb31a* (ENSDARG00000075362)) encodes Whrna and *whrnb* (previously known as *dfnb31b* (ENSDARG00000068166)) encodes Whrnb. Whrna was found to be located at the photoreceptor periciliary region in wild-type larvae (**Fig. 5A** and **Supplemental Fig. 2**). Reduced intensity of the Whrna signal was observed in the retinas of homozygous larvae of both *ush2a* mutants, which was further confirmed by quantification of fluorescence signal intensities (**Fig. 5A**). The same results were observed in homozygous *ush2a^{rmc1}* larvae when an anti-Whrnb antibody was employed (**Fig. 5B** and **Supplemental Fig. 2**). In contrast, the intensity of the Whrnb signal was unaltered in photoreceptors of homozygous *ush2a^{b1245}* larvae as compared to AB* wild-type larvae (**Fig. 5B**).

Zebrafish *ush2a* mutants exhibit elevated levels of photoreceptor apoptosis

Based on the assumption that usherin is required for long-term maintenance of photoreceptor cells, we assessed whether absence of usherin in the zebrafish retina would lead to increased levels of apoptosis in the outer nuclear layer (ONL). Larvae were raised under a 14/10 hours light/dark cycle until 5 dpf. After 5 dpf, they were either raised for an additional 72 hours in regular facility conditions of 300 lux light intensity of a 14hr/10hr light/dark cycle, or exposed to constant light with an intensity of 3000 lux for 72 hours. A slight but significant increase in the amount of apoptotic photoreceptor cells was observed in 8 dpf *ush2a^{rmc1}* larvae raised in normal facility conditions (**Fig. 6A**). These results were consistent with our previously reported data on photoreceptor degeneration in larvae treated with a morpholino targeting an early splice junction in *ush2a* (Ebermann et al., 2010). Subsequently, we assessed the number of apoptotic events in *ush2a^{b1245}* mutant larvae. No significantly elevated levels of cell death in the ONL were observed when these larvae were raised under normal facility conditions (**Fig. 6B**). Constant light rearing with an elevated light intensity of 3000 lux significantly increased the amount of apoptotic cells in the ONL of both mutant alleles as compared to their strain-matched wild-type controls (**Fig. 6A, B**). Variations in the genetic backgrounds of the *rmc1* and *b1245* alleles, variances in the light sources used in the elevated light exposure assay, and other environmental differences between the two facilities where these experiments were conducted could contribute to the observed difference in the absolute number of apoptotic cells.

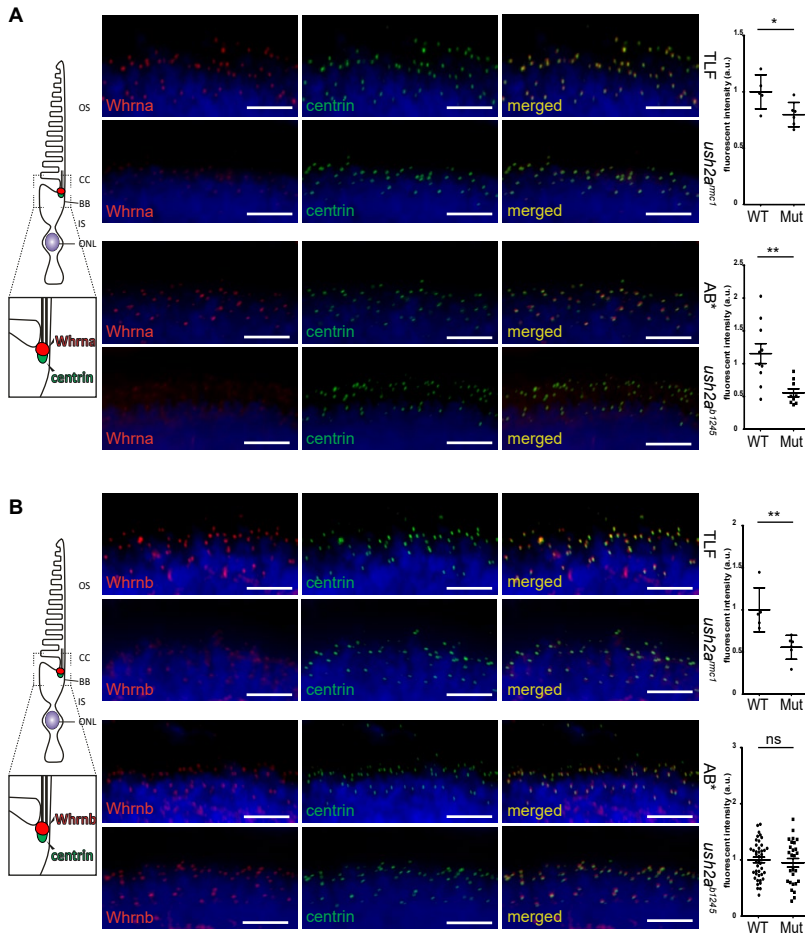


Figure 5. Ablation of usherin affects the localization of Whrna and Whrnb in the zebrafish retina (5 dpf). (A) Intensity of Whrna labeling was significantly reduced in both *ush2a^{mc1}* and *ush2a^{b1245}* mutants as compared to corresponding wild-types (n=35 larvae from 5 biological replicates with *ush2a^{mc1}* mutant larvae and TLF larvae, and n=54 larvae from 7 biological replicates with *ush2a^{b1245}* mutant larvae and AB* larvae). Intensities of fluorescence using antibodies directed against Whrna (red signal) were quantified and plotted as scatter plots next to the corresponding images. Each dot represents the average grey-value per eye (n=5 *ush2a^{mc1}* eyes and n=6 TLF larvae eyes, $p < 0.05$ and n=10 *ush2a^{b1245}* and n=9 AB* eyes, $p < 0.01$, two-tailed unpaired Student's *t*-test). (B) Whrnb labeling was reduced in *ush2a^{mc1}* mutants, but unaltered in *ush2a^{b1245}* mutants compared to corresponding wild-types (n=35 larvae from 5 biological replicates with *ush2a^{mc1}* mutant larvae and TLF larvae, and n=54 larvae from 7 biological replicates with *ush2a^{b1245}* mutant larvae and AB* larvae). Intensity of Whrnb labeling (red signal) was significantly reduced in *ush2a^{mc1}* larvae as compared to wild-type (TLF) larvae (n=5 *ush2a^{mc1}* eyes and n=6 TLF eyes, $p < 0.01$, two-tailed unpaired Student's *t*-test). In *ush2a^{b1245}* larvae, the intensity of Whrnb labeling appeared unaltered as compared to wild-type (AB*) larvae (n=27 eyes for both *ush2a^{b1245}* and AB* wild-type; $p = 0.57$, two-tailed unpaired Student's *t*-test). Nuclei were stained with DAPI (blue signal) and anti-centrin (green signal) was used as a marker for the connecting cilium. Scale bars: 10 μm , dpf: days post fertilization, a.u.: arbitrary units, * indicates $p < 0.05$, ** indicates $p < 0.01$, and ns: not significant.

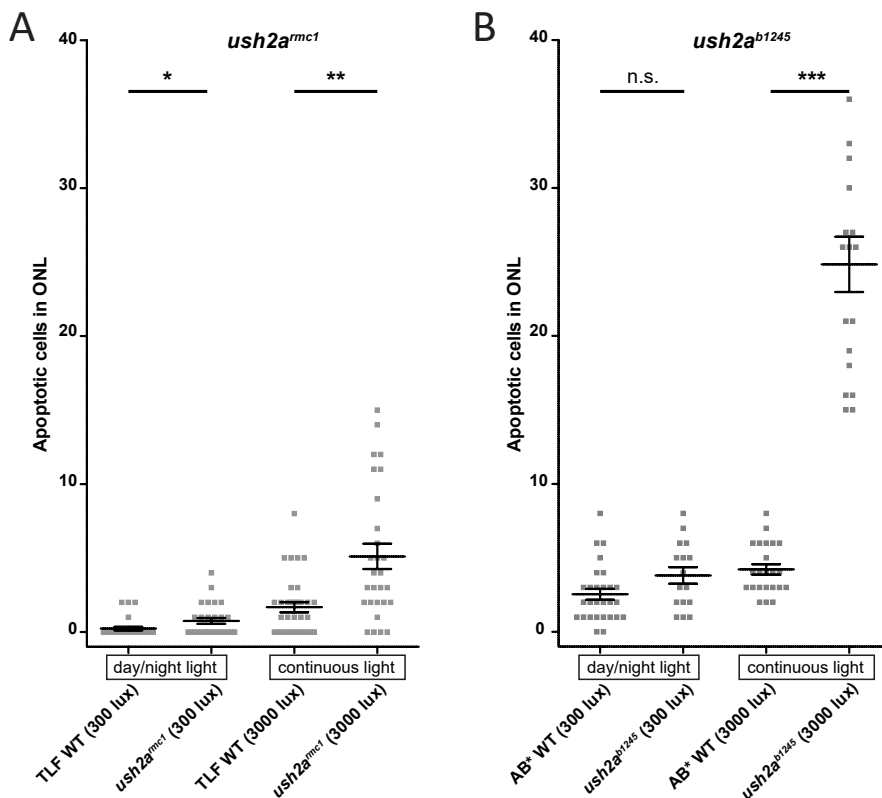


Figure 6. Quantification of apoptotic events in the ONL of zebrafish *ush2a* mutants (8 dpf). Homozygous *ush2a^{mnc1}* and *ush2a^{b1245}* larvae were exposed either to 300 lux in a (14/10h) day/night rhythm or to continuous light at 3000 lux from 5-8 dpf. Individual dots represent the number of apoptotic cells in the ONL per eye. Strain matched wild-type TLF or AB* zebrafish were used as controls. **(A)** TLF and *ush2a^{mnc1}* larvae kept at 300 lux with a day/night cycle showed on average 0.2 (\pm 0.1; 30 eyes) and 0.8 (\pm 0.2; 28 eyes) apoptotic cells per eye, respectively ($p < 0.05$). When kept under 3000 lux of continuous light, 1.7 (\pm 2.0; 34 eyes) and 5.1 (\pm 4.5; 28 eyes) apoptotic cells per eye were observed in TLF and *ush2a^{mnc1}*, respectively ($p < 0.01$). **(B)** AB* and *ush2a^{b1245}* larvae maintained at 300 lux with a day/night cycle showed on average 2.5 (\pm 1.9; 28 eyes) versus 3.8 (\pm 2.3; 16 eyes) apoptotic cells per eye, respectively (n.s.). When kept under 3000 lux of continuous light, on average 4.2 (\pm 1.7; 23 eyes) versus 24.8 (\pm 7.9; 18 eyes) apoptotic cells per eye were observed in AB* and *ush2a^{b1245}*, respectively ($p < 0.0001$). Each point represents the number of apoptotic cells in the ONL per eye and the standard error of the mean are given as error bars. * indicates $p < 0.05$, ** indicates $p < 0.01$, *** indicates $p < 0.0001$, n.s.: not significant (two-tailed Mann-Whitney test); ONL: outer nuclear layer; dpf: days post fertilization.

Because significantly elevated levels of apoptotic events were seen in the ONL of *ush2a^{mnc1}* mutant larvae when kept at facility conditions, we examined whether retinal degeneration was progressive under these conditions. Retinal histology was analyzed for both homozygous *ush2a* mutants at 5 dpf and at 18 months of age, which revealed

that cellular organization and retinal lamination in mutants was indistinguishable from those in wild-type controls. Moreover, photoreceptor outer segments of both *ush2a* mutants had a normal morphology (**Supplemental Fig. 4**). The observed lack of progressive retinal degeneration in these mutants suggests that the rate of photoreceptor apoptosis might be compensated by the rate of photoreceptor regeneration when fish are raised in low-intensity light.

Ush2a mutants show reduced visual function

To assess whether absence of usherin has implications for visual function in the *ush2a^{rmc1}* and *ush2a^{b1245}* mutants, electroretinograms (ERGs) were recorded in 5 dpf *ush2a* mutant larvae and strain- and age-matched wild-type controls that were raised under normal facility conditions. In the zebrafish retina, a small negative a-wave generated by photoreceptor hyperpolarization is immediately followed by a large positive b-wave, generated largely by the depolarization of second-order ON-bipolar cells in response to photoreceptor hyperpolarization (Dowling, 2012). The ERG maximum b-wave amplitudes were significantly reduced in homozygous *ush2a^{rmc1}* larvae as compared to age- and strain-matched wild-type controls (**Fig. 7A, B**). The same result was observed in homozygous *ush2a^{b1245}* larvae (5 dpf) (**Fig. 7C, D**). To investigate whether the decreased inner retinal function was primarily mediated by a decrease in photoreceptor function, we recorded pharmacologically isolated a-waves by abolishing b-waves with glutamate receptor antagonists t-APB and TBOA. Maximum a-wave amplitudes in homozygous *ush2a^{rmc1}* larvae were significantly reduced compared to wild-type larvae (**Fig. 7E, F**). Again, a similar defect was detected in homozygous *ush2a^{b1245}* larvae, in which the maximum a-wave amplitudes were also significantly decreased compared to wild-type controls (**Fig. 7G, H**). Despite the absence of detectable retinal morphological defects, early-onset retinal photoreceptor dysfunction was recorded in both *ush2a* mutants.

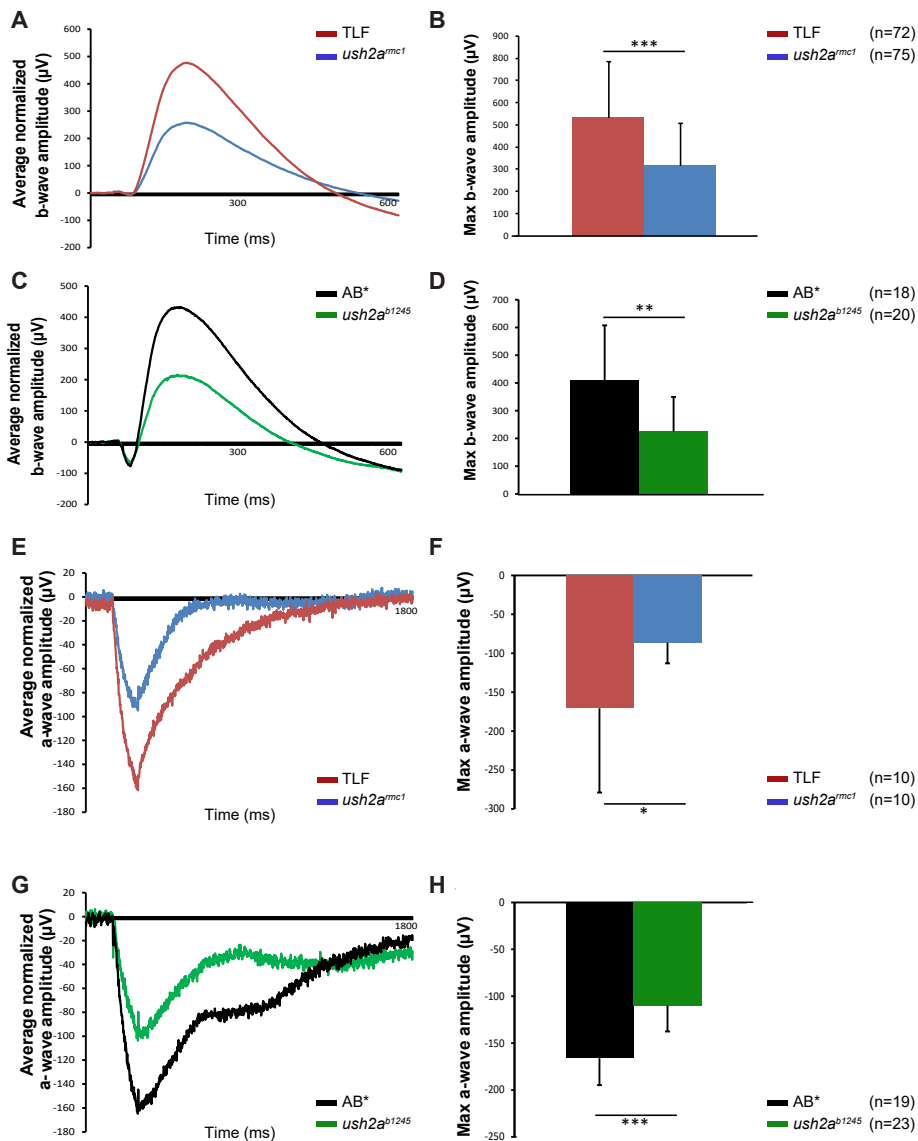


Figure 7. *ush2a* mutants show reduced retinal function. Average ERG traces from a cohort of homozygous *ush2a^{mct1}* and *ush2a^{b1245}* larvae (5 dpf) with age- and strain-matched wild-type controls are depicted. Averages of the maximum ERG amplitudes are plotted as bar graphs \pm standard deviation. **(A-D)** Normalized b-wave amplitudes recorded in both mutants are significantly reduced compared to ERG-traces from wild-type controls (n=72 TLF and n=75 *ush2a^{mct1}*, from 3 biological replicates, $p < 0.001$, two-tailed unpaired Student's *t*-test, and n=20 *ush2a^{b1245}* larvae and n=18 wild-type larvae, from 3 biological replicates, $p < 0.01$, two-tailed unpaired Student's *t*-test). **(E-H)** In both *ush2a* mutants, the a-wave amplitudes are significantly reduced as compared to strain-matched wild-type controls (n=10 for TLF and *ush2a^{mct1}*, from 2 biological replicates, $p < 0.05$, two-tailed unpaired Student's *t*-test, and n=19 for AB* and n=23 for *ush2a^{b1245}*, from 2 biological replicates, $p < 0.001$, two-tailed unpaired Student's *t*-test). * indicates $p < 0.05$, ** indicates $p < 0.01$ and *** indicates $p < 0.001$.

DISCUSSION

In this study we generated and characterized two zebrafish *ush2a* mutant models, *ush2a^{rmc1}* and *ush2a^{b1245}*, in which different domains of usherin were ablated. No signal was detected in photoreceptors of either *ush2a^{rmc1}* or *ush2a^{b1245}* larvae when using an antibody targeting the intracellular C-terminal region. In contrast, truncated usherin was detected at the photoreceptor periciliary region of homozygous *ush2a^{b1245}* larvae when using an N-terminal usherin antibody, but not in *ush2a^{rmc1}*. Absence of full length usherin resulted in reduced whirlin levels at the photoreceptor periciliary region. Furthermore, the *rmc1* allele showed mild levels of photoreceptor degeneration at 8 dpf raised under normal facility conditions, whereas constant light rearing from 5-8 dpf with a light intensity of 3000 lux exacerbated photoreceptor degeneration in both mutants. Finally, both models presented with early-onset retinal dysfunction, as evidenced by significantly reduced ERG a- and b-wave responses recorded at 5 dpf. After complete phenotypic evaluation of both alleles we conclude that the intracellular region of usherin is the most critical region in usherin required for visual function in zebrafish larvae.

Prior to this study, several USH mouse models were generated, which all presented with early-onset hearing defects, with or without vestibular dysfunction, closely resembling human inner ear USH defects (Slijkerman et al., 2017). These models have contributed significantly to understanding the molecular pathology underlying USH-associated hearing loss (Schwander et al., 2009; Tian et al., 2010; Yang et al., 2010). Unfortunately, these mouse models only sporadically recapitulated retinal degeneration seen in USH patients. A spontaneous mutant mouse model, *Kunming*, was described for Usher syndrome type IIa (Yao et al., 2016). This model shows a rapid, early-onset retinal degeneration, but contains mutations in two genes known to be involved in inherited retinal dystrophies: *Ush2a* and *Pde6b*. A targeted *Ush2a* knock-out mouse demonstrates only mild retinal degeneration with late age of onset (Liu et al., 2007). A likely explanation for the discrepancy in phenotypic outcome between mice and humans lies within the anatomical differences between human and mouse photoreceptor cells. The most prominent subcellular locations in human photoreceptor cells where USH1 and USH2 proteins have been found are the calyceal processes and the periciliary membrane (Maerker et al., 2008; May-Simera et al., 2017; Sahly et al., 2012; Sorusch et al., 2017). In rodents, photoreceptor calyceal processes and periciliary membranes are absent or underdeveloped, respectively, compared to humans. In contrast, these structures are well-developed and present in frogs and teleost fish (Slijkerman et al., 2015). Zebrafish mutants or morphants for USH1-associated genes *myo7aa* (Ernest et al., 2000; Wasfy et al., 2014), *cdh23* (Glover et al., 2012; Sollner et al., 2004), *pcdh15* (Seiler et al., 2005) and *ush1c* (Blanco-Sanchez et al., 2014; Phillips et al., 2011) have been described in the literature, most of them showing early-onset retinal dysfunction (Blanco-Sanchez et al.,

2017). Furthermore, we showed that morpholino-induced knock-down of *ush2a* expression induces photoreceptor cell death in zebrafish larvae (Ebermann et al., 2010). In this study we generated and characterized two zebrafish mutant models that will allow us to continue to investigate the molecular pathology underlying *ush2a*-associated retinal dysfunction and future therapeutic strategies.

Although the anatomical similarities between human and zebrafish photoreceptor cells are numerous, some differences have also been noted. Cone photoreceptors of adult teleost fish contain a cilium-like structure with a 9+0 arrangement of microtubule-doublets. This structure, the accessory outer segment (AOS), protrudes from the connecting cilium and projects apically alongside the outer segment, eventually associating with the retinal pigment epithelium (RPE) (Hodel et al., 2014). The function of the AOS is still unclear, but previous reports have suggested that the AOS provides structural support to the outer segment (Yacob et al., 1977) and that it is involved in exchange of metabolites between RPE and cones (Burnside et al., 1993; Hodel et al., 2014; Yacob et al., 1977). Moreover, in response to changes in ambient light conditions and to circadian signals during light-to-dark adaptation of the teleost retina, reversible retinomotor movements take place that result in contraction and elongation of rods and cones to expose the outer segment optimally to incoming light (Hodel et al., 2006; Wagner et al., 1983). It has been postulated that by anchoring the cones to the pigment epithelium, the AOS may preserve the highly organized arrangement of the various types of cones in the fish retina (Yacob et al., 1977). Previous experiments showed that the USH1b protein, myosin VIIa, is localized in the cone AOS (Hodel et al., 2014), and we now discovered that usherin is present in these structures as well. It has been shown that myosin VIIa and usherin, together with *Adgrv1* and whirlin, physically interact to form the ankle-link complex in cochlear hair cells (Michalski et al., 2007). It is therefore tempting to speculate that within the AOS, myosin VIIa and usherin also form a complex that could be of importance for alignment and connection of the AOS to cone outer segments.

In humans, usherin and the other known USH2 proteins, whirlin and ADGRV1, form a dynamic protein complex that is mainly mediated by PDZ-PBM-based interactions (van Wijk et al., 2006; Yang et al., 2010). Previous research using knockout mice showed that usherin, whirlin, and *Adgrv1* are mutually dependent on each other for their localization at the photoreceptor periciliary membrane (Chen et al., 2014; Yang et al., 2010). Whereas *ush2a* and *adgrv1* are present as single copy genes, there are two zebrafish whirlin orthologs (*whrna* and *whrnb*). In larvae of the *ush2a^{rmc1}* allele, in which no usherin could be detected, we observed reduced levels of both *Whrna* and *Whrnb* at the periciliary membrane. In *ush2a^{b1245}* larvae, however, *Whrna* is significantly reduced at the periciliary membrane, whereas *Whrnb* appears unaffected. These observations fit a model in which the ectodomains of usherin and *Adgrv1* interact while the intracellular regions of both proteins are anchored by whirlin (**Fig. 8**), as was previously proposed

by Maerker and co-workers (Maerker et al., 2008; Soroush et al., 2017). Based on the results of the current study, *Whrna* seems to bind the intracellular region of usherin preferentially, whereas *Whrnb* predominantly associates with the intracellular region of *Adgrv1*. Complete absence of usherin (*rmc1* allele) results in absence of both *Whrna* and *Whrnb* at the periciliary membrane and probably the complete USH2 complex including *Adgrv1*, similar to what was observed in the *Ush2a* knockout mouse (Yang et al., 2010). Immunohistochemical analyses using anti-*Adgrv1* antibodies corroborated this hypothesis (**Supplemental Fig. 5**). Absence of the C-terminal cytoplasmic region of usherin (*b1245* allele) apparently affects the association with only the intracellular binding partner *Whrna*, leaving the remainder of the USH2 complex (*Adgrv1* and *Whrnb*) intact (**Fig. 8** and **Supplemental Fig. 5**). Thus, absence of zebrafish usherin affects localization of interaction partner whirlin. The observed differences in localization of both whirlin co-orthologs in the *rmc1* and *b1245* alleles suggest that *Whrna* and *Whrnb* have high binding-affinities for usherin and *Adgrv1*, respectively, and that they most probably have acquired divergent functions during evolution, consistent with the subfunctionalization hypothesis (Force et al., 1999).

The presence of usherin at the periciliary region suggests a role in providing the connecting cilium with structural support. It has been proposed that the periciliary

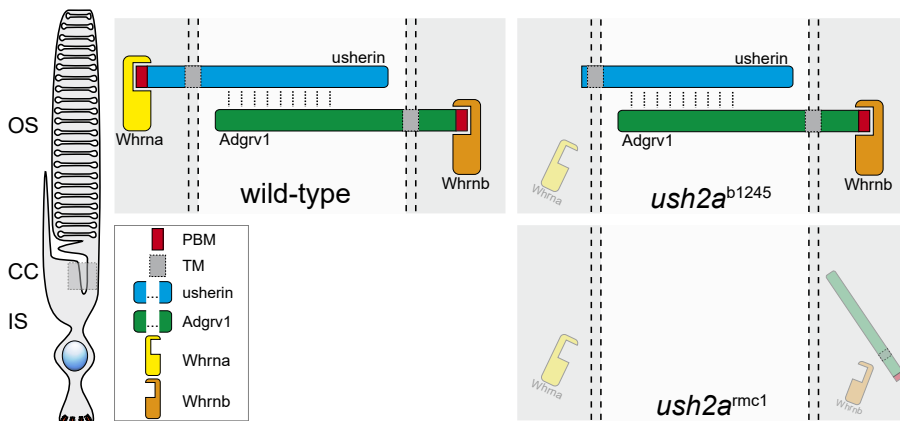


Figure 8. Schematic model of molecular consequences for other USH2 proteins in *ush2a* mutants. The ectodomain of wild-type usherin associates with the ectodomain of *Adgrv1* (indicated by dashed lines). *Whrna* and *Whrnb* bind via a PDZ-PBM-mediated interaction to usherin and *Adgrv1*, respectively. The *ush2a^{rmc1}* allele results in the complete absence of usherin at the periciliary region. As a consequence, localization of *Adgrv1*, *Whrna* and *Whrnb* at the periciliary membrane is also affected. The *ush2a^{b1245}* allele, however, generates a truncated usherin protein that lacks only the C-terminal 62 amino acids and that is still located at the proper subcellular location in the photoreceptor cell. Because *Whrna* is mislocalized in this mutant and *Whrnb* localization is largely unaffected, we propose a model in which *Whrna* has a higher binding affinity for usherin, and *Whrnb* a higher binding affinity for *Adgrv1*. IS: inner segment, OS: outer segment, PBM: PDZ-binding motif.

membrane is physically connected to the connecting cilium by means of interactions between the ectodomains of usherin and Adgrv1 (**Fig. 8**) (Maerker et al., 2008; Sorusch et al., 2017). The photoreceptor apical inner segment and periciliary region are also thought to be involved in docking of trans-Golgi-derived vesicles that contain cargo essential for outer segment formation, maintenance, and function (Falk et al., 2015). The USH protein complex, including usherin, has been proposed to play a role in this process (Maerker et al., 2008). Based on our functional and immunohistochemical data, we propose a dual role for usherin in zebrafish photoreceptors: providing the connecting cilium with (ectodomain-mediated) structural support and participating in vesicle docking and/or signaling mediated by the intracellular region. Moreover, reduced retinal function and increased cell death in the retinal outer nuclear layer combined with the localization of truncated usherin at the periciliary membrane of the *ush2a*^{b1245} mutant, point towards a critical role for the intracellular region of usherin in retinal function, a significant finding for future therapeutic interventions.

The first clinical sign of retinal dysfunction in patients with Usher syndrome is typically night blindness, indicative of rod dysfunction. In zebrafish, rod photoreceptors contribute little to visual function before about 14 dpf (Bilotta et al., 2001; Moyano et al., 2013). In both *ush2a* mutants, however, we observed impaired ERGs at 5 dpf, which is suggestive of early-onset cone dysfunction. Although ERG data of pre-symptomatic patients are typically not available, a recent study demonstrated markedly reduced ERG responses for both rods and cones in adolescent Usher syndrome type 2a patients (Sengillo et al., 2017), consistent with our observations of cone defects by the onset of vision in zebrafish *ush2a* mutants. Furthermore, *USH2A*-associated retinal degeneration in humans has a slow, progressive pathology. Zebrafish, unlike humans, have the ability to regenerate retinal cells lost to injury or disease. Steady cell proliferation from stem-like populations in the ciliary marginal zone persists throughout adult stages (Wan et al., 2016). Acute damage to the retina triggers the reprogramming of Müller glial cells into retinal progenitor cells that are able to differentiate into all major types of retinal neurons including photoreceptors (Wan and Goldman, 2016). Either or both of these regenerative pathways could explain the finding that *ush2a* mutants showed no progressive loss of retinal photoreceptor cells (**Supplemental Fig. 4**) under normal light conditions, although increased levels of photoreceptor apoptosis and impaired visual function were observed within the first week of life when larvae were challenged by exposure to constant illumination with 3000 lux of white light. These observations suggest that sustained exposure to higher light levels throughout life might disrupt the homeostasis between slow degeneration and steady repopulation by regeneration in these mutants. Importantly these observations may have significant implications for light exposure and the use of sunglasses or high-energy wavelength filtering lenses as treatments in Usher syndrome patients. In conclusion, we have shown that zebrafish

ush2a mutants show an early onset retinal dysfunction, mainly in the absence of photoreceptor degeneration. As such they can be used for studying the retinal function of usherin and for the evaluation of therapeutic strategies that are currently being developed for the future treatment of *USH2A*-associated retinal degeneration. For the latter, restored *Whrn* levels at the photoreceptor periciliary membrane and reduced numbers of apoptotic cells in the outer nuclear layer can be used as measures for therapeutic efficacy.

ACKNOWLEDGEMENTS

The authors would like to thank Tom Spanings and Judy Peirce for excellent fish husbandry.

Funding: This study was supported by 'Stichting Nederlands Oogheelkundig Onderzoek', 'Stichting Blindenhulp', 'Stichting Researchfonds Nijmegen', 'Landelijke Stichting voor Blinden en Slechtzienden' to HK and EvW; the Foundation Fighting Blindness USA [grant numbers PPA-0517-0717-RAD to EvW, PPA-0717-0719-RAD to UW], 'Stichting Wetenschappelijk Onderzoek Doof-Blindheid', 'Stichting Ushersyndroom' to EvW, the 'FAUN Stiftung Nuernberg' to UW, 'Forschung contra Blindheit - Initiative Usher syndrome e.V.' to NS and UW; 'JGU Mainz S1 funding' to NS and UW, 'German Research Council (DFG)' [grant number WO848-8/FOR2194 to UW], National Institute of Health [grant numbers HD22486, DC010447, and DC004186 to MW], and Vision for A Cure, The Megan Project, and the many individual donors to the University of Oregon Usher Syndrome Research Fund.

REFERENCES

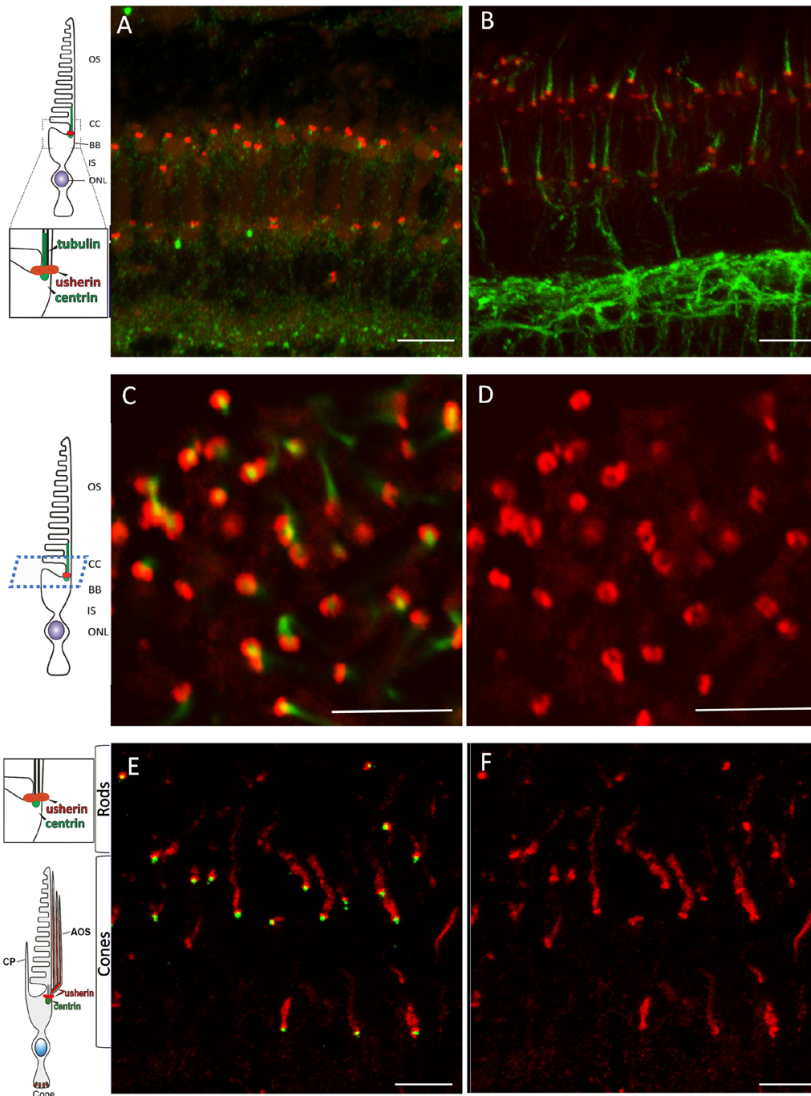
- Adato, A., et al., 2005. Usherin, the defective protein in Usher syndrome type IIA, is likely to be a component of interstereocilia ankle links in the inner ear sensory cells. *Human molecular genetics* 14, 3921-3932.10.1093/hmg/ddi416
- Aller, E., et al., 2010. The *USH2A* c.2299delG mutation: dating its common origin in a Southern European population. *European journal of human genetics: EJHG* 18, 788-793.10.1038/ejhg.2010.14
- Baux, D., et al., 2014. Enrichment of LOVD-USHbases with 152 *USH2A* genotypes defines an extensive mutational spectrum and highlights missense hotspots. *Human mutation* 35, 1179-1186.10.1002/humu.22608
- Bilotta, J., et al., 2001. Rod contributions to the electroretinogram of the dark-adapted developing zebrafish. *Dev Dyn* 222, 564-570.10.1002/dvdy.1188
- Blanco-Sanchez, B., et al., 2014. Complexes of Usher proteins preassemble at the endoplasmic reticulum and are required for trafficking and ER homeostasis. *Disease models & mechanisms* 7, 547-559.10.1242/dmm.014068
- Blanco-Sanchez, B., et al., 2017. Zebrafish models of human eye and inner ear diseases. *Methods Cell Biol* 138, 415-467.10.1016/bs.mcb.2016.10.006
- Burnside, B., et al., 1993. Retinomotor movements in isolated teleost retinal cone inner-outer segment preparations (CIS-COS): effects of light, dark and dopamine. *Experimental eye research* 57, 709-722.10.1006/exer.1993.1179
- Chen, Q., et al., 2014. Whirlin and PDZ domain-containing 7 (PDZD7) proteins are both required to form the quaternary protein complex associated with Usher syndrome type 2. *The Journal of biological chemistry* 289, 36070-36088.10.1074/jbc.M114.610535
- Dowling, J.E., 2012. What can a zebrafish see with only an off-pathway and other fish stories? *J Ophthalmic Vis Res* 7, 97-99
- Ebermann, I., et al., 2010. PDZD7 is a modifier of retinal disease and a contributor to digenic Usher syndrome. *The Journal of clinical investigation* 120, 1812-1823.10.1172/JCI39715
- Ernest, S., et al., 2000. Mariner is defective in myosin VIIA: a zebrafish model for human hereditary deafness. *Human molecular genetics* 9, 2189-2196
- Falk, N., et al., 2015. Specialized Cilia in Mammalian Sensory Systems. *Cells* 4, 500-519.10.3390/cells4030500
- Force, A., et al., 1999. Preservation of duplicate genes by complementary, degenerative mutations. *Genetics* 151, 1531-1545
- Glover, G., et al., 2012. The Usher gene cadherin 23 is expressed in the zebrafish brain and a subset of retinal amacrine cells. *Molecular vision* 18, 2309-2322
- Hartong, D.T., et al., 2006. Retinitis pigmentosa. *Lancet* 368, 1795-1809.10.1016/S0140-6736(06)69740-7
- Hodel, C., et al., 2006. Time course and development of light adaptation processes in the outer zebrafish retina. *Anat Rec A Discov Mol Cell Evol Biol* 288, 653-662.10.1002/ara.20329
- Hodel, C., et al., 2014. Myosin VIIA is a marker for the cone accessory outer segment in zebrafish. *Anat Rec (Hoboken)* 297, 1777-1784.10.1002/ar.22976
- Januschka, M.M., et al., 1987. The ultrastructure of cones in the walleye retina. *Vision Res* 27, 327-341
- Kimmel, C.B., et al., 1995. Stages of embryonic development of the zebrafish. *Dev Dyn* 203, 253-310.10.1002/aja.1002030302

- Lenassi, E., et al., 2014. The effect of the common c.2299delG mutation in *USH2A* on RNA splicing. *Experimental eye research* 122, 9-12.10.1016/j.exer.2014.02.018
- Lenassi, E., et al., 2015. A detailed clinical and molecular survey of subjects with nonsyndromic *USH2A* retinopathy reveals an allelic hierarchy of disease-causing variants. *European journal of human genetics : EJHG* 23, 1318-1327.10.1038/ejhg.2014.283
- Liu, X., et al., 2007. Usherin is required for maintenance of retinal photoreceptors and normal development of cochlear hair cells. *Proceedings of the National Academy of Sciences of the United States of America* 104, 4413-4418.10.1073/pnas.0610950104
- Maerker, T., et al., 2008. A novel Usher protein network at the periciliary reloading point between molecular transport machineries in vertebrate photoreceptor cells. *Human molecular genetics* 17, 71-86.10.1093/hmg/ddm285
- May-Simera, H., et al., 2017. Cilia - The sensory antennae in the eye. *Progress in retinal and eye research* 60, 144-180.10.1016/j.preteyeres.2017.05.001
- McGee, T.L., et al., 2010. Novel mutations in the long isoform of the *USH2A* gene in patients with Usher syndrome type II or non-syndromic retinitis pigmentosa. *Journal of medical genetics* 47, 499-506.10.1136/jmg.2009.075143
- Michalski, N., et al., 2007. Molecular characterization of the ankle-link complex in cochlear hair cells and its role in the hair bundle functioning. *J Neurosci* 27, 6478-6488.10.1523/JNEUROSCI.0342-07.2007
- Millan, J.M., et al., 2011. An update on the genetics of usher syndrome. *Journal of ophthalmology* 2011, 417217.10.1155/2011/417217
- Mou, H., et al., 2017. CRISPR/Cas9-mediated genome editing induces exon skipping by alternative splicing or exon deletion. *Genome biology* 18, 108.10.1186/s13059-017-1237-8
- Moyano, M., et al., 2013. The effects of nicotine on cone and rod b-wave responses in larval zebrafish. *Vis Neurosci* 30, 141-145.10.1017/S0952523813000187
- Overlack, N., et al., 2011. Direct interaction of the Usher syndrome 1G protein SANS and myomegalin in the retina. *Biochimica et biophysica acta* 1813, 1883-1892.10.1016/j.bbamcr.2011.05.015
- Pennings, R.J., et al., 2004. *USH2A* mutation analysis in 70 Dutch families with Usher syndrome type II. *Human mutation* 24, 185.10.1002/humu.9259
- Phillips, J.B., et al., 2011. Harmonin (Ush1c) is required in zebrafish Muller glial cells for photoreceptor synaptic development and function. *Disease models & mechanisms* 4, 786-800.10.1242/dmm.006429
- Reiners, J., et al., 2005. Scaffold protein harmonin (USH1C) provides molecular links between Usher syndrome type 1 and type 2. *Human molecular genetics* 14, 3933-3943.10.1093/hmg/ddi417
- Rinner, O., et al., 2005. Knockdown of cone-specific kinase GRK7 in larval zebrafish leads to impaired cone response recovery and delayed dark adaptation. *Neuron* 47, 231-242.10.1016/j.neuron.2005.06.010
- Sahly, I., et al., 2012. Localization of Usher 1 proteins to the photoreceptor calyceal processes, which are absent from mice. *The Journal of cell biology* 199, 381-399.10.1083/jcb.201202012
- Sandberg, M.A., et al., 2008. Disease course in patients with autosomal recessive retinitis pigmentosa due to the *USH2A* gene. *Investigative ophthalmology & visual science* 49, 5532-5539.10.1167/iovs.08-2009
- Sander, J.D., et al., 2007. Zinc Finger Targeter (ZiFiT): an engineered zinc finger/target site design tool. *Nucleic Acids Res* 35, W599-605.10.1093/nar/gkm349

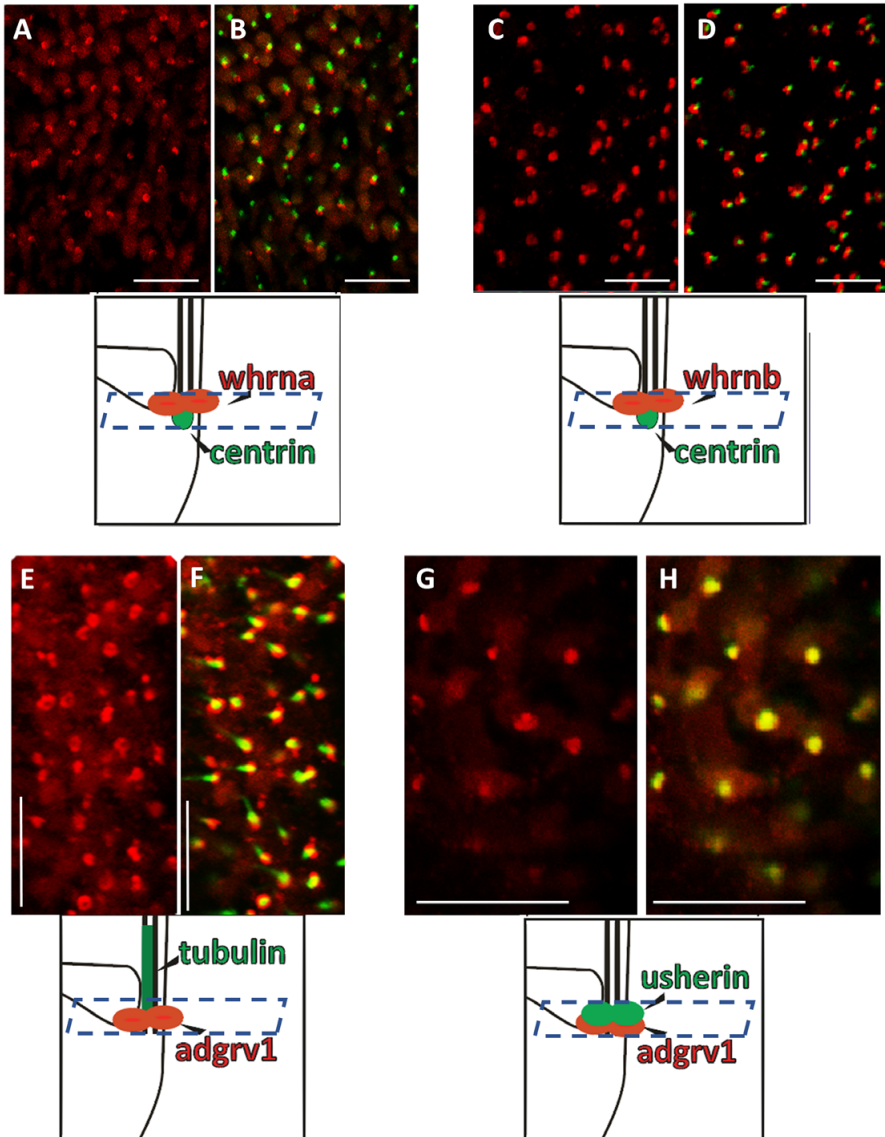
- Schwander, M., et al., 2009. A novel allele of myosin VIIa reveals a critical function for the C-terminal FERM domain for melanosome transport in retinal pigment epithelial cells. *J Neurosci* 29, 15810-15818.10.1523/JNEUROSCI.4876-09.2009
- Sedmak, T., et al., 2009. Immunoelectron microscopy of vesicle transport to the primary cilium of photoreceptor cells. *Methods Cell Biol* 94, 259-272.10.1016/S0091-679X(08)94013-9
- Sedmak, T., Wolfrum, U., 2010. Intraflagellar transport molecules in ciliary and nonciliary cells of the retina. *The Journal of cell biology* 189, 171-186.10.1083/jcb.200911095
- Seiler, C., et al., 2005. Duplicated genes with split functions: independent roles of protocadherin15 orthologues in zebrafish hearing and vision. *Development* 132, 615-623.10.1242/dev.01591
- Sengillo, J.D., et al., 2017. Electroretinography Reveals Difference in Cone Function between Syndromic and Nonsyndromic USH2A Patients. *Scientific reports* 7, 11170.10.1038/s41598-017-11679-y
- Sirisi, S., et al., 2014. Megalencephalic leukoencephalopathy with subcortical cysts protein 1 regulates glial surface localization of GLIALCAM from fish to humans. *Human molecular genetics* 23, 5069-5086.10.1093/hmg/ddu231
- Slijkerman, R., et al., 2017. Molecular Genetics of Usher Syndrome: Current State of Understanding. eLS. John Wiley & Sons, Ltd: Chichester.DOI: 10.1002/9780470015902.a0021456.pub2
- Slijkerman, R.W., et al., 2015. The pros and cons of vertebrate animal models for functional and therapeutic research on inherited retinal dystrophies. *Progress in retinal and eye research* 48, 137-159.10.1016/j.preteyeres.2015.04.004
- Sollner, C., et al., 2004. Mutations in cadherin 23 affect tip links in zebrafish sensory hair cells. *Nature* 428, 955-959.10.1038/nature02484
- Sorusch, N., et al., 2017. Characterization of the ternary Usher syndrome SANS/ush2a/whirlin protein complex. *Human molecular genetics* 26, 1157-1172.10.1093/hmg/ddx027
- Tazetdinov, A.M., et al., 2008. [Molecular genetics of Usher syndrome]. *Genetika* 44, 725-733
- Tian, C., et al., 2010. Ush1c gene expression levels in the ear and eye suggest different roles for Ush1c in neurosensory organs in a new Ush1c knockout mouse. *Brain Res* 1328, 57-70.10.1016/j.brainres.2010.02.079
- van Wijk, E., et al., 2004. Identification of 51 novel exons of the Usher syndrome type 2A (USH2A) gene that encode multiple conserved functional domains and that are mutated in patients with Usher syndrome type II. *American journal of human genetics* 74, 738-744.10.1086/383096
- van Wijk, E., et al., 2006. The DFNB31 gene product whirlin connects to the Usher protein network in the cochlea and retina by direct association with USH2A and VLGR1. *Human molecular genetics* 15, 751-765.10.1093/hmg/ddi490
- Wagner, B., et al., 1983. Morphological evidence for different types of IgG-Fc receptors in group A streptococci. *Zentralbl Bakteriell Mikrobiol Hyg A* 256, 61-71
- Wan, J., Goldman, D., 2016. Retina regeneration in zebrafish. *Curr Opin Genet Dev* 40, 41-47.10.1016/j.gde.2016.05.009
- Wan, Y., et al., 2016. The ciliary marginal zone of the zebrafish retina: clonal and time-lapse analysis of a continuously growing tissue. *Development* 143, 1099-1107.10.1242/dev.133314
- Wasfy, M.M., et al., 2014. myosin 7aa(-/-) mutant zebrafish show mild photoreceptor degeneration and reduced electroretinographic responses. *Experimental eye research* 122, 65-76.10.1016/j.exer.2014.03.007
- Yacob, A., et al., 1977. The accessory outer segment of rods and cones in the retina of the guppy, *Poecilia reticulata* P. (Teleostei). An electron microscopical study. *Cell Tissue Res* 177, 181-193

- Yan, D., Liu, X.Z., 2010. Genetics and pathological mechanisms of Usher syndrome. *Journal of human genetics* 55, 327-335.10.1038/jhg.2010.29
- Yang, J., et al., 2010. Ablation of whirlin long isoform disrupts the USH2 protein complex and causes vision and hearing loss. *PLoS genetics* 6, e1000955.10.1371/journal.pgen.1000955
- Yao, L., et al., 2016. The Time Course of Deafness and Retinal Degeneration in a Kunming Mouse Model for Usher Syndrome. *PloS one* 11, e0155619.10.1371/journal.pone.0155619
- Zou, J., et al., 2011. Whirlin replacement restores the formation of the USH2 protein complex in whirlin knockout photoreceptors. *Investigative ophthalmology & visual science* 52, 2343-2351.10.1167/iops.10-6141

SUPPLEMENTAL FIGURES



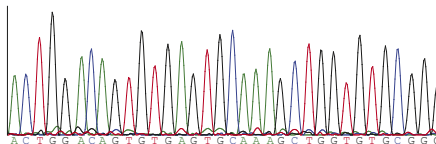
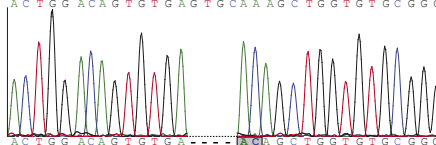
Supplemental Figure 1. Specific organization of usherin within wild-type photoreceptors is revealed by scanning confocal microscopy. (A,B) Anti-usherin antibody localizes in a flattened disc pattern spanning the photoreceptor periciliary region in cross sections of 6dpf wild-type retinas. Tissue co-labeled sequentially with anti-centrin (A) to mark the basal body or acetylated α -tubulin to mark the connecting cilium (B) further defines the region of usherin enrichment between these two structures. (C,D) Transverse sections through the 6dpf larval retina (dotted line on schematic) reveal the usherin localization pattern as a ring at the periciliary region (cilia labeled green in panel C). (E,F) Cross sections of adult retinas labeled for usherin and centrin (E only) show the persistence of the ring structure superior to the basal body in addition to the localization within the accessory outer segments of cone photoreceptors. Scale bars: 5 μ m.



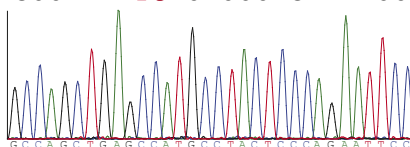
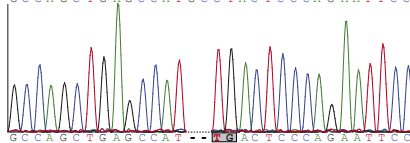
Supplemental Figure 2. Zebrafish USH2 proteins encircle the base of the connecting cilium. (A-D) Transverse sections through the inner-outer segment boundary of 6dpf larval photoreceptors shows whirlin proteins (red; WhrnA: A, B, WhrnB: C, D) at the periciliary region. Centrin marks the basal body/connecting cilium in green. (E-H) In transverse sections of 6dpf larval retinas, Adgrv1 (red) organizes into a concentric ring (E, F) surrounding the connecting cilium (acetylated α -tubulin, green in F); Adgrv1 (red) and usherin (green) localization overlaps in this region (G, H). Scale bars: 5 μ m. Plane of sectioning shown in schematics.

A*ush2a^{mc1}* (c.2337_2342delinsAC; p.Cys780GlnfsTer32)wt: ACTGGACAGTGTGAGTGC~~AAAGCTGGTGTGCGGG~~mut: ACTGGACAGTGTGA **AC**AGCTGGTGTGCGGG

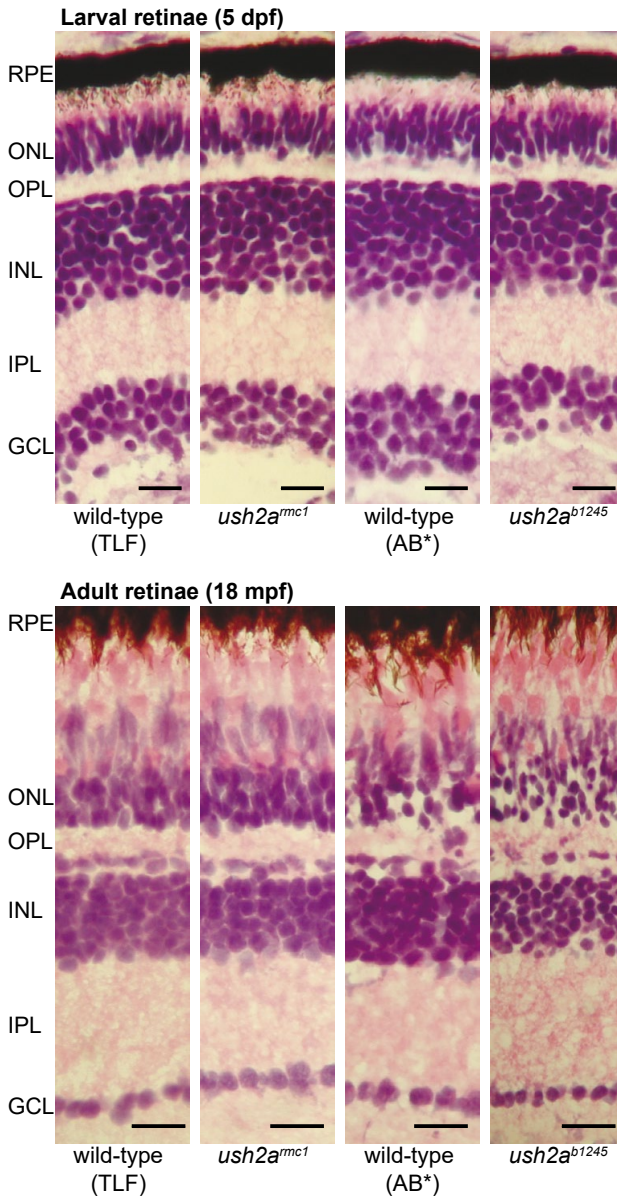
wild-type

*ush2a^{mc1}***B***ush2a^{b1245}* (c.15520_15523delinsTG; p.Ala5174fsTer)wt: GCCAGCTGAGCCATGCCTACTCCCA~~GAAATTC~~mut: GCCAGCTGAGCCAT **TG**ACTCCCA~~GAAATTC~~

wild-type

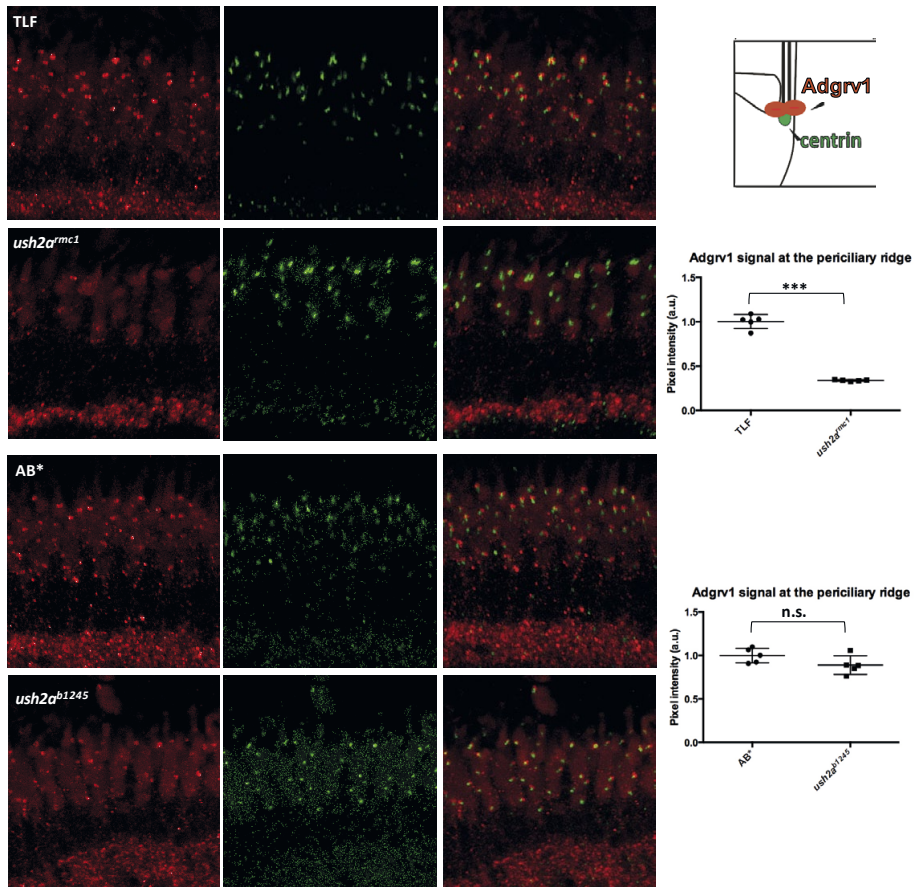
*ush2a^{b1245}***Supplemental Figure 3. DNA sequence traces of homozygous *ush2a^{mc1}* and *ush2a^{b1245}* alleles.**

(A) The *ush2a^{mc1}* allele contains a six basepair deletion ('GTGCAA') and a two basepair insertion ('AC') in *ush2a* exon13 (c.2337_2342delinsAC; p.Cys780GlnfsTer32). Lower sequence traces are derived from larvae homozygous for the *ush2a^{mc1}* allele, whereas the upper sequence traces are derived from strain-matched wild-type larvae. **(B)** Zebrafish homozygous for the *ush2a^{b1245}* allele have a four basepair-deletion ('GCCT') and a two basepair insertion ('TG') in *ush2a* exon71, creating an instant TGA termination codon (c.15520_15523delinsTG; p.Ala5174fsTer). Lower sequence traces are derived from larvae homozygous for the *ush2a^{b1245}* allele, whereas the upper sequence traces are derived from strain-matched wild-type larvae.



Supplemental Figure 4. Histological examination of *ush2a^{mc1}* and *ush2a^{b1245}* zebrafish retinas.

Light microscopy of retinal sections from larval (5 dpf) and adult (18 mpf) zebrafish stained with hematoxylin and eosin. Retinas of wild-type and both mutant alleles are morphologically indistinguishable from wild-type retinas at both ages. (n=7 larvae and n=4 adult eyes (18 mpf) with *ush2a^{mc1}* mutant, *ush2a^{b1245}* mutant, TLF and AB* fish). Dpf: days post fertilization, mpf: months post fertilization, GCL: ganglion cell layer, IPL: inner plexiform layer, OPL: outer plexiform layer, ONL: outer nuclear layer, RPE: retinal pigment epithelium. Scale bars: 10 μ m.



Supplemental Figure 5. Ablation of usherin affects the localization of Adgrv1 in the zebrafish retina (5 dpf). Confocal microscopy of retinal sections from *ush2a* mutants and strain-matched wild-type controls shows a marked reduction in Adgrv1 localization at the periciliary region of *ush2a^{rmc1}* photoreceptors (D-F) compared to those of *ush2a^{b1245}* (K-M) and to wild-type controls (A-C: TLF; H-J: AB*). Signal intensity for the Adgrv1 labeling (red) was calculated for each genotype to quantify the reduction in specific localization (G, N). Scale bars: 10 μ m.

Chapter 2^c



Affinity purification of *in vivo*-assembled whirlin-associated protein complexes from the zebrafish retina

Slijkerman R.W.N.^{1,2}, Hetterschijt L.¹, Peters T.¹, Broekman S.³, Clement A.⁴, Westerfield M.⁴, Phillips J.B.⁴, Junger K.⁵, Boldt K.⁵, De Vrieze E.^{1,6}, Kremer H.^{1,3,6} and Van Wijk E.^{1,6}

¹ Department of Otorhinolaryngology, Radboud University Medical Center, Nijmegen - the Netherlands.

² Radboud Institute for Molecular Life Sciences, Nijmegen - the Netherlands.

³ Department of Human Genetics, Radboud University Medical Center, Nijmegen - the Netherlands.

⁴ University of Oregon, Eugene, Oregon - United States of America.

⁵ Division of Experimental Ophthalmology and Medical Bioanalytics, Center for Ophthalmology, Eberhard-Karls University Tübingen, Tübingen - Germany.

⁶ Donders Institute for Brain, Cognition and Behavior, Nijmegen - the Netherlands.

ABSTRACT

Mutations in *WHRN* lead to Usher syndrome type 2d (USH2d) or to non-syndromic hearing impairment (DFNB31). The *WHRN*-encoded gene product whirlin directly interacts with the intracellular regions of the other two USH2 proteins, usherin and ADGRV1, to collectively make up a transient ankle link complex necessary for maturation of the inner ear hairbundle. In photoreceptors, usherin and ADGRV1 are scaffolded by whirlin and proposed to constitute similar fibrous links between the apical inner segment and the connecting cilium. However, the molecular mechanism of retinal degeneration as a consequence of a compromised USH2 protein complex formation and function remains elusive. Therefore, we aimed to better understand the retinal function of the USH2 proteins by identification of proteins that associate with the key scaffolding protein of the USH2 complex in photoreceptors, whirlin. We generated a transgenic zebrafish that expresses Strep/FLAG-tagged *Whrna* under the control of a photoreceptor-specific promoter. Eyes of these transgenic fish were employed to perform affinity purification of native *Whrna*-associated protein complexes. *Whrna* is one of the two zebrafish orthologs of human whirlin with the highest affinity for usherin, the USH2 protein most often affected in patients with USH2. Mass spectrometry analysis identified 19 co-purified proteins and the human orthologs of at least two of these, *Preso1* and *Kir2.3*, directly interacted with human whirlin in a yeast two-hybrid assay. Future studies assessing the interactions between the here identified co-purified proteins and whirlin in a biologically relevant context will be necessary to evaluate whether a disrupted interaction with whirlin contributes to the development of a retinal phenotype as observed in USH2d patients.

INTRODUCTION

Usher syndrome (USH) is the most frequent cause of inherited deaf-blindness in man. Hallmark symptoms of USH are congenital sensorineural hearing loss and progressive retinal degeneration classified as retinitis pigmentosa (RP). Based on the severity of hearing loss, the onset of retinal degeneration and the presence of vestibular dysfunction, three types of USH can be distinguished: USH1, USH2 and USH3 (Smith et al. 1994). Besides being clinically heterogeneous, USH is also genetically heterogeneous (overview in Slijkerman, Kremer, and Van Wijk 2017). In addition, mutations in several USH-associated genes can also result in non-syndromic forms of hearing impairment or retinal degeneration. USH2 is the most prevalent type of USH and clinically manifests as congenital moderate-to-severe bilateral hearing impairment combined with a progressive loss of visual function that becomes apparent from puberty onwards (Hartel et al. 2016, Pierrache et al. 2016). So far, mutations in *USH2A*, *ADGRV1* or *WHRN* have been associated with USH2.

The proteins encoded by the USH2 genes form dynamic protein complexes in the auditory hair cells and in photoreceptors (Maerker et al. 2008, Zou et al. 2017). In developing hair cells, a quaternary protein complex of the three known USH2 proteins and the paralog of the *WHRN*-encoded protein whirlin, PDZD7, is essential for the maturation of the inner ear sensory hair bundles (Chen et al. 2014, Zou et al. 2017). The extracellular regions of the *USH2A*-encoded protein usherin and the *ADGRV1*-encoded protein ADGRV1 are proposed to interact and form fibrous links, named ankle links, between adjacent stereocilia and between stereocilia and the kinocilium, whereas the intracellular domains are connected with whirlin and PDZD7 (Michalski et al. 2007, Grati et al. 2012, Chen et al. 2014, Zou et al. 2017). In both rod and cone photoreceptors, USH2 proteins are found in close proximity to the connecting cilium, the structure through which proteins are transported from the metabolic inner segment towards the light-sensitive outer segment (van Wijk et al. 2006, Yang et al. 2010). Immuno-electron microscopic analyses demonstrated that whirlin is localized at the photoreceptor periciliary membrane (PCM) (Yang et al. 2010), which is the apical part of the inner segment that folds as a collar-like structure around the connecting cilium. Presumably, whirlin scaffolds a complex of USH2 proteins in photoreceptors similar to that of the ankle links in auditory hair cells, since usherin and ADGRV1 are almost completely absent at the region of the connecting cilium of whirlin knock-out mice (Yang et al. 2010, Chen et al. 2014). The interdependency of USH2 proteins for their proper subcellular localization is further underlined by a reduction of the amount of whirlin and ADGRV1/Adgrv1 proteins at the PCM of usherin-deficient mice and zebrafish (Yang et al. 2010, Dona et al. 2018) and the absence of whirlin and usherin at the periciliary membrane of *Adgrv1* knock-out mice (Yang et al. 2010).

Besides interacting with USH2 proteins, whirlin has also been described to associate with multiple USH1-associated proteins (Belyantseva et al. 2005, Brown, Hardisty-Hughes, and Mburu 2008, Maerker et al. 2008, Riazuddin et al. 2012, Sorusch et al. 2017). The identified interaction partners of whirlin also extend beyond USH-associated proteins. For example, whirlin has been shown to interact with GPSM2, G α i3 and Myosin15a to form a complex that is involved in stereocilia elongation in mice (Mauriac et al. 2017) and whirlin acts as a scaffold protein for the actin-regulating proteins MPP1 (also known as p55) and Eps8 in the mouse stereocilia tip complex (Gosens et al. 2007, Mburu et al. 2010, Manor et al. 2011). In addition to functioning in the inner ear, whirlin connects to the RP-associated protein RPGR and both proteins co-localize at the photoreceptor connecting cilium (Wright, Hong, and Perkins 2012). However, none of the binding partners of whirlin have been identified through the isolation of native, endogenously formed whirlin-associated protein complexes, but were rather identified after GST pull-down assays, yeast two-hybrid screenings and co-immunoprecipitation experiments. Isolation and identification of *in vivo*-assembled whirlin protein complexes from the tissue of interest has therefore the potential to significantly improve the understanding of the function of whirlin and the molecular pathogenesis of USH2. For this reason, we generated a transgenic zebrafish line that stably expresses Strep/FLAG-tagged zebrafish whirlin (SF-Whrna) in photoreceptors. Affinity purification of *in vivo*-assembled SF-Whrna protein complexes from retinal lysates followed by mass-spectrometry analysis, resulted in the identification of multiple novel candidate members of whirlin complexes of which *Lrrc8*-channels, *Preso1* and *Kir2.3* seem most prominent. We confirmed a direct interaction between the human orthologs of *Preso1* and *Kir2.3* with human whirlin and hypothesize that *Kir2.3* could be part of a vesicle handling complex consisting of at least whirlin, *CASK* and *Kir2.3* at the photoreceptor connecting cilium.

MATERIALS AND METHODS

Zebrafish strain and husbandry

Larvae (Tupfel Long Fin, (TLF)) were maintained and raised by standard methods (Kimmel et al., 1995). All experimental procedures were approved by the Animal Experimentation Committee of the Royal Netherlands Academy of Arts and Sciences (Protocol #RU-DEC2016-091).

Antibodies for immunohistochemistry

The following primary antibodies were used for immunohistochemistry: rabbit anti-FLAG (1:1000; #F7425, Sigma Aldrich), mouse anti-centrin (1:500; #04-1624, Merck), rabbit anti-Whrna (1:300; #42700002, Novus Biological), mouse anti-synaptic vesicle

glycoprotein 2A (Sv2a) (1:10; Developmental Studies Hybridoma Bank), anti-GFAP (1:1000; #Z033429, Agilent Technologies), rabbit and guinea-pig anti-Prso1 (1:50, 1:100, 1:200 for all antibodies, kind gifts from Prof. Dr. P. Worley and Prof. Dr. E. Kim). As secondary antibodies for immunohistochemistry, the following Alexa Fluor (AF) conjugated immunoglobulins from Molecular Probes were used at a 1:800 dilution: AF 568-goat anti-rabbit (#A11011), AF 488-goat anti-mouse (#A11029), AF 488-goat anti-rabbit (#A11008) and AF568-goat anti-guinea pig (#A11075).

Generation of transgenic zebrafish

The coding sequence of *Whrna* (ENSDARG00000075362) was amplified by RT-PCR (primers: 5'-GGGGACAGCTTCTTGTACAAAGTGGTCATGAGCACAGACCTGGAGC-3' and 5'-GGGGACAACCTTTGTATAATAAAGTTGCCTACAGAGCCACATTGAACTCTG-3') from whole larvae-derived RNA and used for the generation of a 3' entry vector in a BP recombination using the pDONRP2R-P33' donor vector following instructions in the Multisite Gateway™ cloning (Thermo Fisher Scientific) Manual. Subsequently, using Multisite Gateway™ cloning technology we cloned a 3x photoreceptor regulatory element-1 (PRE-1)-containing zebrafish rhodopsin promoter element (*rho*) (Morrissey et al. 2011), a double Strep and single FLAG-tag (SF) (Gloeckner, Boldt, and Ueffing 2009) and *Whrna* into the pDestTol2CG2destination vector (Kwan et al. 2007). A volume of 1nl, containing 40pg pDestTol2CG2_*rho:SF-Whrna* and 50pg of *in vitro*-transcribed *transposase* mRNA (T7 mMessage mMachine; #AM1344; Ambion Life Sciences, using a linearized pCS2FA-transposase plasmid as template (Kwan et al. 2007)), was injected into 1-cell-stage embryos (F0 generation) (Suster et al. 2009). Subsequently, embryos were analyzed for genome integration of the cassette based on GFP expression in the cardiomyocytes at 2.5 dpf. Positively selected animals were grown into adulthood and outcross with wildtype TLF, of which the offspring (F1) was similarly positively selected for germline transmission of the transgene. Eyes of adult F2 transgenic zebrafish were used for affinity purification experiments.

Retinal histology and immunohistochemistry

Eyes of adult zebrafish (*rho:SF-whrna* and TLF wild-type) or mice (Prso1^{-/-} and C57BL/6 wild-type) were cryoprotected in 10% sucrose in PBS for 30 minutes and subsequently embedded in OCT compound (Tissue-Tek®; #4583; Sakura Finetek U.S.A. inc.) without prior fixation. The embedded samples were frozen using melting isopentane. Cryosections of zebrafish retinas were fixed for 10 minutes with 4% PFA, rinsed 3 times for 10 minutes with PBS and permeabilised with 0.01% Tween-20 in PBS for 20 minutes. Next, sections were rinsed again 3 times for 5 minutes with PBS, incubated with blocking buffer (10% normal goat serum, 2% bovine serum albumin in PBS) for 1 hour and incubated with primary antibodies diluted in blocking buffer at 4°C overnight. Subsequently,

cryosections were rinsed 3 times for 10 minutes with PBS and incubated with secondary antibodies and DAPI (1:8000; #D1306; Molecular Probes) diluted in blocking buffer at room temperature for 1 hour. Finally, sections were mounted with anti-fade Prolong Gold (#P36930; Molecular Probes). Retinal sections were imaged with a Zeiss AxioCam MRC5 camera, mounted on a Zeiss Axio Imager fluorescence microscope.

For immunohistochemical analysis of the *Frmpt4* knock-out and wild-type mice, unfixed cryosections were blocked with 0.1% (w/v) ovalbumin and 0.5% (w/v) fish gelatin in PBS for 30 minutes. Before mounting, sections were fixed with 4% PFA for 10 minutes. The experimental procedure was otherwise similar to the procedure for zebrafish sections.

For histological analysis of the murine retinae, cryosections were fixed with 4% PFA for 10 minutes, stained with toluidine blue and analyzed with a Zeiss Axioskop light microscope. Images were taken with an AxioCam MRC5 camera (Zeiss) camera.

Single-step anti-FLAG affinity purification from zebrafish retina

Adult zebrafish (18-24 months of age) were euthanized by severing of the spinal cord after general anesthesia in 0.1% (v/v) 2-phenoxyethanol. Subsequently, the eyes were removed and the lens and vitreous humor were surgically dissected as described (Cao et al. 2010). Per condition, fourteen eyes were individually homogenized with a pestle using 80 μ l lysis buffer (0.15M NaCl, 0.03M HEPES pH7.8, 1%(v/v) NP40, 10%(v/v) glycerol, 1%(v/v) phosphatase inhibitor cocktail 2 (#P5726-5ML, Sigma-Aldrich), 1%(v/v) Phosphatase Arrest™ III (#786-452, VWR) and a cOplete™ mini protease cocktail tablet (#11836153001, Sigma Aldrich)). After homogenization, total eye extracts were incubated on ice for 15 minutes, pooled and centrifuged (10,000xg) at 4°C for 10 minutes. In parallel, microspin columns (#27-3565-01, VWR) were prepared by adding an anti-FLAG M2 affinity matrix (#A2220, Sigma Aldrich)/lysis buffer mixture (1:1). After centrifugation, beads were washed three times with TBS. All centrifugation steps were performed for 1 minute at 112xg and 4°C, unless otherwise stated. Next, the supernatant of the pooled pre-cleared retinal extracts was added to the column and allowed to bind to the anti-FLAG beads while rotating on an intelli-mixer (25rpm) at 4°C for 1 hour. Subsequently, beads were washed three times with washbuffer (0.15M NaCl, 0.03M HEPES pH 7.8, 0.1% (v/v) NP40, 1%(v/v) phosphatase inhibitor cocktail 2, 1%(v/v) Phosphatase Arrest™ III and cOplete™ mini protease inhibitors) followed by two washing steps with TBS. Elution by competition was performed on ice by addition of 200 μ l FLAG peptide (250 μ g/ml, #F3290, Sigma-Aldrich) in TBS for 15 minutes with gentle agitation every 5 minutes. The eluted proteins were collected by centrifugation, precipitated using chloroform/methanol as described (Gloeckner, Boldt, and Ueffing 2009) and sent out for mass spectrometry analysis.

Western blotting

Protein samples supplemented with sample buffer (sample buffer NuPage LDS (#NP0007, Life Technologies) with a final concentration of 2mM DTT) were denatured at 70°C for 10 minutes. Proteins were resolved on 4-12% NuPage gradient gels (#NP0321BOX, Life Technologies). Subsequently, proteins were electrophoretically transferred onto nitrocellulose membranes, blocked with 5% (w/v) non-fat dry milk (#1706404, Biorad) in PBS-T (PBS supplemented with 0.1% Tween) and analyzed with anti-FLAG monoclonal primary antibodies (1:1,000) and goat anti-rabbit IRDye 800 (1:20,000, #926-3221, LI-COR) secondary antibodies in 0.5% (w/v) non-fat dry milk in PBS-T. Proteins were visualized using the Odyssey Infrared Imaging System (LI-COR, USA).

GST pull-down

For the generation of GST fusion proteins, the coding sequence of zebrafish *whrna* was cloned into a pDest15 expression vector using Gateway cloning™ technology (Thermo Fisher Scientific) and subsequently used for the expression of GST-fused Whrna as previously described (van Wijk et al. 2006). GST-fusion proteins were coupled to glutathion Sepharose 4B beads (#17-0756-01, GE Healthcare) for 2 hours on a rotating wheel at 4°C. Beads with bound fusion proteins were washed twice with STE-buffer (1% (v/v) Sarkosyl, 1% (v/v) Triton X-100, 5 mM 1,4-dithiothreitol (DTT), supplemented with cComplete™ mini protease inhibitors) and three times with TBS-TD (1x TBS supplemented with 1% (v/v) Triton X-100, 2 mM DTT and cComplete™ mini protease inhibitors). Pre-cleared zebrafish retinal extracts were incubated overnight at 4°C with equal amounts of blocked beads with GST or beads with GST-fusion proteins. GST fusion proteins were eluted from the glutathion sepharose 4B beads with 100 mM reduced Glutathione (#G4251, Sigma Aldrich), 5 mM NaCl and 1M TRIS-HCl (pH 8.0) overnight at 4°C. Proteins were precipitated using chloroform/methanol as previously described (Gloeckner, Boldt, and Ueffing 2009) and analyzed by mass spectrometry.

Mass spectrometry analysis

Precipitated proteins were solubilized and proteolytically cleaved using trypsin. LC-MS/MS analysis was performed on Ultimate3000 nanoRSLC systems (Thermo Scientific) coupled to an Orbitrap Fusion Tribrid mass spectrometer (Thermo Scientific) by a nano spray ion source. Tryptic peptide mixtures were injected automatically and loaded at a flow rate of 30 µl/min in 0.1% trifluoroacetic acid in HPLC-grade water onto a nano trap column (300 µm i.d. × 5 mm Precolumn, packed with Acclaim PepMap100 C18, 5 µm, 100 Å; Thermo Scientific). After 3 minutes, peptides were eluted and separated on the analytical column (75 µm i.d. × 25 cm, Acclaim PepMap RSLC C18, 2 µm, 100 Å; Thermo Scientific) by a linear gradient from 2% to 30% of buffer B (80% acetonitrile and 0.08%

formic acid in HPLC-grade water) in buffer A (2% acetonitrile and 0.1% formic acid in HPLC-grade water) at a flow rate of 300 nl/min over 82 minutes. Remaining peptides were eluted by a short gradient from 30% to 95% buffer B in 5 minutes. Analysis of the eluted peptides was done on an LTQ Fusion mass spectrometer. From the high resolution MS pre-scan with a mass range of 335 to 1500, peptide ions were selected for fragment analysis in the Orbitrap depending on intensity (at least 5000 counts) and if they were at least doubly charged. The normalized collision energy for HCD was set to a value of 30 and the resulting fragments were detected in the ion trap analyzer. The lock mass option was activated; the background signal with a mass of 445.12003 was used as lock mass (Olsen et al. 2005). MaxQuant software (version 1.5.3.30) was used to search the raw spectra against the translated Ensembl *Danio rerio*-specific database for identification of gene IDs (Cox and Mann 2008).

Yeast two-hybrid assay

A GAL4-based yeast two-hybrid system (HybriZap, Stratagene) was used to identify the interactions between whirlin and LRRC8A, LRRC8D, Kir2.3 and Preso1. cDNAs encoding LRRC8A (LRRC8A_TM2>3: amino acid (aa) 137-272, LRRC8A_C-term: aa 333-810), LRRC8D (LRRC8D_C-term: aa 378-858) and Kir2.3 (Kir2.3_C-term: aa 162-434) were amplified from HEK293T-derived cDNA and cloned in the pDONR201 vector. Preso1 cDNA fragments (Preso1_fl: aa 1-1322, Preso1_fl Δ PBM: aa 1-1316, Preso1_PDZ: aa 75-165, Preso1_FERM: aa 192-434, Preso1_PDZ+FERM: aa 75-434, Preso1_C-term: aa 1273-1322, Preso1_C-term Δ PBM: aa 1273-1316, Preso1_WW: aa 23-76) were amplified using cDNA clone BC113700 (TransOMIC technologies Inc.) as a template and cloned in pDONR201. Next, LRRC8A/D, Kir2.3 and Preso1 fragments were cloned in a pBD-GAL4/DEST expression vector and full length whirlin was cloned in the pAD-GAL4/DEST expression vector, as previously described (van Wijk et al. 2006). Interactions were analyzed (*in triplo*), using the yeast strains PJ69-4A and -4 α as a host, by the assessment of reporter gene activation, using growth on selective media (*HIS3* and *ADE2* reporter genes) and an X- β -gal colorimetric filter lift assay (*LacZ* reporter gene). All used pBD-expression vectors were confirmed not to autoactivate the reported genes after analysis of growth of the transformed yeast on selective media lacking tryptophan and histidine (WH) or lacking tryptophan, histidine and adenine (WHA).

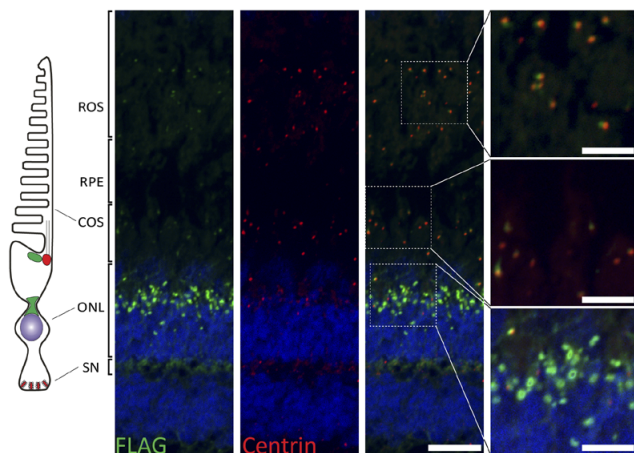
RESULTS

Generation of transgenic zebrafish expressing SF-Whrna in photoreceptors

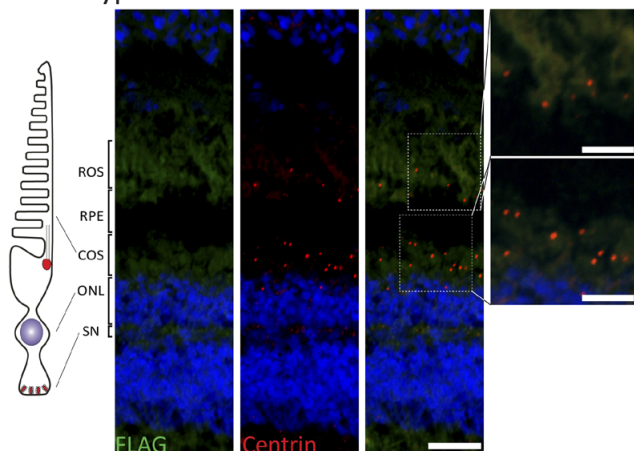
The zebrafish genome contains two orthologs of human *WHRN*, *whrna* and *whrnb*. We have previously demonstrated that *Whrna* has the highest binding affinity for the zebrafish *ush2a*-encoded protein usherin (Dona et al. 2018) and therefore *Whrna* was selected as a target for affinity purification of *in vivo*-assembled protein complexes. We used the Tol2 transposon system to generate a transgenic zebrafish line stably expressing Strep/FLAG-tagged zebrafish *Whrna* (*tg(rho:SF-Whrna)*) in photoreceptors (Suster et al. 2009), to which we hereafter refer as SF-*Whrna*. Expression and localization of SF-*Whrna* in adult zebrafish photoreceptors was confirmed by immunohistochemistry (**Fig. 1**). Part of SF-*Whrna*, visualized by anti-FLAG staining, colocalizes with the connecting cilium marker centrin in both rods and cones of *SF-whrna* transgenic zebrafish (**Fig. 1A, B**). This indicates that SF-*Whrna* can recapitulate the localization of native *Whrna* in the zebrafish photoreceptor (**Fig. 1C**) and is likely to interact with the same proteins as endogenous *Whrna* at the connecting cilium. However, the majority of SF-*Whrna* accumulates in the inner segment of photoreceptors. In several, but not all, studies on murine photoreceptors, whirlin was also observed at the synapse (van Wijk et al. 2006, Maerker et al. 2008, Yang et al. 2010). However, in wild-type adult zebrafish retinas, endogenous *Whrna* could not be detected at the photoreceptor synapse (**Fig. 1C**). Moreover, immunohistochemistry did not reveal co-localization of SF-*Whrna* and the synaptic marker Sv2a (synaptic vesicle glycoprotein 2A) in *SF-whrna* retinas (**Supplemental Fig. 1**).

Affinity purification of SF-Whrna-associated protein complexes from the adult zebrafish retina

After confirming expression of SF-tagged *Whrna*, we investigated whether this protein and associated protein complexes could be isolated from adult *SF-whrna* retinas using a single FLAG-affinity purification step (**Fig. 2A**). Samples of three different stages of anti-FLAG affinity purification were analyzed on western blot (**Fig. 2B**). A protein corresponding to the predicted molecular weight of SF-tagged *Whrna* (83kDa) was identified in *SF-whrna* retinal extracts (inp.) using anti-FLAG antibodies, but not in extracts derived from wild-type retinas. SF-*Whrna* was abundantly present in the eluted sample after affinity purification (elu.), whereas little of the SF-*Whrna* protein could be detected in the flow-through (flo.) that contains the unbound proteins. This indicates that, using this procedure, we were able to purify SF-*Whrna* from lysates of adult transgenic zebrafish eyes.

A *SF-Whrna* retina

B Wild-type retina



C Wild-type retina

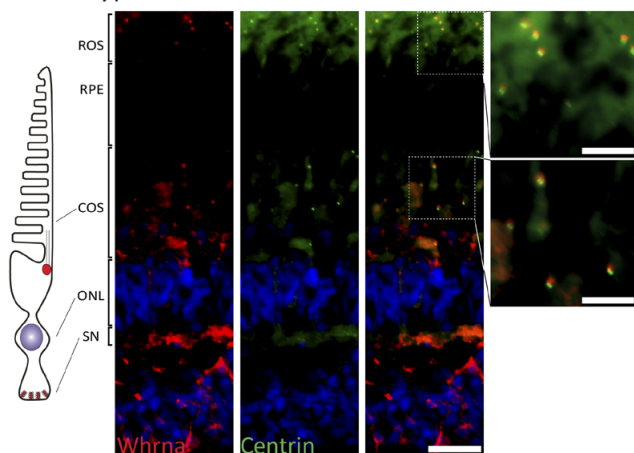


Figure 1. *SF-Whrna* is present in the region of the connecting cilium and in the inner segment of adult *SF-whrna* zebrafish photoreceptors.

(A) Immunohistochemistry using FLAG-recognizing antibodies (green) in the retina of *SF-whrna* zebrafish. Flag-labeling is present in the photoreceptor inner segment and at the base of the connecting cilium where it is partially overlapping with anti-centrin signals (red). (B) The retinas of wild-type TLF zebrafish were used as negative control. No anti-FLAG signal could be detected. (C) Immunohistochemical analysis of wild-type zebrafish retinas using antibodies directed against Whrna. Whrna (red) colocalizes with the connecting cilium marker centrin (green). No specific staining could be observed at the photoreceptor synapses (OPL). COS = cone outersegment, ONL = outer nuclear layer, OPL = outer plexiform layer, ROS = rod outer segment. Scalebars represent 20 μm in the overview pictures and 10 μm in close-up pictures.

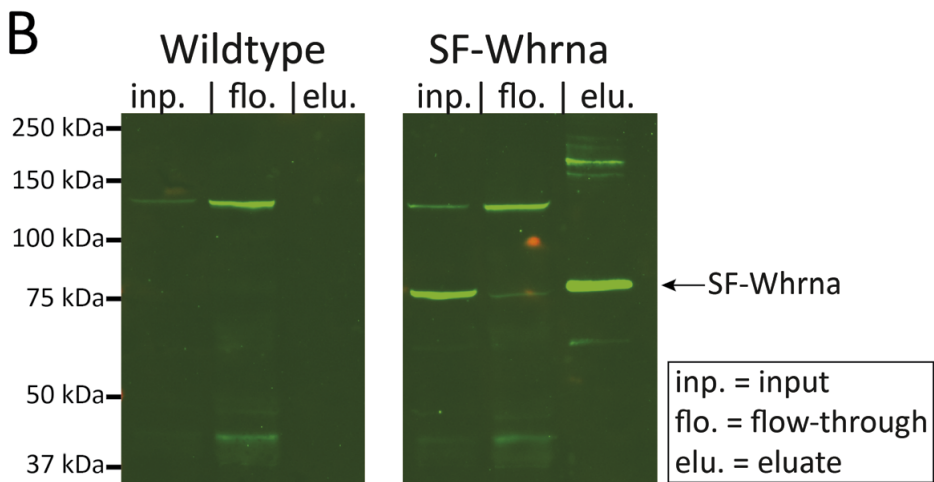
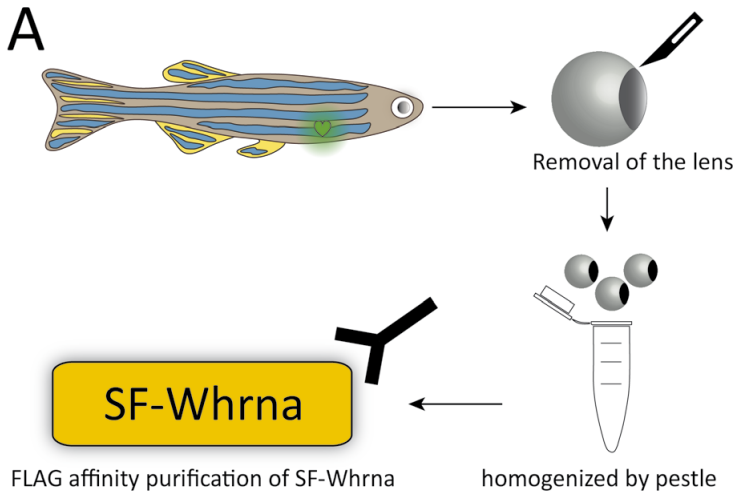


Figure 2. FLAG-affinity purification from *SF-whrna* zebrafish retinas. (A) Schematic overview of the protocol for affinity purification of *in vivo*-assembled SF-Whrna-associated protein complexes. Eyes were sampled from *SF-whrna* zebrafish, after which the lens was surgically removed. The remaining tissue was homogenized in lysis buffer using a pestle and the resulting extract was used as input for an anti-FLAG affinity purification experiment. (B) Western blot analysis of FLAG-tagged proteins in the retinal extract before (inp.) and after (flo.) anti-FLAG affinity purification and after elution of the anti-FLAG-containing beads (elu.). SF-Whrna (83 kDa) is indicated by an arrow. The flow-through (flo.) contains all proteins that are not bound to the anti-FLAG beads and only a minimal amount of SF-Whrna. Non-annotated bands were not further investigated.

Subsequently, a mass spectrometry analysis was performed to identify the isolated SF-Whrna-associated proteins. The resulting peptide sequences were blasted against the translated EMBL zebrafish database (trEMBL) in order to also include non-annotated zebrafish proteins. Keratins are known contaminants of mass spectrometry samples and were therefore removed from the database prior to analysis (**Supplemental Table 1**). Data analysis revealed 795 unique proteins that co-purified with SF-Whrna at least once in the three replicate affinity purification experiments (**Supplemental Table 2**). Nineteen proteins were considered as potential Whrna interaction partners (**Fig. 3**), since they were identified in at least two out of three replicates, but not in eluates derived from wild-type retinas. Except for Whrnb, none of the nineteen repeatedly identified proteins are orthologs of previously identified whirlin-interaction partners.

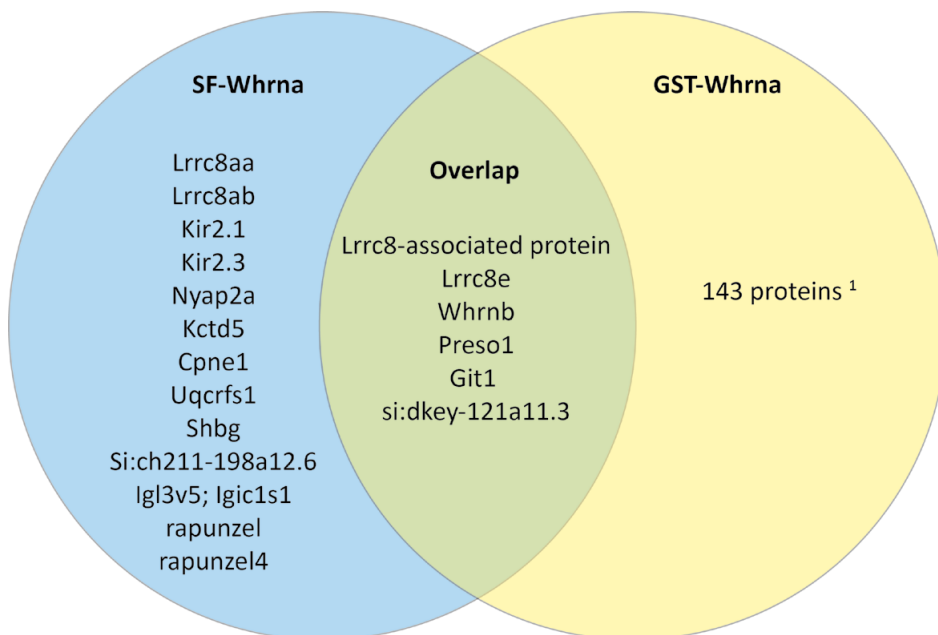


Figure 3. Overview of retrieved SF-Whrna-associated proteins after FLAG-affinity purification or GST pull-down. Proteins that have been identified as candidate Whrna interaction partners, arranged by the purification method (i.e. by FLAG-affinity purification (SF-Whrna) or by GST pull-down (GST-Whrna)). ¹ Proteins retrieved by GST pull-down are listed in **Supplemental Table 3**.

GST-Whrna pull-down analysis from zebrafish retinal extracts

To validate the results obtained from the affinity purification experiments, we performed a glutathione S-transferase (GST) pull-down assay using wild-type zebrafish retinal extracts. The resulting protein samples were analyzed by mass spectrometry and proteins that were identified in two GST-Whrna replicate assays, but not in GST only assays (GST-solo), were regarded as being specific for Whrna (**Supplemental Table 3**).

This resulted in a list of 149 Whrna candidate interaction partners, of which Whrnb is the only zebrafish ortholog of a previously known binding partner of whirlin, as human whirlin is known to homodimerize.

Only six proteins were identified in both the GST-Whrna pull-down assay and the FLAG-affinity purification experiments (**Fig. 3**). Next to Whrnb, two members of the volume regulated anion channel (VRAC) family were retrieved: *Lrrc8e* (leucine-rich repeat-containing 8 subunit e) and the *si:ch211-106h11.1*-encoded protein named 'Novel protein similar to vertebrate leucine rich repeat containing 8 family' (Uniprot: B0S5F3), which shows a high sequence similarity to proteins of the vertebrate leucine-rich repeat-containing 8 family. The VRAC subunits *Lrrc8aa* and *Lrrc8ab* were identified after SF-Whrna affinity purification, but were omitted from the list of proteins identified after GST-Whrna pull-down experiments as several peptides of these proteins were also pulled down from retinal extracts by GST only. Both *Lrrc8aa* and *Lrrc8ab* are orthologs of the human LRRC8 subunit A (LRRC8A), which is also known as SWELL1. With the aforementioned filtering criteria, both protein extraction methods also revealed the *Frmpr4*-encoded protein *Preso1*, *Git1* (G protein-coupled receptor kinase-interacting ArfGAP 1) and *si:dkey-121a11.3* (ortholog of human KIAA1614).

In total, SF-Whrna affinity purification resulted in the identification of 13 proteins that were not identified after GST-Whrna pull-down. Most noteworthy are the two members of the potassium voltage-gated channel subfamily J, named Kir2.1 (encoded by *Kcnj2a* or *Kcnj2b*) and Kir2.3 (encoded by *Kcnj4*), and two paralogs of the zebrafish-specific protein Rapunzel: Rapunzel (encoded by *Rpz*) and Rapunzel 4 (encoded by *Rpz4*). Within the list of 143 proteins that were only isolated after GST-Whrna pull-down analyses, no known USH-related protein complexes or networks were identified upon manual screening.

Whirlin directly associates with *Preso1* and Kir2.3

We selected several of the identified candidate interactors for a cross species validation by investigating the ability of human whirlin to directly bind the human orthologs of candidate interactors in a yeast two-hybrid assay. For this experiment, we selected LRRC8A and LRRC8D because of the consistent retrieval of several *Lrrc8*-channel subunits. Since many of the established protein-protein interactions of whirlin depend on a PDZ (PSD95, Discs large, ZO-1) domain -PDZ binding motif (PBM)-based interaction (van Wijk et al. 2006), we expanded our experiment with proteins containing a predicted PDZ domain or PBM. For this reason, we also included *Preso1* (PDZ-domain and PBM) and Kir2.3 (PBM) (**Fig. 4A**). The orthologs of *Lrrc8e* and Kir2.1 were not included, since only very few peptides of these proteins were identified in the affinity purification and GST-pull-down experiments. For the transmembrane (TM) proteins LRRC8A, LRRC8D and Kir2.3, only the intracellular regions were analyzed for the ability to interact with

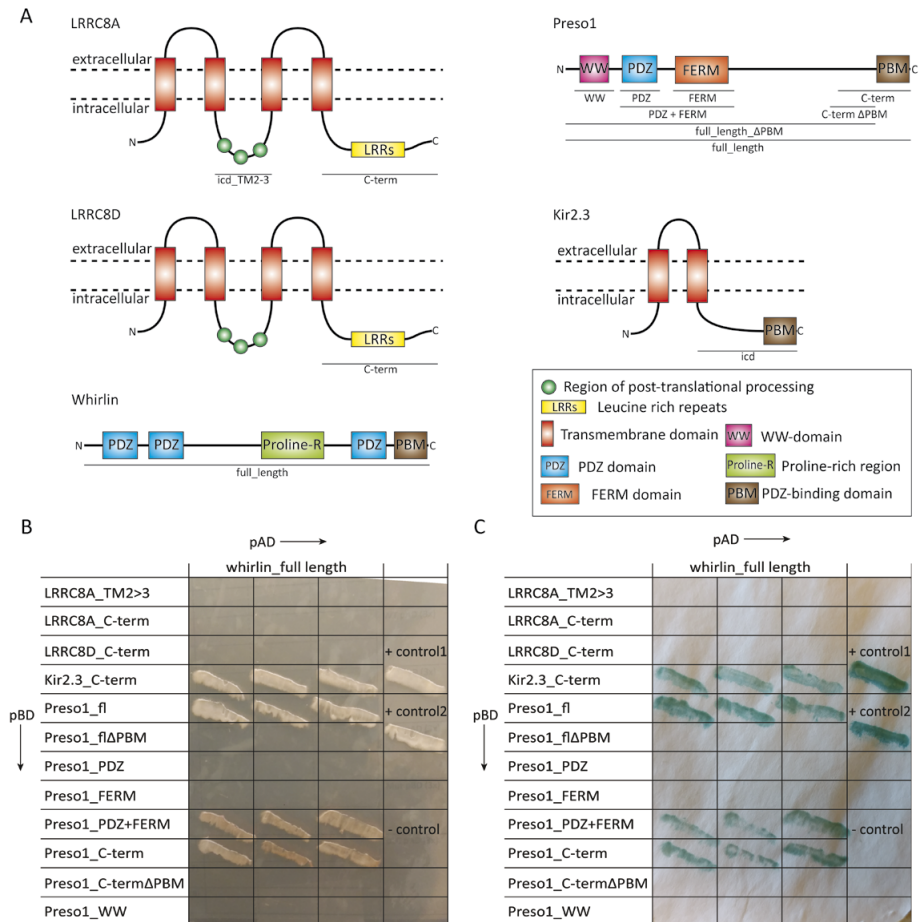


Figure 4. Human whirlin binds directly to Preso1 and Kir2.3, but not to LRRCA8A and LRRCA8D.

(A) Graphical representation of the predicted protein structures of human LRRCA8A, LRRCA8D, whirlin, Preso1 and Kir2.3. Protein fragments that are used in yeast two-hybrid experiments are underlined. **(B)** Yeast two-hybrid reporter gene activation upon binding of whirlin to candidate interactors. The panel shows selective yeast growth after the most stringent amino acid restriction (-WHLA). Plasmids encoding fragments of candidate interactors fused to a DNA binding domain (pBD) are co-expressed in yeast with a plasmid encoding full length whirlin fused to an activator domain (pAD). All combinations of protein fragments, except for controls, were analyzed *in triplo*. **(C)** Analysis of β -galactosidase reporter gene activation in yeast grown on the selective medium as shown in (B). Blue color results from the hydrolysis of the X- β -gal substrate by β -galactosidase and is indicative for an interaction between the two protein fragments. + control 1 and 2 = positive controls and - control = negative control.

full length whirlin. For LRRCA8A, we used the intracellular region between TM2 and TM3 (LRRCA8A_TM2>3) and the C-terminal region that contains a leucine-rich repeat (LRR) domain (LRRCA8A_C-term). For LRRCA8D and Kir2.3, only the C-terminal intracellular regions were used (LRRCA8D_C-term and Kir2.3_icd, respectively) (**Fig. 4A**). The possible

interaction between Preso1 and full length whirlin was investigated in more detail, using full-length Preso1 with or without PBM and multiple (combinations of) protein domains.

The yeast two-hybrid experiments were performed *in triplo* and identified a direct interaction between human full length whirlin and the intracellular region of Kir2.3 and multiple fragments of Preso1 (**Fig. 4B, C**). Interestingly, whirlin directly interacts with full length Preso1, but the interaction is lost when the PBM of Preso1 is removed. The protein fragment containing only the PDZ and FERM domains (PDZ+FERM) of Preso1 was also able to interact with full length whirlin, while the individual PDZ or FERM domains were not. We could not perform reciprocal assays with whirlin fused to the DNA binding domain (BD), as BD-whirlin auto-activates the reporter genes (data not shown). For the same reason, it was not possible to analyze the interaction between whirlin and a Kir2.3_icd fragment without PBM, as expression of BD-Kir2.3_icd Δ PBM also results in an auto-activation of the reporter genes. Taken together, these results indicate that whirlin directly binds to the C-terminal PBM of Preso1 and the intracellular region of Kir2.3.

Analysis of mutant animal models for candidate interactors

To further investigate the functional relevance of the interaction between whirlin and the identified candidate interaction partners, we searched for known mutant animal models. No animals lacking Kir2.3 are described so far. For the whirlin candidate interactor Preso1 (encoded by *Frmpr4*), a knock-out mouse has been described (Hu et al. 2012). This mouse model demonstrated sustained pain signaling due to the loss of a negative feedback on metabotropic glutamate receptor 5 (mGluR5) signaling. Since the retina was never evaluated in these mice, we aimed to determine the subcellular localization of Preso1 in the murine retina and to investigate the effect of absence of Preso1 on retinal morphology. However, using two previously described antibodies we were unable to detect Preso1 in the retina of P19 or P108-old wild-type mice (data not shown) (Lee et al. 2008, Hu et al. 2012). In parallel, we investigated whether the loss of Preso1 affects retinal morphology. Retinal lamination in *Frmpr4*^{-/-} mice was investigated using toluidine blue staining (**Fig. 5A**) and retinal stress was evaluated by immunohistochemical analysis of glial fibrillary acidic protein (GFAP) that has been described as an early marker for photoreceptor degeneration (**Fig. 5B**) (Liu et al. 2007). Both analyses did not reveal any sign of aberrant retinal lamination or retinal degeneration in the *Frmpr4*^{-/-} mouse retina at post-natal day 19 (P19) or at 3 months (P108) of age.

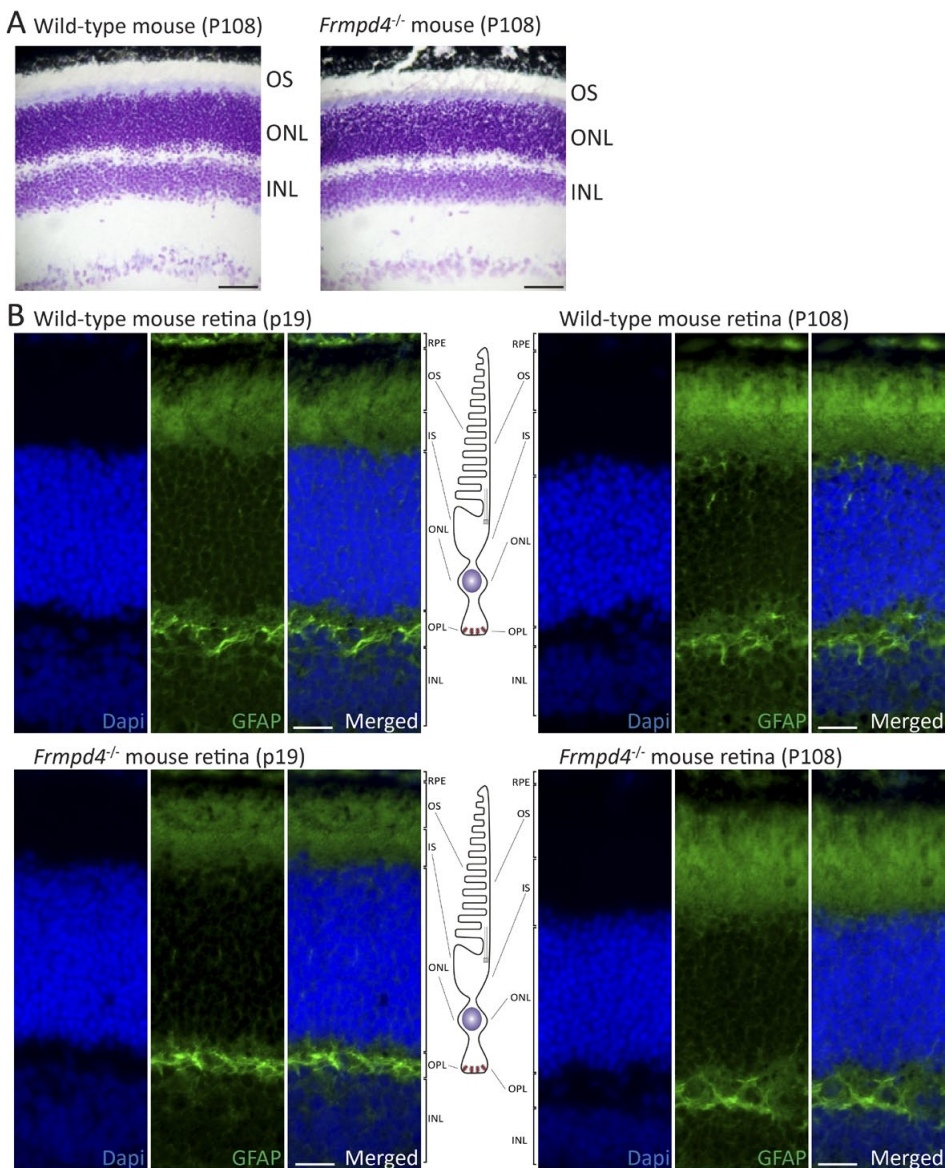


Figure 5. Analysis of the *Frmprd4*^{-/-} mouse retina. (A) The morphology of the *Frmprd4*^{-/-} mouse retina is visualized by toluidine blue staining. No differences were observed in the thickness of the nuclear layers or outer segments between wild-type (left) and *Frmprd4*^{-/-} (right) retinas at post-natal day 108 (P108). (B) Antibodies recognizing GFAP (green signal) were used to analyze retinal sections derived from eyes of either wild-type (upper panel) or *Frmprd4*^{-/-} (lower panel) mice at P19 and P108. In both the wild-type and mutant retina a similar GFAP immunoreactivity is observed exclusively at the OPL, confirming the absence of retinal degeneration in the *Frmprd4*^{-/-} mouse. INL = inner nuclear layer, ONL = outer nuclear layer, OPL = outer plexiform layer, COS = cone outer segment, ROS = rod outer segment, scale bars in (A) represent 60 μ m. In (B), scale bars represent 20 μ m.

DISCUSSION

This study introduces a novel strategy to isolate and identify native Whrna-associated protein complexes from photoreceptors of adult transgenic zebrafish. We compared our approach with a GST pull-down assay that is commonly used for the identification of protein-protein interactions. Our strategy identified several novel candidate Whrna interaction partners (**Fig. 6**), of which human Preso1 and Kir2.3 were validated as direct interactors of human whirlin using a yeast two-hybrid assay. Kir2.3 was not identified in the GST-Whrna pull-down experiments, indicating that our approach likely identified interaction partners of Whrna that were otherwise missed.

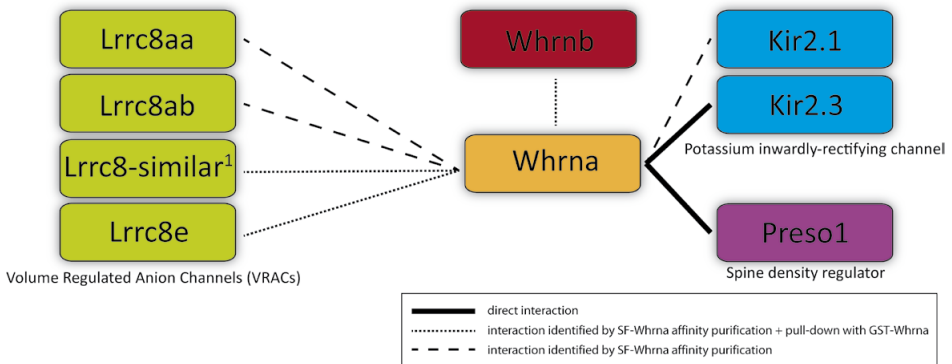


Figure 6. Most prominent candidate interactors of Whrna that have been identified in this study. Whrna candidate binding partners that have been identified in this study are shown. Proteins that only co-purified with SF-Whrna affinity purification are connected by an open dashed line, proteins identified by both SF-Whrna affinity purification and GST-Whrna pull-down assays are connected by a packed dashed line and the proteins of which the human ortholog directly interacted with human full length whirlin are connected by a solid line. ¹ lrrc8-similar = Novel protein similar to vertebrate leucine rich repeat containing 8 family.

Protein-protein interaction studies have unraveled many novel connections with and between proteins involved in Usher syndrome (summarized by Kremer et al. 2006, Boldt et al. 2016, Slijkerman, Kremer, and Van Wijk 2017). However, the mechanism through which the loss of Usher syndrome-associated proteins results in retinal degeneration has not yet been uncovered. The protein-protein interaction assays used to identify novel USH-associated proteins so far relied on non-retinal cell models, such as HEK293T, that lack expression of photoreceptor-specific proteins and on artificial *in vitro* methodologies that are mainly based on over-expression (e.g. yeast two-hybrid, co-immunoprecipitation and GST pull-down). Therefore, we expected that these approaches could have missed biologically relevant interaction partners resulting in a lack of complete understanding of the role of the Usher protein complex in photoreceptors. Although it is in theory possible to culture induced pluripotent stem cell-derived retinal organoids,

this procedure is too expensive and labor intense to yield the number of photoreceptors required for proteomic studies. In contrast, the zebrafish retina contains photoreceptors that are anatomically and functionally comparable to those present in man (Slijkerman et al. 2015). For this reason, we generated a transgenic zebrafish line that expresses an SF-tagged ortholog of one of the key organizers of the Usher protein complex, whirlin (SF-Whrna), in photoreceptors to enable the isolation of *in vivo*-assembled whirlin-associated protein complexes from the biologically relevant cells.

The cassette used for zebrafish transgenesis contains *SF-Whrna* under the control of the zebrafish (3x PRE-1)-1.2 kb ZOP promoter that was previously shown to drive rod-specific gene expression (Morrissey et al. 2011). However, FLAG-recognizing antibodies labeled the periciliary region of both rod (upper row) and cone (lower row) photoreceptors in our experiments, indicating that the promoter in our set-up drives the expression of SF-tagged Whrna in both rods and cones. Since whirlin is endogenously expressed in both photoreceptor types, we used the unexpected additional expression of SF-Whrna in cones to our advantage and did not further investigate the difference with previous studies.

We successfully purified SF-Whrna-associated protein complexes from transgenic adult zebrafish retinas. Subsequently, mass spectrometry of the purified proteins identified the co-purified proteins that are potential direct or indirect interaction partners of Whrna. Strikingly, with the exception of Whrnb, none of the other USH1 and USH2 proteins that have been previously shown to interact with whirlin were identified after applying all the necessary data filtering steps. The USH1 proteins Myo7aa and Myo7ab were retrieved by affinity purification from both SF-Whrna and wild-type retinas and were therefore not regarded as specific interactors of Whrna in this experiment. The absence of the other USH2 proteins, ADGRV1 and usherin, from the list of co-purified proteins might well be due to the large size of these proteins. In addition, also the zebrafish orthologs of previously published non-Usher syndrome-related whirlin interaction partners, such as Ngl-1, Caska/b, Myo15aa and Mpp1, were not found to co-purify with SF-Whrna. We also did not observe any overlap in proteins that co-purified with whirlin in our approaches and those purified from HEK293T cells, except for two peptides of Git1 (Boldt et al. 2016). Several of the mentioned interaction partners of whirlin have previously been demonstrated to exert important functions in the auditory hair cells, but may not form a protein complex with whirlin in photoreceptors.

Interestingly, other studies already indirectly associated Preso1 (encoded by *FRMPD4*) with whirlin by unraveling that both whirlin and Preso1 directly interact with GPSM2, otherwise known as Leu-Gly-Asn repeat-enriched protein (LGN) (Yuzawa et al. 2011, Takayanagi, Yuzawa, and Sumimoto 2015, Mauriac et al. 2017). GPSM2 was not retrieved in our study, but was previously shown to depend on whirlin for its proper localization in the tips of stereocilia and to be required for stereocilia elongation in the

inner ear of mice (Mauriac et al. 2017). In the retina, GPSM2 is present in the photoreceptor inner segments, where it associates with transducin (Nair et al. 2005). Based on the identification of Preso1 as a direct interactor of whirlin, we postulate that Preso1 also co-functions with whirlin in the retina. Using a *Frmpr4* knock-out mouse model, Hu and colleagues previously showed that Preso1 regulates phosphorylation and signaling of group I metabotropic glutamate receptor 5 at the post synaptic density (Hu et al. 2012). However, the retina and cochlea of this mouse model were never evaluated. Preso1 has been prominently detected in the adult retina (Human Proteome Map: Kim et al. 2014) and therefore we investigated whether Preso1 is essential in the murine retina by a morphological analysis of *Frmpr4*^{-/-} retinas and performed immunohistochemistry to determine the localization of Preso1 in the retina. While ample immunoreactivity for Preso1 was observed in the hippocampal neurons that were used as a positive control, no specific Preso1 immunoreactivity was detected in photoreceptors. Preso1 is either not present in the murine photoreceptor or is present in a retina-specific isoform that is not recognised by the employed anti-Preso1 antibodies. Alternative explanations could be that Preso1 is only expressed during certain stages of development, that it is only expressed in dark-adapted retina or that it is only detectable in case of cellular stress. In these cases, loss of Preso1 from the retina could still result in retina defects. However, we did not observe any sign of retinal degeneration in the retina of three months old *Frmpr4*^{-/-} mice, both in thickness of the outer nuclear layer and in expression of the retinal cell stress marker GFAP. Of note, USH2 knock-out mice demonstrate only a mild form of retinal degeneration with a very late onset, which may be similar for the retina of *Frmpr4*^{-/-} mice.

The second protein that was identified as a direct interaction partner of whirlin is Kir2.3, an inwardly-rectifying potassium channel subunit. Kir2.3 proteins are arranged as homomeric channels or form heteromeric channels by association with Kir2.1 (Preisig-Muller et al. 2002), of which also several peptides were co-purified with SF-Whrna. Kir2.3 was previously shown to localize at the post-synaptic membrane of excitatory synapses in the olfactory bulb (Inanobe et al. 2002) and, together with Kir2.1, in the somata of retinal ganglion cells and in photoreceptors (Chen et al. 2004). Functionally, Kir2-channels were indicated to maintain the membrane resting potential near the K⁺ equilibrium potential (Inanobe et al. 2002, Hibino et al. 2010).

The expression of Kir2.3 at the basolateral membrane of renal epithelial cells is positively regulated by a direct interaction with LIN7C, which acts in concert with calcium/calmodulin-dependent serine protein kinase (CASK) (Olsen et al. 2002, Alewine et al. 2006, Alewine et al. 2007). In mammalian neurons, a trimeric complex of CASK, either LIN7A, LIN7B or LIN7C, and APBA1, was shown to be involved in the regulation of pre- and postsynaptic vesicle transport (Misawa et al. 2001). Interestingly, whirlin was initially described as a CASK-interacting protein (CIP98) that was isolated from rat brain-derived

protein extracts (Yap et al. 2003). As such, whirlin was proposed to act as a synaptic adaptor protein for CASK scaffolding proteins (Yap et al. 2003), although we did not detect SF-Whrna at the synapse of adult zebrafish photoreceptors. Expression of mutant LIN7C that lacks the ability to interact with Kir2.3 in polarized MDCK cells, resulted in the accumulation of Kir2.3 in large intracellular vesicles (Alewine et al. 2007). Extensive morphological analyses of whirlin-deficient murine photoreceptors revealed the accumulation of vacuole-like structures at the periciliary membrane (PCM), but no obvious defects at the synapse (Yang et al. 2010). CASK has been found in all retinal synapses, but it is still unclear whether CASK is also present in the region of the photoreceptor connecting cilium (Anjum, Ayoubian, and Schmitz 2014). Possibly, a complex containing whirlin and CASK is anchored at the periciliary membrane by the transmembrane USH2 proteins to regulate the acceptance of Kir2.3-positive vesicles. Downregulation of Kir2.3 expression in mouse medium spiny neurons was shown to induce a hyperpolarized membrane resting potential (Cazorla et al. 2012), resulting in an impaired ability to generate action potentials. Therefore we hypothesize that a controlled acceptance of Kir2.3-containing vesicles at the PCM is highly important for maintaining the excitability of photoreceptors. Future functional analyses using suitable cellular and animal models will unveil whether the interactions between whirlin, Kir2.3 and CASK are indeed biologically relevant in the retina and to what extent a disrupted association with whirlin contributes to the observed retinal phenotype in USH2d patients.

ACKNOWLEDGEMENTS

The authors would like to thank Stef Letteboer and Kaman Wu for their technical assistance with the yeast two-hybrid experiments. Furthermore, we are grateful to Prof. Dr. Paul Worley, Dr. Raozhou Lin and Juhong Zhang (department of Neuroscience, Johns Hopkins University, Baltimore - U.S.A.) for sharing anti-Prso1 antibodies and isolated eyes from the *Fmpd4* knock-out mice; Prof. Dr. Eunjoon Kim and Rynhee Kim (Department of Biological Sciences, Korea Advanced Institute of Science and Technology (KAIST), Daejeon - South Korea) for providing anti-Prso1 antibodies and Prof. Dr. Brendan Kennedy (School Of Biomolecular & Biomed Science, Conway Institute, Dublin - Ireland) for sharing the 3xPRE-ZOP promoter.

REFERENCES

- Alewine, C., B. Y. Kim, V. Hegde, and P. A. Welling. 2007. "Lin-7 targets the Kir 2.3 channel on the basolateral membrane via a L27 domain interaction with CASK." *Am J Physiol Cell Physiol* 293 (6):C1733-41. doi: 10.1152/ajpcell.00323.2007.
- Alewine, C., O. Olsen, J. B. Wade, and P. A. Welling. 2006. "TIP-1 has PDZ scaffold antagonist activity." *Mol Biol Cell* 17 (10):4200-11. doi: 10.1091/mbc.E06-02-0129.
- Anjum, R., H. Ayoubian, and F. Schmitz. 2014. "Differential synaptic distribution of the scaffold proteins Cask and Caskin1 in the bovine retina." *Mol Cell Neurosci* 62:19-29. doi: 10.1016/j.mcn.2014.08.004.
- Belyantseva, I. A., E. T. Boger, S. Naz, G. I. Frolenkov, J. R. Sellers, Z. M. Ahmed, A. J. Griffith, and T. B. Friedman. 2005. "Myosin-XVa is required for tip localization of whirlin and differential elongation of hair-cell stereocilia." *Nat Cell Biol* 7 (2):148-56. doi: 10.1038/ncb1219.
- Boldt, K., J. van Reeuwijk, Q. Lu, K. Koutroumpas, T. M. Nguyen, Y. Texier, S. E. van Beersum, N. Horn, J. R. Willer, D. A. Mans, G. Dougherty, I. J. Lamers, K. L. Coene, H. H. Arts, M. J. Betts, T. Beyer, E. Bolat, C. J. Gloeckner, K. Haidari, L. Hettterschijt, D. Iaconis, D. Jenkins, F. Klose, B. Knapp, B. Latour, S. J. Letteboer, C. L. Marcelis, D. Mitic, M. Morleo, M. M. Oud, M. Riemersma, S. Rix, P. A. Terhal, G. Toedt, T. J. van Dam, E. de Vrieze, Y. Wissinger, K. M. Wu, G. Apic, P. L. Beales, O. E. Blacque, T. J. Gibson, M. A. Huynen, N. Katsanis, H. Kremer, H. Omran, E. van Wijk, U. Wolfrum, F. Kepes, E. E. Davis, B. Franco, R. H. Giles, M. Ueffing, R. B. Russell, R. Roepman, and Uk K. Rare Diseases Group. 2016. "An organelle-specific protein landscape identifies novel diseases and molecular mechanisms." *Nat Commun* 7:11491. doi: 10.1038/ncomms11491.
- Brown, S. D., R. E. Hardisty-Hughes, and P. Mburu. 2008. "Quiet as a mouse: dissecting the molecular and genetic basis of hearing." *Nat Rev Genet* 9 (4):277-90. doi: 10.1038/nrg2309.
- Cao, Z., L. D. Jensen, P. Rouhi, K. Hosaka, T. Lanne, J. F. Steffensen, E. Wahlberg, and Y. Cao. 2010. "Hypoxia-induced retinopathy model in adult zebrafish." *Nat Protoc* 5 (12):1903-10. doi: 10.1038/nprot.2010.149.
- Cazorla, M., M. Shegda, B. Ramesh, N. L. Harrison, and C. Kellendonk. 2012. "Striatal D2 receptors regulate dendritic morphology of medium spiny neurons via Kir2 channels." *J Neurosci* 32 (7):2398-409. doi: 10.1523/JNEUROSCI.6056-11.2012.
- Chen, L., Y. C. Yu, J. W. Zhao, and X. L. Yang. 2004. "Inwardly rectifying potassium channels in rat retinal ganglion cells." *Eur J Neurosci* 20 (4):956-64. doi: 10.1111/j.1460-9568.2004.03553.x.
- Chen, Q., J. Zou, Z. Shen, W. Zhang, and J. Yang. 2014. "Whirlin and PDZ domain-containing 7 (PDZD7) proteins are both required to form the quaternary protein complex associated with Usher syndrome type 2." *J Biol Chem* 289 (52):36070-88. doi: 10.1074/jbc.M114.610535.
- Cox, J., and M. Mann. 2008. "MaxQuant enables high peptide identification rates, individualized p.p.b.-range mass accuracies and proteome-wide protein quantification." *Nat Biotechnol* 26 (12):1367-72. doi: 10.1038/nbt.1511.
- Dona, M., R. Slijkerman, K. Lerner, S. Broekman, J. Wegner, T. Howat, T. Peters, L. Hettterschijt, N. Boon, E. de Vrieze, N. Sorusch, U. Wolfrum, H. Kremer, S. Neuhaus, J. Zang, M. Kamermans, M. Westerfield, J. Phillips, and E. van Wijk. 2018. "Usherin defects lead to early-onset retinal dysfunction in zebrafish." *Exp Eye Res* 173:148-159. doi: 10.1016/j.exer.2018.05.015.
- Gloeckner, C. J., K. Boldt, and M. Ueffing. 2009. "Strep/FLAG tandem affinity purification (SF-TAP) to study protein interactions." *Curr Protoc Protein Sci* Chapter 19:Unit19 20. doi: 10.1002/0471140864.ps1920s57.

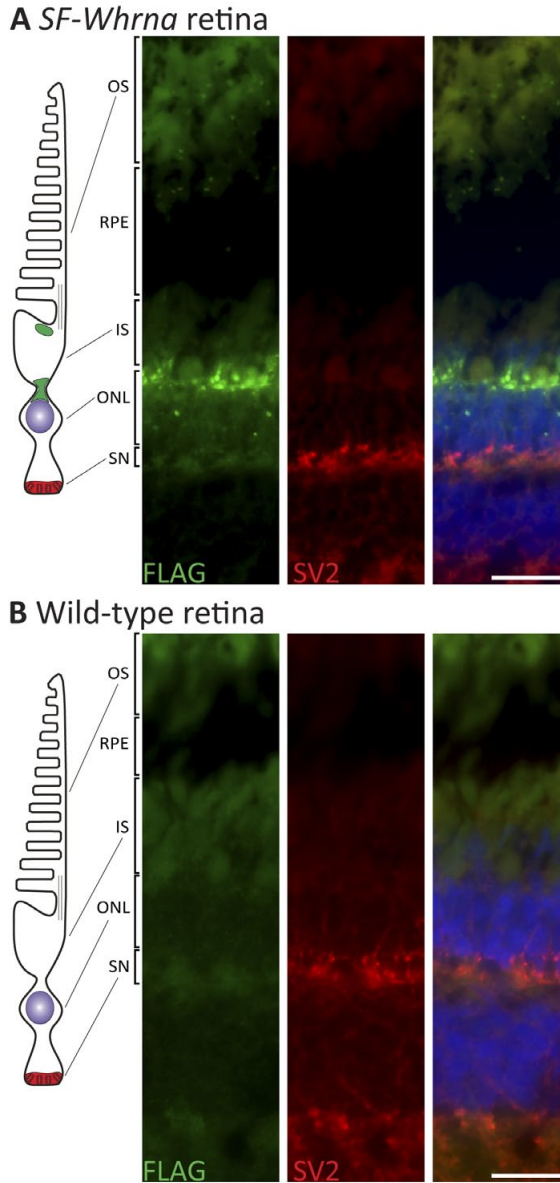
- Gosens, I., E. van Wijk, F. F. Kersten, E. Krieger, B. van der Zwaag, T. Marker, S. J. Letteboer, S. Dusseljee, T. Peters, H. A. Spiereburg, I. M. Punte, U. Wolfrum, F. P. Cremers, H. Kremer, and R. Roepman. 2007. "MPP1 links the Usher protein network and the Crumbs protein complex in the retina." *Hum Mol Genet* 16 (16):1993-2003. doi: 10.1093/hmg/ddm147.
- Grati, M., J. B. Shin, M. D. Weston, J. Green, M. A. Bhat, P. G. Gillespie, and B. Kachar. 2012. "Localization of PDZD7 to the stereocilia ankle-link associates this scaffolding protein with the Usher syndrome protein network." *J Neurosci* 32 (41):14288-93. doi: 10.1523/JNEUROSCI.3071-12.2012.
- Hartel, B. P., M. Lofgren, P. L. Huygen, I. Guchelaar, A. Njoe Kort N. Lo, A. M. Sadeghi, E. van Wijk, L. Tranebjaerg, H. Kremer, W. J. Kimberling, C. W. Cremers, C. Moller, and R. J. Pennings. 2016. "A combination of two truncating mutations in *USH2A* causes more severe and progressive hearing impairment in Usher syndrome type IIa." *Hear Res* 339:60-8. doi: 10.1016/j.heares.2016.06.008.
- Hibino, H., A. Inanobe, K. Furutani, S. Murakami, I. Findlay, and Y. Kurachi. 2010. "Inwardly rectifying potassium channels: their structure, function, and physiological roles." *Physiol Rev* 90 (1):291-366. doi: 10.1152/physrev.00021.2009.
- Hu, J. H., L. Yang, P. J. Kammermeier, C. G. Moore, P. R. Brakeman, J. Tu, S. Yu, R. S. Petralia, Z. Li, P. W. Zhang, J. M. Park, X. Dong, B. Xiao, and P. F. Worley. 2012. "Preso1 dynamically regulates group I metabotropic glutamate receptors." *Nat Neurosci* 15 (6):836-44. doi: 10.1038/nn.3103.
- Inanobe, A., A. Fujita, M. Ito, H. Tomoike, K. Inageda, and Y. Kurachi. 2002. "Inward rectifier K⁺ channel Kir2.3 is localized at the postsynaptic membrane of excitatory synapses." *Am J Physiol Cell Physiol* 282 (6):C1396-403. doi: 10.1152/ajpcell.00615.2001.
- Kim, M. S., S. M. Pinto, D. Getnet, R. S. Nirujogi, S. S. Manda, R. Chaerkady, A. K. Madugundu, D. S. Kelkar, R. Isserlin, S. Jain, J. K. Thomas, B. Muthusamy, P. Leal-Rojas, P. Kumar, N. A. Sahasrabudhe, L. Balakrishnan, J. Advani, B. George, S. Renuse, L. D. Selvan, A. H. Patil, V. Nanjappa, A. Radhakrishnan, S. Prasad, T. Subbannayya, R. Raju, M. Kumar, S. K. Sreenivasamurthy, A. Marimuthu, G. J. Sathe, S. Chavan, K. K. Datta, Y. Subbannayya, A. Sahu, S. D. Yelamanchi, S. Jayaram, P. Rajagopalan, J. Sharma, K. R. Murthy, N. Syed, R. Goel, A. A. Khan, S. Ahmad, G. Dey, K. Mudgal, A. Chatterjee, T. C. Huang, J. Zhong, X. Wu, P. G. Shaw, D. Freed, M. S. Zahari, K. K. Mukherjee, S. Shankar, A. Mahadevan, H. Lam, C. J. Mitchell, S. K. Shankar, P. Satishchandra, J. T. Schroeder, R. Sirdeshmukh, A. Maitra, S. D. Leach, C. G. Drake, M. K. Halushka, T. S. Prasad, R. H. Hruban, C. L. Kerr, G. D. Bader, C. A. Iacobuzio-Donahue, H. Gowda, and A. Pandey. 2014. "A draft map of the human proteome." *Nature* 509 (7502):575-81. doi: 10.1038/nature13302.
- Kremer, H., E. van Wijk, T. Marker, U. Wolfrum, and R. Roepman. 2006. "Usher syndrome: molecular links of pathogenesis, proteins and pathways." *Hum Mol Genet* 15 Spec No 2:R262-70. doi: 10.1093/hmg/ddl205.
- Kwan, K. M., E. Fujimoto, C. Grabher, B. D. Mangum, M. E. Hardy, D. S. Campbell, J. M. Parant, H. J. Yost, J. P. Kanki, and C. B. Chien. 2007. "The Tol2kit: a multisite gateway-based construction kit for Tol2 transposon transgenesis constructs." *Dev Dyn* 236 (11):3088-99. doi: 10.1002/dvdy.21343.
- Lee, H. W., J. Choi, H. Shin, K. Kim, J. Yang, M. Na, S. Y. Choi, G. B. Kang, S. H. Eom, H. Kim, and E. Kim. 2008. "Preso, a novel PSD-95-interacting FERM and PDZ domain protein that regulates dendritic spine morphogenesis." *J Neurosci* 28 (53):14546-56. doi: 10.1523/JNEUROSCI.3112-08.2008.

- Liu, X., O. V. Bulgakov, K. N. Darrow, B. Pawlyk, M. Adamian, M. C. Liberman, and T. Li. 2007. "Usherin is required for maintenance of retinal photoreceptors and normal development of cochlear hair cells." *Proc Natl Acad Sci U S A* 104 (11):4413-8. doi: 10.1073/pnas.0610950104.
- Maerker, T., E. van Wijk, N. Overlack, F. F. Kersten, J. McGee, T. Goldmann, E. Sehn, R. Roepman, E. J. Walsh, H. Kremer, and U. Wolfrum. 2008. "A novel Usher protein network at the periciliary reloading point between molecular transport machineries in vertebrate photoreceptor cells." *Hum Mol Genet* 17 (1):71-86. doi: 10.1093/hmg/ddm285.
- Manor, U., A. Disanza, M. Grati, L. Andrade, H. Lin, P. P. Di Fiore, G. Scita, and B. Kachar. 2011. "Regulation of stereocilia length by myosin XVa and whirlin depends on the actin-regulatory protein Eps8." *Curr Biol* 21 (2):167-72. doi: 10.1016/j.cub.2010.12.046.
- Mauriac, S. A., Y. E. Hien, J. E. Bird, S. D. Carvalho, R. Peyrourou, S. C. Lee, M. M. Moreau, J. M. Blanc, A. Geysler, C. Medina, O. Thoumine, S. Beer-Hammer, T. B. Friedman, L. Ruttiger, A. Forge, B. Nurnberg, N. Sans, and M. Montcouquiol. 2017. "Defective Gpsm2/Galphi3 signalling disrupts stereocilia development and growth cone actin dynamics in Chudley-McCullough syndrome." *Nat Commun* 8:14907. doi: 10.1038/ncomms14907.
- Mburu, P., M. R. Romero, H. Hilton, A. Parker, S. Townsend, Y. Kikkawa, and S. D. Brown. 2010. "Gelsolin plays a role in the actin polymerization complex of hair cell stereocilia." *PLoS One* 5 (7):e11627. doi: 10.1371/journal.pone.0011627.
- Michalski, N., V. Michel, A. Bahloul, G. Lefèvre, J. Barral, H. Yagi, S. Chardenoux, D. Weil, P. Martin, J. P. Hardelin, M. Sato, and C. Petit. 2007. "Molecular characterization of the ankle-link complex in cochlear hair cells and its role in the hair bundle functioning." *J Neurosci* 27 (24):6478-88. doi: 10.1523/JNEUROSCI.0342-07.2007.
- Misawa, H., Y. Kawasaki, J. Mellor, N. Sweeney, K. Jo, R. A. Nicoll, and D. S. Bredt. 2001. "Contrasting localizations of MALS/LIN-7 PDZ proteins in brain and molecular compensation in knockout mice." *J Biol Chem* 276 (12):9264-72. doi: 10.1074/jbc.M009334200.
- Morrissey, M. E., S. Shelton, S. E. Brockerhoff, J. B. Hurley, and B. N. Kennedy. 2011. "PRE-1, a cis element sufficient to enhance cone- and rod- specific expression in differentiating zebrafish photoreceptors." *BMC Dev Biol* 11:3. doi: 10.1186/1471-213X-11-3.
- Nair, K. S., A. Mendez, J. B. Blumer, D. H. Rosenzweig, and V. Z. Slepak. 2005. "The presence of a Leu-Gly-Asn repeat-enriched protein (LGN), a putative binding partner of transducin, in ROD photoreceptors." *Invest Ophthalmol Vis Sci* 46 (1):383-9. doi: 10.1167/iops.04-1006.
- Olsen, J. V., L. M. de Godoy, G. Li, B. Macek, P. Mortensen, R. Pesch, A. Makarov, O. Lange, S. Horning, and M. Mann. 2005. "Parts per million mass accuracy on an Orbitrap mass spectrometer via lock mass injection into a C-trap." *Mol Cell Proteomics* 4 (12):2010-21. doi: 10.1074/mcp.T500030-MCP200.
- Olsen, O., H. Liu, J. B. Wade, J. Merot, and P. A. Welling. 2002. "Basolateral membrane expression of the Kir 2.3 channel is coordinated by PDZ interaction with Lin-7/CASK complex." *Am J Physiol Cell Physiol* 282 (1):C183-95. doi: 10.1152/ajpcell.00249.2001.
- Pierrache, L. H., B. P. Hartel, E. van Wijk, M. A. Meester-Smoor, F. P. Cremers, E. de Baere, J. de Zaeytijd, M. J. van Schooneveld, C. W. Cremers, G. Dagnelie, C. B. Hoyng, A. A. Bergen, B. P. Leroy, R. J. Pennings, L. I. van den Born, and C. C. Klaver. 2016. "Visual Prognosis in USH2A-Associated Retinitis Pigmentosa Is Worse for Patients with Usher Syndrome Type IIa Than for Those with Nonsyndromic Retinitis Pigmentosa." *Ophthalmology* 123 (5):1151-60. doi: 10.1016/j.ophtha.2016.01.021.

- Preisig-Muller, R., G. Schlichthorl, T. Goerge, S. Heinen, A. Bruggemann, S. Rajan, C. Derst, R. W. Veh, and J. Daut. 2002. "Heteromerization of Kir2.x potassium channels contributes to the phenotype of Andersen's syndrome." *Proc Natl Acad Sci U S A* 99 (11):7774-9. doi: 10.1073/pnas.102609499.
- Riazuddin, S., I. A. Belyantseva, A. P. Giese, K. Lee, A. A. Indzhykulia, S. P. Nandamuri, R. Yousaf, G. P. Sinha, S. Lee, D. Terrell, R. S. Hegde, R. A. Ali, S. Anwar, P. B. Andrade-Elizondo, A. Sirmaci, L. V. Parise, S. Basit, A. Wali, M. Ayub, M. Ansar, W. Ahmad, S. N. Khan, J. Akram, M. Tekin, S. Riazuddin, T. Cook, E. K. Buschbeck, G. I. Frolenkov, S. M. Leal, T. B. Friedman, and Z. M. Ahmed. 2012. "Alterations of the CIB2 calcium- and integrin-binding protein cause Usher syndrome type 1J and nonsyndromic deafness DFNB48." *Nat Genet* 44 (11):1265-71. doi: 10.1038/ng.2426.
- Slijkerman, R. W., F. Song, G. D. Astuti, M. A. Huynen, E. van Wijk, K. Stieger, and R. W. Collin. 2015. "The pros and cons of vertebrate animal models for functional and therapeutic research on inherited retinal dystrophies." *Prog Retin Eye Res* 48:137-59. doi: 10.1016/j.preteyeres.2015.04.004.
- Slijkerman, RWN, H. Kremer, and E Van Wijk. 2017. "Molecular Genetics of Usher Syndrome: Current State of Understanding." *eLS. John Wiley & Sons, Ltd: Chichester*. doi: DOI: 10.1002/9780470015902.a0021456.pub2.
- Smith, R. J., C. I. Berlin, J. F. Hejtmancik, B. J. Keats, W. J. Kimberling, R. A. Lewis, C. G. Moller, M. Z. Pelias, and L. Tranebjaerg. 1994. "Clinical diagnosis of the Usher syndromes. Usher Syndrome Consortium." *Am J Med Genet* 50 (1):32-8. doi: 10.1002/ajmg.1320500107.
- Sorusch, N., K. Bauss, J. Plutniok, A. Samanta, B. Knapp, K. Nagel-Wolfrum, and U. Wolfrum. 2017. "Characterization of the ternary Usher syndrome SANS/ush2a/whirlin protein complex." *Hum Mol Genet* 26 (6):1157-1172. doi: 10.1093/hmg/ddx027.
- Suster, M. L., H. Kikuta, A. Urasaki, K. Asakawa, and K. Kawakami. 2009. "Transgenesis in zebrafish with the tol2 transposon system." *Methods Mol Biol* 561:41-63. doi: 10.1007/978-1-60327-019-9_3.
- Takayanagi, H., S. Yuzawa, and H. Sumimoto. 2015. "Structural basis for the recognition of the scaffold protein Frmpd4/Preso1 by the TPR domain of the adaptor protein LGN." *Acta Crystallogr F Struct Biol Commun* 71 (Pt 2):175-83. doi: 10.1107/S2053230X14028143.
- van Wijk, E., B. van der Zwaag, T. Peters, U. Zimmermann, H. Te Brinke, F. F. Kersten, T. Marker, E. Aller, L. H. Hoefsloot, C. W. Cremers, F. P. Cremers, U. Wolfrum, M. Knipper, R. Roepman, and H. Kremer. 2006. "The DFNB31 gene product whirlin connects to the Usher protein network in the cochlea and retina by direct association with USH2A and VLGR1." *Hum Mol Genet* 15 (5):751-65. doi: 10.1093/hmg/ddi490.
- Wright, R. N., D. H. Hong, and B. Perkins. 2012. "RpgORF15 connects to the usher protein network through direct interactions with multiple whirlin isoforms." *Invest Ophthalmol Vis Sci* 53 (3):1519-29. doi: 10.1167/iovs.11-8845.
- Yang, J., X. Liu, Y. Zhao, M. Adamian, B. Pawlyk, X. Sun, D. R. McMillan, M. C. Liberman, and T. Li. 2010. "Ablation of whirlin long isoform disrupts the USH2 protein complex and causes vision and hearing loss." *PLoS Genet* 6 (5):e1000955. doi: 10.1371/journal.pgen.1000955.
- Yap, C. C., F. Liang, Y. Yamazaki, Y. Muto, H. Kishida, T. Hayashida, T. Hashikawa, and R. Yano. 2003. "CIP98, a novel PDZ domain protein, is expressed in the central nervous system and interacts with calmodulin-dependent serine kinase." *J Neurochem* 85 (1):123-34.

- Yuzawa, S., S. Kamakura, Y. Iwakiri, J. Hayase, and H. Sumimoto. 2011. "Structural basis for interaction between the conserved cell polarity proteins Inscuteable and Leu-Gly-Asn repeat-enriched protein (LGN)." *Proc Natl Acad Sci U S A* 108 (48):19210-5. doi: 10.1073/pnas.1110951108.
- Zou, J., Q. Chen, A. Almishaal, P. D. Mathur, T. Zheng, C. Tian, Q. Y. Zheng, and J. Yang. 2017. "The roles of USH1 proteins and PDZ domain-containing USH proteins in USH2 complex integrity in cochlear hair cells." *Hum Mol Genet* 26 (3):624-636. doi: 10.1093/hmg/ddw421.

SUPPLEMENTAL FIGURE AND TABLES



Supplemental figure 1. *SF-Whrna* is absent from the adult photoreceptor synapse. Immunohistochemical stainings of adult (1.5 years old) **(A)** *SF-Whrna* and **(B)** wild-type zebrafish retinas with anti-FLAG antibodies (green signal) and antibodies targeting the synaptic marker Sv2a (red signal). OS = outer segment, IS = inner segment, ONL = outer nuclear layer, SN = synaptic region, scale bar represents 20 μm .

Supplemental table 1. List of keratins that were removed from the mass spectrometry results.
(available upon request)

Supplemental table 2. Proteins identified by SF-Whrna affinity purification or GST-Whrna pull-down assays from adult zebrafish retinal extracts. All proteins that have been identified by mass spectrometry are provided with their respective protein sequence coverage for each experiment. (available upon request)

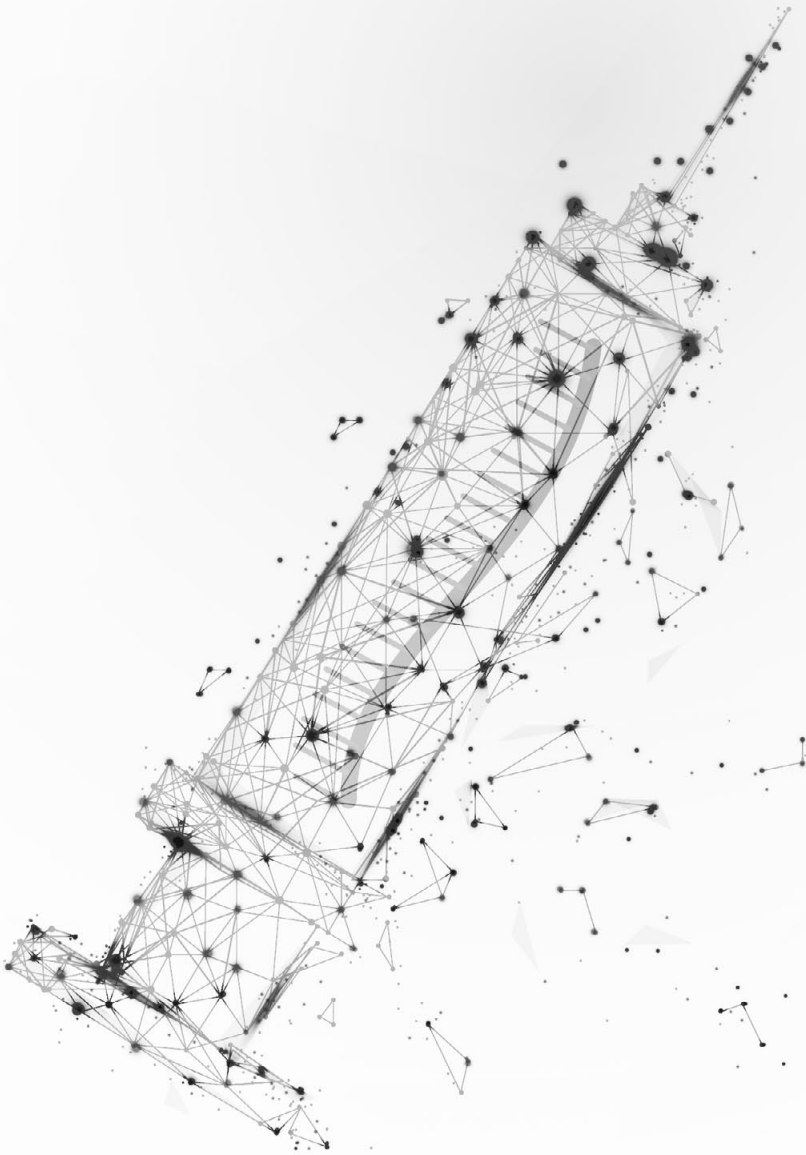
Supplemental table 3. GST-Whrna pull-down assays from lysates of adult zebrafish eyes. The protein identifier and the sequence coverage of 149 proteins are listed that were co-purified with GST-Whrna in two out of two experiments, and not by GST alone. Proteins that have also been identified by FLAG-affinity purification are highlighted in orange. (available upon request)

Chapter 3

A Splice-Based Therapy For *USH2A*-
Associated Retinal Degeneration Due
To The Deep Intronic c.7595-2144A>G
Mutation That Activates PE40



Chapter 3^a



Antisense oligonucleotide design and evaluation of splice-modulating properties using cell-based assays

Ralph W.N. Slijkerman^{1,2}, **Hannie Kremer**^{1,3,4} and **Erwin van Wijk**^{1,4}

¹ Department of Otorhinolaryngology, Radboudumc, Nijmegen, the Netherlands.

² Radboud Institute for Molecular Life Sciences, Nijmegen, the Netherlands.

³ Department of Human Genetics, Radboudumc, Nijmegen, the Netherlands.

⁴ Donders Institute for Brain, Cognition, and Behaviour, Nijmegen, the Netherlands.

Published in *Methods Mol Biol.*, 2018

doi: https://doi.org/10.1007/978-1-4939-8651-4_34

PMID: 30171565

ABSTRACT

Antisense oligonucleotide (AON)-based splice modulation has been proven to hold great promise as a therapeutic strategy for a number of hereditary conditions. AONs are small modified single-stranded RNA or DNA molecules that are complementary to splice enhancer or silencer target sites. Upon pre-mRNA binding, AONs will prevent or stimulate binding of the spliceosome thereby modulating splicing events. AONs can be designed and applied for different genes and genetic disorders as the specificity depends on their nucleotide sequence. Here we provide a guideline for setting up AON-based splice-modulation experiments by describing a detailed protocol to design and evaluate AONs using a combination of *in silico* and *in vitro* analyses.

1. INTRODUCTION

Splicing defects represent a significant proportion of genetic variation underlying inherited disorders [1]. It has, for instance, been estimated that ~20% of the mutations identified for inherited retinal diseases (IRDs) affect pre-mRNA splicing. Non-canonical splice site defects are found in several IRD genes and might be amenable to antisense oligonucleotide (AON)-based splice correction. AONs are small modified single-stranded RNA or DNA molecules that are complementary (antisense) to their target, allowing them to bind to the corresponding pre-mRNA molecule and prevent or enhance the binding of RNA-protein complexes essential for splicing. The lack of binding by the spliceosome often results in the (partial) skipping of the targeted exon, as has been shown for the deep-intronic mutations identified in *USH2A* [2,3] and *CEP290* [4,5], thereby restoring normal splicing. In addition, AONs can force the retention of exons that, due to mutations, are absent in the transcripts of the corresponding gene, by either blocking intronic splice silencer (ISS) sites, exonic splice silencer (ESS) sites or by fusing the sequence of the AON to elements recruiting factors that enhance splicing ("bifunctional" AONs). This has been successfully shown for Spinal Muscular Atrophy [6]. Also, AONs can redirect aberrant splicing as a consequence of (non-canonical) splice site mutations that weaken the original splice acceptor or donor site, by blocking these alternative splice sites. Finally, AONs can also be used to skip (combinations of) exons harboring loss-of-function (e.g. nonsense or frameshift) mutations that do not disrupt the reading frame when skipped. This approach has been successfully applied for large genes encoding (structural) proteins that contain series of repetitive protein domains such as *NOTCH3*, dystrophin or usherin [7-9]. The slightly shortened proteins that result from these skipping events have sufficient residual activity, thereby converting a null allele into a hypomorphic allele.

In order to evaluate the effectiveness of the designed AONs, cellular models expressing the gene of interest, including the identified pathogenic genetic variants, are essential. Genes involved in IRDs, however, are often not or at a very low level expressed in patient-derived cells that are relatively easily accessible (e.g. HUVECs, lymphoblasts or fibroblasts) [2,10]. An alternative method to show the ability and effectiveness of AONs to induce the desired splice-modulation is to develop and use gene- and mutation-specific minigene splice assays (**Fig. 1**) [2]. In this chapter we discuss the guidelines to effectively setup and assess AON-based splice modulation experiments.

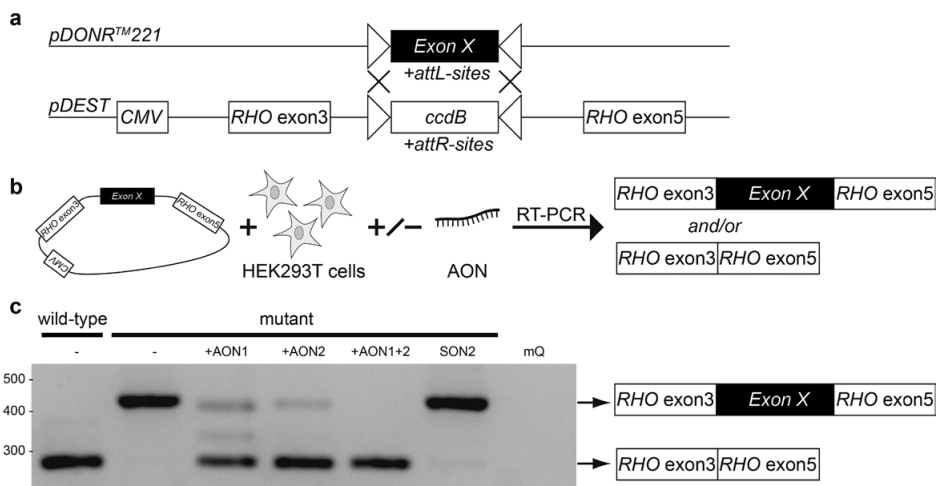


Figure 1. Schematic overview of the experimental procedure to validate AON-induced exon skipping using a minigene splice assay. (A) Using Gateway® cloning technology, an expression clone can be generated after recombination of the *att*-sites in the entry clone (pDONR™221) and destination (pDEST) vector. The resulting expression plasmid contains the exon of interest ('*Exon X*') flanked by *RHO* exons 3 and 5, under the control of a CMV promoter ('CMV'). **(B)** The minigene splice vector can be transfected into HEK293T cells in the presence or absence of AONs. Subsequent transcript analysis by RT-PCR results in transcripts either containing *RHO* exons 3 and 5 or containing the exon of interest ('*Exon X*') flanked by *RHO* exons 3 and 5. **(C)** RT-PCR products can be visualized on an agarose gel. In this example a deep-intronic mutation in gene *X* that results in the inclusion of a pseudoexon, is modeled. RT-PCR analyses after transfection of the wildtype minigene splice vector does not result in the inclusion of *Exon X*, whereas transcript analysis after expression of the mutant minigene splice vector shows a larger product containing *Exon X*. Co-transfection of the mutant minigene splice vector with AONs that target *Exon X* ('AON1' and/or 'AON2') results in splice-corrected transcripts without *Exon X* (lower band). Water (mQ) was used as a negative PCR control, SON2 is a non-binding sense oligonucleotide control.

2. MATERIALS

For generating solutions the use of autoclaved milliQ water is suggested unless stated differently.

2.1 *In silico* analysis

A computer with internet access and a webbrowser are required.

2.2 Ordering AONs

1. Find a supplier and determine the chemical backbone and sugar modifications of choice (see **Note 1**).

2.3 Cloning of a minigene splice assay

1. Forward and reverse primers including *attB* tails, for the generation of Gateway®-compatible PCR amplicons that span the exon of interest including (>500 bp) up- and downstream intronic sequence (see **Note 2**).
2. NucleoSpin® Gel and PCR Clean-up kit (MACHEREY-NAGEL, Düren, Germany).
3. Gateway®BP clonase™ enzyme mix (Thermo Fisher scientific, Carlsbad (CA), USA).
4. Gateway®LR clonase™ enzyme mix (Thermo Fisher scientific, Carlsbad (CA), USA).
5. Gateway pDONR™221 vector (Thermo Fisher scientific, Carlsbad (CA), USA).
6. A pCI-neo-based minigene splice assay destination vector [11].
7. LB agar plates: Dissolve 20 g NaCl, 20 g tryptone and 10 g yeast extract into 750 ml water. Add 30 g agar and fill up to 1 liter. Autoclave the solution and let it cool down to approximately 55 °C. Just before pouring the solution into 9 10 cm plates, add the corresponding antibiotics. Let the plates solidify and subsequently dry for approximately 10 minutes and store them at 4 °C until use.
8. LB medium: Dissolve 20 g NaCl, 20 g tryptone and 10 g yeast extract into 750 ml water. Subsequently, fill up to 1 liter total volume and autoclave the solution. LB medium can be stored at room temperature.
9. NucleoSpin® Plasmid EasyPure DNA extraction kit (MACHEREY-NAGEL, Düren, Germany).

2.4 Cell culture

- 1a. Dulbecco's modified Eagle's medium (DMEM) (see **Note 3**).
- 1b. RPMI 1640 (see **Note 3**).
2. Fetal bovine serum.
3. Penicillin-streptomycin.
4. Sodium pyruvate.
5. Phosphate buffered saline (PBS) 10x: Dissolve 8.1 g NaCl (138 mM), 0.2 g KCl (2.7 mM), 1.15 g Na₂HPO₄·2H₂O (6.5 mM) and 0.2 g KH₂PO₄ (1.5 mM) in 1 liter water. Adjust pH to 6.7 with HCl and autoclave the solution. Dilute 10 times with water before use. PBS can be stored at room temperature.
6. Trypsin 250. Dissolve 2.5 g trypsin in 100 ml 10x PBS and 900 ml water. Sterilize by filtration.
7. Opti-MEM.
- 8a. FuGENE® HD Transfection Reagent.
- 8b. Polyethylenimine (PEI). Dissolve 0.1 g PEI in 1 liter 150 mM NaCl pH 5.5 and adjust pH to 7.8 with HCl. Heat the solution to 80 °C for 4 to 8 hours. Let the solution cool down to room-temperature, sterilize by filtration and store at 4 °C.

9. [optional] Cyclohexamide (see **Note 4**).

2.5 RNA isolation

1. Nucleospin RNA II isolation kit (MACHEREY-NAGEL, Düren, Germany).

2.6 cDNA synthesis

1. SuperScript VILO cDNA synthesis kit (Thermo Fisher Scientific, Carlsbad (CA), USA).

2.7 Polymerase Chain Reaction

1. Q5® High-Fidelity DNA polymerase.
2. dNTPs mix (10 mM each).
3. Gene-specific forward and reverse primer. PCR amplicon should ideally cover multiple flanking exons and not exceed a length of ~1400 bp (see **Note 5**).

2.8 Agarose gel electrophoresis

1. Agarose-gel: Add 150 ml 0.5xTBE buffer to 1.5 g of agarose MP and boil the solution until the agarose is completely dissolved. Cool down to approximately 60 °C before adding ethidium bromide to a final concentration of 0.3 µg/ml. Pour the gel into a gel-tray and let it solidify at room temperature for approximately half an hour (see **Note 6**).

2.9 Quantitative RT-PCR

1. Forward and reverse primers spanning about 100 bp of sequence. Preferably, the amplicon includes an exon-exon boundary to exclude DNA or incompletely processed pre-mRNA molecules (see **Note 7**).
2. GoTaq polymerase mix.

3. METHODS

3.1 Identify target sequence motifs

1. The 'Human Splicing Finder' website (<http://www.umd.be/HSF3/>) can be used to identify exonic splice enhancer (ESE) sites, intronic splice silencer (ISS) sites, or exonic splice silencer (ESS) sites. Click on 'Start an Analysis with HSF3.0' and select 'analyze a sequence' under "Select an analysis type". Subsequently, select 'Pasting your own sequence' under "Choose a sequence by" and paste your sequence of the exon of interest with 50 nucleotides of flanking up- and downstream sequence in the appearing box. Use the 'Proceed to analysis!' but-

ton to see the results. In the second window from the top, named "Graphical representations", click on the tab "Splicing motifs" to unveil all predicted ESE and ISS sequence motifs.

2. For exon skipping purposes, manually identify sequences that contain as many ESE motifs (i.e. SF2/ASF, SRp40, SC35, SRp55, ESE hexamers and putative ESE (PESE) octamers) without covering silencer motifs (i.e. ESS motifs 1-3, Fas ESS and putative ESS (PESS) octamers) motifs [12]. For exon retention purposes, identify sequences that cover as many silencer motifs without covering ESE motifs. Design as many potential AONs as possible, that can be screened for their thermodynamic and intrinsic properties and RNA structure (see **Note 8**). AONs have an optimal length of 17-23 nucleotides. However, the length of AONs can be adjusted to optimize any of the below mentioned properties and is thus not critical in this phase of the design.

3.2 Thermodynamic AON properties and secondary RNA structures

Different AON sequences should be designed that cover the core target sequence as determined above. Since these guidelines are no guarantee that AONs will be effective, it is recommended to design at least three different AONs per target sequence for subsequent *in vitro* evaluation.

1. Analyze the thermodynamic parameters of all candidate AON sequences, starting with the accessibility of the target RNA. Analyze the target sequence for nucleotides that are expected to hybridize to other nucleotides (referred to as 'closed') and those not expected to do so (referred to as 'open'). Go to the online 'mFold' prediction tool (<http://unafold.rna.albany.edu/?q=mfold/RNA-Folding-Form>) to predict the secondary RNA structure of the exon including 50 nucleotides of up- and downstream intronic sequence. Use the default parameters, except for "maximum distance between paired bases" that should be put to value 100, and click on 'fold RNA'. Open '(ss-count file)' under the heading "View ss-count information". This opens a new window in which your input sequence is analyzed for an 'open' conformation per nucleotide, counted for each predicted secondary structure. A higher score represents a more open structure and vice versa as previously explained by Aartsma-Rus [13]. Ideally, each AON targets a combination of predominantly 'open' and 'closed' conformations.
2. Take the AON secondary structure into account using the RNAstructure prediction software (<http://rna.urmc.rochester.edu/RNAstructureWeb/index.html>). Choose for 'Predict a Secondary Structure'. Paste the AON sequence in capital characters (lower case characters will be forced into single strand positions) and tick 'RNA' before hitting 'Submit Query' using default parameters. In order to be

able to effectively bind the target pre-mRNA, the AON structure should have a calculated energy of > -4 kcal/mol.

3. Calculate the free energy of AON-AON complex using the same software tool (<http://rna.urmc.rochester.edu/RNAstructureWeb/index.html>). Choose for 'Predict a Bimolecular Secondary Structure'. Paste the AON sequence in both the white box below 'sequence 1' as well as the box below 'sequence 2', then click on 'submit query'. The free energy should be > -15 kcal/mol.
4. Predict the binding stability of an AON to its target RNA using the mFold software for bimolecular secondary structures. First, predict the free energy for the target sequence without AON by pasting the target sequence in the box under 'Predict a Secondary Structure' (<http://rna.urmc.rochester.edu/RNAstructureWeb/index.html>). Second, use the 'Predict a Bimolecular Secondary Structure'-tool to paste the target sequence as 'sequence 1' and the potential AON sequence as 'sequence 2'. The calculated difference between the first (free energy target) and the second (free energy AON bound to target) analysis should ideally be > 21 kcal/mol.

3.3 Intrinsic AON properties

1. Analyze the AON sequence for the amount of G or C residues. Typically, AONs having a GC-content between 40 and 60% are considered to be appropriate for exon skipping or retention purposes (see **Note 9**).
2. Determine the T_m temperature of the AON sequence using the T_m calculator tool (<https://tmcalculator.neb.com/#!/>). The optimal T_m of an AON is 60 °C. Avoid AONs with a $T_m < 48$ °C.
3. Analyze the uniqueness of the AONs by performing BLASTn searches against the genome of interest. Use the online blast-tool (<https://blast.ncbi.nlm.nih.gov/Blast.cgi>) and choose for "nucleotide BLAST" (= BLASTn). Make sure the proper genome has been selected and paste the AON sequence (FASTA format) into the white box before clicking on 'BLAST'. Homologous genomic sequences are listed. Ideally, there should be only a single hit that is completely identical to the AON. Avoid AONs for which off-target regions with stretches of 15 consecutive identical nucleotides are identified (see **Note 10**).

3.4 Generation of a minigene splice vector

1. Perform a PCR using primers that contain Gateway®-*attB* tails generating an amplicon consisting of the exon of interest together with >500 bp up- and downstream intronic sequences. Extract and purify the PCR product from an agarose gel.

2. Perform a Gateway® BP-recombination reaction to generate an entry clone containing the purified PCR product. Mix 2 µl of the BP clonase buffer, together with 1 µl of the recovered PCR product (~15-150 ng), 150 ng pDONR™221 vector, 4 µl water and 2 µl Gateway®BP clonase™ enzyme mix. Incubate the reaction at 25 °C for two hours. (see **Note 11**).
3. Terminate the Gateway® BP-recombination reaction by adding 1 µl of the Proteinase K solution (2 µg). Vortex briefly. Incubate sample at 37 °C for 10 minutes.
4. Transform 2.5 µl of the BP reaction into DH5α competent cells and plate 200 µl on LB agar plates that contain 100 µg/ml kanamycin as a selection marker for the pDONR™221 vector. Incubate overnight at 37 °C.
5. Inoculate single colonies and culture them overnight (see **Note 12**).
6. Extract plasmid DNA from the bacterial cultures.
7. Sequence-verify the extracted plasmids by Sanger sequencing.
8. Perform a Gateway® LR-recombination reaction to generate a pCI-neo-based minigene splice vector. Mix 2 µl LR clonase buffer with 150 ng of the entry clone, 150 ng pCI-neo-*RHO* ex3-5 destination vector and 2 µl Gateway®LR clonase™ enzyme mix. Incubate the reaction at 25 °C for two hours (see **Note 11**).
9. Repeat steps 3 to 7 in order to obtain the desired pCI-neo-based minigene splice vector.

3.5 Validating AONs *in vitro* using a minigene splice assay

1. Prior to use, dissolve AONs in sterile phosphate-buffered saline (PBS) in an appropriate concentration (see **Note 13**). Aliquot dissolved AONs and store them at -80 °C for later use.
2. Seed transfectable cells, typically HEK293T cells, into a 12-wells plate and culture them until a 50-70% confluency (see **Note 3**) (see **Note 14**) (see **Note 15**).
3. Co-transfect AONs and the minigene splice vector into HEK293T cells using polyethylenimine (PEI). Mix the AON of choice (typically 1 µl of 1 mM stock) (see **Note 16**) and 500 ng of the minigene splice vector with 45 µl PEI and incubate at room temperature for 10 minutes. Add the mixture drop-wise to the cells. There is no need to refresh the medium before collecting the cells for RNA isolation.
4. Harvest the cells approximately 48 hours after transfection. Discard the medium and wash the cells with PBS. Isolate total RNA using the Nucleospin RNA II isolation kit.
5. Perform a cDNA synthesis using the SuperScript VILO cDNA synthesis kit. Add 4 µl of the VILO enzyme mastermix with 500 ng total RNA and adjust the volume to 20 µl using sterile RNase-free water (see **Note 17**). Incubate the mixture in a thermocycler at 25°C for 10 minutes, followed by 42 °C for 60 minutes, 85 °C for 5 minutes and 16 °C forever.

6. The cDNA product that is generated after the reverse transcriptase reaction is directly used as a template in a PCR. Typically, one PCR (25 μ l) contains dNTPs (final concentration of 0.2 mM for each nucleotide), forward and reverse primers (final concentration of 0.2 mM for each primer), 0.5 to 1 μ l (25 to 50 ng) cDNA, 0.25 μ l (0.5 units) Q5 polymerase, and 5 μ l Q5 reaction buffer. Cycling conditions are: 94 °C for 3 minutes, followed by 30 cycles with 94 °C for 20 seconds, T_m °C for 20 seconds and 72 °C for 1 minute. The T_m temperature depends on the primers used and should be optimized on beforehand. The reaction is finalized by a 5 minute incubation step at 72 °C after which the reaction is cooled down to 16 °C until further processing.
7. Analyze the PCR products on an agarose gel (**Fig. 1C**). An estimation of the ratio between normal and splice-modulated transcripts, which is indicative for AON efficacy, can be made. Determine the quantitative splice-modulating efficiency of the AON by RT-qPCR (see section 2.9). Sanger sequencing of the amplified products will reveal whether or not the used AON is capable of inducing the desired splice-modulation.

3.6 *In vitro* validation of AONs using cells endogenously expressing the target pre-mRNA

1. Seed cells of interest into a 12-wells plate (see **Note 14**) and culture to a 50-70% confluency (see **Note 15**). WERI-Rb-1 cells, however, are non-adhesive cells and grow in suspension. We therefore recommend seeding them at a density of 0.9×10^6 cells per well (see **Note 3**). Since many different cell types can be used, AON transfection protocols might need some optimization (see **Note 18**). We have transfected AONs into patient-derived fibroblasts using FuGENE® HD Transfection Reagent or WERI-Rb-1 cells using polyethylenimine (PEI).
- 2a. Transfection using FuGENE® HD Transfection Reagent: mix the AON of choice (typically 1 μ l of a stock-solution) with 3 μ l FuGENE® HD Transfection Reagent and 100 μ l Opti-MEM and incubate at room temperature for 20 minutes. In the meantime, replace the medium on the cells by 900 μ l DMEM medium with supplements. Add the transfection mixture drop-wise to the cells (see **Note 19**).
- 2b. Transfection using PEI: mix the AON of choice (typically 1 μ l of a stock-solution) with 45 μ l PEI and incubate at room temperature for 10 minutes. Subsequently, add the mixture drop-wise to the cells.
3. Approximately 48 hours after transfection (see **Note 4**), collect the cells for transcript analysis using a cell-scraper. Total RNA is isolated, followed by (q)RT-PCR analysis as described under **3.5** points **4-8**.

4. NOTES

1. AONs can be chemically modified in different ways to enhance stability and/or binding affinity. Generally, the backbone that connects the sugar moiety can be modified (e.g. phosphorothioate (PT) addition) and/or the sugar moiety itself can be altered (e.g. addition of a 2'-O-methyl group (2'-OMe) or a 2'-O-(2-methoxyethyl) group (2'-MOE)). Alternatively, the sugar moiety can be internally coupled to create a 'locked nucleic acid' (LNA) or can be exchanged for a morpholino-ring (PMO). For a comprehensive overview of different AON chemistries, read Khvorova and Watts (2017) [14].
2. Design a forward and reverse primer that generate the amplicon with the sequence of interest. Add a Gateway®-compatible *attB1* tail to the forward primer (5'-GGGGACAAGTTTGTACAAAAAAGCAGGCT-XXX-3') and *attB2* tail to the reverse primer (5'-GGGGACCACTTTGTACAAGAAAGCTGGGT-YYY-3'). XXX indicates the forward primer sequence and YYY indicates the reverse primer sequence from 5' to 3'.
3. Culture primary fibroblast cells in DMEM supplemented with 20% fetal bovine serum, 1% sodium pyruvate and 1% penicillin-streptomycin. Culture HEK293T cells in DMEM supplemented with 10% fetal bovine serum, 1% sodium pyruvate and 1% penicillin-streptomycin and culture WERI-Rb-1 cells in RPMI 1640 supplemented with 10% fetal bovine serum, 1% sodium pyruvate and 1% penicillin-streptomycin.
4. In case transcripts undergo nonsense-mediated decay, the medium can be exchanged by cyclohexamide (use at 100 µg/ml final concentration)-containing medium 24 hours after supplementing AONs.
5. Ideally an amplicon should cover flanking exons as well as the exon of interest. AON-induced exon skipping can influence the in- and exclusion of other exons [15]. Also, the total amplicon length should be chosen in such a way that exon skipping results in a markedly different-sized PCR product that can be readily distinguished after agarose gel electrophoresis.
6. Casted agarose gels can be stored at 4 °C for up to one month when properly sealed in order to prevent them from drying out.
7. Primers for qPCR can be designed using the NCBI primer design tool (<https://www.ncbi.nlm.nih.gov/tools/primer-blast/>). Use standard settings, but adjust the PCR product size range to 70 - 120 bp and the primer melting temperature range to 59 - 61 °C.
8. AONs targeting intron-exon or exon-intron boundaries are not always the most effective in skipping or retaining exons. Splice sites often contain higher percentages of A and U-residues, resulting in a weaker AON-RNA binding as compared

to more GC-rich regions. Also, exonic sequences often are more suitable to find a unique AON-target sequence than intronic sequences and splice sites.

9. GC-content of AONs is important, as a higher GC% leads to a higher AON-RNA binding strength. A GC > 60% in a given AON can result in a strong self-hybridization and render these AONs unable to bind to target pre-mRNA sequences.
10. Preferably, the AON sequence has only one homologous region in the target genome. However, if there are no other options, mismatches in the AON's middle region are expected to disrupt binding more than those at either ends of the AON.
11. We have experienced that extending the incubation time at 25 °C from two hours to overnight enhances the recombination efficiency for difficult reactions.
12. As a rule of thumb, we generally analyze three clones per reaction.
13. Typically AONs are used in a final concentration of 0.1 to 10 μM.
14. Also 6-well plates can be used to scale up the experiment. We have successfully performed splice modulation experiments in a 6-well plate using 1 ml of AON-containing medium per well.
15. All cell culture reagents should be pre-warmed to the same temperature as at which the cells are cultured.
16. Using a cocktail of AONs can be more effective than using a single AON. For the most optimal exon skipping result, make sure the target sequences do not overlap. Some exons are only partially skipped when using a single AON and therefore might need a combination of AONs to induce complete exon skipping.
17. In order to avoid unnecessary use of reagents, this reaction is scalable.
18. AONs can cross the cell membrane unaided. Supplementing naked AONs to the culture medium is often sufficient to induce exon skipping in cells, although the use of a transfection reagent significantly enhances the AON uptake efficiency.

ACKNOWLEDGEMENTS

The authors received funding from 'Stichting Ushersyndroom' (HK and EvW); the Foundation Fighting Blindness USA (grant PPA-0517-0717-RAD) and 'Stichting Wetenschappelijk Onderzoek Doof-Blindheid' (EvW) for the research that led to the protocol.

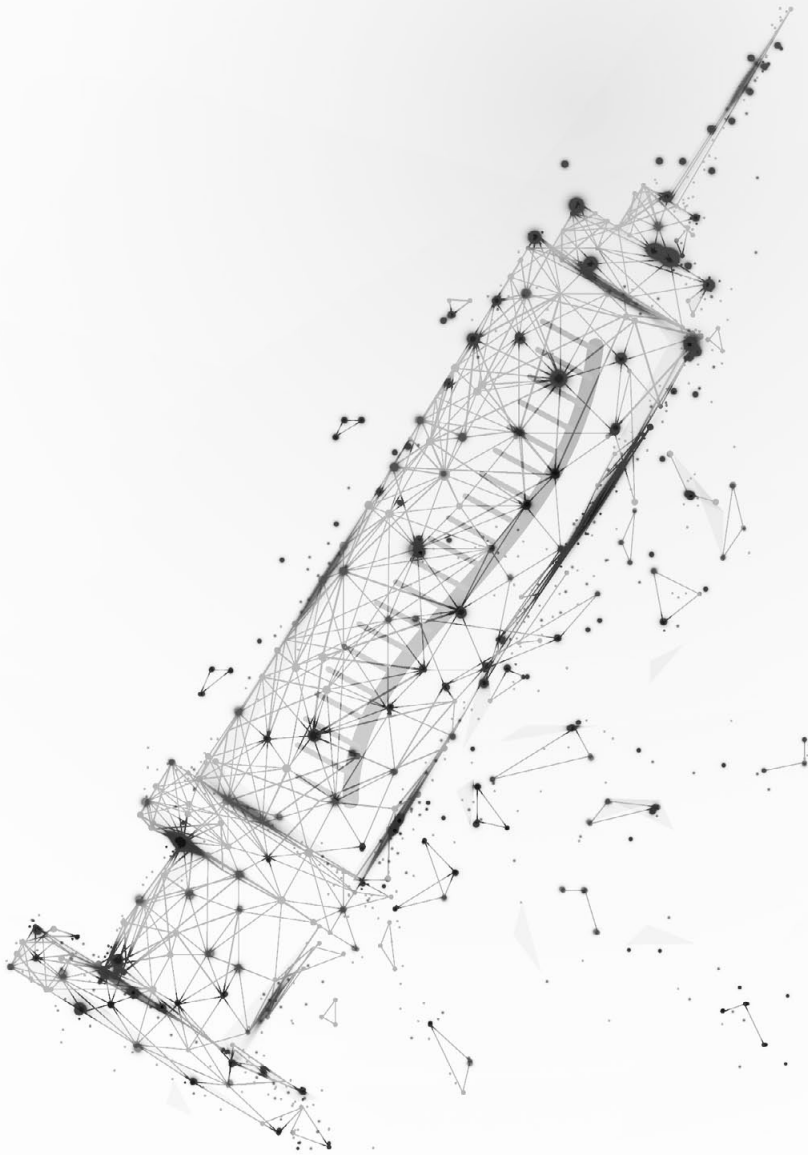
Conflict of Interest

EvW is employed by Radboudumc and inventor on a patent (PCT/EP2015/065736) for antisense oligonucleotide-based exon skipping. Radboudumc has licensed the rights to the patent exclusively to ProQR Therapeutics. As the inventor, EvW is entitled to a share of any future royalties paid to Radboudumc, should the therapy eventually be brought to the market.

REFERENCES

1. Liu MM, Zack DJ (2013) Alternative splicing and retinal degeneration. *Clin Genet* 84 (2):142-149. doi:10.1111/cge.12181
2. Slijkerman RW, Vache C, Dona M et al. (2016) Antisense Oligonucleotide-based Splice Correction for *USH2A*-associated Retinal Degeneration Caused by a Frequent Deep-intronic Mutation. *Mol Ther Nucleic Acids* 5 (10):e381. doi:10.1038/mtna.2016.89
3. Liquori A, Vache C, Baux D et al. (2016) Whole *USH2A* Gene Sequencing Identifies Several New Deep Intronic Mutations. *Hum Mutat* 37 (2):184-193. doi:10.1002/humu.22926
4. Collin RW, den Hollander AI, van der Velde-Visser SD et al. (2012) Antisense Oligonucleotide (AON)-based Therapy for Leber Congenital Amaurosis Caused by a Frequent Mutation in *CEP290*. *Mol Ther Nucleic Acids* 1:e14. doi:10.1038/mtna.2012.3
5. Gerard X, Perrault I, Hanein S et al. (2012) AON-mediated Exon Skipping Restores Ciliation in Fibroblasts Harboring the Common Leber Congenital Amaurosis *CEP290* Mutation. *Mol Ther Nucleic Acids* 1:e29. doi:10.1038/mtna.2012.21
6. Skordis LA, Dunckley MG, Yue B et al. (2003) Bifunctional antisense oligonucleotides provide a trans-acting splicing enhancer that stimulates *SMN2* gene expression in patient fibroblasts. *Proc Natl Acad Sci U S A* 100 (7):4114-4119. doi:10.1073/pnas.0633863100
7. Rutten JW, Dauwerse HG, Peters DJ et al. (2016) Therapeutic *NOTCH3* cysteine correction in *CADASIL* using exon skipping: in vitro proof of concept. *Brain* 139 (Pt 4):1123-1135. doi:10.1093/brain/aww011
8. van Wijk E, Dona M, Slijkerman R et al. (2017) Antisense Oligonucleotide-induced Skipping of *USH2A* exon13 Restores Visual Function in Zebrafish. *Invest Ophth Vis Sci* 58 (8):2490-2490
9. Aoki Y, Yokota T, Nagata T et al. (2012) Bodywide skipping of exons 45-55 in dystrophic *mdx52* mice by systemic antisense delivery. *Proc Natl Acad Sci U S A* 109 (34):13763-13768. doi:10.1073/pnas.1204638109
10. Allikmets R, Singh N, Sun H et al. (1997) A photoreceptor cell-specific ATP-binding transporter gene (*ABCR*) is mutated in recessive Stargardt macular dystrophy. *Nat Genet* 15 (3):236-246. doi:10.1038/ng0397-236
11. Sangermano R, Bax NM, Bauwens M et al. (2016) Photoreceptor Progenitor mRNA Analysis Reveals Exon Skipping Resulting from the *ABCA4* c.5461-10T-->C Mutation in Stargardt Disease. *Ophthalmology* 123 (6):1375-1385. doi:10.1016/j.ophtha.2016.01.053
12. Aartsma-Rus A, van Vliet L, Hirschi M et al. (2009) Guidelines for antisense oligonucleotide design and insight into splice-modulating mechanisms. *Mol Ther* 17 (3):548-553. doi:10.1038/mt.2008.205
13. Aartsma-Rus A (2012) Overview on AON design. *Methods Mol Biol* 867:117-129. doi:10.1007/978-1-61779-767-5_8
14. Khvorova A, Watts JK (2017) The chemical evolution of oligonucleotide therapies of clinical utility. *Nat Biotechnol* 35 (3):238-248. doi:10.1038/nbt.3765
15. Singh NN, Seo J, Rahn SJ et al. (2012) A multi-exon-skipping detection assay reveals surprising diversity of splice isoforms of spinal muscular atrophy genes. *PLoS One* 7 (11):e49595. doi:10.1371/journal.pone.0049595

Chapter 3^b



Antisense oligonucleotide-based splice correction for *USH2A*-associated retinal degeneration caused by a frequent deep-intronic mutation.

Slijkerman R.W.N.^{1,2,5}, Vaché C.^{3,4,5}, Dona M.^{1,2}, García-García G.⁴, Claustres M.^{3,4}, Hetterschijt L.^{1,5}, Peters T.A.^{1,5}, Hartel B.P.^{1,6}, Pennings R.J.^{1,5}, Millan J.M.⁷, Aller E.⁷, Garanto A.^{5,8}, Collin R.W.^{5,8}, Kremer H.^{1,5,8}, Roux A.F.^{3,4,^} Van Wijk E.^{1,5,^}

⁵ Two first authors have contributed equally.

[^] Two last authors have contributed equally.

¹ Department of Otorhinolaryngology, Radboudumc, Nijmegen, the Netherlands.

² Radboud Institute for Molecular Life Sciences, Radboudumc, Nijmegen, the Netherlands.

³ Laboratoire de Génétique Moléculaire, CHU Montpellier, Montpellier, France.

⁴ Laboratoire de Génétique de Maladies Rares EA 7402, Université de Montpellier, Montpellier, France.

⁵ Donders Institute for Brain, Cognition, and Behaviour, Nijmegen, the Netherlands.

⁶ Radboud Institute for Health Sciences, Radboudumc, Nijmegen, the Netherlands.

⁷ Grupo de Investigación en Biomedicina Molecular, Celular y Genómica, and CIBERER, Madrid, Spain.

⁸ Department of Human Genetics, Radboudumc, Nijmegen, the Netherlands.

Published in *Molecular Therapy—Nucleic Acids*, 2016

doi: 10.1038/mtna.2016.89

PMID: 27802265

ABSTRACT

Usher syndrome (USH) is the most common cause of combined deaf-blindness in man. The hearing loss can be partly compensated by providing patients with hearing aids or cochlear implants, but the loss of vision is currently untreatable. In general, mutations in the *USH2A* gene are the most frequent cause of USH explaining up to 50% of all patients worldwide. The first deep-intronic mutation in the *USH2A* gene (c.7595-2144A>G) was reported in 2012, leading to the insertion of a pseudoexon (PE40) into the mature *USH2A* transcript. When translated, this PE40-containing transcript is predicted to result in a truncated non-functional USH2A protein. In this study, we explored the potential of antisense oligonucleotides (AONs) to prevent aberrant splicing of *USH2A* pre-mRNA as a consequence of the c.7595-2144A>G mutation. Engineered 2'-O-methylphosphorothioate AONs targeting the PE40 splice acceptor site and/or exonic splice enhancer regions displayed significant splice correction potential in both patient derived fibroblasts and a minigene splice assay for *USH2A* c.7595-2144A>G, whereas a non-binding sense oligonucleotide had no effect on splicing. Altogether, AON-based splice correction could be a promising approach for the development of a future treatment for *USH2A*-associated retinitis pigmentosa caused by the deep-intronic c.7595-2144A>G mutation.

INTRODUCTION

Usher syndrome (USH) and nonsyndromic retinitis pigmentosa (NSRP) are forms of inherited retinal dystrophies. Usher syndrome is clinically and genetically heterogeneous and by far the most common cause of inherited deaf-blindness in man, with a prevalence of approximately 1 in 6,000 individuals.¹ Based on the presence and progression of the clinical symptoms, Usher syndrome can be classified in three types: type 1 (USH1), type 2 (USH2), and type 3 (USH3). Approximately two-third of Usher syndrome patients suffer from type 2,² of whom up to 85% have mutations in *USH2A*.³ USH2 patients present with congenital hearing impairment, which can be partly compensated by hearing aids or cochlear implants,⁴ and retinitis pigmentosa (RP). NSRP is more prevalent than Usher syndrome, occurring in 1 per 4,000 individuals worldwide,⁵ of whom up to 23% can be explained by mutations in *USH2A*.^{6,7} Both USH2 and NSRP patients with mutations in *USH2A* develop night blindness in their late teens as a consequence of photoreceptor degeneration.⁸ This night blindness subsequently progresses from peripheral vision loss towards legal blindness around the end of the sixth decade of life.⁹ However, USH2 patients have an earlier and faster decline of visual function as compared to NSRP patients with *USH2A* mutations.¹⁰

Usher syndrome and other retinal dystrophies for long have been considered as incurable disorders. However, recent preclinical studies and ongoing phase 1/2 clinical trials using gene augmentation therapy led to promising results in selected groups of Usher syndrome, Leber congenital amaurosis and retinitis pigmentosa patients carrying mutations in *MYO7A*^{11–14} (ClinicalTrials.gov; NCT02065011) or *RPE65*^{15–18}. However, *USH2A* gene augmentation is hampered as the size of its coding sequence (15,606 bp; Genbank NM_206933) exceeds the cargo capacity of the currently available vehicles used for delivery (e.g., adenoassociated or lentiviral vectors). An alternative to gene augmentation is gene correction by for instance CRISPR/Cas9-based targeted genome repair. Although promising preclinical advances have been made, gene repair is not yet fully developed for clinical applications.¹⁹

Mutations in *USH2A* are mostly private and so far more than 600 different mutations have been reported which are distributed all over the gene (e.g., nonsense and missense mutations, deletions, duplications, large rearrangements, and variants that affect splicing (USHbases; <http://www.lovd.nl/USH2A>)).^{20,21} However, there are a few mutations that originate from a common ancestor (e.g., c.2299delG; p.Glu767fs and c.2276G>T; p.Cys759Phe) and are therefore observed more frequently.^{21–23}

In 2012, the first deep-intronic mutation (c.7595-2144A>G) in *USH2A* was reported for which also an ancestral event was suggested in association with the rare variant c.6049+76A>T.²⁴ This mutation creates a high-quality splice donor site in intron 40, resulting in the incorporation of a 152-nt pseudoexon (PE40) into the mature transcript²⁴

and is predicted to lead to a premature termination of translation (p.Lys2532Thrfs*56). With a 4% frequency, this deep-intronic mutation represents the second most frequent Usher syndrome type 2A-causing mutation (Usher syndrome type 2A-patient cohort from Montpellier (n = 562), unpublished data). Recently, three additional deep-intronic mutations were identified in *USH2A*,²⁵ emphasizing the contribution and frequency of deep-intronic mutations to the pathology of Usher syndrome. Subsequent diagnostic screening of the c.7595-2144A>G mutation in Usher syndrome patient cohorts identified multiple patients with the mutation in a homo- or compound heterozygous state.^{21,24,26-30} In addition, this mutation is reported (*in trans* to p.Arg4192His) in a patient with NSRP,²⁶ suggesting a wide distribution of the c.7595-2144A>G mutation in both USH and NSRP patients.

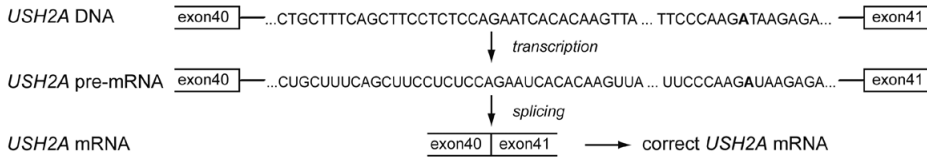
In this study, we explored the potential of antisense oligonucleotides (AONs) to redirect splicing in patient-derived fibroblasts harboring a heterozygous *USH2A* c.7595-2144A>G mutation. Both in fibroblasts and in a minigene splice assay, AONs showed promising preclinical potential to correct aberrant splicing, which might be of benefit for *USH2A* c.7595-2144A>G patients in the future.

RESULTS

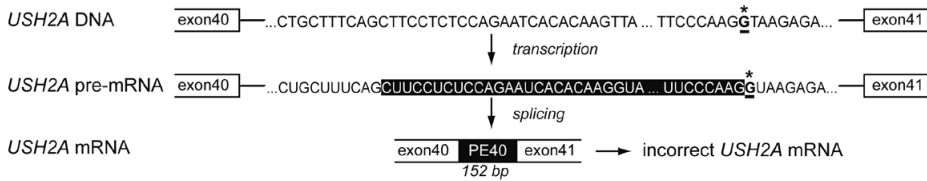
The deep-intronic c.7595-2144A>G mutation in *USH2A* creates a high-quality splice donor site that leads to a partial exonification of intron 40 (152 nt; PE40) into the mature mRNA²⁴ (**Fig. 1A, B**). This results in a predicted frameshift and premature termination of translation. The aim of this study is to assess the effectiveness of AONs targeting the PE40 region thereby specifically induce PE40 skipping from *USH2A* pre-mRNA containing the c.7595-2144A>G mutation (**Fig. 1C**).

Previous studies demonstrated highest exon-skipping efficiencies using AONs targeting exonic splice enhancer (ESE) motifs recognized by human SRSF2 (SC35), SRSF1 (SF2/ASF) and SRSF5, instead of intron-exon boundaries or other types of splice enhancers.^{31,32} Hence, AONs have been designed (sequences in **Table 1**) encompassing most predicted SRSF2, SRSF1, and SRSF5 ESE sequence motifs. AON1 targets five predicted SRSF1, two SRSF2, five SRSF5, and two hexamer ESE sequences, while AON2 targets two SRSF2 and one SRSF5 motifs (**Supplemental Fig. 1**). Guidelines for AON design further dictate that AONs should target partially open and partially closed pre-mRNA structures, which is the case for both AON1 (10 closed and 13 open nucleotides) and AON2 (13 closed and 7 open nucleotides). Thermodynamic criteria for AON design include a free energy higher than -4 kcal/mol for self-folding, a free energy higher than -15 kcal/mol for self-dimerisation and a preferable binding energy higher than 20 kcal/mol.³³ All these criteria were met in the design of both AON1 and 2 (**Table 1**).

A Wildtype *USH2A*



B Mutant *USH2A* (c.7595-2144A>G)



C Mutant *USH2A* (c.7595-2144A>G) + AON

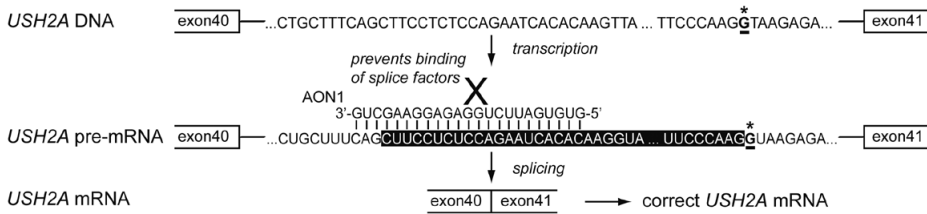


Figure 1. *USH2A* splicing and principle of AON-based splice correction. (A) In wild-type alleles, *USH2A* exons 40 and 41 are recognized and fused during splicing of *USH2A* pre-mRNA. **(B)** In case the c.7595-2144A>G mutation is present (indicated with an asterisk), a high-quality splice donor site is created. As a result, the 152 nt directly upstream are recognized as a pseudoexon and incorporated into *USH2A* mRNA (highlighted with a black background). **(c)** Addition of AONs complementary to PE40 can potentially prevent binding of splice factors to that region (indicated by a cross), thereby excluding PE40 from the mature *USH2A* transcript.

Table 1. Sequences of designed 2'-OMePT AONs.

Name	Sequence
AON1	5'-GTGTGATTCTGGAGAGGAAGCTG-3'
AON2	5'-CCCTTAAAGCCAGCATACA-3'
SON2	5'-TGTATGCTGGCTTTTAAGGG-3'

Fibroblasts from an USH2 patient, having the *USH2A* c.7595-2144A>G (p.Lys2532Thrfs*56) and c.10636G>A (p.Gly3546Arg) mutations in compound heterozygosity, were obtained in order to evaluate the splice correction potential of both AONs. In order to be able to detect PE40-containing *USH2A* transcripts, NMD inhibition using cycloheximide was needed (**Supplementary Fig. 2**). Unexpectedly, without NMD inhibition also the *USH2A* allele containing the c.10636G>A (p.Gly3546Arg) missense mutation could not be amplified. This could be the result of quantity-associated detection problems or alternatively could be because the missense variant has an effect on splicing, resulting in an out of frame transcript that is subjected to NMD. However, after NMD inhibition, the presence of this mutation could be confirmed by sequence analysis whereas no indications for alternative splice events were obtained. Subsequent quantitative RT-PCR analyses revealed that the relative *USH2A* transcript levels in the patient-derived and control fibroblasts were $0.12 \pm 0.05\%$ and $0.10 \pm 0.03\%$ as compared to the expression levels of the housekeeping gene *GUSB*, respectively. Because of the extremely low expression levels in fibroblasts, *USH2A* could only be detected after using a highly sensitive reverse transcriptase, as was already reported by others.²⁷

USH2A transcripts from patient-derived fibroblasts were analyzed by RT-PCR using primers in exon 39 (forward) and exon 42 (reverse) which revealed the inclusion of PE40 in mature *USH2A* mRNA (**Fig. 2A**), as expected. Transfection of these fibroblasts with either AON1, AON2 or with a cocktail of AON1+2 together in a final concentration of 0.5 $\mu\text{mol/l}$, resulted in a significant skipping of PE40 (**Fig. 2A**), whereas no aberrant splice events were observed when transfecting these AONs in control fibroblasts (**Fig. 2A**). RT-qPCR analyses showed that the total amount of *USH2A* transcripts was not significantly altered in AON-treated cells as compared to SON2-treated cells (AON1: $p = 0.0797$; AON2: $p = 0.2039$; AON1+2: $p = 0.6491$ (two-tailed Student's *t*-test); **Supplementary Fig. 3**), which indicates that the PE40-containing transcript is not degraded but instead is converted into the wild-type transcript as a consequence of AON-treatment. We next calculated the relative amount of PE40 incorporation into the *USH2A* transcript by comparing PCR fragment intensities on gel. The ratio of PE40 incorporation was calculated for every PCR product. Around half of the *USH2A* transcripts from untransfected patient fibroblasts contained PE40 (0.56 ± 0.03 (ratio \pm SEM)) (**Fig. 2B**). We observed a minimal difference in the average ratio of PE40 incorporation between untransfected cells and cells transfected with a nonbinding sense oligonucleotide (SON2; 0.44 ± 0.04) ($p = 0.0216$) (**Fig. 2B**), which might be explained by natural variation as a consequence of low *USH2A* transcript levels. Patient fibroblasts transfected with either AON1 or AON2 separately (1 $\mu\text{mol/l}$), showed a significantly lower average ratio of PE40 incorporation (0.15 ± 0.03 ; $p < 0.0001$ and 0.23 ± 0.04 ; $p < 0.01$, respectively) as compared to SON2 (**Fig. 2B**). Cotransfecting AON1+2 in a 1:1 ratio with the same final concentration of 1 $\mu\text{mol/l}$ resulted in the nearly complete exclusion of PE40 (0.08 ± 0.02 ; $P < 0.0001$ when

compared to SON2) (**Fig. 2B**). AONs 1 and 2 thus both showed the ability to induce skipping of PE40 in patient-derived fibroblasts, however the highest degree of splice correction was induced using a cocktail of AON1+2.

Quantification of the splice redirection potential of the AONs using RT-qPCR analyses appeared to be technically challenging as a result of very low *USH2A* expression levels in fibroblasts, especially in the case of compound heterozygous mutations. For this reason, we set up an *in vitro* minigene splice assay, based on the pCI-NEO plasmid (**Fig. 3A**).³⁴ The genomic region of *USH2A* PE40 (both wild-type and mutant), surrounded by 722 bp up- and 636 bp downstream sequence, was cloned between *RHO* exons 3 and 5

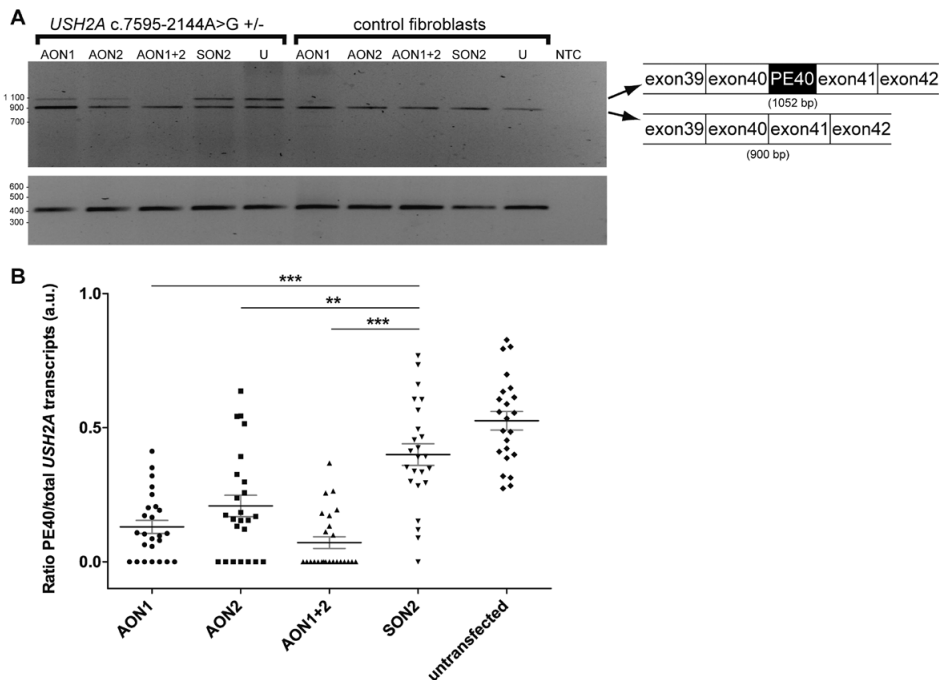


Figure 2. AON-based splice correction in patient-derived fibroblasts. (A) One representative sample of each AON treatment is shown, both for patient-derived and control fibroblasts (upper panel). The upper band represents *USH2A* containing PE40, whereas the lower band is *USH2A* lacking PE40. *ACTB* amplification is shown as a loading control (lower panel). **(B)** For every PCR analysis the PE40/(PE40+*USH2A* lacking PE40) transcript ratio was calculated from the gel intensities of PCR products normalized for their fragment length and plotted as a dot, with the mean ratio represented by a horizontal line. Samples in which the *USH2A* transcript lacking PE40 was not amplified were excluded from calculations, which was the case for four datapoints (one in both AON2 and SON2 and two in the non-AON treated cells). An unpaired two-tailed Student's t-test was used to compare calculated ratios between AON-treated and SON-treated patient-derived fibroblasts, showing a significant reduction of PE40 incorporation in all three AON treatment (AON1, AON2, and AON1+2) conditions (indicated by ***($p < 0.001$) or **($p < 0.01$)). Grey error bars: SEM; NTC: negative template control; U: untreated control; a.u.: arbitrary units.

to model splice defects as seen in *USH2A* patients with the c.7595-2144A>G mutation. Indeed, as a consequence of the mutation,^{24,26} the mutant minigene splice assay only yielded a transcript consisting of *RHO* exon 3-*USH2A* PE40-*RHO* exon 5 whereas the wild-type minigene splice assay only resulted in a transcript containing *RHO* exons 3 and 5 (**Fig. 3B**).

Using an *USH2A* PE40 minigene splice assay, we tried to induce PE40-skipping from the artificial RNA using the same AONs as used to transfect fibroblasts. Cotransfection of the PE40 mutant minigene (1 µg) with 0.5 µmol/l of either AON1 or AON2, resulted in both cases in a combination of corrected and non-corrected transcripts (**Fig. 3B**; 274 bp (corrected) versus 426 bp (noncorrected)). Subsequent sequence analysis of the noncorrected PCR product derived from AON1-treated samples revealed that the first 12 bp of PE40 were lacking as a consequence of a second cryptic splice acceptor site use. This was neither observed in patient-derived fibroblasts treated with AON1 nor in AON2-treated samples. In addition, the AON1-treated minigene splice assay displayed

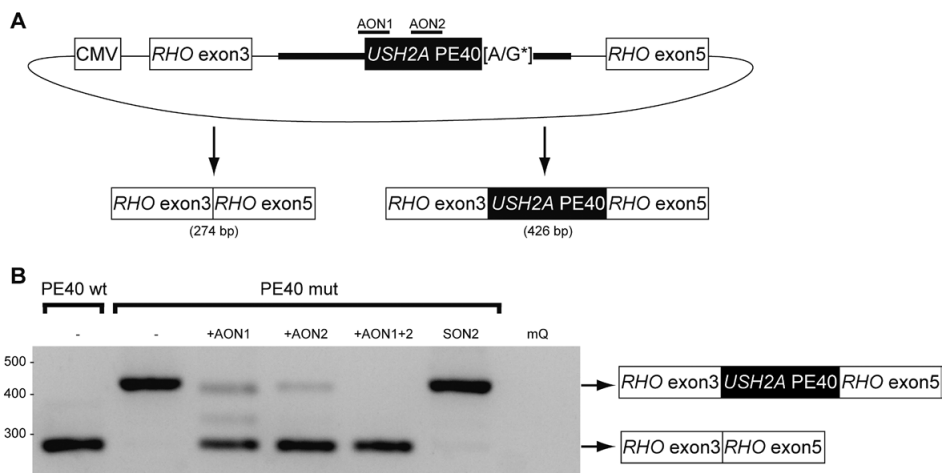


Figure 3. *USH2A* PE40 minigene splice assay to assess AON efficacy *in vitro*. (A) Schematic representation of the minigene splice assay, with the nucleotide corresponding to the *USH2A* c.7595-2144A>G substitution highlighted with an asterisk. The genomic *USH2A* PE40 sequence (indicated with a black background “*USH2A* PE40”) and flanking sequences (indicated with a fat black line) were cloned between *RHO* exons 3 and 5. The targeting sequence of AON1 and AON2 is schematically indicated above the *USH2A* PE40 region. (B) RT-PCR analysis of *RHO* ex3-*USH2A* PE40 wild-type/mutant-*RHO* ex5 RNAs, isolated from transfected HEK293T cells that were cultured in the absence or presence of AON1, AON2, or AON1 and 2 together. AONs are directed against the aberrant *USH2A* PE40 and used in a final concentration of 0.5 µmol/l. The upper bands represent the aberrant *RHO-USH2A* PE40 splice product (426 or 414 bp when AON1-treated), whereas the lower bands represent the corrected transcript without *USH2A* PE40 (274 bp). Also an intermediate splice product was observed after AON1 treatment. SON2 is a nonbinding control sense oligonucleotide and cotransfection into HEK293T cells with the minigene splice assay only gives rise to the aberrant splice product. Water (mQ) was used as a negative control.

a faint intermediate splice product, most probably resulting from partially skipped PE40 (**Fig. 3B**). Sequence analysis of the lower, presumably corrected fragment, showed that it indeed represents correct splicing of *RHO* exon 3 to exon 5. To exclude AON-induced effects on PE40 splicing independent of the targeted sequence, we reversed the sequence of AON2 into a sense orientation (SON2). Cotransfecting the PE40 mutant minigene splice assay with the nonbinding SON2 did not result in splice modulation of PE40, demonstrating the specificity of the result obtained with the antisense sequences (**Fig. 3C**). These results were in total agreement with the results obtained from AON-treated patient-derived fibroblasts (**Fig. 2A, B**). Since both AONs 1 and 2 showed exon-skipping potential using the minigene splice assay, we next lowered AON concentrations ranging from 1.0 to 0.01 $\mu\text{mol/l}$ in order to determine the minimal concentration at which the AONs were still able to induce significant PE40 splice redirection. As shown in **Fig. 4A, B**, for both AON1 and AON2, we observed a gradual decrease of PE40-containing transcripts to coincide with increasing concentrations of AON. When cotransfecting AON1 and 2 as a cocktail, a similar PE40-skipping effect was seen (**Fig. 4C**). However, in

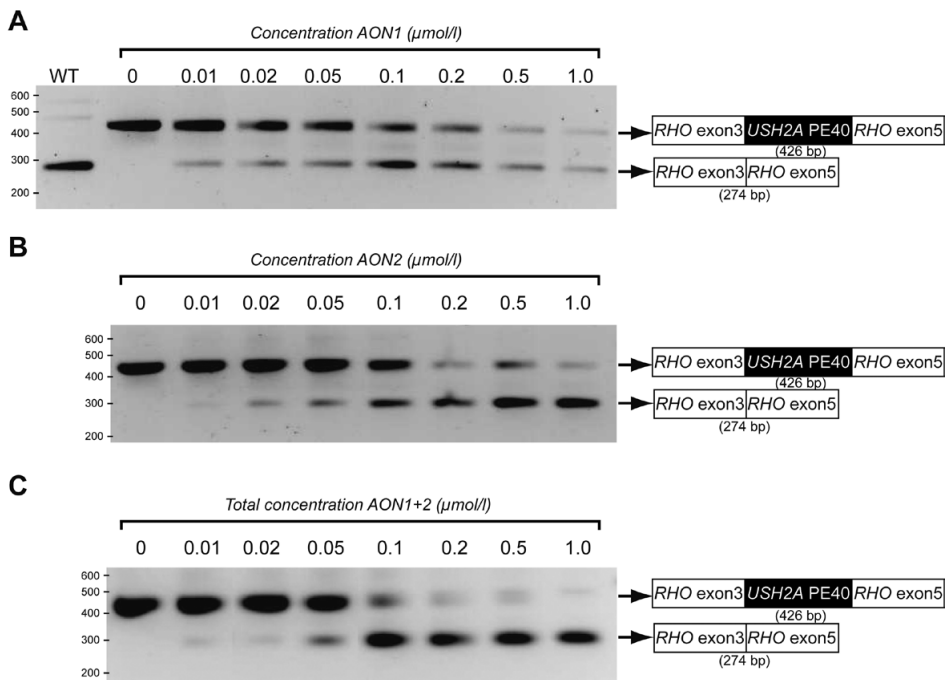


Figure 4. Dose-dependent AON-induced splice correction of *USH2A* using a minigene splice assay. RT-PCR analysis of *RHO* ex3-*USH2A* PE40 mutant-*RHO* ex5 transcripts isolated from transfected HEK293T cells that were cultured in the absence or presence of different end-concentrations of AON1 (**A**), AON2 (**B**), or AON1+2 (**C**), ranging from 0 to 1.0 $\mu\text{mol/l}$. PCR (30 cycles) was performed from *RHO* exon 3 to exon 5, in order to specifically amplify minigene splice assay derived cDNA. The lower band (274 bp) represents the transcript without *USH2A* PE40.

contrast to what we observed for both AON1 and 2 individually, a steep turning point in splice redirection potential was seen between a total AON concentration of 0.1 and 0.05 $\mu\text{mol/l}$. In addition, we observed a decrease in target transcripts when applying AON1 at higher concentrations (0.5 or 1 $\mu\text{mol/l}$) to our minigene splice assay (**Fig. 4A**), which we attributed as the result of toxicity.

In conclusion, we were able to show that designed AONs are able to induce PE40-skipping in both patient-derived fibroblasts and in vitro minigene splice assays.

DISCUSSION

Mutations in *USH2A* that affect splicing are responsible for Usher syndrome type 2 and autosomal recessive retinitis pigmentosa. Recent identification of four deep-intronic mutations leading to inclusion of PEs underlines the importance of this pathogenic mechanism,^{24,25} that was underestimated a few years ago. In this work, we used the c.7595-2144A>G mutation, which represents the second most frequent *USH2A* mutation in some populations, as a model to initiate the development of an AON-based therapy for *USH2A*-associated retinitis pigmentosa.

Mutations that affect pre-mRNA splicing represent a significant fraction of disease-causing mutations, in a variety of inherited disorders.^{35,36} Different strategies have been employed to correct the resulting splice defects, of which AON treatment seems most promising. AONs do not alter endogenous transcription levels and also their relative ease in design and low production costs can be regarded favorable for AON-based therapies.^{35,37} The sequence-specific properties of AONs make them suitable for interfering with splicing processes for different therapeutic purposes.^{38,39} Next to skipping of (pseudo)exons, AONs have been shown to be able to retain exons that are skipped as a consequence of splice site mutations.^{40,41} In addition, AONs can be used to alter the ratio between two naturally occurring alternatively spliced transcripts.³⁸

Several preclinical proof-of-concept studies for AON-based RNA splice modulation therapy have been performed, showing promising results for different genetic disorders such as Leber congenital amaurosis, Hutchinson-Gilford progeria syndrome, spinal muscular atrophy or Duchenne muscular dystrophy.^{31,42-48} As a consequence, AONs are now in or beyond different phase 1, 2, or 3 clinical trials to evaluate their therapeutic potential and biosafety.⁴⁹⁻⁵¹ No major adverse effects have been observed in patients with Duchenne muscular dystrophy after subcutaneous injections with Drisapersen, however mild-to-moderate reactions at the site of injection and proteinuria have been observed in most cases.⁵² Increasing doses of Drisapersen above 6 mg/kg are less well tolerated and lead to inflammatory responses.⁵³ The phosphorothioate backbone can be immunostimulatory mainly via the nucleic acid recognizing toll like receptors (TLRs)

3, 7, 8 and 9⁵⁴. Although not proven, direct delivery into the eye will most probably circumvent systemic exposure of AONs to TLRs due to the presence of a blood-retinal barrier, however, TLR3 expression has also been observed in retinal pigment epithelium cells.⁵⁵ 2'-O-methyl modification of the riboses within the phosphorothioate backbone has been described to prevent activation of TLR7-9, but not of TLR3⁵⁶. As TLR3 recognizes double stranded DNA,⁵⁶ it is not expected that a TLR3-activated inflammatory response will be induced upon an intraocular delivery of AONs.⁵⁷

Different guidelines to aid AON design have been described by others.^{33,37} AONs complementary to exonic splice enhancer (ESE) motifs that are targeted by Ser-Arg-rich splice modulators, in particular SRSF1 (SF2/ASF), SRSF2 (formerly known as SC35) and SRSF5, have been shown to be most effective in exon skipping.³⁷ Also, it has been shown that effective AONs often bind close to the splice acceptor site and the free energy of the AON-target complex is higher than that of the target complex and that of the AON individually.³⁷ By adopting these guidelines we have designed two different AONs and examined the exon skipping potential after single AON addition or after addition of a cocktail consisting of the two AONs. AON1 has been designed to target five predicted SRSF1, two SRSF2, five SRSF5, and two hexamer ESE sequence motifs, thereby overlapping the PE40 splice acceptor site. The use of AON1 in combination with a minigene splice assay results in the use of an alternative splice acceptor site 12 nt downstream of the regular PE40 splice acceptor site. Although this effect has not been observed in fibroblasts treated with AON1 and/or AON2, we cannot rule out that, due to the low level of *USH2A* expression, we are unable to detect any alternatively spliced transcripts. In line with other studies, suggesting that the use of a cocktail of AONs is often more potent than using a single AON,⁵⁸⁻⁶⁰ our results show that a combination of AON1+2 is indeed more potent than using either AON individually.

In our study, we show *USH2A* splice correction in biologically nonrelevant patient-derived fibroblasts and minigene splice assays. However, this does not result in the production of functional *USH2A* protein. In order to evaluate the effect of AON-induced splice correction on the level of photoreceptor maintenance and function, physiological relevant cellular and/or animal models will be crucial. Using iPSC technology, it is possible to generate photoreceptor-like cells from patient-derived keratinocytes or fibroblasts, which has already been shown for an *USH2A* patient having the c.7595-2144A>G mutation in compound heterozygosity with the c.12575G>A; p.Arg4192His mutation.²⁶ The use of photoreceptor-like cells will enable the assessment of potential AON-induced off-target effects by sequencing total RNA from those artificial eyecups. For the evaluation of visual function, animal models will be essential. However, the currently available *Ush2a* knockout mouse model only shows a mild retinal degeneration with a very late age of onset.⁶¹ Zebrafish can be an attractive alternative model for studying Usher syndrome-related retinal degeneration.⁶² Electroretinogram (ERG) traces have been shown

to be significantly attenuated in zebrafish *Myo7a* (USH1b), *Ush1c* (USH1c), and *Pcdh15b* (USH1f) mutants and morphants.^{63–65} In addition, morpholino-induced knockdown of zebrafish *ush2a* results in moderate levels of early-onset photoreceptor degeneration in larvae (5 days postfertilization).⁶⁶ Although the effect of human mutations on splicing is not always recapitulated in non-human species,⁶⁷ the c.7595-2144A>G mutation results in a consensus (“GTAAG”) splice donor site. Recent advances in CRISPR/Cas9 technology now enable the generation of a humanized locus for the *USH2A* PE40 intronic sequence in zebrafish. Future research will determine whether the effect of the c.7595-2144A>G mutation is recapitulated in a humanized zebrafish, and whether this model will be suitable to evaluate the effect of AON-induced splice correction on the level of visual function.

Once an animal model is present, the next challenge will be the delivery of AONs to photoreceptor cells. Systemic drug administration is one possible route for treating retinal disorders. However, retinal transfer of drugs from the circulating blood is strictly regulated by two blood–ocular barrier systems, the blood–aqueous barrier and the blood–retinal barrier.^{45,68,69} In order to effectively overcome these physical barriers, AONs need to be delivered directly into the human eye, either via injections of naked AONs into the vitreous humor or by using a stabilizing vehicle (e.g., recombinant virus, designed nanoparticles, cell penetrating peptides, exosomes, or liposomes).^{35,70,71} Once present in the eye, naked AONs have proven to be able to freely diffuse into all cells of the retina to interfere with splicing.⁴⁵ When using naked AONs, it will be needed to repeatedly supplement photoreceptor cells with AONs, since effectiveness will be lost over time due to AON degradation or wash out. Intravitreal injections in mice have demonstrated that 2'-O-methylphosphorothioate AONs are effective in photoreceptor cells for at least one month and probably longer.⁴⁵ Therefore, we speculate that patients will need a few intravitreal AON administrations per year.

A durable splice correction effect is likely to be achieved by administration of an AAV vector expressing AON sequences linked to a modified U7 small nuclear RNA (U7 snRNA). Via this route, it will be possible to induce the same therapeutic effect as with naked AONs, but presumably with a long-lasting effect.^{72–74} However, traditionally AAVs are unable to cross the retinal layers from vitreous humor into photoreceptor cells due to the presence of a diffusive barrier made up by the inner limiting membrane.⁷⁵ In addition, also the presence of neutralizing antibodies may reduce successful photoreceptor infection from intravitreally injected AAVs.⁷⁶ For this reason, AAVs will need to be injected subretinally, limiting the targeted retinal area.⁷⁷ However, a recent study presented a promising rAAV serotype which can be efficiently delivered intravitreally.⁷⁸ After transduction, the rAAV DNA strands will form very stable episomal structures, from which transcription can take place. Since photoreceptor cells are nondividing cells, integration in their genome is not a pre-requisite for success and therefore the use of

rAAVs instead of integrating (retro)viruses will lower the risk of potential side effects without reducing AON effectiveness.

Besides presenting with retinal degeneration, Usher syndrome patients suffer from congenital hearing impairment. Usher proteins have been shown to be the structural components of the fibrous links between hair cell stereocilia and essential for proper hair bundle formation and function (reviewed by Kremer *et al.*⁷⁹). *USH1C* encodes harmonin, a protein directly connected to the *USH2A* protein in both hair cells and photoreceptors.⁸⁰ Treatment of an *Ush1c* mouse model with splice modulating AONs anytime during the first thirteen days after birth, results in a restored orientation and function of cochlear hair bundles.⁸¹ Treatment on this mouse from post-natal day 16 onwards, which corresponds to five months of gestation in humans, shows no beneficial effects anymore. Therefore, AON-based splice correction will probably only be effective when administered during or prior to the development of inner ear hair bundles.

In conclusion, this study shows that administration of engineered AONs to fibroblasts of an individual affected by Usher syndrome almost fully restores a splice defect that is caused by the frequent deep-intronic c.7595-2144A>G mutation in *USH2A*. Although promising on transcript level, future research is needed to determine the therapeutic potential of AON-based splice correction as a treatment to stop or slow down the progression of this devastating blinding aspect of Usher syndrome and isolated *USH2A*-associated retinitis pigmentosa.

MATERIALS AND METHODS

Antisense oligonucleotides

The sequence of *USH2A* PE40 was analyzed for the presence of exonic splice enhancer motifs using the online ESE finder 3.0 program (<http://rulai.cshl.edu/cgi-bin/tools/ESE3/esefinder.cgi?process=home>) with standard settings. The presence of RESCUE-ESE sites was determined using the RESCUE-ESE tool (<http://genes.mit.edu/burgelab/rescue-ese/>). AONs were subsequently designed to each cover multiple SRSF1, SRSF2, SRSF5, or hexamers in PE40. Furthermore, the energetically most stable secondary structure of *USH2A* PE40 (including 25 nucleotides of flanking sequence both up- and downstream) was predicted using the RNAstructure software (<http://rna.urmc.rochester.edu/rnastructure.html>).⁸² In addition, we picked sequences to be targeted by AONs predicted as “partially open”. With the same webtool, also thermodynamic criteria were evaluated: free energy of the AON, of the AON-AON complexes and of binding energy between the AON and its target sequence.³³ AONs according above criteria were designed with a Tm of 58 °C and a GC% between 40–60%. The uniqueness of the AON target sequences was determined by BLAST analysis. The two most optimal AONs were

purchased from Eurogentec (Liège, Belgium) containing 2'-O-methyl modified riboses and a phosphorothioate backbone (sequences are presented in **Table 1**). As a nonbinding control, a sense orientation of AON2 was also acquired (named SON2). AONs were dissolved in phosphate-buffered saline (PBS) before use.

USH2A qPCR analysis

Total RNA was isolated from fibroblasts using the Nucleospin RNA II isolation kit (MACHEREY-NAGEL #740955.50, Düren, Germany), according to manufacturer's protocol. Subsequently, 0.5–1.0 µg of total RNA was used for cDNA synthesis with SuperScript III RT (Life Technologies, #11755050, Carlsbad, CA). *USH2A* was subsequently amplified using forward primer 5'-CCAGGGAAAAGAGCAGAGTG-3' (exon 28) and reverse primer 5'-GATAGCCTCGCATGAAGGAG-3' (exon 29). The housekeeping gene *GUSB* was used as a reference using the forward primer 5'-AGAGTGGTGCTGAGGATTGG-3' (exon 2) and reverse primer 5'-GACACGCTAGAGCATGAGGG-3' (exon 3). GoTaq (Promega A6001) was used to amplify *USH2A* and *GUSB* cDNA in triplicate in a 7500 HT qPCR machine. Analysis of the qPCR data was performed with 7500 software (version 2.3), with the CT-threshold set manually. Subsequently, *USH2A/GUSB* ratios were calculated to obtain relative *USH2A* transcript levels.

Minigene splice assays

A plasmid containing the genomic region of *RHO* encompassing exons 3–5 inserted at the EcoRI/SalI sites in the pCI-NEO vector³⁴ was adapted to the Gateway cloning system, as previously described.⁸³ Using Gateway cloning technology, human *USH2A* PE40 (wild-type and mutant) together with 722 bp of 5'-flanking and 636 bp of 3'-flanking intronic sequence was inserted in the vector.

Cell culture

HEK293T cells were cultured in Dulbecco's modified Eagle's medium (DMEM) (Sigma-Aldrich D0819, St. Louis, MO) supplemented with 10% (v/v) fetal bovine serum (Sigma-Aldrich, F7524) and 1% penicillin-streptomycin (Sigma-Aldrich, P4333). Primary fibroblasts of an *USH2* patient, with compound heterozygous *USH2A* mutations (c.7595-2144A>G and c.10636G>A), were cultured in DMEM (Sigma-Aldrich, D0819) supplemented with 20% fetal bovine serum (Sigma-Aldrich, F7524), 1% sodium pyruvate (Sigma-Aldrich, S8636) and 1% penicillin-streptomycin (Sigma-Aldrich P4333). All cells were passaged twice a week.

Transfection of AONs in patient-derived fibroblasts

Fibroblasts were seeded at a concentration of 5.0×10^5 cells/well in a 12-well plate. Cells were subsequently transfected with AONs using FuGENE HD Transfection Reagent

(Promega, E2311, Madison, WI) according to manufacturer's instructions, in quintuplicate. Twenty-four hours after transfection, cells were treated for an additional 16 hours with cycloheximide (Sigma-Aldrich, C4859—final concentration of 100 µg/ml in DMEM medium with all supplements as described before) prior to RNA isolation in order to inhibit nonsense-mediated decay of the *USH2A* PE40-containing transcripts.

Transfection of AONs and minigene splice assay in HEK293T cells

One day before transfection, 5.0×10^5 HEK293T cells were seeded in each well of a 12-well plate, in a total volume of 0.9 ml medium containing all supplements as described before. Transfection mixtures were prepared by combining 1 µl AON in a desired concentration as indicated in the graphs, 500 ng of plasmid DNA and 45 µl polyethylenimine transfection reagent (PEI). Mixtures were incubated at room temperature for 10 minutes, before being dropwise added to the cells. Forty-eight hours after transfection, cells were collected using a cell scraper and washed with 1x PBS prior to RNA isolation.

RNA isolation and RT-PCR

Total RNA was isolated from transfected HEK293T or fibroblasts using the Nucleospin RNA II isolation kit (MACHEREY-NAGEL, 740955.50, Düren, Germany), according to manufacturer's protocol. Subsequently, 0.5–1.0 µg of total RNA was used for cDNA synthesis with iScript cDNA synthesis kit (Bio-Rad, 170–8891) or SuperScript III RT (Life Technologies, 11755050) for HEK293T and primary fibroblasts, respectively. For the splice correction experiments with the minigene splice assay, part of the cDNA was amplified under standard PCR conditions using Q5 polymerase (New England Biolabs, M0491L, Ipswich, MA) and using forward primer 5'-CGGAGGTCAACAACGAGTCT-3' and reverse primer 5'-AGGTGTAGGGGATGGGAGAC-3' that are designed for exons 3 and 5 of the human *RHO* gene, respectively. For the splice correction experiments in fibroblasts, part of the *USH2A* cDNA was amplified under standard PCR conditions using Q5 polymerase and the primers 5'-GCTCTCCAGATACCAACTCC-3' and 5'-GATTCACATGCCTGACCCCTC-3' designed for exons 39 and 42, respectively. A PCR amplifying *ACTB* cDNA using forward primer 5'-ACTGGGACGACATGGAGAAG-3' and reverse primer 5'-CTTACCACCACAGCTGAGA-3' was employed as a control for the amount of lysed cell material. Every cDNA sample was analysed in quintuplicate, yielding in total 25 datapoints per AON. PCR products were separated on a standard 1% agarose gel. Fragments presumably representing correctly and aberrantly spliced *USH2A* were excised from the gel, purified using Nucleospin Extract II isolation kit (MACHEREYNAGEL, 740609) and sequenced from both strands with the ABIPRISM Big Dye Terminator Cycle Sequencing V2.0 Ready Reaction kit and the ABIPRISM 3730 DNA analyzer (Applied Biosystems, Foster City, CA).

Quantification of PCR product intensities and ratio calculation

PCR products were size separated on a 1% agarose gel, and DNA was visualized using ethidium bromide. Gels were photographed with an Isogen Life sciences imager using ProXima AQ-4 (v3.0) software and subsequently quantified with ImageJ (v1.46r) software. Both PE40-containing fragments and *USH2A* fragments lacking PE40 were covered in a square with an equal surface area, from which the intensity profile was subsequently generated. The peaks' bases were closed manually by drawing a horizontal line, after which the surface of the peaks was calculated, representing *USH2A* PE40-containing transcripts and transcripts lacking PE40. These values were transferred to Microsoft Excel 2007 and normalized for their product size (i.e. 1,052 or 900 bp). The total amount of *USH2A* transcripts (i.e. the sum of PE40-containing and PE40-lacking band intensities) and the PE40 transcript ratio (i.e., PE40-containing transcripts divided by total *USH2A* transcripts) was calculated per condition. Samples in which the *USH2A* transcript lacking PE40 was not amplified were excluded from calculations, which was the case for four PCR products (one in both AON2 and SON2 and two samples in the non-AON-treated cells). Each gel image was analyzed twice, from which the average was plotted in a dot-plot using GraphPad Prism (v5.03, GraphPad Software, San Diego, CA). Statistical analyses were subsequently performed with a two-tailed unpaired Student's *t*-test using GraphPad Prism.

ACKNOWLEDGMENTS

The authors would like to thank the CIBERER biobank (Valencia, Spain) for sharing *USH2A* patient-derived primary fibroblasts. This work is financially supported by the Dutch Organisation for Scientific research (I Veni grant 016.136.091; E.V.W.), the Dutch Organisation for Health Research and Development (ZonMW E-rare grant "Eur-USH" 40-42900-98-1006; E.V.W.), the Dutch eye foundations (Stichting Nederlands Oogheelkundig Onderzoek, SAFDOR and Stichting Blindenhulp; E.V.W. and H.K.), the French national union of blind and visually impaired people (UNADEV; A-FR), and the French National Research Agency (E-rare grant "Eur-USH" ANR-12-RARE-006-03; CV). The work in this manuscript has been patented under number PCT/EP2015/065736. E.V.W. reports being employed by Radboudumc and inventor on this patent. Radboudumc has licensed the rights to the patent exclusively to ProQR Therapeutics. As the inventor, E.V.W. is entitled to a share of any future royalties paid to Radboudumc, should the therapy eventually be brought to the market.

REFERENCES

1. Kimberling, WJ, Hildebrand, MS, Shearer, AE, Jensen, ML, Halder, JA, Trzupke, K et al. (2010). Frequency of Usher syndrome in two pediatric populations: Implications for genetic screening of deaf and hard of hearing children. *Genet Med* 12: 512–516.
2. Millán, JM, Aller, E, Jaijo, T, Blanco-Kelly, F, Gimenez-Pardo, A and Ayuso, C (2011). An update on the genetics of usher syndrome. *J Ophthalmol* 2011: 417217.
3. Yan, D and Liu, XZ (2010). Genetics and pathological mechanisms of Usher syndrome. *J Hum Genet* 55: 327–335.
4. Sadeghi, AM, Cohn, ES, Kimberling, WJ, Halvarsson, G and Möller, C (2013). Expressivity of hearing loss in cases with Usher syndrome type IIA. *Int J Audiol* 52: 832–837.
5. Hartong, DT, Berson, EL and Dryja, TP (2006). Retinitis pigmentosa. *Lancet* 368: 1795–1809.
6. Seyedahmadi, BJ, Rivolta, C, Keene, JA, Berson, EL and Dryja, TP (2004). Comprehensive screening of the *USH2A* gene in Usher syndrome type II and nonsyndromic recessive retinitis pigmentosa. *Exp Eye Res* 79: 167–173.
7. McGee, TL, Seyedahmadi, BJ, Sweeney, MO, Dryja, TP and Berson, EL (2010). Novel mutations in the long isoform of the *USH2A* gene in patients with Usher syndrome type II or non-syndromic retinitis pigmentosa. *J Med Genet* 47: 499–506.
8. Blanco-Kelly, F, Jaijo, T, Aller, E, Avila-Fernandez, A, López-Molina, MI, Giménez, A et al. (2015). Clinical aspects of Usher syndrome and the *USH2A* gene in a cohort of 433 patients. *JAMA Ophthalmol* 133: 157–164.
9. Sandberg, MA, Rosner, B, Weigel-DiFranco, C, McGee, TL, Dryja, TP and Berson, EL (2008). Disease course in patients with autosomal recessive retinitis pigmentosa due to the *USH2A* gene. *Invest Ophthalmol Vis Sci* 49: 5532–5539.
10. Pierrache, LH, Hartel, BP, van Wijk, E, Meester-Smoor, MA, Cremers, FP, de Baere, E et al. (2016). Visual prognosis in *USH2A*-associated retinitis pigmentosa is worse for patients with Usher syndrome type IIA than for those with nonsyndromic Retinitis Pigmentosa. *Ophthalmology* 123: 1151–1160.
11. Hashimoto, T, Gibbs, D, Lillo, C, Azarian, SM, Legacki, E, Zhang, XM et al. (2007). Lentiviral gene replacement therapy of retinas in a mouse model for Usher syndrome type 1B. *Gene Ther* 14: 584–594.
12. Lopes, VS, Boye, SE, Louie, CM, Boye, S, Dyka, F, Chiodo, V et al. (2013). Retinal gene therapy with a large *MYO7A* cDNA using adeno-associated virus. *Gene Ther* 20: 824–833.
13. Colella, P, Trapani, I, Cesi, G, Sommella, A, Manfredi, A, Puppo, A et al. (2014). Efficient gene delivery to the cone-enriched pig retina by dual AAV vectors. *Gene Ther* 21: 450–456.
14. Zallocchi, M, Binley, K, Lad, Y, Ellis, S, Widdowson, P, Iqbal, S et al. (2014). ElAV-based retinal gene therapy in the shaker1 mouse model for usher syndrome type 1B: development of UshStat. *PLoS One* 9: e94272.
15. Bainbridge, JW, Smith, AJ, Barker, SS, Robbie, S, Henderson, R, Balaggan, K et al. (2008). Effect of gene therapy on visual function in Leber's congenital amaurosis. *N Engl J Med* 358: 2231–2239.
16. Cideciyan, AV, Aleman, TS, Boye, SL, Schwartz, SB, Kaushal, S, Roman, AJ et al. (2008). Human gene therapy for RPE65 isomerase deficiency activates the retinoid cycle of vision but with slow rod kinetics. *Proceed Natl Acad Sci USA* 105, 15112–15117.

17. Hauswirth, WW, Aleman, TS, Kaushal, S, Cideciyan, AV, Schwartz, SB, Wang, L et al. (2008). Treatment of leber congenital amaurosis due to RPE65 mutations by ocular subretinal injection of adeno-associated virus gene vector: short-term results of a phase I trial. *Hum Gene Ther* 19: 979–990.
18. Maguire, AM, Simonelli, F, Pierce, EA, Pugh, EN Jr, Mingozzi, F, Bennicelli, J et al. (2008). Safety and efficacy of gene transfer for Leber's congenital amaurosis. *N Engl J Med* 358: 2240–2248.
19. Savić, N and Schwank, G (2016). Advances in therapeutic CRISPR/Cas9 genome editing. *Transl Res* 168: 15–21.
20. Roux, AF, Faugère, V, Vaché, C, Baux, D, Besnard, T, Léonard, S et al. (2011). Four-year follow-up of diagnostic service in USH1 patients. *Invest Ophthalmol Vis Sci* 52: 4063–4071.
21. Baux, D, Blanchet, C, Hamel, C, Meunier, I, Larrieu, L, Faugère, V et al. (2014). Enrichment of LOVD-USHbases with 152 *USH2A* genotypes defines an extensive mutational spectrum and highlights missense hotspots. *Hum Mutat* 35: 1179–1186.
22. Aller, E, Larrieu, L, Jaijo, T, Baux, D, Espinós, C, González-Candelas, F et al. (2010). The *USH2A* c.2299delG mutation: dating its common origin in a Southern European population. *Eur J Hum Genet* 18: 788–793.
23. Pennings, RJ, Te Brinke, H, Weston, MD, Claassen, A, Orten, DJ, Weekamp, H et al. (2004). *USH2A* mutation analysis in 70 Dutch families with Usher syndrome type II. *Hum Mutat* 24: 185.
24. Vaché, C, Besnard, T, le Berre, P, García-García, G, Baux, D, Larrieu, L et al. (2012). Usher syndrome type 2 caused by activation of an *USH2A* pseudoexon: implications for diagnosis and therapy. *Hum Mutat* 33: 104–108.
25. Liquori, A, Vaché, C, Baux, D, Blanchet, C, Hamel, C, Malcolm, S et al. (2016). Whole *USH2A* gene sequencing identifies several new deep intronic mutations. *Hum Mutat* 37: 184–193.
26. Tucker, BA, Mullins, RF, Streb, LM, Anfinson, K, Eystone, ME, Kaalberg, E et al. (2013). Patient-specific iPSC-derived photoreceptor precursor cells as a means to investigate retinitis pigmentosa. *Elife* 2: e00824.
27. Steele-Stallard, HB, Le Quesne Stabej, P, Lenassi, E, Luxon, LM, Claustres, M, Roux, AF et al. (2013). Screening for duplications, deletions and a common intronic mutation detects 35% of second mutations in patients with *USH2A* monoallelic mutations on Sanger sequencing. *Orphanet J Rare Dis* 8: 122.
28. Krawitz, PM, Schiska, D, Krüger, U, Appelt, S, Heinrich, V, Parkhomchuk, D et al. (2014). Screening for single nucleotide variants, small indels and exon deletions with a next-generation sequencing based gene panel approach for Usher syndrome. *Mol Genet Genomic Med* 2: 393–401.
29. Aparisi, MJ, Aller, E, Fuster-García, C, García-García, G, Rodrigo, R, Vázquez-Manrique, RP et al. (2014). Targeted next generation sequencing for molecular diagnosis of Usher syndrome. *Orphanet J Rare Dis* 9: 168.
30. Sodi, A, Mariottini, A, Passerini, I, Murro, V, Tachyla, I, Bianchi, B et al. (2014). *MYO7A* and *USH2A* gene sequence variants in Italian patients with Usher syndrome. *Mol Vis* 20: 1717–1731.
31. Collin, RW, den Hollander, AI, van der Velde-Visser, SD, Bennicelli, J, Bennett, J and Cremers, FP (2012). Antisense oligonucleotide (AON)-based therapy for Leber congenital amaurosis caused by a frequent mutation in CEP290. *Mol Ther Nucleic Acids* 1: e14.

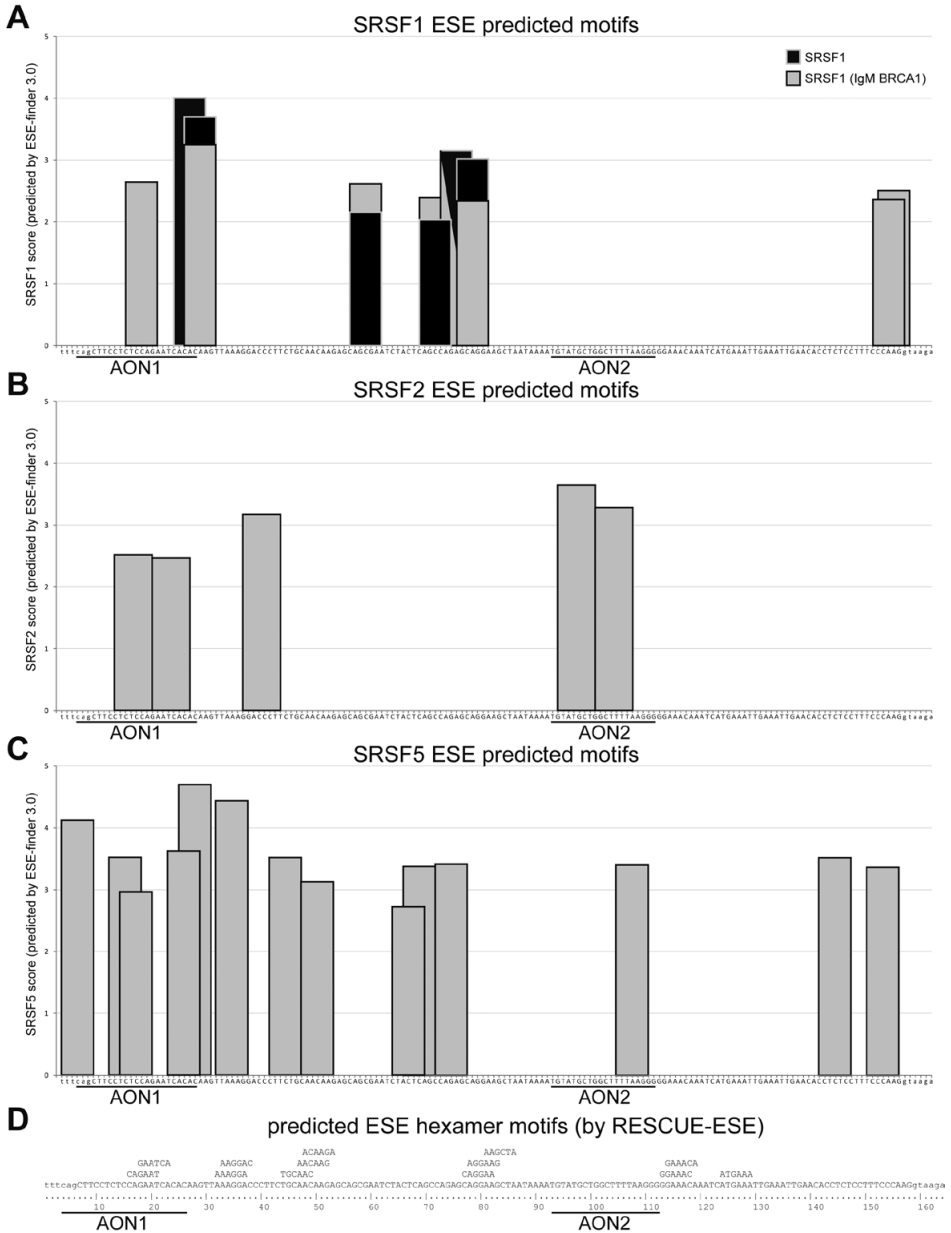
32. Aartsma-Rus, A, Houllberghs, H, van Deutekom, JC, van Ommen, GJ and 't Hoen, PA (2010). Exonic sequences provide better targets for antisense oligonucleotides than splice site sequences in the modulation of Duchenne muscular dystrophy splicing. *Oligonucleotides* 20: 69–77.
33. Aartsma-Rus, A (2012). Overview on AON design. *Methods Mol Biol* 867: 117–129.
34. Gamundi, MJ, Hernan, I, Muntanyola, M, Maseras, M, López-Romero, P, Alvarez, R et al. (2008). Transcriptional expression of cis-acting and trans-acting splicing mutations cause autosomal dominant retinitis pigmentosa. *Hum Mutat* 29: 869–878.
35. Hammond, SM and Wood, MJ (2011). Genetic therapies for RNA mis-splicing diseases. *Trends Genet* 27: 196–205.
36. Wang, GS and Cooper, TA (2007). Splicing in disease: disruption of the splicing code and the decoding machinery. *Nat Rev Genet* 8: 749–761.
37. Aartsma-Rus, A, van Vliet, L, Hirschi, M, Janson, AA, Heemskerk, H, de Winter, CL et al. (2009). Guidelines for antisense oligonucleotide design and insight into splice-modulating mechanisms. *Mol Ther* 17: 548–553.
38. Siva, K, Covello, G and Denti, MA (2014). Exon-skipping antisense oligonucleotides to correct missplicing in neurogenetic diseases. *Nucleic Acid Ther* 24: 69–86.
39. Gerard, X, Garanto, A, Rozet, JM and Collin, RW (2016). Antisense Oligonucleotide Therapy for Inherited Retinal Dystrophies. *Adv Exp Med Biol* 854: 517–524.
40. Igreja, S, Clarke, LA, Botelho, HM, Marques, L and Amaral, MD (2016). Correction of a Cystic Fibrosis Splicing Mutation by Antisense Oligonucleotides. *Hum Mutat* 37: 209–215.
41. Skordis, LA, Dunckley, MG, Yue, B, Eperon, IC and Muntoni, F. (2003). Bifunctional antisense oligonucleotides provide a trans-acting splicing enhancer that stimulates SMN2 gene expression in patient fibroblasts. *Proceed Natl Acad Sci USA* 100, 4114–4119.
42. Scaffidi, P and Misteli, T (2005). Reversal of the cellular phenotype in the premature aging disease Hutchinson-Gilford progeria syndrome. *Nat Med* 11: 440–445.
43. Cirak, S, Feng, L, Anthony, K, Arechavala-Gomez, V, Torelli, S, Sewry, C et al. (2012). Restoration of the dystrophin-associated glycoprotein complex after exon skipping therapy in Duchenne muscular dystrophy. *Mol Ther* 20: 462–467.
44. Hua, Y, Sahashi, K, Hung, G, Rigo, F, Passini, MA, Bennett, CF et al. (2010). Antisense correction of SMN2 splicing in the CNS rescues necrosis in a type III SMA mouse model. *Genes Dev* 24: 1634–1644.
45. Gérard, X, Perrault, I, Munnich, A, Kaplan, J and Rozet, JM (2015). Intravitreal injection of splice-switching oligonucleotides to manipulate splicing in retinal cells. *Mol Ther Nucleic Acids* 4: e250.
46. Garanto, A, Chung, DC, Duijkers, L, Corral-Serrano, JC, Messchaert, M, Xiao, R et al. (2016). In vitro and in vivo rescue of aberrant splicing in CEP290-associated LCA by antisense oligonucleotide delivery. *Hum Mol Genet* (epub ahead of print).
47. Gerard, X, Perrault, I, Hanein, S, Silva, E, Bigot, K, Defoort-Delhemmes, S et al. (2012). AON-mediated exon skipping restores ciliation in fibroblasts harboring the common Leber congenital amaurosis CEP290 mutation. *Mol Ther Nucleic Acids* 1: e29.
48. Parfitt, DA, Lane, A, Ramsden, CM, Carr, AJ, Munro, PM, Jovanovic, K et al. (2016). Identification and correction of mechanisms underlying inherited blindness in human iPSC-derived optic cups. *Cell Stem Cell* 18: 769–781.

49. Miller, TM, Pestronk, A, David, W, Rothstein, J, Simpson, E, Appel, SH et al. (2013). An anti-sense oligonucleotide against SOD1 delivered intrathecally for patients with SOD1 familial amyotrophic lateral sclerosis: a phase 1, randomized, first-in-man study. *Lancet Neurol* 12: 435–442.
50. Koo, T and Wood, MJ (2013). Clinical trials using antisense oligonucleotides in duchenne muscular dystrophy. *Hum Gene Ther* 24: 479–488.
51. Goemans, NM, Tulinius, M, van den Akker, JT, Burm, BE, Ekhart, PF, Heuvelmans, N et al. (2011). Systemic administration of PRO051 in Duchenne's muscular dystrophy. *N Engl J Med* 364: 1513–1522.
52. Voit, T, Topaloglu, H, Straub, V, Muntoni, F, Deconinck, N, Campion, G et al. (2014). Safety and efficacy of drisapersen for the treatment of Duchenne muscular dystrophy (DEMAND II): an exploratory, randomized, placebo-controlled phase 2 study. *Lancet Neurol* 13: 987–996.
53. Flanigan, KM, Voit, T, Rosales, XQ, Servais, L, Kraus, JE, Wardell, C et al. (2014). Pharmacokinetics and safety of single doses of drisapersen in non-ambulant subjects with Duchenne muscular dystrophy: results of a double-blind randomized clinical trial. *Neuromuscul Disord* 24: 16–24.
54. Yu, FS and Hazlett, LD (2006). Toll-like receptors and the eye. *Invest Ophthalmol Vis Sci* 47: 1255–1263.
55. Kumar, MV, Nagineni, CN, Chin, MS, Hooks, JJ and Detrick, B (2004). Innate immunity in the retina: Toll-like receptor (TLR) signaling in human retinal pigment epithelial cells. *J Neuroimmunol* 153: 7–15.
56. Richardt-Pargmann, D and Vollmer, J (2009). Stimulation of the immune system by therapeutic antisense oligodeoxynucleotides and small interfering RNAs via nucleic acid receptors. *Ann N Y Acad Sci* 1175: 40–54.
57. Kole, R and Krieg, AM (2015). Exon skipping therapy for Duchenne muscular dystrophy. *Adv Drug Deliv Rev* 87: 104–107.
58. Aartsma-Rus, A, Kaman, WE, Weij, R, den Dunnen, JT, van Ommen, GJ and van Deutekom, JC (2006). Exploring the frontiers of therapeutic exon skipping for Duchenne muscular dystrophy by double targeting within one or multiple exons. *Mol Ther* 14: 401–407.
59. Adams, AM, Harding, PL, Iversen, PL, Coleman, C, Fletcher, S and Wilton, SD (2007). Antisense oligonucleotide induced exon skipping and the dystrophin gene transcript: cocktails and chemistries. *BMC Mol Biol* 8: 57.
60. Wilton, SD, Fall, AM, Harding, PL, McClorey, G, Coleman, C and Fletcher, S (2007). Antisense oligonucleotide-induced exon skipping across the human dystrophin gene transcript. *Mol Ther* 15: 1288–1296.
61. Liu, X, Bulgakov, OV, Darrow, KN, Pawlyk, B, Adamian, M, Liberman, MC et al. (2007). Usherin is required for maintenance of retinal photoreceptors and normal development of cochlear hair cells. *Proceed Natl Acad Sci USA* 104, 4413–4418.
62. Slijkerman, RW, Song, F, Astuti, GD, Huynen, MA, van Wijk, E, Stieger, K et al. (2015). The pros and cons of vertebrate animal models for functional and therapeutic research on inherited retinal dystrophies. *Prog Retin Eye Res* 48: 137–159.
63. Wasfy, MM, Matsui, JI, Miller, J, Dowling, JE and Perkins, BD (2014). Myosin 7aa(-/-) mutant zebrafish show mild photoreceptor degeneration and reduced electroretinographic responses. *Exp Eye Res* 122: 65–76.

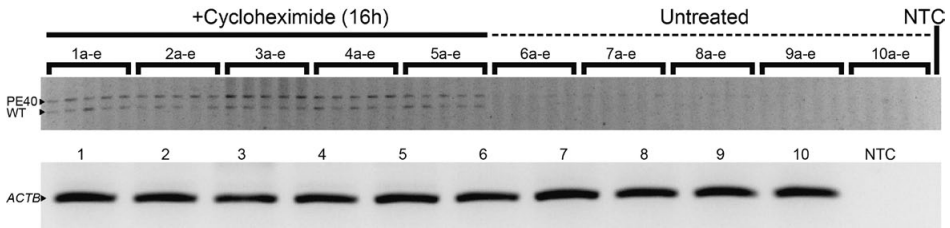
64. Phillips, JB, Blanco-Sanchez, B, Lentz, JJ, Tallafuss, A, Khanobdee, K, Sampath, S et al. (2011). Harmonin (Ush1c) is required in zebrafish Müller glial cells for photoreceptor synaptic development and function. *Dis Model Mech* 4: 786–800.
65. Seiler, C, Finger-Baier, KC, Rinner, O, Makhankov, YV, Schwarz, H, Neuhaus, SC et al. (2005). Duplicated genes with split functions: independent roles of protocadherin15 orthologues in zebrafish hearing and vision. *Development* 132: 615–623.
66. Ebermann, I, Phillips, JB, Liebau, MC, Koenekoop, RK, Schermer, B, Lopez, I et al. (2010). PDZD7 is a modifier of retinal disease and a contributor to digenic Usher syndrome. *J Clin Invest* 120: 1812–1823.
67. Garanto, A, Duijkers, L and Collin, RW (2015). Species-dependent splice recognition of a cryptic exon resulting from a recurrent intronic CEP290 mutation that causes congenital blindness. *Int J Mol Sci* 16: 5285–5298.
68. Raghava, S, Hammond, M and Kompella, UB (2004). Periocular routes for retinal drug delivery. *Expert Opin Drug Deliv* 1: 99–114.
69. Janoria, KG, Gunda, S, Boddu, SH and Mitra, AK (2007). Novel approaches to retinal drug delivery. *Expert Opin Drug Deliv* 4: 371–388.
70. Falzarano, MS, Passarelli, C and Ferlini, A (2014). Nanoparticle delivery of antisense oligonucleotides and their application in the exon skipping strategy for Duchenne muscular dystrophy. *Nucleic Acid Ther* 24: 87–100.
71. Wada, S, Uruse, T, Hasegawa, Y, Ban, K, Sudani, A, Kawai, Y et al. (2014). Aib-containing peptide analogs: cellular uptake and utilization in oligonucleotide delivery. *Bioorg Med Chem* 22: 6776–6780.
72. Gedicke-Hornung, C, Behrens-Gawlik, V, Reischmann, S, Geertz, B, Stimpel, D, Weinberger, F et al. (2013). Rescue of cardiomyopathy through U7snRNA-mediated exon skipping in Mybpc3-targeted knock-in mice. *EMBO Mol Med* 5: 1128–1145.
73. Geib, T and Hertel, KJ (2009). Restoration of full-length SMN promoted by adenoviral vectors expressing RNA antisense oligonucleotides embedded in U7 snRNAs. *PLoS One* 4: e8204.
74. Goyenvalle, A, Vulin, A, Foucherousse, F, Leturcq, F, Kaplan, JC, Garcia, L et al. (2004). Rescue of dystrophic muscle through U7 snRNA-mediated exon skipping. *Science* 306: 1796–1799.
75. Dalkara, D, Kolstad, KD, Caporale, N, Visel, M, Klimczak, RR, Schaffer, DV et al. (2009). Inner limiting membrane barriers to AAV-mediated retinal transduction from the vitreous. *Mol Ther* 17: 2096–2102.
76. Kotterman, MA, Yin, L, Strazzeri, JM, Flannery, JG, Merigan, WH and Schaffer, DV (2015). Antibody neutralization poses a barrier to intravitreal adeno-associated viral vector gene delivery to non-human primates. *Gene Ther* 22: 116–126.
77. Li, Q, Miller, R, Han, PY, Pang, J, Dinculescu, A, Chiodo, V et al. (2008). Intraocular route of AAV2 vector administration defines humoral immune response and therapeutic potential. *Mol Vis* 14: 1760–1769.
78. Dalkara, D, Byrne, LC, Klimczak, RR, Visel, M, Yin, L, Merigan, WH et al. (2013). In vivo-directed evolution of a new adeno-associated virus for therapeutic outer retinal gene delivery from the vitreous. *Sci Transl Med* 5: 189ra76.
79. Kremer, H, van Wijk, E, Märker, T, Wolfrum, U and Roepman, R (2006). Usher syndrome: molecular links of pathogenesis, proteins and pathways. *Hum Mol Genet* 15 Spec No 2: R262–R270.

80. Reiners, J, van Wijk, E, Märker, T, Zimmermann, U, Jürgens, K, te Brinke, H et al. (2005). Scaffold protein harmonin (USH1C) provides molecular links between Usher syndrome type 1 and type 2. *Hum Mol Genet* 14: 3933–3943.
81. Lentz, JJ, Jodelka, FM, Hinrich, AJ, McCaffrey, KE, Farris, HE, Spalitta, MJ et al. (2013). Rescue of hearing and vestibular function by antisense oligonucleotides in a mouse model of human deafness. *Nat Med* 19: 345–350.
82. Reuter, JS and Mathews, DH (2010). RNAstructure: software for RNA secondary structure prediction and analysis. *BMC Bioinformatics* 11: 129.
83. Yariz, KO, Duman, D, Seco, CZ, Dallman, J, Huang, M, Peters, TA et al. (2012). Mutations in OTOGL, encoding the inner ear protein otogelin-like, cause moderate sensorineural hearing loss. *Am J Hum Genet* 91: 872–882.

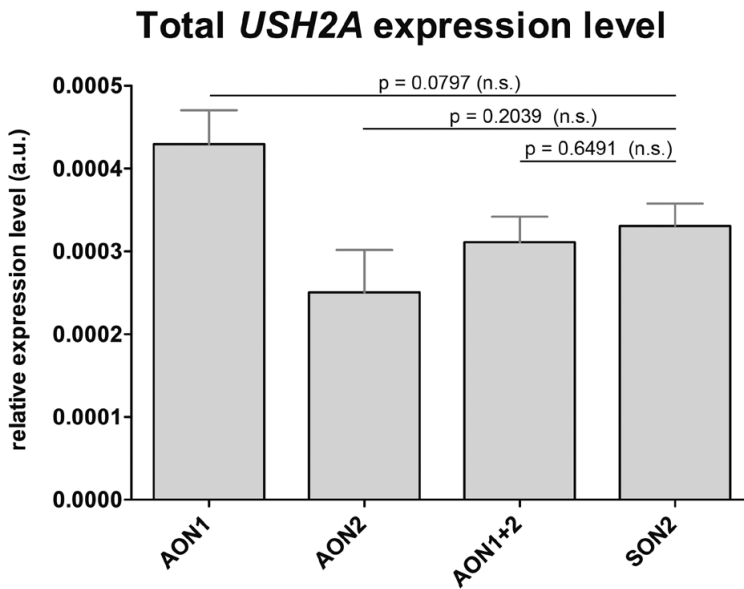
SUPPLEMENTAL FIGURES



Supplemental Figure 1. Predicted ESE sequence motifs in *USH2A* PE40.

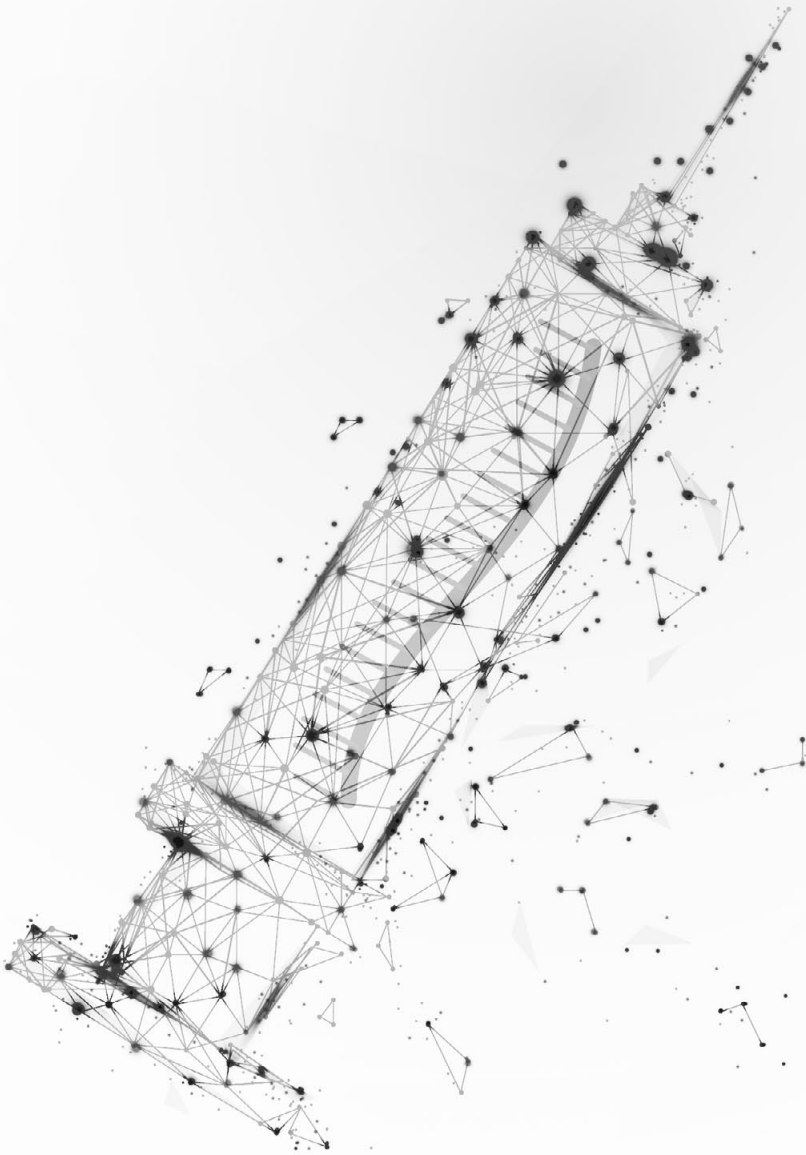


Supplemental Figure 2. Cycloheximide treatment induces stabilization of PE40 containing transcripts.



Supplemental Figure 3. Quantification of total *USH2A* transcript level after AON treatment of fibroblasts.

Chapter 3_c



Poor splice site recognition in a humanized zebrafish knock-in model for the recurrent deep-intronic c.7595-2144A>G mutation in *USH2A*

Slijkerman, R.W.N.^{1,2}, Goloborodko, A.³, Broekman, S.^{1,4}, De Vrieze, E.^{1,4}, Hetterschijt, L.^{1,4}, Peters, T.A.^{1,4}, Gerits, M.³, Kremer, H.^{1,3,4}, Van Wijk, E.^{1,4}

¹ Department of Otorhinolaryngology, Radboudumc, Nijmegen, The Netherlands

² Radboud Institute for Molecular Life Sciences, Radboudumc, Nijmegen, The Netherlands

³ Department of Human genetics, Radboudumc, Nijmegen, The Netherlands

⁴ Donders Institute for Brain, Cognition, and Behaviour, Nijmegen, The Netherlands

Published in *Zebrafish*, 2018

doi: <https://doi.org/10.1089/zeb.2018.1613>

PMID: 30281416

ABSTRACT

The frequent deep-intronic c.7595-2144A>G mutation in intron 40 of *USH2A* generates a high quality splice donor site, resulting in the incorporation of a pseudoexon (PE40) into the mature transcript that is predicted to prematurely terminate usherin translation. Aberrant *USH2A* pre-mRNA splicing could be corrected in patient-derived fibroblasts using antisense oligonucleotides. With the aim to study the effect of the c.7595-2144A>G mutation and *USH2A* splice redirection on retinal function, a humanized zebrafish knock-in model was generated in which 670 basepairs of *ush2a* intron 40 were exchanged for 557 basepairs of the corresponding human sequence using an optimized CRISPR/Cas9-based protocol. However, in the retina of adult homozygous humanized zebrafish only $7.4 \pm 3.9\%$ of *ush2a* transcripts contained the human PE40 sequence and immunohistochemical analyses revealed no differences in usherin expression and localization between the retina of humanized and wildtype zebrafish larvae. Nevertheless, we were able to partially correct aberrant *ush2a* splicing using a PE40-targeting antisense morpholino. Our results indicate a clear difference in splice site recognition by the human and zebrafish splicing machinery. Therefore we propose a protocol in which the effect of human splice-modulating mutations is studied in a zebrafish-specific cell-based splice assay prior to the generation of a humanized zebrafish knock-in model.

INTRODUCTION

Patients with Usher syndrome (USH) have congenital hearing impairment and develop a progressive loss of vision as a consequence of retinitis pigmentosa (RP). The first symptoms of RP become apparent during the second decade of life and often result in legal blindness around the age of 60 years¹. Hearing aids and cochlear implants can partly ameliorate the auditory phenotype, but for the loss of vision currently no treatment options are available². Mutations in *USH2A* are the leading cause of Usher syndrome explaining 50 to 70% of all patients worldwide³. Defects in this gene are also the most prevalent cause of non-syndromic retinitis pigmentosa (NSRP) thereby accounting for 12-25% of all cases^{3,4}. In total, over 600 different mutations have been identified in *USH2A* that are spread throughout the gene (USHbases; <http://www.lovd.nl/USH2A>)^{5,6}. Most mutations in *USH2A* are unique or are only found in a few patients. However, at least three mutations are known to be derived from a common ancestor and are therefore seen more commonly: c.2299delG (p.Glu767fs*21), c.2276G>T (p.Cys759Phe) and c.7595-2144A>G (p.Lys2532Thrfs*56)^{6,7}.

The c.7595-2144A>G mutation is the first identified deep-intronic mutation in *USH2A*, described by Vaché *et al.* in 2012⁷. This mutation represents 4% of all pathogenic *USH2A* alleles identified in a French cohort of 562 Usher syndrome patients, making c.7595-2144A>G the second most frequently found mutation in *USH2A* in France⁸. The c.7595-2144A>G mutation creates a high quality splice donor site in intron 40, leading to the incorporation of a pseudoexon (PE40) into the mature *USH2A* mRNA⁷. Translation of PE40-containing *USH2A* transcripts is predicted to result in a truncated protein (p.Lys2532Thrfs*56) due to a premature termination of translation. We have previously demonstrated that antisense oligonucleotides (AONs) targeting PE40 are able to prevent aberrant *USH2A* pre-mRNA splicing as a consequence of the c.7595-2144A>G mutation in both a minigene splice assay and patient-derived fibroblasts⁸. Splice-corrected *USH2A* transcripts are expected to result in a restored synthesis of usherin protein and as such, potentially halt the progression of visual dysfunction in patients with *USH2A*-associated RP caused by the c.7595-2144A>G mutation.

To evaluate the effect of PE40-splice correction at the level of visual function, an animal model is pivotal. A mouse model with a loss of function mutation in *Ush2a* develops mild retinal degeneration with a late age of onset⁹. In contrast, we have recently shown that retinal function is impaired in two different *ush2a* zebrafish mutants, already at five days post fertilization¹⁰. Furthermore, the similar retinal morphology and photoreceptor anatomy as compared to man^{8,11}, make zebrafish an attractive model organism to assess the effect of the *USH2A* c.7595-2144A>G mutation *in vivo* and to evaluate the effect of AON-induced PE40 splice correction at the level of visual function.

In this study, we employed CRISPR/Cas9 technology to generate a humanized zebrafish *ush2a* knock-in model that contains 557 bp of human *USH2A* intron 40, including the c.7595-2144A>G mutation. Zebrafish homozygous for the humanized PE40 allele only sporadically showed inclusion of human PE40 into the mature zebrafish *ush2a* transcript, whereas the effect of the c.7595-2144A>G mutation is fully penetrant in patient-derived fibroblasts. To aid future projects that aim to generate humanized zebrafish models with the purpose of assessing splice-modulating mutations, we have developed a zebrafish-specific minigene splice assay to evaluate splice-site recognition by the zebrafish splicing machinery.

MATERIAL AND METHODS

Zebrafish ethics, husbandry and spawning

Animal experiments were conducted in accordance with the Dutch guidelines for care and use of laboratory animals, with the approval of the Animal Experimentation Committee (Dier Experimenten Commissie [DEC]) of the Royal Netherlands Academy of Arts and Sciences (Koninklijke Nederlandse Akademie van Wetenschappen [KNAW]) (Protocol #RU-DEC 2012–301). Embryos were obtained from natural spawning zebrafish. Zebrafish were maintained and raised according standard methods ¹².

CRISPR/Cas9 design

In order to identify the PE40-homologous region in zebrafish, we aligned the human *USH2A* PE40 sequence with the zebrafish *ush2a* sequence using Align X software (Vector NTI Advance 11.0) with a *Gap opening penalty* of 15 and a *Gap extension penalty* of 6.66. A gRNA targeting the human *USH2A* PE40 homologous region in zebrafish *ush2a* intron 40 was designed using the online ZiFiT-Targeter (<http://zifit.partners.org/>) ¹³. Subsequently, oligonucleotides (5'-TAGGGGGAAACGGGGAACGTGA-3' and 5'-AAACTCACGTTCCCGTTTCCC-3') were ordered from Integrated DNA Technologies. The oligonucleotides were cloned into a pDR274 vector and subsequently used as a template in an *in vitro* transcription reaction as previously described ¹⁰. To assess the efficiency of the designed gRNA, wildtype Tüpfel Longfin (TL) zebrafish embryos at a one-cell stage were injected with 1 nl of a mixture containing gRNA (180 ng/μl), Cas9 protein (250 ng/μl; PNA Bio, CP-01), KCl (0.2 M) and phenol red (0.05%; Sigma, P0290) as described below. At 2.5 days post fertilization, individual embryos were analyzed for the presence of desired mutational events by heteroduplex analysis, using the 5'-CACAAGGACCTCTGCAATGC-3' (forward) and 5'-GCAGAAGGGAAAACAAGAGC -3' (reverse) primers. For the generation of humanized *ush2a* alleles, we co-injected the gRNA with Cas9 mRNA that was synthesized from a zebrafish codon-optimized Cas9-

containing vector (pT3TS-nCas9n; Addgene plasmid 46757). This vector was linearized by XbaI (New England Biolabs, #R0145S) and the Cas9-encoding fragment was *in vitro* transcribed using the mMESSAGE mMACHINE® T3 Transcription kit (Ambion life technologies, #AM1348) according to manufacturer's protocol. Obtained transcripts were purified using the MEGAclean™ Transcription Clean-Up Kit (Ambion life technologies, #AM1908).

Donor template vector design and cloning

Two donor template vectors were cloned containing either the human wildtype or mutant PE40 *USH2A* sequence, in order to respectively generate the humanized *ush2a^{hum/hum}* and *ush2a^{PE40/PE40}* zebrafish lines. Each donor template contains 557 bp of human *USH2A* intron 40 sequence (with or without the c.7595-2144A>G mutation) and two homology arms. The entire template for homology directed repair was flanked by the CRISPR target sites. The left homology arm (forward: 5'-TCACGTTCCCCGTTTCCCCCAGGCAATACGACAGGGTTATACCG-3' and reverse: 5'- AATACAATGAAAAGCATTTAAGTTGCCATCTA-3') and the right homology arm (forward: 5'- TAGTTCACGTGATTTAAGGCTTGGCGGCCCGC-3' and reverse: 5'- TCACGTTCCCCGTTTCCCCCGGGAGAAGGCAATTATTACAACTG-3') including the gRNA target sequence (underlined) were amplified in a standard PCR reaction using Q5 DNA polymerase (BioKé, #M0491L, Leiden - The Netherlands) with zebrafish genomic DNA as a template. The 557 bp of human *USH2A* intron 40 including PE40 was amplified from patient-derived genomic DNA isolated from fibroblasts, using forward primer 5'-TGCTTTTCATTGTATTAGCAAACCTACCCAAT-3' and reverse primer 5'-TAAATCACGTGAACCTATCAAACCTGTGAGCATC-3'). Subsequently, the PCR products were combined by fusion PCR, cloned into a pCR4-TOPO-vector using the TOPO® TA Cloning® Kit (Thermo Fisher Scientific, 450030, Waltham, MA, USA) and phenol:chloroform extracted prior to microinjection.

Microinjections

Injection needles (World Precision Instruments, TW120F-3) were prepared using a micropipette puller (Sutter Instrument Company, Model P-97). In order to generate the humanized alleles, we injected each zebrafish embryo with *Cas9* mRNA (250 pg), gRNA (180 pg), KCl (0.2 M), phenol red (0.05%), a *ku70* targeting morpholino (1.5 ng) and a template vector (25 pg). Injections were performed using a Pneumatic Picopump pv280 (World Precision Instruments) injector. After injection, embryos were kept at 28°C in E3 embryo medium (5 mM NaCl, 0.17 mM KCl, 0.33 mM CaCl₂, 0.33 mM MgSO₄, supplemented with 0.1% methylene blue).

Morpholinos

An *upf1* splice-blocking morpholino (5'-ttttgggagtttatactggtgtgc-3'), a human *USH2A* PE40 targeting morpholino (5'-ggtccttaactgtgtgattctgg-3'), a *ku70* splice-blocking morpholino (5'-AACTTTTTAGGCTCACCTGCATAGT-3') and a standard control morpholino (5'-CCTTTACCTCAGTTACAATTTATAC-3') (Gene Tools Inc., USA) were used in this study. Morpholinos were diluted to 50 ng/nl stock-solutions in MilliQ water.

Genotyping zebrafish

Genomic DNA was isolated from finclips of adult zebrafish by incubation in 75 µl lysis buffer (40 mM NaOH and 0.2 mM EDTA (Invitrogen, #15575-038)) at 95 °C for 20 minutes. The isolated genomic DNA was ten times diluted and used as a template in two PCR reactions with standard conditions. Primers used for amplification of the wildtype zebrafish *ush2a* allele are 5'-CACAAAGGACCTCTGCAATGC-3' and 5'-GCTTGAATGAATTGCACTGCT-3'. Primers used for the amplification of the introduced wildtype and PE40 human sequence are 5'-CTGGCTTTAAGGGGAAAC-3' and 5'-GCTTGAATGAATGCACTGCT-3'. The presence or absence of the PE40-inducing c.7595-2144A>G mutation was confirmed by sanger sequencing.

Transcript analysis

Pools of 15 *ush2a*^{PE40/PE40}, *ush2a*^{hum/hum} or wildtype larvae, or single adult zebrafish eyes were used to isolate total RNA. Samples were snap frozen in liquid nitrogen and subsequently homogenized in Qiazol (Qiagen, 79306) using a 25-gauge 16 mm needle. Total RNA was isolated using Qiazol extraction followed by isopropanol precipitation. Extracted total RNA was further purified and DNase treated using a NucleoSpin® RNA II Isolation kit (Macherey-Nagel, 740955) according to manufacturer's protocol. Subsequently, 0.3-1.0 µg of total RNA was used for cDNA synthesis using SuperScript VILO mastermix reverse transcriptase (Life Technologies, 11755050). PE40 incorporation in zebrafish *ush2a* transcripts was assessed in a PCR analysis using a forward primer in *ush2a* exon 39 (5'-ACGATGAGACGACCACCTTC-3') and a reverse primer in *ush2a* exon 41 (5'-CGCTGGAGGGTGTATTATAG-3'). Similarly, *upf1* splicing was assessed using a forward primer in *upf1* exon 1 (5'-GCGTCCAGTGGAGAAGAGAG-3') and a reverse primer in *upf1* exon 3 (5'-TGCAAAACCACTTCTTGCTG-3'). To visualize PE40 incorporation in patient-derived fibroblasts, a forward primer in *USH2A* exon 39 (5'-GCTCTCCCAGATACCAACTCC-3') and a reverse primers in *USH2A* exon 42 (5'-GAGGGTCAGGCATGTGAATC-3') were used.

Quantitative analysis of *ush2a* transcripts

Quantitative RT-PCR (RT-qPCR) was used to measure expression levels of *ush2a* transcripts. To determine levels of wildtype *ush2a* transcripts (*ush2a_wildtype*), a forward primer spanning the boundary of *ush2a* exons 40 and 41 (5'-TGTTTACTGCACAAGA-

CAGG-3') and reverse primer in *ush2a* exon 41 (5'-GGGCTGAGATGGAGGAGAC-3') were used. The levels of PE40-containing *ush2a* transcripts (*ush2a*_PE40) were determined using the PE40-specific forward primer 5'-CTACTCAGCCAGAGCAGGAAG-3' and reverse primer 5'-GAGAGGACTGGTGGTCAAC-3' in *ush2a* exon 41. The housekeeping gene *rpl13a* was used as a reference using the forward primer 5'-TCTGGAGGACTGTAAGAGGTATGC-3' and reverse primer 5'-AGACGCACAATCTTGAGAGCAG-3'. *ush2a* and *rpl13a* amplicons were amplified in triplicate using GoTaq DNA polymerase (Promega, #A6001) on a 7900 HT qPCR machine. Analysis of the qPCR data was performed with 7900 software (version 2.4), using the same threshold for all target genes. Expression of *ush2a*_wildtype and *ush2a*_PE40 was calculated relative to *rpl13a* expression using the $2^{-\Delta\text{dCT}}$ method. Next, the amount of PE40-containing *ush2a* transcripts was calculated as the percentage of total *ush2a* transcripts. The latter was calculated as the sum of *ush2a*_wildtype and *ush2a*_PE40 transcripts.

Immunofluorescence

Unfixed living zebrafish larvae (5 dpf) were cryoprotected with 10% sucrose in cold PBS for 20 minutes, prior to embedding in TissueTek (Sakura) and hereafter slowly frozen down using melting isopentane. After that, cryosections were made at a thickness of 7 μm , dried for at least two hours and subsequently permeabilized for 20 minutes with 0.01% Tween20 in PBS, followed by a 1 hour blocking step with blocking solution (10% normal goat serum and 2% bovine serum albumin in PBS). Antibodies diluted in blocking buffer were incubated overnight at 4 °C. Secondary antibodies were also diluted in blocking buffer and incubated together with DAPI (1:8000; D1306; Molecular Probes) for 1 hour. The following primary antibodies and dilutions were used: rabbit anti-usherin-C (1:500; #27640002; Novus Biological) and mouse anti-centrin (1:500; #04-1624; Millipore). Secondary antibodies (Alexa Fluor 488 goat anti-mouse (A11029) and Alexa Fluor 568 goat anti-rabbit (A11011)) derived from Molecular Probes, were used in a 1:800 dilution. Sections were post-fixed with 4% PFA for 10 minutes and mounted with Prolong Gold Anti-fade (Molecular Probes) and analyzed using an Axioskop2 Mot plus fluorescence microscope (Zeiss) equipped with an AxioCam MRC5 camera (Zeiss). Images were processed using Axiovision 4.3 (Zeiss) and Adobe Photoshop (Adobe Systems).

Generation of zebrafish minigene splice vector

A plasmid containing the genomic region encompassing exons 3 through 5 of zebrafish *opn1ws2*, inserted at the EcoRI/Sall sites in the pCI-NEO vector, was adapted to the Gateway cloning system and used for in vivo splicing assays. The plasmid was digested with HpaI (cat no. R0105S, New England Biolabs, Ipswich, MA), resulting in the opening of the vector between exons 3 and 4. Subsequently, a blunt-end Gateway cloning cas-

sette containing attR1 and attR2 sites was cloned in the linearized pCI-neo vector using the Rapid DNA Ligation Kit (catalog no., 11635379001; Roche) to generate pCI-NEO-*opn1sw2* exon3-5/DEST. Using Gateway cloning technology (Thermo Fisher Scientific), 557 bp of human *USH2A* intron 40 sequence (with or without the c.7595-2144A>G mutation) was cloned into the pDONR201, resulting in an pENTR vector. Mutagenesis PCR was performed to introduce the different mutations in the splice-acceptor site. The different pENTR vectors were validated by Sanger sequencing, and 150 ng of each were cloned into the destination vector pCI-NEO-*opn1sw2* exon3-5/DEST by using the Gateway LR Clonase enzyme mix (Thermo Fisher Scientific).

Culturing and transfection of zebrafish cells

Zendo-1 cells were kindly provided by Dr. Jeroen den Hertog and cultured in L15 medium (Sigma Aldrich, L1518) supplemented with 15% v/v FCS (Sigma F7524), 1% v/v penicillin/streptomycin (Sigma Aldrich P4333), 0.5% v/v isoleucine and 1% v/v alanyl-guanyl (Sigma Aldrich, G8541) at 28°C. Cells were passaged twice per week using a standard trypsin (Thermo Fisher Scientific, DF0152-15-9, Carlsbad (CA), USA) protocol. One day before transfection, cells were seeded in a six wells plate. Transfection of 1 µg plasmid was performed using Lipofectamine® 2000 (Life Technologies, 11668019) in Opti-MEM (Life Technologies, 31985047) medium according manufacturer's protocol. Two days after transfection, the cells were collected using a cell scraper and washed with 1x PBS prior to RNA isolation using the Nucleospin RNA II isolation kit (MACH-EREY-NAGEL #740955.50, Düren, Germany), according to manufacturer's protocol. 1.0 µg of total RNA was used for cDNA synthesis using SuperScript VILO mastermix reverse transcriptase (Life Technologies, #11755050). PE40 incorporation was subsequently analyzed in a standard PCR using Q5 DNA polymerase (BioKé, #M0491L, Leiden - The Netherlands) with forward primer 5'-TGAATCCTACGTCATGTTCC-3' and reverse primer 5'-CCTGAGATGAAGAAGAAGCC-3'.

RESULTS

Generation of a humanized *ush2a* knock-in zebrafish model

To determine the preferred zebrafish genomic site for incorporation of human *USH2A* PE40, we searched for the PE40 homologous sequence in zebrafish *ush2a* intron 40. After sequence alignment, a region with 48.7% sequence similarity to the human *USH2A* PE40 sequence was identified (**Fig. 1a**). Next, the CRISPR/Cas9 system was exploited to exchange this sequence for the human *USH2A* PE40 sequence. A guide RNA that was predicted to specifically target the *USH2A* PE40-homologous region in the zebrafish genome was designed for which the efficiency in generating double strand

breaks (DSBs) was determined. Small insertions and deletions were found in 13 out of 16 (81%) screened larvae (2 dpf) that were injected with a cocktail of gRNA and *Cas9* protein. Subsequently, we generated a donor template vector to be used by the homology-directed repair (HDR) branch of the DNA repair pathway. The donor template vector contained 557 bp of human sequence, consisting of PE40 and 208 bp upstream and 197 bp downstream flanking sequence. The human sequence was flanked by a left (890 bp) and right (1026 bp) homology arm (**Fig. 1b**). Since injection of a cocktail of gRNA, *Cas9* mRNA and donor template vector did not result in the integration of a detectable amount of human PE40 into the zebrafish genome two days after injection ($n=24$, four pools of eight larvae each), we tried to improve the observed knock-in efficiency by introducing two adjustments to the CRISPR/*Cas9* protocol (**Fig. 1c**). First, the gRNA target sequence flanked by a non-canonical PAM site ('NAG') was added to the donor template vector both upstream of the left and downstream of the right homology arm (**Fig. 1b**, indicated by black triangles). It was previously demonstrated by Irion and colleagues that adding these gRNA target sites resulted in a 20-fold increase of the favored knock-in event as compared to using a donor template vector without those sites¹⁴. Furthermore, we improved the efficiency of homology-directed DNA repair (HDR) by inhibition of the non-homologous end joining (NHEJ) DNA repair pathway. The latter was achieved by morpholino-induced suppression of *Ku70* expression, which is a key component of NHEJ-mediated DNA repair¹⁵. Previous research determined that injecting 5.0 ng *ku70*-targeting morpholino into the yolk of zebrafish embryos resulted in optimal NHEJ-inhibition. We injected different amounts of this morpholino (0.1, 0.5 and 1.0 ng) into one-cell staged embryos to determine the effect on *ku70* pre-mRNA splicing (**Supplemental Fig. 1**). We estimated that the volume of the embryonic cells in the cleavage phase comprises approximately 30% of the volume of the complete embryo, and therefore decided to further increase the dose of *ku70*-targeting morpholino to roughly match the concentration that results from injecting 5.0 ng morpholino in the yolk. To generate knock-in zebrafish, we therefore injected a cocktail of 1.5 ng of *ku70*-targeting morpholino, 180 pg of gRNA, 250 pg of *Cas9* mRNA, and 25 pg of the donor vector containing gRNA target sites into zebrafish embryos at a one-cell stage stage (**Fig. 1c**). Two days after injection, twenty individual larvae were screened for the genomic incorporation of the human wildtype or PE40-mutant *USH2A* donor sequence. We confirmed that 3 out of 20 (15%) injected larvae were positive for the mutant PE40 *USH2A* donor sequence. The remainder of the batch of injected zebrafish was raised and outcrossed with strain-matched wildtype zebrafish. The offspring was analyzed for the presence of the human *USH2A* PE40 sequence using a genomic PCR-based assay with a forward primer in the human PE40 sequence and a reverse primer downstream of the right homology arm. Hereby, we found that four out of 19 (21%) adult zebrafish showed germline transmission of the humanized *ush2a* allele. Subsequently, the four germline

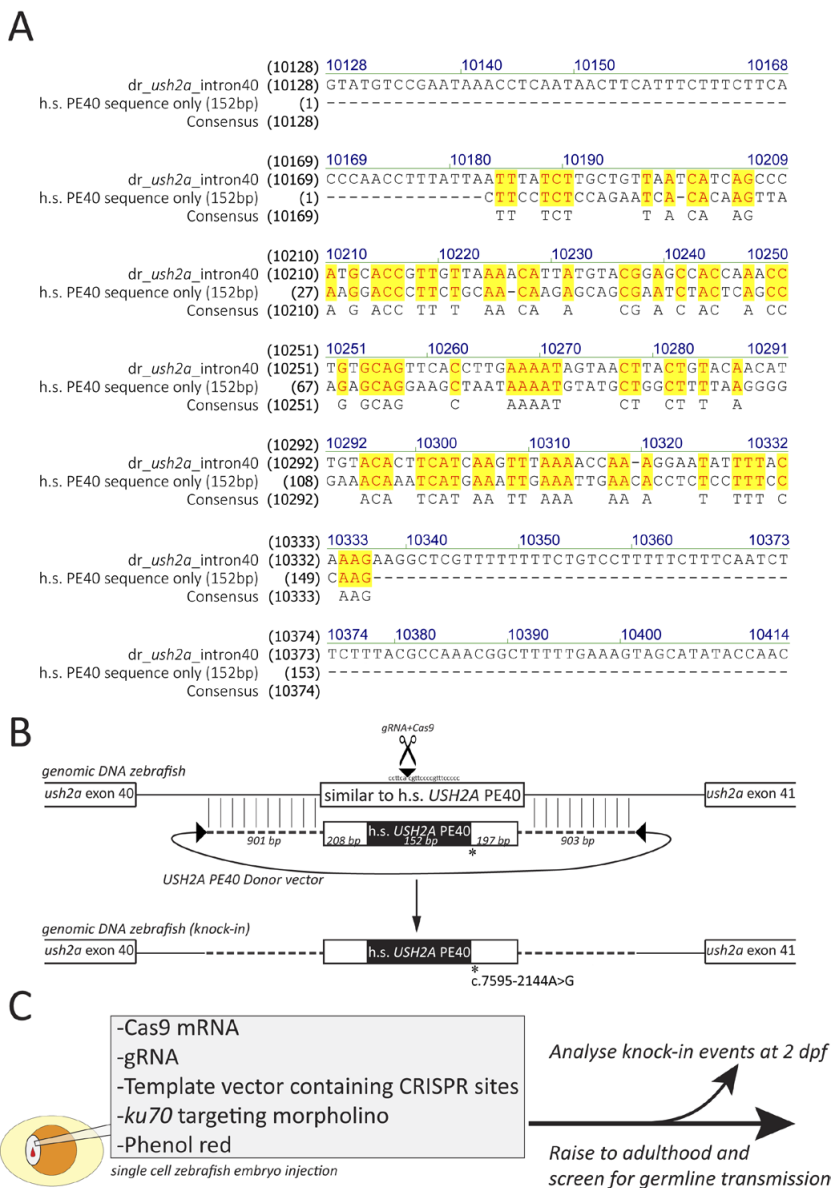


Figure 1. Strategy for the generation of a humanized *ush2a*^{PE40/PE40} transgenic zebrafish model. (A) Sequence alignment using the human *USH2A* PE40 sequence identified a region with 48.7% sequence similarity in zebrafish *ush2a* intron 40. (B) Schematic overview of the designed template vector that was used to exchange the zebrafish *ush2a* PE40-corresponding region for the human *USH2A* PE40 sequence. Black triangles indicate gRNA target sites, which are added next to a non-canonical PAM ('NAG') site in the vector backbone. Homology arms both up- and downstream are indicated by a dashed line and the human derived sequence is boxed with PE40 in black. The resulting knock-in genotype is schematically presented below the template vector. (C) Composition of the injection mixture that was injected into one-cell-stage TL embryos.

positive zebrafish (two females and two males) were crossed and their progeny (F1) was genotyped by PCR analyses (**Fig. 2a**) followed by Sanger sequencing (**Fig. 2b-e**). The F1 zebrafish that were heterozygous for the knock-in allele were used to generate homozygous (F2) knock-in fish that contained 557 bp of the human *USH2A* sequence with the deep-intronic c.7595-2144A>G mutation (*ush2a*^{PE40/PE40}). The humanized zebrafish with the wildtype *USH2A* intron 40 sequence (*ush2a*^{hum/hum}) was generated using the same strategy. The *ush2a*^{PE40/PE40} and *ush2a*^{hum/hum} lines were distinguished from each other by Sanger sequencing. Homozygous knock-in fish were viable, fertile and displayed no behavioral or morphological abnormalities.

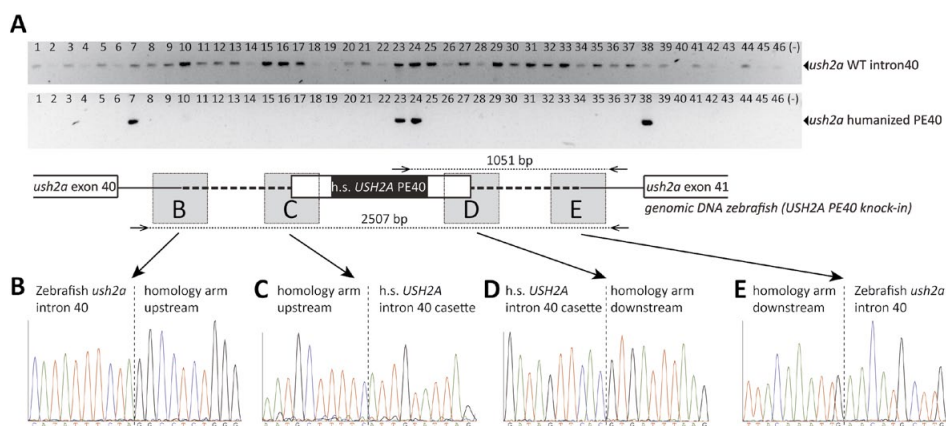


Figure 2. Validation of the integration of human *USH2A* PE40 in zebrafish *ush2a* intron 40. (A) Integration of human PE40 was assessed by genomic PCR analysis. Four adult humanized zebrafish (F1) were identified that were heterozygous for the presence of the humanized PE40 allele (lanes 7, 23, 24, and 38). (B-E) Chromatograms derived from an amplicon spanning the complete PE40 cassette including up- and downstream homology arms. The sequence junction between zebrafish *ush2a* intron 40 and the upstream homology arm (B), the upstream homology arm and the human *USH2A* sequence (C), the human *USH2A* sequence and the downstream homology arm (D) and the downstream homology arm and zebrafish *ush2a* intron 40 (E) are indicated by a grey box. Chromatograms corresponding to the sequence junctions are shown. The vertical dashed lines indicate the sequence junction.

Transcriptional analysis of *ush2a* in the humanized zebrafish model

The effect of the human c.7595-2144A>G mutation on zebrafish *ush2a* pre-mRNA splicing was analyzed in larvae and adult eyes derived from *ush2a*^{PE40/PE40} transgenic fish. An RT-PCR analysis using primers in *ush2a* exon 39 (forward) and exon 41 (reverse) demonstrated that the majority of transcripts did not contain human *USH2A* PE40 (**Fig. 3a**). *ush2a* transcripts of the *ush2a*^{hum/hum} zebrafish larvae did not contain any human *USH2A* sequences, indicating that the incorporation of human *USH2A* PE40 sequence in the *ush2a* transcript is the result of the c.7595-2144A>G mutation. Sequence analyses

of the larger PCR products revealed the incorporation of human PE40 between zebrafish *ush2a* exons 40 and 41. In some transcripts also an alternative splice acceptor site was used, 12 nucleotides downstream of the original PE40 splice acceptor site (**Fig. 3b**, grey box). Quantitative RT-PCR analyses were performed to determine the ratio between PE40-containing transcripts and transcripts that lack PE40. In *ush2a*^{PE40/PE40} larvae, 4.4%

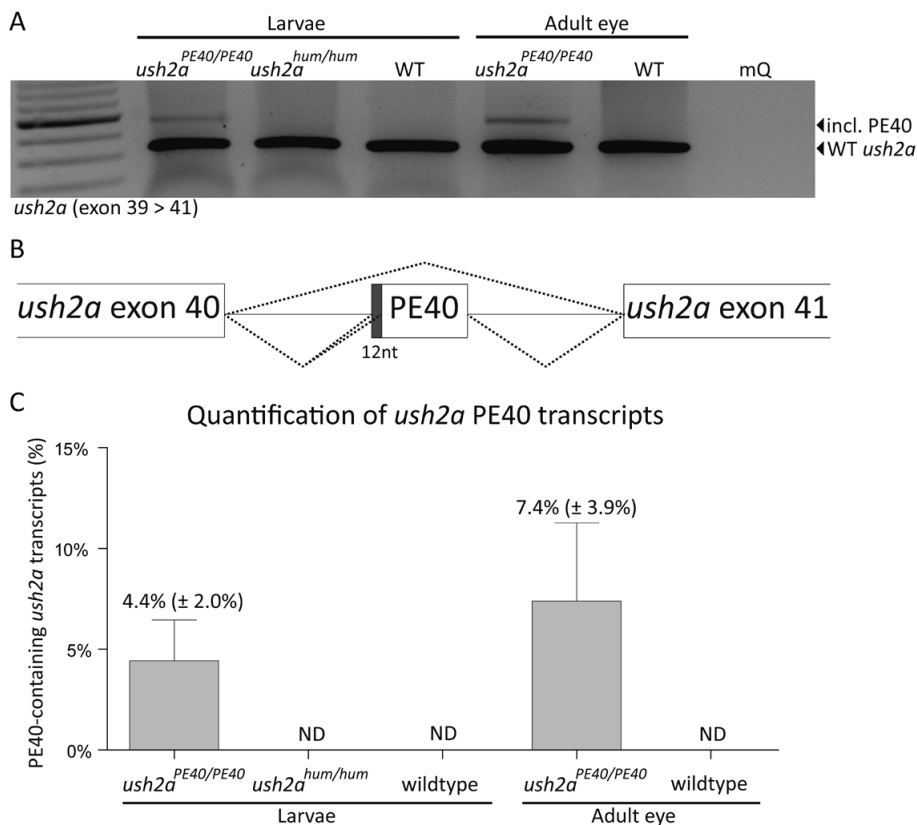


Figure 3. Human *USH2A* PE40 incorporation in zebrafish *ush2a* transcripts. (A) The level of human *USH2A* PE40 incorporation into the zebrafish *ush2a* transcript is analyzed by RT-PCR using cDNA derived from *ush2a*^{PE40/PE40}, *ush2a*^{hum/hum} and wildtype larvae, and *ush2a*^{PE40/PE40} and wildtype adult eyes. The upper band represents *ush2a* transcripts containing PE40, whereas the lower band represents wild-type zebrafish *ush2a* transcripts. **(B)** *ush2a* splicing in *ush2a*^{PE40/PE40} transgenic zebrafish resulted in a combination of wild-type *ush2a* transcripts (upper dashed lines) and *ush2a* transcripts that contain PE40 (lower dashed line). Sporadically, also an alternative splice acceptor site is used in human *USH2A* PE40, leading to a transcript that lacks the initial 12 nucleotides of PE40 (indicated in grey) **(C)** Quantitative RT-PCR analyses to determine the relative amount of PE40-containing *ush2a* transcripts in *ush2a*^{PE40/PE40}, *ush2a*^{hum/hum} and wildtype larvae, and *ush2a*^{PE40/PE40} and wildtype adult eyes. Data are expressed as mean ± SD. For transcript analysis, RNA from 2 pools of 15 larvae were used, and RNA from 6 individual adult eyes was used per genotype. One-way ANOVA followed by Holm-Sidak's multiple comparisons test revealed no significant differences between groups. ND = not detectable.

($\pm 2.0\%$) of *ush2a* transcripts were aberrantly spliced as a consequence of the introduced human *USH2A* c.7595-2144A>G mutation and contain either the complete PE40 sequence or PE40 lacking the first 12 nucleotides. Approximately 7.4% ($\pm 3.9\%$) of *ush2a* transcripts derived from *ush2a*^{PE40/PE40} adult eyes contained human *USH2A* PE40 (**Fig. 3c**). Previous experiments using a *RHO*-based minigene splice assay in human embryonic kidney (HEK293T) cells showed that the effect of the c.7595-2144A>G mutation on pre-mRNA splicing is fully penetrant, since c.7595-2144A>G results in incorporation of PE40 in all observed minigene-derived transcripts⁸. This result was confirmed in fibroblasts derived from a patient with a homozygous *USH2A* c.7595-2144A>G mutation (**Supplemental Fig. 2**). For this reason, we hypothesized that PE40-containing *ush2a* transcripts are either rapidly degraded via nonsense-mediated decay (NMD) or that human *USH2A* PE40 is poorly recognized by the zebrafish splicing machinery. However, quantification of *ush2a* transcripts in larvae from previously generated *ush2a* mutant zebrafish (*ush2a*^{rmc1/rmc1} and *ush2a*^{b1245/b1245})¹⁰, as well as the *ush2a*^{PE40/PE40} zebrafish, showed no reduction in total amount of *ush2a* transcripts compared to age and strain matched wildtypes (**Supplemental Fig. 3**). To rule out any potential contribution of NMD-pathway to the degradation of PE40-containing *ush2a* transcripts, we used a previously published splice-blocking morpholino targeting *upf1* that was shown to inactivate the NMD pathway¹⁶. *upf1* pre-mRNA splicing was indeed significantly altered in the *ush2a*^{PE40/PE40} larvae after morpholino injection (**Fig. 4a**). After Sanger sequencing we

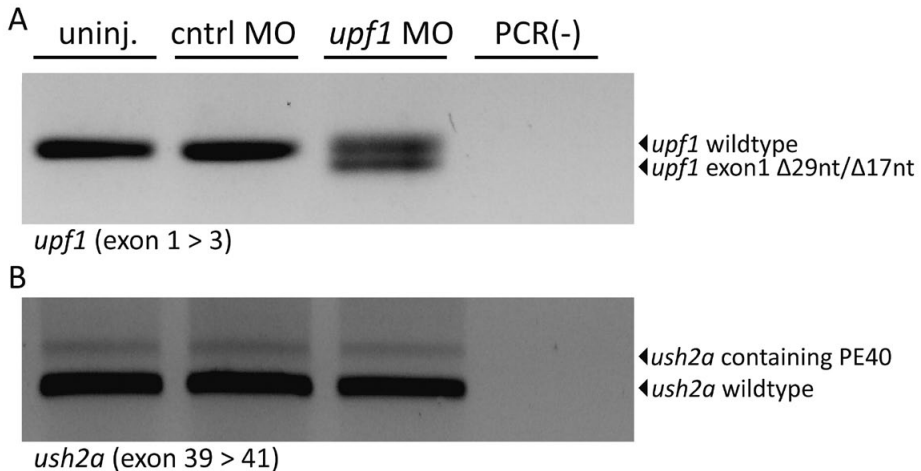


Figure 4. *Ush2a*^{PE40/PE40} transcript analysis after NMD inhibition by *upf1* knock-down. (A) Characterization of the effect of the *upf1* ex1 spMO at 2 dpf by RT-PCR analysis. Injection of 3 ng *upf1* splice-blocking morpholino resulted in the partial skipping of 17 or 29 nt at the 3' end of *upf1* exon 1, leading to premature termination of Upf1 translation. **(B)** Characterization of the effect of NMD inhibition on stabilization of PE40-containing *ush2a* transcripts by RT-PCR analysis (2 dpf). PCR (-): MQ water PCR control; cntrl MO: control morpholino.

identified that the upper *upf1* fragment corresponds to the wildtype transcript, whereas the lower fragment contains a mixture of transcripts lacking the 3' 29 or 17 nucleotides of *upf1* exon 1. At 1 dpf, no correctly spliced *upf1* could be detected (**Supplemental Fig. 4**), although *ush2a* transcripts could not be detected yet at this developmental stage. At 2.5 dpf, the amount of correctly splice *upf1* mRNA was still strongly reduced. While similar levels of alternative *upf1* splicing were previously shown to inhibit NMD¹⁶, we did not observe an increase or stabilization of PE40-containing *ush2a* transcripts (**Fig. 4b**). We therefore conclude that PE40-containing *ush2a* transcripts are not amenable to NMD in zebrafish and that human *USH2A* PE40 is poorly recognized by the zebrafish splicing machinery.

Morpholino-based splice redirection in *ush2a*^{PE40/PE40} zebrafish

Although with low efficiency, human *USH2A* PE40 was incorporated in part of the zebrafish *ush2a* transcripts. This provided us the opportunity to use a PE40-targeting antisense morpholino in order to redirect aberrant splicing *in vivo*. We previously designed antisense oligonucleotides capable of correcting aberrant splicing of *USH2A* pre-mRNA as a consequence of the c.7595-2144A>G mutation⁸. A PE40-targeting morpholino (PE40_MO) was designed with a sequence that was highly similar to our previously used AON1. RT-PCR analysis using cDNA derived from MO-injected *ush2a*^{PE40/PE40} larvae showed that injection of 1 ng of PE40_MO already induced splice correction (**Fig. 5a**). The ratio between PE40-containing *ush2a* transcripts and transcripts lacking PE40 was determined by quantitative RT-PCR analyses after injection of 3 ng PE40_MO. Although not statistically significant, morpholino (3 ng) treatment decreased the amount of PE40-containing *ush2a* transcripts from 4.4% (\pm 2.0%) in untreated *ush2a*^{PE40/PE40} larvae to 1.3% (\pm 0.03%) (**Fig. 5b**), while the total amount of *ush2a* transcripts was not altered after treatment (**Fig 5c**).

Immunohistochemical analyses of zebrafish retinas

Inclusion of PE40 in the *ush2a* transcript is predicted to result in a frameshift and premature termination of usherin translation. In order to study the effect on usherin expression and localization, retinal cryosections from wildtype (WT), knock-out (*ush2a*^{rmc1/rmc1}), *ush2a*^{PE40/PE40} and *ush2a*^{PE40/PE40} larvae treated with PE40-targeting morpholinos (*ush2a*^{PE40/PE40} + MO) were analyzed at 5 dpf by immunohistochemistry. The overall morphology and retinal lamination was similar in all analyzed retinas. Usherin was absent from the retina of homozygous *ush2a*^{rmc1/rmc1} larvae, confirming the specificity of the used anti-usherin antibody (**Fig. 6b**). No differences in usherin localization or expression were observed between wildtype and *ush2a*^{PE40/PE40} larvae (**Fig. 6a, c**). *Ush2a* splice correction after PE40_MO injection also had no detectable effect on the level of usherin expression (**Fig. 6d**). These results illustrate that the low abundance of aber-

rantly spliced *ush2a* transcripts does not affect the level of usherin protein expression and usherin localization in the retina.

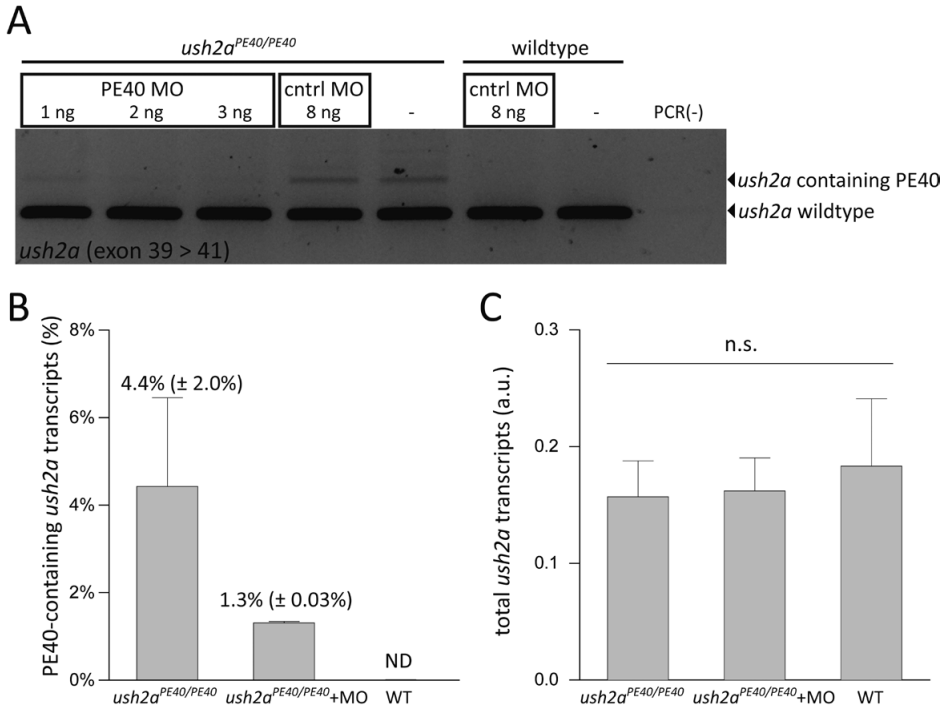


Figure 5. *Ush2a* splice correction in *ush2a*^{PE40/PE40} using a PE40-targeting morpholino. (A) *ush2a* transcripts containing PE40 (upper bands) or transcripts lacking PE40 (lower bands) were amplified by RT-PCR and visualized on an agarose gel. *Actb* amplification is shown as a loading control. PCR(-) is a negative template control. **(B)** Quantitative RT-PCR analysis of transcripts derived from either wild-type larvae (WT), untreated *ush2a*^{PE40/PE40} larvae (*ush2a*^{PE40/PE40}) or *ush2a*^{PE40/PE40} larvae injected with 3 ng of PE40 targeting morpholino (*ush2a*^{PE40/PE40} + MO). Per condition, the amount of PE40 inclusion in the *ush2a* transcript is presented as the percentage of total *ush2a* transcripts. Data are expressed as mean ± SD of 2 pools of 15 larvae per condition. **(C)** The total amount of *ush2a* transcripts (sum of PE40-containing transcripts and transcripts lacking PE40) is plotted as a bar graph. All values are normalized to *rpl13a* expression. Data are expressed as mean ± SD of 2 pools of 15 larvae per condition. One-way ANOVA followed by Holm-Sidak's multiple comparisons test revealed no significant differences between groups. ND = not detectable.

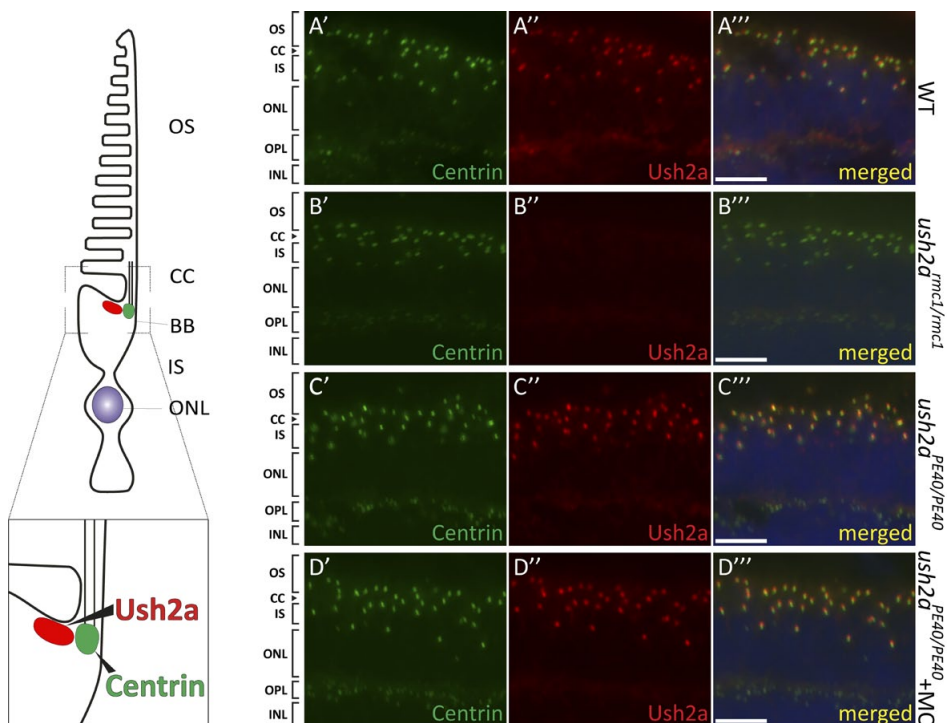


Figure 6. Immunohistochemical analyses using anti-usherin in zebrafish larval retinas (5 dpf). Retinal cryosections of wild-type (WT) (A), *ush2a^{mcl/mcl}* knock-out (B), *ush2a^{PE40/PE40}* (C) and morpholino-injected *ush2a^{PE40/PE40}* (D) larvae were analyzed for usherin expression and localization (red signal). Anti-centrin antibodies (green) were used to mark the connecting cilium. Nuclei were stained with DAPI (blue signal). BB: basal body, CC: connecting cilium, IS: inner segment, ONL: outer nuclear layer, OS: outer segment. Scale bar: 10 μ m.

Splice site optimization for the recognition of human *USH2A* PE40 by the zebrafish splicing machinery

We were intrigued by the vast difference in amount of *ush2a* transcripts that contain PE40 in *ush2a^{PE40/PE40}* larvae as compared to *USH2A* transcripts in patient-derived fibroblasts (**Supplemental fig. 1**)⁸. Since we hypothesized that PE40 might be poorly recognized by the zebrafish splicing machinery, we used a splice site prediction tool ("Berkeley Drosophila Genome Project" http://www.fruitfly.org/seq_tools/splice.html) to analyze the strength of the PE40 splice acceptor and splice donor sites. Scores can range from 0 (extremely weak) to 1.0 (extremely strong). The PE40 splice acceptor site scored <0.1 and the PE40 splice donor site scored 1.0. Next, we compared the human *USH2A* PE40 splice acceptor and splice donor sequences with the human and zebrafish splice site consensus sequences as presented by Abril and colleagues¹⁷ (**Fig 7a, b**). We identified three positions in the splice acceptor site of *USH2A* PE40 that were markedly different between the human and zebrafish splice acceptor consensus sequence (G at

-8, AAG at -11/-12/-13 and C at +1) (**Fig. 7b**). In order to optimize the weak PE40 splice acceptor site, 'AAG' at position -11/-12/-13 was substituted by 'TTT' (M1) and 'C' at position +1 was substituted by 'G' (M2). *In silico* splice-site prediction after the introduction of M1 showed an increase in the strength of the splice acceptor site from <0.1 to 0.96. Introduction of M2 increased the splice acceptor site score to 0.60. A combination of M1 and M2 resulted in a splice acceptor site score of 0.99 (**Fig. 7b**). In order to examine whether PE40 recognition by the zebrafish splicing machinery could be enhanced by changing these positions in the splice acceptor site, we developed a zebrafish-specific minigene splice assay. For this, a pCI-neo-based vector was generated that contained the genomic sequence of zebrafish *opn1sw2* spanning exons 3 to 5. Human PE40 flanked by 250 bp up- and downstream sequence was cloned between *opn1sw2* exons 3 and 4 (**Fig. 7c**). We next introduced M1 and M2 in the minigene splice vector (**Fig. 7c**) and analyzed the transcripts by RT-PCR after transfection in a zebrafish epithelium-derived cell line (Zendo-1) (**Fig. 7d**). The low level of human *USH2A* PE40 recognition as a consequence of the c.7595-2144A>G mutation by the zebrafish splicing machinery was mimicked in the zebrafish-specific minigene splice assay (**Fig. 7d**, lane 2). Introduction of either M1 or M1+2 in addition to the c.7595-2144A>G mutation resulted in the incorporation of PE40 in nearly all transcripts (**Fig. 7d**, lanes 4 and 8). The contribution of M2 was only minor (**Fig. 7d**, lane 2 versus 6). Furthermore, the effect of M1, M2 and M1+2 was fully dependent on the presence of the c.7595-2144A>G mutation (**Fig. 7d**, lanes 1, 3, 5 and 7).

DISCUSSION

In this study we generated a humanized zebrafish model using an optimized CRISPR/Cas9-based protocol. Our aim was to elucidate the pathogenic mechanism underlying *USH2A*-associated retinal dysfunction as a consequence of the deep-intronic c.7595-2144A>G mutation and to determine the therapeutic potential of antisense oligonucleotide-based correction of aberrant *ush2a* pre-mRNA splicing *in vivo*⁸. However, human *USH2A* pseudoexon 40 was significantly less efficiently incorporated into the zebrafish *ush2a* transcript than it was in fibroblasts of a patient homozygous for the c.7595-2144A>G mutation.

CRISPR/Cas9-based genome editing has been frequently used to generate cellular and animal models with random insertions and deletions. However, models generated by precise genome editing are only sporadically described¹⁸. Supplementing the CRISPR/Cas9 system with a template vector could theoretically result in alleles that have incorporated the provided template sequence by a homology-directed repair (HDR)-based mechanism. However, using this strategy we were unable to detect any

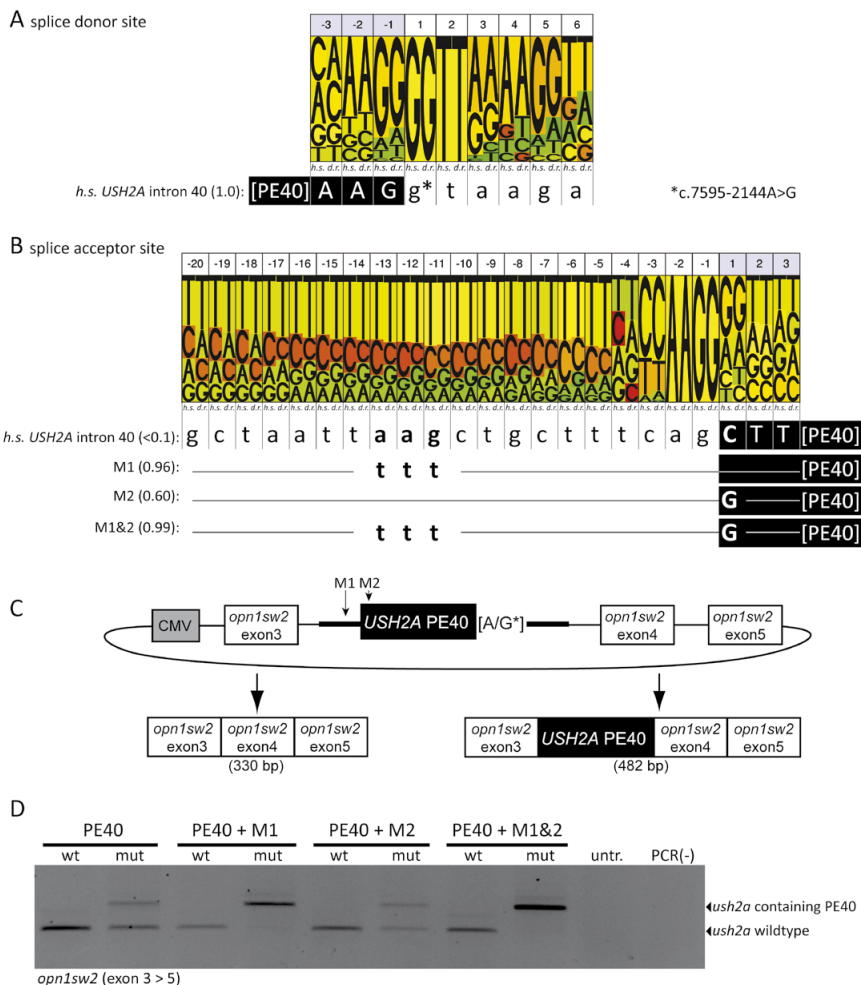


Figure 7. Optimization of human *USH2A* PE40 splice acceptor site for improved recognition by the zebrafish splicing machinery. (A) The nucleotide distribution of the splice donor site found in man (*h.s.*) and zebrafish (*d.r.*) is displayed for both species per position in one column¹⁷. The PE40 splice donor sequence is presented under the splice donor sites with the c.7595-2144A>G mutation, indicated by an asterisk, present on the +1 position relative to the last nucleotide of PE40. (B) Similar as in (A), the PE40 splice acceptor sequence is presented under the consensus splice acceptor sites as used in human (*h.s.*) and zebrafish (*d.r.*). Based on these comparisons, we choose two sites (M1 and M2) that were each predicted to result in a stronger PE40 splice acceptor site, the predicted strength of the splice acceptor site is indicated in brackets. (C) A zebrafish-specific minigene splice assay containing the human *USH2A* PE40 with flanking sequences cloned between zebrafish *opn1sw2* exon 3 and exons 4 + 5 was generated. The plasmids, either containing the c.7595-2144A>G mutation (mut) or not (wt), included M1, M2 or M1+2 (indicated by vertical arrows). (D) The effect of the introduction of M1 and/or M2 on recognition of human *USH2A* PE40 after expression in zebrafish epithelial cells (*Zendo-1*) determined by RT-PCR using primers targeting *opn1sw2* exon 3 and 5. The upper band represents transcripts that contain *USH2A* PE40 whereas the lower bands represent *opn1sw2* transcripts lacking *USH2A* PE40. untr.: untransfected cells, PCR(-): negative template PCR control.

knock-in events in zebrafish larvae. The efficiency of this method is limited by non-homologous end joining (NHEJ), an alternative DNA repair pathway that competes with homology-directed repair (HDR). Therefore, we exploited an improved HDR-mediated knock-in strategy containing two adjustments to the existing protocol. First, to promote HDR at the expense of NHEJ, we downregulated the expression of *ku70*, which is a key component of NHEJ-mediated DNA repair. The same effect can also be achieved by supplementing target cells with a small molecule inhibitor of NHEJ, such as SCR7, L755507 or resveratrol¹⁹⁻²¹. In case of zebrafish embryos, morpholino-induced inhibition of NHEJ is preferred due to the temporal effect of morpholinos. For this reason, potential morpholino-induced toxicity is diminished after a few days, which is uncertain when using SCR7, L755507 or resveratrol in zebrafish larvae. A further increase of the HDR-mediated knock-in efficiency by approximately three-fold might be achieved by overexpression of Rad52, a protein known to be involved in HDR²². Our second improvement was based on previously published experiments in HEK293T cells that demonstrated a more efficient HDR-mediated repair when using a linear DNA template as compared to using a circular template vector²³. We used the design of Irion and colleagues who showed a significant improvement of the HDR-based knock-in efficiency in zebrafish when adding gRNA target sites up- and downstream of the left and right homology arms, respectively, presumably resulting in the excision of the fragment *in vivo* while circumventing toxic effects that are often observed after injection of linear DNA¹⁴. By adding gRNA target sites in the template vector and blocking NHEJ-mediated repair, we were able to significantly increase the efficiency of HDR and introduce the human PE40 sequence into the zebrafish genome in a targeted manner.

Knock-in animal models recapitulating splice defects as observed in various inherited disorders have been generated with the purpose of studying disease pathology and evaluating potential therapeutic strategies²⁴⁻²⁹. For Usher syndrome type Ic, a humanized mouse has been generated to model the consequences of the recurrent c.216G>A mutation in *USH1C*³⁰. The c.216G>A mutation activates a cryptic splice donor site that results in the skipping of the last 35 nucleotides of exon 3 in both humans and this mouse model, although the original splice donor site is predicted to be stronger than the c.216G>A-activated cryptic splice site³⁰. Humanized zebrafish models for deep-intronic mutations resulting in pseudoexon inclusion have not been generated to our knowledge. Nevertheless, zebrafish have been used to model splice-site mutations, for instance by disrupting the splice donor site in intron 14 of *col6a1* to mimic exon 14 skipping as observed in patients with collagen I defects (known as Bethlem myopathy)³¹. However, some animal models fail to recapitulate human splice defects, which is also the case for our humanized *USH2A* zebrafish knock-in model. As our data suggests that PE40-containing *ush2a* transcripts are not subjective to NMD, we expect that the zebrafish splicing machinery does not efficiently recognize human *USH2A* PE40.

As human and zebrafish consensus splice-site sequences are highly similar¹⁷, it is difficult to predict the efficiency of human splice-site recognition by the zebrafish splicing machinery purely based on bio-informatic analyses. The consensus splice-site sequences in man and mouse are also highly comparable. Nevertheless, differences in human splice-site recognition by the murine and human splice machinery have recently been reported after modeling a deep-intronic mutation in *CEP290* (c.2991+1655A>G) and a SNP (c.315-48C) in *FECH*^{32,33}. Further assessment of the observed inter-species differential splicing revealed that only the splicing machinery of non-human primates, but not that of dog, mouse or *Drosophila*, efficiently recognizes human (pseudo)exons³⁴. Splicing depends on a combination of small nuclear ribonucleoproteins that are formed at both the splice donor site of an exon and the splice acceptor site of the following exon in combination with a branch point sequence in between the two exons. These three genomic motifs are essential, but regulation of splicing involves also many other factors such as regulatory proteins and epigenetic marks that could differ between species. Therefore, even though splice consensus sequences are highly similar between man and zebrafish, a difference in any regulatory condition could explain a species-dependent differential splicing of PE40. This once more illustrates the complexity of the splicing processes in different species, and highlights the importance to take these differences into account prior to generating humanized animal models to mimic disorders caused by splice-modulating mutations.

As human *USH2A* PE40 is poorly recognized by the zebrafish splicing machinery, we introduced an *in vitro* zebrafish-specific minigene splice assay to *a priori* verify human splice-site recognition for future modeling of human (pseudo-)exons in zebrafish. Using this assay, we noticed that modification of the splice acceptor site was sufficient for a near complete recognition of human PE40 by the zebrafish splicing machinery in cultured zebrafish epithelial Zendo-1 cells, although the translational value of this assay still needs to be proven in future *in vivo* experiments.

ACKNOWLEDGEMENTS

The authors would like to thank Dr. Jeroen den Hertog for sharing his zebrafish-derived Zendo-1 cell line. Also, the authors are grateful that Drs. Josep Abril and Roderic Guigo shared their figure on consensus splice site differences between human and zebrafish. Furthermore, the authors would like to thank Tom Spanings for excellent fish husbandry. The study was supported by the Foundation Fighting Blindness (grant PPA-0517-0717-RAD to EvW), Stichting Wetenschappelijk Onderzoek Doof-Blindheid (to EvW) and Stichting Ushersyndroom (to EvW and HK).

AUTHOR DISCLOSURE STATEMENT

No competing financial interests exist.



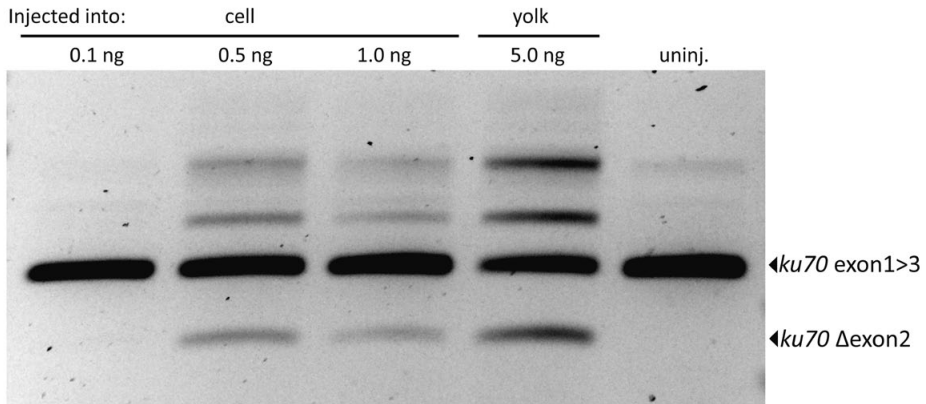
REFERENCES

1. Sandberg MA, Rosner B, Weigel-DiFranco C, McGee TL, Dryja TP, Berson EL: Disease course in patients with autosomal recessive retinitis pigmentosa due to the USH2A gene. *Investigative ophthalmology & visual science*. 2008;49:5532-9.
2. Hartel BP, van Nierop JWJ, Huinck WJ, Rotteveel LJC, Mylanus EAM, Snik AF, et al.: Cochlear Implantation in Patients With Usher Syndrome Type IIa Increases Performance and Quality of Life. *Otol Neurotol*. 2017;38:e120-e7.
3. McGee TL, Seyedahmadi BJ, Sweeney MO, Dryja TP, Berson EL: Novel mutations in the long isoform of the USH2A gene in patients with Usher syndrome type II or non-syndromic retinitis pigmentosa. *Journal of medical genetics*. 2010;47:499-506.
4. Seyedahmadi BJ, Rivolta C, Keene JA, Berson EL, Dryja TP: Comprehensive screening of the USH2A gene in Usher syndrome type II and non-syndromic recessive retinitis pigmentosa. *Experimental eye research*. 2004;79:167-73.
5. Roux AF, Faugere V, Vache C, Baux D, Besnard T, Leonard S, et al.: Four-year follow-up of diagnostic service in USH1 patients. *Investigative ophthalmology & visual science*. 2011;52:4063-71.
6. Baux D, Blanchet C, Hamel C, Meunier I, Larrieu L, Faugere V, et al.: Enrichment of LOVD-USHbases with 152 USH2A genotypes defines an extensive mutational spectrum and highlights missense hotspots. *Human mutation*. 2014;35:1179-86.
7. Vache C, Besnard T, le Berre P, Garcia-Garcia G, Baux D, Larrieu L, et al.: Usher syndrome type 2 caused by activation of an USH2A pseudoexon: implications for diagnosis and therapy. *Human mutation*. 2012;33:104-8.
8. Slijkerman RW, Vache C, Dona M, Garcia-Garcia G, Claustres M, Hetterschijt L, et al.: Anti-sense Oligonucleotide-based Splice Correction for USH2A-associated Retinal Degeneration Caused by a Frequent Deep-intronic Mutation. *Molecular therapy Nucleic acids*. 2016;5:e381.
9. Liu X, Bulgakov OV, Darrow KN, Pawlyk B, Adamian M, Liberman MC, et al.: Usherin is required for maintenance of retinal photoreceptors and normal development of cochlear hair cells. *Proceedings of the National Academy of Sciences of the United States of America*. 2007;104:4413-8.
10. Dona M, Slijkerman RWN, Lerner KM, Broekman S, Wegner J, Howat TA, et al.: Usherin defects lead to early-onset retinal dysfunction in zebrafish. *Experimental Eye Research*. 2018;173:148-159.
11. Slijkerman RW, Song F, Astuti GD, Huynen MA, van Wijk E, Stieger K, et al.: The pros and cons of vertebrate animal models for functional and therapeutic research on inherited retinal dystrophies. *Progress in retinal and eye research*. 2015;48:137-59.
12. Westerfield M: *The Zebrafish Book: A Guide for the Laboratory Use of Zebrafish Danio ("Brachydanio Rerio")*: University of Oregon; 2007.
13. Sander JD, Zaback P, Joung JK, Voytas DF, Dobbs D: Zinc Finger Targeter (ZiFiT): an engineered zinc finger/target site design tool. *Nucleic acids research*. 2007;35:W599-605.
14. Irion U, Krauss J, Nusslein-Volhard C: Precise and efficient genome editing in zebrafish using the CRISPR/Cas9 system. *Development*. 2014;141:4827-30.
15. Bladen CL, Navarre S, Dynan WS, Kozlowski DJ: Expression of the Ku70 subunit (XRCC6) and protection from low dose ionizing radiation during zebrafish embryogenesis. *Neuroscience letters*. 2007;422:97-102.

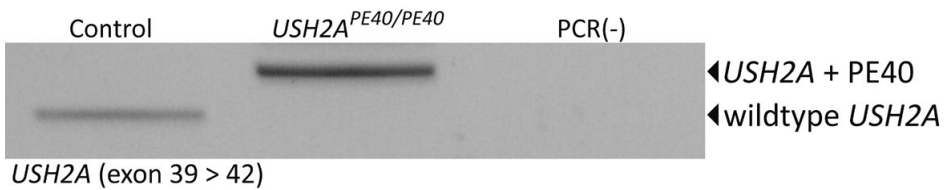
16. Witkopp N, Huntzinger E, Weiler C, Sauliere J, Schmidt S, Sonawane M, et al.: Nonsense-mediated mRNA decay effectors are essential for zebrafish embryonic development and survival. *Molecular and cellular biology*. 2009;29:3517-28.
17. Abril JF, Castelo R, Guigo R: Comparison of splice sites in mammals and chicken. *Genome research*. 2005;15:111-9.
18. Albadri S, Del Bene F, Revenu C: Genome editing using CRISPR/Cas9-based knock-in approaches in zebrafish. *Methods*. 2017;121-122:77-85.
19. Maruyama T, Dougan SK, Truttmann MC, Bilate AM, Ingram JR, Ploegh HL: Increasing the efficiency of precise genome editing with CRISPR-Cas9 by inhibition of nonhomologous end joining. *Nature biotechnology*. 2015;33:538-42.
20. Chu VT, Weber T, Wefers B, Wurst W, Sander S, Rajewsky K, et al.: Increasing the efficiency of homology-directed repair for CRISPR-Cas9-induced precise gene editing in mammalian cells. *Nature biotechnology*. 2015;33:543-8.
21. Li G, Zhang X, Zhong C, Mo J, Quan R, Yang J, et al.: Small molecules enhance CRISPR/Cas9-mediated homology-directed genome editing in primary cells. *Scientific reports*. 2017;7:8943.
22. Shao S, Ren C, Liu Z, Bai Y, Chen Z, Wei Z, et al.: Enhancing CRISPR/Cas9-mediated homology-directed repair in mammalian cells by expressing *Saccharomyces cerevisiae* Rad52. *Int J Biochem Cell Biol*. 2017;92:43-52.
23. Song F, Stieger K: Optimizing the DNA Donor Template for Homology-Directed Repair of Double-Strand Breaks. *Molecular therapy Nucleic acids*. 2017;7:53-60.
24. Gladman JT, Bebee TW, Edwards C, Wang X, Sahenk Z, Rich MM, et al.: A humanized *Smn* gene containing the *SMN2* nucleotide alteration in exon 7 mimics *SMN2* splicing and the SMA disease phenotype. *Human molecular genetics*. 2010;19:4239-52.
25. Hims MM, Shetty RS, Pickel J, Mull J, Leyne M, Liu L, et al.: A humanized *IKBKAP* transgenic mouse models a tissue-specific human splicing defect. *Genomics*. 2007;90:389-96.
26. Morini E, Dietrich P, Salani M, Downs HM, Wojtkiewicz GR, Alli S, et al.: Sensory and autonomic deficits in a new humanized mouse model of familial dysautonomia. *Human molecular genetics*. 2016;25:1116-28.
27. Vadolas J, Nefedov M, Wardan H, Mansooriderakshan S, Voullaire L, Jamsai D, et al.: Humanized beta-thalassemia mouse model containing the common IVSI-110 splicing mutation. *The Journal of biological chemistry*. 2006;281:7399-405.
28. Yang Y, Swaminathan S, Martin BK, Sharan SK: Aberrant splicing induced by missense mutations in *BRCA1*: clues from a humanized mouse model. *Human molecular genetics*. 2003;12:2121-31.
29. Lewis J, Yang B, Kim R, Sierakowska H, Kole R, Smithies O, et al.: A common human beta globin splicing mutation modeled in mice. *Blood*. 1998;91:2152-6.
30. Lentz J, Pan F, Ng SS, Deininger P, Keats B: *Ush1c216A* knock-in mouse survives Katrina. *Mutat Res*. 2007;616:139-44.
31. Radev Z, Hermel JM, Elipot Y, Breaud S, Arnould S, Duchateau P, et al.: A TALEN-Exon Skipping Design for a Bethlehem Myopathy Model in Zebrafish. *PLoS one*. 2015;10:e0133986.
32. Garanto A, van Beersum SE, Peters TA, Roepman R, Cremers FP, Collin RW: Unexpected *CEP290* mRNA splicing in a humanized knock-in mouse model for Leber congenital amaurosis. *PLoS one*. 2013;8:e79369.

33. Barman-Aksozen J, P CW, Bansode VB, Koentgen F, Trub J, Pelczar P, et al.: Modeling the ferrochelatase c.315-48C modifier mutation for erythropoietic protoporphyria (EPP) in mice. *Dis Model Mech.* 2017;10:225-33.
34. Garanto A, Duijkers L, Collin RW: Species-dependent splice recognition of a cryptic exon resulting from a recurrent intronic CEP290 mutation that causes congenital blindness. *International journal of molecular sciences.* 2015;16:5285-98.

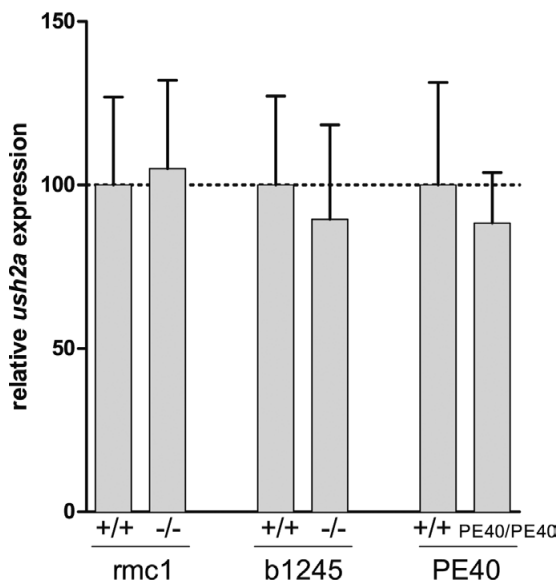
SUPPLEMENTAL FIGURES



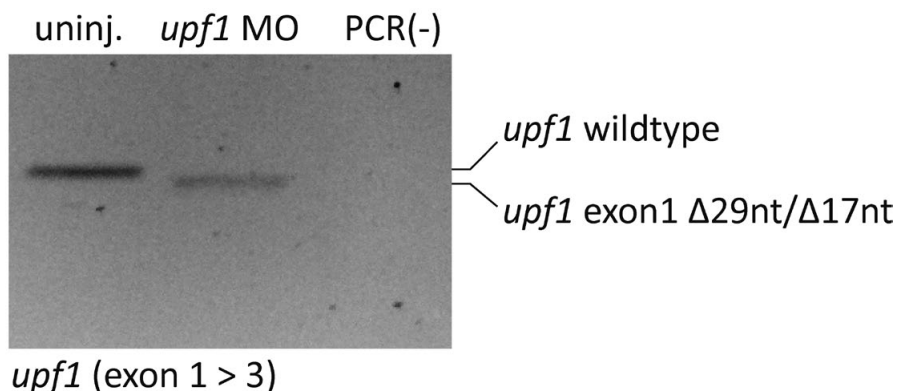
Supplemental figure 1. Characterization of the effect of the *ku70* splice-blocking morpholino (2 dpf). Injection of various amounts of morpholinos (0.1-1.0 ng) resulted in the skipping of *ku70* exon2 or in the (partial) retention of intron2, leading to a premature termination of translation. PCR fragments were analyzed by Sanger sequencing.



Supplemental figure 2. *USH2A* transcript analysis in fibroblasts derived from a patient with a homozygous deep-intronic c.7595-2144A>G mutation in *USH2A*. Alternative splicing in fibroblasts from a control individual (Control) and fibroblasts from a patient that is homozygous for the *USH2A* c.7595-2144A>G mutation (*USH2A*^{PE40/PE40}) is compared using an amplicon spanning PE40 (i.e. *USH2A* exon 39 to 42). The upper band represents transcripts that contain PE40, whereas the lower band represents *USH2A* transcripts without PE40. PCR(-): MilliQ water PCR control.



Supplemental figure 3. Quantitative RT-PCR of total *ush2a* transcripts in wildtype and mutant *ush2a* larvae. *ush2a* expression in *ush2a*^{*rmc1/rmc1*}, *ush2a*^{*b1245/b1245*} and *ush2a*^{*PE40/PE40*} mutant larvae is expressed as percentage of *ush2a* expression in wildtype larvae of the same genetic background. *ush2a* expression is determined relative to *rpl13a*. Data are expressed as mean ± SD (n = 2-5 pools of larvae).



Supplemental figure 4. *upf1* transcript analysis after morpholino knockdown. Characterization of the effect of the *upf1* ex1 spMO at 1 dpf by RT-PCR analysis. Injection of 3 ng *upf1* splice-blocking morpholino in *ush2a*^{*PE40/PE40*} larvae resulted in aberrant *upf1* splicing in 100% of transcripts.

Chapter 4

Skipping Of *ush2a* Exon 13 Prevents Retinal Dysfunction In A Mutant Zebrafish Model

Slijkerman, R.W.N.^{1,2} *, Dona, M.^{1,2} *, Broekman, S.³, Van Diepen, H.⁴, Adamson, P.⁴, Venselaar, H.^{2,5}, Zang, J.⁵, Neuhauss, S.C.⁵, Kremer, H.^{1,3,7}, Van Wijk, E.^{1,7}

** The first two authors are shared first authors*

¹ Department of Otorhinolaryngology, Radboudumc, Nijmegen, the Netherlands

² Radboud Institute for Molecular Life Sciences, Nijmegen, the Netherlands

³ Department of Human Genetics, Radboudumc, Nijmegen, the Netherlands

⁴ ProQR Therapeutics, Leiden, the Netherlands

⁵ CMBI, Radboudumc, Nijmegen, the Netherlands

⁶ University of Zürich, Institute of Molecular Life Sciences, Zürich, Switzerland.

⁷ Donders Institute for Brain, Cognition, and Behaviour, Nijmegen, the Netherlands



ABSTRACT

Usher syndrome (USH) is the most common cause of combined deafblindness in man. Mutations in ten different genes have been associated with USH, but approximately half of all USH patients can be explained by mutations in *USH2A*. In addition, mutations in *USH2A* are the most frequent cause of nonsyndromic retinitis pigmentosa. So far, three founder mutations have been identified in *USH2A*, of which two (c.2299delG; p.Glu767fs and c.2276G>T; p.Cys759Phe) are located in exon 13. Therefore, this study explores the potential of *USH2A* exon 13-skipping as a future treatment option to prevent or halt the progression of retinal dysfunction. *USH2A* transcripts lacking exon 13 are predicted to result in the synthesis of a shortened usherin in which EFG Lam domains 5, 6 and 7 are missing and EGF-Lam domains 4 and 8 are fused into an EGF-like domain. To examine the effect of *ush2a* exon 13-skipping at the level of visual function, we injected zebrafish embryos containing a homozygous protein truncating mutation in this exon with antisense phosphorodiamidate morpholino oligomers (PMOs). PMOs successfully induced the skipping of exon 13 and treatment resulted in the production of a shortened usherin that correctly localizes in the region of the zebrafish photoreceptor connecting cilium. Furthermore, treated larvae demonstrated a rescue of ERG responses, indicative for an improved retinal function. In conclusion, proof of concept was obtained for exon skipping as a future treatment for *USH2A*-associated retinitis pigmentosa caused by mutations in exon 13.

INTRODUCTION

Usher syndrome (USH) is the most common cause of inherited deafblindness in man, with a prevalence of approximately 1 in 20,000 individuals (Kimberling et al. 2010). Three clinical types of USH (USH1-3) can be distinguished based on the severity and progression of the hearing impairment, the age at which the initial visual problems are diagnosed and the presence or absence of vestibular dysfunction (Smith et al. 1994). Approximately two third of patients with USH suffer from USH2, which is characterized by congenital moderate to severe bilateral sensorineural hearing impairment in combination with a slowly progressive loss of visual function as a consequence of retinitis pigmentosa (RP) (Millan et al. 2011, Pierrache et al. 2016). Around 85% of USH2 cases are explained by mutations in *USH2A* (Yan and Liu 2010). In addition, defects in this gene are also among the most prevalent causes of non-syndromic RP (nsRP), accounting for 12-25% of all cases (Seyedahmadi et al. 2004, Hartong, Berson, and Dryja 2006, McGee et al. 2010).

The USH2 auditory phenotype can be partially compensated by providing patients with hearing aids or cochlear implants (Hartel et al. 2017). However, for the progressive loss of vision currently no treatment options are available. Vision loss is the result of a gradual deterioration of photoreceptors, with an onset of visual complaints at an average age of 15 years for patients with USH2 and 25 years for patients with nsRP (Pierrache et al. 2016). This provides a window of opportunity for therapeutic intervention to prevent retinal degeneration prior to the manifestation of visual complaints. Several gene augmentation therapies for *RPE65*-, *MERTK*-, *ABCA4*-, *CHM*-, *MYO7A*-, or *RS1*-associated retinal degeneration are currently under clinical evaluation (Grob et al. 2016, DiCarlo, Mahajan, and Tsang 2018). Furthermore, supplementing the retina of a whirlin-deficient mouse with a healthy cDNA copy of *Whrn*, resulted in the restoration of the USH2 protein complex in photoreceptors (Zou et al. 2011). However, the development of *USH2A* gene augmentation therapy is severely hampered by the size of the coding sequence (15,606 nucleotides), which largely exceeds the cargo capacity of the currently used viral vehicles for gene delivery. Using CRISPR/Cas9 gene editing technology, researchers were able to successfully repair the prevalent *USH2A* c.2299delG mutation in patient-derived fibroblasts, albeit with a very low efficiency (Fuster-Garcia et al. 2017). In addition to low repair efficiencies, also potential off-target effects hamper clinical application of gene editing strategies at present. Therefore, the development of alternative, tailored therapeutic strategies is needed to compensate for the defects in *USH2A* in order to prevent *USH2A*-associated retinal degeneration in the future.

The transcript encoding the long isoform of usherin is built up by 71 coding exons, in which over 600 different mutations have been identified (Baux et al. 2014). In addition, four deep-intronic mutations have been reported to underlie USH2 (Vache et al.

2012, Liquori et al. 2016). Many mutations in *USH2A* are private, but three mutations are derived from a common ancestor and are therefore seen more frequently: c.2299delG, p.Glu767fs; c.2276G>T, p.Cys759Phe; and c.7595-2144A>G, p.Lys2532Thrfs*56 (Slijkerman et al. 2016, Pennings et al. 2004, Aller et al. 2010, Baux et al. 2014). The c.2299delG and c.2276G>T mutations are most common, representing 27.8% and 7.1% of all pathogenic *USH2A* alleles, respectively, and are both in exon 13 (Baux et al. 2014). As this exon consists of a multiple of three nucleotides, skipping the exon could result in the production of a slightly shortened protein with a potential residual function.

In this study we explored the potential of *USH2A* exon 13 as a future therapeutic target for *USH2A*-associated retinal degeneration using our previously characterized *ush2a^{rmc1/rmc1}* zebrafish as a model (Dona et al. 2018). Antisense phosphorodiamidate morpholino oligomers (PMOs) were able to specifically induce the skipping of *ush2a* exon 13 in zebrafish larvae, which resulted in the expression of *usherin* Δ ex13 that properly localized at the photoreceptor periciliary membrane and in a restored retinal function. In summary, proof of concept was obtained for an exon skipping strategy as a potential future treatment option for patients with RP as a consequence of (a) mutation(s) in *USH2A* exon 13.

MATERIAL AND METHODS

In silico modelling of the effect of *USH2A* exon 13 skipping on EGF-lam protein domain structure

Models of the separate EGF-lam domains were built using the modelling script in the YASARA (Krieger et al. 2002) and WHAT IF (Vriend 1990) Twinset with standard parameters. The separate domain sequences were used, resulting in a model for each domain based on PDB files 4AQS (domain 4, 45% sequence identity), 3TBD (domain 5, 46% sequence identity), 4AQS (domain 6, 44% sequence identity), 5LF2 (domain 7, 51% sequence identity, and 1KLO (domain 8, 41% sequence identity) (<https://www.rcsb.org/>). To create the fusion model of domains 4 and 8, we used the model for domain 4 as template and swapped the C-terminal residues for their corresponding residues in domain 8. A subsequent energy minimization was performed to remove big errors.

Zebrafish housing and maintenance

Experimental procedures were conducted according to international and institutional guidelines (RU-DEC, 2012-301). Tupfel long fin (TLF) zebrafish and the previously described *ush2a^{rmc1/rmc1}* mutants with the c.2337_2342delsinsAC (p.Cys780GlnfsTer32) mutation (Dona et al. 2018) were used. Zebrafish eggs were obtained from natural spawning. Larvae were maintained and raised by standard methods (Westerfield 2007).

PMO design and microinjection

PMOs were designed by first assessing the target sequence for SRSF2 (SC35) exonic splice enhancer sites (threshold of 3.0) using the online ESE finder 3.0 tool (http://krainer01.cshl.edu/cgi-bin/tools/ESE3/ese_finder.cgi?process=home). Zebrafish *ush2a* exon 13-targeting PMOs were synthesized by Gene Tools, LCC (USA). PMOs were dissolved in mQ water in a stock concentration of 50 mg/μl and stored at -20°C. One nl of an injection mix (1-4 ng per PMO and 50% (v/v) 0.5% phenol red) was injected into the yolk of 1- to 2-cell-stage embryos with a Pneumatic PicoPump pv280 (World Precision Instruments). After injection, embryos were raised at 28.5°C in E3 embryo medium (5 mM NaCl, 0.17 mM KCl, 0.33 mM CaCl₂, and 0.33 mM MgSO₄) supplemented with 0.1% (w/v) methylene blue. PMO sequences are listed in **Table 1**.

Table 1. Antisense PMO sequences targeting zebrafish *ush2a* exon 13.

Name	Sequence (5'>3')	Targeted motifs
PMO-N1	GCATTTCTGTGGCTGTGACCCATG	SC35 motif 3 and 4
PMO-N2	GTTCTCTGCACCAGTTCTGTAATCC	SC35 motif 5 and 6
PMO-N3	TAAGTGGTCAGTGTATCTGCCTACC	SC35 motif 18
PMO-P2	AACGGTCACAGGTTAGACCTAAAATAA	Splice acceptor and SC35 motif 1
PMO-P3	GTTACAACGGTCACAGGTTAGACCTAAA	Splice acceptor and SC35 motif 1
PMO-P4	AAGCACTAACCTGGTTTACAGGTTCCAC	Splice donor and SC35 motif 19 and 20
Control PMO	CCTCTTACCTCAGTTACAATTATAC	-

Transcript analysis

Pools of 10-15 larvae (3 dpf, unless otherwise stated) were snap frozen in liquid nitrogen and subsequently homogenized in 500 μl Qiazol (Qiagen, #79306) using a 25 gauge 16 mm needle. Total RNA was isolated using phenol:chloroform extraction and precipitated using isopropanol. Extracted total RNA was further purified and DNase treated using the Nucleospin RNA extraction kit (MACHEREY-NAGEL #740955.50) according to manufacturer's instructions. cDNA synthesis from 1 μg of total RNA using SuperScript VILO reverse transcriptase kit (#11755050; ThermoFisher Scientific) was performed, followed by PCR amplification (primers in zebrafish *ush2a* exon 11 (5 pmol; 5'-AGCGCTGTGCGAGTCTCTTC-3'; fwd) and exon 14 (5 pmol; 5'-CTGTGACCGGTCAGT-GATGG-3'; rev)) using Q5 HF DNA polymerase (# M0491L; New England Biolabs). Amplified fragments were analyzed by agarose gel electrophoresis (1% agarose in 0.5xTBE) and used for Sanger sequencing.

Immunohistochemistry and quantification of fluorescence signals

Immunohistochemistry on zebrafish larval eyes using rabbit anti-usherin-C (1:500; #27640002; Novus Biological) and mouse anti-centrin (1:500; #04-1624) antibodies, the secondary antibodies Alexa Fluor 568 goat anti-rabbit (1:8000, A11011, Molecular Probes) and Alexa Fluor 488 goat anti-mouse (1:8000, A11029, Molecular Probes) with DAPI (1:8000; D1306; Molecular Probes) and subsequent quantification of the signals has been performed as previously described (Dona et al. 2018). Plotting of the data and statistical analyses were performed using GraphPad Prism v5.03. Saturated intensity grey values (value of 255) were excluded from the datasets (five datapoints for wild-type samples, seven datapoints for PMO-treated samples and none for untreated *ush2a^{rmc1/rmc1}*), since these values are likely derived from artifacts.

Electroretinogram (ERG) recordings

ERG recordings were performed on isolated larval eyes (6 dpf) as previously described (Sirisi et al. 2014). Larvae were dark-adapted for a minimum of 30 minutes prior to the measurements and subsequently handled under dim red illumination. Larvae were placed on a filter paper in the middle of a plastic recording chamber which was filled with 1% agarose, the reference electrode was inserted into the agarose. The eye to be measured was removed by a loop made of tungsten wire. The loop was placed behind the eye and was pressed down to cut the optic nerve. Meanwhile forceps were used to pull the body and discard it. The isolated eye was then positioned to face the light source. Under visual control via a standard microscope equipped with red illumination (Stemi 2000C, Zeiss, Oberkochen, Germany), a glass microelectrode with an opening of approximately 20 μm at the tip was placed against the center of the cornea. This electrode was filled with E3 medium (5 mM NaCl, 0.17 mM KCl, 0.33 mM CaCl₂ and 0.33 mM MgSO₄), the same in which the embryos were raised and held. The electrode was moved with a micromanipulator (M330R, World Precision Instruments Inc., Sarasota, USA). A custom-made stimulator was invoked to provide light pulses of 100 ms duration, with a light intensity of 7000 lux. It uses a ZEISS XBO 75W light source and a fast shutter (Uni-Blitz Model D122, Vincent Associates, Rochester, NY, USA) driven by a delay unit interfaced to the main ERG recording setup. Electronic signals were amplified 1000 times by a pre-amplifier (P55 A.C. Pre-amplifier, Astro-Med. Inc, Grass Technology) with a band pass between 0.1 and 100 Hz, digitized by DAQ Board NI PCI-6035E (National Instruments) via NI BNC-2090 accessories and displayed via self-developed NI Labview program.

RESULTS

Formation of EGF-like fusion domain after targeted *USH2A* exon 13 skipping

Wild-type usherin is predicted to contain ten EGF-lam domains (<http://smart.embl-heidelberg.de/>). EGF-lam domains typically contain eight cysteine residues that pairwise interact by a covalent disulfide bond, necessary for protein folding and stability. These EGF-lam domains in usherin harbor multiple protein truncating mutations. Also, 22 out of the 80 cysteine residues in these EGF-lam domains have been found to be mutated in patients with *USH2A*-associated RP (*USH2A* LOVD mutation database, <http://www.lovd.nl/USH2A>), of which five reside within exon 13. Unpaired cysteine residues contain a reactive free thiol group that can induce unwanted multimerization or crosslinking with other proteins. The in frame skipping of exon 13 is predicted to result in the fusion of parts of EGF-lam domains 4 and 8 into a functionally related EGF-like domain (**Fig. 1A**). EGF-like domains contain six cysteine residues that together create three disulfide bonds, created by cysteines 1+3, 2+4 and 5+8 in the fused EGF-like domain (Wouters et al. 2005). There are 16 amino acids between the fifth and sixth cysteine residue in the EGF-like 4-8 fusion domain, which is different from the canonical EGF-like cysteine spacing, namely 8 amino acids. However, 3D homology modelling predicted normal disulphide bridge formation within the EGF-like 4-8 fusion domain, supporting a favorable effect of exon 13 skipping (**Fig. 1B**). Therefore, skipping of *USH2A* exon 13 is predicted to result in a shortened protein with a potential residual function, when expressed.

Design and validation of splice modulating antisense morpholinos

To validate exon 13 skipping as a therapeutic strategy, we employed our previously characterized mutant zebrafish (*ush2a*^{*rmc1/rmc1*}) that contains a frameshift-inducing mutation in *ush2a* exon 13 (Dona et al. 2018). The length of *USH2A* exon 13 is reasonably well conserved between human (642 nucleotides) and zebrafish (648 nucleotides). Therefore, three antisense PMOs were designed to target the zebrafish *ush2a* exon 13 splice acceptor (PMO-P2, PMO-P3) or splice donor sites (PMO-P4). Previous studies demonstrated a positive correlation between the exon skipping efficiency of antisense oligonucleotides and the presence of exonic splice enhancer (ESE) motifs recognized by splice factors SRSF2 (SC35), SRSF1 (SF2/ASF) and SRSF5 or other types of splice enhancers (Aartsma-Rus et al. 2009). We analyzed the sequence of zebrafish *ush2a* exon 13 for the presence of SC35 splice factor binding sites using the online ESE finder 3.0 program (<http://krainer01.cshl.edu/cgi-bin/tools/ESE3/ese finder.cgi?process=home>). Using a stringent threshold of 3.0, the algorithm identified twenty predicted SC35 splice factor binding sites (**Fig. 2**), based on which three additional PMOs (PMO-N1, PMO-N2

and PMO-N3) were designed following the previously published guidelines for AON design (Aartsma-Rus 2012) (sequences in **Table 1**).

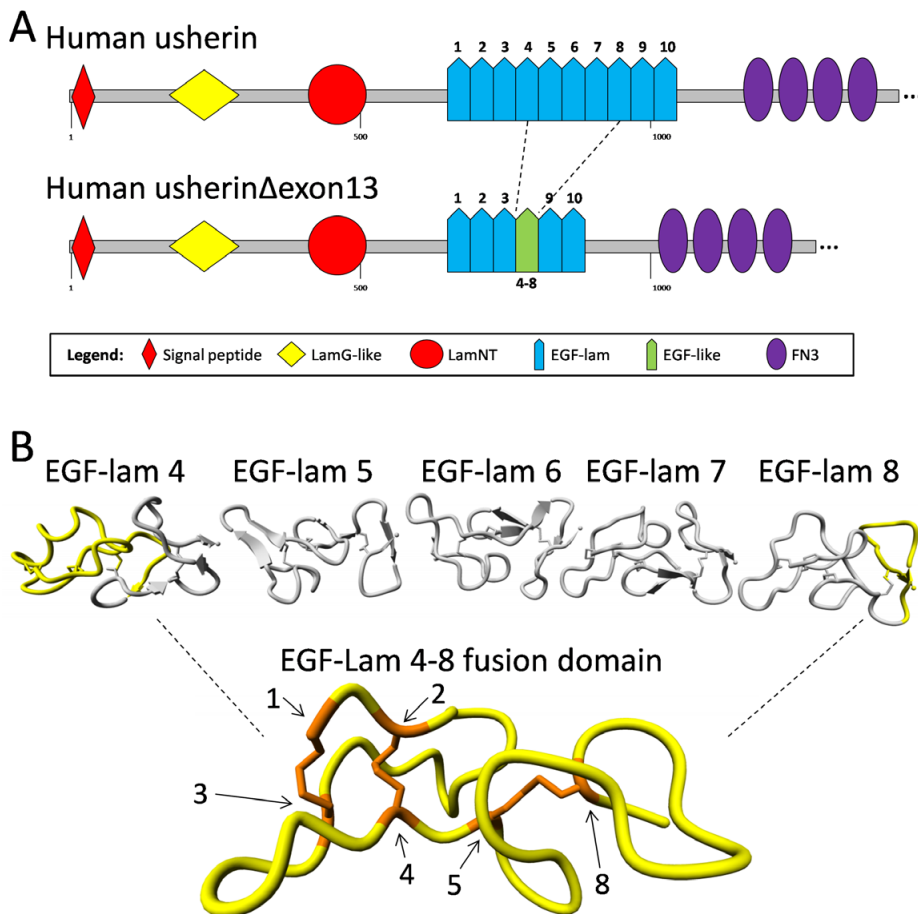


Figure 1. *In silico* modelling of usherin after exon 13 skipping. (A) Schematic representation of the domain architecture of wild-type usherin and usherin Δ exon13. Individual EGF-lam domains are numbered. Skipping of exon 13 results in the exclusion of EGF-lam domains 5, 6 and 7 as well as the partial exclusion of EGF-lam domains 4 and 8. The remaining amino acids of EGF-lam domains 4 and 8 are predicted to form an EGF-like domain with six cysteine residues. The fusion site of this domain is located between the fifth cysteine residue of EGF-lam domain 4 and the eighth cysteine derived from EGF-lam 8. **(B)** 3D homology modelling predicts the formation of a properly folded EGF-like domain with normal disulphide bridge formations. The predicted structures of usherin EGF-lam domains 4 (left) to 8 (right) are shown. The amino acids that are encoded by *USH2A* exon 13 are depicted in grey and predicted to be absent after translation of *USH2A* Δ exon13 transcripts. Cysteine residues that are present in the EGF-like fusion domain are numbered and indicated in orange. The cysteine residues numbered 1 to 5 are derived from EGF-lam domain 4, whereas residue 8 is derived from EGF-lam domain 8.

Different doses (2, 4 or 8 pg) of individual PMOs were injected into the yolk of one- to two-cell stage wild-type zebrafish embryos to assess their efficacy in *ush2a* exon 13 skipping. RT-PCR analyses revealed that PMO-N1, PMO-P2 and PMO-P3 were able to induce a significant skipping of exon 13, whereas PMO-N2, PMO-N3 or PMO-P4 were not (**Supplemental Fig. 1**). Since PMO-N1 targets a different region of exon 13 than PMO-P2 and PMO-P3 (**Fig. 2**), we assessed whether the injection of a combination of PMO-N1 with either PMO-P2 or PMO-P3 would result in an enhanced efficiency in exon 13 skipping. For this purpose, different doses of the PMO-cocktails PMO-N1 + P2 and PMO-N1 + P3 (2+2 pg, 3+3 pg and 4+4 pg) were injected in wild-type embryos. *ush2a* transcript analysis at three days post injection revealed a near complete skipping of zebrafish *ush2a* exon 13 already after injection of the lowest dose of PMOs (2+2 pg) (**Fig. 3A**). Sanger sequencing of the PCR products confirmed the precise skipping of *ush2a* exon 13, since exon 12 is directly fused to exon 14 (**Fig. 3B**).

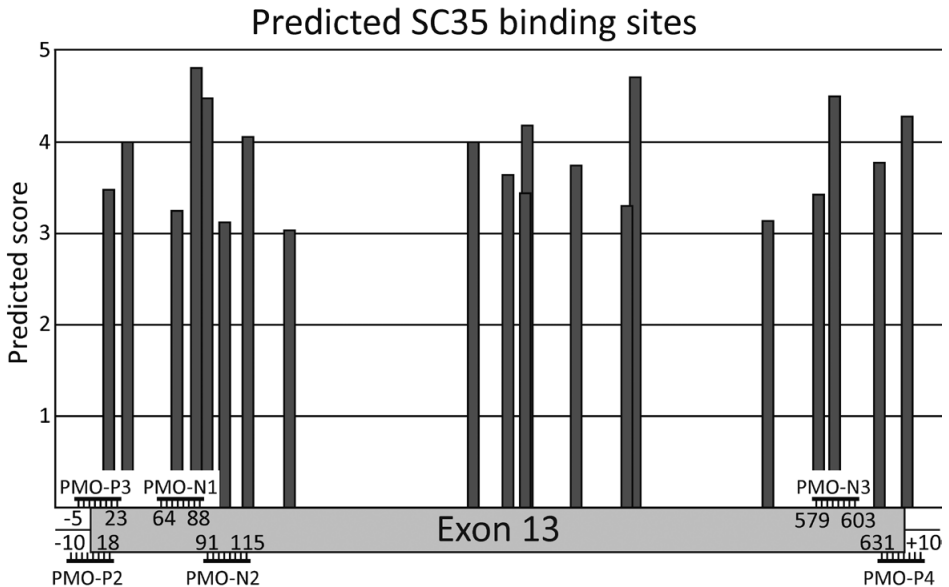


Figure 2. SC35 splice factor binding sites in *ush2a* exon 13. Target sites of the individual PMOs are indicated in the plot. Numbers indicate the first and last nucleotide of the PMO target sequences in zebrafish *ush2a* exon 13. The bars represent the SC35 splice factor binding sites. Prediction scores are indicated on the Y-axis and the *ush2a* sequence on the X-axis.

Ush2a exon 13 skipping restores ERG b-wave amplitudes in *ush2a^{rmc1/rmc1}* larvae

We previously reported that electroretinogram (ERG) traces are significantly reduced in *ush2a^{rmc1/rmc1}* larvae (Dona et al. 2018). Here, we recorded ERGs from *ush2a^{rmc1/rmc1}* larvae that were treated with combinations of *ush2a* exon 13-targeting PMOs (PMO-N1

+ P2 (4+4 pg) (n=14); PMO-N1 + P3 (4+4 pg) (n=25)) or control PMOs (8 pg) (n=14). Larvae were derived from the same clutch. ERGs recorded from uninjected age-, strain-, and clutch-matched wild-type (n=10) and *ush2a^{rmc1/rmc1}* (n=11) larvae were used as controls. We first confirmed the efficiency of *ush2a* exon 13 skipping by RT-PCR analysis of RNA derived from PMO-injected larvae (**Fig. 4A**). Uninjected and control PMO-injected *ush2a^{rmc1/rmc1}* mutant larvae demonstrated a significantly reduced b-wave amplitude as compared to age- and strain-matched wild-type larvae ($p < 0.05$ (uninjected) and $p < 0.01$ (control PMO-injected)) (**Fig. 4B, C**). We observed significantly increased b-wave amplitudes after injection of either PMO combination (PMO-N1 + P2 (4+4 pg) or PMO-N1 + P3 (4+4 pg)) as compared to untreated or control PMO-injected *ush2a^{rmc1/rmc1}* larvae, which is indicative of an improved excitation of the secondary neurons. The ERG b-wave amplitudes recorded in *ush2a^{rmc1/rmc1}* larvae after injection with exon 13-targeting PMOs were not different from those recorded in age- and strain-matched wild-type larvae (**Fig. 4B, C**).

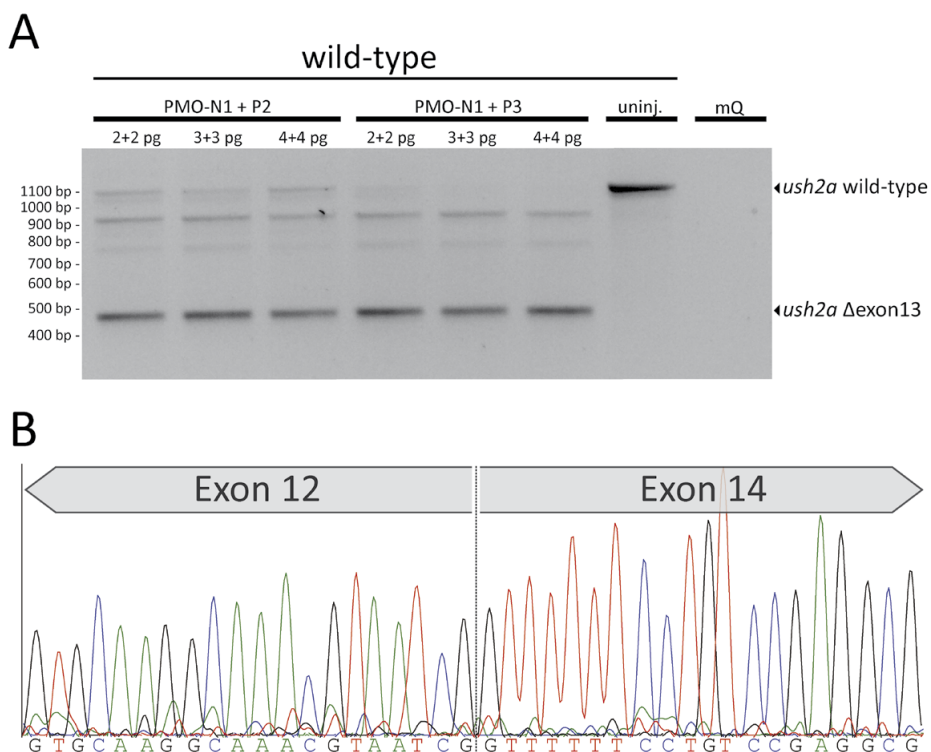


Figure 3. *ush2a* exon 13 skipping potential of combinations of morpholinos in wild-type zebrafish larvae. (A) RT-PCR analyses to evaluate the *ush2a* exon 13 skipping potential of different combinations of PMOs (PMO-N1 + P2 and PMO-N1 + P3). (B) Chromatogram of the lower fragment (488 bp) showing a perfect skipping of *ush2a* exon 13 after PMO treatment.

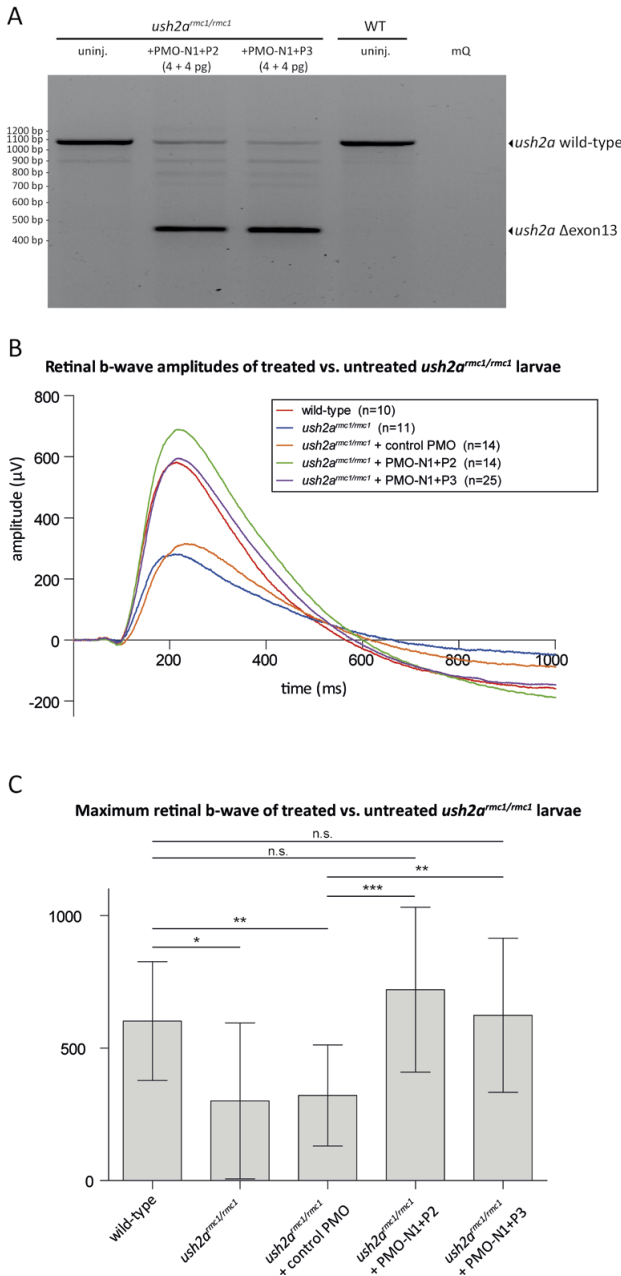


Figure 4 Morpholino-induced exon 13 skipping restores ERG b-wave amplitudes in *ush2a^{mcl1/rmc1}* larvae.

(A) *ush2a* transcript analysis after injection of *ush2a* exon 13-targeting PMOs. The larger PCR product (1096 bp, indicated by '*ush2a* wild-type') represents wild-type spliced *ush2a* transcripts, whereas the smaller product (448 bp, indicated by '*ush2a* Δexon 13') represents *ush2a* transcripts lacking exon 13. **(B)** Average ERG b-wave amplitudes recorded in a cohort of uninjected or control PMO-injected *ush2a^{mcl1/rmc1}* larvae (5-6 dpf) and age- and strain-matched wild-type controls. Skipping of *ush2a* exon 13 from *ush2a^{mcl1/rmc1}* larvae restored ERG b-wave amplitudes to wild-type levels ('n' in the legend panel indicates the number of injected larvae in 2 biological replicates). **(C)** Average maximum b-wave amplitudes recorded in uninjected ($p < 0.05$, indicated by '*') and control PMO-injected ($p < 0.01$, indicated by '**') *ush2a^{mcl1/rmc1}* larvae are significantly reduced as compared to those recorded in wild-type controls (n=10 wild-type, n=11 uninjected *ush2a^{mcl1/rmc1}* and n=14 control PMO-injected *ush2a^{mcl1/rmc1}*, 2 biological replicates; two-tailed unpaired Student's *t*-test). B-wave amplitudes recorded in PMO-N1 + P2- ($p < 0.001$, indicated by '****') or PMO-N1 + P3-injected ($p < 0.01$, indicated by '**') *ush2a^{mcl1/rmc1}* larvae are significantly higher as compared to ERG-traces from control PMO-injected *ush2a^{mcl1/rmc1}* mutants from the same clutch, while not being significantly different from b-wave amplitudes recorded from uninjected wild-type larvae (PMO-N1 + P2 injected *ush2a^{mcl1/rmc1}* (n=14), PMO-N1 + P3 injected *ush2a^{mcl1/rmc1}* (n=25) and wild-types (n=10); 2 biological replicates; two-tailed unpaired Student's *t*-test). n.s., not significant.

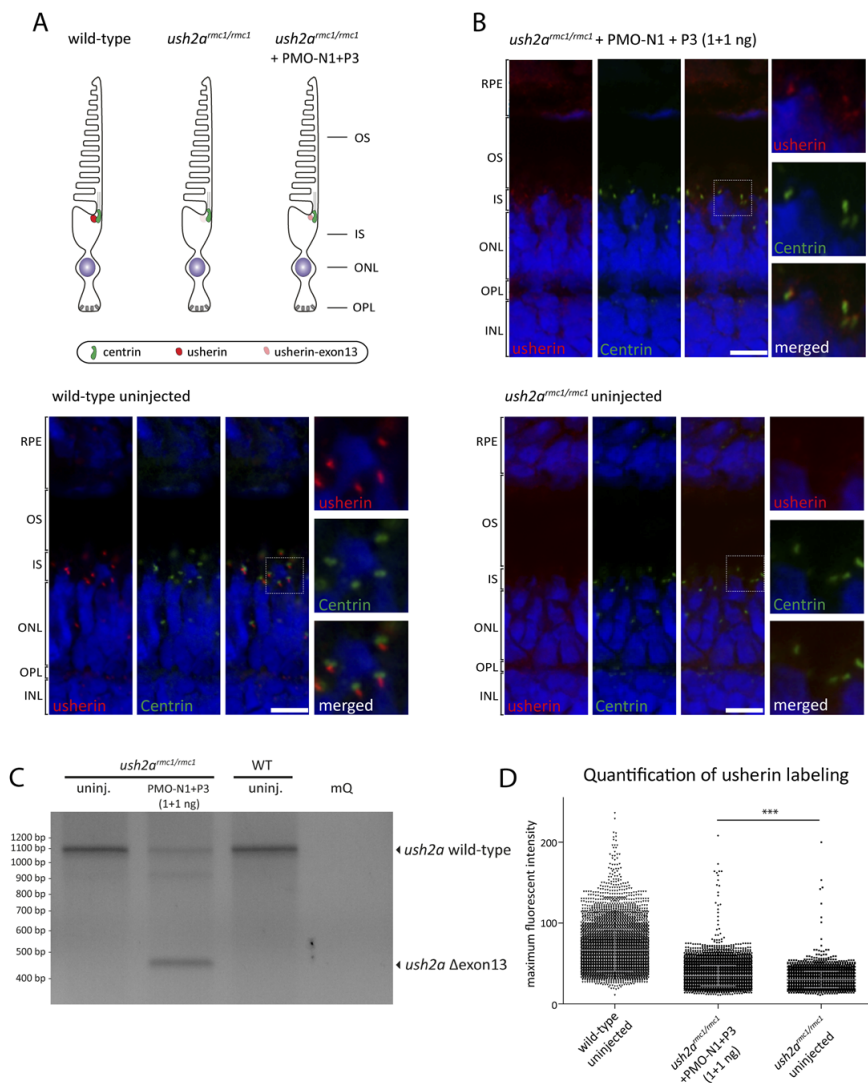


Figure 5. Skipping of *ush2a* exon 13 partially restores the expression of usherin in the photoreceptor periciliary region. (A) Schematic presentation of usherin localization in the zebrafish retina. Usherin (red) or usherin Δ exon13 (pink) localize at the photoreceptor periciliary region, adjacent to the connecting cilium marked by centrin (green). Photoreceptors from *ush2a^{mc1/mc1}* larvae completely lack usherin. (B) Subcellular localization of usherin in radial cryosections of larval (5 dpf) zebrafish retinae using anti-usherin-C antibodies (red signal). Nuclei were stained with DAPI (blue signal). In wild-type larvae, usherin is present in the photoreceptor periciliary region. In *ush2a^{mc1/mc1}* larvae, no specific usherin signal could be detected. Skipping of *ush2a* exon 13 in *ush2a^{mc1/mc1}* larvae (*ush2a^{mc1/mc1}* + MO-N1+P3 (1+1 ng)) resulted in a partial restoration of usherin expression and localization. RPE: retinal pigment epithelium; OS: outer segment; CC: connecting cilium; IS: inner segment; ONL: outer nuclear layer; OPL: outer plexiform layer; IPL: inner plexiform layer. Scale bars represent 20 μ m. (C) Transcript analysis confirmed that injection of MO-N1+P3 (1+1 ng) efficiently induces *ush2a* exon 13 skipping in *ush2a^{mc1/mc1}* larvae.

Figure 5. Skipping of *ush2a* exon 13 partially restores the expression of usherin in the photoreceptor periciliary region. (continued)

The upper band represents *ush2a* transcripts with a wild-type pattern of transcript splicing (WT), whereas the lower band represents *ush2a* transcripts lacking exon 13 (Δ exon13). **(D)** Quantification of usherin labeling (red signal) in the photoreceptor periciliary region in PMO-treated *ush2a^{rmc1/rmc1}* larvae as compared to wild-type and untreated *ush2a^{rmc1/rmc1}* larvae. Each datapoint in the scatter graph displays the intensity grey value of a single photoreceptor. Exon 13 skipping results in a significant increase of fluorescence intensity as compared to untreated *ush2a^{rmc1/rmc1}* mutants (34.98 ± 0.14 grayscale value in PMO-treated retinas versus 30.04 ± 0.16 grayscale value in untreated retinas; $p < 0.001$ (indicated by '***', two-tailed Student's t-test)). The average grayscale intensity value as measured in wild-type retinas was significantly higher as compared to PMO-treated *ush2a^{rmc1/rmc1}* retinas (66.42 ± 0.32 versus 34.98 ± 0.14 ; $p < 0.001$). In total, 10 to 12 eyes were analyzed per condition and genotype, of which 31 sections (6580 connecting cilia) of wild-type, 43 sections (8474 connecting cilia) of PMO-treated and 21 sections (4201 connecting cilia) of untreated *ush2a^{rmc1/rmc1}* larvae were analyzed.

Usherin Δ exon13 is expressed and localizes in the photoreceptor periciliary region

We next determined whether skipping of zebrafish *ush2a* exon 13 in the *ush2a^{rmc1/rmc1}* mutant larvae resulted in the synthesis of a shortened usherin protein (usherin Δ exon13) (**Fig. 5A**). Antibodies directed against the intracellular region of zebrafish usherin were used to stain unfixed cryosections of wild-type larvae, uninjected *ush2a^{rmc1/rmc1}* larvae and *ush2a^{rmc1/rmc1}* larvae in which *ush2a* exon 13 skipping was induced by PMO injection (**Fig. 5B**, red signal). The connecting cilium was marked by antibodies directed against centrin (**Fig. 5B**, green signal). In wild-type larvae usherin localizes in the periciliary region, as expected. In the retina of uninjected *ush2a^{rmc1/rmc1}* larvae no usherin could be detected. In PMO-treated *ush2a^{rmc1/rmc1}* larvae a partial restoration of usherin expression was detected with a proper subcellular localization. The intensity of the anti-usherin fluorescence signals was quantified using an automated Fiji script, after confirmation of the exon 13 skipping efficiency in the injected larvae (**Fig. 5C**). Skipping of *ush2a* exon 13 resulted in a small but significant increase of the average fluorescence intensity as compared to untreated larvae from the same clutch (34.98 ± 0.14 (Δ exon 13) versus 30.04 ± 0.16 (untreated); $p < 0.001$ (two-tailed Student's t-test)) (**Fig. 5D**). This further corroborated that exon 13-skipping resulted in the synthesis of usherin Δ exon13.

DISCUSSION

In this study we used PMOs targeting *ush2a* exon 13 to evaluate exon skipping as a therapeutic strategy for the future treatment of *USH2A*-associated retinal dysfunction. A zebrafish model with a frameshift mutation in *ush2a* exon 13 (*ush2a*^{*rmc1/rmc1*}) lacks usherin in the region of the photoreceptor connecting cilium and displays early-onset retinal dysfunction (Dona et al. 2018). We here show that skipping of *ush2a* exon 13 in larvae of this mutant resulted in a partially restored expression of usherin in the region of the photoreceptor connecting cilium. Furthermore, exon 13-skipping restored ERG b-wave amplitudes, indicative of an improved retinal function. Our study therefore provides proof of concept for an exon skipping strategy as a potential future treatment for *USH2A*-associated retinal dysfunction as a consequence of mutations in exon 13, such as the recurrent c.2299delG or c.2276G>T mutations.

In the inner ear, usherin is essential for the maturation of hair bundles that are located at the apex of hair cells. Usherin and ADGRV1 together form the transient ankle links between adjacent stereocilia and between the tallest stereocilium and the kinocilium (Michalski et al. 2007). Hair bundle formation and subsequent mechanotransduction requires a very strict and tightly regulated spacing between adjacent stereocilia. This is further corroborated by the extremely high conservation of the length and domain architecture of the usherin protein throughout the complete vertebrate lineage (Dona et al. 2018). Also in the Anthozoan *Nematostella vectensis* usherin has the same architecture (Tucker 2010). In the latter, Usher proteins are proposed to have a similar function in the maturation of stereocilia on cnidocytes, which are specialized cells that fire a barb and thread upon touch stimulation (Michel, Sabourault, and Petit 2018). In the retina, the large extracellular tails of usherin and ADGRV1 have been proposed to interact and together bridge the gap between the opposing membranes of the photoreceptor connecting cilium and periciliary region (Maerker et al. 2008, Sorousch et al. 2017). In contrast to the situation in the inner ear hair cells, usherin seems redundant for the initial development and function of photoreceptors (Maerker et al. 2008), but rather fulfills a post-developmental role. As such, usherin seems to be particularly important for photoreceptor maintenance (Liu et al. 2007). Therefore, therapeutic strategies that rescue the expression of usherin in the functional retina could potentially prevent or slow down the progression of photoreceptor degeneration and, as such, preserve visual function in patients.

Many mutations in *USH2A* are private and evenly distributed over the gene. They include nonsense, frame-shift, splice-modulating, and missense variants. It is generally believed that RP due to mutations in this gene is caused by a loss-of-function mechanism, although endoplasmic reticulum-stress has been suggested as the disease mechanism for missense mutations (Tucker et al. 2013). An alternative for gene aug-

mentation therapy is the skipping of exons harboring pathogenic mutations, which has already been shown to have a high therapeutic potential for Duchenne Muscular Dystrophy (DMD) and Cerebral Autosomal Dominant Arteriopathy with Subcortical Infarcts and Leukoencephalopathy (CADASIL). This approach is particularly interesting for large genes encoding (structural) proteins that contain series of repetitive protein domains. Dystrophin, encoded by the *DMD* gene, is a rod-shaped structural linker protein consisting of a stretch of 24 spectrin-like domains flanked by protein-protein interaction domains that are used to connect the F-actin cytoskeleton to β -dystroglycan (Mendell et al. 2013, Mendell et al. 2016). Protein truncating mutations in *DMD* give rise to the severe DMD, whereas missense mutations generally result into the milder Becker Muscular Dystrophy (BMD) (Monaco et al. 1988). This genotype-phenotype correlation was the basis of the rationale to correct the *DMD* reading frame as a therapeutic strategy. This was further corroborated by the identification of partial in frame deletions of *DMD* in patients with BMD (Nakamura et al. 2016, Nakamura et al. 2017). Indeed, induced skipping of *DMD* exon 51 in patients with a protein truncating mutation in this exon resulted in an increase of dystrophin-positive fibers and a delayed muscle degeneration (Aoki et al. 2012). Usherin is a large structural protein that contains repetitive EGF-lam and FN3 domains. The in frame *USH2A* exon 13, the exon in which two founder mutations have been identified, encodes part of a stretch of ten EGF-lam domains, that is proposed to form a stiff rod-like element (Beck, Hunter, and Engel 1990, Campbell and Bork 1993, Yurchenco and Cheng 1993). Skipping of this exon could therefore well result in the expression of a slightly shortened protein with residual function.

Exons should meet certain criteria in order to be eligible as a target in therapeutic exon-skipping approaches (Niks and Aartsma-Rus 2017). The exclusion of the target exon from the transcript should not result in a frameshift. Furthermore, the target exon should not encode any essential protein domains. In addition, the Δ exon transcript should give rise to a protein that is able to fold properly. For example, mutations in *NOTCH3* typically result in the loss or gain of a cysteine residue in one of the 34 EGF-like domains and clinically manifest as CADASIL (Rutten et al. 2014). The skipping of selected, mutated exons was shown to result in the formation of EGF-like fusion domains that are structurally similar to wild-type EGF-like domains. The resulting shortened *NOTCH3* protein was shown to undergo normal processing and to retain ligand-induced activation (Rutten et al. 2016). In line with Rutten *et al.*, *USH2A* exon 13 also seems to fulfill the criteria for exon-skipping. This in frame exon (642 nucleotides) encodes multiple EGF-lam domains and *in silico* predictions and 3D homology modelling demonstrated that EGF-lam domains 4 and 8, that are both in part encoded by exon 13, fuse into a properly folded EGF-like domain after skipping of *USH2A* exon 13. However, the spacing between cysteine residues 5 and 6 in the resulting EGF-like 4-8 fusion domain of usherin Δ exon13 is 16 amino acids, which significantly differs from the reported consensus spacing (8

amino acids) in EGF-like domains. A certain variation in spacing between the fifth and sixth cysteine residue in EGF-like domains is tolerated and has been reported (<http://smart.embl-heidelberg.de/>). For example, the spacing between cysteine residues 5 and 6 in EGF-like domains 1 and 2 of UMODL1, a transmembrane protein in which variants have been suggested to be associated with high myopia in the Japanese population (Nishizaki et al. 2009), is 18 and 15 amino acids, respectively.

To assess the functionality of the usherin Δ exon13 protein, we employed the recently published *ush2a^{rmc1/rmc1}* zebrafish mutant, which has a homozygous protein truncating mutation in exon 13 and shows an early onset retinal dysfunction (Dona et al. 2018). First of all, a small but significant increase in usherin labeling at the photoreceptor periciliary membrane of PMO-treated *ush2a^{rmc1/rmc1}* larvae was observed, which indicates that *ush2a* Δ exon13 transcripts result in the synthesis of a shortened usherin that is able to properly localize in the retina. Furthermore, PMO-induced skipping of the mutated exon 13 resulted in completely restored ERG b-wave amplitudes, indicative of a restored visual function. ERG responses were recorded in larvae (5-6 dpf), which are known to have an immature retina. Rods do not significantly contribute to the zebrafish ERG until 15 dpf and therefore all responses recorded in these larvae are expected to be cone-derived (Branchek 1984, Bilotta, Saszik, and Sutherland 2001). Patients with *USH2A*-associated RP often present with night-blindness as the initial symptom of retinal dysfunction, indicating a primary dysfunction of the rods. However, it was recently reported that both rod and cone responses were markedly reduced in the ERGs of adolescent *USH2a* patients (Sengillo et al. 2017). Therefore, a restored ERG response in zebrafish *ush2a^{rmc1/rmc1}* larvae upon exon 13 skipping is promising for a beneficial effect in patients. In summary, we confirmed that usherin Δ exon13 is functional based on the partially restored usherin expression and improved retinal function in PMO-treated *ush2a^{rmc1/rmc1}* larvae.

The minimal amount of usherin Δ exon13 that is required for a normal retinal function is still unknown. Although, individuals that carry a heterozygous loss of function mutation in *USH2A* are asymptomatic, indicating that about 50% of usherin would theoretically be sufficient. The level of usherin Δ exon13 expression and localization in PMO-treated zebrafish larvae has been determined based on fluorescence intensity measurements after immunohistochemistry. Surprisingly little usherin Δ exon13 was detected in the retina of injected larvae, even though retinal function was completely restored. This either indicates that only a minor amount of usherin is sufficient for retinal function, or that the total amount of usherin expression after PMO treatment was significantly underestimated. Quantification of protein expression levels based on immunohistochemistry is semi-quantitative at best. More direct quantification methods, such as Western blotting, would be more accurate although these are technically challenging due to the large size of usherin. Alternatively, restoration of expression

and subcellular localization of key usherin interaction partners, such as *Whrna* and *Whrnb*, which have been previously shown to be reduced in untreated *ush2a^{rmc1/rmc1}* larvae (Dona et al. 2018), could serve as biomarker for therapeutic efficacy. In addition, functional analyses can be extended with visual-motor response measurements, which were previously found to be attenuated in *ush2a^{rmc1/rmc1}* larvae (Dona, Van den Bos, and Van Wyk Manuscript in preparation).

In conclusion, proof of concept was obtained for exon-skipping as a potential therapeutic strategy for *USH2A*-associated RP. Zebrafish and human photoreceptor anatomy and morphology is highly similar (Slijkerman et al. 2015). As such, we expect that skipping of *USH2A* exon 13 in patients with a mutation in this exon will likely result in a similar beneficial effect as observed in zebrafish. However, future studies using iPSC-derived 3D retinal organoids generated from skin biopsies of patients having mutations in *USH2A* exon 13 and subsequent Phase I/II clinical trials will determine the translational value of the results obtained from our zebrafish studies.

ACKNOWLEDGEMENTS

The authors would like to thank Tom Spanings for excellent fish husbandry. The authors would like to acknowledge The Microscopic Technology Center of the RIMLS for facilitating the use of the Airyscan microscope.

This study was financially supported by 'Stichting Nederlands Oogheelkundig Onderzoek', 'Stichting Blindenhulp', 'Stichting Researchfonds Nijmegen', 'Landelijke Stichting voor Blinden en Slechtienden' to HK and EvW; the Foundation Fighting Blindness USA [grant number PPA-0517-0717-RAD to EvW], 'Stichting Wetenschappelijk Onderzoek Doof-Blindheid', 'Stichting Ushersyndroom' to EvW, and the Dutch Organisation for Scientific research (NWO Veni grant 016.136.091; to EvW).

CONFLICT OF INTEREST

The work in this manuscript has been patented under number PCT/EP2015/065736. EvW reports being employed by Radboudumc and inventor on this patent. Radboudumc has licensed the rights to the patent exclusively to ProQR Therapeutics. As the inventor, EvW is entitled to a share of any future royalties paid to Radboudumc, should the therapy eventually be brought to the market.

REFERENCES

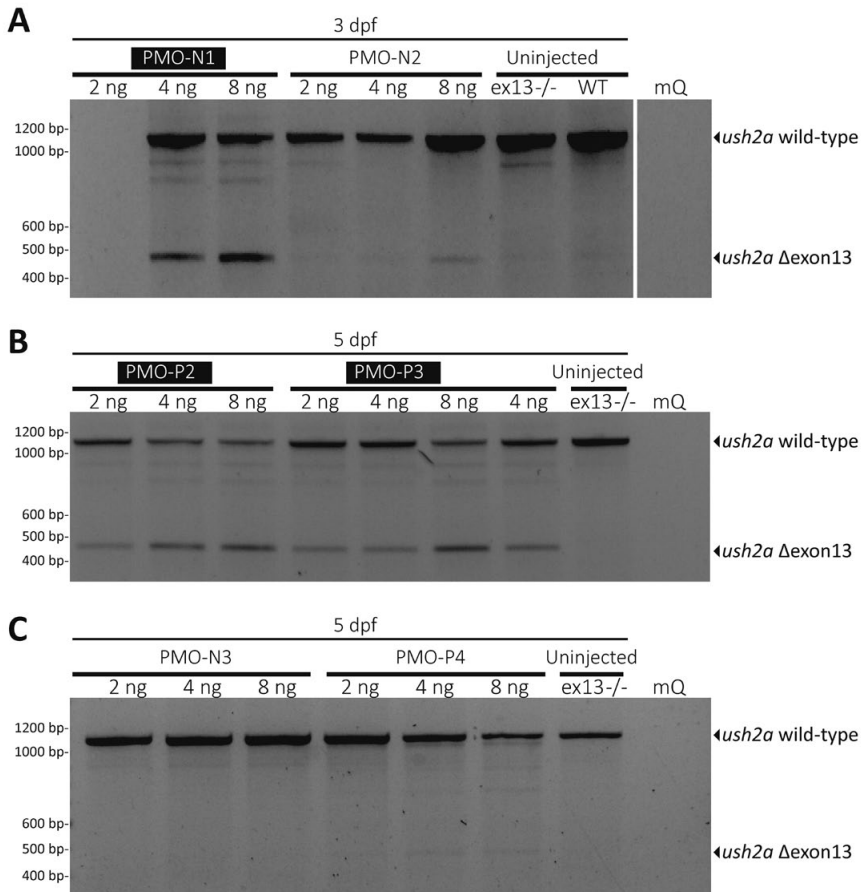
- Aartsma-Rus, A. 2012. "Overview on AON design." *Methods Mol Biol* 867:117-29. doi: 10.1007/978-1-61779-767-5_8.
- Aartsma-Rus, A., L. van Vliet, M. Hirschi, A. A. Janson, H. Heemskerk, C. L. de Winter, S. de Kimpe, J. C. van Deutekom, P. A. t Hoen, and G. J. van Ommen. 2009. "Guidelines for antisense oligonucleotide design and insight into splice-modulating mechanisms." *Mol Ther* 17 (3):548-53. doi: 10.1038/mt.2008.205.
- Aller, E., L. Larrieu, T. Jaijo, D. Baux, C. Espinos, F. Gonzalez-Candelas, C. Najera, F. Palau, M. Claustres, A. F. Roux, and J. M. Millan. 2010. "The *USH2A* c.2299delG mutation: dating its common origin in a Southern European population." *Eur J Hum Genet* 18 (7):788-93. doi: 10.1038/ejhg.2010.14.
- Aoki, Y., T. Yokota, T. Nagata, A. Nakamura, J. Tanihata, T. Saito, S. M. Duguez, K. Nagaraju, E. P. Hoffman, T. Partridge, and S. Takeda. 2012. "Bodywide skipping of exons 45-55 in dystrophic mdx52 mice by systemic antisense delivery." *Proc Natl Acad Sci U S A* 109 (34):13763-8. doi: 10.1073/pnas.1204638109.
- Baux, D., C. Blanchet, C. Hamel, I. Meunier, L. Larrieu, V. Faugere, C. Vache, P. Castorina, B. Puech, D. Bonneau, S. Malcolm, M. Claustres, and A. F. Roux. 2014. "Enrichment of LOVD-USHbases with 152 *USH2A* genotypes defines an extensive mutational spectrum and highlights mis-sense hotspots." *Hum Mutat* 35 (10):1179-86. doi: 10.1002/humu.22608.
- Beck, K., I. Hunter, and J. Engel. 1990. "Structure and function of laminin: anatomy of a multidomain glycoprotein." *FASEB J* 4 (2):148-60.
- Bilotta, J., S. Saszik, and S. E. Sutherland. 2001. "Rod contributions to the electroretinogram of the dark-adapted developing zebrafish." *Dev Dyn* 222 (4):564-70. doi: 10.1002/dvdy.1188.
- Branchek, T. 1984. "The development of photoreceptors in the zebrafish, brachydanio rerio. II. Function." *J Comp Neurol* 224 (1):116-22. doi: 10.1002/cne.902240110.
- Campbell, I. D., and P. Bork. 1993. "Epidermal Growth Factor-Like Modules." *Current Opinion in Structural Biology* 3 (3):385-392. doi: Doi 10.1016/S0959-440x(05)80111-3.
- DiCarlo, J. E., V. B. Mahajan, and S. H. Tsang. 2018. "Gene therapy and genome surgery in the retina." *J Clin Invest* 128 (6):2177-2188. doi: 10.1172/JCI120429.
- Dona, M., R. Slijkerman, K. Lerner, S. Broekman, J. Wegner, T. Howat, T. Peters, L. Hetterschijt, N. Boon, E. de Vrieze, N. Sorusch, U. Wolfrum, H. Kremer, S. Neuhauss, J. Zang, M. Kamermans, M. Westerfield, J. Phillips, and E. van Wijk. 2018. "Usher1 defects lead to early-onset retinal dysfunction in zebrafish." *Exp Eye Res* 173:148-159. doi: 10.1016/j.exer.2018.05.015.
- Dona, M., R. Van den Bos, and E. Van Wyk. Manuscript in preparation. Behavioral assays to measure visual function in zebrafish larvae.
- Fuster-Garcia, C., G. Garcia-Garcia, E. Gonzalez-Romero, T. Jaijo, M. D. Sequedo, C. Ayuso, R. P. Vazquez-Manrique, J. M. Millan, and E. Aller. 2017. "*USH2A* Gene Editing Using the CRISPR System." *Mol Ther Nucleic Acids* 8:529-541. doi: 10.1016/j.omtn.2017.08.003.
- Grob, S. R., A. Finn, T. D. Papakostas, and D. Elliott. 2016. "Clinical Trials in Retinal Dystrophies." *Middle East Afr J Ophthalmol* 23 (1):49-59. doi: 10.4103/0974-9233.173135.
- Hartel, B. P., J. W. I. van Nierop, W. J. Huinck, L. J. C. Rotteveel, E. A. M. Mylanus, A. F. Snik, H. P. M. Kunst, and R. J. E. Pennings. 2017. "Cochlear Implantation in Patients With Usher Syndrome Type IIa Increases Performance and Quality of Life." *Otol Neurotol* 38 (6):e120-e127. doi: 10.1097/MAO.0000000000001441.

- Hartong, D. T., E. L. Berson, and T. P. Dryja. 2006. "Retinitis pigmentosa." *Lancet* 368 (9549):1795-809. doi: 10.1016/S0140-6736(06)69740-7.
- Kimberling, W. J., M. S. Hildebrand, A. E. Shearer, M. L. Jensen, J. A. Halder, K. Trzuppek, E. S. Cohn, R. G. Weleber, E. M. Stone, and R. J. Smith. 2010. "Frequency of Usher syndrome in two pediatric populations: Implications for genetic screening of deaf and hard of hearing children." *Genet Med* 12 (8):512-6. doi: 10.1097/GIM.0b013e3181e5afb8.
- Liquori, A., C. Vache, D. Baux, C. Blanchet, C. Hamel, S. Malcolm, M. Koenig, M. Claustres, and A. F. Roux. 2016. "Whole *USH2A* Gene Sequencing Identifies Several New Deep Intronic Mutations." *Hum Mutat* 37 (2):184-93. doi: 10.1002/humu.22926.
- Liu, X., O. V. Bulgakov, K. N. Darrow, B. Pawlyk, M. Adamian, M. C. Liberman, and T. Li. 2007. "Usherin is required for maintenance of retinal photoreceptors and normal development of cochlear hair cells." *Proc Natl Acad Sci U S A* 104 (11):4413-8. doi: 10.1073/pnas.0610950104.
- Maerker, T., E. van Wijk, N. Overlack, F. F. Kersten, J. McGee, T. Goldmann, E. Sehn, R. Roepman, E. J. Walsh, H. Kremer, and U. Wolfrum. 2008. "A novel Usher protein network at the periciliary reloading point between molecular transport machineries in vertebrate photoreceptor cells." *Hum Mol Genet* 17 (1):71-86. doi: 10.1093/hmg/ddm285.
- McGee, T. L., B. J. Seyedahmadi, M. O. Sweeney, T. P. Dryja, and E. L. Berson. 2010. "Novel mutations in the long isoform of the *USH2A* gene in patients with Usher syndrome type II or non-syndromic retinitis pigmentosa." *J Med Genet* 47 (7):499-506. doi: 10.1136/jmg.2009.075143.
- Mendell, J. R., N. Goemans, L. P. Lowes, L. N. Alfano, K. Berry, J. Shao, E. M. Kaye, E. Mercuri, Group Eteplirsen Study, and D. M. D. Italian Network Telethon Foundation. 2016. "Longitudinal effect of eteplirsen versus historical control on ambulation in Duchenne muscular dystrophy." *Ann Neurol* 79 (2):257-71. doi: 10.1002/ana.24555.
- Mendell, J. R., L. R. Rodino-Klapac, Z. Sahenk, K. Roush, L. Bird, L. P. Lowes, L. Alfano, A. M. Gomez, S. Lewis, J. Kota, V. Malik, K. Shontz, C. M. Walker, K. M. Flanigan, M. Corridore, J. R. Kean, H. D. Allen, C. Shilling, K. R. Melia, P. Sazani, J. B. Saoud, E. M. Kaye, and Group Eteplirsen Study. 2013. "Eteplirsen for the treatment of Duchenne muscular dystrophy." *Ann Neurol* 74 (5):637-47. doi: 10.1002/ana.23982.
- Michalski, N., V. Michel, A. Bahloul, G. Lefevre, J. Barral, H. Yagi, S. Chardenoux, D. Weil, P. Martin, J. P. Hardelin, M. Sato, and C. Petit. 2007. "Molecular characterization of the ankle-link complex in cochlear hair cells and its role in the hair bundle functioning." *J Neurosci* 27 (24):6478-88. doi: 10.1523/JNEUROSCI.0342-07.2007.
- Michel, V., C. Sabourault, and C. Petit. 2018. "Sea anemone as a model to study Usher proteins interactions in inner ear hair bundle." *ARO Abstracts*.
- Millan, J. M., E. Aller, T. Jaijo, F. Blanco-Kelly, A. Gimenez-Pardo, and C. Ayuso. 2011. "An update on the genetics of usher syndrome." *J Ophthalmol* 2011:417217. doi: 10.1155/2011/417217.
- Monaco, A. P., C. J. Bertelson, S. Liechti-Gallati, H. Moser, and L. M. Kunkel. 1988. "An explanation for the phenotypic differences between patients bearing partial deletions of the DMD locus." *Genomics* 2 (1):90-5.
- Nakamura, A., N. Fueki, N. Shiba, H. Motoki, D. Miyazaki, H. Nishizawa, Y. Echigoya, T. Yokota, Y. Aoki, and S. Takeda. 2016. "Deletion of exons 3-9 encompassing a mutational hot spot in the DMD gene presents an asymptomatic phenotype, indicating a target region for multiexon skipping therapy." *J Hum Genet* 61 (7):663-7. doi: 10.1038/jhg.2016.28.

- Nakamura, A., N. Shiba, D. Miyazaki, H. Nishizawa, Y. Inaba, N. Fueki, R. Maruyama, Y. Echigoya, and T. Yokota. 2017. "Comparison of the phenotypes of patients harboring in-frame deletions starting at exon 45 in the Duchenne muscular dystrophy gene indicates potential for the development of exon skipping therapy." *J Hum Genet* 62 (4):459-463. doi: 10.1038/jhg.2016.152.
- Niks, E. H., and A. Aartsma-Rus. 2017. "Exon skipping: a first in class strategy for Duchenne muscular dystrophy." *Expert Opin Biol Ther* 17 (2):225-236. doi: 10.1080/14712598.2017.1271872.
- Pennings, R. J., H. Te Brinke, M. D. Weston, A. Claassen, D. J. Orten, H. Weekamp, A. Van Aarem, P. L. Huygen, A. F. Deutman, L. H. Hoefsloot, F. P. Cremers, C. W. Cremers, W. J. Kimberling, and H. Kremer. 2004. "USH2A mutation analysis in 70 Dutch families with Usher syndrome type II." *Hum Mutat* 24 (2):185. doi: 10.1002/humu.9259.
- Pierrache, L. H., B. P. Hartel, E. van Wijk, M. A. Meester-Smoor, F. P. Cremers, E. de Baere, J. de Zaeytijd, M. J. van Schooneveld, C. W. Cremers, G. Dagnelie, C. B. Hoyng, A. A. Bergen, B. P. Leroy, R. J. Pennings, L. I. van den Born, and C. C. Klaver. 2016. "Visual Prognosis in USH2A-Associated Retinitis Pigmentosa Is Worse for Patients with Usher Syndrome Type IIa Than for Those with Nonsyndromic Retinitis Pigmentosa." *Ophthalmology* 123 (5):1151-60. doi: 10.1016/j.ophtha.2016.01.021.
- Rutten, J. W., H. G. Dauwerse, D. J. Peters, A. Goldfarb, H. Venselaar, C. Haffner, G. J. van Ommen, A. M. Aartsma-Rus, and S. A. Lesnik Oberstein. 2016. "Therapeutic NOTCH3 cysteine correction in CADASIL using exon skipping: in vitro proof of concept." *Brain* 139 (Pt 4):1123-35. doi: 10.1093/brain/aww011.
- Rutten, J. W., J. Haan, G. M. Terwindt, S. G. van Duinen, E. M. Boon, and S. A. Lesnik Oberstein. 2014. "Interpretation of NOTCH3 mutations in the diagnosis of CADASIL." *Expert Rev Mol Diagn* 14 (5):593-603. doi: 10.1586/14737159.2014.922880.
- Sengillo, J. D., T. Cabral, K. Schuerch, J. Duong, W. Lee, K. Boudreault, Y. Xu, S. Justus, J. R. Sparrow, V. B. Mahajan, and S. H. Tsang. 2017. "Electroretinography Reveals Difference in Cone Function between Syndromic and Nonsyndromic USH2A Patients." *Sci Rep* 7 (1):11170. doi: 10.1038/s41598-017-11679-y.
- Seyedahmadi, B. J., C. Rivolta, J. A. Keene, E. L. Berson, and T. P. Dryja. 2004. "Comprehensive screening of the USH2A gene in Usher syndrome type II and non-syndromic recessive retinitis pigmentosa." *Exp Eye Res* 79 (2):167-73. doi: 10.1016/j.exer.2004.03.005.
- Sirisi, S., M. Folgueira, T. Lopez-Hernandez, L. Minieri, C. Perez-Rius, H. Gaitan-Penas, J. Zang, A. Martinez, X. Capdevila-Nortes, P. De La Villa, U. Roy, A. Alia, S. Neuhaus, S. Ferroni, V. Nunes, R. Estevez, and A. Barrallo-Gimeno. 2014. "Megalencephalic leukoencephalopathy with subcortical cysts protein 1 regulates glial surface localization of GLIALCAM from fish to humans." *Hum Mol Genet* 23 (19):5069-86. doi: 10.1093/hmg/ddu231.
- Slijkerman, R. W., F. Song, G. D. Astuti, M. A. Huynen, E. van Wijk, K. Stieger, and R. W. Collin. 2015. "The pros and cons of vertebrate animal models for functional and therapeutic research on inherited retinal dystrophies." *Prog Retin Eye Res* 48:137-59. doi: 10.1016/j.preteyeres.2015.04.004.
- Slijkerman, R. W., C. Vache, M. Dona, G. Garcia-Garcia, M. Claustres, L. Hetterschijt, T. A. Peters, B. P. Hartel, R. J. Pennings, J. M. Millan, E. Aller, A. Garanto, R. W. Collin, H. Kremer, A. F. Roux, and E. Van Wijk. 2016. "Antisense Oligonucleotide-based Splice Correction for USH2A-associated Retinal Degeneration Caused by a Frequent Deep-intronic Mutation." *Mol Ther Nucleic Acids* 5 (10):e381. doi: 10.1038/mtna.2016.89.

- Smith, R. J., C. I. Berlin, J. F. Hejtmancik, B. J. Keats, W. J. Kimberling, R. A. Lewis, C. G. Moller, M. Z. Pelias, and L. Tranebjaerg. 1994. "Clinical diagnosis of the Usher syndromes. Usher Syndrome Consortium." *Am J Med Genet* 50 (1):32-8. doi: 10.1002/ajmg.1320500107.
- Sorusch, N., K. Bauss, J. Plutniok, A. Samanta, B. Knapp, K. Nagel-Wolfrum, and U. Wolfrum. 2017. "Characterization of the ternary Usher syndrome SANS/*ush2a*/whirlin protein complex." *Hum Mol Genet* 26 (6):1157-1172. doi: 10.1093/hmg/ddx027.
- Tucker, B. A., R. F. Mullins, L. M. Streb, K. Anfinson, M. E. Eyestone, E. Kaalberg, M. J. Riker, A. V. Drack, T. A. Braun, and E. M. Stone. 2013. "Patient-specific iPSC-derived photoreceptor precursor cells as a means to investigate retinitis pigmentosa." *Elife* 2:e00824. doi: 10.7554/eLife.00824.
- Tucker, R. P. 2010. "Expression of usherin in the anthozoan *Nematostella vectensis*." *Biol Bull* 218 (2):105-12. doi: 10.1086/BBLv218n2p105.
- Vache, C., T. Besnard, P. le Berre, G. Garcia-Garcia, D. Baux, L. Larrieu, C. Abadie, C. Blanchet, H. J. Bolz, J. Millan, C. Hamel, S. Malcolm, M. Claustres, and A. F. Roux. 2012. "Usher syndrome type 2 caused by activation of an *USH2A* pseudoexon: implications for diagnosis and therapy." *Hum Mutat* 33 (1):104-8. doi: 10.1002/humu.21634.
- Westerfield, Monte. 2007. *The Zebrafish Book: A Guide for the Laboratory Use of Zebrafish Danio ("Brachydanio Rerio")*: University of Oregon.
- Wouters, M. A., I. Rigoutsos, C. K. Chu, L. L. Feng, D. B. Sparrow, and S. L. Dunwoodie. 2005. "Evolution of distinct EGF domains with specific functions." *Protein Sci* 14 (4):1091-103. doi: 10.1110/ps.041207005.
- Yan, D., and X. Z. Liu. 2010. "Genetics and pathological mechanisms of Usher syndrome." *J Hum Genet* 55 (6):327-35. doi: 10.1038/jhg.2010.29.
- Yurchenco, P. D., and Y. S. Cheng. 1993. "Self-assembly and calcium-binding sites in laminin. A three-arm interaction model." *J Biol Chem* 268 (23):17286-99.
- Zou, J., L. Luo, Z. Shen, V. A. Chiodo, B. K. Ambati, W. W. Hauswirth, and J. Yang. 2011. "Whirlin replacement restores the formation of the *USH2* protein complex in whirlin knockout photoreceptors." *Invest Ophthalmol Vis Sci* 52 (5):2343-51. doi: 10.1167/iovs.10-6141.

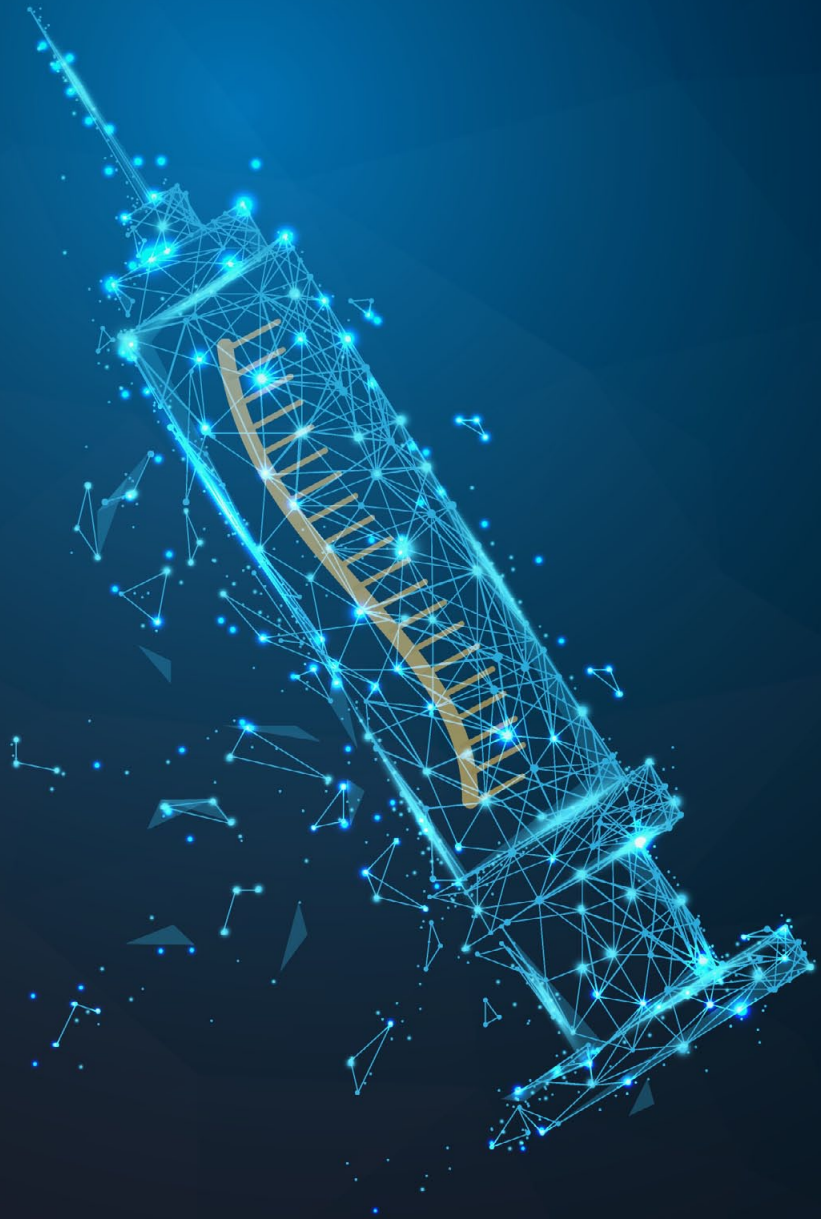
SUPPLEMENTAL FIGURES



Supplemental Figure 1. Evaluation of the *ush2a* exon 13 skipping potential of different PMOs. (A-C) PMOs that are able to induce *ush2a* exon 13-skipping are marked with a black bar. Transcripts with a wild-type splicing pattern lead to a PCR product of 1096 nucleotides and *ush2a* Δ exon 13 transcripts to a PCR product of 448 nucleotides. PMO-N1, PMO-P2 and PMO-P3 (indicated with a black bar) show a significant exon 13 skipping potential after injection in zebrafish embryos. The PMO-P3 (4 ng) sample was run twice on the agarose gel. RT-PCR analysis of the PMO-N1 (2 ng) sample failed for technical reasons. Injection of PMO-N2, PMO-N3 and PMO-P4 did not result in a significant skipping of *ush2a* exon 13. Efficacy of PMOs N1 and N2 was tested at 3 days post injection. The effect of PMO-N3, PMO-P2, PMO-P3 and PMO-P4 was evaluated at 5 days post injection. mQ: negative (water) control.

Chapter 5

General Discussion And Future Perspectives



ADDRESSING DEFECTS IN *USH2A* TO TREAT USHER SYNDROME OR NON-SYNDROMIC RETINITIS PIGMENTOSA

It is devastating to lose both the auditory and visual senses as it will significantly reduce a person's ability to perceive the world. Hearing aids and cochlear implants can partially compensate for severe to profound hearing impairment, but so far vision loss caused by progressive retinal degeneration as a consequence of retinitis pigmentosa (RP) is untreatable in patients with Usher syndrome. The development of therapeutic strategies will therefore have a large impact on patients and society. As mutations underlying Usher syndrome are most frequently found in *USH2A* (McGee et al. 2010) and mutations in *USH2A* are also the most frequent cause of non-syndromic RP (nsRP) (Seyedahmadi et al. 2004), the research described in this thesis focused on the development of a potential treatment option for *USH2A*-associated disease. To do so, the zebrafish is extensively used to model *USH2A*-associated retinal dysfunction (**chapter 2b**), to further unravel the function of the USH2 protein complex by isolation of *in vivo*-assembled Usher syndrome-associated protein complexes (**chapter 2c**) and to develop and validate a therapeutic exon skipping strategy targeting *USH2A* transcripts (**chapter 3 and 4**). These studies provide a better understanding of the role of USH2 proteins, such as usherin, in the retina and attempt to lay a solid foundation to delay retinal degeneration in patients in the future. In this chapter, the impact of the studies in this thesis will be discussed as well as future challenges.

IMPROVEMENTS IN GENETICALLY DIAGNOSING PATIENTS WITH USHER SYNDROME

Patients with Usher syndrome type 2a are born hearing impaired and usually fail the Newborn Hearing Screening Test. The first clinical signs of RP become apparent around puberty and therefore the clinical diagnosis of Usher syndrome is eventually made in the third decade of life at a mean age of 26 years (Pierrache et al. 2016). However, due to the introduction of genetic screening for hearing impairment in out-patient-clinics over the past decades, patients with Usher syndrome are nowadays often diagnosed before the onset of the retinal phenotype. A genetic diagnosis early in life is important as it will provide patients with a general understanding of the disease and as such will provide a prognosis for future functioning. Also other family members might benefit from a genetic diagnosis in their family planning. Furthermore, genetic therapies are developed for specific genetic defects and therefore knowledge of the genotype could make patients potentially eligible for treatment. In addition, the identification of pathogenic mutations in novel or known genes could result in the development of therapeutic op-

tions, since existing treatment options could be redirected to newly identified mutations and genes. Currently, the underlying genetic cause of disease is most often identified by sequencing the coding regions of a patient's genome, referred to as 'exome sequencing'. By exome sequencing the underlying genetic defect is identified in approximately 63% of patients with RP (Haer-Wigman et al. 2017), and in 33.5% of patients with hearing impairment (Zazo Seco et al. 2017). For patients with USH, exome sequencing results in approximately 70 to 75% of the cases in a genetic diagnosis (Krawitz et al. 2014, Besnard et al. 2014). This percentage can be increased to 93 when combining exome sequencing with analyzing copy number variations, as observed in a cohort of Usher syndrome cases (Bonnet et al. 2016). However, the remaining 7% of Usher syndrome patients require an alternative strategy to identify the underlying genetic defect. Future genetic diagnostics should therefore include the analysis of intronic and regulatory sequences by using whole genome sequencing and transcript analysis.

Whole genome sequencing (WGS) will play a more and more important role in future DNA diagnostics to also identify deep-intronic mutations. These mutations could be ideal candidates for an AON-based splice redirection therapy, as was demonstrated for the *USH2A* c.7595-2144A>G mutation in this thesis (**chapter 3b**). Currently, the high costs prevent the application of genome sequencing in routine DNA diagnostics. However, this might change as costs have been continuously decreased during the last decade, driven by the ongoing rat-race for the first '\$1000 dollar genome' (Mardis 2006, Park and Kim 2016). Once financially feasible, the extraction of the underlying genetic defect from all benign intronic variants will raise another limitation for the applicability of genome sequencing. The pathogenicity of genetic variants that lead to alterations in amino acid sequence (e.g. missense variants) or in expression levels (e.g. nucleotide variants in regulatory sequences) can be addressed by *in vitro* cell-based assays or require the generation of a model organism containing the variant to evaluate the impact on a functional level. On the other hand, splice-modulating variants, that result in a (partial) skipping of exons or in the incorporation of a pseudoexon, can be identified by transcriptome sequencing. In order to analyze *USH2A* pre-mRNA splicing, it is essential to have access to cells that express the gene. As patient-derived photoreceptors and hair cells cannot be extracted without causing permanent damage, there is a high need for alternative assays and cellular models to analyze the effects of potential splice-interfering variants *in vitro*.

In **chapter 3b**, we used patient-derived fibroblasts to analyze the effect of the deep-intronic c.7595-2144A>G mutation on *USH2A* pre-mRNA splicing, despite the extremely low level of *USH2A* expression in these cells. A more robust expression of *USH2A* can be obtained by dedifferentiating patient-derived fibroblasts or blood cells into induced pluripotent stem cells (iPSCs). Subsequently, *USH2A* expression is further increased when iPSCs are differentiated into photoreceptor-like cells, but this is

a labor-intensive and time-consuming process. Alternatively, splicing can be analyzed by cloning midgene vectors that contain, if possible, multiple exons and introns of the same gene (Sangermano et al. 2018) (**chapter 3b and 3c**). In conclusion, extending DNA diagnostics by WGS in combination with transcript analysis will expand the mutational spectrum of *USH2A* by the identification of novel deep-intronic splice-modulating variants, which can be targets for an AON-based splice correction therapy.

ZEBRAFISH AS A MODEL TO STUDY THE FUNCTION OF USH2 PROTEINS

Zebrafish as an animal model to study USH2A-associated retinitis pigmentosa

Wild-type and knock-out mice have been pivotal in understanding the role of Usher proteins in the inner ear (overview in **chapter 1**). The retina of mice deficient for genes associated with Usher syndrome type 2, however, is generally only mildly affected. Studying retinal dysfunction as a consequence of defects in *USH2A*, therefore requires different models. As the human retina is a highly specialized tissue with many different cell-types, mimicking retinal architecture in a dish is challenging. Furthermore, iPSC-derived photoreceptors are currently not yet perfectly suited to study the function of usherin, as they have an underdeveloped outer segment, connecting cilium and periciliary region. Additionally, the lack of supporting cells prevents the formation of a mature retina using iPSC-derived photoreceptors, which makes these cultures unsuitable to use in functional assays such as electroretinogram (ERG) measurements at this point. Therefore, we used the zebrafish retina to study the effect of usherin depletion. The zebrafish is an attractive model organisms to study the effect of mutations in *ush2a* at the level of retinal function, since photoreceptor anatomy is highly similar in man and zebrafish (reviewed in **chapter 2a**). Also, usherin is highly conserved between zebrafish and man (**chapter 2b**). Various other benefits that underline the suitability of the zebrafish to study inherited retinal dystrophies are described after comparing all vertebrate animal models used in retinal research (**chapter 2a**). However, the capacity of zebrafish to regenerate damaged cells and tissues is a disadvantage for studying a progressive retinal degenerative disorder (**chapter 2b**). Blocking the regeneration in zebrafish might induce a progressive retinal phenotype. For this reason, two temperature-sensitive mutant zebrafish that have been classified as regeneration deficient, *nightcap (ncp)* or *no blastema (nbl)*, could potentially be used (Poss et al. 2002, Makino et al. 2005). These two mutant zebrafish were shown to lack cone photoreceptor regeneration upon light damage after a temperature shift. Alternatively, other organisms such as pigs, sheep, cats, dogs or non-human primates that are used to study inherited retinal dystrophies (**chapter 2a**) (Mowat et al. 2017, Ikeda et al. 2018, Ross et al. 2012, Rah et al. 2005),

without the ability to regenerate photoreceptors, could be used for studying the long-term effect of *USH2A* mutations. Although progressive retinal degeneration might be prevented by its regenerative capacities, the zebrafish is still an excellent model to study the pathogenesis underlying *ush2a*-associated retinal dysfunction (**chapter 2b**).

Functions of the *USH2* interactome

The specific loss of the intracellular region of usherin leads to a reduced visual function in zebrafish as determined by ERG recordings, even when the extracellular region of usherin is still anchored and present at the proper subcellular location (*ush2a*^{b1245} mutant zebrafish) (**chapter 2b**). Apart from the suggested structural role for usherin in maintaining the proper spacing between the apical inner segment and the connecting cilium, together with ADGRV1 (Maerker et al. 2008), our data indicate that the intracellular region of usherin has an additional function. The localization of whirlin, one of the key organizers of the Usher protein complex at the photoreceptor periciliary membrane, depends on the presence of the intracellular region of usherin in photoreceptors of both zebrafish (**chapter 2b**) and mouse (Yang et al. 2010). As loss of function mutations in *USH2A* probably also result in the absence of whirlin at specific subcellular regions of the human photoreceptor, unraveling the function(s) of whirlin is likely instrumental in understanding the underlying pathogenic mechanisms of retinal degeneration in Usher syndrome type 2 and may lead to the development of novel mechanism-based therapeutic strategies.

One way to unravel the molecular function of whirlin is the identification of novel interacting proteins. These interactors can potentially be used as biomarkers for monitoring disease progression or assessing future therapeutic efficacy. Previous research aiming on the dissection of the Usher interactome used conventional cell-based co-purification assays or pull-down techniques (Kremer et al. 2006, Reiners et al. 2006, Bauss et al. 2014, Boldt et al. 2016, Sorusch et al. 2017). However, the cells that were generally used, such as HEK293T, lack the expression of photoreceptor-specific proteins. As such, these previous assays could have missed important clues for photoreceptor-specific functions. Pull-down experiments using retinal lysates can detect interactions with retina-specific proteins, but fail to detect *in vivo*-assembled protein modules. To address previous shortcomings and to expand the whirlin interactome in the retina, we generated a transgenic zebrafish that expresses Strep/FLAG-tagged Whrna (SF-Whrna) in photoreceptors. We used the eyes of this zebrafish for the isolation of *in vivo*-assembled SF-Whrna-associated protein complexes (**chapter 2c**). This approach yielded Preso1 (encoded by *FRMPD4*), LRRC8-channel subunits and Kir2.3-channel subunits as novel Whrna-associated candidate interaction partners.

Preso1 points towards a role in α -transducin translocation. It has been reported that the retina of whirlin knock-out mice contains an elevated threshold, from 200 lux

to 700 lux light intensity, for the light-dependent translocation of α -transducin from the outer to the inner segment of rod photoreceptors (Tian et al. 2014). The retention of α -transducin in the outer segment under light conditions is believed to result in the observed photoreceptor degeneration in these mice, as well as in mice lacking myosin VIIa (Tian et al. 2014). Transducin, a heterotrimeric G-protein consisting of an α , β and γ subunit, is essential in the visual cycle. The inactive α -subunit (α -transducin) binds GDP and interacts with the other two subunits for anchoring in the outer segment disk membrane (Slepek and Hurley 2008). Light-activated rhodopsin activates α -transducin by inducing the conversion of GDP to GTP. Subsequently, α -transducin is released from the other subunits and activates phosphodiesterases (PDEs). In the wild-type mouse retina, bright light stimulation leads to the accumulation of 90% of activated α -transducin in the inner segment of rods within ten minutes of light exposure, possibly to alleviate the rods from light sensitivity and metabolic stress (Tian et al. 2014, Sokolov et al. 2002). The subsequent deactivation of α -transducin is considered to be the activating step that will heterotrimerize α -, β - and γ -transducin and relocate the complex to the membrane of outer segment disks (Slepek and Hurley 2008, Lobanova et al. 2007). Therefore, the increased light intensity threshold for α -transducin translocation in the whirler mouse retina may be indicative for an impaired deactivation of α -transducin. Preso1, identified as a direct interaction partner of whirlin, directed our attention to the GAP-inhibiting protein G protein signaling modulator 2 (GPSM2, also known as LGN). In the inner ear, GPSM2 is an interaction partner of both whirlin and Preso1 and known to be essential for stereocilia elongation (Mauriac et al. 2017). Interestingly, GPSM2 is also present in the rod inner segment where it sequesters inactive α -transducin (Kerov, Natochin, and Artemyev 2005). These studies indicate that whirlin, Preso1 and GPSM2 may act as regulatory complex of inactive α -transducin by preventing reallocation to the outer segment disk membrane under bright light conditions. Based on our findings, a similar retinal phenotype as observed in patients with Usher syndrome type 2 might occur in individuals with mutations in *GPSM2* or *FRMPD4*. However, patients with mutations in *FRMPD4* have not been described to display retinal defects and mutations in *GPSM2* have only been reported in patients clinically diagnosed with Chudley-McCullough Syndrome (OMIM: 609245), of which typical features include congenital sensorineural hearing loss and complex brain malformations, without retinal degeneration. The oldest patient described with mutations in *GPSM2* was at an age of 26 years when undergoing the clinical examinations (Doherty et al. 2012). Potential retinal dysfunction as a consequence of *GPSM2* mutations may become apparent later in life. To determine whether or not murine *Frmpd4* is essential for the maintenance of photoreceptors, it would be essential to analyze the retina of *Frmpd4* knock-out mice for α -transducin cycling defects and signs of retinal degeneration after treatment of a similar lighting regime (>700 lux light intensity) as the whirler mouse model by Tian *et al.* (2014). In conclusion,

our result that whirlin is able to directly interact with Preso1 points towards a possible function of whirlin, Preso1 and GPSM2 in the deactivation of α -transducin in rods.

Studying the direct interaction between whirlin and Kir2.3 might well provide a better understanding of and how whirlin is involved in the regulation of vesicle docking at the base of the photoreceptor connecting cilium (**chapter 2c**), as has been suggested by others (Maerker et al. 2008, Sorusch et al. 2017, Overlack et al. 2011). Kir2.3 is a voltage-gated potassium channel that transports extracellular potassium into the cell (Hibino et al. 2010). The presence of Kir2.3 in the cell membrane is balanced by the amount of Kir2.3-containing vesicles that is allowed to dock and by the amount of Kir2.3 that is again retrieved from the target membrane. At the target membrane, the docking process is regulated by TIP-1, which prevents the docking of Kir2.3-containing vesicles, and a complex of CASK and LIN7C to accept these vesicles (Yan et al. 2009). Dark-adapted photoreceptors have a continuous influx of sodium ions via cGMP-dependent Na^+ -channels (Trudeau and Zagotta 2003). To counteract this influx, sodium ions are actively pumped out of the photoreceptor by Na^+/K^+ -channels (encoded by the *SLC24* gene family, reviewed by Schnetkamp et al. 2014), thereby inducing an influx of K^+ ions. Upon light-induced activation of the visual cycle, cGMP is converted into GMP which induces the closure of cGMP-dependent Na^+ -channels. As a consequence, the photoreceptor membrane hyperpolarizes, since the still open K^+ -channels result in a decrease of the intracellular K^+ concentration. An equilibrium in the K^+ concentration may be reached by an upregulation of inwardly rectifying Kir2.3-channels in the outer membrane of light-adapted photoreceptors. We hypothesize that the latter process is organized by a protein complex containing at least whirlin, CASK and LIN7C (**chapter 2c**). Future studies analyzing the dark/light-associated membrane shuttling of Kir2.3 could possibly elucidate whether or not Kir2.3-channels play a role in balancing the potassium concentration in light-adapted rods and unravel the potential regulatory function of whirlin as anchor for the upregulation of Kir2.3 expression at the membrane.

GENE EDITING

CRISPR/Cas9 technology

Editing genomic DNA by altering the nucleotide sequence has been pivotal in studying a broad spectrum of human diseases by the generation of cellular and animal models. Patients would benefit from genome editing when the underlying mutation could be repaired *in vivo* or when the technique is used to evaluate variants of unknown pathogenicity that are discovered in exome sequencing or WGS efforts. For instance, the long debate about the contribution of a *Pde6b* nucleotide variant and/or a viral intronic insertion to the retinal phenotype in the *rd1* mouse model has recently come

to an end after using a CRISPR/Cas9 approach to independently repair either of the two potentially causative variants (Wu et al. 2016). Several targeted genome modification methods have been developed in the past years, such as homologous recombination, transcription activator-like effector nucleases (TALENs) and Zinc-finger nucleases (ZFNs). These methods are generally difficult to use due to their complex design and their dependence on specific sequence motifs (described in **chapter 2a**). The introduction of the clustered regularly interspaced short palindromic repeats (CRISPR)/Cas9 system has positively changed the ease of genome editing (Cong et al. 2013). The system is capable of inducing DNA double strand breaks (DSBs) in a targeted manner (**Fig. 1**) and introduces mutations with an unprecedented ease and efficiency. The introduction of this system marks the beginning of a booming era of genome editing (Jinek et al.

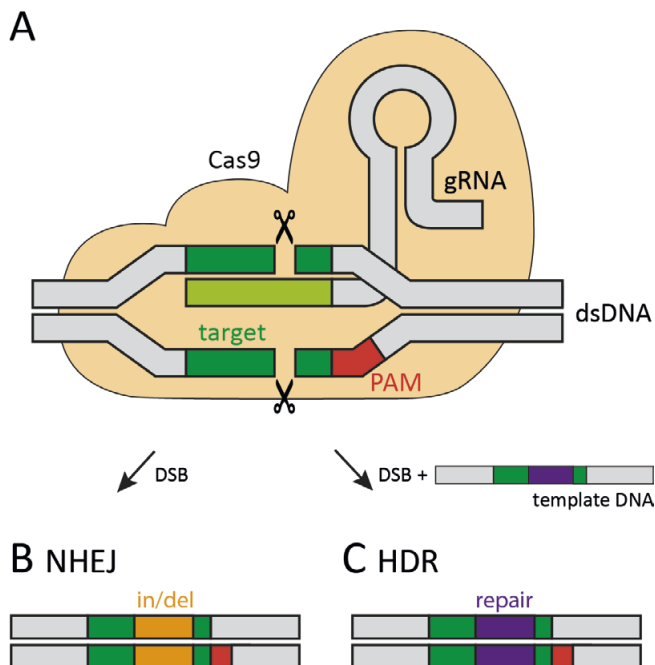


Figure 1. Schematic overview of the CRISPR/Cas9 complex bound to DNA. (A) Cas9 (indicated in brown color) is the endonuclease that can induce a double strand break (DSB). To direct Cas9 to the target DNA (in green), a guide RNA (gRNA) that binds Cas9 and that is complementary to the target DNA is essential. In addition, the protospacer adjacent motif (PAM, indicated in red) is necessary for Cas9 to bind and cleave the target DNA sequence. Upon a DSB, there are two major natural DNA repair mechanisms to fuse the two DNA-ends together. **(B)** Non-homologous end joining (NHEJ) directly ligates the two DNA ends and potentially results in the introduction of small insertions or deletions (in/del). **(C)** Alternatively, homology-directed repair (HDR) uses a template DNA sequence that is either present on the second allele or supplemented to the CRISPR/Cas9 components to precisely repair the broken DNA strands (repair). Figure adapted from: <https://commons.wikimedia.org/wiki/File:GRNA-Cas9.png>.

2012, Cong et al. 2013, Jinek et al. 2013, Cho et al. 2013). The CRISPR/Cas9 technology has been extensively used in the research presented in this thesis to generate zebrafish models for *ush2a* (**chapters 2b** and **4c**), but also holds great promise for a clinical use. Currently, however, the two major hurdles for a clinical application of CRISPR/Cas9 are potential off-target DNA editing and the low efficiency of homology-directed gene repair in differentiated cells. Recent developments to address these issues, in addition to what has already been described in **chapter 2a** and **4c**, will be discussed in more detail in the following sections.

Reduction of CRISPR/Cas9-induced off-target effects

Efforts are ongoing to design gRNAs that lead to reduced off-target binding without affecting on-target effects, such as reducing the length of gRNAs (Fu et al. 2014), the addition of two G-nucleotides to the 5' end of a gRNA (Cho et al. 2014), the development of off-target prediction software based on sequence similarity to other genomic sequences (Doench et al. 2016) or the use of 'nickases' and derivatives thereof (Ran et al. 2013). To further reduce off-target binding of Cas9, both the labs led by Keith Young and Feng Zhang have experimentally optimized the Cas9 protein by mutating the amino acids that have been identified in being responsible for non-specific Cas9-DNA binding (Kleinstiver et al. 2016, Slaymaker et al. 2016). Further research revealed that it was not the weakened binding to DNA that increased the specificity of Cas9 to induce double strand breaks (DSBs), but that the proofreading domain REC3 in Cas9 triggers a state of inactivity upon mismatches (Chen et al. 2017). By exploiting this knowledge, a hyper-accurate Cas9 variant (HypaCas9) was created that contains an improved proofreading capacity with even less off-target effects while not reducing on-target efficiency (Chen et al. 2017). Simultaneously, other endonucleases that are similar to Cas9 have been discovered, such as smaller Cas9 variants or Cpf1 (Ran et al. 2015, Zetsche et al. 2015). Reduction of the levels of off-target editing by combining the optimizations on gRNA design and endonucleases might improve the applicability of *in vivo* gene editing as a future therapeutic strategy.

Low HDR-based repair efficiencies hamper clinical use of CRISPR/Cas9-mediated gene repair

Endonucleases, such as Cas9, induce a DSB that is repaired by DNA repair mechanisms. Subsequently, the DSB is generally repaired by either non-homologous end joining (NHEJ)-based repair that results in small insertions or deletions or homology directed repair (HDR) that results in the precise repair of the damaged DNA strand by using a donor sequence as template. However, post-mitotic cells generally do not depend on HDR to repair a DSB, but rather use NHEJ-mediated DNA repair. *In vivo* DNA repair mechanisms in photoreceptors are not extensively studied. As photoreceptors

are fully differentiated, non-dividing cells, it can be expected that HDR-based gene repair in photoreceptors may not be as straightforward as observed in mitotic cells *in vitro*. The first study using CRISPR/Cas9-mediated correction of a mutation underlying Usher syndrome has recently been published (Fuster-Garcia et al. 2017). However, only 1.7% of the *USH2A* alleles in patient-derived fibroblasts containing the c.2299delG mutation was repaired. These results illustrate that an *in vivo* repair of this mutation in non-dividing photoreceptors will most probably be difficult and highly inefficient. Furthermore, differences between species could have to be taken into account when translating results derived from animal models to man. In contrast to the human retina, in which the lens and cornea filter UV-light, mice have a fourth cone type that is sensitive for UV light. As a consequence, the murine retina is exposed to elevated levels of UV-light compared to humans and therefore potentially needs more active DNA repair mechanisms (Yanik et al. 2017). Taking into account that gene editing relies on HDR-mediated DNA repair, *in vivo* validated lab-results using murine retinas could therefore overrepresent the efficiency of gene repair as would be obtained when applied to the human retina. However, also in rat photoreceptors Suzuki and colleagues were not able to knock-in a DNA sequence of interest using a homology template construct after introduction of a DSB, despite the presence of UV-sensitive cones in the rat retina (Suzuki et al. 2016). When using an adapted donor vector that contains homology-independent targeted integration (HITI)-sites, the authors were able to generate a NHEJ-dependent method for a targeted genomic sequence integration in retinal cells. Using this method, the missing exon 2 of *Mertk* could be successfully inserted at the right position in the genome of photoreceptors of the Royal College of Surgeons rat to avoid RP from manifesting (Suzuki et al. 2016). Future clinical applications of genome editing in retinal cells therefore potentially need to rely on an NHEJ- instead of an HDR-mediated strategy for efficient DNA repair.

Alternative strategies using CRISPR/Cas9 to potentially treat Usher syndrome

Besides precisely repairing a mutation, disruption of a dominant pathogenic allele could already alleviate the phenotype. However, applications for Usher syndrome seem to be limited due to the recessive inheritance pattern of the disease. Nevertheless, part of the retinal phenotype in patients with Usher syndrome might be caused by ER-stress as a consequence of misfolded proteins due to missense mutations (Tucker et al. 2013). Silencing of the corresponding pathogenic allele might therefore potentially circumvent ER-stress-induced apoptosis of photoreceptors. Dominant mutations in *RHO* are a common cause of RP (8-10%) (Latella et al. 2016), in which photoreceptor degeneration due to ER-stress plays an important role in the clinical manifestation (Comitato et al. 2016). Lower levels of rhodopsin expression do not lead to haploinsufficiency, thereby

making it possible to use CRISPR/Cas9 to disrupt the mutated allele without the need for an additional gene augmentation strategy (Bakondi et al. 2016). Both a mouse and rat model containing dominant mutations in *Rho* (S334* in rat and P23H in mouse) were protected from retinal degeneration after *in vivo* treatment (Bakondi et al. 2016, Latella et al. 2016). The same strategy has been performed to silence a dominant allele for *KRT12* in mice, in which the mutation creates a PAM site that was used for allele-specific targeting of the Cas9 (Courtney et al. 2016). Gene disruption of pathogenic *USH2A* alleles that induce ER-stress might therefore be part of a future therapeutic approach to treat Usher syndrome when future gene augmentation strategies allow this for *USH2A*.

Alternatively, future applications of CRISPR/Cas9-based editing might not only be applied to DNA, but rather focus on transcripts. Editing of transcripts circumvents the generation of potential off-target mutations in the genome with a long-lasting effect, since any off-target effects on RNA level will be transient as they will be 'washed out' by newly generated transcripts. Consequently, life-time administration is required, which enables the clinician to optimize dosage regimes to yield sufficient amounts of repaired transcripts. Cas9 can be directed to target RNA molecules by addition of a PAMmer that introduces a protospacer adjacent motif (PAM) *in trans* (Nelles et al. 2016). More recently, an endogenous RNA endonuclease family (Cas13a (also known as C2c2), Cas13b, Cas13c and Cas13d) has been identified, functionally similar to Cas9 or Cpf1 (Abudayyeh et al. 2016, Shmakov et al. 2017, Smargon et al. 2017, Yan et al. 2018, Konermann et al. 2018). RNA editing can also be achieved by coupling the RNA editing enzyme Adenosine Deaminase Acting on RNA (ADAR2) to an inactive ('dead') Cas13b, which circumvents the need for an RNA sequence protospacer flanking site (PFS, similar to PAM in DNA) motif. ADAR2 deaminates adenosine into inosine, the latter being functionally similar to guanosine, and is therefore more specific (Cox et al. 2017). Collectively, these studies highlight the feasibility of RNA editing as future alternative to repairing mutations at the level of DNA.

AON-INDUCED SPLICE REDIRECTION

AONs as splice modulating molecules

Gene editing or gene augmentation seem promising therapeutic strategies for several hereditary disorders, but are not yet readily available for clinical application to treat patients with Usher syndrome type 2a. Next to the previously mentioned limitations for gene editing, the large protein coding sequence of *USH2A* currently hampers a gene augmentation strategy. Full length *USH2A* cDNA (15.6 kb) exceeds by far the 4.7 kb cargo capacity of currently available therapeutic AAV vectors. To develop a treatment for the near future, we focused on splice modulation. Others have demonstrated that

splicing can be redirected by application of either antisense oligonucleotides (AONs), other small molecules or modified proteins (Pagliarini, La Rosa, and Sette 2017). Small molecules can, for instance, stabilize the binding of splice factors to the 5' splice site of *SMN2* exon 7 and thereby efficiently induce exon inclusion (Woll et al. 2016). Similarly, when modifying exon-specific U1 snRNAs (ExSpe U1s), the same result could be achieved (Dal Mas et al. 2015). However, the ease of design by following existing *in silico* guidelines make AONs easily adaptable for many target transcripts and AONs are therefore the preferred splice-modulating molecules (Aartsma-Rus 2012, Aartsma-Rus et al. 2009). AONs can be therapeutically used in two ways (Scotti and Swanson 2016). First, upon binding to mRNA, an RNase-mediated degradation of the targeted mRNA molecule can be induced. Secondly, AONs can bind to pre-mRNA and thereby block certain motifs from being recognized by the spliceosome. Depending on the sequence motif that is targeted, AONs result in the skipping or inclusion of exons from or in the mature transcript, respectively.

Usher syndrome is a recessively inherited disease which holds an advantage for splice modulation therapy. Correction of only part, presumably half or less, of the transcripts is already expected to prevent or halt the progression of the phenotype. Therefore, besides patients that are homozygous for the *USH2A* c.7595-2144A>G mutation or mutations in *USH2A* exon 13, also patients that are compound heterozygous for these mutations are eligible for an AON-based PE40 or exon 13 exon-skipping treatment, increasing the population that could benefit from one therapy.

Future clinical evaluation of retinal AON treatment

The clinical development of AONs targeting *USH2A* PE40 (**chapters 3B and 3C**) or *USH2A* exon 13 (**chapter 4**) could potentially benefit from the experiences of clinical studies using a similar approach. Splice-modulating AONs have been evaluated for the treatment of Duchene muscular dystrophy (DMD) and spinal muscular dystrophy (SMA). Currently, for both diseases AON treatments have obtained market authorization. Eteplirsen (Exondys51, Sarepta Therapeutics), a phosphorodiamidate morpholino oligomer (PMO) was approved for treating DMD in the U.S.A. in September 2016 (Lim, Maruyama, and Yokota 2017, Aartsma-Rus and Krieg 2017), while in Europe Eteplirsen is currently under review at the European Medicines Agency (EMA) ¹. Nusinersen (Spinraza, Biogen), a 2'-O-methoxyethyl (2'OMOE) phosphorothioate-modified AON, was allowed to treat SMA in both the U.S.A. (December 2016) and Europe (April 2017) (Ottesen 2017, Press release EMA 2017 ²). An exon skipping AON similar to Eteplirsen, named Dris-

1 <https://muscular dystrophy news.com/2017A/01/03/chmp-reviewing-etepilrsen-as-duchenne-muscular-dystrophy-treatment-in-europe/>

2 First medicine for spinal muscular atrophy: http://www.ema.europa.eu/docs/en_GB/document_library/Press_release/2017/04/WC500226270.pdf

apersen and based on a 2'OMe PT backbone, was rejected for market approval by the Food and Drug Administration (FDA) in early 2016 due to the lack of substantial clinical benefit. This led to questions on the design of the trial (Hoffman and McNally 2014). The primary outcome measurement in this trial was the distance that DMD patients walked during a six-minute walking test. Mainly older individuals were included in the trial, as it was anticipated that these individuals could potentially show a larger improvement during the six-minute walking test (Hoffman and McNally 2014). However, muscle cells in patients degenerate and are replaced by fibrofatty tissue. As younger patients still have a larger amount of myofibers, they are probably more suitable to determine the effectiveness of a treatment (Merlini and Sabatelli 2015). Similar to the irreversible degeneration of muscle fibers in DMD patients, also degenerated photoreceptors in patients with *USH2A*-associated retinal degeneration will not be restored upon splice redirection therapy. The best clinical effect can therefore be expected when initiating treatment in an early or even pre-symptomatic stage of the disease to prevent photoreceptors from degenerating.

The amount of usherin that results from splice redirection treatment cannot be directly quantified in the patient's retina. Similar difficulties have been observed in the design of clinical studies that analyzed the effect of *DMD* splice correction in muscle tissue. Also, several semi-quantitative methods have been used, such as western blotting of the large dystrophin protein (427 kDa) or immunofluorescence analysis of tissue, that made the comparison of different experiments challenging (Merlini and Sabatelli 2015). Future evaluations should therefore make use of more sophisticated methods of imaging and analysis of patient-derived material, such as mass spectrometry or other quantitative techniques (Merlini and Sabatelli 2015). But, protein levels alone are not always directly correlated to disease progression as became apparent when two Eteplirsen treated patients lost their ability to walk despite of an observed consistent increase in dystrophin-positive fibers (Merlini and Sabatelli 2015, Mendell et al. 2013). Instead of a six minute functional walking test for DMD patients, researchers pointed out that the primary outcome measurement to analyze treatment efficacy should be focused on monitoring cell defects and the underlying pathomechanism of disease (Aartsma-Rus 2014, Merlini and Sabatelli 2015). Evaluation of iPSC-derived photoreceptors containing defects in *USH2A* pointed towards a possible increase in ER stress as a consequence of protein accumulation (Tucker et al. 2013). Thioflavin T, a fluorescent dye that binds protein aggregates and is otherwise known as Pittsburgh Compound-B, is already used to image plaque formation in patients with Alzheimer's disease (Cai, Innis, and Pike 2007) and could therefore potentially also be employed as *in vivo* monitor of retinal ER-stress (Beriault and Werstuck 2013).

Novel readouts for photoreceptor functioning could also be determined by studying the identified interaction partners of the *USH2* proteins. In **chapter 2c** we found

novel whirlin-interaction candidates (Preso1, Kir2.3 and LRRC8-channels) that may have a function in the homeostasis of K^+ -ions or other molecules. We and others already demonstrated that whirlin and usherin are mutually dependent on each other for their localization at the photoreceptor periciliary membrane (**chapter 2b**) (Yang et al. 2010), making the presence of whirlin at this subcellular compartment a biomarker for proper localization of usherin. In contrast, the *RPE65*-encoded retinal pigment epithelium-specific isomerohydrolase RPE65 is an enzyme that functions in the visual cycle. Patients with mutations in *RPE65* present with severe retinal dystrophies in the form of either Leber congenital amaurosis or early-onset RP (Astuti et al. 2016). Upon *RPE65* gene augmentation therapy, the visual function of these patients could be partially rescued as became clear in an obstacle course (Maguire et al. 2008). Treated patients had an increased ability to navigate through the course, which was indicative for a clinical success. Since photoreceptors in patients with Usher syndrome degenerate slowly, such a visual improvement is probably not to be expected when functional usherin expression is restored. Therefore, a detailed phenotypic analysis of multiple patients, performed by a combination of methods and techniques, could potentially generate an accurate model for the future distinguishment of a therapeutic benefit from the natural course of the disease (Sujirakul et al. 2015, Lambertus et al. 2017).

TREATMENT POSSIBILITIES FOR HEARING IMPAIRMENT IN PATIENTS WITH USHER SYNDROME TYPE 2

Besides retinal degeneration, patients with USH demonstrate congenital progressive hearing impairment. Since the retina is clinically unaffected during childhood, there is likely a window of opportunity for therapeutic intervention and therefore the research in this thesis was mainly focused on prevention of retinal degeneration. Furthermore, there is currently no treatment for *USH2A*-associated RP, whereas hearing aids or cochlear implants can partially compensate for the hearing loss (Hartel et al. 2017). However, these devices are far from perfect. Cochlear implants give a broad spatial neuronal activation due to the limited number and size of the electrodes, leading to poor frequency resolution and poor speech recognition in a noisy environment (Zeng 2017). Therefore, the development of additional treatment options for the inner ear is desired. Once the clinical effect of exon skipping is validated for the retina, it could also be explored as potential treatment for the progressive hearing impairment in patients with Usher syndrome type 2a.

Fibrous-links between stereocilia and between stereocilia and the kinocilium are, among other proteins, made up and anchored by USH1- and USH2-proteins and are essential for normal cochlear development (overview in **chapter 1**). In mice, the cochlea

matures until around postnatal day twenty. Hence, augmentation of USH-associated genes in the immature cochlea of mouse models that are defective for *Ush1c* or *Whrn* rescued hearing when delivered at the first days after birth (Pan et al. 2017, Isgrig et al. 2017). Similarly, vestibular function of a mouse model with defects in *Ush1c* could be restored upon AON-based splice correction at day one after birth (Vijayakumar et al. 2017), whereas the effectiveness of treatment decreased when performed at 4, 5 or 15 days after birth. This coincides with the completion of vestibular hair cell development in mice between postnatal day two and ten (Vijayakumar et al. 2017). The same holds true for the functional rescue of hearing in this mouse model, since preservation of outer hair cell function requires AON treatment before postnatal day five in order to be effective (Ponnath et al. 2018). In contrast, the human cochlea is already mature at birth and hair cells do not regenerate. Therefore, the therapeutic strategies that were employed postnatally in the mouse cochlea, seem not applicable to humans.

Confirming a post-developmental role of usherin in the cochlea will determine whether or not patients with mutations in *USH2A* might benefit from a postnatally applied treatment to halt the progressive deterioration of hearing. Comparing patients with two protein truncating mutations in *USH2A* with patients having one or two missense mutations in this gene demonstrated that hearing impairment in the first group is more severe and progressive, thereby possibly indicating a post-developmental role for usherin (Hartel et al. 2016). However, usherin could not be detected in mature stereocilia of rats when using an antibody against the intracellular region (van Wijk et al. 2006) and also mass spectrometry data from inner and outer hair cells from adult mice did not detect any usherin (Liu et al. 2014). In contrast, usherin-encoding transcripts were identified after RT-PCR analysis using RNA derived from adult rat and mouse cochlear tissue (Huang et al. 2002). This implies that either the smaller usherin isoform A has a function in the adult cochlea, that the protein is present in undetectable amounts or that usherin functions in other cell types than hair cells in the mature cochlea. Indeed, immunohistochemical analysis of the spiral ganglion cells demonstrated the presence of usherin, ADGRV1 and whirlin in the cell bodies of the spiral ganglion neurons in adult rats (van Wijk et al. 2006). As for photoreceptors, dysfunction of neurons in the spiral ganglia as a consequence of mutations in *USH2A* might only become apparent later in life leading to progression of the hearing impairment in patients. Also, a cochlea-specific exon has been identified that encodes an additional 24 amino acids in the intracellular region of usherin, suggesting a cochlea-specific function (Adato et al. 2005). Using the cochlea-specific intracellular domain of usherin to screen for candidate interactors, by for instance yeast two-hybrid screenings using a cDNA library derived from matured cochlea or even spiral ganglion cells, could unravel the post-developmental role of usherin in the cochlea.

In contrast to therapeutic strategies that are applied on matured cells containing a defect in Usher syndrome-associated genes, future stem cell-based therapeutic strategies potentially can replace non-functional hair cells by *in vitro* grown hair cells to reverse the hearing phenotype. However, stem cell-based strategies are under development and currently not ready for clinical application. Both autologous transplantation options as well as allogeneic options are exploited. The first option would be ideal as it will prevent potential immune responses after supplementation. An autologous cell transplant, however, requires repairing the mutation that underlies the hearing impairment before resupplementation. The first human subject has recently been treated by an autologous CRISPR/Cas9-treated T-cell injection in a phase I study against lungcancer (ClinicalTrials.gov Identifier: NCT02793856) (Cyranoski 2016). Although the resupplemented T-cells in this study contained a disruption of the gene coding for the PD-1 protein ("Programmed Death-1") instead of a precisely repaired mutation. For this purpose, patient-derived fibroblasts should be dedifferentiated into iPSCs, repaired and subsequently be differentiated into sensory epithelia prior to be supplemented to the cochlea (Koehler et al. 2013, Oshima et al. 2010). However, besides gene repair and differentiation protocols that have to be optimized, also difficulties in the supplementation of stem cell-based therapies into the cochlea limit the clinical application at present. Reaching the cochlea is difficult and each surgical procedure contains the risk of damaging the delicate membranous labyrinth. Furthermore, supplemented cells should be able to mature and integrate into the existing neuronal network *in situ* without the risk of developing into tumorous tissues. Other than the supplementation of stem cells, research focuses on activating the regenerative capacity in man that, for instance, has been observed in avian hair cells. Quiescent murine supporting cells could be activated to develop into hair cells upon supplementation of mice cochlear explants devoided of hair cells with a cocktail of small molecules (McLean et al. 2017). Since these regenerated cells still contain the underlying genetic defect, also regeneration strategies have to be combined with gene repair.

AONs have a demonstrated capacity to prevent *USH2A*-associated retinal dysfunction (**chapter 4**) and would therefore be a logical first choice to also apply in the inner ear as treatment. The cochlea is protected from the systemic blood circulation by endothelial cells in the stria vascularis that are connected by tight junctions, known as the blood-labyrinth barrier (Jahnke 1975, Shi 2016). Therefore, the organ of Corti or spiral ganglia can be best reached by AONs through diffusion in the perilymph (reviewed by Swan et al. 2008). AONs can enter the perilymph after diffusion through the round window membrane, to which they can be delivered by intratympanic injection. For a durable effect, transport vehicles that slowly release AONs, such as microimplants (Arnold et al. 2005), biodegradable hydrogels (Endo et al. 2005, Paulson et al. 2008) or encapsulating nanoparticles (Tamura et al. 2005, Ge et al. 2007, Kim et al. 2015), are

under development. Alternatively, AONs can be directly delivered into the inner ear upon cochleostomy, but this method has the risk to induce the formation of hydrops or fibrosis (Ishiyama et al. 2016). A further option is injection into the endolymphatic sac, of which injections of adenoviral vectors resulted in the targeting of mainly the marginal cells in the striavascularis and the supporting cells in the organ of Corti (Yamasoba et al. 1999). Once the cell type responsible for the *USH2A*-associated progressive hearing impairment has been unraveled, the appropriate method of AON addition into the inner ear can be determined.

SPLICE MODULATION THERAPY FOR USHER SYNDROME

The aim of the research described in this thesis was to evaluate the potential of splice modulation as therapeutic strategy for patients with Usher syndrome type 2a. Pre-clinical proof-of-concept for this exon skipping approach was obtained using a zebrafish model with a protein truncating mutation in *ush2a* exon13 (**chapter 2b** and **4**). The predicted domains in usherin are conserved between zebrafish and man and the overall photoreceptor morphology is highly similar between the two species (**chapter 2b**). Therefore, the effect of *ush2a* exon 13 skipping in zebrafish is likely indicative for a therapeutic effect of exon 13 skipping in patients with mutations in the orthologous exon. Additionally, the genetic architecture of *USH2A* exon 13 is similar between zebrafish and man, allowing for a similar AON design. Indeed, ongoing efforts show that AONs designed to target human *USH2A* exon 13 are able to induce exon 13 skipping in iPSC-derived photoreceptor precursor cells (unpublished data). The next step is to clinically evaluate the effect of exon skipping in order to determine whether AON-induced skipping of *USH2A* exon 13 will be safe and will stop or slow down the progression of retinal degeneration in patients.

The number of patients with Usher syndrome that would benefit from an exon skipping therapy is highest for *USH2A* exon 13. However, using the experiments from this thesis as guidelines for AON design, efficacy testing and the validation in patient-derived cells or in animal models (**chapter 3** and **4**) for other exons, more patients could benefit relatively quickly. Additionally, also a combination of exons could potentially be skipped to increase the amount of patients that are eligible for an exon skipping therapy (Aslesh, Maruyama, and Yokota 2018). A similar treatment is expected to be applicable to prevent visual dysfunction as a consequence of a mutation in other genes encoding large Usher proteins with a repetitive domain structure, such as ADGRV1, protocadherin-15 or cadherin-23. Based on the results in this thesis, a therapeutic option for patients with selected mutations in *USH2A* might be in sight.

REFERENCES

- Aartsma-Rus, A. 2012. "Overview on AON design." *Methods Mol Biol* 867:117-29. doi: 10.1007/978-1-61779-767-5_8.
- Aartsma-Rus, A. . 2014. "Dystrophin Analysis in Clinical Trials." *J Neuromuscul Dis* 1 (1):41-53.
- Aartsma-Rus, A., and A. M. Krieg. 2017. "FDA Approves Eteplirsen for Duchenne Muscular Dystrophy: The Next Chapter in the Eteplirsen Saga." *Nucleic Acid Ther* 27 (1):1-3. doi: 10.1089/nat.2016.0657.
- Aartsma-Rus, A., L. van Vliet, M. Hirschi, A. A. Janson, H. Heemskerk, C. L. de Winter, S. de Kimpe, J. C. van Deutekom, P. A. t Hoen, and G. J. van Ommen. 2009. "Guidelines for antisense oligonucleotide design and insight into splice-modulating mechanisms." *Mol Ther* 17 (3):548-53. doi: 10.1038/mt.2008.205.
- Abudayyeh, O. O., J. S. Gootenberg, S. Konermann, J. Joung, I. M. Slaymaker, D. B. Cox, S. Shmakov, K. S. Makarova, E. Semenova, L. Minakhin, K. Severinov, A. Regev, E. S. Lander, E. V. Koonin, and F. Zhang. 2016. "C2c2 is a single-component programmable RNA-guided RNA-targeting CRISPR effector." *Science* 353 (6299):aaf5573. doi: 10.1126/science.aaf5573.
- Adato, A., G. Lefevre, B. Delprat, V. Michel, N. Michalski, S. Chardenoux, D. Weil, A. El-Amraoui, and C. Petit. 2005. "Usherin, the defective protein in Usher syndrome type IIA, is likely to be a component of interstereocilia ankle links in the inner ear sensory cells." *Hum Mol Genet* 14 (24):3921-32. doi: 10.1093/hmg/ddi416.
- Arnold, W., P. Senn, M. Hennig, C. Michaelis, K. Deingruber, R. Scheler, H. J. Steinhoff, F. Riphagen, and K. Lamm. 2005. "Novel slow- and fast-type drug release round-window microimplants for local drug application to the cochlea: an experimental study in guinea pigs." *Audiol Neurootol* 10 (1):53-63. doi: 10.1159/000082575.
- Aslesh, T., R. Maruyama, and T. Yokota. 2018. "Skipping Multiple Exons to Treat DMD-Promises and Challenges." *Biomedicines* 6 (1). doi: 10.3390/biomedicines6010001.
- Astuti, G. D., M. Bertelsen, M. N. Preising, M. Ajmal, B. Lorenz, S. M. Faradz, R. Qamar, R. W. Collin, T. Rosenberg, and F. P. Cremers. 2016. "Comprehensive genotyping reveals RPE65 as the most frequently mutated gene in Leber congenital amaurosis in Denmark." *Eur J Hum Genet* 24 (7):1071-9. doi: 10.1038/ejhg.2015.241.
- Bakondi, B., W. Lv, B. Lu, M. K. Jones, Y. Tsai, K. J. Kim, R. Levy, A. A. Akhtar, J. J. Breunig, C. N. Svendsen, and S. Wang. 2016. "In Vivo CRISPR/Cas9 Gene Editing Corrects Retinal Dystrophy in the S334ter-3 Rat Model of Autosomal Dominant Retinitis Pigmentosa." *Mol Ther* 24 (3):556-63. doi: 10.1038/mt.2015.220.
- Bauss, K., B. Knapp, P. Jores, R. Roepman, H. Kremer, E. V. Wijk, T. Marker, and U. Wolfrum. 2014. "Phosphorylation of the Usher syndrome 1G protein SANS controls Magi2-mediated endocytosis." *Hum Mol Genet* 23 (15):3923-42. doi: 10.1093/hmg/duu104.
- Beriault, D. R., and G. H. Werstuck. 2013. "Detection and quantification of endoplasmic reticulum stress in living cells using the fluorescent compound, Thioflavin T." *Biochim Biophys Acta* 1833 (10):2293-301. doi: 10.1016/j.bbamcr.2013.05.020.
- Besnard, T., G. García-García, D. Baux, C. Vaché, V. Faugère, L. Larrieu, S. Léonard, J. M. Millan, S. Malcolm, M. Claustres, and A. F. Roux. 2014. "Experience of targeted Usher exome sequencing as a clinical test." *Mol Genet Genomic Med* 2 (1):30-43. doi: 10.1002/mgg3.25.

- Boldt, K., J. van Reeuwijk, Q. Lu, K. Koutroumpas, T. M. Nguyen, Y. Texier, S. E. van Beersum, N. Horn, J. R. Willer, D. A. Mans, G. Dougherty, I. J. Lamers, K. L. Coene, H. H. Arts, M. J. Betts, T. Beyer, E. Bolat, C. J. Gloeckner, K. Haidari, L. Hetterschijt, D. Iaconis, D. Jenkins, F. Klose, B. Knapp, B. Latour, S. J. Letteboer, C. L. Marcelis, D. Mitic, M. Morleo, M. M. Oud, M. Riemersma, S. Rix, P. A. Terhal, G. Toedt, T. J. van Dam, E. de Vrieze, Y. Wissinger, K. M. Wu, G. Apic, P. L. Beales, O. E. Blacque, T. J. Gibson, M. A. Huynen, N. Katsanis, H. Kremer, H. Omran, E. van Wijk, U. Wolfrum, F. Kepes, E. E. Davis, B. Franco, R. H. Giles, M. Ueffing, R. B. Russell, R. Roepman, and Uk K. Rare Diseases Group. 2016. "An organelle-specific protein landscape identifies novel diseases and molecular mechanisms." *Nat Commun* 7:11491. doi: 10.1038/ncomms11491.
- Bonnet, C., Z. Riahi, S. Chantot-Bastaraud, L. Smagghe, M. Letexier, C. Marcaillou, G. M. Lefevre, J. P. Hardelin, A. El-Amraoui, A. Singh-Estivalet, S. Mohand-Said, S. Kohl, A. Kurtenbach, I. Slieso-raityte, D. Zobor, S. Gherbi, F. Testa, F. Simonelli, S. Banfi, A. Fakir, D. Glavac, M. Jarc-Vidmar, A. Zupan, S. Battelino, L. Martorell Sampol, M. A. Claveria, J. Catala Mora, S. Dad, L. B. Moller, J. Rodriguez Jorge, M. Hawlina, A. Auricchio, J. A. Sahel, S. Marlin, E. Zrenner, I. Audo, and C. Petit. 2016. "An innovative strategy for the molecular diagnosis of Usher syndrome identifies causal biallelic mutations in 93% of European patients." *Eur J Hum Genet* 24 (12):1730-1738. doi: 10.1038/ejhg.2016.99.
- Cai, L., R. B. Innis, and V. W. Pike. 2007. "Radioligand development for PET imaging of beta-amyloid (A β)--current status." *Curr Med Chem* 14 (1):19-52.
- Chen, J. S., Y. S. Dagdas, B. P. Kleinstiver, M. M. Welch, A. A. Sousa, L. B. Harrington, S. H. Sternberg, J. K. Joung, A. Yildiz, and J. A. Doudna. 2017. "Enhanced proofreading governs CRISPR-Cas9 targeting accuracy." *Nature* 550 (7676):407-410. doi: 10.1038/nature24268.
- Cho, S. W., S. Kim, J. M. Kim, and J. S. Kim. 2013. "Targeted genome engineering in human cells with the Cas9 RNA-guided endonuclease." *Nat Biotechnol* 31 (3):230-2. doi: 10.1038/nbt.2507.
- Cho, S. W., S. Kim, Y. Kim, J. Kweon, H. S. Kim, S. Bae, and J. S. Kim. 2014. "Analysis of off-target effects of CRISPR/Cas-derived RNA-guided endonucleases and nickases." *Genome Res* 24 (1):132-41. doi: 10.1101/gr.162339.113.
- Comitato, A., M. T. Di Salvo, G. Turchiano, M. Montanari, S. Sakami, K. Palczewski, and V. Marigo. 2016. "Dominant and recessive mutations in rhodopsin activate different cell death pathways." *Hum Mol Genet* 25 (13):2801-2812. doi: 10.1093/hmg/ddw137.
- Cong, L., F. A. Ran, D. Cox, S. Lin, R. Barretto, N. Habib, P. D. Hsu, X. Wu, W. Jiang, L. A. Marraffini, and F. Zhang. 2013. "Multiplex genome engineering using CRISPR/Cas systems." *Science* 339 (6121):819-23. doi: 10.1126/science.1231143.
- Courtney, D. G., J. E. Moore, S. D. Atkinson, E. Maurizi, E. H. Allen, D. M. Pedrioli, W. H. McLean, M. A. Nesbit, and C. B. Moore. 2016. "CRISPR/Cas9 DNA cleavage at SNP-derived PAM enables both in vitro and in vivo KRT12 mutation-specific targeting." *Gene Ther* 23 (1):108-12. doi: 10.1038/gt.2015.82.
- Cox, D. B. T., J. S. Gootenberg, O. O. Abudayyeh, B. Franklin, M. J. Kellner, J. Joung, and F. Zhang. 2017. "RNA editing with CRISPR-Cas13." *Science* 358 (6366):1019-1027. doi: 10.1126/science.aaq0180.
- Cyranoski, D. 2016. "CRISPR gene-editing tested in a person for the first time." *Nature* 539 (7630):479. doi: 10.1038/nature.2016.20988.
- Dal Mas, A., M. E. Rogalska, E. Bussani, and F. Pagani. 2015. "Improvement of SMN2 pre-mRNA processing mediated by exon-specific U1 small nuclear RNA." *Am J Hum Genet* 96 (1):93-103. doi: 10.1016/j.ajhg.2014.12.009.

- Doench, J. G., N. Fusi, M. Sullender, M. Hegde, E. W. Vaimberg, K. F. Donovan, I. Smith, Z. Tothova, C. Wilen, R. Orchard, H. W. Virgin, J. Listgarten, and D. E. Root. 2016. "Optimized sgRNA design to maximize activity and minimize off-target effects of CRISPR-Cas9." *Nat Biotechnol* 34 (2):184-191. doi: 10.1038/nbt.3437.
- Doherty, D., A. E. Chudley, G. Coghlan, G. E. Ishak, A. M. Innes, E. G. Lemire, R. C. Rogers, A. A. Mhanni, I. G. Phelps, S. J. Jones, S. H. Zhan, A. P. Fejes, H. Shahin, M. Kanaan, H. Akay, M. Tekin, Forge Canada Consortium, B. Triggs-Raine, and T. Zelinski. 2012. "GPSM2 mutations cause the brain malformations and hearing loss in Chudley-McCullough syndrome." *Am J Hum Genet* 90 (6):1088-93. doi: 10.1016/j.ajhg.2012.04.008.
- Endo, T., T. Nakagawa, T. Kita, F. Iguchi, T. S. Kim, T. Tamura, K. Iwai, Y. Tabata, and J. Ito. 2005. "Novel strategy for treatment of inner ears using a biodegradable gel." *Laryngoscope* 115 (11):2016-20. doi: 10.1097/01.mlg.0000183020.32435.59.
- Fu, Y., J. D. Sander, D. Reyon, V. M. Cascio, and J. K. Joung. 2014. "Improving CRISPR-Cas nuclease specificity using truncated guide RNAs." *Nat Biotechnol* 32 (3):279-284. doi: 10.1038/nbt.2808.
- Fuster-Garcia, C., G. Garcia-Garcia, E. Gonzalez-Romero, T. Jaijo, M. D. Sequedo, C. Ayuso, R. P. Vazquez-Manrique, J. M. Millan, and E. Aller. 2017. "USH2A Gene Editing Using the CRISPR System." *Mol Ther Nucleic Acids* 8:529-541. doi: 10.1016/j.omtn.2017.08.003.
- Ge, X., R. L. Jackson, J. Liu, E. A. Harper, M. E. Hoffer, R. A. Wassel, K. J. Dormer, R. D. Kopke, and B. J. Balough. 2007. "Distribution of PLGA nanoparticles in chinchilla cochleae." *Otolaryngol Head Neck Surg* 137 (4):619-23. doi: 10.1016/j.otohns.2007.04.013.
- Haer-Wigman, L., W. A. van Zelst-Stams, R. Pfundt, L. I. van den Born, C. C. Klaver, J. B. Verheij, C. B. Hoyng, M. H. Breuning, C. J. Boon, A. J. Kievit, V. J. Verhoeven, J. W. Pott, S. C. Sallevelt, J. M. van Hagen, A. S. Plomp, H. Y. Kroes, S. H. Lelieveld, J. Y. Hehir-Kwa, S. Castelein, M. Nelen, H. Scheffer, D. Lugtenberg, F. P. Cremers, L. Hoefsloot, and H. G. Yntema. 2017. "Diagnostic exome sequencing in 266 Dutch patients with visual impairment." *Eur J Hum Genet* 25 (5):591-599. doi: 10.1038/ejhg.2017.9.
- Hartel, B. P., M. Lofgren, P. L. Huygen, I. Guchelaar, A. Njoe Kort N. Lo, A. M. Sadeghi, E. van Wijk, L. Tranebjaerg, H. Kremer, W. J. Kimberling, C. W. Cremers, C. Moller, and R. J. Pennings. 2016. "A combination of two truncating mutations in USH2A causes more severe and progressive hearing impairment in Usher syndrome type IIa." *Hear Res* 339:60-8. doi: 10.1016/j.heares.2016.06.008.
- Hartel, B. P., J. W. I. van Nierop, W. J. Huinck, L. J. C. Rotteveel, E. A. M. Mylanus, A. F. Snik, H. P. M. Kunst, and R. J. E. Pennings. 2017. "Cochlear Implantation in Patients With Usher Syndrome Type IIa Increases Performance and Quality of Life." *Otol Neurotol* 38 (6):e120-e127. doi: 10.1097/MAO.0000000000001441.
- Hibino, H., A. Inanobe, K. Furutani, S. Murakami, I. Findlay, and Y. Kurachi. 2010. "Inwardly rectifying potassium channels: their structure, function, and physiological roles." *Physiol Rev* 90 (1):291-366. doi: 10.1152/physrev.00021.2009.
- Hoffman, E. P., and E. M. McNally. 2014. "Exon-skipping therapy: a roadblock, detour, or bump in the road?" *Sci Transl Med* 6 (230):230fs14. doi: 10.1126/scitranslmed.3008873.
- Huang, D., J. D. Eudy, E. Uzvolgyi, J. R. Davis, C. B. Talmadge, D. Pretto, M. D. Weston, J. E. Lehman, M. Zhou, T. A. Seemayer, I. Ahmad, W. J. Kimberling, and J. Sumegi. 2002. "Identification of the mouse and rat orthologs of the gene mutated in Usher syndrome type IIa and the cellular source of USH2A mRNA in retina, a target tissue of the disease." *Genomics* 80 (2):195-203.

- Ikeda, Y., K. M. Nishiguchi, F. Miya, N. Shimozawa, J. Funatsu, S. Nakatake, K. Fujiwara, T. Tachibana, Y. Murakami, T. Hisatomi, S. Yoshida, Y. Yasutomi, T. Tsunoda, T. Nakazawa, T. Ishibashi, and K. H. Sonoda. 2018. "Discovery of a Cynomolgus Monkey Family With Retinitis Pigmentosa." *Invest Ophthalmol Vis Sci* 59 (2):826-830. doi: 10.1167/iovs.17-22958.
- Isgrig, K., J. W. Shteamer, I. A. Belyantseva, M. C. Drummond, T. S. Fitzgerald, S. Vijayakumar, S. M. Jones, A. J. Griffith, T. B. Friedman, L. L. Cunningham, and W. W. Chien. 2017. "Gene Therapy Restores Balance and Auditory Functions in a Mouse Model of Usher Syndrome." *Mol Ther* 25 (3):780-791. doi: 10.1016/j.ymthe.2017.01.007.
- Ishiyama, A., J. Doherty, G. Ishiyama, A. M. Quesnel, I. Lopez, and F. H. Linthicum. 2016. "Post Hybrid Cochlear Implant Hearing Loss and Endolymphatic Hydrops." *Otol Neurotol* 37 (10):1516-1521. doi: 10.1097/MAO.0000000000001199.
- Jahnke, K. 1975. "The fine structure of freeze-fractured intercellular junctions in the guinea pig inner ear." *Acta Otolaryngol Suppl* 336:1-40.
- Jinek, M., K. Chylinski, I. Fonfara, M. Hauer, J. A. Doudna, and E. Charpentier. 2012. "A programmable dual-RNA-guided DNA endonuclease in adaptive bacterial immunity." *Science* 337 (6096):816-21. doi: 10.1126/science.1225829.
- Jinek, M., A. East, A. Cheng, S. Lin, E. Ma, and J. Doudna. 2013. "RNA-programmed genome editing in human cells." *Elife* 2:e00471. doi: 10.7554/eLife.00471.
- Kerov, V. S., M. Natochin, and N. O. Artemyev. 2005. "Interaction of transducin-alpha with LGN, a G-protein modulator expressed in photoreceptor cells." *Mol Cell Neurosci* 28 (3):485-95. doi: 10.1016/j.mcn.2004.10.010.
- Kim, D. K., S. N. Park, K. H. Park, C. W. Park, K. J. Yang, J. D. Kim, and M. S. Kim. 2015. "Development of a drug delivery system for the inner ear using poly(amino acid)-based nanoparticles." *Drug Deliv* 22 (3):367-74. doi: 10.3109/10717544.2013.879354.
- Kleinstiver, B. P., V. Pattanayak, M. S. Prew, S. Q. Tsai, N. T. Nguyen, Z. Zheng, and J. K. Joung. 2016. "High-fidelity CRISPR-Cas9 nucleases with no detectable genome-wide off-target effects." *Nature* 529 (7587):490-5. doi: 10.1038/nature16526.
- Koehler, K. R., A. M. Mikosz, A. I. Molosh, D. Patel, and E. Hashino. 2013. "Generation of inner ear sensory epithelia from pluripotent stem cells in 3D culture." *Nature* 500 (7461):217-21. doi: 10.1038/nature12298.
- Konermann, Silvana, Peter Lotfy, Nicholas J. Brideau, Jennifer Oki, Maxim N. Shokhirev, and Patrick D. Hsu. 2018. "Transcriptome Engineering with RNA-Targeting Type VI-D CRISPR Effectors." *Cell*. doi: 10.1016/j.cell.2018.02.033.
- Krawitz, P. M., D. Schiska, U. Krüger, S. Appelt, V. Heinrich, D. Parkhomchuk, B. Timmermann, J. M. Millan, P. N. Robinson, S. Mundlos, J. Hecht, and M. Gross. 2014. "Screening for single nucleotide variants, small indels and exon deletions with a next-generation sequencing based gene panel approach for Usher syndrome." *Mol Genet Genomic Med* 2 (5):393-401. doi: 10.1002/mgg3.92.
- Kremer, H., E. van Wijk, T. Marker, U. Wolfrum, and R. Roepman. 2006. "Usher syndrome: molecular links of pathogenesis, proteins and pathways." *Hum Mol Genet* 15 Spec No 2:R262-70. doi: 10.1093/hmg/ddl205.
- Lambertus, S., N. M. Bax, A. Fakin, J. M. Groenewoud, B. J. Klevering, A. T. Moore, M. Michaelides, A. R. Webster, G. J. van der Wilt, and C. B. Hoyng. 2017. "Highly sensitive measurements of disease progression in rare disorders: Developing and validating a multimodal model of retinal degeneration in Stargardt disease." *PLoS One* 12 (3):e0174020. doi: 10.1371/journal.pone.0174020.

- Latella, M. C., M. T. Di Salvo, F. Cocchiarella, D. Benati, G. Grisendi, A. Comitato, V. Marigo, and A. Recchia. 2016. "In vivo Editing of the Human Mutant Rhodopsin Gene by Electroporation of Plasmid-based CRISPR/Cas9 in the Mouse Retina." *Mol Ther Nucleic Acids* 5 (11):e389. doi: 10.1038/mtna.2016.92.
- Lim, K. R., R. Maruyama, and T. Yokota. 2017. "Eteplirsen in the treatment of Duchenne muscular dystrophy." *Drug Des Devel Ther* 11:533-545. doi: 10.2147/DDDT.S97635.
- Liu, H., J. L. Pecka, Q. Zhang, G. A. Soukup, K. W. Beisel, and D. Z. He. 2014. "Characterization of transcriptomes of cochlear inner and outer hair cells." *J Neurosci* 34 (33):11085-95. doi: 10.1523/JNEUROSCI.1690-14.2014.
- Lobanova, E. S., S. Finkelstein, H. Song, S. H. Tsang, C. K. Chen, M. Sokolov, N. P. Skiba, and V. Y. Arshavsky. 2007. "Transducin translocation in rods is triggered by saturation of the GTPase-activating complex." *J Neurosci* 27 (5):1151-60. doi: 10.1523/JNEUROSCI.5010-06.2007.
- Maerker, T., E. van Wijk, N. Overlack, F. F. Kersten, J. McGee, T. Goldmann, E. Sehn, R. Roepman, E. J. Walsh, H. Kremer, and U. Wolfrum. 2008. "A novel Usher protein network at the periciliary reloading point between molecular transport machineries in vertebrate photoreceptor cells." *Hum Mol Genet* 17 (1):71-86. doi: 10.1093/hmg/ddm285.
- Maguire, A. M., F. Simonelli, E. A. Pierce, E. N. Pugh, Jr., F. Mingozzi, J. Bencicelli, S. Banfi, K. A. Marshall, F. Testa, E. M. Surace, S. Rossi, A. Lyubarsky, V. R. Arruda, B. Konkle, E. Stone, J. Sun, J. Jacobs, L. Dell'Osso, R. Hertle, J. X. Ma, T. M. Redmond, X. Zhu, B. Hauck, O. Zelenai, K. S. Shindler, M. G. Maguire, J. F. Wright, N. J. Volpe, J. W. McDonnell, A. Auricchio, K. A. High, and J. Bennett. 2008. "Safety and efficacy of gene transfer for Leber's congenital amaurosis." *N Engl J Med* 358 (21):2240-8. doi: 10.1056/NEJMoa0802315.
- Makino, S., G. G. Whitehead, C. L. Lien, S. Kim, P. Jhavar, A. Kono, Y. Kawata, and M. T. Keating. 2005. "Heat-shock protein 60 is required for blastema formation and maintenance during regeneration." *Proc Natl Acad Sci U S A* 102 (41):14599-604. doi: 10.1073/pnas.0507408102.
- Mardis, E. R. 2006. "Anticipating the 1,000 dollar genome." *Genome Biol* 7 (7):112. doi: 10.1186/gb-2006-7-7-112.
- Mauriac, S. A., Y. E. Hien, J. E. Bird, S. D. Carvalho, R. Peyrourou, S. C. Lee, M. M. Moreau, J. M. Blanc, A. Geysler, C. Medina, O. Thoumine, S. Beer-Hammer, T. B. Friedman, L. Ruttiger, A. Forge, B. Nurnberg, N. Sans, and M. Montcouquiol. 2017. "Defective Gpsm2/Galphi3 signalling disrupts stereocilia development and growth cone actin dynamics in Chudley-McCullough syndrome." *Nat Commun* 8:14907. doi: 10.1038/ncomms14907.
- McGee, T. L., B. J. Seyedahmadi, M. O. Sweeney, T. P. Dryja, and E. L. Berson. 2010. "Novel mutations in the long isoform of the *USH2A* gene in patients with Usher syndrome type II or non-syndromic retinitis pigmentosa." *J Med Genet* 47 (7):499-506. doi: 10.1136/jmg.2009.075143.
- McLean, W. J., X. Yin, L. Lu, D. R. Lenz, D. McLean, R. Langer, J. M. Karp, and A. S. B. Edge. 2017. "Clonal Expansion of Lgr5-Positive Cells from Mammalian Cochlea and High-Purity Generation of Sensory Hair Cells." *Cell Rep* 18 (8):1917-1929. doi: 10.1016/j.celrep.2017.01.066.
- Mendell, J. R., L. R. Rodino-Klapac, Z. Sahenk, K. Roush, L. Bird, L. P. Lowes, L. Alfano, A. M. Gomez, S. Lewis, J. Kota, V. Malik, K. Shontz, C. M. Walker, K. M. Flanigan, M. Corridore, J. R. Kean, H. D. Allen, C. Shilling, K. R. Melia, P. Sazani, J. B. Saoud, E. M. Kaye, and Group Eteplirsen Study. 2013. "Eteplirsen for the treatment of Duchenne muscular dystrophy." *Ann Neurol* 74 (5):637-47. doi: 10.1002/ana.23982.
- Mertini, L., and P. Sabatelli. 2015. "Improving clinical trial design for Duchenne muscular dystrophy." *BMC Neurol* 15:153. doi: 10.1186/s12883-015-0408-z.

- Mowat, F. M., K. J. Gervais, L. M. Occelli, M. J. Annear, J. Querubin, J. W. Bainbridge, A. J. Smith, R. R. Ali, and S. M. Petersen-Jones. 2017. "Early-Onset Progressive Degeneration of the Area Centralis in RPE65-Deficient Dogs." *Invest Ophthalmol Vis Sci* 58 (7):3268-3277. doi: 10.1167/iops.17-21930.
- Nelles, D. A., M. Y. Fang, M. R. O'Connell, J. L. Xu, S. J. Markmiller, J. A. Doudna, and G. W. Yeo. 2016. "Programmable RNA Tracking in Live Cells with CRISPR/Cas9." *Cell* 165 (2):488-96. doi: 10.1016/j.cell.2016.02.054.
- Oshima, K., K. Shin, M. Diensthuber, A. W. Peng, A. J. Ricci, and S. Heller. 2010. "Mechanosensitive hair cell-like cells from embryonic and induced pluripotent stem cells." *Cell* 141 (4):704-16. doi: 10.1016/j.cell.2010.03.035.
- Ottesen, E. W. 2017. "ISS-N1 makes the First FDA-approved Drug for Spinal Muscular Atrophy." *Transl Neurosci* 8:1-6. doi: 10.1515/tnsci-2017-0001.
- Overlack, N., D. Kilic, K. Bauss, T. Marker, H. Kremer, E. van Wijk, and U. Wolftrum. 2011. "Direct interaction of the Usher syndrome 1G protein SANS and myomegalin in the retina." *Biochim Biophys Acta* 1813 (10):1883-92. doi: 10.1016/j.bbamcr.2011.05.015.
- Pagliarini, V., P. La Rosa, and C. Sette. 2017. "Faulty RNA splicing: consequences and therapeutic opportunities in brain and muscle disorders." *Hum Genet* 136 (9):1215-1235. doi: 10.1007/s00439-017-1802-y.
- Pan, B., C. Askew, A. Galvin, S. Heman-Ackah, Y. Asai, A. A. Indzhykulian, F. M. Jodelka, M. L. Hastings, J. J. Lentz, L. H. Vandenberghe, J. R. Holt, and G. S. Geleoc. 2017. "Gene therapy restores auditory and vestibular function in a mouse model of Usher syndrome type 1c." *Nat Biotechnol* 35 (3):264-272. doi: 10.1038/nbt.3801.
- Park, S. T., and J. Kim. 2016. "Trends in Next-Generation Sequencing and a New Era for Whole Genome Sequencing." *Int Neurolog J* 20 (Suppl 2):S76-83. doi: 10.5213/inj.1632742.371.
- Paulson, D. P., W. Abuzeid, H. Jiang, T. Oe, B. W. O'Malley, and D. Li. 2008. "A novel controlled local drug delivery system for inner ear disease." *Laryngoscope* 118 (4):706-11. doi: 10.1097/MLG.0b013e31815f8e41.
- Pierrache, L. H., B. P. Hartel, E. van Wijk, M. A. Meester-Smoor, F. P. Cremers, E. de Baere, J. de Zaeytijd, M. J. van Schooneveld, C. W. Cremers, G. Dagnelie, C. B. Hoyng, A. A. Bergen, B. P. Leroy, R. J. Pennings, L. I. van den Born, and C. C. Klaver. 2016. "Visual Prognosis in *USH2A*-Associated Retinitis Pigmentosa Is Worse for Patients with Usher Syndrome Type IIa Than for Those with Nonsyndromic Retinitis Pigmentosa." *Ophthalmology* 123 (5):1151-60. doi: 10.1016/j.ophtha.2016.01.021.
- Ponnath, A., F. F. Depreux, F. M. Jodelka, F. Rigo, H. E. Farris, M. L. Hastings, and J. J. Lentz. 2018. "Rescue of Outer Hair Cells with Antisense Oligonucleotides in Usher Mice Is Dependent on Age of Treatment." *J Assoc Res Otolaryngol* 19 (1):1-16. doi: 10.1007/s10162-017-0640-x.
- Poss, K. D., A. Nechiporuk, A. M. Hillam, S. L. Johnson, and M. T. Keating. 2002. "Mps1 defines a proximal blastemal proliferative compartment essential for zebrafish fin regeneration." *Development* 129 (22):5141-9.
- Rah, H., D. J. Maggs, T. N. Blankenship, K. Narfstrom, and L. A. Lyons. 2005. "Early-onset, autosomal recessive, progressive retinal atrophy in Persian cats." *Invest Ophthalmol Vis Sci* 46 (5):1742-7. doi: 10.1167/iops.04-1019.
- Ran, F. A., L. Cong, W. X. Yan, D. A. Scott, J. S. Gootenberg, A. J. Kriz, B. Zetsche, O. Shalem, X. Wu, K. S. Makarova, E. V. Koonin, P. A. Sharp, and F. Zhang. 2015. "In vivo genome editing using *Staphylococcus aureus* Cas9." *Nature* 520 (7546):186-91. doi: 10.1038/nature14299.

- Ran, F. A., P. D. Hsu, C. Y. Lin, J. S. Gootenberg, S. Konermann, A. E. Trevino, D. A. Scott, A. Inoue, S. Matoba, Y. Zhang, and F. Zhang. 2013. "Double nicking by RNA-guided CRISPR Cas9 for enhanced genome editing specificity." *Cell* 154 (6):1380-9. doi: 10.1016/j.cell.2013.08.021.
- Reiners, J., K. Nagel-Wolfrum, K. Jurgens, T. Marker, and U. Wolfrum. 2006. "Molecular basis of human Usher syndrome: deciphering the meshes of the Usher protein network provides insights into the pathomechanisms of the Usher disease." *Exp Eye Res* 83 (1):97-119. doi: 10.1016/j.exer.2005.11.010.
- Ross, J. W., J. P. Fernandez de Castro, J. Zhao, M. Samuel, E. Walters, C. Rios, P. Bray-Ward, B. W. Jones, R. E. Marc, W. Wang, L. Zhou, J. M. Noel, M. A. McCall, P. J. DeMarco, R. S. Prather, and H. J. Kaplan. 2012. "Generation of an inbred miniature pig model of retinitis pigmentosa." *Invest Ophthalmol Vis Sci* 53 (1):501-7. doi: 10.1167/iov.11-8784.
- Sangermano, R., M. Khan, S. S. Cornelis, V. Richelle, S. Albert, A. Garanto, D. Elmelik, R. Qamar, D. Lugtenberg, L. I. van den Born, R. W. J. Collin, and F. P. M. Cremers. 2018. "ABCA4 midigenes reveal the full splice spectrum of all reported noncanonical splice site variants in Stargardt disease." *Genome Res* 28 (1):100-110. doi: 10.1101/gr.226621.117.
- Schnetkamp, P. P., A. H. Jalloul, G. Liu, and R. T. Szerencsei. 2014. "The SLC24 family of K(+)-dependent Na(+)-Ca(2)(+) exchangers: structure-function relationships." *Curr Top Membr* 73:263-87. doi: 10.1016/B978-0-12-800223-0.00007-4.
- Scotti, M. M., and M. S. Swanson. 2016. "RNA mis-splicing in disease." *Nat Rev Genet* 17 (1):19-32. doi: 10.1038/nrg.2015.3.
- Seyedahmadi, B. J., C. Rivolta, J. A. Keene, E. L. Berson, and T. P. Dryja. 2004. "Comprehensive screening of the *USH2A* gene in Usher syndrome type II and non-syndromic recessive retinitis pigmentosa." *Exp Eye Res* 79 (2):167-73. doi: 10.1016/j.exer.2004.03.005.
- Shi, X. 2016. "Pathophysiology of the cochlear intrastrial fluid-blood barrier (review)." *Hear Res* 338:52-63. doi: 10.1016/j.heares.2016.01.010.
- Shmakov, S., A. Smargon, D. Scott, D. Cox, N. Pyzocha, W. Yan, O. O. Abudayyeh, J. S. Gootenberg, K. S. Makarova, Y. I. Wolf, K. Severinov, F. Zhang, and E. V. Koonin. 2017. "Diversity and evolution of class 2 CRISPR-Cas systems." *Nat Rev Microbiol* 15 (3):169-182. doi: 10.1038/nrmicro.2016.184.
- Slaymaker, I. M., L. Gao, B. Zetsche, D. A. Scott, W. X. Yan, and F. Zhang. 2016. "Rationally engineered Cas9 nucleases with improved specificity." *Science* 351 (6268):84-8. doi: 10.1126/science.aad5227.
- Slepak, V. Z., and J. B. Hurley. 2008. "Mechanism of light-induced translocation of arrestin and transducin in photoreceptors: interaction-restricted diffusion." *IUBMB Life* 60 (1):2-9. doi: 10.1002/iub.7.
- Smargon, A. A., D. B. T. Cox, N. K. Pyzocha, K. Zheng, I. M. Slaymaker, J. S. Gootenberg, O. A. Abudayyeh, P. Essletzbichler, S. Shmakov, K. S. Makarova, E. V. Koonin, and F. Zhang. 2017. "Cas13b Is a Type VI-B CRISPR-Associated RNA-Guided RNase Differentially Regulated by Accessory Proteins Csx27 and Csx28." *Mol Cell* 65 (4):618-630 e7. doi: 10.1016/j.molcel.2016.12.023.
- Sokolov, M., A. L. Lyubarsky, K. J. Strissel, A. B. Savchenko, V. I. Govardovskii, E. N. Pugh, Jr., and V. Y. Arshavsky. 2002. "Massive light-driven translocation of transducin between the two major compartments of rod cells: a novel mechanism of light adaptation." *Neuron* 34 (1):95-106.
- Sorusch, N., K. Bauss, J. Plutniok, A. Samanta, B. Knapp, K. Nagel-Wolfrum, and U. Wolfrum. 2017. "Characterization of the ternary Usher syndrome SANS/ush2a/whirlin protein complex." *Hum Mol Genet* 26 (6):1157-1172. doi: 10.1093/hmg/ddx027.

- Sujirakul, T., M. K. Lin, J. Duong, Y. Wei, S. Lopez-Pintado, and S. H. Tsang. 2015. "Multimodal Imaging of Central Retinal Disease Progression in a 2-Year Mean Follow-up of Retinitis Pigmentosa." *Am J Ophthalmol* 160 (4):786-98 e4. doi: 10.1016/j.ajo.2015.06.032.
- Suzuki, K., Y. Tsunekawa, R. Hernandez-Benitez, J. Wu, J. Zhu, E. J. Kim, F. Hatanaka, M. Yamamoto, T. Araoka, Z. Li, M. Kurita, T. Hishida, M. Li, E. Aizawa, S. Guo, S. Chen, A. Goebel, R. D. Soligalla, J. Qu, T. Jiang, X. Fu, M. Jafari, C. R. Esteban, W. T. Berggren, J. Lajara, E. Nunez-Delgado, P. Guillen, J. M. Campistol, F. Matsuzaki, G. H. Liu, P. Magistretti, K. Zhang, E. M. Callaway, K. Zhang, and J. C. Belmonte. 2016. "In vivo genome editing via CRISPR/Cas9 mediated homology-independent targeted integration." *Nature* 540 (7631):144-149. doi: 10.1038/nature20565.
- Swan, E. E., M. J. Mescher, W. F. Sewell, S. L. Tao, and J. T. Borenstein. 2008. "Inner ear drug delivery for auditory applications." *Adv Drug Deliv Rev* 60 (15):1583-99. doi: 10.1016/j.addr.2008.08.001.
- Tamura, T., T. Kita, T. Nakagawa, T. Endo, T. S. Kim, T. Ishihara, Y. Mizushima, M. Higaki, and J. Ito. 2005. "Drug delivery to the cochlea using PLGA nanoparticles." *Laryngoscope* 115 (11):2000-5. doi: 10.1097/01.mlg.0000180174.81036.5a.
- Tian, M., W. Wang, D. Delimont, L. Cheung, M. Zallocchi, D. Cosgrove, and Y. W. Peng. 2014. "Photoreceptors in whirler mice show defective transducin translocation and are susceptible to short-term light/dark changes-induced degeneration." *Exp Eye Res* 118:145-53. doi: 10.1016/j.exer.2013.10.021.
- Trudeau, M. C., and W. N. Zagotta. 2003. "Calcium/calmodulin modulation of olfactory and rod cyclic nucleotide-gated ion channels." *J Biol Chem* 278 (21):18705-8. doi: 10.1074/jbc.R300001200.
- Tucker, B. A., R. F. Mullins, L. M. Streb, K. Anfinson, M. E. Eyestone, E. Kaalberg, M. J. Riker, A. V. Drack, T. A. Braun, and E. M. Stone. 2013. "Patient-specific iPSC-derived photoreceptor precursor cells as a means to investigate retinitis pigmentosa." *Elife* 2:e00824. doi: 10.7554/eLife.00824.
- van Wijk, E., B. van der Zwaag, T. Peters, U. Zimmermann, H. Te Brinke, F. F. Kersten, T. Marker, E. Aller, L. H. Hoefsloot, C. W. Cremers, F. P. Cremers, U. Wolfrum, M. Knipper, R. Roepman, and H. Kremer. 2006. "The DFNB31 gene product whirlin connects to the Usher protein network in the cochlea and retina by direct association with USH2A and VLGR1." *Hum Mol Genet* 15 (5):751-65. doi: 10.1093/hmg/ddi490.
- Vijayakumar, S., F. F. Depreux, F. M. Jodelka, J. J. Lentz, F. Rigo, T. A. Jones, and M. L. Hastings. 2017. "Rescue of peripheral vestibular function in Usher syndrome mice using a splice-switching antisense oligonucleotide." *Hum Mol Genet* 26 (18):3482-3494. doi: 10.1093/hmg/ddx234.
- Woll, M. G., H. Qi, A. Turpoff, N. Zhang, X. Zhang, G. Chen, C. Li, S. Huang, T. Yang, Y. C. Moon, C. S. Lee, S. Choi, N. G. Almstead, N. A. Naryshkin, A. Dakka, J. Narasimhan, V. Gabbeta, E. Welch, X. Zhao, N. Risher, J. Sheedy, M. Weetall, and G. M. Karp. 2016. "Discovery and Optimization of Small Molecule Splicing Modifiers of Survival Motor Neuron 2 as a Treatment for Spinal Muscular Atrophy." *J Med Chem* 59 (13):6070-85. doi: 10.1021/acs.jmedchem.6b00460.
- Wu, W. H., Y. T. Tsai, S. Justus, T. T. Lee, L. Zhang, C. S. Lin, A. G. Bassuk, V. B. Mahajan, and S. H. Tsang. 2016. "CRISPR Repair Reveals Causative Mutation in a Preclinical Model of Retinitis Pigmentosa." *Mol Ther* 24 (8):1388-94. doi: 10.1038/mt.2016.107.
- Yamasoba, T., M. Yagi, B. J. Roessler, J. M. Miller, and Y. Raphael. 1999. "Inner ear transgene expression after adenoviral vector inoculation in the endolymphatic sac." *Hum Gene Ther* 10 (5):769-74. doi: 10.1089/10430349950018526.

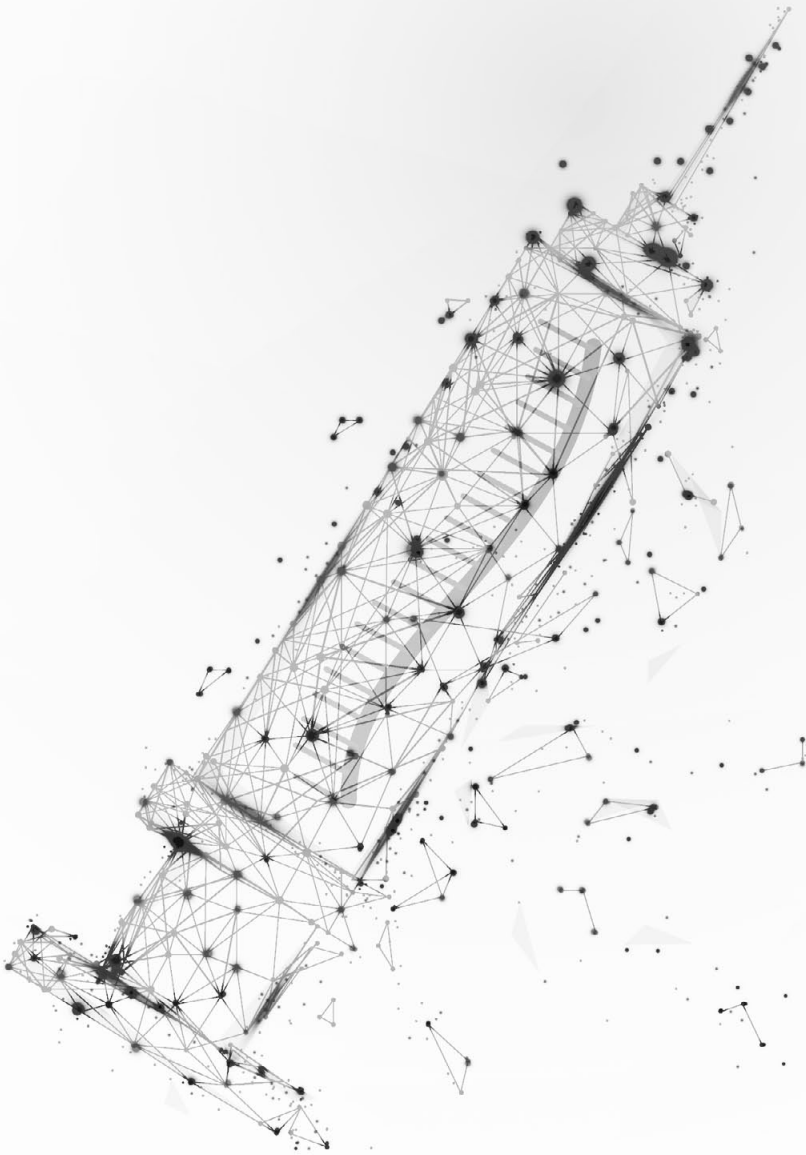
- Yan, Winston X., Shaorong Chong, Huaibin Zhang, Kira S. Makarova, Eugene V. Koonin, David R. Cheng, and David A. Scott. 2018. "Cas13d Is a Compact RNA-Targeting Type VI CRISPR Effector Positively Modulated by a WYL-Domain-Containing Accessory Protein." *Molecular Cell*. doi: 10.1016/j.molcel.2018.02.028.
- Yan, X., H. Zhou, J. Zhang, C. Shi, X. Xie, Y. Wu, C. Tian, Y. Shen, and J. Long. 2009. "Molecular mechanism of inward rectifier potassium channel 2.3 regulation by tax-interacting protein-1." *J Mol Biol* 392 (4):967-76. doi: 10.1016/j.jmb.2009.07.060.
- Yang, J., X. Liu, Y. Zhao, M. Adamian, B. Pawlyk, X. Sun, D. R. McMillan, M. C. Liberman, and T. Li. 2010. "Ablation of whirlin long isoform disrupts the USH2 protein complex and causes vision and hearing loss." *PLoS Genet* 6 (5):e1000955. doi: 10.1371/journal.pgen.1000955.
- Yanik, M., B. Muller, F. Song, J. Gall, F. Wagner, W. Wende, B. Lorenz, and K. Stieger. 2017. "In vivo genome editing as a potential treatment strategy for inherited retinal dystrophies." *Prog Retin Eye Res* 56:1-18. doi: 10.1016/j.preteyeres.2016.09.001.
- Zazo Seco, C., M. Wesdorp, I. Feenstra, R. Pfundt, J. Y. Hehir-Kwa, S. H. Lelieveld, S. Castelein, C. Gilissen, I. J. de Wijs, R. J. Admiraal, R. J. Pennings, H. P. Kunst, J. M. van de Kamp, S. Tammaing, A. C. Houweling, A. S. Plomp, S. M. Maas, P. A. de Koning Gans, S. G. Kant, C. M. de Geus, S. G. Frints, E. K. Vanhoutte, M. F. van Dooren, M. H. van den Boogaard, H. Scheffer, M. Nelen, H. Kremer, L. Hoefsloot, M. Schraders, and H. G. Yntema. 2017. "The diagnostic yield of whole-exome sequencing targeting a gene panel for hearing impairment in The Netherlands." *Eur J Hum Genet* 25 (3):308-314. doi: 10.1038/ejhg.2016.182.
- Zeng, F. G. 2017. "Challenges in Improving Cochlear Implant Performance and Accessibility." *IEEE Trans Biomed Eng* 64 (8):1662-1664. doi: 10.1109/TBME.2017.2718939.
- Zetsche, B., J. S. Gootenberg, O. O. Abudayyeh, I. M. Slaymaker, K. S. Makarova, P. Essletzbichler, S. E. Volz, J. Joung, J. van der Oost, A. Regev, E. V. Koonin, and F. Zhang. 2015. "Cpf1 is a single RNA-guided endonuclease of a class 2 CRISPR-Cas system." *Cell* 163 (3):759-71. doi: 10.1016/j.cell.2015.09.038.

Chapter 6

In Brief



Chapter 6^a



Summary And Conclusions

Usher syndrome is the most common cause of combined deaf- and blindness. Approximately 1 in 6,000 individuals has bi-allelic mutations in either one of the ten Usher-associated genes that lead to this autosomal recessively inherited disorder. Three clinical types of Usher syndrome can be distinguished, USH1, USH2 and USH3, based on the age of onset, the presence or absence, the severity and the progression of these symptoms (overview in **Chapter 1**). The majority of patients present with Usher syndrome type 2 (USH2), which is characterized by congenital moderate-to-severe bilateral hearing impairment and retinitis pigmentosa (RP) that becomes apparent around the end of the second decade of life. About 85% of USH2 patients have mutations in *USH2A*. Additionally, mutations in *USH2A* are the most frequent cause of autosomal recessively inherited non-syndromic RP (arRP). For this reason, the aim of the research in this thesis was to (1) improve the understanding of the underlying molecular pathogenesis of USH2-associated retinal degeneration and (2) to evaluate the potential of splice modulation as a future treatment option for patients with mutations in *USH2A*.

Usher-associated proteins have a restricted expression profile and are predominantly expressed in the inner ear hair cells and retinal photoreceptors, in which they exert a specialized function. Hence, designing *in vitro* assays to study the USH2 proteins is challenging. The role of USH-associated proteins in the inner ear has been largely determined by studying wild-type and knock-out mouse models for the associated Usher syndrome genes, but the retina in these mice models is mostly not, or only mildly, affected. This indicates the presence of anatomical or physiological differences between murine and human photoreceptors that limit the suitability of rodent models to study the pathogenesis of Usher syndrome-associated retinal degeneration. To identify these and other differences between vertebrate animal models, we reviewed all species for which animal models for inherited retinal dystrophies have been generated and characterized. We compared their retinal morphology, the observed phenotypes and discussed their suitability for different research purposes (**chapter 2a**). Based on the comparative analyses in **chapter 2a**, the zebrafish was identified as an attractive model organism to study Usher-associated proteins and was therefore used as model to study the role of USH2 proteins and complexes in the retina. **Chapter 2b** describes the generation and characterization of two targeted *ush2a* knock-out zebrafish models (*ush2a^{rmc1/rmc1}* and *ush2a^{b1245/b1245}*). Analysis of the mutant retinas demonstrated that *ush2a^{rmc1/rmc1}* mutant zebrafish completely lack the *ush2a*-encoded protein usherin, whereas in the retina of *ush2a^{b1245/b1245}* zebrafish usherin could still be detected with antibodies recognizing the N-terminal ectodomain. We concluded that usherin lacking the intracellular region is still properly localizing to the photoreceptor periciliary membrane of *ush2a^{b1245/b1245}* mutant zebrafish. Both mutants showed a reduced retinal function as was determined by electroretinogram recordings from homozygous larvae, largely in the absence of apoptotic photoreceptors. Challenging these mutants with constant bright light for 72

hours resulted in a significant increase in the amount of apoptotic cells in the outer nuclear layer (ONL) as compared to strain- and age-matched wild-types. Histological analysis of adult mutant zebrafish eyes revealed no signs of progressive retinal degeneration, possibly due to the regenerative capacities of zebrafish. In conclusion, these zebrafish mutants are considered to be suitable for studying *USH2A*-associated retinal dysfunction and will likely play an important role in the future in elucidating the retinal pathogenesis that leads to photoreceptor degeneration in patients with Usher syndrome.

To better understand the molecular function of the USH2 protein complex(es) in the retina, we expanded the known USH2 protein interactome by the identification of novel candidate interacting partners of the USH2 scaffold protein whirlin (**Chapter 2c**). We generated a transgenic zebrafish that expresses Strep/FLAG-tagged Whrna (SF-Whrna), the whirlin ortholog with the highest binding-affinity for usherin, under the control of a photoreceptor-specific promoter. A single-step affinity purification was performed to isolate Whrna-associated protein complexes from the adult zebrafish retina and subsequent mass spectrometry analysis unveiled that these complexes consisted of, among others, Preso1, Kir2.3 and LRRC8-channels. The human orthologs of Kir2.3 and Preso1 directly interacted with human whirlin in a yeast two-hybrid assay, indicating that our novel approach is able to identify relevant novel interactors. Furthermore, Preso1 was already indirectly associated with whirlin in the inner ear and Kir2.3 has been shown to be part of a CASK-mediated mechanism of vesicle acceptance. Based on these data, we hypothesize that Kir2.3 channels, together with whirlin, LIN7C, CASK, and potentially other proteins, are involved in the regulation of cargo vesicle acceptance at the base of the photoreceptor connecting cilium.

In **Chapter 3**, we demonstrate that AONs are able to correct aberrant *USH2A* pre-mRNA splicing caused by the deep intronic c.7595-2144A>G mutation in *USH2A* intron 40. The c.7595-2144A>G mutation generates a high quality splice donor site that results in the inclusion of a 152 nucleotide pseudoexon (PE40) into the mature *USH2A* transcript predicted to result in premature termination of usherin translation. Pseudoexons are ideal targets for an AON-based treatment, since splice correction results in a wild-type transcript. To identify AONs with efficient exon skipping characteristics, we compiled a step-by-step protocol (**chapter 3a**). The designed AONs targeting *USH2A* PE40 were able to efficiently redirect *USH2A* splicing in fibroblasts from patients with the c.7595-2144A>G mutation (**chapter 3b**). To evaluate the effect of AON-based splice correction at the level of retina function, we generated a CRISPR/Cas9-based humanized zebrafish model in which human *USH2A* PE40 with flanking sequences was introduced in intron 40 of the zebrafish *ush2a* gene (**chapter 3c**). However, human *USH2A* PE40 was poorly recognized by the zebrafish splicing machinery. For this reason, we developed a zebrafish-specific cell-based minigene splice assay to evaluate human splice site recognition

by the zebrafish splicing machinery, prior to generating humanized zebrafish knock-in models. In case of *USH2A* PE40, we adapted the human PE40 splice acceptor site towards the zebrafish splice acceptor consensus sequence. This modification resulted in a significantly improved recognition of human PE40 by the zebrafish splicing machinery. In conclusion, we have shown that AONs are able to efficiently prevent the inclusion of PE40 in the *USH2A* transcript in patient-derived fibroblasts. These results indicate that AON-based splice correction has the potential to become a future treatment option for patients with *USH2A*-associated retinal degeneration caused by the c.7595-2144A>G mutation.

Chapter 4 describes the effect of zebrafish *ush2a* exon 13 skipping on retina function. Using an optimized dose of exon 13-targeting morpholinos, exon 13 could be efficiently skipped from *ush2a* transcripts in zebrafish larvae. Treatment of our previously generated *ush2a*^{rmc1/rmc1} mutant zebrafish with these morpholinos resulted in a partial rescue of usherin expression at the photoreceptor periciliary membrane and in restored electroretinogram b wave amplitudes. Therefore, this study provides *in vivo* proof-of-concept that early retinal dysfunction as a consequence of mutations in *ush2a* exon 13 can be rescued by skipping of this exon in zebrafish.

In conclusion, the studies described in this thesis use cell and zebrafish models to expand the USH2 protein network with novel interaction candidates and to provide proof-of-concept for an exon skipping as a therapeutic strategy. Future research will determine whether AON-induced skipping of exon 13 in selected patients with *USH2A*-associated retinal degeneration results in a similar therapeutic effect in man (**chapter 5**). By following the protocol described in **chapter 3a**, AONs can be relatively easily designed to target other (combinations of) exons in *USH2A* or other USH genes. Therefore, once AONs targeting *USH2A* exon 13 have proven to be effective in halting or preventing retinal degeneration, potentially also patients with mutations in other exons, either in *USH2A* or other USH genes, could similarly benefit from a splice redirection therapy in the future (**chapter 5**).

Chapter 6^b



Samenvatting En Conclusies

Usher syndroom is de meest voorkomende oorzaak van gecombineerde doofheid en blindheid. Ongeveer 1 op de 6.000 personen heeft bi-allelische mutaties in één van de tien met Usher syndroom geassocieerde genen. Er zijn drie klinische typen Usher syndroom te onderscheiden, USH1, USH2 en USH3, op basis van de leeftijd waarop de ziekte tot uiting komt, en de aan- of afwezigheid, de ernst en progressie van de symptomen (overzicht in **hoofdstuk 1**). De meerderheid van de patiënten presenteert zich met Usher syndroom type 2 (USH2) dat wordt gekenmerkt door aangeboren, matige tot ernstige bilaterale gehoorstoornissen en retinitis pigmentosa (RP) die rond het einde van de tiener jaren tot uiting komt. Ongeveer 85% van de patiënten met USH2 heeft mutaties in het *USH2A*-gen. Bovendien zijn mutaties in dit gen de meest voorkomende oorzaak van autosomaal recessief overervende niet-syndromale RP (arRP). Om deze redenen was het doel van het onderzoek in dit proefschrift om (1) het inzicht te vergroten in de onderliggende moleculaire pathogenese van USH2-geassocieerde retinadegeneratie en (2) om het mogelijk positieve effect te onderzoeken van splice-modulatie als toekomstige behandeloptie voor patiënten met mutaties in *USH2A*.

De eiwitten gecodeerd door de USH-genen komen beperkt tot expressie en zijn voornamelijk aanwezig in de haarcellen van het binnenoer en de fotoreceptoren in de retina, waarin ze een specifieke functie vervullen. Daarom is het ontwerpen van *in vitro* testen om de USH2-eiwitten te bestuderen een uitdaging. De rol van USH-eiwitten in het binnenoer werd grotendeels bepaald door het bestuderen van wild-type en knock-out muismodellen voor genen die geassocieerd zijn met Usher syndroom, maar het netvlies in deze muismodellen is meestal niet, of slechts licht, afwijkend. Dit toont de aanwezigheid van anatomische of fysiologische verschillen aan tussen menselijke fotoreceptoren en die van de muis. Door deze verschillen zijn knaagdiermodellen ongeschikt om de pathogenese van retinadegeneratie bij Usher syndroom te bestuderen. Om deze en andere verschillen tussen de gewervelde dieren te identificeren, hebben we alle soorten met elkaar vergeleken waarvan diermodellen voor een erfelijke retinadystrofie zijn gegenereerd en gekarakteriseerd. We keken hierbij naar de morfologie van de retina, de waargenomen fenotypes en we bediscussieerden hun geschiktheid voor verschillende onderzoeksdoeleinden (**hoofdstuk 2a**). Op basis van deze vergelijkende analyses werd de zebrafish geïdentificeerd als een aantrekkelijk modelorganisme om USH-eiwitten te bestuderen en werd deze als model gebruikt om de rol van USH2-eiwitten en -complexen in het netvlies te bestuderen. **Hoofdstuk 2b** beschrijft het genereren en karakteriseren van twee *ush2a* knock-out zebrafish modellen (*ush2a^{rmc1/rmc1}* en *ush2a^{b1245/b1245}*). Analyse van de *ush2a^{rmc1/rmc1}* zebrafish toonde aan dat het door *ush2a* gecodeerde eiwit usherin mist. Daarentegen kon in de retina van de *ush2a^{b1245/b1245}* zebrafish usherin nog steeds worden gedetecteerd met antilichamen die het N-terminale ectodomein herkennen. Deze analyses lieten zien dat usherin zonder de intracellulaire regio nog steeds goed gelokaliseerd is in het periciliaire membraan van fotoreceptoren in de

ush2a^{b1245/b1245} zebnavis. Beide mutanten vertoonden een verminderde netvliesfunctie zoals werd bepaald door elektroretinografie van homozygoot-mutante larven met in hun netvlies weinig apoptotische fotoreceptoren. Het blootstellen van deze mutanten aan fel licht gedurende 72 uur resulteerde in een significante toename van het aantal apoptotische cellen in de buitenste nucleaire laag (ONL) ten opzichte van wild-type larven met dezelfde genetische achtergrond en leeftijd na deze blootstelling. Histologische analyse van ogen van volwassen mutante zebnavissen liet geen tekenen zien van progressieve retinadegeneratie. Dit is mogelijk het gevolg van de regeneratieve vermogens van de zebnavis. Concluderend worden deze zebnavis mutanten geschikt geacht voor het bestuderen van *USH2A*-geassocieerde retina disfunctie. Daarom zullen deze vissen waarschijnlijk een belangrijke rol gaan spelen bij het ophelderen van de moleculaire mechanismen die leiden tot fotoreceptor degeneratie bij patiënten met Usher syndroom.

Om de moleculaire functie van de *USH2*-eiwitcomplexen in het netvlies beter te begrijpen, hebben we nieuwe (kandidaat) interactiepartners van het *USH2*-eiwit whirlin geïdentificeerd (**hoofdstuk 2c**). We hebben een transgene zebnavis gemaakt die Strep/FLAG-getagd Whrna (SF-Whrna), de whirlin-ortholoog in zebnavis met de hoogste bindingsaffiniteit voor usherin, onder de controle van een fotoreceptor specifieke promotor tot expressie brengt. Door middel van een enkele affiniteitszuivering werden Whrna-geassocieerde eiwitcomplexen uit de retina van volwassen zebnavissen geïsoleerd en met behulp van massaspectrometrie geanalyseerd. De geïsoleerde eiwitcomplexen bevatten onder andere Preso1, Kir2.3 en componenten van LRRC8-kanalen. De humane orthologen van Kir2.3 en Preso1 lieten een directe interactie zien met het menselijke whirlin in een 'yeast two-hybrid'-test, wat aangeeft dat onze nieuwe benadering in staat is om relevante nieuwe interactoren te identificeren. Bovendien was Preso1 al eerder indirect geassocieerd met whirlin in het binnenoer en is aangetoond dat Kir2.3 deel uitmaakt van een CASK-gemedieerd mechanisme van het aannemen van transportblaasjes in de cel. Op basis van deze gegevens veronderstellen we dat Kir2.3-kanalen, samen met whirlin, LIN7C, CASK en mogelijk andere eiwitten, betrokken zijn bij de regulatie en het aannemen van transportblaasjes aan de basis van het 'connecting' cilium in fotoreceptoren.

In **Hoofdstuk 3** laten we zien dat antisense oligonucleotiden (AONs) de afwijkende splicing van *USH2A* pre-mRNA kunnen corrigeren die wordt veroorzaakt door de diep-intronische c.7595-2144A>G mutatie in *USH2A* intron 40. De c.7595-2144A>G mutatie genereert een splice donor site van hoge kwaliteit die resulteert in de inclusie van een pseudoexon (PE40) in het mature *USH2A*-transcript. Deze inclusie wordt voorspeld te resulteren in voortijdige beëindiging van de usherin-eiwitsynthese. Pseudoexonen zijn ideale targets voor behandeling met AONs, omdat correctie van de afwijkende splicing (exon-skipping) resulteert in een normaal mRNA. Om AONs met efficiënte exon-

skipping kenmerken te identificeren, hebben we een stapsgewijs protocol opgesteld (**hoofdstuk 3a**). De ontworpen AONs, gericht tegen *USH2A* PE40, waren in staat om *USH2A* RNA-splicing efficiënt te corrigeren in fibroblasten van patiënten met de c.7595-2144A>G mutatie (**hoofdstuk 3b**). Om het effect van de AONs op retina functie te evalueren, hebben we met CRISPR/Cas9 een gehumaniseerd zebrafismodel gemaakt waarin het menselijke *USH2A* PE40 met flankerend DNA is geïntroduceerd in intron 40 van het zebrafish *ush2a*-gen (**hoofdstuk 3c**). Het menselijke *USH2A* PE40 werd echter slecht herkend door de zebrafis splicing-machinerie. Om deze reden hebben we een test ontwikkeld, waarbij we gebruik maken van gekweekte zebrafiscellen, om de herkenning van humane splice-sites door de zebrafis splicing-machinerie te evalueren, voorafgaand aan het genereren van gehumaniseerde zebrafismodellen. In het geval van *USH2A* PE40 hebben we de menselijke PE40 acceptor site aangepast aan de consensus sequentie van de zebrafis acceptor site. Deze modificatie resulteerde in een significant verbeterde herkenning van het menselijke PE40 door de zebrafis splicing-machinerie. Concluderend hebben we aangetoond dat AONs in staat zijn de inclusie van PE40 in het *USH2A*-RNA efficiënt te voorkomen in fibroblasten afkomstig van patiënten. Deze resultaten laten zien dat splice-correctie met AONs potentie heeft als toekomstige behandelmethode voor retinadegeneratie bij patiënten met de c.7595-2144A>G mutatie.

In **hoofdstuk 4** is het effect beschreven van het overslaan van zebrafis *ush2a* exon 13 op retinafunctie. Met een geoptimaliseerde dosis morfolino's gericht tegen exon 13, kan dit exon efficiënt worden overgeslagen in *ush2a*-RNA in zebrafislarven. Behandeling van onze eerder gegenereerde *ush2a*^{*rmc1/rmc1*} mutante zebrafis met deze morfolino's resulteerde in een gedeeltelijk herstel van de aanwezigheid van usherin in het periciliaire membraan van fotoreceptoren. Ook werd er een herstel van de amplitude van b-golven gemeten bij electroretinografie. Daarom biedt deze studie *in vivo* 'proof of concept' dat vroege retinadisfunctie als gevolg van mutaties in *ush2a* exon 13 kan worden voorkomen door het overslaan van dit exon in de zebrafis.

Samenvattend kunnen we stellen dat de in dit proefschrift beschreven studies met cel- en zebrafis-modellen het USH2-eiwitnetwerk hebben uitgebreid en 'proof of concept' hebben geleverd voor het overslaan van een exon als therapeutische strategie. Toekomstig onderzoek zal bepalen of overslaan van exon 13 van het *USH2A*-gen met behulp van AONs bij specifieke patiënten met retinadegeneratie resulteert in een vergelijkbaar therapeutisch effect in de mens (**hoofdstuk 5**). Door het volgen van het protocol dat is beschreven in **hoofdstuk 3a**, kunnen AONs relatief eenvoudig worden ontworpen om andere (combinaties van) exonen over te slaan in *USH2A* of andere genen geassocieerd met Usher syndroom. Als AONs gericht tegen *USH2A* exon 13 effectief blijken te zijn in het stoppen of voorkomen van retinadegeneratie, kunnen mogelijk ook patiënten met mutaties in andere exonen, hetzij in *USH2A* of andere USH-genen, in de

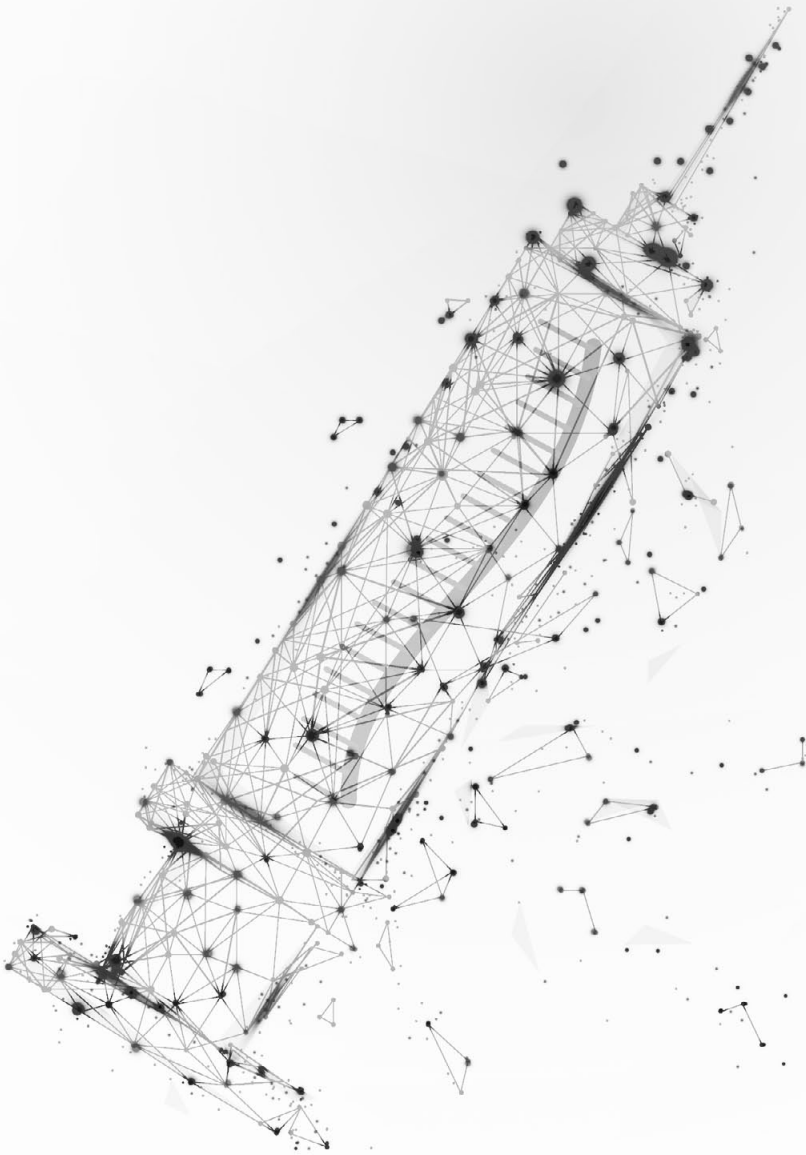
toekomst profiteren van een behandeling die afwijkende splicing van RNA corrigeert
(hoofdstuk 5).

Chapter 7

About The Author



Chapter 7A



List Of Publications

Slijkerman, RWN, Goloborodko, A, Hetterschijt, L, Peters, T, Gerits, M, Kremer, H, Van Wijk, E – *Poor splice-site recognition in a humanized zebrafish knock-in model for the recurrent deep-intronic c.7595-2144A>G mutation in USH2A*. Zebrafish, 2018, Doi: <https://doi.org/10.1089/zeb.2018.1613>

[PMID: 30281416]

Messchaert M, Dona M, Broekman S, Peters T, Serrano JC, **Slijkerman RWN**, Van Wijk E, Collin RWJ – *Eyes shut homolog (eys) is important for the maintenance of retinal architecture and visual function in zebrafish*. PLoS One, 2018, 13(7):e0200789, Doi: <https://doi.org/10.1371/journal.pone.0200789>

[PMID: 30052645]

Dona M*, **Slijkerman RWN***, Lerner KM, Broekman S, Wegner J, Howat TA, Peters T, Hetterschijt L, Boon N, De Vrieze E, Sorusch N, Wolfrum U, Kremer H, Neuhauss SC, Zang J, Kamermans M, Westerfield M[#], Phillips JB[#] and Van Wijk E[#] – *Usherin defects lead to early-onset retinal dysfunction in zebrafish*. Experimental Eye Research, 2018, Volume 173, Pages 148-159, Doi: <https://doi.org/10.1016/j.exer.2018.05.015>

[PMID: 29777677]

Slijkerman RWN, Kremer H and Van Wijk E – book chapter: *Antisense oligonucleotide design and evaluation of splice-modulating properties using cell-based assays*. Exon Skipping and Inclusion Therapies, Methods Mol Biol., 2018, pages 519-530, Doi: https://doi.org/10.1007/978-1-4939-8651-4_34.

[PMID: 30171565]

Slijkerman RWN, Kremer H, Van Wyk, E – *Molecular Genetics of Usher Syndrome: Current State of Understanding*. Encyclopedia of life sciences (eLS), 2017, Doi: <https://doi.org/10.1002/9780470015902.a0021456.pub2>

Slijkerman RWN*, Vaché C*, Dona M, García-García G, Claustres M, Hetterschijt L, Peters TA, Hartel BP, Pennings RJ, Millan JM, Aller E, Garanto A, Collin RW, Kremer H, Roux AF and Van Wijk E – *Antisense Oligonucleotide-based Splice Correction for USH2A-associated Retinal Degeneration Caused by a Frequent Deep-intronic Mutation*. Mol Ther Nucleic Acids. 2016;5:e381. Doi: 10.1038/mtna.2016.89.

[PMID: 28131284]

Slijkerman RWN*, Song F*, Astuti GD*, Huynen MA, van Wijk E, Stieger K and Collin RW – *The pros and cons of vertebrate animal models for functional and therapeutic research on inherited retinal dystrophies*. Prog Retin Eye Res. 2015 Sep;48:137-59. Doi: 10.1016/j.preteyeres.2015.04.004. Review.

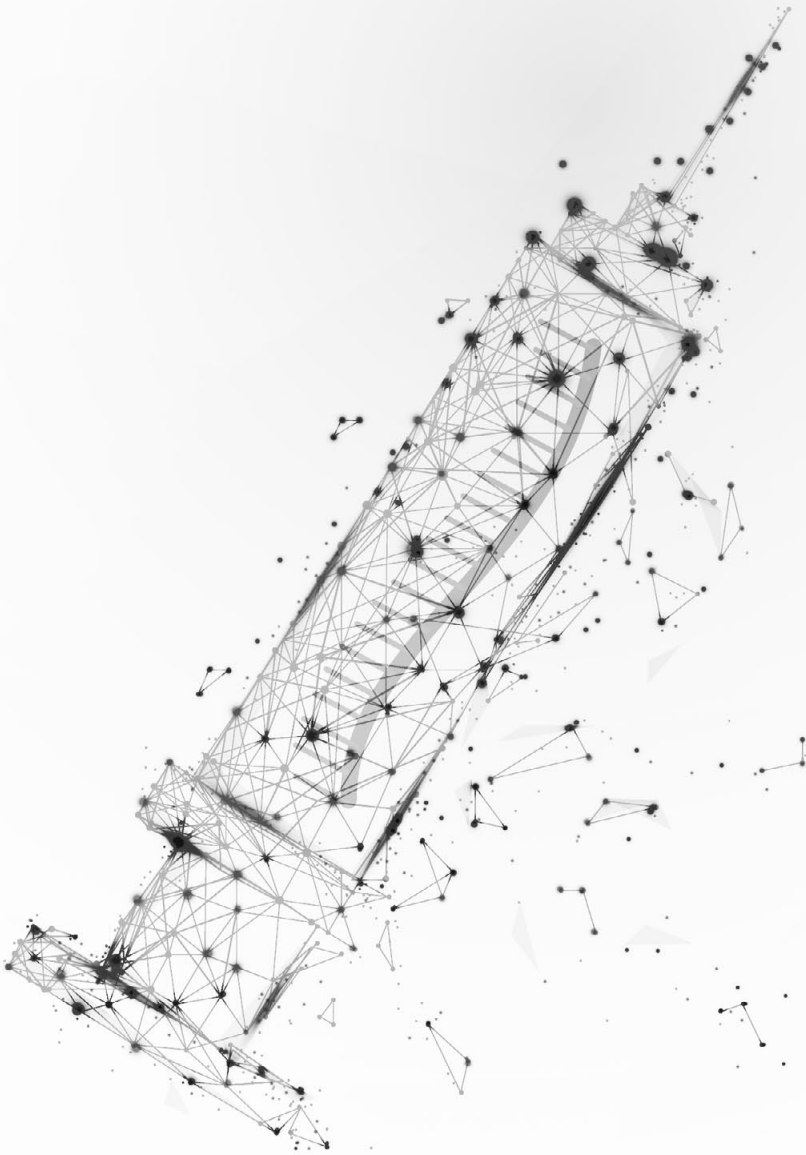
[PMID: 25936606]

Dona M*, Bachmann-Gagescu R*, Texier Y, Toedt G, Hetterschijt L, Tonnaer EL, Peters TA, van Beersum SE, Bergboer JG, Horn N, de Vrieze E, **Slijkerman RWN**, van Reeuwijk J, Flik G, Keunen JE, Ueffing M, Gibson TJ, Roepman R, Boldt K, Kremer H, van Wijk E – *NINL and DZANK1 Co-function in Vesicle Transport and Are Essential for Photoreceptor Development in Zebrafish*. PloS Genet. 2015 Oct 20;11(10):e1005574. Doi: 10.1371/journal.pgen.1005574.

[PMID: 26485514]

*/# Authors contributed equally

Chapter 7B



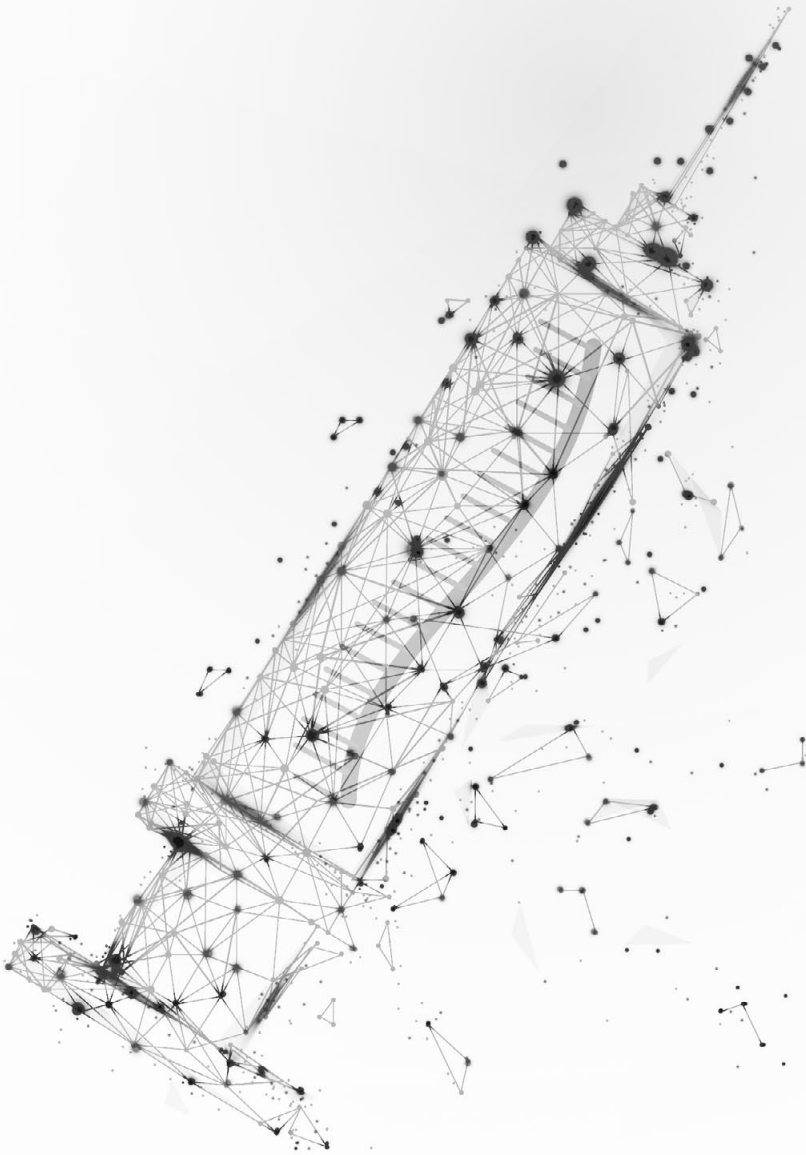
Curriculum Vitae

Ralph Slijkerman is geboren op 26 februari 1990 te Terneuzen. Nadat hij hier de lagere en middelbare school heeft voltooid, is hij in de zomer van 2008 verhuisd naar Nijmegen om daar de bacheloropleiding Moleculaire Levenswetenschappen aan de Radboud Universiteit te starten. Tegelijkertijd is hij bij scouting vereniging E.O.S. St. Hubertus te Terneuzen van jeugdlid 'overgevlogen' naar



verkennerleiding en is daar nog steeds actief. Tijdens de bachelorfase van zijn studie is Ralph actief geweest in een commissie van studievereniging V.C.M.W. Sigma en heeft hij wiskunde bijles gegeven aan een havo-leerling via stichting Studo. De bachelorstudie werd in 2011 afgerond met een zebra-vis-gerelateerde stage binnen de onderzoeksgroep van professor dr. Gert Flik. Tijdens de gelijknamige masteropleiding heeft Ralph zijn eerste onderzoeksstage in de groep van dr. Peter Willems in het RIMLS voltooid, waar hij werkte aan een FRET-gebaseerde biosensor in spiercellen van patiënten met afwijkingen in de mitochondriën. In zijn tweede masterstage werd polymerase recycling bestudeerd in de groep van professor dr. Torben Heick Jensen te Aarhus (Denemarken). Tijdens de masterfase was Ralph medeorganisator van een tweewekse studiereis naar Zweden en Noorwegen. In 2013 heeft hij de masteropleiding voltooid met het *judicium bene meritum*. Daaropvolgend is Ralph als promovendus in de groep van professor dr. Hannie Kremer en dr. Erwin van Wyk begonnen werken aan het ontrafelen van en therapie ontwikkeling voor het Usher syndroom, met dit proefschrift als resultaat. Tijdens het promotieonderzoek heeft hij het RIMLS Ph.D. programma gevolgd en heeft hij twee masterstudenten begeleid met hun wetenschappelijke eindstage. Naast zijn promotie onderzoek was Ralph sinds 2015 actief bij Stichting denktank Edison-Nijmegen, waar een interdisciplinaire groep denkers maatschappelijke vraagstukken probeert op te lossen door out-of-the-box ideeën te genereren. Het geven van de winnende pitch bij de Leiden weekend business challenge in februari 2017 was hiervan een hoogtepunt. Aansluitend aan zijn promotie onderzoek heeft Ralph in 2018 zijn carrière vervolgd als Science and Business Fellow bij Janssen Vaccines & Prevention B.V. te Leiden, onderdeel van de Johnson and Johnson Family of Companies.

Chapter 7c



Acknowledgements

“Wetenschap is topsport” wordt wel eens gezegd. Echter is het succes van die topsporter altijd mede-afhankelijk van het ondersteunende team. Er zijn heel veel mensen die ik tegen ben gekomen tijdens mijn Ph.D.-traject waarvan ik (veel) geleerd heb en/of mij op de een of andere manier gemotiveerd hebben. Hoewel ik slechts een selectie hieronder persoonlijk bedank, zijn ook niet-genoemde een waardevolle aanvulling voor mij geweest!

Erwin, ik voelde mij vereerd dat je mij hebt uitgekozen tijdens de sollicitatierondes om aan jouw eerste eigen project te werken: ‘Eur-USH’. Tijdens onze gezamenlijke overleggen werkte jouw steevast enthousiasme aanstekelijk bij mij. In combinatie met jouw onuitputtelijke wetenschappelijke kennis voel ik mij bevoorrecht om jou als co-promoter te hebben getroffen. Met de gelijktijdige afronding van twee promovendi onder jouw hoede, was er behoorlijk wat leeswerk te doen. Ik hoop dat dit boekje je daarbij voldoening geeft voor die genomen moeite!

Hannie, als promotor stond je iets verder van mijn onderzoek af. Desalniettemin is dit boekje mede gevormd dankzij jouw grondige opmerkingen op zowel wetenschappelijk als punctueel grammaticaal vlak. Je hebt me geleerd om altijd kritisch te zijn over proefopzetten, redematies en manuscripten, iets waar ik veel van heb geleerd en de rest van mijn carrière profijt van zal ondervinden!

Ronald, het was interessant om jouw (soms andere) invalshoek vanuit de kliniek te ervaren. Samen met Erwin heb jij de patiëntzorg en genetisch onderzoek weten te combineren, wat leidt tot een ijzersterke formule. Bedankt om ook mij de klinische invalshoek te laten zien, waar ik met name in mijn afsluitende discussie veel aan heb gehad!

Theo, Scherven brengen geluk is een oud gezegde. Mijn geluk is dat ik samen met jou heb mogen werken aan verschillende van mijn hoofdstukken, waardoor mijn thesis gedecoreerd is met zeer fraaie immunohistochemie! Jouw expertise en enthousiasme voor deze tak van de wetenschap heb ik vanaf mijn eerste dag bewonderd. Ik wil je bedanken voor alle moeite die je hebt gestopt om mij hierbij te ondersteunen, met name voor de Preso1 kleuringen in mijn laatste jaar, en voor jouw open houding waardoor ik altijd bij je terecht kon om ‘lopende zaken’ te evalueren.

Lisette, jij was degene die mij bij ‘binnenkomst’ wegwijs hebt gemaakt bij genetica zodat ik gelijk goed aan de slag kon. Later was je cruciaal in mijn ‘TAP’-experimenten. Maar ook zeker wil ik je bedanken voor de gezelligheid die je in het lab bracht!

Sanne, binnen korte tijd heb jij jezelf het zebra-vis onderzoek helemaal eigen gemaakt en daar heb ik de vruchten van kunnen plukken! Bedankt voor al je snelle antwoorden en hulp in het lab!

Margo, als mede-promovendus is jouw verdediging een mooi voorbeeld voor de mijne! Bij jou moet ik nog altijd aan die ene 1 april grap denken: ‘die met dat oog’. Veel succes met jouw vervolg carrière.

Erik, op de een of andere manier liepen onze gesprekken meer dan eens uit in een levendige discussie, zowel gevraagd als ongevraagd. Ik heb hier stiekem altijd erg van genoten en met name tijdens het schrijfproces vond ik dit een welkome afwisseling. Daarnaast ben ik je dankbaar voor de input die je mij hebt gegeven bij het 'TAP hoofdstuk'.

Dames (KaMan, Ideke, Machteld, Mariam, Brooke, Sylvia, Cenna and Minh) en Stef van het eiwit-lab, we hebben de eerste twee jaar van mijn promotietraject het lab gedeeld en ik heb het hier altijd erg naar mijn zin gehad met jullie. Ook toen wij drie labs verder zaten, kwam ik nog altijd graag langs om tips en tricks voor de yeast two-hybrid experimenten op te doen of mijn ervaringen van het schrijfproces en afronding te delen...! **KaMan**, jou wil ik in het bijzonder bedanken voor de leuke en interessante gesprekken die we gehad hebben. Een kopje koffie met jou heeft mij nooit verveeld! Veel succes met je vervolg carrière!

De Zebrafish And Therapy (Z.A.T.)-lab collega's (Muriël, Dyah, Lonneke, Julio, Alex, Matthijs, Anita, Tamara), met jullie heb ik met veel plezier samen in één lab gewerkt. Specifiek wil ik **Muriël** en **Lonneke** benoemen, want met jullie was het nooit saai in en buiten 'ons' lab! **Muriël**, bedankt dat jij me wilt bijstaan als paranimf! Het succes van het Z.A.T.-lab dagje-uit dat we samen hebben georganiseerd kunnen we nu mooi herhalen!

Alle voormalige kantoormaatjes (Margo, Armen, Renske, Judith, Benjamin (a.k.a. Bennie), Euginia, Marjolein, Ideke, Machteld, Evelien en Marije), met de meesten van jullie heb ik nogal wat tijd doorgebracht. Gelukkig bleven we erin geloven (in meer of mindere mate) dat er licht aan het einde van de tunnel moest zijn en dat blijkt er dus ook echt te zijn! Bedankt dat jullie altijd open stonden om een praatje te maken over wat dan ook! Ik wens jullie veel plezier en succes met jullie onderzoeken en vervolg carrière!

Beste collega's van de **oogheelkunde** in Nijmegen en **Ronald** 'uit Groningen', wat was het enorm leuk om jullie beter te leren kennen in onze gezamenlijke appartementen tijdens ARVO '16 in Seattle. En **Roos**, onze road-trip door Californië, die we na afloop hebben gemaakt, was erg tof!

Milou en **Alex**, jullie waren de twee studenten die ik heb begeleid tijdens mijn promotie onderzoek. Dankzij jullie enthousiasme en gedrevenheid waren veel collega Ph.D.-studenten jaloers op mij! Jullie harde en goede werken heeft dan ook daadwerkelijk iets kunnen toevoegen aan mijn onderzoek en leverde jullie een wel verdiende coauteurschap bij het zebavis knock-in paper op (hoofdstuk 3c). Veel succes in jullie vervolg carrière, Alex met jouw Ph.D. onderzoek in Göttingen en Milou met ambities in de medische wereld!

Medeleiding, met jullie heb ik de afgelopen jaren graag samengewerkt om de verkenners een uitdagend programma aan te bieden en om andere projecten binnen

scouting voor elkaar te krijgen. Ondanks dat ik niet altijd aanwezig kan zijn, heb ik het hier wel altijd naar mijn zin.

Denktank Edison-Nijmegen (o.a. Tom, Rob, Moana, Niels, Bernadette, Anne, Jesse, Niek, Jelle, Koen, Rogier, Joris, Nicole en Sanne), wat heb ik het enorm naar mijn zin gehad met jullie. Ik vond het altijd erg interessant om met onze brainstormsessies nieuwe ideeën aan te dragen bij een gemeente, een zorginstelling of bij de politie, om er maar een paar te noemen. Daarnaast was het natuurlijk een groot plezier tijdens onze jaarlijkse weekendjes in bijvoorbeeld Brugge en Nancy! Echter, de kers op de taart van mijn tijd bij Edison was toch wel het winnen van de weekend business challenge bij HubSpot Leiden! Doordat wij elkaar erg goed konden aanvullen, hebben we in een weekend een oersterk concept weten te pitchen! Ik weet zeker dat ook de toekomstige denkers nog veel interessante ideeën weten voort te brengen, want het interdisciplinaire concept van Edison is enorm waardevol!

Tim en Loek, ik vond het altijd leuk om elkaar minimaal jaarlijks weer te zien bij de tweedaagse RIMLS Ph.D.-retreat. We hadden hier altijd uitdagende wetenschappelijk discussies, waarbij één thema centraal stond: 'The sky is the limit'. Tim, in het bijzonder bedankt voor het delen van de kamer tijdens de retreat!

Tjeerd, Donny, Peter, Ivo, Floris en Niels, we hebben samen veel mooie avonturen meegemaakt! En of dit nu in Nijmegen, Goes, Stockholm, Aarhus, Den Haag, Eindhoven, Keulen, Leiden of ergens anders was, maakte daarbij weinig uit. Ik kijk uit naar onze toekomstige avonturen die we ongetwijfeld nog zullen gaan beleven! **Peter en Niels**, ik wens jullie veel plezier en succes met jullie promotietrajecten! **Tjeerd**, ik vind het top dat jij mij ondersteunt als paranimf tijdens mijn verdediging. Wellicht is je wetenschappelijke kennis over zebavissen en Usher net niet genoeg om mij bij te staan mocht dat nodig zijn, ik weet dat ik sowieso op je kan rekenen om er een mooi feest van te maken!

Tjeerd, Bob en andere fietsfanaten. De vele kilometers en mooie tochten die we samen hebben gereden waren voor mij een leuke afwisseling met het dagelijkse werk. **Lot**, in het bijzonder wil ik jou enorm bedanken voor de gastvrijheid tijdens de Fiets-Elfstedentocht. Deze tocht van 235 km lang was voor mij één groot feest waarbij ik mijn ogen heb uitgekeken!

Sven, Myrna, Tineke en Eric, ik waardeer het altijd erg om zo goed verzorgd te worden tijdens een 'weekendje Zeeland'. Met plezier heb ik dan ook vaak uit proberen leggen hoe het ook al weer zat met dat DNA, RNA en die 'antisense' streepjes. Pa, Ma, bedankt dat jullie mij hebben geleerd om door te zetten en mij altijd hebben gestimuleerd en aangemoedigd om mijn interesses te volgen. Dit boekje is daar het resultaat van!

Chapter 7^D



RIMLS Portfolio

PHD PORTFOLIO

Name PhD student:	R.W.N. Slijkerman	PhD period:	01-10-2013 until 30-11-2017
Department:	Otorhinolaryngology	Promotor(s):	Prof.dr. H.M.J. Kremer Dr. H.A.R. van Wijk Dr. R.J.E. Pennings
Graduate school:	Radboud Institute for Molecular Life Sciences	Co-promotor(s):	

TRAINING ACTIVITIES	Year(s)	ECTS
a) Courses & Workshops		
- Graduate Course 2014	2014	2
- Masterclass: Novel therapies for inherited retinal dystrophies	2014	0.2
- Scientific Integrity course	2015	1.0
- Laboratory animal science course	2015	3.0
- Writing course: 'effectieve schrijfstrategiën' by Joy de Jong	2016	3.0
- Advanced conversation English by Loraine Faulds	2017	1.5
b) Seminars & Lectures	2013-2017	3.85
c) (Inter)national Symposia & Congresses		
- Annual Meeting EUR-USH (Nijmegen)	2013	0.2
- Symposium: Novel therapies for inherited retinal dystrophies	2014	0.1
- Symposium: RIMLS New Frontiers	2013-2016	2.0
- PhD retreat ^{*,*,#}	2014-2017	3.0
- USHER symposium Boston [*]	2014	1.0
- Maastricht/Nijmegen Science day	2015	0.25
- Vision Camp (Leibertingen) [#]	2015	1.0
- E-rare annual meeting (Barcelona)	2016	0.25
- DOPS symposium ^{*,*}	2015, 2016	1.5
- ARVO 2016 (Seattle) [#]	2016	1.75
d) Other		
- Journal club department Human Genetics, Radboudumc ^{*,#}	2015, 2016	2.0
- Theme discussion department Human Genetics, Radboudumc ^{*,#}	2016, 2017	0.5
TEACHING ACTIVITIES	Year(s)	ECTS
e) Lecturing		
- EyeTN course: lecture	2015	0.1
- Practical guidance 1st year BMW students	2016	0.5
f) Other		
- Supervising master student MLS (Alex Goloborodko)	2014-2015	2.0
- Supervising master student Medicine (Milou Gerits)	2016	2.0
- Honours students: tour around the zebrafish facility	2016	0.1
TOTAL		32.8

* Poster presentation

Oral presentation

